CATALYTIC TRANSFORMATIONS ENABLED BY DUAL NICKELPHOTOREDOX MANIFOLDS

Bradley Higginson

UNIVERSITAT ROVIRA i VIRGILI

Catalytic transformations enabled by dual nickel-photoredox manifolds

Bradley Higginson

DOCTORAL THESIS
2022

Catalytic transformations enabled by dual nickel-photoredox manifolds

Bradley Higginson

DOCTORAL THESIS

Supervised by Prof Rubén Martín Romo

Institut Català d'Investigació Química (ICIQ)
Universitat Rovira i Virgili (URV)
Department of Analytical Chemistry & Organic Chemistry

Tarragona 2022

“Life is a roller coaster, just got to ride it”

- Ronan Keating

Prof. Ruben Martin Romo, Group Leader at the Institute of Chemical Research of Catalonia (ICIQ) and Research Professor of the Catalan Institution for Research and Advanced Studies (ICREA),

STATES that the present study, entitled “Catalytic transformations enabled by dual nickel-photoredox manifolds”, presented by Bradley Higginson for the award of the degree of Doctor, has been carried out under his supervision at the Institute of Chemical Research of Catalonia (ICIQ).

Tarragona, September 2022

Doctoral Thesis Supervisor

Users, RubÈn MartÌn Romo

Firmado digitalmente por Users, RubÈn MartÌn Romo
Fecha: 2022.09.12 14:08:55 +02'00'

Prof. Ruben Martin Romo

List of Publications

At the time of printing, the results reported herein have been published as:

1. **Higginson, B**.; Sanjosé-Orduna, J.; Gu, Y.; Martin, R. Nickel-Catalyzed Photodehalogenation of Aryl Bromides. *Synlett* **2021**, *32* (16), 1633–1636. https://doi.org/10/gj5rxq.
2. *Buendia, M. B.; ***Higginson, B**.; Kegnæs, S.; Kramer, S.; Martin, R. Redox-Neutral Ni-Catalyzed Sp3 C–H Alkylation of α-Olefins with Unactivated Alkyl Bromides. *ACS Catal.* **2022**, *12* (7), 3815–3820. https://doi.org/10/gqfs55.

* Indicates co-authorship

Table of Contents

Acknowledgements

The first person I would like to thank is of course, **Prof. Ruben Martin**. Thank you for your undying faith in my capabilities as a chemist. It has been a constant reassurance that even my wildest ideas may be viable. You have overseen my growth as a chemistry, from an incompetent wet chemist to someone who can take their ideas and get them into a flask. Thank you for your guidance and creating an environment of great chemistry by your *judicious* choice of chemists.

Secondly, I would like to thank the members of my committee, **Dr Igor Larrosa**, **Dr Arkaitz Correa**, and **Dr Fabio Julia** for accepting our invitation to read and assess my work.

I would also like to acknowledge the collaborators that I have worked with during my time as a PhD. Dr **Mikkel B. Buendia** and his supervisors Prof. **Søren Kegnæs,** Dr **Søren Kramer**. Thank you for a very fruitful collaboration on the allylic C-H functionalisation!! The work we produced I am very proud of, and it was great to get to know you when you visited the institute. Prof. **Martin Oestreich**, thank you for accepting me into your group to attempt some new chemistry that I still hold some hope for, both you and your group taught me a lot about myself and chemistry. As well as just how much I miss a university campus. I am forever appreciative for the opportunity to work in your group.

I am grateful for all those at ICIQ who work behind the scenes to make the ~~smooth~~ running of the institute. The lab technicians that made our lives easier, but most importantly **David Sadaba** whose organisational skills and dedication to making our lab run is awe inspiring. The research support area of ICIQ has been useful, so thank you for your help.

I would like to thank the funding body which provided the money **La Caixa**. The project that gave rise to these results received the support of a fellowship from “la Caixa” Foundation (ID 100010434). The fellowship code is 11660031. This project has received funding from the European Union´s Horizon 2020 research and innovation programme under the Marie Skłodowska-Curie grant agreement No. 713673.

Without this funding I would not have met my **Lacaixitos**. The “networking” events (getting bevved) allowed me to meet some truly wonderful scientists from across the world, but most importantly it allowed me to meet the Barcelona gang. The girls from *Balboa*, **Aru**, **Silvia**, and **Yas** will forever be in my heart, thank you, your presence and love has been felt from the first days of meeting you. **Poonam**, **Enrico**, **Loic**, **Ivan** and **Paloma**, **Ivan, Christophe, Theodora**, **Ifeanyi** (my roomie), **Ignasi**, **Luca**, **Max**… If I had to pour my heart for about each and every one of you my thesis would be twice as long, and your cups would be full. Thank you for being a part of this journey and I hope our paths are entwined for the rest of our time.

The **Ruben Alumni**, the Martini PhD-inis that were there from the beginning **Andreu**, **Raul** (mi hermano), **Marino**, thank you for welcoming me with open arms to the group, I wouldn't have had such a good time without all of you! **Yang Yang** and **Yiting** thank you for an awful project that may finally see the light of day! **Rosie,** you have been such a source of brightness, I hope we get to change the world of academia and don't just have to observe the terrible goings on. **Shang-zheng** the absolute chemistry machine, I am still in awe of your abilities as a chemist. **Craig** you are really an excellent chemist and a good person, I just hope I don't have to compete against you for any positions!

The post-doc alumni of our group are vast and are all worthy of mention! **Jacob**, you're a true chemistry hero and I have thoroughly enjoyed our time together in the group and thank you from the bottom of my heart for all of the thesis help. **Riccardo**, from visiting student to postdoc! Thank you for being a close friend and sounding board for some crazy ideas. **Matt,** the rugby lad behaviour was such an enjoyable energy to have in the group and you're dearly missed. From home to away, **Robert**, you and your family are a delight! I miss you all and I hope to visit Berlin when I can. **Hongfei**, **Jessica,** and **Jose**, the terrible three! I miss your energy and constant back and forth. **Ciro**, I genuinely nearly forgot you, but I am glad I checked my *spam*, it's been an experience to spend so much time with you and your interesting mind. Thank you to the rest of the postdoc alumni that have helped guide me through this ride of a PhD, the beers, the coffees, and the discourse. Thank you also to the visiting students, most importantly **Pascal** who came onto the enantioselective C-H project and struggled with me for a few months, it was a great time to get to know you.

The Martinis in its **current iteration**, Of course I have to start with the PhDs and wish you all the best of luck for the future, you're going to need it ;). **Laura**, the industry chemist stuck doing an academic PhD, unlucky, thank you for your attitude and wit and especially the Catalan abstract, I truly would not have this doctorate without this translation. **Carlotta**, it's been super nice to get to know you and your pragmatism over the years, remember that the PhD will finish! **Julien**, my French baby you are a gem of a human, and I am glad you are struggling in our lab with CO_2 it's a joy to watch you fail like I did; adversity brings strength, and you will be a better chemist for it, just keep going! **Julia (Paula)**, from the heights of bravas from Alicante to the depths of those from Tarragona, you are a joyous human, and it is good to have your energy in 2.12 we desperately needed it! **Adrian,** your Instagram captions are the best, keep partying <3, **Fei**, *HEY* my dear friend, push push push and I hope that your chemistry stops being sh*t and starts being good. **Dmitry**, the frustrated wet chemist turning to computational, your projects have been far worse than mine and I hope the switch to *in silico* helps you to get where you want, you deserve it.

Wen-jun, the machine-like spirit is astounding keep on grinding out those papers! **Jinhong**, you are such a lovely energy in the lab of 2.7 I hope to see your work go places. **Xinyang**, it has been very enjoyable to share the lab space with you over these years, I hope your projects work out and enable you to get where you want to go. **Hui** and **Hao**, the two newbies who are doing more social events than I ever did in my first year, keep the social light alive it will really help in those harder times. And finally, the current postdocs. **Franz** the Berlin boy, your vitality has reinvigorated me to just keep pushing, and your feedback on all manner of problems has been a blessing, may we party until our mid-40s. **Roman** clearly a theatre kid and my *twin*, you always ask me the right questions to make me feel really stupid, it's frustrating but necessary so thank you, a big xaxi. Also, my undying gratitude to you both for helping me with this thesis, many many beers are on me. **Jesus**, it's been super nice to get to know you over lunch and coffees! **Santosh**, it has been a real pleasure to get to know you.

Mum, of course you are the most important, my rock, the strongest most supportive and fantastic soul I know. Without your continued support, your love, your energy, and happiness I would not have made it here, I would not be me and I am forever thankful for you and everything you have ever done. The **Harris',** your strength knows no bounds, thank you for being there and supporting me, maybe one day I will get a proper job. **Tia**, I know that things may not be how we thought they would; I am struggling to find the poetic sentiment that I would like, but you've been on this journey with me, this is our achievement, thank you for your support and continuous love over the distance and time. The **Higginsons** thank you for all of your support and strength. **Heather**, I really don't know where to start but you are still the only person to visit me in TGN and this really means the whole world to me, I am truly grateful for our friendship. **Jess**, you are going to be a doctor too, but not a real doctor like me, a medical doctor so a lot more boring but a lot more useful. **The Barrow Boys** who have been a stabilising place and home for this journey, thank you. Lastly, **The University Gang** too, we absolutely do not see each other enough but I am so grateful to have you still very much present in my life.

And to all those I have stupidly missed because my memory recall is absolutely abysmal but have shared a place in my heart and life. Thank you.

Preface

The presented thesis has been performed at the Institute for Chemical Research of Catalonia (ICIQ) under the supervision of Professor Ruben Martin. The thesis is divided into five chapters: a general introduction, three research chapters, and a concluding chapter that summarises the Thesis. Each of the research chapters consists of an introduction and a summary of the aims of the project, followed by a discussion of the experimental results, and an experimental section.

Chapter 1, "General introduction" background themes and concepts are introduced concerning the application of photochemistry to organic synthesis. The concepts addressed will aid in the understanding of the works presented in the following chapters. Relevant literature is also presented concerning the combination of nickel and photoredox catalysis.

Chapter 2, "Development of an enantioselective C(sp^3)-H functionalisation technique harnessing metallatriplet catalysis" describes the preliminary development of an enantioselective C(sp^3)-H arylation of α-ether functionalities. The work done has tried to establish an optimised reaction for the enantioselective C-H functionalisation using a commercially available phosphinooxazoline ligand. Judicious choice of ketone and light source proved critical in the development of this reaction technique.

Chapter 3, "C(sp^3)-H functionalisation of allylic bonds", discloses the development of an allylic C(sp^3)-H functionalisation to achieve the translocated alkylation of terminal olefins. This methodology is redox neutral in nature and is characterised by its mild reaction conditions, absence of strong base, and excellent selectivity for the translocated site of reactivity. The technique is then extended to use gaseous olefins and arylation. Preliminary evidence is described which suggests that bromide radicals are involved. This work was conducted in collaboration with Dr Mikkel B. Buendia (primary bromides and mechanistic studies), my contribution of this work was the development of the secondary bromide series and extension of the work to arylation. This work is published in *ACS Catal.* **2022**, *12* (7), 3815–3820.

Chapter 4, "Nickel mediated proto- and deuterodehalogenation of aryl bromides using visible light", describes the development of a photoredox catalyst free hydrodehalogenation of aryl bromides using nickel under visible light irradiation. The reaction uses a substoichiometric amount of cesium iodide to achieve general reductive conditions. The mild conditions and a benign hydrogen source – THF – are used to afford a broad range of hydrodehalogenated aryl bromides. The technique is extended to deuterodehalogenation of aryl bromides using THF-d_8 as the deuterium source. The work described was conducted in collaboration with Dr Jesus Sanjosé-Orduna (mechanistic studies), and Yiting Gu (preliminary optimisation). This work is published in *Synlett* **2021**, *32* (16), 1633–1636.

Chapter 5, "Concluding remarks", the chapter summarises the presented works.

Glossary

4dMebpy: 4,4'-dimethyl-2,2'-bipyridine

4,7-dOMePhen: 4,7-dimethoxy-1,10-phenanthroline

5dCF$_3$bpy: 5,5'-bis(trifluoromethyl)-2,2'-bipyridine

AT: Atom Transfer
- XAT – Halogen Atom Transfer
- HAT – Hydrogen Atom Transfer

BDE: Bond Dissociation Energy

BDFE: Bond Dissociation Free Energy

B-E-P: Bell-Evans-Polanyi

BET: Back Electron Transfer

Bpy: 2,2'-bipyridine

CFL: Compact Fluorescent Light Bulb

CHD: 1,4-cyclohexadiene

COD: 1,5-cyclooctadiene

conPET: consecutive photoinduced electron transfer

DCI: 4,5-Dicyanoimidazole

Dcyb: 1, 4-(dicyclohexylphosphino)butane

dFCF3ppy: 2-(2,4-difluorophenyl)-5-(trifluoromethyl)pyridine

DG: Directing group

DMDC: dimethyldicarbonate

DME: 1,2-dimethoxyethane

dOMeBP: 4,4'dimethoxybenzophenone

dppe: 1,2-(Diphenylphosphino)ethane

dtbbpy: 4,4'-di-tert-butylbipyridine

EtOAc: ethyl acetate

E_{ox}: Reduction potential for molecule E[M/M$^{\bullet+}$]

E_{red}: Reduction potential for molecule E[M$^{\bullet-}$/M]

EDA: Electron Donor Acceptor

EnT: Energy Transfer

FG: Functional group

HOMO: Highest Occupied Molecular Orbital

hv: abbreviation used for "light"

NHPI: N-Hydroxyphthalimide

NIS: N-iodosuccinimide

NN: Bidentate ligand with two nitrogen donors

PBDE: polybrominated diphenyl ethers

PP: Bidentate ligand with two phosphine donors

PS / PC: Photosensitiser / Photocatalyst

Q: Quencher

RI: Reactive Intermediate

RP: Radical Precursor

SCE: Standard Calomel Electrode

SET: Single electron Transfer

SOMO: Singularly occupied molecular orbital

TBACl: Tetrabutyl ammonium chloride

TfOH: trifluoromethanesulfonic acid

THF: tetrahydrofuran

TS: Transition State

ttbtpy: 4, 4', 4'' tri-tert--butyl 2, 2': 6, 2''-terpyridine

YK: (4-methoxyphenyl) (4'-(trifluoromethyl) phenyl)methanone

Abstract

Over the past two decades, photoredox chemistry has undergone a renaissance that has seen a huge range of new reactivity developed. Access to innovative reaction manifolds and techniques has led to the creation of an expansive literature pool.[i] Combination of photoredox catalysis and transition metals has dramatically enhanced the synthetic organic chemist's toolbox,[ii] with the workhorse metal of this platform being nickel.

In line with the Martin Groups research themes of inert bond functionalisation and nickel mediated transformations, this doctoral thesis will focus on the combination of nickel with photoredox chemistry. The works presented consist of an enantioselective C(sp^3)-H functionalisation of α-ether bonds (chapter 2). A metallaphotoredox mediated allylic C(sp^3)-H alkylation using unactivated alkyl bromides (chapter 3). Finally, a photocatalyst free, visible light mediated, hydrodehalogenation of aryl bromides employing a nickel-phosphine catalyst (chapter 4).

The functionalisation of inert C(sp^3)-H bonds constitutes one of the holy grails of chemistry. Selective use of a C-H bond as a functional handle would open new synthetic routes and streamline synthesis. Despite the advantages of direct C(sp^3)-H functionalisation the reaction still remains a challenge, although photoredox platforms are becoming increasingly useful.[iii]

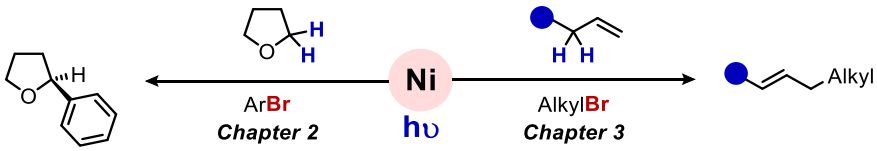

Figure 0.1.Nickel catalysed C(sp^3)-H bond functionalisation.

An additional layer of complexity would be the direct enantioselective functionalisation of C(sp^3)-H bonds which would constitute a powerful technique to access valuable chiral molecules from benign starting materials. To this end, we have developed a metallatriplet platform that affords the direct enantioselective functionalisation of C(sp^3)-H bonds (Chapter 2). The technique developed uses 390 nm light and a benzophenone catalyst in conjunction with a chiral nickel catalyst (Scheme 0.1, *left*) to afford the enantioenriched α-arylated ether.

i. McAtee, R. C.; McClain, E. J.; Stephenson, C. R. J. Illuminating Photoredox Catalysis. *Trends in Chemistry* **2019**, *1* (1), 111–125. https://doi.org/10.1016/j.trechm.2019.01.008.

ii. Chan, A. Y.; Perry, I. B.; Bissonnette, N. B.; Buksh, B. F.; Edwards, G. A.; Frye, L. I.; Garry, O. L.; Lavagnino, M. N.; Li, B. X.; Liang, Y.; Mao, E.; Millet, A.; Oakley, J. V.; Reed, N. L.; Sakai, H. A.; Seath, C. P.; MacMillan, D. W. C. Metallaphotoredox: The Merger of Photoredox and Transition Metal Catalysis. *Chem. Rev.* **2022**, *122* (2), 1485–1542. https://doi.org/10/gpnfxv.

iii.Holmberg-Douglas, N.; Nicewicz, D. A. Photoredox-Catalyzed C-H Functionalization Reactions. *Chemical Reviews* **2021**. https://doi.org/10.1021/acs.chemrev.1c00311.

An additional benefit of C(sp^3)-H functionalisation is the retention of functional groups which can be used in a subsequent synthetic step, the olefin functional handle remains one of the most synthetically versatile motifs in chemistry.[iv] An allylic C-H functionalisation technique would retain this valuable motif whilst increasing molecular complexity. Allylic C-H bond oxidation or C-X bond forming reactions has seen widespread development.[v] However the corresponding C-C bond forming reaction, especially forming C(sp^3)-C(sp^3) linkages remains challenging.

A technique that regioselectively alkylates the C(sp^3)-H bond with a general electrophile would be of value to the community. With this in mind, we developed a metallaphotoredox platform that combines a nickel complex with a photocatalyst to afford the redox-neutral alkylation of allylic C-H bonds (Chapter 3). The mild nature of this technique is highlighted by the broad scope and excellent control over the site selectivity of the protocol. Furthermore, preliminary evidence suggests the presence of bromide radicals as the abstracting species.

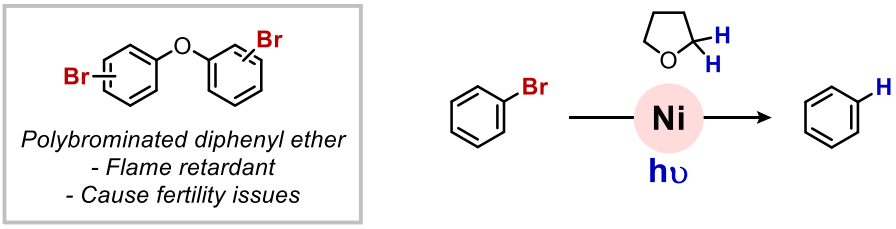

Figure 0.2. Nickel catalysed reduction of aryl bromides.

Brominated arenes have found widespread use in agrochemical and industrial applications due to their resistance to degradation. This general resistance can be problematic when disposal is required, furthermore oxidative techniques produce toxic by-products. Therefore, a reductive step is required before incineration.[vi] The hydrodehalogenation of arylbromides was commonly observed in Chapter 2 as an undesirable side product due to abstraction of a hydrogen from THF. With the problematic disposal of aryl bromides in mind we believed that a technique that uses THF as the hydrogen source could offer a mild and environmentally benign method to reduce aryl bromides (Chapter 4). To this end we developed a platform that dehalogenates a range of aryl bromides under visible light irradiation that requires only a substoichiometric amount cesium iodide salt. The reaction is then extended to the deuterodehalogenation of aryl bromides using THF-d_8

iv.Carruthers, W.; Coldham, I. MODERN METHODS OF ORGANIC SYNTHESIS. pp 315-369. https://doi.org/10/gfvbzj.
v. Kazerouni, A. M.; McKoy, Q. A.; Blakey, S. B. Recent Advances in Oxidative Allylic C–H Functionalization *via* Group IX-Metal Catalysis. *Chem. Commun.* **2020**, *56* (87), 13287–13300. https://doi.org/10/ggpm7k.
vi. Alonso, F.; Beletskaya, I. P.; Yus, M. Metal-Mediated Reductive Hydrodehalogenation of Organic Halides. *Chemical Reviews* **2002**, *102* (11), 4009–4092. https://doi.org/10/ft5wxh.

CHAPTER 1.

General Introduction

Introduction

1.1. Photochemistry

1.1.1. A brief history

Many chemical reactions require an input of energy.[1] The most typical form in a laboratory environment is heat. Nature, on the other hand, employs a much more energetic form - light. Chemists often take inspiration from nature and the application of light as an energy form is not an exception.[2] Documented cases of reactions promoted by sunlight go back centuries, one such example is the observation made by Tromsdorff in 1834 where crystals of α-santonin turn yellow and then burst under exposure to sunlight.[3] This reaction was revisited by chemists in the 1960s,[4] and studied computationally in the 2000s.[5] Updating historical literature with modern techniques and perspectives can lead to new and diverse reactivity, benefitting both chemistry and the broader society. However, the merger of visible light and organic synthesis was initially met with difficulty. The interaction of light and simple organic molecules is weak, so harnessing the power of light in a lab environment is not trivial.

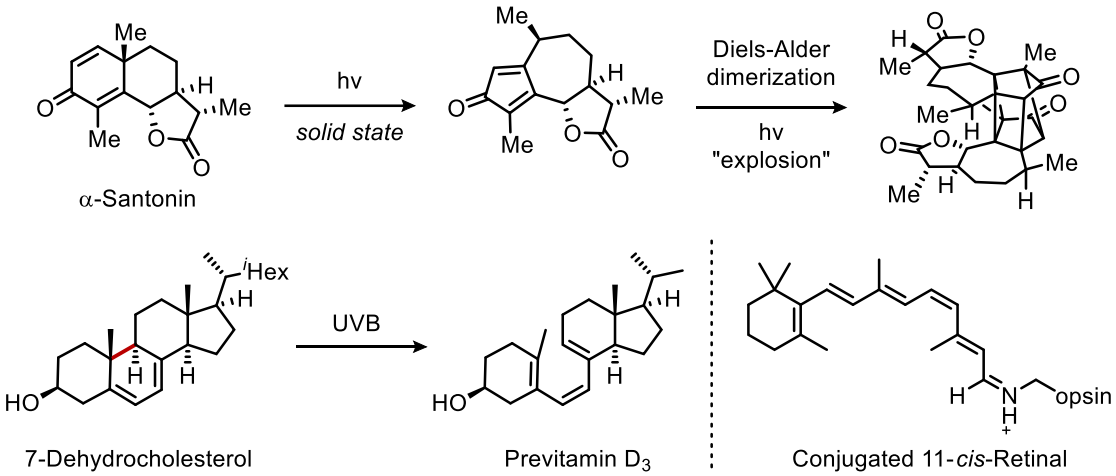

Figure 1.1.1. The elucidation of α-santonin's mechanism of explosion. Nature uses all forms of light.

Nature has circumvented this by using π extended systems such as retinal; or by exploiting high energy UV irradiation (i.e., in the synthesis of previtamin D_3 from 7-dehydrocholesterol, Figure 1.1.1). Taking inspiration from nature, sunlight was initially explored, Ciamician left sealed bottles in the sun for weeks or months at a time.[6] However, the discontinuous nature of sunlight (weather, night, seasons) and the poor interaction of visible light with many organic molecules made synthetic organic photochemistry an underdeveloped field. However, the fundamental study of light interacting with matter certainly flourished.

1.1.2. Fundamental understanding

The first law of photochemistry – The Grotthus Draper law – states that *"radiation must be absorbed by a chemical substance in order for a photochemical reaction to occur."* A molecule that absorbs a photon undergoes an electronic change from its ground state electronic configuration (M) to an excited state (Figure 1.1.2., often denoted with an asterisk, i.e., M*). The energy gap (ΔE) between the occupied molecular orbital and the unoccupied molecular orbital is equal to the energy of light (hv) where h is Planck's constant and v is the wavelength of light. (ΔE = hv).

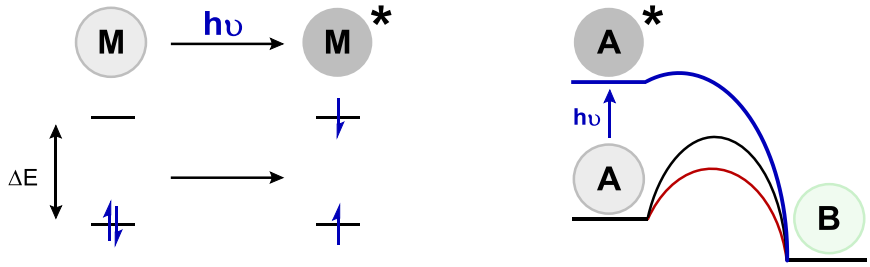

Figure 1.1.2. Electronic change of M when interacting with light. Cartoon showing catalysed, uncatalysed, and light promoted transformations.

The energy and reactivity of this excited state is considerably altered when compared to the ground state. The highly energetic nature is one of the key advantages that photochemistry has over thermal chemistry. Reactions are heated in the hope that the thermal input is sufficient to overcome the necessary energetic barriers, or a catalyst is introduced to lower or alter these barriers. The energy of an excited state within a photochemical process is already high and often greater than the energy barrier in which thermal chemistry is trying to overcome. This means that processes which cannot proceed with thermal chemistry readily do so in a photochemical setting.

Photochemistry also has societal benefits. The photon is often hailed as one of the greenest reagents in chemistry; a non-invasive, non-toxic, and a renewable reagent that imparts a controllable amount of energy on a system.[7] The "green" world of photochemistry was first suggested by Ciamician,[8] but it hasn't been until the past few decades where this has been realised in organic synthesis.[9] Again, the difficulties in photochemistry are due to the poor interaction of most organic matter with visible light. The use of UV has been used historically, but this requires specialised equipment. Shifting photochemistry into the visible spectrum could allow for cheap light sources and regular laboratory equipment to be used, two techniques have been used to do this, electron donor-acceptor (EDA) complexation and photosensitisation.

1.1.3. Electron Donor-Acceptor complexes

It is well known that strongly coloured solutions can form upon mixing two colourless organic compounds, this observation is the result of transient interactions between molecules.[10] The coloured interactions are often attributed to EDA complexes which are formed when electronically differentiated molecules interact within a system and have been rigorously studied by Mulliken.[11] Typically, electron rich donor (D) and electron poor acceptor (A) molecules will form these species (Figure 1.1.3). The new molecular aggregate formed absorb light at lower wavelengths than the individual components due to the electronic coupling of the frontier molecular orbitals.

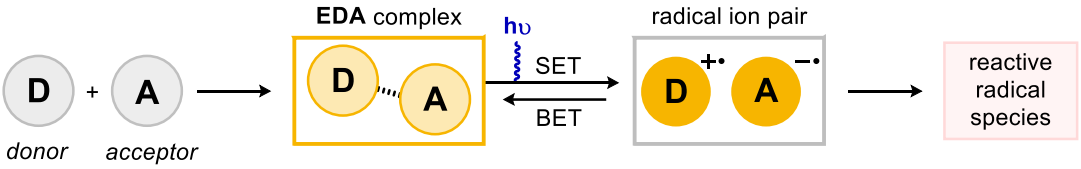

Figure 1.1.3. EDA complexation generates radical ion pair intermediates.

The presence of EDA complexes can be identified by the appearance of a charge-transfer band in the UV/Vis spectrum. Absorption of a photon with a wavelength within this charge-transfer band can trigger a charge separation through single electron transfer (SET) from the donor to the acceptor molecule, creating a radical ion pair. The most common pathway which this radical ion pair takes is a back electron transfer (BET) to reform the ground-state EDA complex. However, if the individual components can escape, then it is possible to generate radical species which can undergo radical reactivity.

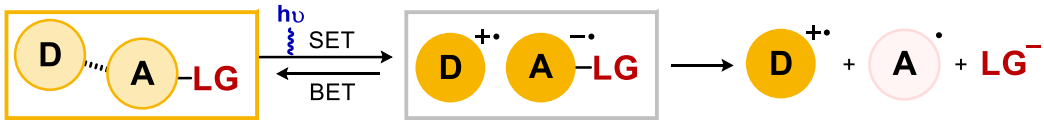

Figure 1.1.4. Installing a leaving group enables irreversible fragmentation to generate free radicals.

Although the fundamental photophysics of EDA complexes have been studied for several decades,[12] the synthetic utility of EDA complexes has been hampered due to BET.[13] To overcome this barrier, chemists have installed leaving groups (LG) that fragment upon formation of the radical ion pair to give the neutral radical and ionic LG (Figure 1.1.4).[14] The electrostatic attraction between the radical ion pair is removed so cage escape is facile and a neutral radical can undergo typical reactivity. Although EDA complex have received considerable attention, the generality of the technique is limited because it is reliant upon favourable interactions between the reactants. A more universally applicable concept is photosensitisation, where a photosensitive molecule absorbs light to form an excited state and can transfer the energy into the system by electron transfer.

1.1.4. Photosensitisation

Photosensitive molecules usually absorb within the visible spectrum or at lower wavelength UV (~ 390 nm). The process begins by absorption of a photon by the photosensitiser (PS) which is promoted to an excited state (PS*), the excited state will then interact with another molecule in the system, often called a “quencher” (Q) which is where photosensitisers impart the energy into the system.

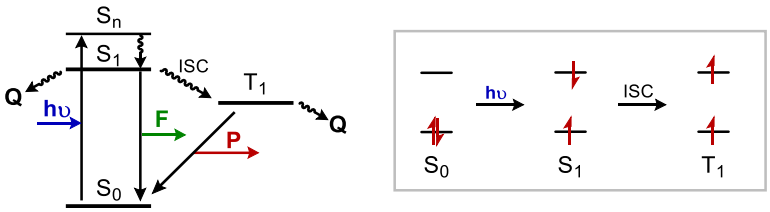

Figure 1.1.5. Jablonski diagram and the spin arrangement in the depicted states.

Jablonski diagrams (Figure 1.1.5, left) are used to picture the movement of the electron. Upon absorbing a photon equivalent to the energy gap, **hv**, an electron is promoted to a high energy singlet state (S_n), followed by instantaneous relaxation to the lowest singlet state (S_1). S_1 has a natural radiative lifetime, which means that the excited state will relax to S_0 with the emission of a photon, *fluorescence*, if no other processes deactivate it. The lifetime of S_1 is on the *micro*second to *nano*second (10^{-6}-10^{-9} s) range. If the rate of a competitive deactivation is slower than this (i.e., 10^{-5} s) then fluorescence will be the default mode of deactivation.

The singlet state can transition through a spin forbidden inversion to a triplet state (T_n), called *intersystem crossing* (ISC). T_n can be the lowest energy triplet state (T_1) or relax to this from a higher triplet state. T_1 is more stable than S_1, due to the forbidden nature of relaxation to the ground state. Emissive deactivation of this state is called *phosphorescence*, the natural radiative lifetime of T_1 is longer in the range of milliseconds to decaseconds (10^{-3}-10^{2} s).

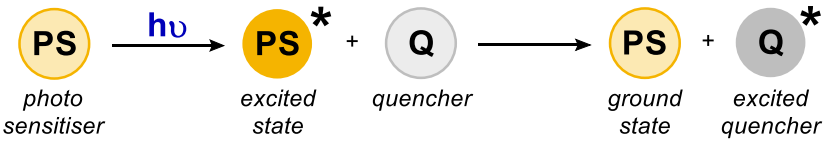

Figure 1.1.6. The excited state photocatalyst is quenched.

As mentioned, for an excited state photosensitiser to impart the energy into a system, a bimolecular interaction with a suitable molecule or “quencher” (**Q**) must occur (Figure 1.1.6). This is more realistic from T_1 due to its long-lived nature, although singlet sensitisation can also occur. Upon quenching PS*, the quenching molecule becomes excited, and the PS returns to the ground state. The nature of the electron transfer to the quenching molecule is especially important.

Introduction

Quenching

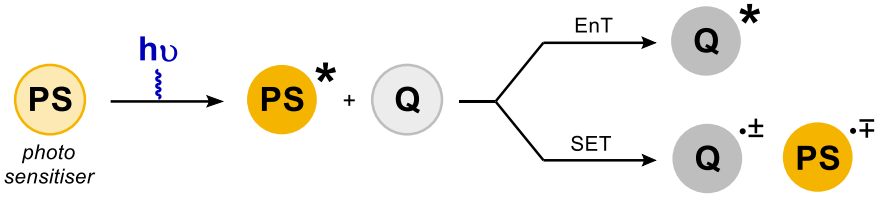

Figure 1.1.7. Photosensitisers transfer energy to a molecule through an EnT or SET mechanism.

There are two types of quenching event which PS* can undergo (Figure 1.1.7). The first is a bimolecular electron exchange with a **Q** to obtain the **Q***. We will refer to this process as an energy transfer (EnT) event, of which there are two distinct mechanisms: Dexter EnT, which is the direct exchange of the electrons and will produce a triplet **Q***. Forster EnT is a coulombic interaction that induces excitation through dipole oscillation and can only produce a singlet **Q***.[15]

The second is a bimolecular electron transfer to form a radical ion pair ($\mathbf{Q}^{\bullet\pm}$ $PS^{\bullet\mp}$), where the electron is donated in a unidirectional fashion, such that one of the molecules is reduced, and the other oxidised. Similar to the charge transfer within an EDA complex, it is commonly referred to as a SET process.

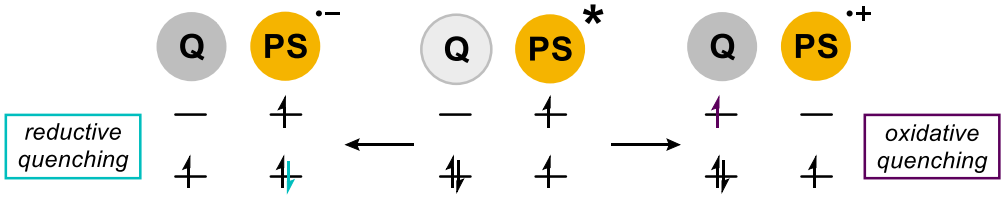

Figure 1.1.8. Oxidative or reductive quenching of the excited state photosensitiser.

Due to the unpaired nature of PS*, either an oxidative or reductive quenching event can occur. The pathway is dependent upon the reduction potentials of the excited state photosensitiser and the molecule. If Q can donate an electron, the photocatalyst is reduced ($PS^{\bullet-}$) and **Q** is oxidised to the radical cation ($\mathbf{Q}^{\bullet+}$), *reductive quenching*. Conversely if Q can accept an electron, then the photocatalyst is oxidised ($PS^{\bullet+}$) and **Q** reduced to the radical anion ($\mathbf{Q}^{\bullet-}$), *oxidative quenching*.

Photosensitisation has significantly contributed towards the application of light to organic synthesis, however historical photosensitisers often required UV irradiation.[16] A challenge to this working principal was developed when a visible light absorbing dye was applied as a photosensitiser under irradiation from common household light bulbs.

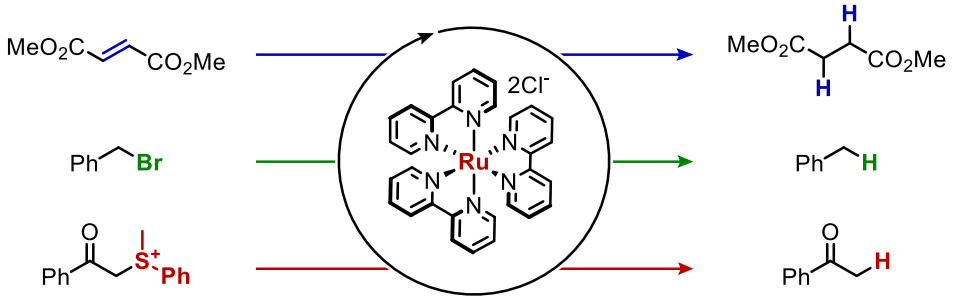

Figure 1.1.9. Olefin reduction, Kellog (blue); benzylic bromide reduction, Tanaka (green); sulfonium reduction, Pak (red).

Three initial reports were described by Kellog,[17] Tanaka,[18] and Pac.[19] The well-studied ruthenium dye was used to enable the photoreduction of three classes of reactant using dihydropyridines. $Ru(bpy)_3^{2+}$ is an important complex in inorganic photochemistry and has played a vital role in many fields.[20] The main transition that accounts for the photochemistry of $Ru(bpy)_3^{2+}$ is an intense absorption at 452 nm corresponding to a Metal-to-Ligand Charge Transfer (MLCT) from the t_{2g} orbital on the metal to the π* orbital of the ligand.[21]

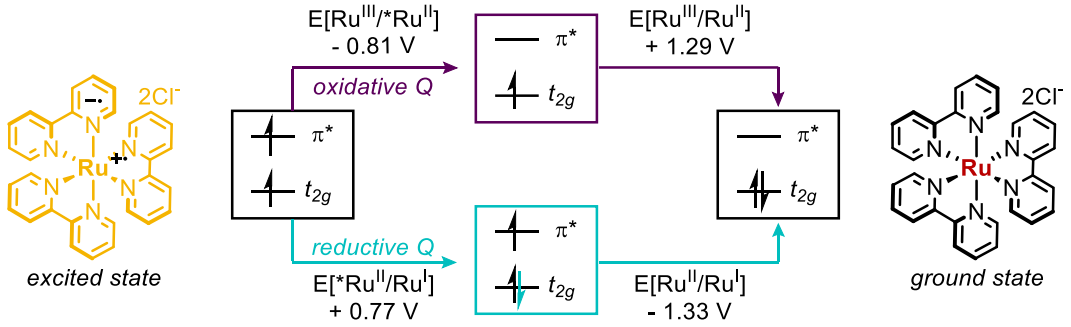

Figure 1.1.10. Reduction potentials of the four possible single electron transfers.

This MLCT can be envisioned as a ruthenium oxidation and ligand reduction (Figure 1.1.10). The unpaired nature of the excited state means that it can behave as a reductant ($E[Ru^{III}/*Ru^{II}]$ = - 0.81 V *vs* SCE) or as an oxidant ($E[*Ru^{II}/Ru^{I}]$ = + 0.77 V *vs* SCE). The intermediate states then behave as an oxidant ($E[Ru^{III}/Ru^{II}]$ = + 1.29 V *vs* SCE) or reductant ($E[Ru^{II}/Ru^{I}]$ = - 1.33 V *vs* SCE) respectively, to regenerate the ground state catalyst.

Although the use of this dye as a photosensitiser was a significant paradigm shift and served as inspiration to some remarkable publications: Wilmer,[22] Deronzier,[23] Fukuzumi,[24] Sauvage,[25] and Okada.[26] The overarching perspective of synthetic chemists was not reorientated and the widespread uptake of photochemistry by organic chemists took several more decades.

1.2. A modern take on photochemistry – photoredox catalysis

1.2.1. The renaissance

It was not until the late 2000s, where the works of Macmillan,[27] Yoon,[28] and Stephenson[29] brought to light three reactions which captured the interest of the community. The works take inspiration from those of the 1980s, but the diversity of the reactions presented highlighted the potential of this field. Macmillan developed an enantioselective α-alkylation of aldehydes, Yoon, a [2+2] cycloaddition and Stephenson a benzylic bromide reduction. All these processes utilized the ruthenium dye, $Ru(bpy)_3Cl_2$ (Figure 1.2.1).

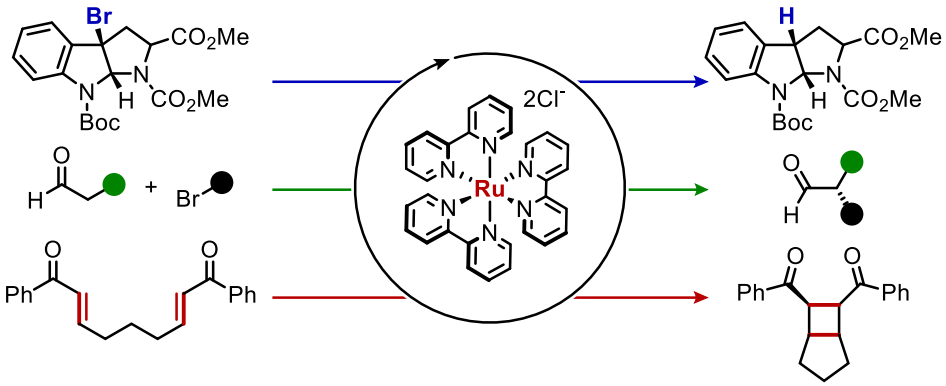

Figure 1.2.1. Stephenson's reduction of alkyl bromides (blue), Macmillan's enantioselective α-aldehyde alkylation (green), Yoon's [2+2] cycloaddition (red).

Each paper references "photoredox catalysis" and whilst it has been used previously,[30] the context in which it is used here clearly resonated with the community. Furthermore, emphasis was put on useable set ups that simply required commercial compact fluorescent light (CFL) bulbs placed close to the reaction vessel. One of the key contributing factors to the impact of these publications is the diversity of the reactivity which is highlighted. They suggest a greater synthetic potential than the three seminal reductions using dihydropyridines.

Whilst these are typically referred to as the seminal works that reinvigorated photochemistry in the modern era, there are some techniques that are sometimes overlooked, for example the decarboxylative technique developed by Hatanaka and co-workers.[31] As well as a palladium catalysed Sonogashira coupling that uses $Ru(bpy)_3Cl_2$ (Figure 1.4.3) and preceded the "metallaphotoredox" renaissance.[32]

1.2.2. Reduction and oxidation

The utility of photoredox catalysis is the generation of transient open shell intermediates under ambient reaction conditions without photoexciting other substrates within the reaction.[33] By employing external photosensitisers/photocatalysts, access to higher energy states of photo-insensitive molecules is facile. The unpaired nature of the photocatalyst means that both oxidation and reduction of the photocatalyst must occur to regenerate the ground state. Creating a unique opportunity where both oxidative and reductive SET events happen in the same reaction vessel. This has not been realised with stoichiometric reductants and oxidants due to their inherent incompatibilities until recently.[34] Additionally, the redox events can be close together on the reaction coordinate or far apart allowing for a huge array of complex reactions to be realised.

1.2.3. Redox neutral

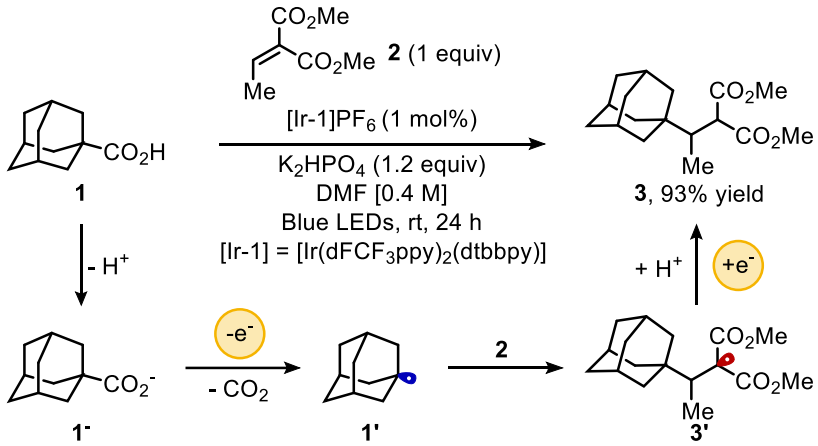

Figure 1.2.2. Giese reaction, oxidative generation from carboxylic acid.

Macmillan and co-workers used aliphatic unactivated carboxylic acids as radical precursors in a Giese addition (Figure 1.2.2).[35] The reaction exploits the nature of photocatalysis to access a radical precursor that would be difficult to use in a net reductive environment or from tin hydride species, which are typically used.[36] The reaction proceeds through reductive quenching of the excited state photocatalyst ($E[^*Ir^{III}/Ir^{II}]$ = + 1.21 V *vs* SCE) by the *in situ* generated carboxylate (E_{ox} ~ + 1.16 V *vs* SCE) to form the alkyl radical upon release of carbon dioxide. Radical addition of the electron rich alkyl radical **1'** into the electron deficient Michael acceptor forms radical adduct **3'**. Reduction of **3'** by the reduced photocatalyst ($E[Ir^{III}/Ir^{II}]$ = - 1.37 V *vs* SCE) and protonation affords the desired product **3** and regenerates the photocatalyst.

Introduction

This redox neutral reaction highlights that the SET events can be temporally separated as three processes need to occur after the initial SET - decarboxylation, diffusion, radical addition - before the second reduction occurs.

The net redox-neutral nature of photoredox catalysis is particularly interesting because it allows for unique reactivity to be developed. However, photoredox chemistry can also be exploited for its ability to generate radical intermediates under ambient conditions, from novel precursors. As such, the desired transformation may be net oxidative or reductive in nature. To access this type of reactivity a sacrificial electron donor or acceptor can be introduced to compensate for the undesired SET event.

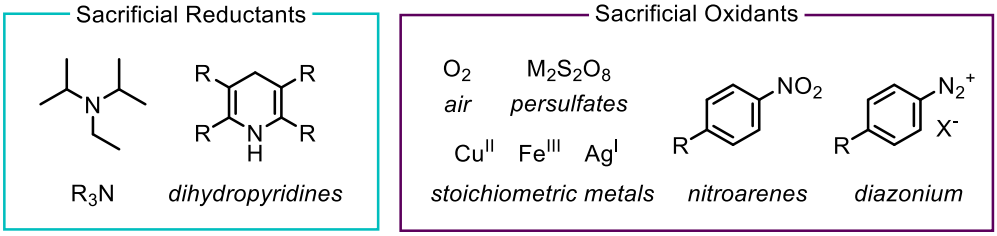

Figure 1.2.3. Sacrificial reductants, reductively quench the photocatalyst and become oxidised. vice versa.

Tertiary amines and dihydropyridines are cheap, readily available sacrificial reductants. Low oxidation potentials mean that they are readily oxidised to the radical cation and allow for the photoredox catalyst to act as a reducing agent. They have been widely applied within photoredox chemistry.[37] Sacrificial oxidants, such as air, persulfates, and N-X oxidants are examples of sacrificial oxidants. However, there are issues surrounding the formation of reactive oxygen species or incorporation into the final products.[38] Additionally, nitro arenes,[39] viologens,[40] and aryl diazonium salts have seen use but are not free from difficulties.[41]

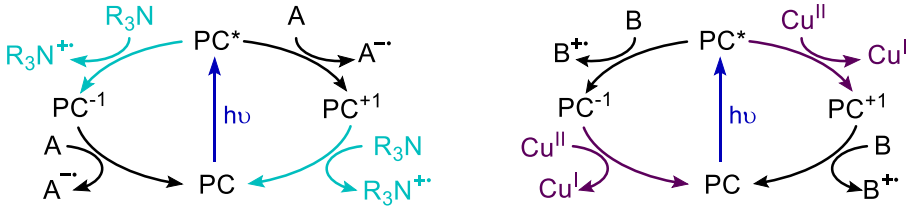

Figure 1.2.4. Using a terminal quencher allows for net reductive or oxidative processes.

A terminal reductant, such as triethylamine (Figure 1.2.4) will reductively quench an excited state photocatalyst PC* by donating an electron to form the radical cation. It could also regenerate an oxidised photocatalyst PC^{+1}. This enables the photocatalyst to behave solely as a reductant. A terminal oxidant, in this case copper (II) salts, can oxidatively quench PC*, or regenerate the ground state catalyst from PC^{-1} allowing for the photocatalyst to behave as a net oxidant.

1.2.4. Net reductive photoredox catalysis

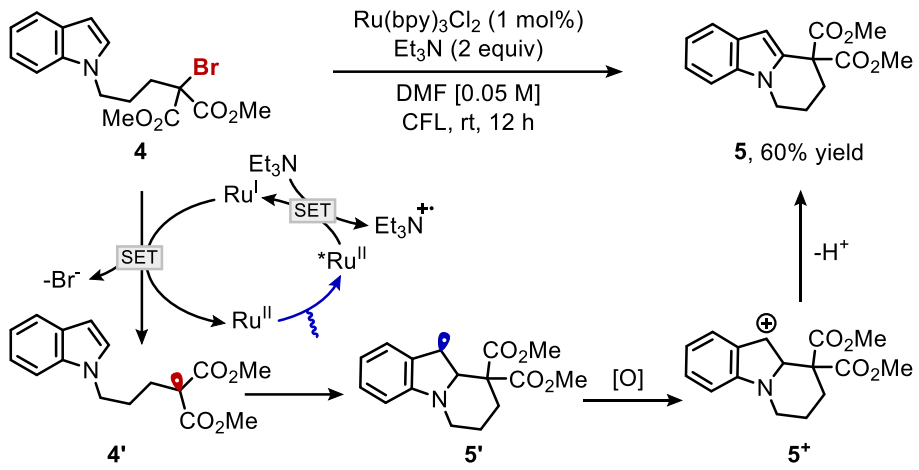

Figure 1.2.5. Net reductive conditions for C-C bond forming reactions.

Tertiary amines are especially well recognised within the context of photoredox chemistry.[42] The C-C bond forming reaction developed by Stephenson uses triethylamine as a terminal reductant to afford the desired transformation (Figure 1.2.5). Triethylamine is oxidised (E_{ox} = + 0.71 V) to the radical cation by reductive quenching of the excited state ruthenium photocatalyst ($E[*Ru^{II}/Ru^{I}]$ = + 0.77 V) to form Ru (I). The radical cation decomposes under the reaction conditions. Ru (I) injects an electron into the bromomalonate functional handle of **4** to regenerate the ground state ruthenium catalyst. Fragmentation of the transient radical anion with loss of bromide anion liberates **4'**. The electrophilic radical undergoes a radical cyclisation to form the benzylic radical **5'**. Oxidation of **4'** to carbocation **5$^+$,** followed by deprotonation gives product **5**.

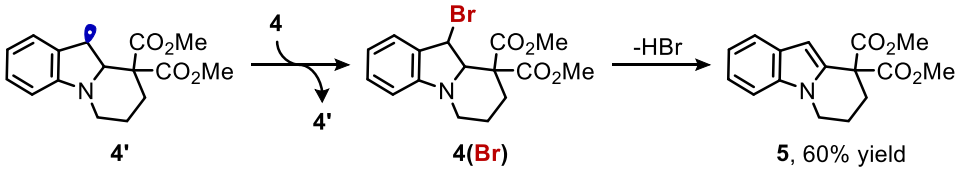

Figure 1.2.6. Alternative chain propogation mechanism.

It is also possible that intermediate **4'** undergoes a halogen atom abstraction from the bromomalonate **4** liberating benzylic bromide **4**(**Br**) (Figure 1.2.6). Base mediated elimination of HBr would yield the same product **5**. Additionally, the halogen atom transfer would propagate the reaction by directly forming **4'** without the need for a reductive quenching cycle. This reaction serves to illustrate that the full redox cycle should be accounted for, for efficient reactivity.

Introduction

1.2.5. Net oxidative photoredox catalysis

Net oxidative photoredox chemistry is a less explored field when compared to the reductive works. As mentioned, the issues surrounding the terminal oxidants stem from the generation of highly reactive oxygen species;[43] or the incorporation of the oxidant into the product.[44] For example, Selectfluor can be used as an oxidant in a photocatalytic scenario, however the fluorine is incorporated into the product of the reaction, as demonstrated by Sammis *et. al*.[45]

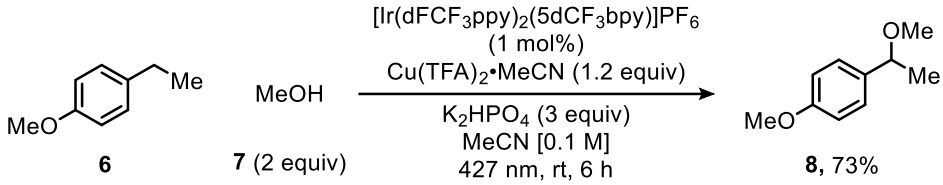

Figure 1.2.7. Yoon and co-workers benzylic alkoxylation.

Copper (II) salts are known radical oxidants that would avoid the generation of reactive oxygen species and will not be incorporated into the final product. Yoon and co-workers, inspired by the works of Kochi, used copper (II) trifluoroacetate as a stoichiometric terminal oxidant in the intermolecular benzylic alkoxylation (Figure 1.2.7).[46]

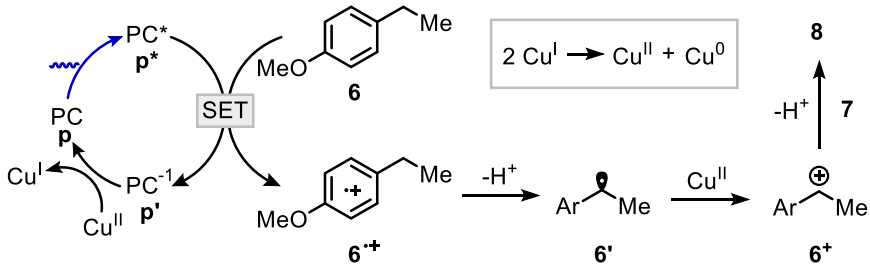

Figure 1.2.8. Mechanism of oxidation and the disproportionation reaction (grey box).

The mechanistic understandings of this reaction are quite difficult due to the well-matched reduction potentials.[47] One possible pathway is depicted (Figure 1.2.8), a reductive quenching of the excited state photocatalyst ($E[*Ir^{III}/Ir^{II}]$ = + 1.68 V) by arene (**6**, E_{ox} = + 1.52 V) to form the radical cation **6**$^{\bullet+}$. Deprotonation of **6**$^{\bullet+}$ by the base affords the benzylic radical **6'**, copper (II) salt reacts rapidly with the benzylic radical to form the benzylic cation **6**$^{+}$. Trapping with the methanol nucleophile forms the desired product **8**. Copper (II) salt regenerates the ground state photocatalyst through a second SET event. Theoretically, the reaction requires at least two equivalents of copper, however only 1.2 equivalents of copper are used, the authors justified this by a disproportionation reaction between two copper (I) species to copper (II) and copper (0). By exploiting the ability of photoredox chemistry to access radicals the works of Yoon highlight that copper can be a cheap and benign oxidant for net oxidative photoredox chemistry.

1.2.6. Chromoselective photoredox catalysis

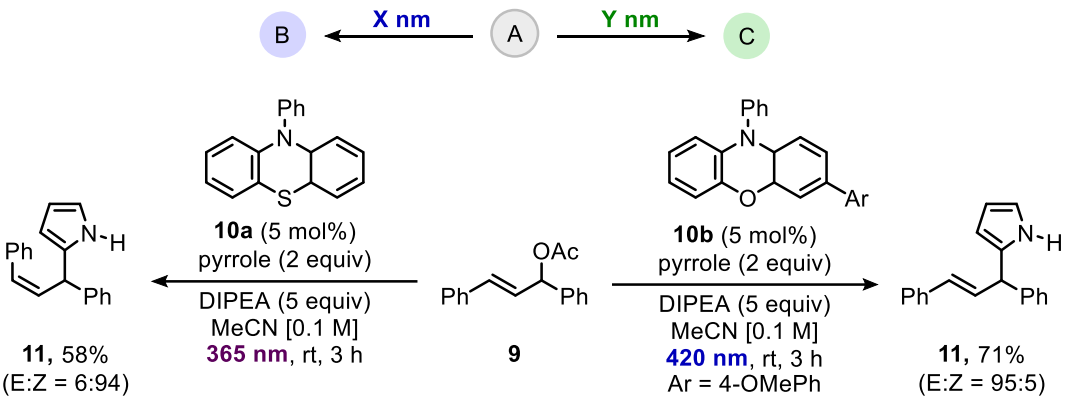

Figure 1.2.9. Chromoselective catalysis, demonstrated by isomer access.

There are still areas of photochemistry that are underexplored, for example, chromoselective transformations, where different wavelengths of light result in different products (Figure 1.2.9).[48] One example of this is the chromoselective allylation of N-heterocycles to selectively access the *E* or *Z* isomer.[49] The selective allylation of pyrrole was achieved with choice of both the photocatalyst and the wavelength of light. The presence of **10a** under 365 nm was found to isomerise the starting material *E*-**9** entirely to *Z*-**9**. Whereas under 420 nm irradiation, the isomerisation was negligible, allowing for selective formation of *E*-**11** under the appropriate photocatalytic conditions. The isomerisation of double bonds by visible light photocatalysis is well studied, but the ability to access different products by choice of light source is an interesting concept. The external nature of the light source means that reactivity can simply be switched off, making photochemistry safer than radical initiated reactions which can sometimes runaway.[50]

The opportunities presented as well as those still being discovered are what make organic photoredox chemistry such an interesting field. Over the past two decades, development in photocatalyst and reaction design have enabled organic chemists to take full advantage of the opportunities that photochemistry presents. Initial development of photoredox chemistry used the well-studied $Ru(bpy)_3Cl_2$ photocatalyst. The relative ease of understanding within organic photoredox catalysis can be owed to the exceptional works of those in the broader area of photochemistry and photophysics. The first applied photocatalysts were not designed for organic synthesis but for photovoltaic,[51] electroluminescent,[52] or sensing technologies.[53] Since the arena of organic photocatalysis has shown such promise there has been considerable effort invested in the redirection of such molecules from their original purpose to photoredox catalysts.

1.2.7. The photocatalyst

Photocatalysts come in many forms, but we will focus on homogenous molecular photocatalysts. The gap between the HOMO and LUMO is the controlling factor for light absorption, the $S_0 \rightarrow S_1$ transition. Due to ISC and molecule rearrangements, the energy of the $S_0 \rightarrow S_1$ transition is not equal to the energy available to the reaction system. Increasing the HOMO-LUMO gap is used to increase the relative energy available to a system, however above certain wavelengths direct photoexcitation of the substrates can occur which may lead to undesirable side reactions. Therefore, a balance must be found, in this regard many photocatalysts are tuned for the purple/blue wavelengths of light between 400-460 nm.

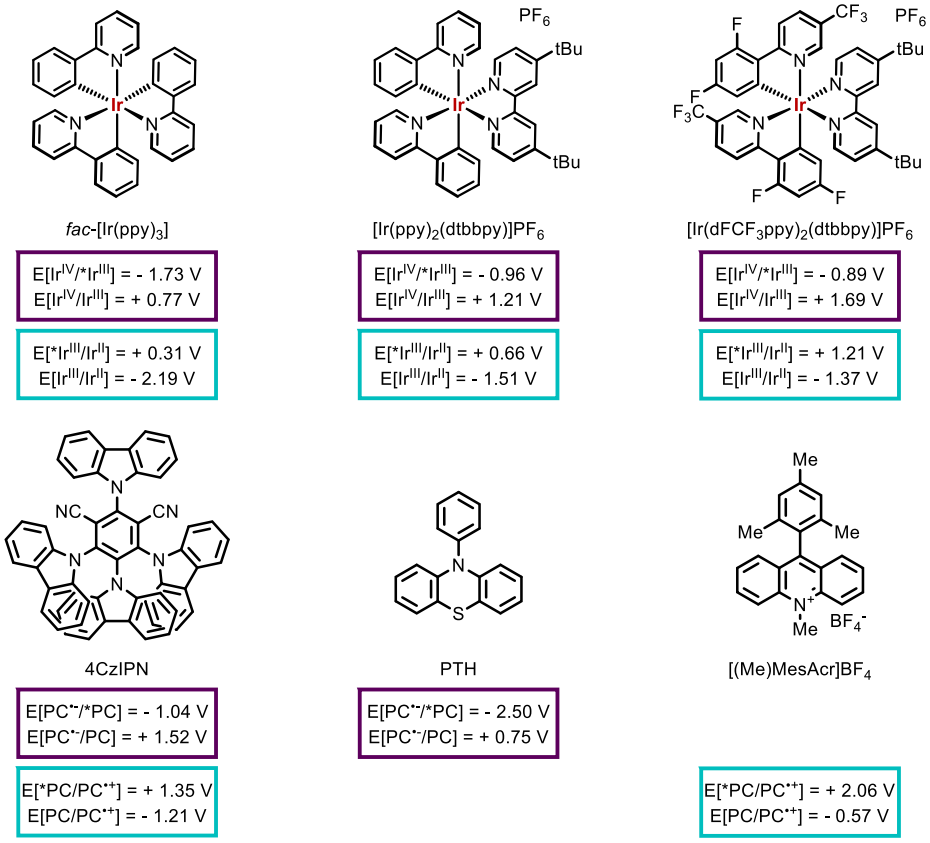

Figure 1.2.10. Common photoredox catalysts and their reduction potentials.

The redox potentials of the photocatalyst are important to the reactivity of the photocatalysts (Figure 1.2.10).[54] The excited state and ground state reduction potentials are intrinsically linked by the Gibbs energy of electron transfer.[55] This effectively means that whilst the reduction potential of an excited state may be high, the corresponding ground state reduction potentials will be low. This is illustrated by *fac*-Ir(ppy)$_3$ and its reductive quenching potentials.

Applications for highly oxidising or reducing photocatalysts such as the mesityl acridinium or 10-phenylphenothiazine (PTH) lines of photocatalysts are well established,[56] however the relatively low ground state reduction potentials in comparison to their excited states can severely limit the available chemistry. Thus, efforts have been made to access more balanced catalysts.[57]

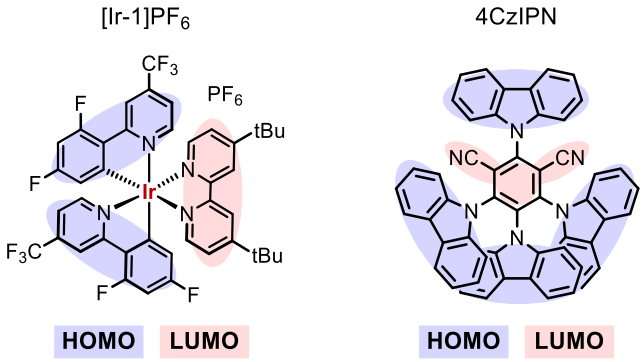

Figure 1.2.11. The location of the HOMO and LUMO are critical for light absorption and redox potentials.

A modular system that allows for the individual tuning of the HOMO and LUMOs is a valuable method, which would allow for the redox properties of the photocatalyst to be tailored. The standout photocatalysts of this decade are iridium polypyridyl complexes of the type $[Ir(CN)_2(NN)]$. Adjustments on the cyclometalated ligands directly effects the LUMO and leave the HOMO relatively unchanged. The opposite is also true and modification of the NN ligand directly effects the HOMO but does not affect the LUMO.[58] Another modular photocatalyst is the 4CzIPN motif, 4CzIPN is a thermally activated delayed fluorescent (TADF) material,[59] designed by Adachi and co-workers in 2012 and was specifically designed to have a high energy triplet state by spatially separating the HOMO and LUMOS (Figure 1.2.11).

The photocatalyst design and properties are responsible for the chemical transformations available, and there is a huge array of complex and intricately designed reactions that have exploited the design of photocatalysts to access new chemical space.

We will examine the application of photocatalysts to organic synthesis, with particular emphasis on the formation of C-C bonds. C-X bond formation through photoredox chemistry is expansive and generally beyond the scope of this thesis. Due to the radical nature of photoredox chemistry, it is appropriate to have an understanding of radical stability, especially C-centred radicals.

1.3. Photoredox catalysis and synthesis

1.3.1. The stability of carbon centred radicals

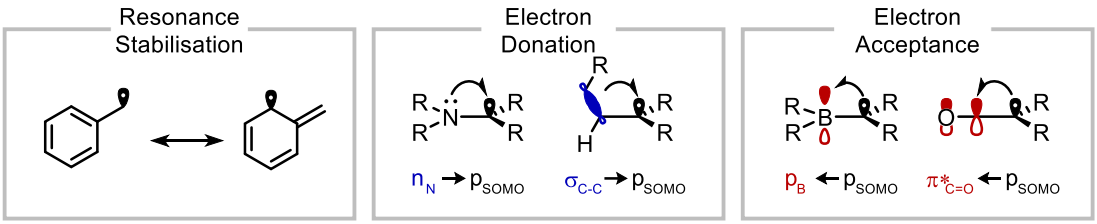

Figure 1.3.1. Three methods to induce radical stablisation.

Radical stability is a fundamental principal and plays a pivotal role in the arena of photoredox chemistry because carbon centred radicals undergo a plethora of bond forming reactions.[60]

Three primary effects stabilise carbon centred radicals (Figure 1.3.1)[61]: (a) resonance, (b) electron donation, and (c) electron acceptance. a) resonance effects are identical to the analogous cationic or anionic resonances, when in conjugation with a π system, the radical can delocalise across the system. b) electron rich sites donate electrons through non-bonding lone pairs (n_N), or bonding orbitals ($\sigma_{C\text{-}C}$). Donation to the singularly occupied molecular orbital (SOMO) induces stability by lowering the overall energy of the system but raises the SOMO's energy. c) electron acceptance of a radical, is analogous to resonance stabilisation. An empty p orbital (p_B) or unsaturated system ($\pi^*_{C=O}$) can accept the SOMO, lowering the energy of the system and the SOMO.

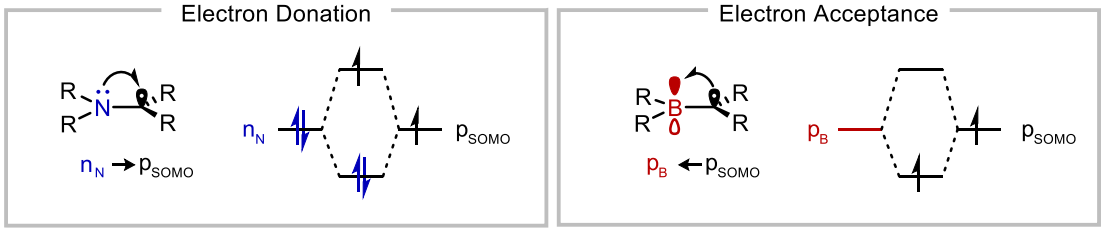

Figure 1.3.2. Effect on the frontier molecular orbitals of the SOMO.

The stability of the radical and its environment is critical in understanding the reactivity (Figure 1.3.2). Electron donating groups increase the energy of the SOMO, which in turn creates a more nucleophilic radical. An electron withdrawing substituent lowers the energy of the SOMO and increases the electrophilicity of the radical. The electronic environment of the radical is often termed, "philicity" and is a transition state effect. It is important for understanding the outcomes of many radical reactions.[62] The reactivity is similar to polar reactivity; nucleophilic entities prefer to react with electrophilic species and *vice versa.*

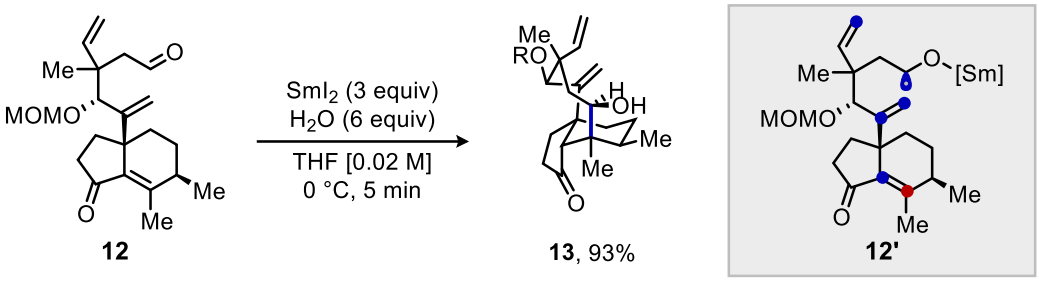

Figure 1.3.3. Reisman and co-workers exquisite 8-endo-trig cyclisation in the synthesis of pleuromutilin.

A beautiful example of how the philicity of the radical can influence reactivity is highlighted in the work of Reisman and co-workers and the total-synthesis of pleuromutilin (Figure 1.3.3).[63] Although this technique is not photoredox in nature it serves to highlight how the philicity of the radical is highly influential in the outcome of the reaction. The radical generated by SmI_2 (**12'**) has five possible cyclisation modes, highlighted as blue or red dots. The α-oxy radical is nucleophilic in nature (blue) due to the donation of the lone pair of oxygen, it is therefore a nucleophilic species and will react preferentially with electrophilic sites. Of the 5 possible cyclisation events, there is only one electrophilic site, highlighted in red **12'**. The nucleophilic radical reacts at this site with exquisite site selectivity to give cyclised product **13** in 93% yield.

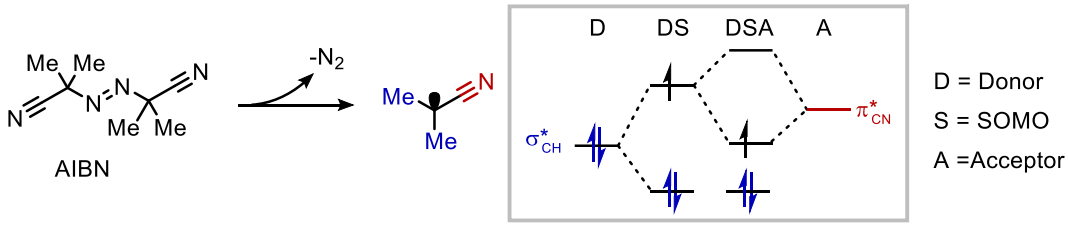

Figure 1.3.4. Thermal decomposition of AIBN highlights the captodative stabilisation.

The combination an electron withdrawing and electron donating groups α to the radical has an enhanced stabilising effect called a "captodative effect".[64] The synergistic stabilisation by both substituents is highlighted by AIBN, the radical formed upon decomposition of AIBN has both electron donating substituents (two methyl) and an electron withdrawing group (cyano) makes the radical thermodynamically stable and is one of the reasons why AIBN is so widely used as a radical initiator.

1.3.2. Generating radicals through photoredox catalysis

Although the energy of visible light and photocatalysts can promote electrons from the ground state of a molecule to the excited state, the electron transfer does not always lead to a productive bond forming event. There are often BET or radiationless decays that lead to non-productive pathways. Several approaches have been developed to disfavour BET.

Radical precursors and SET

The introduction of radical precursors is one such example. Although electron transfer events are fundamental to photoredox catalysis, many functional groups are not readily amenable to oxidation or reduction to form radical ion pairs. Exceptions exist such as carboxylic acids and trialkyl amines, but the vast majority of functional groups are not trivial to apply in a photoredox setting. By transforming latent functionalities into more activated radical precursors (RPs), this issue can be circumvented. RPs have seen considerable development over the past decades to allow for generation of radicals from a wide range of native functional groups.[65]

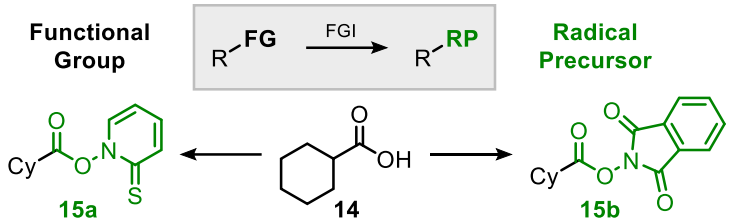

Figure 1.3.5. A functional group interconversion to radical precursor.

The carboxylic acid functionality is a prime example (**14,** Figure 1.3.5), whilst methods exist to directly generate the carbon centred radical through oxidation/decarboxylation,[66] the oxidation potential of carboxylate groups (E_{ox} = +1.11 V *vs* SCE) means that this can be challenging. Activation by esterification has been widely applied. The seminal works in this context by Barton (**15a**),[67] as well as Okada (**15b**)[26] highlight the improved reactivity that carboxylic acid derivatives can have on photochemical reactions.[68]

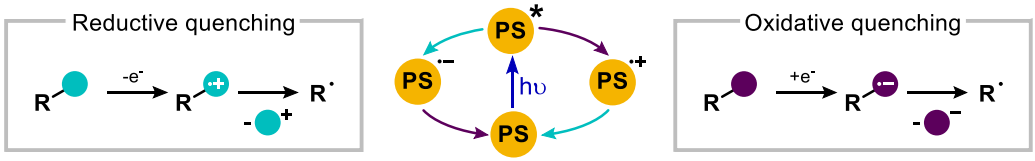

Figure 1.3.6. Radical precursors quench the photocatalyst through reduction or oxidation.

The nature of the radical precursor is important in determining which SET event occurs, some precursors will be oxidised through a reductive quenching event of the PS* or to regenerate the ground state from $PS^{\bullet+}$ (Figure 1.3.6). Others through oxidative quenching or regeneration of $PS^{\bullet-}$.

The first SET determines the second SET in a redox neutral scenario. For example, if the initial SET is an oxidative quenching, then an oxidation must be enabled later in the reaction, or the photocatalytic cycle will not close. The radical precursor is essential in this step, to be able to access both an oxidative quencher and reductive quencher from the same functional group is highly beneficial because it allows for divergency in reactivity.

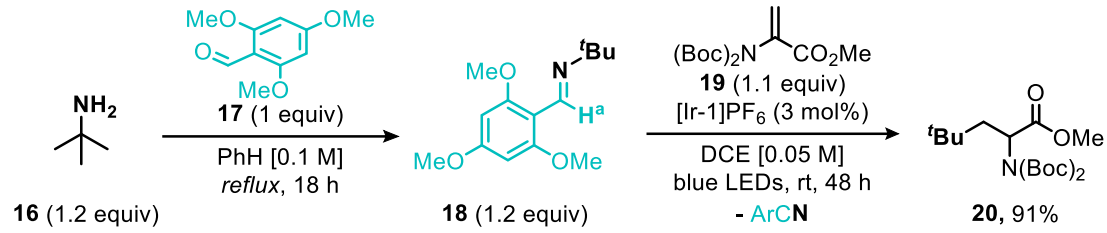

Figure 1.3.7. Deaminative Giese addition through the formation of an oxidisable imine precursor.

Deaminative strategies can access reactive intermediates from what are commonly seen as inert C-N bonds by functional group interconversion to a radical precursor. Rovis and co-workers developed radical precursor **18** (Figure 1.3.7).[69] The electron rich arene substituent reductively quenches an excited state photocatalyst to form the radical cation and reduced photocatalyst. Deprotonation of the radical cation (at **H^a**) releases benzonitrile and the *tert*-butyl radical. Giese addition of the radical into **19** followed by reduction and protonation of the adduct liberates the desired product **20**. This strategy exploits an initial reductive quenching event so a second reductive quenching event closes the photoredox cycle.

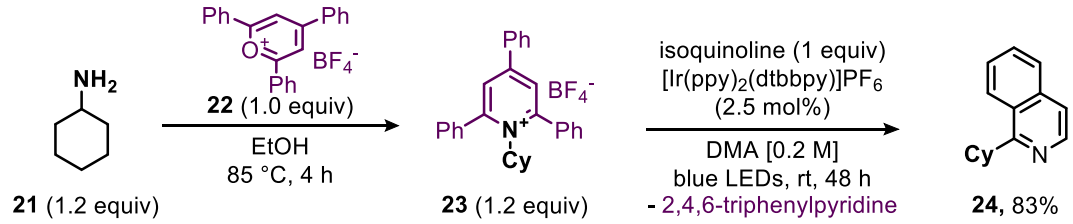

Figure 1.3.8. Deaminative Minisci addition through the formation of a reducible Katritzky salt.

Conversely, Glorius and co-workers used Katritzky salt **23** as an oxidative quenching radical precursor (Figure 1.3.8). Katritzky salts readily accept an electron from the excited state photocatalyst in an oxidative quenching event to form a neutral radical and oxidised photocatalyst. The radical formed fragments to give cyclohexyl radical and neutral pyridine. Radical addition into isoquinoline followed by oxidation of the amine radical by the photocatalyst regenerates the ground state photocatalyst and product **24** upon deprotonation.[70] The divergency of the functional group interconversion to imine (**18**) or Katritzky salt (**23**) allows for a broader variety of deaminative strategies to be developed.

Introduction

Radical precursors and EDA complexes

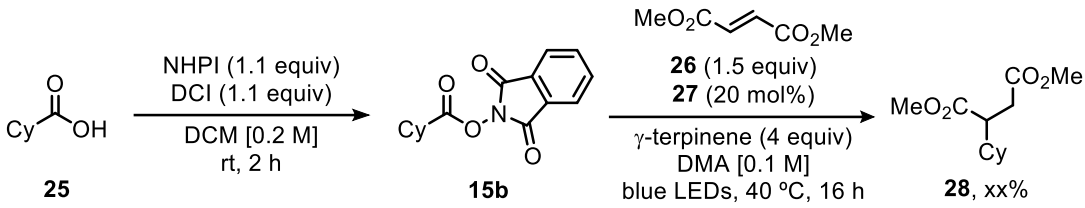

Figure 1.3.9. Catalytic EDA complexation in synthesis from Melchiorre.

Although the injection of an electron into the radical precursors through a SET mechanism is widely applied, EDA complexes and EnT are becoming more relevant. A general and catalytic manifold for EDA formation was disclosed by Melchiorre and co-workers in 2021 (Figure 1.3.9).[71] Direct application of the *in situ* formed NHP esters afforded the Giese addition. The use of γ-terpinene is essential because this reaction is net reductive.

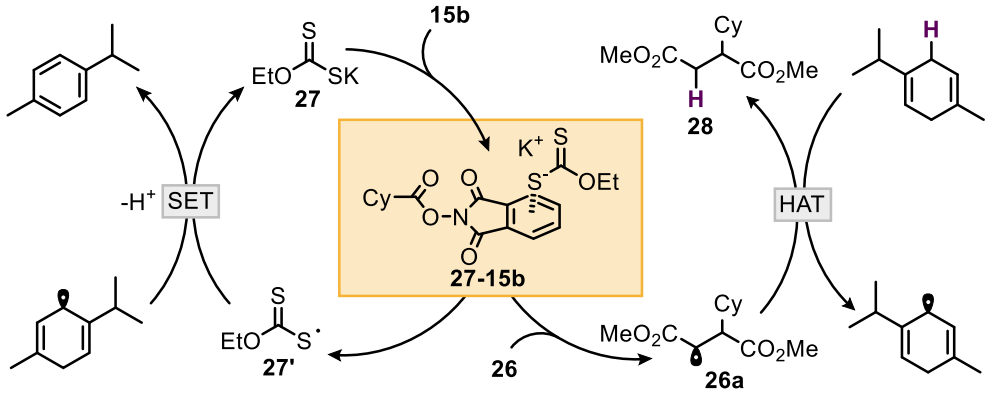

Figure 1.3.10. Mechanism for catalytic EDA complexation.

The reaction proceeds by EDA complexation of electron rich xanthogenate (**27**) with the electron deficient NHP ester **15b** to form EDA complex [**27-15b**]. Photoexcitation of [**27-15b**] transfers an electron from to a SET from **27** to **15b**, which liberates neutral thiyl radical (**27'**) and the radical anion of **15b**, rapid fragmentation of the radical anion gives cyclohexyl radical. Radical conjugate addition of the cyclohexyl radical into acceptor **26** to intermediate **26a**. HAT from γ-terpinene forms the desired product **28** (Figure 1.3.10). The catalyst (**27**) is regenerated from the γ-terpinene radical and the neutral thiyl radical (**27'**), through a SET event.

This technique shows that EDA complexation can be a viable strategy for the fragmentation of radical precursors in a catalytic manor. As reaction conditions and photocatalysts are developed, it is possible to generate radicals from native functional groups without the need for the radical precursors.[72]

1.3.3. Atom transfer

Halogen atom transfer

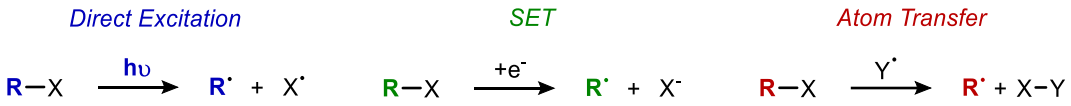

Figure 1.3.11. Three techniques to homolytically cleave an R-X bond.

Three techniques have been used to generate carbon centred radicals from alkyl halides (Figure 1.3.11): direct excitation using high energy UV light; single electron transfer which often requires high reduction potentials; and "atom transfer." An atom transfer, in this case a "halogen atom transfer" (XAT), is where a halogen is abstracted by a radical species (Y•) to form a strong Y-X bond and the carbon centred radical. The formation of radicals through atom transfer events has undergone a revival due to the advent of photoredox catalysis but has been used historically too.[73]

Figure 1.3.12. Halogen atom transfer using α-amine radicals developed by Leonori and co-workers.

Leonori and co-workers developed a general halogen atom transfer technique using α-amino alkyl radicals as the halogen abstracting agent. The alkyl radical generated upon XAT was employed in three scenarios: *ipso*-deuteration, Giese alkylation (Figure 1.3.12), and Giese allylation.[74]

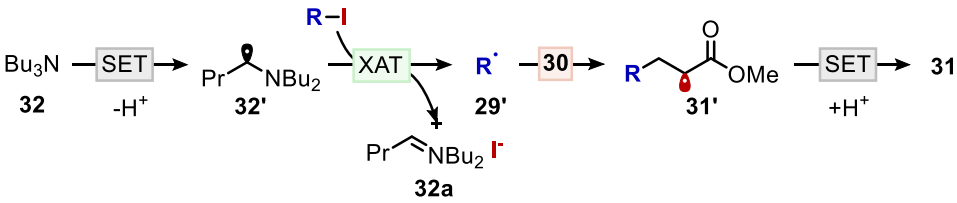

Figure 1.3.13. The mechanistic proposal of XAT mediated by tributylamine

The ability for α-amino radicals to abstract halogen atoms is well founded, and formation of the stable iminium salt provides a thermodynamic sink. The reaction proceeds through reductive quenching of the excited state photocatalyst (E[*PC/PC•⁻] = + 1.35 V vs SCE) by tributylamine (**32,** E_{ox} = + 0.71 V *vs* SCE), followed by deprotonation to create the α-amino radical (**32'**). Halogen atom transfer with alkyl iodide forms iminium iodide salt (**32a**) and alkyl radical **29',** radical conjugate addition of **29'** into **30** generates the radical adduct **31'**. Single electron transfer from the reduced photocatalyst (**p'**, [PC/PC•⁻] = − 1.10 V *vs* SCE) to **31'** followed by protonation closes the photoredox cycle and liberates the desired product **31** (Figure 1.3.13).

Introduction

Hydrogen Atom Transfer

The archetypal atom transfer reaction is hydrogen atom transfer (HAT) which is the transfer of a proton and electron in a single kinetic step. HAT is found across chemistry but particularly in the fields of polymer, biological and synthetic chemistry. The prevalence of HAT in synthetic organic chemistry is because it can readily enable the functionalisation of C(sp^3)-H bonds which has been a long sought-after transformation. HAT will be discussed in much greater detail in Chapter 2 and Chapter 3. Macmillan and co-workers used a thiol co-catalyst to afford the arylation of benzylic ethers under photocatalytic conditions (Figure 1.3.14).

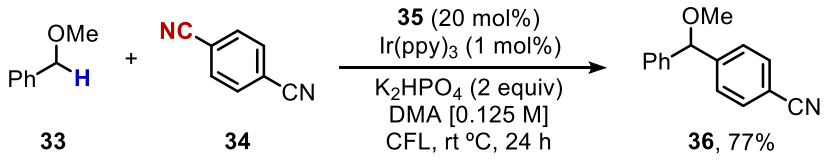

Figure 1.3.14. Hydrogen atom transfer reaction developed by Macmillan and co-workers.

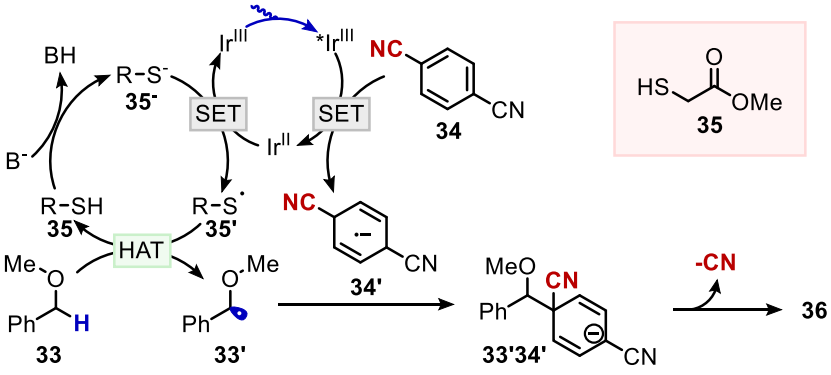

Figure 1.3.15. Mechanism of HAT mediated by thiol organocatalyst.

The reaction mechanism (Figure 1.3.15) consists of an oxidative quenching of the photoexcited iridium photocatalyst ($E[*Ir^{III}/Ir^{II}]$ = - 1.73 V *vs* SCE) by dicyanobenzene (**34,** E_{red} = - 1.61 V *vs* SCE) to form an iridium (II) species and the persistent radical anion **34'**. A proton coupled electron transfer is proposed for the oxidation of the thiol due to the discrepancy between the reduction potentials of the photocatalyst ($E[Ir^{III}/Ir^{II}]$ = + 0.77 V vs SCE) and the thiol (**35,** E_{ox} = + 0.85 V *vs* SCE). The base forms thiolate **35^-,** oxidation of **35^-** to thiyl radical **35'** is facile. **35'** undergoes a HAT event with the benzylic ether to generate radical **33'**. Radical-radical coupling of **33'** and **34'** gives the anionic intermediate **33'34'** which rapidly rearomatizes by elimination of the cyanide anion to the desired α-arylated ether **36**. The use of the thiol co-catalyst is an excellent example of a dual-catalytic manifold. "Dual catalysis" is the use of two catalytic cycles in one reaction vessel. By combining two modes of catalysis a broader range of reactivity can be accessed.

1.3.4. Dual catalysis

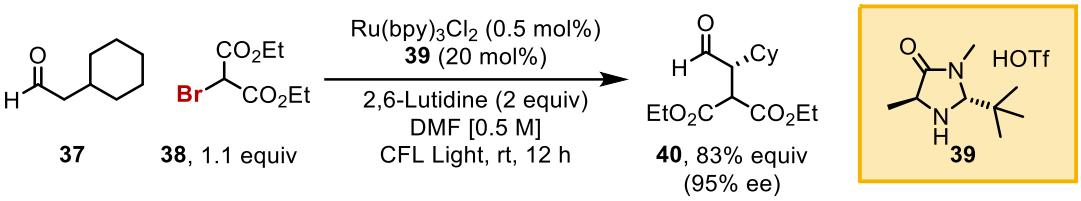

Figure 1.3.16. Dual catalytic strategy by Macmillan and co-workers.

One of the seminal works from Macmillan uses dual-catalysis to afford enantioselective α-arylation of aldehydes under mild conditions (Figure 1.3.16).[27] The work combines the use of a chiral amine catalyst and photoredox catalysis to afford the alkylation which would be difficult through a two-electron pathway.

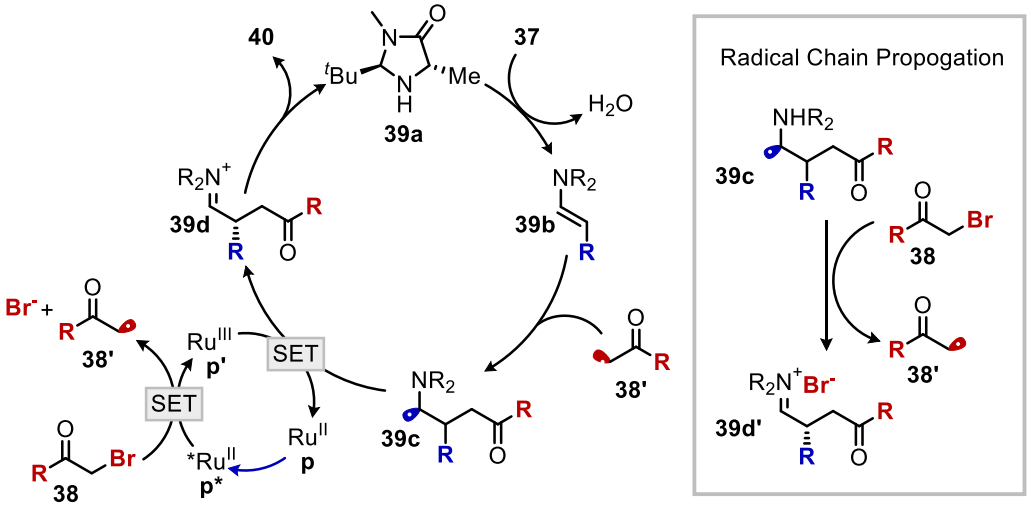

Figure 1.3.17. Mechanism of Macmillan's dual catalytic strategy. Radical chain propagation proposed by Yoon.

The proposed mechanism (Figure 1.3.17), condensation of the chiral amine catalyst with aldehyde (**37**) forms the enamine (**39b**) with loss of water. The photoexcited ruthenium photocatalyst is a strong reductant ($E[Ru^{III}/*Ru^{II}]$ = - 0.81 V *vs* SCE) injection of the electron into the carbonyl of **38** to form the radical anion is quickly followed by fragmentation with release of the bromide anion and creates the alkyl radical **38',** as well as the oxidised ruthenium (III) **p'**. Radical addition of electron deficient **38'** into electron rich enamine **39b** liberates the radical adduct **39c**. **p'** can oxidise ($E[Ru^{III}/Ru^{II}$ = + 1.29 V *vs* SCE) the α-amine radical **39c** to the iminium cation **39d** and regenerate the ground state ruthenium. Hydrolysis of the iminium species liberates the amine catalyst and product.

However, Yoon and co-workers suggested an alternative mechanism of action upon studying the reaction in more detail, specifically the quantum yields.[75] The authors suggest a chain propagation is a more likely scenario where α-amine radical **39c** abstracts a bromide from **38** to form **38'** and **39d'**.

1.4. Merging Metals and Photocatalysts

1.4.1. Introduction

Transition metal catalysis has had a profound impact on the chemical community and is a cornerstone of the synthetic chemist's toolbox.[76] The diverse range of reactions has largely been due to extensive ligand development. Two of the most well-developed ligand series are the Buchwald-Hartwig ligands,[77] and the Hoveyda-Grubbs catalysts.[78]

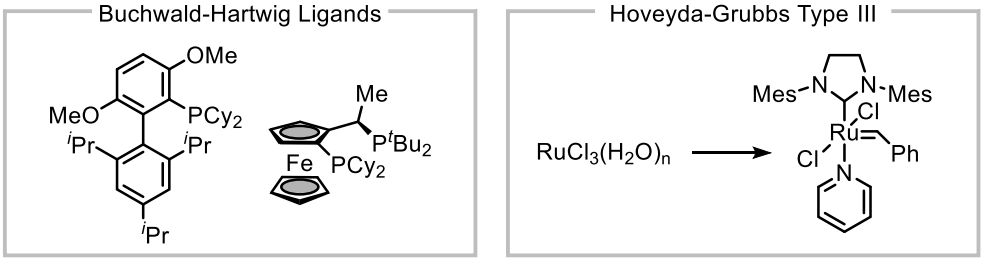

Figure 1.4.1. The Buchwald-Hartwig and Grubbs catalysts are two of the most developed ligand series within chemistry.

The effect of ligands on the steric and electronic environment is highly influential on the fundamental steps within a transition metal catalysed reaction. However, the degree of control over the reaction is limited. Another method to influence the course of the reaction is by oxidation state modulation.

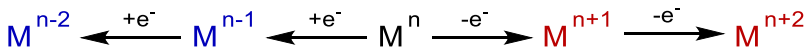

Figure 1.4.2. A change of oxidation state fundamentally changes reactivity.

Historically this technique required stoichiometric oxidants or reductants which inherently changes the reactivity of the overall system and may be incompatible with other elements of the desired catalytic cycle. The use of stoichiometric oxidants and reductants has enabled a range of transition metal catalysed reactions. For example, C-N reductive elimination from high valent copper species in the Chan-Evans-Lam coupling;[79] Or C-O bond forming reactions from the likes of Sanford and Yu.[80] Reductive manifolds on the other hand have enabled cross-electrophile coupling including the functionalisation of CO_2.[81]

The incorporation of stoichiometric oxidants or reductants has fundamental implications for the overall reaction system. Photoredox catalysis offers the unique opportunity of modulating the oxidation states of the transition metals but retains a redox neutral manifold. The area has had such an impact on synthetic organic chemistry that it has been extensively reviewed.[82]

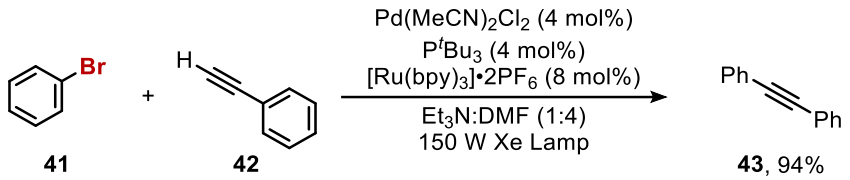

Figure 1.4.3. Osawa and co-workers' copper free Sonogashira coupling.

One of the first dual catalytic strategy was disclosed by Osawa and co-workers in 2007 who developed a palladium catalysed Sonogashira cross-coupling using the $Ru(bpy)_3Cl_2$ photocatalyst in place of the commonly employed copper co-catalyst.[32] This inspired the early works of Sandford and co-workers in this field with palladium.[83] However, the oxidation states of palladium are not particularly suited for a SET scenario, typically palladium favours even electron states (0, 2, 4). Metals that can access odd electron states are much more amenable to the SET environment of photoredox chemistry. Copper in this regard has been applied because it can access oxidation states of one to three, indeed Sanford developed a dual catalytic strategy with copper for the trifluoromethylation of boronic acids in early 2012.[84]

1.4.2. Nickel metallaphotoredox

Another late transition metal that is known to access odd electron states is nickel.[85] Nickel has seen an increase in use over the past few decades, largely driven by the ability to access sp^3 cross coupling scenarios.[86] Furthermore, nickel can access odd electron states ($Ni^{0/I/II/III}$), this was exploited in several thermal single electron transfer type cross-coupling.[87] Nickel is an ideal candidate to be used in conjunction with a SET photoredox platform. Additionally, low lying *d* orbitals which make electronic transitions relatively easy and can allow for direct photoexcitation with higher energy visible light. Or in a complementary fashion, triplet photosensitisation can also be used. The nickel platform is primarily based on the formation of electrophilic nickel (II) species which rapidly capture radicals (nucleophilic radicals) to generate a high-valent nickel (III) intermediates which undergoes reductive elimination to form many C-C and difficult C-X linkages. The diversity of bond formation is complemented by the plethora of reactions which nickel has already been established in, including chain walking.[88] Indeed, it is one of the most visible metals in the metallaphotoredox field.[89]

Introduction

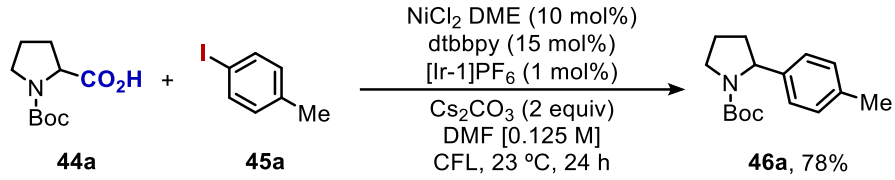

Figure 1.4.4. Macmillan and Doyle's decarboxylative cross-coupling.

The use of nickel in a dual catalytic scenario was exemplified by MacMillan/Doyle and co-workers in 2014.[90] The seminal studies enabled carboxylic acids (**44a**) to be used as the radical precursors in decarboxylative arylation technique. Independently Molander and co-workers reported an analogous technique using alkyl potassium trifluoroborate salts and aryl bromides (**44b**/**45b**).[91]

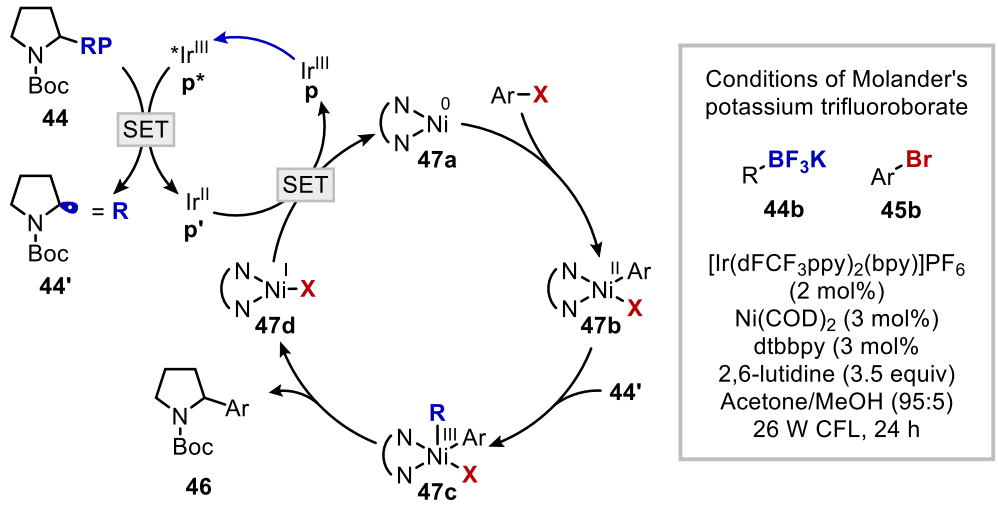

Figure 1.4.5. Mechanistic rationale for both Macmillan and Molander's photoredox cross-coupling.

An initial two electron reduction of the nickel (II) precatalyst to form a nickel (0) intermediate **47a** is proposed. Oxidative addition of aryl iodide **45** to form the electrophilic nickel (II) aryl iodide complex **47b**. Upon photoexcitation an oxidising excited state is accessed ($E[*Ir^{III}/Ir^{II}]$ = + 1.21 V *vs* SCE) which can oxidise the carboxylate (E_{ox} = + 1.11 V vs SCE) to the O-centred radical which rapidly decarboxylates to the nucleophilic radical **44'**. Radical addition of **44'** into **47b** generates a high valent nickel (III) intermediate, **47c**, which rapidly reductively eliminates to the desired product **46** and nickel (I) **47d**. SET from the reduced photocatalyst **p'** ($E[Ir^{III}/Ir^{II}]$ = - 1.37 V *vs* SCE) reduces **47d** ($E[Ni^{I}/Ni^{0}]$ ~ - 1.11 V *vs* SCE) to **47a** and closes both catalytic cycles.

Using carboxylic acids as pronucleophiles serves to highlight the possibility that new synthetic handles can be used within a cross-coupling scenario. Although the advances in transition metal cross-coupling have been considerable, the scope of both nucleophile and electrophile have been restricted to two electron systems,[92] whilst difficult native and inert bond functionalisation have been realised,[93] the reactions are still restricted to polar type chemistry.

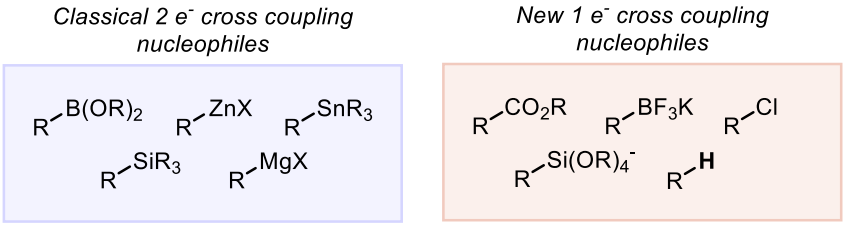

Figure 1.4.6. Classic cross-coupling nucleophiles vs *novel pro nucleophiles*

Metallaphotoredox chemistry has the advantage of opening a variety of new coupling partners through the nature of single electron transfer.[94] A large number of previously inert synthetic handles could accessed (Figure 1.4.6), only being revealed upon SET. This has allowed for novel disconnections and interesting defunctionalisation reactions to be enabled.

1.4.3. Inert bond functionalisation

The alcohol structural motif is prevalent within chemical space, and the ability to use them as a reactive partner through a deoxygenative bond forming reaction would be beneficial to organic synthesis. Indeed, the use of alcohols in this manner has enabled a wide range of reactions to be realised, however many of these techniques require sulphur or phosphorus reagents which are incompatible with transition metals,[95] or laborious pre-activation steps.[96]

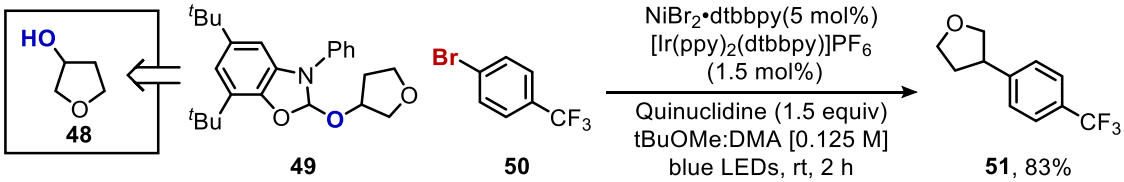

Figure 1.4.7. C-O bond functionalisation by pre-functionalisation of the free alcohol.

To this end Macmillan and co-workers approached the situation by an *in-situ* pre-activation of alcohols using stoichiometric N-heterocyclic carbenes.[97] The pre-activation step is simple, simply stirring the alcohol with NHC to form **49** which is directly applied to the reaction without purification. This technique is broad in scope and highly selective for the C-O bond defunctionalisation. Inert bond functionalisations are often derived from a two-electron polar chemistry perspective but radical chemistry offers an alternative perspective. The extension towards one of the most fundamental native functional handles, C(sp^3)-H bonds has seen considerable progress and will

be discussed in chapter 2/3. In the scenarios we have seen, the combination of metal and photoredox catalysis are largely dual or triple catalytic scenarios. Although direct excitation of transition metal intermediates has become a versatile strategy for bond construction.[98]

1.4.4. Direct photoexcitation of nickel

Although the use of photocatalysts with nickel is well studied, the corresponding direct photoexcitation of nickel has not received quite as much attention.[99] Doyle and co-workers studied the photoexcitation of nickel (II) aryl halide complexes in 2018.[100] and showed that there was in fact a geometrical change of the nickel from square planar to tetrahedral.

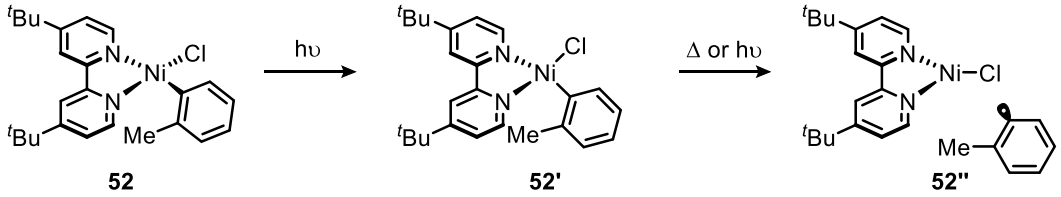

Figure 1.4.8. Photoexcitation leads to a tetrahedral triplet d-d state.

A follow up paper in 2020 by the same group using spectroscopy and DFT studies to rectify their initial incorrect assignment of a long-lived triplet MLCT state (Figure 1.4.8).[101] The ultrafast photophysical studies suggest that the initial MLCT decays to a long-lived (~ 4 ns) triplet d-d state which has a tetrahedral geometry (**52'**). This tetrahedral state weakens the Ni-Aryl bond which allows for the bond homolysis. This work sets a framework which may allow for further development of photocatalyst free nickel catalysed transformations. Indeed, there are a number of reactions that now do not require an exogenous photocatalyst including C-O,[102] C-C,[103] and C-N bond forming reactions.

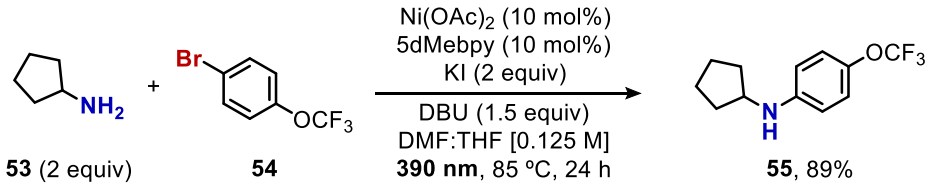

Figure 1.4.9. Buchwald-Hartwig amination enabled by UV irradiation.

Indeed, an initial report by Miyake and co-workers showed that a Buchwald-Hartwig amination could be enabled by direct photoexcitation of nickel.[104] The disclosed reaction was later refined by Xue and co-workers to expand the strategy, enabling an impressive scope of C-N bond forming reactions using low wavelength UV light (390nm, Figure 1.4.9).[105] The direct excitation of a nickel species holds some considerable promise.

1.5. The outlook

Photoredox chemistry has some exceptional advantages over thermal chemistry, however there are also a number of issues that surround photochemistry, particularly for application to large scale reactions and industrial applications. The scale up issues are related to the Beer-Lambert Law (Equation 2). Which relates the absorbance (A) to the Molar absorption coefficient (ε), the molar concentration (c) and the path length (l).

$$A = \varepsilon c l \tag{2}$$

Each of these factors is related to the efficiency of which a photoredox reaction can run as the reaction vessels get larger, light can only penetrate so far into the reaction, as such you can do not get reactivity throughout the reaction vessel and only at the points of light source. It is also one of the reasons why photoreactions must be quite dilute so light can penetrate through the system.

Another noticeable disadvantage to photochemistry is the quantum yield of many reactions. Quantum yield is the number of photons that lead to a productive bond forming reaction. For many photoredox reactions that have been developed, quantum yields are considerably low. This inevitably leads to issues surrounding the green metrics for photoredox chemistry. Inefficiencies surrounding quantum yield are exacerbated when the previous issues are compounded. Initially, the photon has to be generated which requires an electrical input. The light has to pass through the reaction vessels wall which can lead to a reduced number of photons. Then, only certain wavelengths of light will be absorbed by the photocatalyst, these three preliminary steps are not 100% efficient and are then further reduced by the quantum yield of the reaction. Electrochemistry on the other hand offers an almost direct injection of an electron with faradic efficiencies that are comparatively high.

Finally, the maximum energy of a visible light photon is 3.1 eV at 400 nm, accounting for energy losses through intersystem crossing, and molecule rearrangements impose limits on the available energy within a photoredox system.[106]

1.6. Summary

To conclude, this chapter has described the key concepts and themes which the thesis will build upon. Relevant examples of synthetically useful and mechanistically interesting reactions have been presented with the aim of highlighting the diverse reactivity that photoredox catalysis can afford.

The maturing platform of photoredox chemistry has enabled unique reaction platforms and will continue to do so. However, there are still fundamental areas of photocatalysis that need to be addressed for sustained and continued development. Although the current field is an age away from the initial discoveries and developments of the early pioneers, there is some distance to go before photochemistry is widely applied in synthetic organic chemistry.

1.7. General objective of the Doctoral Thesis

Visible light photoredox chemistry has witnessed a dramatic development over the past decades, with a plethora of reactions being enabled through SET or EnT processes. Despite these realisations there are still many chemical transformations that remain elusive, particularly in the field of native C-H functionalisation. The Martin group has already established a connection to the field of inert bond functionalisation, developing many inert bond functionalisations. This thesis is aimed at creating new photoredox techniques that can access elusive *inert bond* functionalisations, particularly in the synthesis of C-C bonds. Additionally, the expansion of photomediated metal-catalysed processes without the requirement of a photocatalyst would be a particularly interesting platform. To this end, the following objectives have been targeted:

1. To develop an *enantioselective* C(sp^3)-H bond arylation enabled by the metallatriplet platform developed within the group.

2. To develop the sp^3-sp^3 cross coupling of allylic C(sp^3)-H bonds and *unactivated alkyl bromides* opening potential routes for increased sp^3 character in molecular scaffolds.

3. Exploit the photochemical behaviour of nickel to access the hydrodehalogenation of arylbromides using THF as the hydrogen source. With the potential to expand to deuterodehalogenation.

1.8. References

1. Greiner, W.; Neise, L.; Stöcker, H. *Thermodynamics and Statistical Mechanics*; Classical theoretical physics; Springer-Verlag: New York, 1995.

2. Roth, H. D. The Beginnings of Organic Photochemistry. *Angew. Chemie Int. Ed. English* **1989**, *28* (9), 1193–1207. https://doi.org/10.1002/anie.198911931.

3. Trommsdorff, H. Ueber Santonin. *Ann. der Pharm.* **1834**, *11* (2), 190–207. https://doi.org/10.1002/jlac.18340110207.

4. a) Barton, D. H. R.; Mayo, P. de; Shafiq, M. Photochemical Transformations. Part I. Some Preliminary Investigations. *J. Chem. Soc.* **1957**, No. 0, 929–935. https://doi.org/10/djvgnn.
b) Matsuura, T.; Sata, Y.; Ogura, K.; Mori, M. Protoinduced Reactions. XXIII. A Novel Photorearranement of Santonin in the Solid State. *Tetrahedron Letters* **1968**, *9* (44), 4627–4630. https://doi.org/10/fdh5kc.

5. Natarajan, A.; K. Tsai, C.; I. Khan, S.; McCarren, P.; N. Houk, K.; A. Garcia-Garibay, M. The Photoarrangement of α-Santonin Is a Single-Crystal-to-Single-Crystal Reaction: A Long-Kept Secret in Solid-State Organic Chemistry Revealed. *Journal of the American Chemical Society* **2007**, *129* (32), 9846–9847. https://doi.org/10.1021/ja073189o.

6 Albini, A.; Fagnoni, M. 1908: Giacomo Ciamician and the Concept of Green Chemistry. *ChemSusChem* **2008**, *1* (1–2), 63–66. https://doi.org/10.1002/cssc.200700015.

7. Albini, A.; Fagnoni, M. The Greenest Reagent in Organic Synthesis: Light; Tundo, P., Esposito, V., Eds.; Springer Netherlands: Dordrecht, 2008; pp 173–189.

8. Ciamician, G. MODERN Civilization Is the daughter of Coal, for This Offers to Mankind the Solar. *Science* **1912**, *XXXVI* (No), 926.

9. Albini, A.; Fagnoni, M. Green Chemistry and Photochemistry Were Born at the Same Time. *Green Chem.* **2004**, *6* (1), 1. https://doi.org/10/c5b3fv.

10. Foster, R. Electron Donor-Acceptor Complexes. *J. Phys. Chem.* **1980**, *84* (17), 2135–2141. https://doi.org/10/c2692v.

11. Mulliken, R. S. Structures of Complexes Formed by Halogen Molecules with Aromatic and with Oxygenated Solvents1. *J. Am. Chem. Soc.* **1950**, *72* (1), 600–608. https://doi.org/10/d242tg.

12. a) Mulliken, R. S. Molecular Compounds and Their Spectra. II. *J. Am. Chem. Soc.* **1952**, *74* (3), 811–824. https://doi.org/10/dt2zr6.
b) Mulliken, R. S. Molecular Compounds and Their Spectra. III. The Interaction of Electron Donors and Acceptors. *J. Phys. Chem.* **1952**, *56* (7), 801–822. https://doi.org/10/c63pct.

13. Crisenza, G. E. M.; Mazzarella, D.; Melchiorre, P. Synthetic Methods Driven by the Photoactivity of Electron Donor–Acceptor Complexes. J. Am. Chem. Soc. 2020, 142 (12), 5461–5476. https://doi.org/10/gqfp83.

14 See references 17-22 in [*ref 13*]

15 a) Strieth-Kalthoff, F.; James, M. J.; Teders, M.; Pitzer, L.; Glorius, F. Energy Transfer Catalysis Mediated by Visible Light: Principles, Applications, Directions. *Chem. Soc. Rev.* **2018**, *47* (19), 7190–7202. https://doi.org/10/gqfqgp.
b) Strieth-Kalthoff, F.; Glorius, F. Triplet Energy Transfer Photocatalysis: Unlocking the Next Level. *Chem* **2020**, *6* (8), 1888–1903. https://doi.org/10.1016/j.chempr.2020.07.010.

16. a) Spada, L. T.; Foote, C. S. Electron-Transfer Photooxidation. 3. Detection of Radical-Ion Intermediates in the Cyanoaromatic-Sensitized Photooxidation of Trans- and Cis-Stilbene. *J. Am. Chem. Soc.* **1980**, *102* (1), 391–393. https://doi.org/10/dk5ntw.
b) Elliott, L. D.; Berry, M.; Harji, B.; Klauber, D.; Leonard, J.; Booker-Milburn, K. I. A Small-Footprint, High-Capacity Flow Reactor for UV Photochemical Synthesis on the Kilogram Scale. *Org. Process Res. Dev.* **2016**, *20* (10), 1806–1811. https://doi.org/10/f9cmm9.

17 Hedstrand, D. M.; Kruizinga, W. H.; Kellogg, R. M. Light Induced and Dye Accelerated Reductions of Phenacyl Onium Salts by 1,4-Dihydropyridines. *Tetrahedron Letters* **1978**, *19* (14), 1255–1258. https://doi.org/10.1016/S0040-4039(01)94515-0.

18. Hironaka, K.; Fukuzumi, S.; Tanaka, T. Tris(Bipyridyl)Ruthenium(II)-Photosensitized. *J. CHEM. SOC. PERKIN TRANS. II* **1984**, 1705. https://doi.org/10.1039/P29840001705.

19 Pac, C.; Ihama, M.; Yasuda, M.; Miyauchi, Y.; Sakurai, H. Ru(Bpy)32+-Mediated Photoreduction of Olefins with 1-Benzyl-1,4-Dihydronicotinamide: A Mechanistic Probe for Electron-Transfer Reactions of NAD(P)H-Model Compounds. *Journal of the American Chemical Society* **1981**, *103* (21), 6495–6497. https://doi.org/10.1021/ja00411a040.

20. Kalyanasundaram, K. Photophysics, Photochemistry and Solar Energy Conversion with Tris(Bipyridyl)Ruthenium(II) and Its Analogues. *Coordination Chemistry Reviews* **1982**, *46*, 159–244. https://doi.org/10/bx7q8r.

21. Roundhill, D. M. Photochemistry, Photophysics, and Photoredox Reactions of $Ru(bpy)_3^{2+}$ and Related Complexes. In *Photochemistry and Photophysics of Metal Complexes*; Springer US: Boston, MA, 1994; pp 165–215. https://doi.org/10.1007/978-1-4899-1495-8_5.

22. a) Goren, Z.; Willner, I. Photochemical and Chemical Reduction of Vicinal Dibromides via Phase Transfer of 4,4'-Bipyridinium Radical: The Role of Radical Disproportionation. *J. Am. Chem. Soc.* **1983**, *105* (26), 7764–7765. https://doi.org/10/b5bm5s.
b) Maidan, R.; Goren, Z.; Becker, J. Y.; Willner, I. Application of Multielectron Charge Relays in Chemical and Photochemical Debromination Processes. The Role of Induced Disproportionation of N,N'-Dioctyl-4,4'-Bipyridinium Radical Cation in Two-Phase Systems. *J. Am. Chem. Soc.* **1984**, *106* (21), 6217–6222. https://doi.org/10/cxvpgk.

23. Cano-Yelo, H., Deronzier, A. Photocatalysis Of the Pschorr Reaction by Tris-(2,2´-Bypyridyl) Ruthenium (II) In the Phenanthrene Series. *J. Chem. Soc. Perkin Trans*. **1984**, *2*, 1093.

24. Fukuzumi, S., Mochizuki, S., Tanaka, T. J. Photocatalytic Reduction of Phenacyl Halides By 9,10-Dihydro-10-Methylacridine: Control Between the Reduction and Oxidative Quenching Pathways of Tris (Bipyridine)Ruthenium Complex Utilizing an Acid Catalysis. *Phy. Chem.* **1990**, *94*, 722.

25. Kern, J.-M., Sauvage, J.-P. Photoassisted C-C Coupling Via Electron Transfer to Benzylic Halides by Bis (Di-Imine) Copper(I) Complex. *J. Chem. Soc. Chem. Commun.* **1987**, 546.

26. Okada, K.; Okamoto, K.; Morita, N.; Okubo, K.; Oda, M. Photosensitized Decarboxylative Michael Addition through N-(Acyloxy)Phthalimides via an Electron-Transfer Mechanism. *J. Am. Chem. Soc.* **1991**, *113* (24), 9401–9402. https://doi.org/10/bgnf8r.

27.Nicewicz, D. A.; MacMillan, D. W. C. Merging Photoredox Catalysis with Organocatalysis: The Direct Asymmetric Alkylation of Aldehydes. *Science* **2008**, *322* (5898), 77–80. https://doi.org/10/bk3fnb.

28. Ischay, M. A.; Anzovino, M. E.; Du, J.; Yoon, T. P. Efficient Visible Light Photocatalysis of [2+2] Enone Cycloadditions. *J. Am. Chem. Soc.* **2008**, *130* (39), 12886–12887. https://doi.org/10/dmsdjd.

29. Narayanam, J. M. R.; Tucker, J. W.; Stephenson, C. R. J. Electron-Transfer Photoredox Catalysis: Development of a Tin-Free Reductive Dehalogenation Reaction. *J. Am. Chem. Soc.* **2009**, *131* (25), 8756–8757. https://doi.org/10/fr7sg2.

30. Fukuzumi, S., Mochizuki, S., Tanaka, T. J. Photocatalytic Reduction of Phenacyl Halides By 9,10-Dihydro-10-Methylacridine: Control Between the Reduction and Oxidative Quenching Pathways of Tris (Bipyridine)Ruthenium Complex Utilizing an Acid Catalysis. *Phy. Chem.* **1990**, *94*, 722.

31. Yoshimi, Y.; Itou, T.; Hatanaka, M. Decarboxylative Reduction of Free Aliphatic Carboxylic Acids by Photogenerated Cation Radical. *Chem. Commun.* **2007**, No. 48, 5244–5246. https://doi.org/10/fkm5pf.

32. Osawa, M.; Nagai, H.; Akita, M. Photo-Activation of Pd-Catalyzed Sonogashira Coupling Using a Ru/Bipyridine Complex as Energy Transfer Agent. *Dalton Trans.* **2007**, No. 8, 827–829. https://doi.org/10/dfk4mb.

33. Albini, A.; Fagnoni, M. The Greenest Reagent in Organic Synthesis: Light. In *Green Chemical Reactions*; Tundo, P., Esposito, V., Eds.; NATO Science for Peace and Security Series; Springer Netherlands: Dordrecht, 2008; pp 173–189. https://doi.org/10.1007/978-1-4020-8457-7_8.

34. Gong, Y.; Su, L.; Zhu, Z.; Ye, Y.; Gong, H. Nickel-Catalyzed Thermal Redox Functionalization of $C(Sp^3)$−H Bonds with Carbon Electrophiles. *Angew Chem Int Ed* **2022**, *61* (22). https://doi.org/10/gqm6tz.

35. An initial publication which is limited to benzylic: Miyake, Y.; Nakajima, K.; Nishibayashi, Y. Visible Light-Mediated Oxidative Decarboxylation of Arylacetic Acids into Benzyl Radicals: Addition to Electron-Deficient Alkenes by Using Photoredox Catalysts. *Chem. Commun.* **2013**, *49* (71), 7854–7856. https://doi.org/10/gqmxpf.
b) Macmillans work: Chu, L.; Ohta, C.; Zuo, Z.; MacMillan, D. W. C. Carboxylic Acids as A Traceless Activation Group for Conjugate Additions: A Three-Step Synthesis of (±)-Pregabalin. *J. Am. Chem. Soc.* **2014**, *136* (31), 10886–10889. https://doi.org/10/f6cpgp.

36. Crespi, S.; Fagnoni, M. Generation of Alkyl Radicals: From the Tyranny of Tin to the Photon Democracy. *Chemical Reviews* **2020**, *120* (17), 9790–9833. https://doi.org/10/gqfc94.

37. Wang, P.-Z.; Chen, J.-R.; Xiao, W.-J. Hantzsch Esters: An Emerging Versatile Class of Reagents in Photoredox Catalyzed Organic Synthesis. *Org. Biomol. Chem.* **2019**, *17* (29), 6936–6951. https://doi.org/10/gqm8xx.

38. Fabry, D. C.; Rueping, M. Merging Visible Light Photoredox Catalysis with Metal Catalyzed C–H Activations: On the Role of Oxygen and Superoxide Ions as Oxidants. *Acc. Chem. Res.* **2016**, *49* (9), 1969–1979. https://doi.org/10/f84swz.

39. DiRocco, D. A.; Rovis, T. Catalytic Asymmetric α-Acylation of Tertiary Amines Mediated by a Dual Catalysis Mode: N-Heterocyclic Carbene and Photoredox Catalysis. *J. Am. Chem. Soc.* **2012**, *134* (19), 8094–8097. https://doi.org/10/f3zmxm.

40. Ischay, M. A.; Lu, Z.; Yoon, T. P. [2+2] Cycloadditions by Oxidative Visible Light Photocatalysis. *J. Am. Chem. Soc.* **2010**, *132* (25), 8572–8574. https://doi.org/10/dx78md.

41. Cano-Yelo, H.; Deronzier, A. Photo-Oxidation of Some Carbinols by the Ru(II) Polypyridyl Complex-Aryl Diazonium Salt System. *Tetrahedron Letters* **1984**, *25* (48), 5517–5520. https://doi.org/10/d2k9n3.

42. Ho, T.-I.; Chow, Y. L. Photochemistry of Amines, and Amino Compounds. In *The Chemistry of Functional Groups*; Patai, S., Ed.; John Wiley & Sons, Ltd: Chichester, UK, 1996; pp 683–745. https://doi.org/10.1002/047085720X.ch15.

43. Rettig, I. D.; McCormick, T. M. Enrolling Reactive Oxygen Species in Photon-to-Chemical Energy Conversion: Fundamentals, Technological Advances, and Applications. *Advances in Physics: X* **2021**, *6* (1), 1950049. https://doi.org/10/gqpkc7.

44. Reed, N. L.; Yoon, T. P. Oxidase Reactions in Photoredox Catalysis. *Chem. Soc. Rev.* **2021**, *50* (5), 2954–2967. https://doi.org/10/ggmxqr.

45. Rueda-Becerril, M.; Mahé, O.; Drouin, M.; Majewski, M. B.; West, J. G.; Wolf, M. O.; Sammis, G. M.; Paquin, J.-F. Direct C–F Bond Formation Using Photoredox Catalysis. *J. Am. Chem. Soc.* **2014**, *136* (6), 2637–2641. https://doi.org/10/ggm4zn.

46. Lee, B. J.; DeGlopper, K. S.; Yoon, T. P. Site-Selective Alkoxylation of Benzylic C−H Bonds by Photoredox Catalysis. *Angewandte Chemie International Edition* **2020**, *59* (1), 197–202. https://doi.org/10/gpnf27.

47. The potentials of the iridium, copper and arene are all matched well so it is difficult to discern which pathway this reaction takes. The arene radical cation can be generated by both the *IrIII or the IrIV complex. Additionally, the copper (II) salt can regenerate the ground state photocatalyst from IrII and quench the *IrIII.

Arene (Eox = + 1.52 V) **vs** (E[IrIV/III] = + 1.94 V) **or** (E[*IrIII/IrII] = + 1.68 V)
(E(CuII/CuI) = + 0.38 V) **vs** (E[IrIV/*IrIII] = - 0.43 V) **or** (E[IrIII/IrII] = - 0.69 V)

48. Markushyna, Y.; Savateev, A. Light as a Tool in Organic Photocatalysis: Multi-photon Excitation and Chromoselective Reactions. *European Journal of Organic Chemistry* **2022**. https://doi.org/10.1002/ejoc.202200026.

49. Martínez-Gualda, A. M.; Cano, R.; Marzo, L.; Pérez-Ruiz, R.; Luis-Barrera, J.; Mas-Ballesté, R.; Fraile, A.; de la Peña O'Shea, V. A.; Alemán, J. Chromoselective Access to Z- or E- Allylated Amines and Heterocycles by a Photocatalytic Allylation Reaction. *Nat Commun* **2019**, *10* (1), 2634. https://doi.org/10/ggmxj8.

50 Although, it must be noted that it is possible to get radical chain mechanisms within photocatalysis where the PC simply behaves as a photoinitiator, many radical chains will terminate quickly without light.

51 a) Kalyanasundaram, K.; Grätzel, M. Applications of Functionalized Transition Metal Complexes in Photonic and Optoelectronic Devices. *Coordination Chemistry Reviews* **1998**, *177* (1), 347–414. https://doi.org/10/fd63r6.
b) Narayan, M. R. Review: Dye Sensitized Solar Cells Based on Natural Photosensitizers. *Renewable and Sustainable Energy Reviews* **2012**, *16* (1), 208–215. https://doi.org/10/dfwgm3.

52. Slinker, J.; Bernards, D.; Houston, P. L.; Abruña, H. D.; Bernhard, S.; Malliaras, G. G. Solid-State Electroluminescent Devices Based on Transition Metal Complexes. *Chem. Commun.* **2003**, No. 19, 2392–2399. https://doi.org/10/c4q2dp.

53. Li, L.; Yu, B.; Zhang, X.; You, T. A Novel Electrochemiluminescence Sensor Based on Ru(Bpy)32+/N-Doped Carbon Nanodots System for the Detection of Bisphenol A. *Analytica Chimica Acta* **2015**, *895*, 104–111. https://doi.org/10/f7vnt6.

54. [Ir] + Acridinium: Prier, C. K.; Rankic, D. A.; MacMillan, D. W. C. Visible Light Photoredox Catalysis with Transition Metal Complexes: Applications in Organic Synthesis. *Chem. Rev.* **2013**, *113* (7), 5322–5363. https://doi.org/10/gdj5t5.
4CzIPN: Shang, T.-Y.; Lu, L.-H.; Cao, Z.; Liu, Y.; He, W.-M.; Yu, B. Recent Advances of 1,2,3,5-Tetrakis(Carbazol-9-Yl)-4,6-Dicyanobenzene (4CzIPN) in Photocatalytic Transformations. *Chem. Commun.* **2019**, *55* (38), 5408–5419. https://doi.org/10/gpnftg.
PTH: Speck, F.; Rombach, D.; Wagenknecht, H.-A. N-Arylphenothiazines as Strong Donors for Photoredox Catalysis – Pushing the Frontiers of Nucleophilic Addition of Alcohols to Alkenes. *Beilstein J. Org. Chem.* **2019**, *15* (1), 52–59. https://doi.org/10/ggprn2.

55. *The IUPAC Compendium of Chemical Terminology: The Gold Book*, 4th ed.; Gold, V., Ed.; International Union of Pure and Applied Chemistry (IUPAC): Research Triangle Park, NC, 2019. *"Gibbs energy of photoinduced electron transfer"* https://doi.org/10.1351/goldbook.

56. **Acridinium:** Joshi-Pangu, A.; Lévesque, F.; Roth, H. G.; Oliver, S. F.; Campeau, L.-C.; Nicewicz, D.; DiRocco, D. A. Acridinium-Based Photocatalysts: A Sustainable Option in Photoredox Catalysis. *J. Org. Chem.* **2016**, *81* (16), 7244–7249. https://doi.org/10/f8zfxn.
PTH: McCarthy, B. G.; Pearson, R. M.; Lim, C.-H.; Sartor, S. M.; Damrauer, N. H.; Miyake, G. M. Structure–Property Relationships for Tailoring Phenoxazines as Reducing Photoredox Catalysts. *J. Am. Chem. Soc.* **2018**, *140* (15), 5088–5101. https://doi.org/10/gdjwg6.

57. Speckmeier, E.; Fischer, T. G.; Zeitler, K. A Toolbox Approach to Construct Broadly Applicable Metal-Free Catalysts for Photoredox Chemistry: Deliberate Tuning of Redox Potentials and Importance of Halogens in Donor-Acceptor Cyanoarenes. *Journal of the American Chemical Society* **2018**, *140* (45), 15353–15365. https://doi.org/10.1021/jacs.8b08933.

58. a) Teegardin, K.; Day, J. I.; Chan, J.; Weaver, J. Advances in Photocatalysis: A Microreview of Visible Light Mediated Ruthenium and Iridium Catalyzed Organic Transformations. *Org. Process Res. Dev.* **2016**, *20* (7), 1156–1163. https://doi.org/10/gmvcqw.
b) Dumur, F. Recent Advances on Visible Light Metal-Based Photocatalysts for Polymerization under Low Light Intensity. *Catalysts* **2019**, *9* (9), 736. https://doi.org/10/ggvb7p.
c) Tamayo, A. B.; Alleyne, B. D.; Djurovich, P. I.; Lamansky, S.; Tsyba, I.; Ho, N. N.; Bau, R.; Thompson, M. E. Synthesis and Characterization of Facial and Meridional Tris-Cyclometalated Iridium(III) Complexes. *J. Am. Chem. Soc.* **2003**, *125* (24), 7377–7387. https://doi.org/10/frr9rp.
d) Lowry, M. S.; Goldsmith, J. I.; Slinker, J. D.; Rohl, R.; Pascal, R. A.; Malliaras, G. G.; Bernhard, S. Single-Layer Electroluminescent Devices and Photoinduced Hydrogen Production from an Ionic Iridium(III) Complex. *Chem. Mater.* **2005**, *17* (23), 5712–5719. https://doi.org/10/bvb4xf.

59. Uoyama, H.; Goushi, K.; Shizu, K.; Nomura, H.; Adachi, C. Highly Efficient Organic Light-Emitting Diodes from Delayed Fluorescence. *Nature* **2012**, *492* (7428), 234–238. https://doi.org/10/jzp.

60. Matsui, J. K.; Lang, S. B.; Heitz, D. R.; Molander, G. A. Photoredox-Mediated Routes to Radicals: The Value of Catalytic Radical Generation in Synthetic Methods Development. *ACS Catal.* **2017**, *7* (4), 2563–2575. https://doi.org/10/ggprkr.

61. Kato, K.; Osuka, A. Platforms for Stable Carbon-Centered Radicals. *Angewandte Chemie International Edition* **2019**, *58* (27), 8978–8986. https://doi.org/10/gfvfcp.

62. Parsaee, F.; Senarathna, M. C.; Kannangara, P. B.; Alexander, S. N.; Arche, P. D. E.; Welin, E. R. Radical Philicity, and Its Role in Selective Organic Transformations. *Nature Reviews Chemistry* **2021**, *5* (7), 486–499. https://doi.org/10.1038/s41570-021-00284-3.

63. Farney, E. P.; Feng, S. S.; Schäfers, F.; Reisman, S. E. Total Synthesis of (+)-Pleuromutilin. *J. Am. Chem. Soc.* **2018**, *140* (4), 1267–1270. https://doi.org/10/gfxbpj.

64. Viehe, H. G.; Janousek, Z.; Merenyi, R.; Stella, L. The Captodative Effect. *Acc. Chem. Res.* **1985**, *18* (5), 148–154. https://doi.org/10/b597f9.

65. Crespi, S.; Fagnoni, M. Generation of Alkyl Radicals: From the Tyranny of Tin to the Photon Democracy. *Chem.Rev.* **2020**, *120* (17), 9790–9833. https://doi.org/10/ggfc94.

66. Li, P.; Zbieg, J. R.; Terrett, J. A. A Platform for Decarboxylative Couplings via Photoredox Catalysis: Direct Access to Carbocations from Carboxylic Acids for Carbon–Oxygen Bond Formation. *ACS Catal.* **2021**, *11* (17), 10997–11004. https://doi.org/10/gpnfzk.

67. Ling, T.; Poupon, E.; Rueden, E. J.; Theodorakis, E. A. Synthesis of (−)-Ilimaquinone via a Radical Decarboxylation and Quinone Addition Reaction. *Org. Lett.* **2002**, *4* (5), 819–822. https://doi.org/10/cnpnw2.

68. Xuan, J.; Zhang, Z.-G.; Xiao, W.-J. Visible-Light-Induced Decarboxylative Functionalization of Carboxylic Acids and Their Derivatives. *Angewandte Chemie International Edition* **2015**, *54* (52), 15632–15641. https://doi.org/10/f3jsrm.

69. Ashley, M. A.; Rovis, T. Photoredox-Catalyzed Deaminative Alkylation via C–N Bond Activation of Primary Amines. *J. Am. Chem. Soc.* **2020**, *142* (43), 18310–18316. https://doi.org/10/ghft5n.

70. Klauck, F. J. R.; James, M. J.; Glorius, F. Deaminative Strategy for the Visible-Light-Mediated Generation of Alkyl Radicals. *Angewandte Chemie - International Edition* **2017**, *56* (40), 12336–12339. https://doi.org/10.1002/anie.201706896.

71. de Pedro Beato, E.; Spinnato, D.; Zhou, W.; Melchiorre, P. A General Organocatalytic System for Electron Donor–Acceptor Complex Photoactivation and Its Use in Radical Processes. *J. Am. Chem. Soc.* **2021**, *143* (31), 12304–12314. https://doi.org/10/gpnfx4.

72. Zhang, K.; Chang, L.; An, Q.; Wang, X.; Zuo, Z. Dehydroxymethylation of Alcohols Enabled by Cerium Photocatalysis. *J. Am. Chem. Soc.* **2019**, *141* (26), 10556–10564. https://doi.org/10/gqfjbn.

73. Juliá, F.; Constantin, T.; Leonori, D. Applications of Halogen-Atom Transfer (XAT) for the Generation of Carbon Radicals in Synthetic Photochemistry and Photocatalysis. *Chem. Rev.* **2022**, *122* (2), 2292–2352. https://doi.org/10/ggm2px.

74. Constantin, T.; Zanini, M.; Regni, A.; Sheikh, N. S.; Juliá, F.; Leonori, D. Aminoalkyl Radicals as Halogen-Atom Transfer Agents for Activation of Alkyl and Aryl Halides. *Science* **2020**, *367* (6481), 1021–1026. https://doi.org/10/ggm32q.

75. Cismesia, M. A.; Yoon, T. P. Characterizing Chain Processes in Visible Light Photoredox Catalysis. *Chem. Sci.* **2015**, *6* (10), 5426–5434. https://doi.org/10/gqpkwn.

76 a) Crawley, M. L.; Trost, B. M. Applications of Transition Metal Catalysis in Drug Discovery and Development: An Industrial Perspective; John Wiley & Sons: Hoboken, 2012.
b) Masters, C. Homogeneous Transition-Metal Catalysis: A Gentle Art; Science paperbacks; Chapman and Hall: London, 1981.

77. a) Fors, B. P.; Watson, D. A.; Biscoe, M. R.; Buchwald, S. L. A Highly Active Catalyst for Pd-Catalyzed Amination Reactions: Cross-Coupling Reactions Using Aryl Mesylates and the Highly Selective Monoarylation of Primary Amines Using Aryl Chlorides. *J. Am. Chem. Soc.* **2008**, *130* (41), 13552–13554. https://doi.org/10/dcqwzx.
b) Hartwig, J. F. Evolution of a Fourth Generation Catalyst for the Amination and Thioetherification of Aryl Halides. *Acc. Chem. Res.* **2008**, *41* (11), 1534–1544. https://doi.org/10/czjbkp.

78. Trnka, T. M.; Grubbs, R. H. The Development of L 2 X 2 RuCHR Olefin Metathesis Catalysts: An Organometallic Success Story. *Acc. Chem. Res.* **2001**, *34* (1), 18–29. https://doi.org/10/bts9r9.

79.Finck, L.; Oestreich, M.; Klare. F. T., H. The Chan–Evans–Lam Coupling. *Synfacts* **2022**, *18* (07), 0772. https://doi.org/10/gqpq5z.

80. a) Wang, X.; Lu, Y.; Dai, H.-X.; Yu, J.-Q. Pd(II)-Catalyzed Hydroxyl-Directed C−H Activation/C−O Cyclization: Expedient Construction of Dihydrobenzofurans. *J. Am. Chem. Soc.* **2010**, *132* (35), 12203–12205. https://doi.org/10/d6dbxm.
b) Hickman, A. J.; Sanford, M. S. High-Valent Organometallic Copper, and Palladium in Catalysis. *Nature* **2012**, *484* (7393), 177–185. https://doi.org/10/gqpkwp.

81. Börjesson, M.; Moragas, T.; Martin, R. Ni-Catalyzed Carboxylation of Unactivated Alkyl Chlorides with CO2. *J. Am. Chem. Soc.* **2016**, *138* (24), 7504–7507. https://doi.org/10/ghjvtc.

82. a) Chan, A. Y.; Perry, I. B.; Bissonnette, N. B.; Buksh, B. F.; Edwards, G. A.; Frye, L. I.; Garry, O. L.; Lavagnino, M. N.; Li, B. X.; Liang, Y.; Mao, E.; Millet, A.; Oakley, J. V.; Reed, N. L.; Sakai, H. A.; Seath, C. P.; MacMillan, D. W. C. Metallaphotoredox: The Merger of Photoredox and Transition Metal Catalysis. *Chemical Reviews* **2021**. https://doi.org/10/gpnfxv.
b) Prier, C. K.; Rankic, D. A.; MacMillan, D. W. C. Visible Light Photoredox Catalysis with Transition Metal Complexes: Applications in Organic Synthesis. *Chemical Reviews* **2013**, *113* (7), 5322–5363. https://doi.org/10.1021/cr300503r.
c) Shaw, M. H.; Twilton, J.; MacMillan, D. W. C. Photoredox Catalysis in Organic Chemistry. *J. Org. Chem.* **2016**, *81* (16), 6898–6926. https://doi.org/10/gdj5nb.

83. Kalyani, D.; McMurtrey, K. B.; Neufeldt, S. R.; Sanford, M. S. Room-Temperature C–H Arylation: Merger of Pd-Catalyzed C–H Functionalization and Visible-Light Photocatalysis. *J. Am. Chem. Soc.* **2011**, *133* (46), 18566–18569. https://doi.org/10/dbzhzt.

84. Ye, Y.; Sanford, M. S. Merging Visible-Light Photocatalysis and Transition-Metal Catalysis in the Copper-Catalyzed Trifluoromethylation of Boronic Acids with CF 3 I. *J. Am. Chem. Soc.* **2012**, *134* (22), 9034–9037. https://doi.org/10/gdj5ns.

85. Schley, N. D.; Fu, G. C. Nickel-Catalyzed Negishi Arylations of Propargylic Bromides: A Mechanistic Investigation. *J. Am. Chem. Soc.* **2014**, *136* (47), 16588–16593. https://doi.org/10/f6r2z5.
Jahn, U. Radicals in Transition Metal Catalyzed Reactions? Transition Metal Catalyzed Radical Reactions? A Fruitful Interplay Anyway. In *Radicals in Synthesis III*; Heinrich, M., Gansäuer, A., Eds.; Topics in Current Chemistry; Springer: Berlin, Heidelberg, 2012; pp 323–451. https://doi.org/10.1007/128_2011_288.

86. Ananikov, V. P. Nickel: The “Spirited Horse” of Transition Metal Catalysis. *ACS Catal.* **2015**, *5* (3), 1964–1971. https://doi.org/10/gjs84r.

87. a) Tasker, S. Z.; Standley, E. A.; Jamison, T. F. Recent Advances in Homogeneous Nickel Catalysis. *Nature* **2014**, *509* (7500), 299–309. https://doi.org/10/f53rpn.
b) Biswas, S.; Weix, D. J. Mechanism and Selectivity in Nickel-Catalyzed Cross-Electrophile Coupling of Aryl Halides with Alkyl Halides. *J. Am. Chem. Soc.* **2013**, *135* (43), 16192–16197. https://doi.org/10/ghjv4g.
c) Weix, D. J. Methods and Mechanisms for Cross-Electrophile Coupling of Csp2 Halides with Alkyl Electrophiles. *Acc. Chem. Res.* **2015**, *48* (6), 1767–1775. https://doi.org/10/ghjv35.

88. a) Sahoo, B.; Bellotti, P.; Juliá-Hernández, F.; Meng, Q.-Y.; Crespi, S.; König, B.; Martin, R. Site-Selective, Remote Sp3 C−H Carboxylation Enabled by the Merger of Photoredox and Nickel Catalysis. *Chemistry – A European Journal* **2019**, *25* (38), 9001–9005. https://doi.org/10/ghjvrz.
b) Song, L.; Fu, D.-M.; Chen, L.; Jiang, Y.-X.; Ye, J.-H.; Zhu, L.; Lan, Y.; Fu, Q.; Yu, D.-G. Visible-Light Photoredox-Catalyzed Remote

Difunctionalizing Carboxylation of Unactivated Alkenes with CO2. *Angewandte Chemie International Edition* **2020**, *59* (47), 21121–21128. https://doi.org/10/ggpr5v.

89. Vila, C. Merging Visible-Light-Photoredox and Nickel Catalysis. *ChemCatChem* **2015**, *7* (12), 1790–1793. https://doi.org/10/f275nz.
b) Gui, Y.-Y.; Sun, L.; Lu, Z.-P.; Yu, D.-G. Photoredox Sheds New Light on Nickel Catalysis: From Carbon–Carbon to Carbon–Heteroatom Bond Formation. *Org. Chem. Front.* **2016**, *3* (4), 522–526. https://doi.org/10/ggprks.
c) Tellis, J. C.; Kelly, C. B.; Primer, D. N.; Jouffroy, M.; Patel, N. R.; Molander, G. A. Single-Electron Transmetalation via Photoredox/Nickel Dual Catalysis: Unlocking a New Paradigm for Sp3–Sp2 Cross-Coupling. *Acc. Chem. Res.* **2016**, *49* (7), 1429–1439. https://doi.org/10/f8whhg.
d) Milligan, J. A.; Phelan, J. P.; Badir, S. O.; Molander, G. A. Alkyl Carbon–Carbon Bond Formation by Nickel/Photoredox Cross-Coupling. *Angewandte Chemie International Edition* **2019**, *58* (19), 6152–6163. https://doi.org/10/gfv8kk.
e) Zhu, C.; Yue, H.; Chu, L.; Rueping, M. Recent Advances in Photoredox and Nickel Dual-Catalyzed Cascade Reactions: Pushing the Boundaries of Complexity. *Chem. Sci.* **2020**, *11* (16), 4051–4064. https://doi.org/10/gmbvdt.

90. Zuo, Z.; Ahneman, D. T.; Chu, L.; Terrett, J. A.; Doyle, A. G.; MacMillan, D. W. C. Merging Photoredox with Nickel Catalysis: Coupling of α-Carboxyl Sp3-Carbons with Aryl Halides. *Science* **2014**, *345* (6195), 437–440. https://doi.org/10.1126/science.1255525.

91. Tellis, J. C.; Primer, D. N.; Molander, G. A. Single-Electron Transmetalation in Organoboron Cross-Coupling by Photoredox/Nickel Dual Catalysis. *Science* **2014**, *345* (6195), 433–436. https://doi.org/10/f6bnn3.

92. a) Miyaura, Norio.; Suzuki, Akira. Palladium-Catalyzed Cross-Coupling Reactions of Organoboron Compounds. *Chem. Rev.* **1995**, *95* (7), 2457–2483. https://doi.org/10/d9mtxs.
b) Fu, G. C. The Development of Versatile Methods for Palladium-Catalyzed Coupling Reactions of Aryl Electrophiles through the Use of P(t-Bu)3 and PCy3 as Ligands. *Acc. Chem. Res.* **2008**, *41* (11), 1555–1564. https://doi.org/10/dcgnzh.
c) Martin, R.; Buchwald, S. L. Palladium-Catalyzed Suzuki−Miyaura Cross-Coupling Reactions Employing Dialkylbiaryl Phosphine Ligands. *Acc. Chem. Res.* **2008**, *41* (11), 1461–1473. https://doi.org/10/brq3k6.

93. Cornella, J.; Zarate, C.; Martin, R. Metal-Catalyzed Activation of Ethers via C–O Bond Cleavage: A New Strategy for Molecular Diversity. *Chem. Soc. Rev.* **2014**, *43* (23), 8081–8097. https://doi.org/10/ghjvtt.

94. Chan, A. Y.; Perry, I. B.; Bissonnette, N. B.; Buksh, B. F.; Edwards, G. A.; Frye, L. I.; Garry, O. L.; Lavagnino, M. N.; Li, B. X.; Liang, Y.; Mao, E.; Millet, A.; Oakley, J. V.; Reed, N. L.; Sakai, H. A.; Seath, C. P.; MacMillan, D. W. C. Metallaphotoredox: The Merger of Photoredox and Transition Metal Catalysis. *Chem. Rev.* **2022**, *122* (2), 1485–1542. https://doi.org/10/gpnfxv.

95 Barton, D. H. R. & McCombie, S. W. A new method for the deoxygenationof secondary alcohols. J. Chem. Soc. Perkin Trans. 1 16, 1574–1585. (1975).
Zhang, L. & Koreeda, M. Radical deoxygenation of hydroxyl groups via phosphites. J. Am. Chem. Soc. 126, 13190–13191 (2004).

96. Zhang, X. & MacMillan, D. W. C. Alcohols as latent coupling fragments for metallaphotoredox catalysis: sp3 –sp2 cross-coupling of oxalates with aryl halides. J. Am. Chem. Soc. 138, 13862–13865 (2016).

97. Dong, Z.; MacMillan, D. W. C. Metallaphotoredox-Enabled Deoxygenative Arylation of Alcohols. *Nature* **2021**, *598* (7881), 451–456. https://doi.org/10/gmn4zd.

98. Cheung, K. P. S.; Sarkar, S.; Gevorgyan, V. Visible Light-Induced Transition Metal Catalysis. *Chem. Rev.* **2022**, *122* (2), 1543–1625. https://doi.org/10/gm7q8z.

99. Wenger, O. S. Photoactive Nickel Complexes in Cross-Coupling Catalysis. *Chemistry – A European Journal* **2021**, *27* (7), 2270–2278. https://doi.org/10/ggpr3s.

100. Shields, B. J.; Kudisch, B.; Scholes, G. D.; Doyle, A. G. Long-Lived Charge-Transfer States of Nickel(II) Aryl Halide Complexes Facilitate Bimolecular Photoinduced Electron Transfer. *J. Am. Chem. Soc.* **2018**, *140* (8), 3035–3039. https://doi.org/10/ggm2sr.

101. a) Yang, L.; Lu, H.-H.; Lai, C.-H.; Li, G.; Zhang, W.; Cao, R.; Liu, F.; Wang, C.; Xiao, J.; Xue, D. Light-Promoted Nickel Catalysis: Etherification of Aryl Electrophiles with Alcohols Catalyzed by a NiII-Aryl Complex. *Angewandte Chemie International Edition* **2020**, *59* (31), 12714–12719. https://doi.org/10/ggpr48.
b) Welin, E. R.; Le, C.; Arias-Rotondo, D. M.; McCusker, J. K.; MacMillan, D. W. C. Photosensitized, Energy Transfer-Mediated Organometallic Catalysis through Electronically Excited Nickel(II). *Science* **2017**, *355* (6323), 380–385. https://doi.org/10/f9n4sh.

102. a) Shen, X.; Li, Y.; Wen, Z.; Cao, S.; Hou, X.; Gong, L. A Chiral Nickel DBFOX Complex as a Bifunctional Catalyst for Visible-Light-Promoted Asymmetric Photoredox Reactions. *Chem. Sci.* **2018**, *9* (20), 4562–4568. https://doi.org/10/gpnft2.
b) Abdiaj, I.; Horn, C. R.; Alcazar, J. Scalability of Visible-Light-Induced Nickel Negishi Reactions: A Combination of Flow Photochemistry, Use of Solid Reagents, and In-Line NMR Monitoring. *J. Org. Chem.* **2019**, *84* (8), 4748–4753. https://doi.org/10/ggpr46.
c) Abdiaj, I.; Fontana, A.; Gomez, M. V.; de la Hoz, A.; Alcázar, J. Visible-Light-Induced Nickel-Catalyzed Negishi Cross-Couplings by Exogenous-Photosensitizer-Free Photocatalysis. *Angewandte Chemie International Edition* **2018**, *57* (28), 8473–8477. https://doi.org/10/ggpr47.

103. Li, G.; Yang, L.; Liu, J.-J.; Zhang, W.; Cao, R.; Wang, C.; Zhang, Z.; Xiao, J.; Xue, D. Light-Promoted C–N Coupling of Aryl Halides with Nitroarenes. *Angewandte Chemie International Edition* **2021**, *60* (10), 5230–5234. https://doi.org/10/gmq58x.

104. Lim, C.-H.; Kudisch, M.; Liu, B.; Miyake, G. M. C–N Cross-Coupling via Photoexcitation of Nickel–Amine Complexes. *J. Am. Chem. Soc.* **2018**, *140* (24), 7667–7673. https://doi.org/10/gdts93.

105. Song, G.; Nong, D.-Z.; Li, J.-S.; Li, G.; Zhang, W.; Cao, R.; Wang, C.; Xiao, J.; Xue, D. General Method for the Amination of Aryl Halides with Primary and Secondary Alkyl Amines via Nickel Photocatalysis. *J. Org. Chem.* **2022**, *87* (15), 10285–10297. https://doi.org/10/ggm89j.

106. Widness, J. K.; Enny, D. G.; McFarlane-Connelly, K. S.; Miedenbauer, M. T.; Krauss, T. D.; Weix, D. J. CdS Quantum Dots as Potent Photoreductants for Organic Chemistry Enabled by Auger Processes. *J. Am. Chem. Soc.* **2022**. https://doi.org/10/ggfn3b.

UNIVERSITAT ROVIRA I VIRGILI
CATALYTIC TRANSFORMATIONS ENABLED BY DUAL NICKELPHOTOREDOX MANIFOLDS
Bradley Higginson

UNIVERSITAT ROVIRA I VIRGILI
CATALYTIC TRANSFORMATIONS ENABLED BY DUAL NICKELPHOTOREDOX MANIFOLDS
Bradley Higginson

CHAPTER 2.

Development of an enantioselective C(sp3)-H functionalisation technique harnessing metallatriplet catalysis

Enantioselective C-H

2.1. Introduction

The direct functionalisation of carbon-hydrogen bonds is a highly sought-after transformation.[107] The potential to rapidly build structural complexity by using latent functionalities is desirable because it can streamline synthetic routes, unlock new chemical space and lead to previously unobtainable transformations.[108] The C-H bond is ubiquitous in nature, providing the structural backbone for many organic molecules. Thus, selectively functionalising a specific C-H bond within an array of C-H environments can be challenging. The selectivity issues are compounded by the high thermodynamic stability and low pKa values of many C-H bonds which means that they are often regarded as inert. Mild strategies must be found that leave sensitive functional groups intact whilst being sufficiently reactive to functionalise the desired C-H bond.

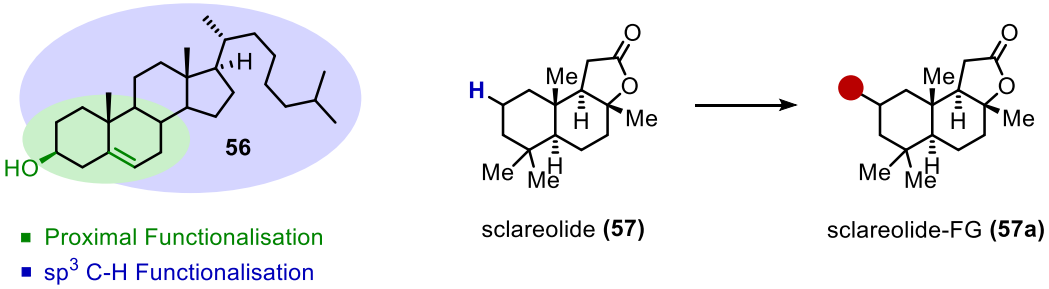

Figure 2.1.1. Proximal functionalisation vs selective C(sp^3)-H functionalisation. A typical Stille coupling and the equivalent C(sp^2)-H functionalisation technique

An interesting model to consider is Cholesterol (**56,** Figure 2.1.1) which possesses only a few native functional groups (i.e. the alcohol and the alkene) the degree of derivatisation starting from this molecule is generally limited to proximal functionalisation (green). However, if we could enable the selective functionalisation of one of the many carbon-hydrogen bond environments then a huge array of derivatives could be synthesised (blue). Cholesterol may still be some distance from effective C-H functionalisation due to its complexity; however, a pertinent case study is sclareolide (**57**) where several groups have enabled C-H functionalisation at the indicated hydrogen on the A ring of the steroid.[109] The selectivity of this reaction uses the inherent reactivity of the C-H bond to dictate the reactivity, however enzymes have been selectively oxidising specific C-H bonds on complex structures for millennia by using a macromolecular architecture to guide the selectivity.[110] However, this macromolecular structure can be difficult to replicate in a lab environment; it can also be too specific for a general transformation to be enabled.[111] Although we can take inspiration from nature and expand the tools available for C-H functionalisation.

2.1.2. Late-stage functionalisation

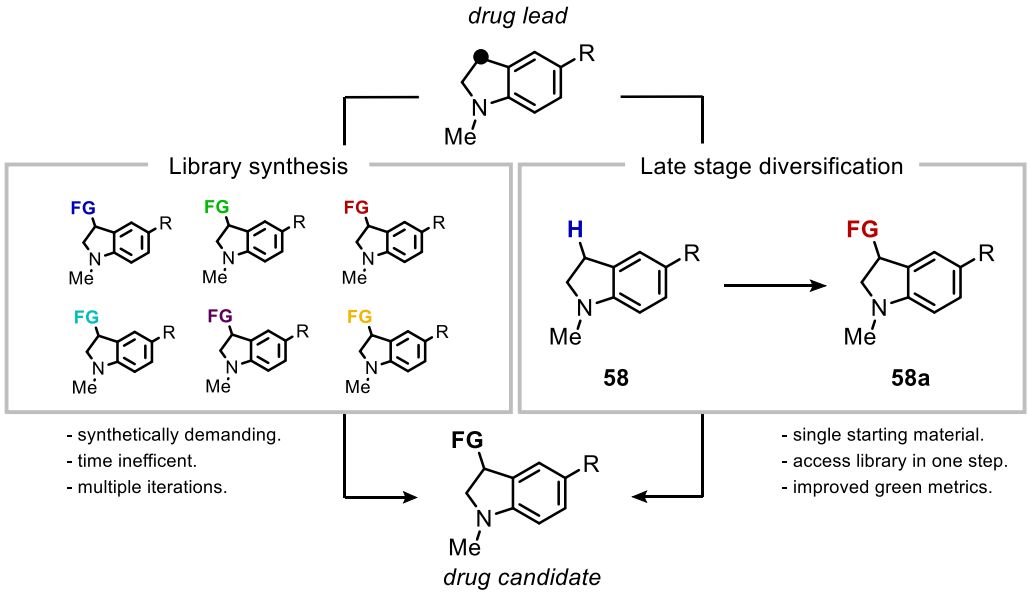

Figure 2.1.2. A schematic that highlights the difference between library synthesis and C-H functionalisation.

The advantages of C-H functionalisation techniques are multifold. This transformation is highly regarded in medicinal chemistry and the applicability to late-stage functionalisation (LSF) of natural products and drug leads is well founded.[112] The traditional method for lead-to-hit was highly synthetic in nature (Figure 2.1.2), relying on multiple synthetic transformations to derive a library of drug candidates through a library synthesis approach. The synthesis of these derivatives may require different synthetic routes, and the presence of the functionality may reduce yields of later steps, or prevent the synthesis being achieved, all adding to both cost and time. By employing a C-H functionalisation techniques from a promising lead, direct functionalisation at the site of interest could be enabled to access a huge range of derivatives, reducing time, cost, and waste.[113]

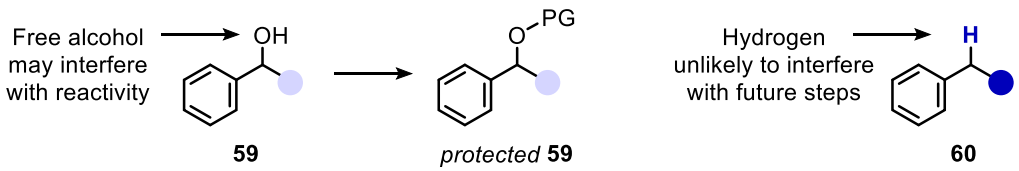

Figure 2.1.3. Free alcohol may need protecting, C-H functionalisation avoids these steps.

The unreactive nature of the C-H bond means that it rarely undergoes undesirable side reactions, nor will it inhibit the desired reactivity of earlier steps, thus limiting the need for protecting group installations, for example, the alcohol motif (**59,** Figure 2.1.3) may need to be protected to prevent interference with other synthetic steps.[114] Each of these advantages also feeds into a more green approach to synthesis, thus C-H functionalisation can be a tool for green chemists.[115]

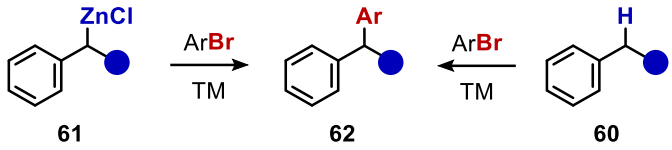

Figure 2.1.4. Negishi cross-coupling requires some ynthetic steps to form the organometallic reagent.

Typical cross coupling reactions require organometallic reagents which need to be synthesised and are often unstable to air or moisture (Figure 2.1.4), for example the zincate used in a Negishi cross-coupling reaction is kinetically unstable. An analogous C-H functionalisation technique would remove both stability and synthetic considerations. Again, reducing synthetic steps as well as by-products, which may be difficult to dispose of.

Because of the rewarding nature of this field, there has been considerable development over the past century within two distinct spheres, C-H to Carbon-Carbon (C-C) and C-H to Carbon-Heteroatom (C-X) bond forming reactions.[116] In the context of this work we will focus exclusively on the formation of C-C bonds. However, we will primarily focus on *inert* C-H bonds; thus enolate,[117] domino metalation-functionalisation,[118] and C(sp)-H bond functionalisation will not be considered.[119]

2.1.3. C-H hybridisation

Figure 2.1.5. Hybridisation of the C-H bond determines the available reactivity

The hybridisation of the C-H bond plays a crucial role in the available techniques (Figure 2.1.5). There have been tremendous advancements in sp^2 hybridised systems, the presence of the unsaturated π system facilitates interaction with organometallic species.[120] The typical mode of activation for this hybridisation is through two electron chemistry and is complemented by the acidified nature of sp^2 hybridised C-H bond with respect to their sp^3 counterparts.[121]

$C(sp^3)$-H systems on the other hand, rarely possess such coordinating abilities, and often have many more individual environments. The ability to functionalise $C(sp^3)$-H bonds has typically proceeded through single electron chemistry (*vide infra*), which generates highly reactive carbon centred radicals.

2.1.4. Traditional methods for C(sp^3)-H functionalisation

Although the first C(sp^3)-H functionalisations were observed through the direct oxidative addition of highly reactive, low valent, noble metals to alkanes (Figure 2.1.6).[122] The direct formation of a C-M from a C-H bond is now recognised as its own subfield, "C-H activation".[123] Tremendous development over the past decades has enabled a wide variety of transformations, but high temperatures and a propensity for C(sp^2)-H functionalisation make these techniques challenging in a C(sp^3)-H scenario, although there are notable examples within the literature.[124]

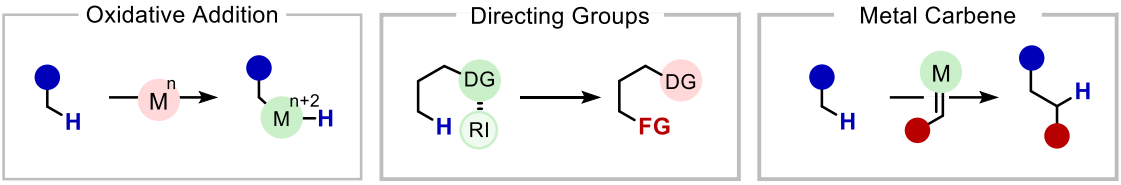

Figure 2.1.6. Traditional techniques to functionalise C-H bonds. M = Metal, DG = Directing Group, RI = Reactive intermediate.

Directing groups operate by placing a reactive intermediate (RI) within proximity to the desired C(sp^3)-H bond, both metal-catalysed and metal-free reactions are able afford excellent site selectivities and occur under much milder conditions than non-directed scenarios.[125, 126] Although these strategies have greatly improved selectivity, the directing group needs to be installed and de-installed for synthetically relevant molecules.[127] Metal carbene chemistry has also played a vital role in the development of C(sp^3)-H functionalisation and are often highly selective and mild in nature, selectivity is based on the inherent reactivity of the C-H bond.[128] However, the methods are often sensitive to steric environment and require stabilised carbene precursors which severely limits the scope of such reactions. A general and practical method based on fundamental thermodynamic parameters as a guiding principle would be a great benefit to the chemical community.

2.1.5. Hydrogen Atom Transfer (HAT)

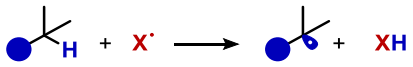

Figure 2.1.7. HAT offers an alternative approach and has fundamental thermodynamic considerations.

Hydrogen Atom Transfer (HAT) offers a complimentary approach to the above techniques and is described as "*the transfer of a proton and an electron in a single kinetic step"*(Figure 2.1.7).[129] The selectivity of HAT is derived from the fundamental thermodynamic and kinetic parameters of the C-H bond. The main contributing factors are bond dissociation energy (*thermodynamic*) and radical philicity (*kinetic*).

Enantioselective C-H

Furthermore, due to the radical nature of abstraction, reactive carbon centred radicals are generated which are of high synthetic value.[130] The widely applicable nature of HAT and its versatility as a platform for substrate functionalisation has been covered in many reviews.[131]

2.1.6. Bond Dissociation Energy (BDE)

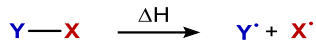

Bond dissociation energy (BDE) is the related enthalpy change when a bond **Y**-**X** is homolytically cleaved to give **Y**• and **X**•. The enthalpy change of this reaction is a temperature dependent parameter, so BDE are defined at 0 K. Historically, HAT reactions have been analysed using the Bell-Evans-Polanyi (B-E-P) relations (Equation 1) which relates the energy barrier of a reaction to the enthalpy.[132] The enthalpy of reaction in the case of HAT reactions is closely correlated to the bond dissociation energy.[133]

$$E_a = E_0 + \alpha \Delta H \qquad (1)$$

The activation energy of a reference reaction (E_a) is proportional to the difference in the enthalpy of reaction (ΔH), modulated by the position along the reaction coordinate (α). If the abstracting species has a higher BDE than the C-H bond, then the reaction is exothermic because a stronger bond is made at the sacrifice of a weaker bond, so the barrier of activation is lowered. This is a simplistic model, and there have been several efforts to develop the theory to include other factors that may influence the reactivity (*vide infra*).[134] Impressive work by Mayer et al. has tried to shift the perspective from B-E-P relations to a Marcus theory-based model.[135] The work takes into consideration several variables, including entropic factors, and highlight that bond dissociation free energies (BDFEs) are more relevant for accurate prediction of reactivity.

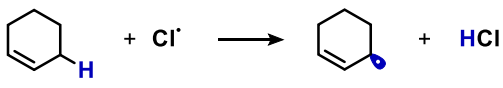

BDE (HCl) = 102 kcal mol^{-1}
BDE (CH) = 83.2 kcal mol^{-1}

Figure 2.1.8. Allylic C-H bonds in the presence of chloride radicals will be abstracted on thermodynamic grounds

However, both B-E-P and Marcus theory rely on the abstracting species bond strength as a predictor. Furthermore, the vast majority of HAT reactions have small entropic values, although some exceptions exist. BDEs are usually sufficient for approximating the outcome of a reaction. Additionally, the use of BDEs is considerably more convenient because they are prevalent within chemical society and readily available.[136] Bearing this in mind, the main question to consider when approximating the outcome of a HAT event is:

"Is the bond dissociation energy of one species greater than the other?"

If the answer is yes, the abstraction is thermodynamically favourable. Consider the reaction of a chloride radical with an allylic C(sp^3)-H (Figure 2.1.8), the BDE of HCl is 101 kcal mol^{-1} which is 18.8 kcal mol^{-1} higher than the allylic C-H bond, thus the forward reaction is highly thermodynamically favourable. Although the thermodynamic parameters play a considerable role in the progress of HAT, there are other considerations that must be taken into account. For example, the difference between the rate of hydrogen abstraction by methyl and trifluoromethyl radicals cannot solely be rationalised through thermodynamic considerations.[137] The reactivity change certainly comes down to electronic or polar considerations.

2.1.7. Radical Philicity

Radical reactions are neutral in nature, however there are well documented polar effects that dramatically influence the outcome of the reaction. These polar effects operate in the transition state and are referred to as radical philicity.[138] In relation to C-H functionalisation, the nature of the HAT reagent will influence which H-atom is abstracted.[139]

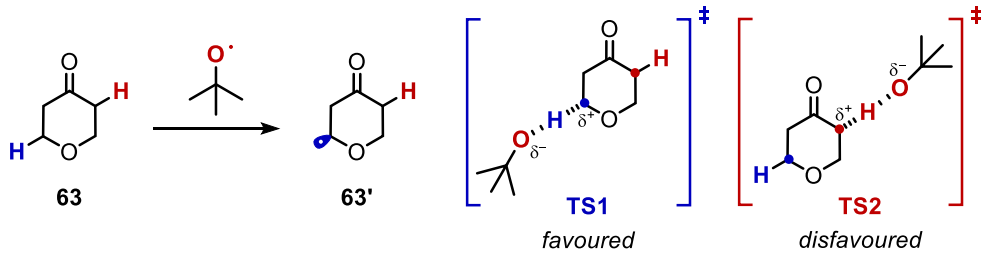

Figure 2.1.9.

Electrophilic HAT reagents have been extensively studied due to the traditional methods of generating them. Decomposition of di-tertbutyl peroxide liberates two *tert*-butoxy radicals, this electrophilic reagent prefers to abstract hydridic protons as opposed to acidic protons. In the example (Figure 2.1.9) the hydridic proton α to the ether of **63** is abstracted preferentially because the build-up of partial positive charge at the α-carbon in the transition state (**TS1**) can be stabilised by the lone pair of the oxygen.[140] Whereas at the inductively withdrawing α-carbonyl site (**TS2**), the positive charge is destabilised. This leads to the formation of **63'** only.

Although the abstraction of the electron poor hydrogen may still occur on a thermodynamic basis, the kinetics of the reaction highly favour the abstraction at the α-ether. Polarity matching lowers the activation barrier of the HAT process, rendering a more facile event.[141]

Polarity inversion catalysts can also be used to select a different polarity C-H bond, but this is beyond the scope of this thesis.[142] The ability to select an electronically differentiated C(sp^3)-H bond is of critical importance and can be reliant upon the medium in which the reactions are conducted.[143] By introducing certain additives or solvents, alternative selectivity can be accessed.

2.1.8. Medium effects

The most frequently abstracted C(sp^3)-H bonds in HAT functionalisations are typically next to stabilising groups. Common stabilising groups are heteroatomic, or π systems – benzylic/allylic. Heteroatoms like oxygen and nitrogen are able to donate the lone pair of electrons into the SOMO. This means that the stability can be highly dependent upon the medium of the reaction because interaction with the solvent or additive may adjust or completely remove the ability of the lone pair to donate. Quantum chemical calculations by Chan and Radom have used alcohol as a model substrate to assess the effects on the bond dissociation enthalpies under different protonation states.[144]

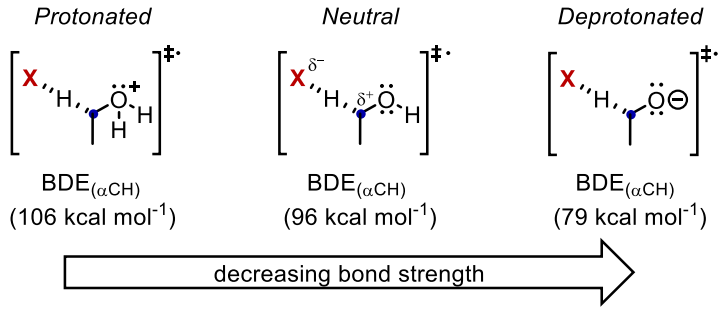

Figure 2.1.10. The transition states are equivalent in each C-H abstraction, but the protonation or deprotonation of the alcohol dramatically effects the energy of the transition state and thus the BDE of the α-CH.

We will focus on the stabilisation of the α-proton, which is afforded by conjugation of the lone pair. If we take an electrophilic abstracting agent (**X**) there is build-up of positive charge at the a-carbon in the transition state. The calculated BDE of the α-CH under neutral conditions is 96 kcal mol^{-1} (Figure 2.1.10). However, if the alcohol is protonated then the lone pair cannot donate, and abstraction is disfavoured. The calculated of BDE is raised by 10 kcal mol^{-1} and may be further exacerbated by the presence of the cationic species – electrostatic repulsion. Deprotonation on the other hand, affords considerably greater electron density and thus stabilisation of the positive charge in the transition state, the calculated BDE is 17 kcal mol^{-1} lower than the neutral alcohol. The use of medium effects can therefore be exploited to control selectivity. However, the (de)activation must be balanced with the properties of the resultant species. For example, the deprotonated alcohol is considerably more basic and so may interfere with other areas of the reaction. More subtle interactions may also influence the reactivity for example coordination of Lewis acids and bases, as well as hydrogen bonding regimes.[145]

2.1.9. Steric influences.

The steric influence of HAT is often overlooked in favour of BDE, philicity, and medium influences. However, there are some subtle and useful examples where steric considerations can play a role in selectivity.[146] The most typical form of steric control comes on ring systems, where the conformation of the ring can favour the abstraction of one hydrogen over another, simply by the choice of the abstracting species.[147]

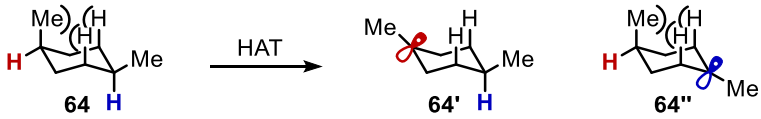

Figure 2.1.11. Abstraction of the red hydrogen minimises steric clash.

The abstraction of a hydrogen can be used to release strain.[148] For example, the red hydrogen of substituted cyclohexane **64** will be abstracted over the blue hydrogen although though they are both tertiary sites. (Figure 2.1.11). HAT at the red position releases the steric clash of the hydrogens and methyl group by planarization upon formation of the carbon centred radical.

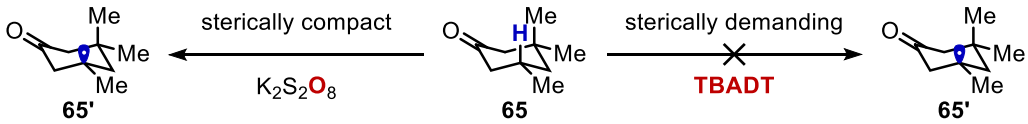

Figure 2.1.12. Bulky hydrogen atom transfer agents may not be able to abstract sterically crowded C-H bonds.

Additionally, the size of the HAT reagent used is important because larger HAT reagents may be too bulky to interact with the substrate effectively, whereas the use of a smaller reagent may be able to abstract the desired hydrogen (Figure 2.1.12).[149] With these factors in mind, it is possible to address the HAT agent and how the design of such species is critical in this field.

2.1.10. HAT development and photochemistry as a new vector

The development of HAT reagents and catalysts has been extensive due to the impact that these species have had on the chemical community. Over the past decade this arena has been reinvigorated due to the influence of photoredox chemistry, which allows for mild generation of radical species which are employed as HAT agents in C(sp^3)-H functionalisation.[150]

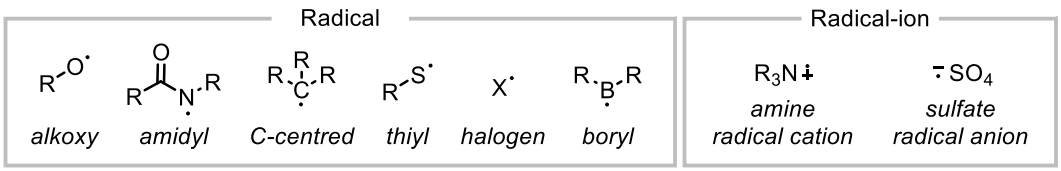

Figure 2.1.13. Common HAT species

Typical HAT reagents are heteroatomic in nature allowing for a more thermodynamically favourable event since many X-H bonds have higher BDEs than C-H bonds (Figure 2.1.13). Although there has been development of carbon centred HAT reagent, the relatively similar philicities and bond dissociation energies means that the reverse reaction can be favourable.[151]

Early HAT reactions required the thermal[152] (or light[153]) decomposition of peroxo species, or by *initiator mediated* reactions. As the arena progressed the desire to access milder or more selective agents became of critical importance.

2.1.11. Photoredox catalysis

Since HAT reagents are open shell intermediates, photoredox catalysis has the potential to unlock this transformation.[154] Oxidisable groups such as amines,[155] can readily generate open shell species through SET (Figure 2.1.14, blue). Stronger bonds such as amides and alcohols require proton-coupled electron transfer (PCET) to generate appropriate HAT abstracting agents (Figure 2.1.14, green).[156] As the area of photoredox HAT is developed, the range of available HAT reagents has only increased, and a wide variety of tailored reagents are employed.[157]

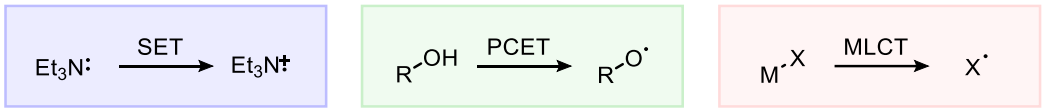

Figure 2.1.14. Photoredox catalysed HAT generation

Additionally, charge transfer (CT) scenarios have enabled the formation of abstracting species. The most prominent of which is the metal-ligand charge transfer (MLCT) type reactivity (Figure 2.1.14, red). The direct photoexcitation of metal-oxo species has been used historically, but often results in an oxidation of the C-H bond through radical rebound, rather than a C-C bond forming reaction.[158] More recently, the direct or photosensitised MLCT of metal halide complexes has gained momentum.[159] This process generates halogen radicals (X•) which act as HAT agents upon cage escape from the metal complex.

The mechanistic distinction between direct excitation of a complex and photosensitisation is quite important. We will use Fagnoni's notation. *Indirect HAT* (*i*-HAT)[160] – where a photocatalyst or sensitiser generates the radical species (X•) through an SET or EnT mechanism. *direct* HAT (*d*-HAT) – where the direct excitation of a molecule generates the appropriate abstracting species, such that PC* is equivalent to X•.

Indirect excitation has dominated the current field due to the modularity of the systems. Direct excitation on the other hand has played a more historical role.

2.1.12. Indirect HAT

The reason for *i*-HATs importance is its modular design, the absorption of light is independent to the abstracting species. The only required feature is that one of the reduction potentials match between the photoredox catalyst and the HAT species. This allows for the toolbox of photocatalysts to be used in conjunction with both traditional and newly developed HAT catalysts. Due to the oxidative nature of C-H functionalisation, typical HAT reagents are generated through the reductive quenching of a photoredox cycle. Although there are some examples that proceed through oxidative quenching.[161]

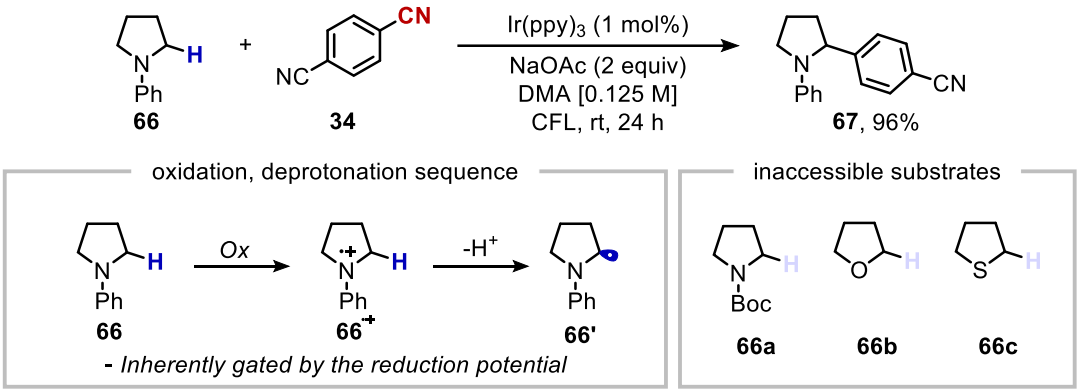

Figure 2.1.15. C(sp^3)-H functionalisation of amines through an oxidation-deprotonation sequence. The oxidation of some functional groups is practically unviable.

Macmillan's seminal work in this field (Figure 2.1.15), does not use a HAT catalyst but instead proceeds by an oxidation-deprotonation sequence.[162] Absorption of a photon by the iridium complex generates a highly reducing species ($E[^*Ir^{III}/Ir^{II}]$ = - 1.73 V *vs* SCE) which is quenched by the 1,4-dicyanobenzene (**67**, E_{ArCN} = - 1.61 V *vs* SCE) to form a persistent radical anion and the oxidised Iridium complex. The ground state iridium is sufficiently oxidising ($E[Ir^{III}/Ir^{II}]$ = + 0.77 V *vs* SCE) to remove an electron from amine **66** to form the radical cation, **66**$^{\bullet+}$. The radical cation dramatically acidifies the α-proton (lowering the pKa by approximately 40) due to hyperconjugation, deprotonation generates a nucleophilic α-amino radical. Radical-radical coupling and elimination of the cyanide anion liberates the α-arylated amine. This reaction has been studied in exceptional detail by Swierk.[163]

However, one of the key drawbacks of this technique is the limited ability to access the radical. The method relies upon oxidation of an appropriate functional group, such that the overall method is inherently reduction-potential gated. To access a general C(sp^3)-H functionalisation, a HAT catalyst can be employed. The use of thiols as HAT species has received considerable attention,[164] which inspired Macmillan to develop the C(sp^3)-H functionalisation of non-oxidisable groups and was discussed previously in chapter 1 (Figure 1.3.15.).[165]

Enantioselective C-H

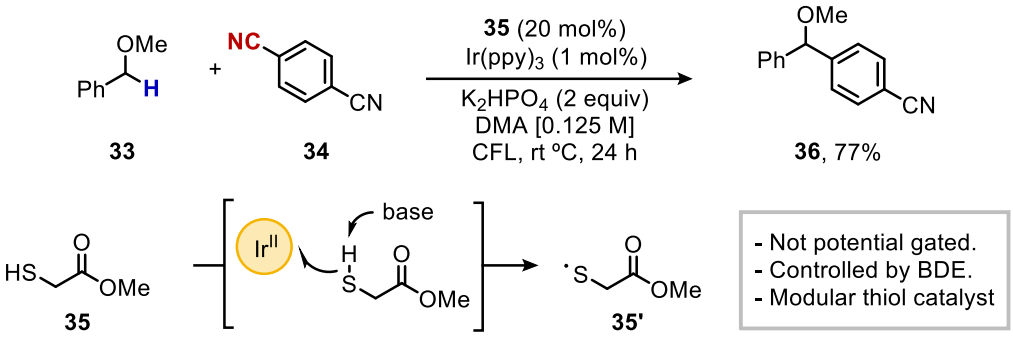

Figure 2.1.16. Thiol catalyst for the C(sp^3)-H arylation of benzylic ethers with benzonitrile derivatives.

The $Ir(ppy)_3$ and electron deficient benzonitrile derivatives act as an effective platform for the discovery of new radical species. A PCET mechanism is proposed due to the discrepancy between the reduction potentials of the photocatalyst ($E[Ir^{III}/Ir^{II}]$ = + 0.77 V vs SCE) and the thiol (**35,** E_{red} = + 0.85 V *vs* SCE). The presence of the base allows for the transfer of a proton and electron to form the thiyl radical (**35'**) (Figure 2.1.16).

The bond dissociation energies of the involved species suggest that the abstraction of the benzylic ether proton (**33**, BDE_{CH} = 85.8 kcal mol^{-1}) would be thermodynamically favoured (BDE_{SH} = 87.2 kcal mol^{-1}).[166] The philicity of the species also suggests a kinetically viable reaction, because the α-ether radical is nucleophilic and the thiol radical electrophilic. After abstraction, radical-radical coupling of the α-ether radical and benzonitrile radical anion, followed by rearomatisation through the elimination of the cyanide liberates the α-arylated ether.

The technique was extended to also couple with imines,[167] methylation from methanol,[168] and a variation of the minisci reaction.[169] Whilst these classical radical reactions can construct a versatile array of molecules and linkages of various hybridisation. The introduction of transition metals to this field has had added another degree of complexity and many opportunities.

2.1.13. Combining HAT with transition metals

The combination of transition metals and photoredox catalysis has been discussed. However, the presence of the metal can introduce some problems, such as the incompatibility between HAT catalysts and transition metal centres. The thiol HAT catalyst is an excellent example of this, due to the ability of thiols to poison metal catalysts.

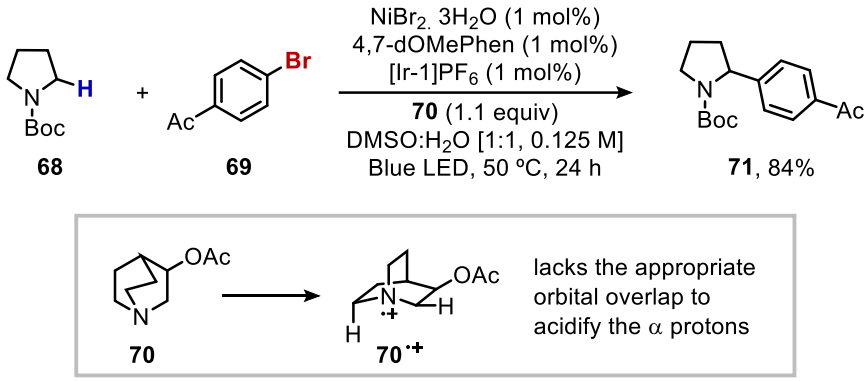

Figure 2.1.17. C(sp^3)-H arylation using nickel, photoredox catalyst, and quinuclidine.

To address these limitations Macmillan developed a quinuclidine based HAT reagent (**70**, Figure 2.1.17).[170] The oxidation of most amines greatly acidifies the α-proton due to hyperconjugation, however the quinuclidine catalyst does not have the appropriate orbital overlap to acidify the protons, leading to a much longer-lived amine radical cation which can abstract the C-H bond to afford the intermolecular C(sp^3)-H arylation.

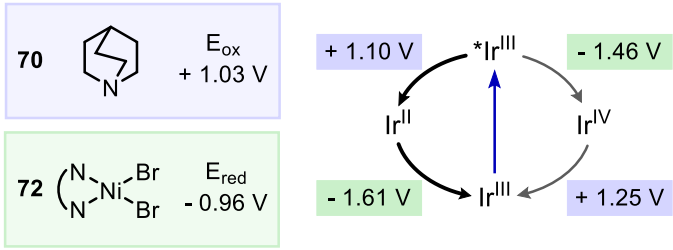

Figure 2.1.18. Reduction potential values of The quenching species and Ir photocatalyst.

The reaction's mechanism was subject to a detailed computational study.[171] Upon visible light excitation, the excited state photocatalyst can undergo either a reductive quenching event with Quinuclidine (**70**) (E_{red} = + 1.03 V) or an oxidative quenching event with a nickel (II) complex **a** ($E[Ni^{II}/Ni^{I}]$ = - 0.96 V) species. Quantum calculations and reduction potential comparisons suggest that both pathways are feasible, but under the reaction conditions the reductive quenching event with Q is more likely due to the higher concentration of this species in the reaction system.

Enantioselective C-H

The proposed mechanistic cycle is supported by detailed and comparative DFT calculations and is shown in Figure 2.1.19. Oxidation of **70** to the radical cation **70$^{\bullet+}$** by the excited iridium photocatalyst. **70$^{\bullet+}$** can readily abstract the hydrogen atom from substrate **68** to form the carbon centred radical **68'** and the protonated quinuclidine **70H^{+}**, calculations placed this event as not only thermodynamically feasible, exergonic by 8.0 kcal mol^{-1}; but also kinetically rapid with a low free energy barrier ($\Delta G^{\ddagger}$ = 9.5 kcal mol^{-1}). The quick and selective formation of **68'** is consistent with the experimental evidence.

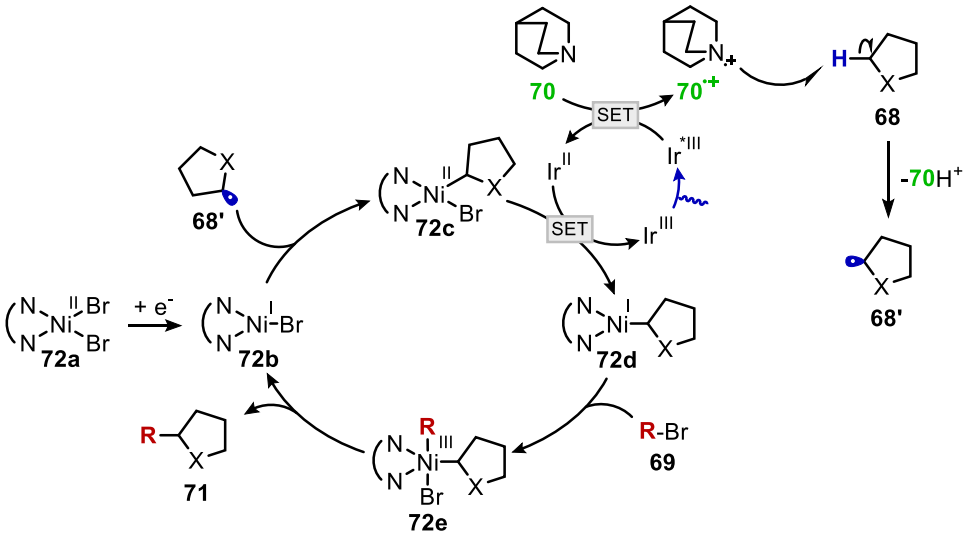

Figure 2.1.19. The mechanistic proposal supported by DFT calculations.

The nickel (II) precatalyst **72a** is reduced by single electron transfer to form the on-cycle nickel (I) complex **72b**. The authors highlight that a second single electron reduction to form a nickel (0) species is thermodynamically unfavourable. Radical addition of **68'** to **72b** creates a nickel (II) alkyl complex **72c**, the reduction of **72c** to **72d** by the ground state iridium (II) is a thermodynamically feasible step. Oxidative addition of aryl bromide **69** generates a nickel (III) complex **72e** which rapidly reductively eliminates to form the desired cross coupled product **71** and regenerate the initial nickel complex **72b**.

In contrast to the aforementioned work, transition metal halides are known to undergo MLCT to liberate halide radicals which are well suited for the abstraction of C(sp^3)-H bonds due to the reasonably high BDEs and electrophilic nature. Individual reports by Molander,[172] Doyle,[173] and Murakami[174] that achieve the arylation of C(sp^3)-H bonds by exploiting MLCT type pathways.

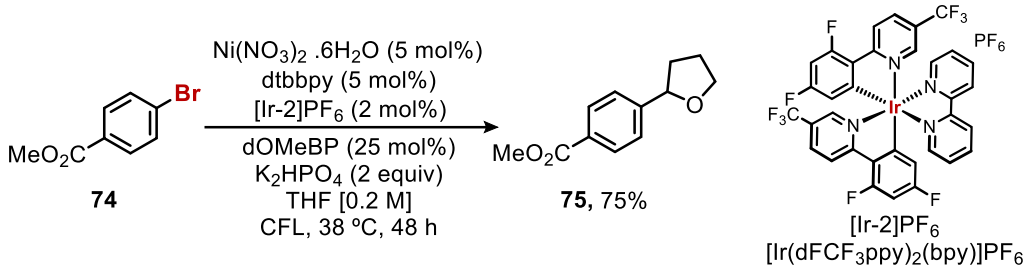

Figure 2.1.20. Molander and co-worker's EnT C(sp³)-H arylation.

Molander and co-workers use a nickel-iridium dual catalytic platform with a co-photocatalyst of dimethoxybenzophenone (dOMeBP) to afford the radical coupling of THF with aryl bromides **74** (Figure 2.1.20), the C(sp³)-H precursor is used as solvent. The authors emphasise an EnT mechanism where the triplet state of the iridium photocatalyst sensitises the putative nickel aryl bromide complex (**77**) to generate the bromine radical. Kinetic isotope studies of this reaction suggest that the reaction is "near-thermoneutral", which may indicate that bromine radicals are responsible for the HAT.[175] Bromine radicals are philicity matched to form the THF radical. The nucleophilic THF radical is able to add to the electrophilic nickel complex (**77**) which reductively eliminates to regenerate a nickel (0) complex and form the desired arylated product **78**.

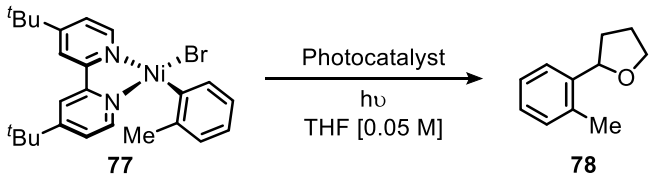

PC	E_{ox}	Emission Wavelength	Result
none	-	-	no reaction
[Ir-2]	+ 1.21 V	470 nm	**78** formed
$[Ru(bpz)_3]2PF_6$	+ 1.45 V	591 nm	no reaction
$[9\text{-MesAcr}]ClO_4$	+ 2.05 V	~590 nm	no reaction
none (UV light)	-	-	**78** formed

Figure 2.1.21. Energy transfer to complex 77 is suggested.

The energy transfer mechanism was proposed, and evidence provided by reaction of the nickel complex **77** in the presence of different photocatalysts. If the reaction mechanism would proceed through an oxidative SET to generate a nickel (III) intermediate (*vide infra*) then more oxidising photocatalysts would generate **78**. However, in this case, more oxidising photocatalysts with lower triplet energies did ***not*** provide **78**. This correlation may be indicative of EnT type pathway. This is in contrast to Doyle and co-worker's published article (Figure 2.1.22), where they provided evidence for oxidation of the nickel (II) intermediate to nickel (III) before photoelimination of the chloride radical could occur. The photoelimination of chloride radicals from nickel (III) complexes to form chloride radicals has been studied by Nocera and served as inspiration to this work.[176]

Enantioselective C-H

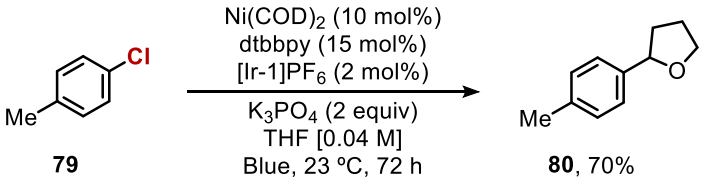

Figure 2.1.22. The conditions employed by Doyle and co-workers.

The conditions employed by Doyle make use of a nickel (0) precatalyst and an iridium photocatalyst in conjunction with a phosphate base. The C(sp^3)-H precursor is used as solvent. The authors propose an oxidation-photoelimination step and provide some evidence for this.

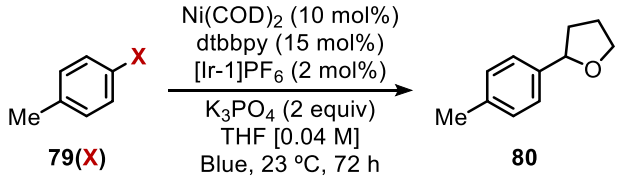

X =	Additive	80 (%)
Cl	-	68%
Br	-	10%
I	-	5%
I	TBACl	51%

Figure 2.1.23. The effect of aryl halide source.

Chloride anion is shown to be essential for reactivity (Figure 2.1.23). The reaction is influenced by the aryl halide source, moving from chloride to iodide, the reaction is inhibited. But including an external source of chloride anion (TBACl) restores the reactivity in the iodide.

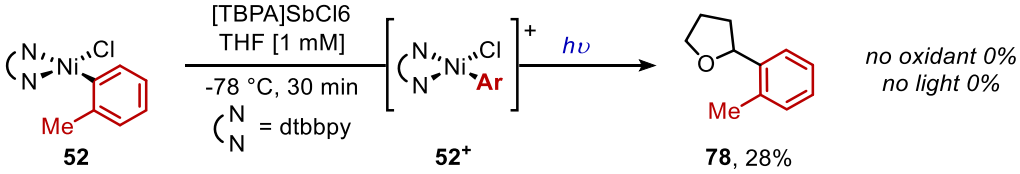

Figure 2.1.24. Evidence for the oxidation-excitation pathway.

Additionally, evidence was provided for the oxidation-photoexcitation mechanism (Figure 2.1.24) – akin to the work by Nocera *et. al*. The nickel (II) aryl chloride complex (**52**) was shown to only form product only when *both* oxidised and irradiated with visible light, removing either parameter does not lead to a productive pathway. The full mechanistic proposal is depicted in Figure 2.1.25.

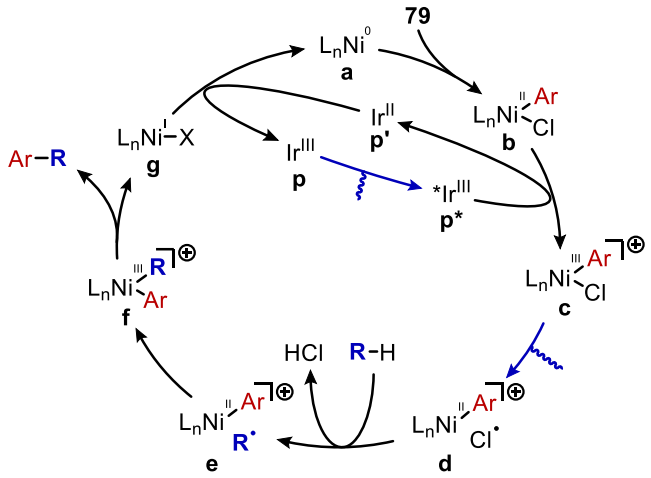

Figure 2.1.25. The mechanistic cycle proposed by Doyle and coworkers.

The initial step is the oxidative addition of aryl chloride **77** into the ligated nickel (0) species **a**, to liberate the nickel (II) aryl chloride **b**. Irradiation of the iridium complex would generate a highly oxidising excited state (**p*,** $E[*Ir^{III}/Ir^{II}]$ = + 1.21 V *vs* SCE) which is able to oxidise **b** ($E[Ni^{III}/Ni^{II}]$ = + 0.85 V *vs* SCE) to nickel (III) intermediate **78**.

A second photoexcitation event of **78c** releases the chlorine radical which upon cage escape from **78d** is capable of abstracting the appropriate C(sp^3)-H bond. Radical combination of the nucleophilic radical and the nickel (II) species **78e** liberates the Ni (III) aryl-alkyl chloride **f**. Rapid reductive elimination forms the product and a nickel (I) intermediate **g**. The nickel species can undergo a SET event ($E[Ni^{II}/Ni^{I}]$ = − 1.17 V *vs* SCE) with the iridium (II) ($E[Ir^{III}/Ir^{II}]$ = − 1.37 V *vs* SCE) to regenerate **a** and close both catalytic cycles. These seminal works on the cross coupling of aryl bromides with C(sp^3)-H derived nucleophiles led to an expansion of the available chemical space, and the ability to form sp^2-sp^n linkages has been well studied.

For example, the presented works have been expanded to generate C(sp^3)-C(sp^3) bonds, acylation,[177] or formylation of aryl halides,[178] However, the above *i*-HAT techniques require the use of iridium polypyridyl complexes, and sometimes require a secondary co-photocatalyst (Molander) or HAT catalyst (Macmillan). One of the principal advantages of photoredox catalysis is the improved “green metrics” of the reaction, requiring noble metal polypyridyl complexes goes against this. Furthermore, the expensive cost and low earth abundance of the iridium may limit scale up of the reaction. The ability to directly access an excited state that can abstract a hydrogen atom would be beneficial by reducing the number of components in a reaction and could be considerably cheaper, especially if the species is a simple organic molecule.

2.2. Direct HAT

Direct HAT (*d*-HAT) offers this possibility, photoexcitation of a molecule leads directly to an excited state that can abstract a hydrogen atom. Carbonyl and carbonyl like systems (Z=O) are the most relevant moieties in this field because the excitation of these species generates an O-centred radical that are likened to an alkoxy radical.[179] Although there are examples in the literature which do not belong to the Z=O class, they are quite limited.[180] One of the key issue with *d*-HAT is that the photocatalysts typically require higher energy light. Modern organic photochemistry has largely avoided UV photocatalysts with greater emphasis being placed on the "visible" spectrum, i.e. high intensity blue and purple lights.

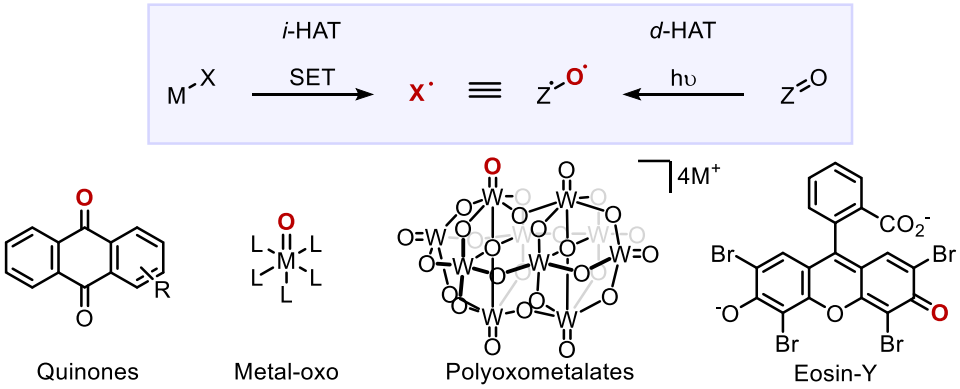

Figure 2.2.1. Comparison of iHat and dHAT. Some relevant Z=O species.

Quinones,[181] metal-oxo, and Eosin Y have been investigated.[182] Polyoxometalates (POMs) of the early transition metals found widespread applications historically. Of the various POMs, the decatungstate (DT) salts of the form $[W_{10}O_{32}]^{4-}$ have established themselves to be an exceptionally versatile platform.[183] One of the critical problems with the decatungstate catalyst is the low modularity. The physical properties of this catalyst cannot be readily adjusted. Metal-oxo species have greater modularity, but often require significant ligand development.[158] A modular system allows for tailoring of the reactivity to achieve the desired transformation.

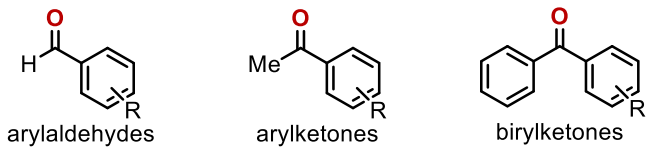

Figure 2.2.2. The aryl ketone motif is very prevalent within the context of HAT

Aryl ketones and aldehydes are modular systems for HAT (Figure 2.2.2), and have seen extensive use within this field, fundamental studies of photoreduction mean there is a wealth of knowledge to work with. These catalysts have shown excellent utility across many platforms and are a privileged motif within organic photochemistry.

2.2.1. Benzophenone as a photocatalyst

The benzophenone (**BP**) structure has a historical significance within photochemistry,[184] and the nature of the ground state and excited state has been subject to extensive study. We will discuss some of the photophysical properties of benzophenones due to their application within this thesis. Upon photoexcitation an excited singlet state of **BP** will be populated (^{S}**BP**), rapid intersystem crossing occurs to generate the triplet state. The triplet excited state of benzophenone catalysts (^{T}**BP**) is the predominant reactive state due to the efficient ISC event.[185]

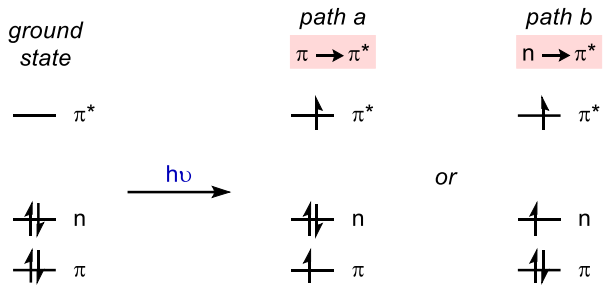

Figure 2.2.3. The transitions upon visible light excitation.

The transitioning electron is highly influential to the reactivity of the excited state. There are two main transitions (Figure 2.2.3): *path a,* the promotion of an electron residing in the carbonyl π system to the π* orbital (^{T}**BP**[π, π*]); or *path b* the promotion of a lone-pair electron from the oxygen to the π* orbital (^{T}**BP**[n, π*]). The UV/vis spectrum of benzophenone shows three features, a broad feature at 350 nm, corresponding to the ^{T}**BP**[n, π*].[186] A broad shoulder at 280 nm, which corresponds to the ^{T}**BP**[π, π*] transition. The absorption peaks show inverse solvatochromic shifts with increasing polarity of solvent ^{T}**BP**[n, π*] shifts to the blue region, whereas ^{T}**BP**[π, π*] shifts into the red region, the [n, π*] transition is characterised by this blue shift.[187]

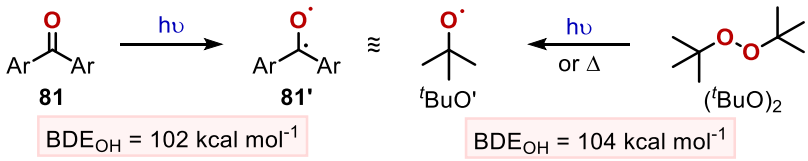

Figure 2.2.4. Photoexcitation of biaryl ketones generates a tert-butoxy radical equivalent.

The ^{T}**BP**[n,π*] transition is the most important transition synthetically because of the character this transition generates. An elongation of the C=O bond, with a shift from sp^2 to sp^3 hybridisation and an increase in spin density on the oxygen atom.[188] The increased spin density on the oxygen atom imbues a “biradical-type” triplet state. Which can allow for photosensitisation,[189] radical addition,[190] and most importantly – HAT.[191]

2.2.2. HAT from excited state benzophenone

The hydrogen abstracting ability of biaryl ketones has been known for over 60 years,[192] and the photoreduction of biaryl ketones has been studied extensively, HAT from an appropriate solvent is often proposed. As previously discussed **^{T}BP**[n, π*] is the prominent HAT state due to the increased spin density at oxygen and the reactivity has been likened to that of a *tert*-butoxy radical (Figure 2.2.4). The electrophilic nature of the oxygen based radical, means that hydridic protons are more readily abstracted to generate nucleophilic carbon centred radicals. The formation of α-amine radicals is particularly useful due to the highly nucleophilic nature of these radicals. Benzophenone catalysts selectively abstract the C(sp^3)-H bond at the α-amine position. Understandings gained through the photoreduction of benzophenone by amines led to this conclusion.[193] And there have been several applications to C-C bond forming reactions through radical conjugate addition,(Figure 2.2.5).[194]

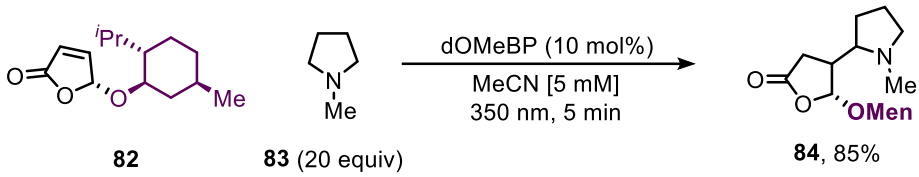

Figure 2.2.5. Radical conjugate addition Hoffman and co-workers, ref 194a.

Although the use of UV has been largely avoided in the modern era of photochemistry, the benzophenone photocatalyst has seen a resurgence. With an early report by Inoue and co-workers in 2014 using stoichiometric benzophenone under high power mercury lamp irradiation to afford a C(sp^3)-H alkenylation (Figure 2.2.6).[195]

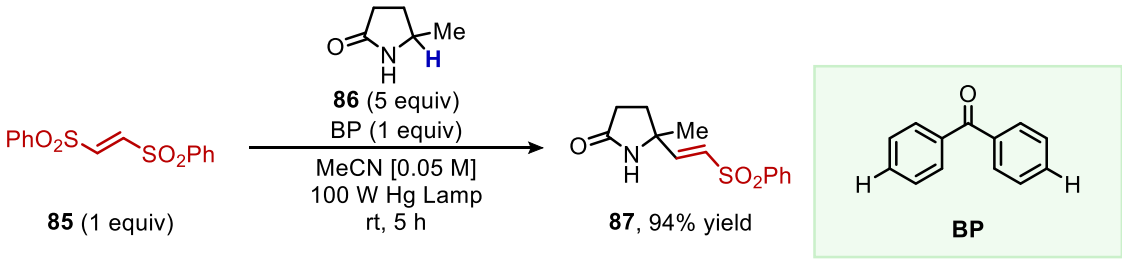

Figure 2.2.6. Inoue and co-workers used stoichiometric benzophenone to afford the C-H functionalisation

The reaction proceeds by photoexcitation of the benzophenone to generate the **^{T}BP**[n, π*] which abstracts the electronically matched α-amine hydrogen to form the nucleophilic radical. HAT is thermodynamically favourable, and polarity matched. Radical conjugate addition of the nucleophilic radical to the electron deficient acceptor followed by elimination of the sulfonate radical or anion liberates the desired product **xb** in 94% yield. The stoichiometric use of benzophenone was later improved to be catalytic in a report by Guin *et. al.*(Figure 2.2.7).[196]

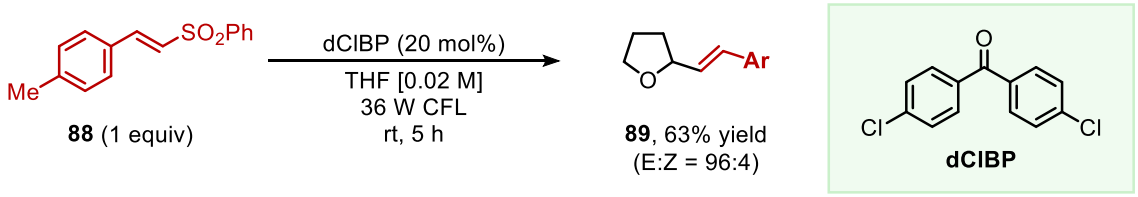

Figure 2.2.7. dichlorobenzophenone used in catalytic quantities under visible light irradiation

Changing from BP to the dichlorinated analogue **dClBP** enabled the catalytic use of the photosensitiser under CFL irradiation to afford the alkenylated THF **2a** in 63% yield and good E:Z ratio. The alkyn- and alkenylation of C(sp^3)-H bonds uses the C-H precursor as solvent. The benzophenone catalyst may not be the only abstracting species within the reaction medium, as the authors proposed that the sulfonate radical generated upon radical elimination could act as either an oxidant for the **dClBP** or abstract the α-ether C-H bond to propagate the reaction. The use of benzophenone catalysts in simple organic transformations has found some novel applications, for example the selective electrophilic fluorination of toluene C(sp^3)-H bonds,[197]

2.2.3. Metallatriplet catalysis.

There is an area that shows exceptional potential, triplet ketones have been shown to reduce nickel species *via* photoexcitation, the seminal works of Chow,[198] and Murakami in this field highlight the synergy between benzophenone and nickel.[199] These works serve as an excellent platform to develop a combined transition metal catalysed reaction with the benzophenone behaving as a photocatalyst. Martin and co-workers built upon these initial works to develop an inert C(sp^3)-H bond arylation and alkylation using a benzophenone catalyst under CFL irradiation (Figure 2.2.8).[200]

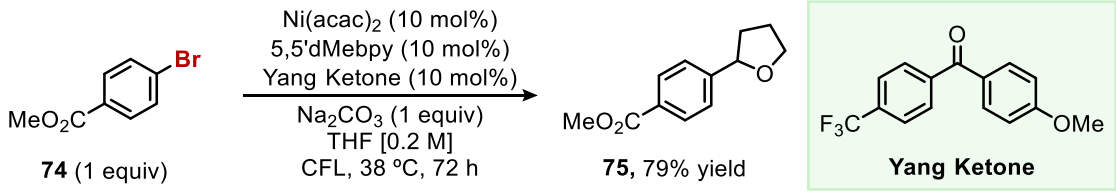

Figure 2.2.8. The C(sp^3)-H bond functionalisation developed by Martin and co-workers.

The biaryl ketone developed, **YK**, uses a "push-pull" electronic system. The higher photochemical activity of this ketone has been tentatively ascribed to a higher molar coefficient in the visible region at reaction concentration. Additionally, the lifetime of the ketyl radical is extended with this electronic bias. The ketyl radical is an essential intermediate because it is required to turn over the nickel catalyst. One of the drawbacks of this reaction is the requirement for the C-H precursor to be used as solvent. Although efforts were made to reduce this large excess to super stoichiometric quantities, 10 equivalents are still required.

Enantioselective C-H

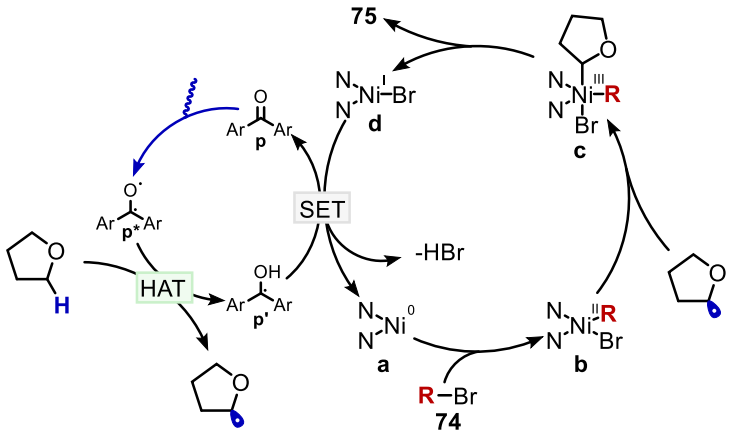

Figure 2.2.9. Mechanistic proposal for the biaryl ketone mediated C-H functionalisation.

The proposed pathway (Figure 2.2.9), a ligated nickel (0) species **a** is formed by photoreduction of $Ni(acac)_2$. Oxidative addition with arylbromide to generate an *electrophilic* aryl nickel (II) bromide (**b**). **b** could then accept the nucleophilic radical which is formed through HAT from the triplet excited state benzophenone (**p***, $BDE_{(Ph2CO^*)} \approx 104$ kcal mol^{-1}). The aryl-alkyl nickel (III) bromide (**c**) rapidly reductively eliminates to form the product and a nickel (I) species (**d**). The highly reducing ketyl radical of **YK** formed upon deprotonation of the C•-OH species ($E_{red} = -2.05$ V)[201] reduces **d** to **a** through a SET process ($E[Ni^I/Ni^0] \approx -1.13$ V).[202] The development of this work has been followed up by several works that combine biaryl ketones with nickel including the benzylation of aryl bromides,[203] acylchlorides/surrogates,[204] and dicarbofunctionalisation.[205]

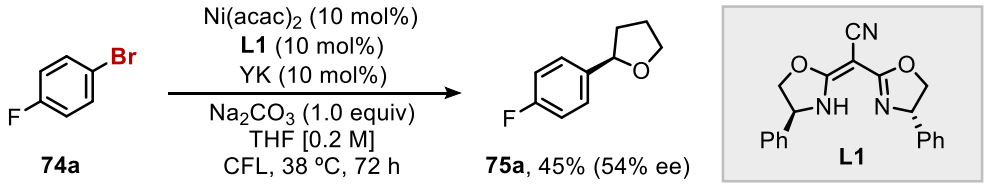

Figure 2.2.10. Enantioselective variant of the C(sp^3)-H arylation.

Additionally, the work by Martin highlighted one key feature, the ability to directly, enantioselectivity functionalise a C(sp^3)-H bond. Whilst the yield and enantioinduction were moderate, the ability to enantioselectivity functionalise the C(sp^3)-H position was not previously possible. The coupling of enantioselective transformations with visible-light driven catalysis has also seen considerable interest due to the sustainability that light mediated transformations offer. Enantioselective functionalisation within a photochemical sphere has seen some considerable development since the seminal report from Macmillan.[27] With some exemplary techniques developed such as chiral at metal photocatalysts;[206] phosphoric acid mediated radical additions;[207] and hydrogen bonding deracemization techniques.[208]

However, the ability to directly enantioselectivity functionalise the C(sp^3)-H bond would be an attractive endeavour.[209] Although exploration of this technique has been quite limited, with metal-carbene chemistry being some of the only available techniques.[210]

2.2.4. Enantioselectivity in C[sp^3]-H functionalisation

At the time of publication, the enantioselective version of the C(sp^3)-H functionalisation developed by Martin and co-workers was one of the first examples of a direct enantioselective C(sp^3)-H functionalisation by means of a HAT reagent. Although Doyle had previously reported an oxidation-deprotonation sequence.[211]

Since the initial publication by Martin and co-workers, the field has seen considerable development because of the synthetic value of such a reaction.[212] The most widely used motif in this scenario is the benzylic C(sp^3)-H, for three critical reasons:

1. The stability of the generated radical upon HAT allows for a reasonably long-lived species, which can undergo a bimolecular reaction with the nickel.
2. The large steric bulk of the aryl ring in comparison to the alkyl chain enhances enantioinduction.
3. The C-H precursor is often needed in *super* stoichiometric amounts which means that cheap and available starting materials are desired, therefore alkyl-arenes are excellent candidates.

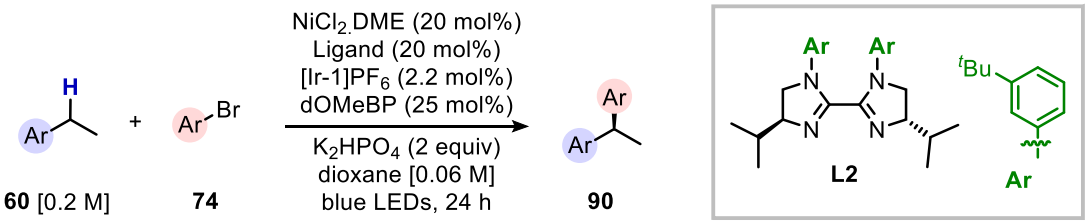

Figure 2.2.11. Enantioselective benzylic arylation using aryl bromides

The first paper on the aryl bromide series developed by Lu *et al* (Figure 2.2.11).[213] produces 1,1-biaryl compounds **90** in good yields and enantioselectivities (up to 92% ee). The use of [Ir-1] and dOMeBP cocatalyst is believed to generate the bromide radical through triplet energy transfer.[Ref] The C-H precursor is often used as solvent, although it was shown that appreciable yields could be afforded with 4 equivalents of **60**. Extension of this work enabled cinnamic acid derivatives to be arylated at the benzylic position.[214]

Enantioselective C-H

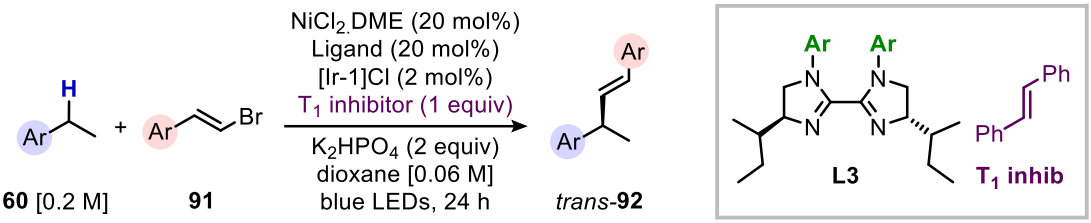

Figure 2.2.12. Enantioselective benzylic vinylation using vinyl bromides and a triplet inhibitor.

The benzylic arylation of the Lu and co-workers was followed up with the vinyl bromide series (Figure 2.2.12).[215] The use of stilbene as a triplet inhibitor and the chloride salt of [Ir-1] was critical in achieving high E:Z ratios by reducing the isomerisation of the double bond.

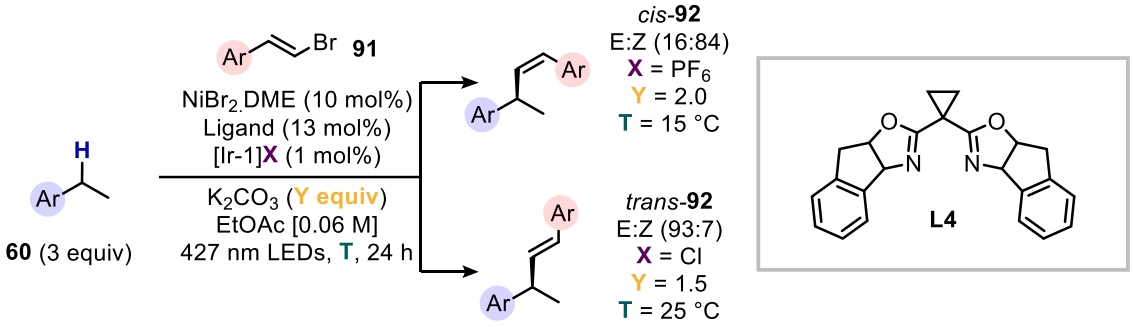

Figure 2.2.13. Enantio and stereoselective vinylation of benzylic C-H bonds.

Huo and co-workers developed the vinyl bromide series further in 2021 (Figure 2.2.13).[216] Achieving excellent control over the stereochemical outcome of the double bond by simply changing the counteranion of the iridium photocatalyst and adjusting the temperature. The [PF_6] anion at 15 °C was effective for the synthesis of Z alkenes, whereas the [Cl] anion preferentially formed the E isomer at 25 °C. The origin of this selectivity is tentatively ascribed to the improved ability of the PF_6 anion to isomerise the double bond.[217] Additionally the C-H precursor **60** could be used in 3.

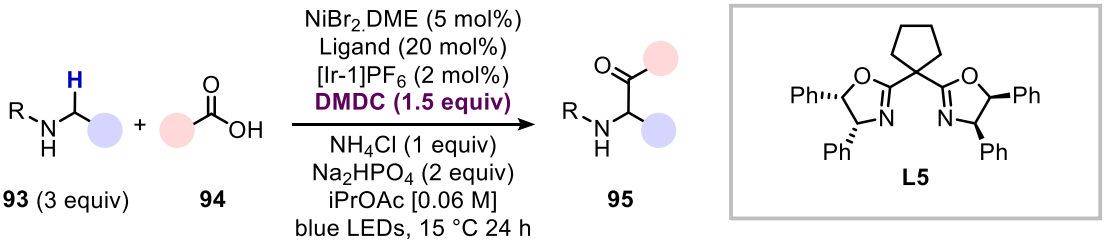

Figure 2.2.14. Enantioselective acylation of α-amine C(sp^3)-H bonds using carboxylic acids

One of the key advantages of nickel is its ability to use *non-classical* electrophiles in cross coupling scenarios.[218] This was effectively demonstrated by Huo and co-workers (Figure 2.2.14), for the generation of enantioenriched α-amino ketones from carboxylic acid feedstocks.[219]

The carboxylic acid was initially activated *in situ* using dimethyldicarbonate and ammonium chloride. In a follow up paper enantioenriched α-aryl ketones and esters could be accessed by employing activated carboxylic acids and chloroformates respectively using benzylic C-H bonds.[220] Murakami was able to generate chiral α-aryl amides using isocyanates, although this single example is only achieved in 34% yield with low enantioselectivity (74% ee).[221]

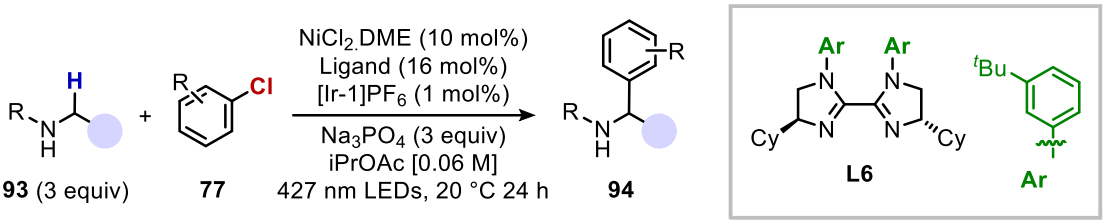

Figure 2.2.15. Enantioselective arylation at the α-amine position using aryl chlorides.

The α-arylation of amines was achieved by Huo and co-workers in 2022 (Figure 2.2.15).[222] The ligand employed is typically used within the sphere of enantioselective C(sp3)-H functionalisations developed by Huo, the steric bulk at the *meta*- position of the aryl ring is claimed to increase the rigidity of the ligand, which in turn increases the steric bulk.

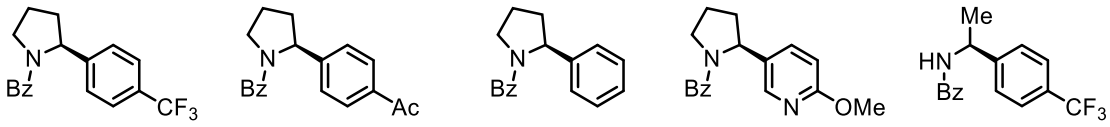

94a, 76% (92% ee) | **94b,** 69% (91% ee) | **94c**, 42% (81% ee) | **94d**, 81% (88% ee) | **94e**, 61% (95% ee)

Figure 2.2.16. Small scope of the enantioselective arylation of α-amines.

The scope of the reaction developed by Huo and co-workers (Figure 2.2.16) consists of a range of aryl- and heteroaryl chlorides which generally produce the desired cross-coupled product in good yields and enantioselectivities ranging from 70% to 97%. The general reactivity profile requires electron deficient aryl chlorides, when moving to neutral aryl chlorides (**94c**) there is a drop in both yield and enantioselectivity. Heteroaromatic chlorides often require a substituent close to a coordinating atom to disfavour coordination to the nickel centre. Lastly acyclic amines can be used in this reaction and affords the desired cross coupled product in reasonable yield.

We believed that the benzophenone platform would be an ideal candidate for the generation of an enantioselective sp^2-sp^3 cross coupling platform, with the potential for the formation of enantioselective sp^3-sp^3 linkages.

2.3. General aim of the project

At the outset of our investigations, the ability to forge C-C bonds through C(sp^3)-H functionalisation had made significant progress. However, there was limited literature precedent for the direct enantioselective C(sp^3)-H functionalisation which would be of exceptional value to the community.

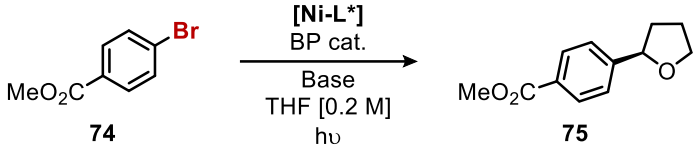

Figure 2.3.1. Proposed reaction scheme for the project

We anticipated that the metallaphotoredox platform developed within our group would be an excellent starting point to enable this transformation (Figure 2.3.1). Firstly, there was already some established enantioinduction using this technique. Secondly, the modular and noble metal free approach is not only synthetically useful, but the departure from noble metal photocatalysts is particularly beneficial from both an economic and ecological perspective. Finally, the absence of highly oxidising SET events opens a range of available phosphine ligands which are typically avoided when using iridium based photocatalysts. The proposed mechanistic cycle Figure 2.3.2 is identical to Figure 2.2.9Figure 2.2.9, however the ligand employed will be chiral as to impose enantioselective influence.

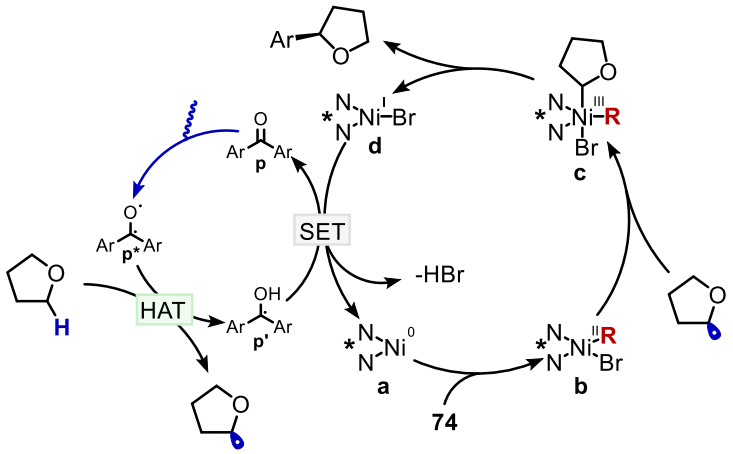

Figure 2.3.2. The mechanistic proposal using a chiral ligand.

2.4. Optimisation

2.4.1. Nitrogen based ligands

The initial reaction conditions developed were applied directly to a ligand screen, although a larger amount of ketone was used (20 mol% *vs* 10 mol% in the published paper). The same reaction set up using CFL irradiation for 72 h without fan assisted cooling. The initial screen of ligands was to assess a range of the parameters, including conversion, product yield of **75** and enantioinduction.

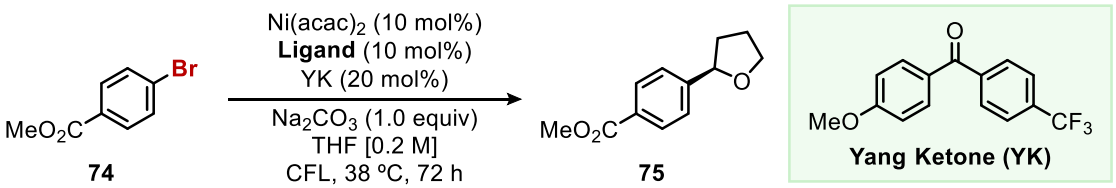

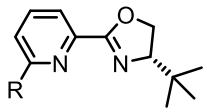

L7, (R=H) 72% (27% ee)
L8, (R=Me), 47% (10% ee)[a]

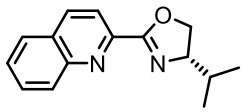

L9, 45% (0% ee)

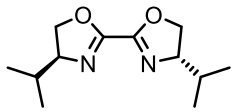

L10, 21% (29% ee)

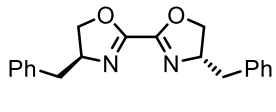

L11, 53% (26% ee)

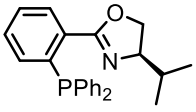

L12, 14% (89% ee)

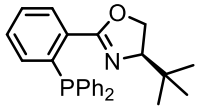

L13, 1% (-)

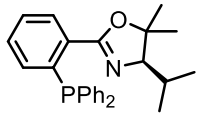

L14, 0% (-)[b]

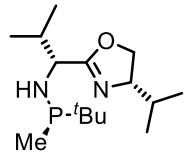

L15, 54% (0% ee)[c]

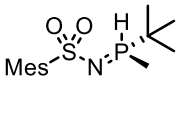

L16, 31% (0% ee)[c]

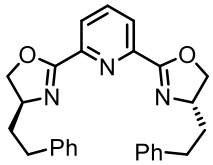

L17, 0%

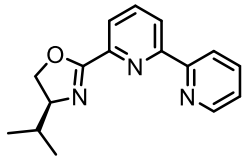

L18, 26% (6% ee)[d]

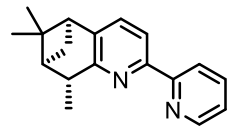

L19, 42% (22% ee)[d]

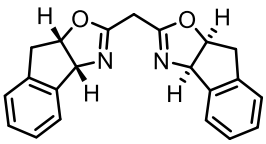

L20, 0% (-)

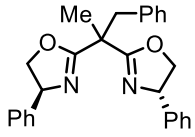

L21, 10% (0% ee)

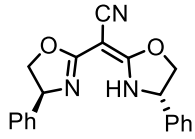

L22, 39% (-43% ee)

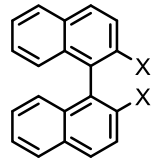

(X=O) **L23^{O},** 12% (0% ee)
(X=NH_2) **L24^{N},** 0% (0% ee)

Figure 2.4.1. Reaction conditions: (74) (0.2 mmol), Ni(acac)$_2$ (0.02 mmol) L7-L24 (0.02 mmol), YK (0.04 mmol), Na_2CO_3 (0.2 mmol), THF (1 mL), 38 °C under CFL lights. GC conversion/yield determined using decane as internal standard, ee% determined by SFC of crude reaction mixture. a) Ligand prepared by Dr Yaya Duan b) 33% protodehalogenated side product. c) Ligands kindly donated by Riera lab. d) ligands syntesised by visiting student Pascal Eisele.

Enantioselective C-H

The results of the screen are shown in Figure 2.4.1. The N^N bidentate ligands are similar to the bipyridine ligand employed in the original protocol. PyrOx ligand (**L7**) gave good reactivity, achieving 72% yield but only a slight enantiomeric excess was observed (27% ee). Increasing the steric bulk in the six position of the pyridine (**L8**) was detrimental to the reaction, with a lower yield and enantioselectivity. This could be due to the parasitic unligated reaction which gives 15% yield, or possibly problems with binding of the ligand (pyridine 0.4 equiv enhanced the reaction to 25% yield). QuinOx ligand (**L9**) yielded 45% of the cross coupled product with no enantioinduction. BiOx ligands (**L10, L11**) also enabled this transformation but gave poorer yields although retained similar enantioselectivities. Chiral P^N ligands which have been used extensively in enantioselective transformations were then assessed.[223]

The iPr-Phox ligand (**L12**) gave some promising results although deviation from this motif showed just how sensitive this reaction is to the steric environment, with sterically demanding *tert*-butyl group (**L13**) giving only traces of product, and functionalisation at the 2 position of the oxazoline ring to increase the steric demand (**L14**) also inhibited the reaction. Additional ligands kindly provided by the Riera lab (**L15, L16**), which have been used in iridium and cobalt catalysed reactions,[224] gave reasonable yields but did not impose any enantioselectivity.

Tridentate box type ligands (**L17, L18**) were not effective at forming **75** nor did they imbue any enantioselectivity. Chiral bipyridine (**L19**) gave similar enantioinduction to the PyrOx ligand and yields of 42%.[225] N^N ligands with a sp^3 break in the backbone (**L20, L21**) did not perform well, this could be attributed to the poor stabilisation of an odd electron count nickel species. When a degree of delocalisation was re-established (Semi-Corrin **L22**) the reactivity was restored. Binol (**L23^O**) gave a poor yield of 10%, and no enantioselectivity. The amine analogue (**L23^N**) was unreactive.

2.4.2. Phosphine Ligands

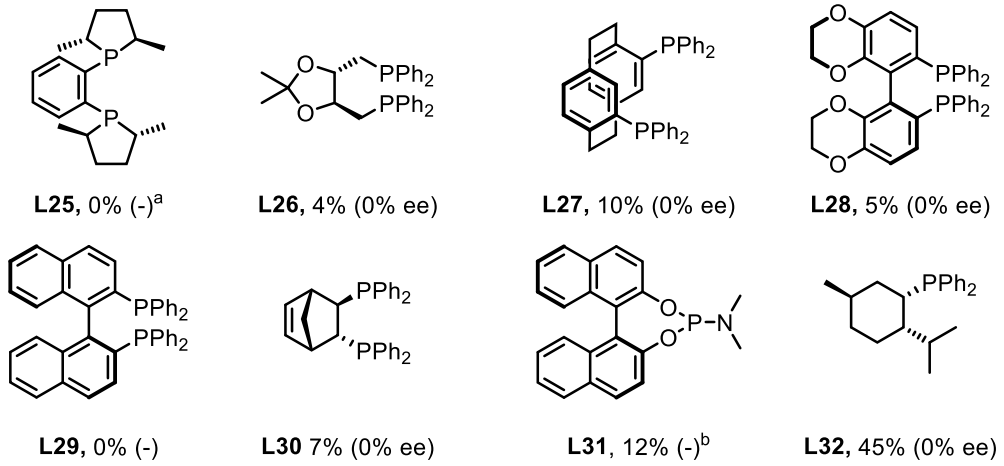

L25, 0% (-)[a] **L26,** 4% (0% ee) **L27,** 10% (0% ee) **L28,** 5% (0% ee)

L29, 0% (-) **L30** 7% (0% ee) **L31**, 12% (-)[b] **L32,** 45% (0% ee)

Figure 2.4.2 Reaction conditions: (74) (0.2 mmol), $Ni(acac)_2$ (0.02 mmol) L25-L26 (0.02 mmol) L31/32 (0.04 mmol), Yang Ketone (0.04 mmol), Na_2CO_3 (0.2 mmol), THF (1 mL), 38 °C under CFL lights. GC conversion/yield determined using decane as internal standard, ee% determined by SFC of crude reaction mixture. a) 88% protodehalogenation side product. b) 53% protodehalogenation side product.

The advantages of *d*-HAT have previously been discussed and the ability to access chiral P^P ligands is particularly beneficial. The lack of highly oxidising photocatalysts means phosphine ligands can readily be employed without deleterious oxidation of the phosphine. To this end a range of bidentate and monodentate chiral phosphines were assessed. Disappointingly the phosphine series performed very poorly. (*R*, *R*)-Me-DUPHOS (**L25**) provided 88% yield of the hydrodehalogenated product and no yield of the desired product **75**. Low yields of the product were afforded by **L26-L28** although no enantioinduction was observed. Binap (**L28**) and the hydrogenated binap derivative (**L29**) gave no conversion to the desired product. norbornene derived diphosphine gave very low yields (**L30**). Monodentate phosphines (**L31, L32**) performed marginally better likely by stabilising reactive intermediates since there was no enantioinduction.

The results of the phosphine screen highlighted that this may not be a trivial transformation. One possible reason for the failure of this screen is the increased steric bulk surrounding the nickel centre, it is clear from **L12-L14** that increasing the steric bulk too much is detrimental to the reaction conditions. Additionally, phosphines donate considerably more electron density onto the metal centre when compared to the nitrogen ligands like bipyridine. This could have two effects on the reactivity, increasing the reduction potential of the nickel species to be outside of the range of the benzophenone catalyst, and reducing the electrophilicity of the nickel centre so radical addition from the nucleophilic entity is disfavoured. With this screen of ligands conducted, it was decided to take the commercially available iPr-Phox (**L12**) on for further screening of the reactivity.

Enantioselective C-H

2.4.3. Base screen

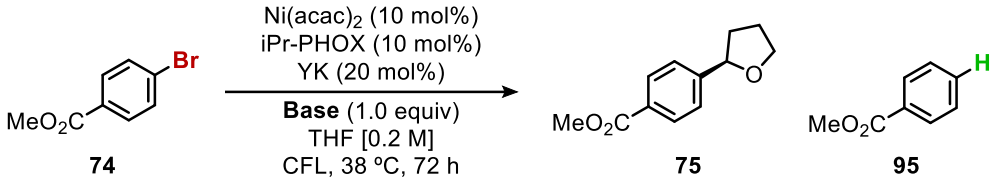

74 **75** **95**

Entry	*Base*	**74** (%)	**75** (%)	**95** (%)	*ee* (%)
1	Na_2CO_3	52	14	13	89
2	$NaHCO_3$	42	12	0	87
3	K_2CO_3	80	4	14	-
4	Cs_2CO_3	85	3	10	-
5	Li_2CO_3	67	5	0	-
6	$(NH_4)_2CO_3$	95	0	0	-
7	NaOtBu	100	0	0	-
8	K_3PO_4	55	3	5	-
9	K_2HPO_4	44	10	5	90
10	DBU	51	8	0	-
11	DIPEA	41	1	0	-
12	DIPA	47	7	0	-
13	Lutidine	67	0	0	-

Figure 2.4.3 . Reaction conditions: (74) (0.1 mmol), Ni(acac)₂ (0.01 mmol) iPr-Phox (0.01 mmol), Yang Ketone (0.02 mmol), Base (0.1 mmol), THF (0.5 mL), 38 °C under CFL lights. GC conversion/yield determined using decane as internal standard, ee% determined by SFC of crude reaction mixture.

Next, we investigated the effect of the base on the reaction system (Figure 2.4.3), inorganic bases (*entry 1 – 9*) afforded **74** in varying degrees of success. Sodium carbonate (*entry 1*) afforded the desired product in 14% yield. The weaker base $NaHCO_3$ (*entry 2*) also afforded the desired product but with a reduced mass balance. The potassium and caesium salts (*entry 3 + 4*) dramatically increased the hydrodehalogenation side reaction to **95**. Lithium carbonate provided **75** in 5% yield (*entry 5*). Employing ammonium carbonate base gave no conversion (*entry 6*).

Strong bases like sodium tertbutoxide shut down the reaction completely, with no conversion (*entry 7*). Phosphate bases were also assessed, affording the product in 10% yield (*entry 9*). The slightly higher solubility led to the hypothesis that a fully soluble base could be beneficial to this reaction system since it would reduce the particles in the system which can be problematic in visible light mediated reactions.

The homogenous organic bases (*entry 10-13*) provided, clear and particulate free solutions but the reactivity was not improved, although DBU (*entry 10*) and diisopropylamine (*entry 12*) provided the desired cross coupled product in 8% and 7% yield respectively, not an improvement over the sodium carbonate.

2.4.4. Cosolvent

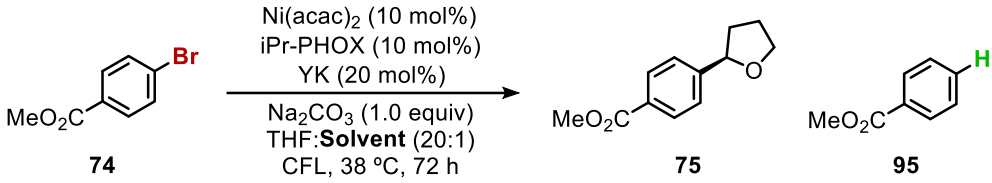

Entry	*Solvent*	**74** (%)	**75** (%)	**95** (%)	ee (%)
0	*none*	55	14	0	89
1	DMAc	50	3	2	-
2	DMSO	36	10	3	-
3	MeCN	49	15	1	90
4	Acetone	41	21	3	89
5	D_2O	54	11	4	90
6	PhH	89	0	0	-

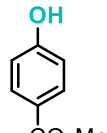

96

Figure 2.4.4. Reaction conditions: (74) (0.1 mmol), Ni(acac)$_2$ (0.01 mmol) iPr-Phox (0.01 mmol), Yang Ketone (0.02 mmol), Na_2CO_3 (0.1 mmol), THF (0.5 mL), cosolvent (25 µl) 38 °C under CFL lights. GC conversion/yield determined using decane as internal standard, ee% determined by SFC of crude reaction mixture.

The cosolvent screen was performed using small amounts of cosolvent (20:1) to prevent a complete shutdown of the reaction (Figure 2.4.4). Solvents are very well known to have an influence on the n-pi* transition which may be critical in improving reactivity. The introduction of dimethylacetamide (*entry 1*), typically a good solvent for nickel catalysed processes shut down the product forming reaction. DMSO (*entry 2*) was also a poor cosolvent. Acetonitrile is a particularly inert solvent for benzophenone catalysis,[226] and improved the reaction yield slightly although the mass balance of the reaction was lower (*entry 3*) Acetone also had a similar effect (*entry 4*). No new peaks by NMR or GC could be identified, for example, the radical addition into acetonitrile or α-arylated acetone have been observed in other reactions but were not identified.[227] The use of D_2O (*entry 5*) liberated phenol **96**. The phenol was quite difficult to see by GC and could explain the poor mass balance across other reaction parameters. Benzene (*entry 6*) which is the solvent used in the published work was not useful in this scenario.

Enantioselective C-H

2.4.5. Acetone cosolvent

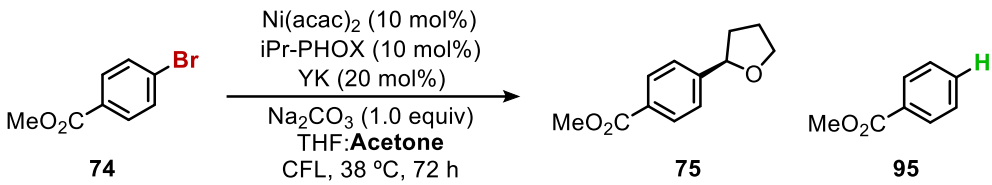

74 **75** **95**

Entry	*Acetone*	**74** (%)	**75** (%)	**95** (%)	ee (%)
0	25 µl	28	21	3	89
1	50 µl	76	22	0	90
2	100 µl	69	20	0	90
3	200 µl	70	21	6	90
4	500 µl	65	18	0	90
5[a]	500 µl	73	8	0	90

Figure 2.4.5 Reaction conditions: (74) (0.1 mmol), Ni(acac)2 (0.01 mmol) iPr-Phox (0.01 mmol), Yang Ketone (0.02 mmol), Na2CO3 (0.1 mmol), THF (0.5 mL), cosolvent (xx µl). 38 °C under CFL lights. GC conversion/yield determined using decane as internal standard, ee% determined by SFC of crude reaction mixture. a) Acetone used as solvent w/ THF ~12.3 equiv.

With the positive result from Figure 2.4.4 *entry 4* in hand, we decided to assess whether the volume of the added acetone had an influence on the reactivity (Figure 2.4.5). The reactivity remained consistent with increasing volumes of acetone. Additionally, the use of THF as a super stoichiometric reaction partner (12.3 equiv) rather than as solvent (*entry 5*) afforded the desired product in 8% yield which is a very promising result. One of the limitations of several C(sp^3)-H functionalisation techniques is that the C-H precursor is used in great excess, this could be enabling the reaction to be run at a more reasonable stoichiometry. Although acetone increased the yield of the desired product **75**, it was not taken forward as a permanent change to the reaction conditions.

2.4.6. Bromide Additive

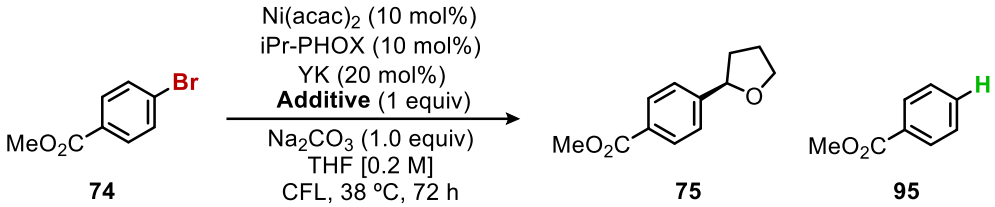

Entry	*Additive (1 equiv)*	**74** (%)	**75** (%)	**95** (%)	ee (%)
0	*none*	52	14	0	89
1	LiBr	98	0	0	-
2	NaBr	56	4	25	-
3	KBr	72	20	2	90
4[a]	KBr	67	24	4	90
5	$ZnBr_2$	83	0	6	-

Figure 2.4.6 Reaction conditions: (74) (0.1 mmol), Ni(acac)₂ (0.01 mmol) iPr-Phox (0.01 mmol), Yang Ketone (0.02 mmol), Na_2CO_3 (0.1 mmol), additive (0.1 mmol) THF (0.5 mL), 38 °C under CFL lights. GC conversion/yield determined using decane as internal standard, ee% determined by SFC of crude reaction mixture. a) 100 ul acetone as additive

The stabilisation of the intermediates is critical for control over the reaction. Introducing halide salts has been beneficial to some of the reactions conducted within the group. The introduction of salts could help in either stabilising or destabilising the intermediates formed. Thus a small additive screen was assessed (Figure 2.4.6)

Bromide salts were chosen to avoid the deleterious Finkelstein products which have been observed.[228] The use of LiBr (*entry 1*) and $ZnBr_2$ (*entry 5*) reduced the reactivity considerably. Introduction of stoichiometric NaBr (*entry 2,* a by-product of the reaction) increased the dehalogenation of the aryl bromide, which was not anticipated because this salt should form within the reaction conditions. KBr (*entry 3*) improved the mass balance of the reaction as well as the yield.

The rationale behind this is somewhat difficult to explain but it could be the displacement of the [$acac^-$] ligands in a key reaction step or the presence of a more Lewis acidic potassium cation. The reaction was also conducted in the presence of one hundred microlitres of acetone (*entry 4*) which liberated slightly more product than without. With the idea that the **X** ligand of the reaction may be essential to the reactivity we decided to test the nickel precursor.

2.4.7. Nickel Precatalyst

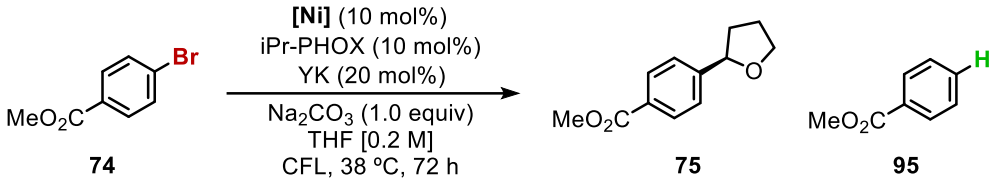

Entry	*Nickel Precatalyst*	**74** (%)	**75** (%)	**95** (%)	ee (%)
0	$Ni(acac)_2$	52	14	0	89
1	$Ni(acac)_2$ (5 mol%)	94	4	0	-
2	$Ni(Facac)_2 .H_2O$	72	6	3	-
3	$NiCl_2$	77	17	0	90
4	$NiBr_2$	83	0	0	-
5	NiI_2	61	0	8	-

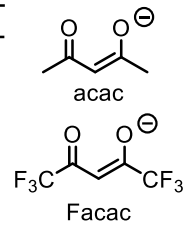

Figure 2.4.7. Reaction conditions: (74) (0.1 mmol), [Ni] (0.01 mmol) iPr-Phox (0.01 mmol), Yang Ketone (0.02 mmol), Na_2CO_3 (0.1 mmol), THF (0.5 mL), 38 °C under CFL lights. GC conversion/yield determined using decane as internal standard, ee% determined by SFC of crude reaction mixture.

The nickel precatalyst screen (Figure 2.4.7), showed that the use of lower nickel loadings was highly detrimental to the reaction (*entry 1*) although **75** was the only observed product in this reaction. The decreasing the electron density of the acac ligand also hampered the reaction outcome (*entry 2*). However, the use of $NiCl_2$ (*entry 3*) was positive with slightly more product formed at 17% yield of **75**. The bromide and iodide precatalysts (*entry 4 and 5*) did not afford the product.

2.4.8. Benzophenone derivatives

One of the issues with the benzophenone catalyst is its poor absorption in the visible spectrum (Figure 2.4.8). CFLs are required due to the presence of a peak in the emission spectrum centred at 396 nm. Shifting the absorption spectrum into the visible region could be of great benefit.

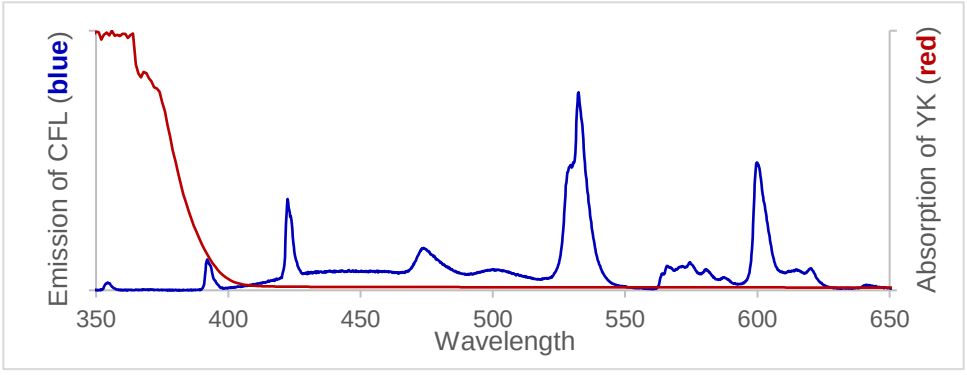

Figure 2.4.8. Emission spectrum of CFLs and the absorption spectra of the yang ketone at reaction concentration.

2.4.9. UV/Vis of benzophenone derivatives.

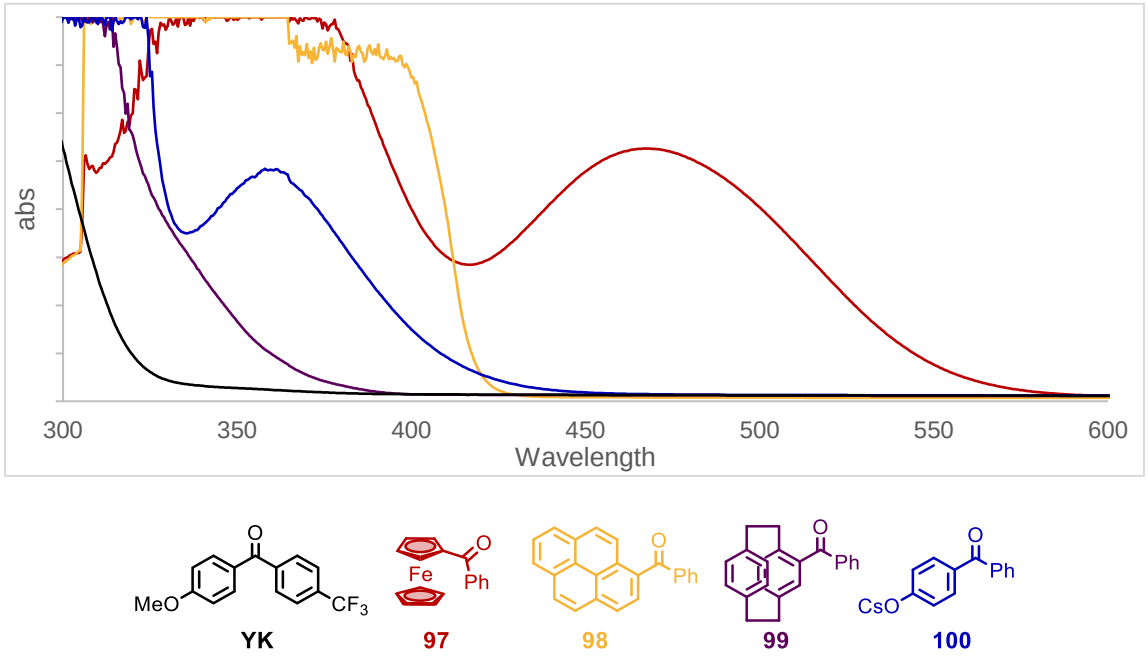

Figure 2.4.9. UV/Vis spectrum of the synthesised ketones in THF.

There is some evidence to suggest that shifting the absorption into the visible region can retain the n-pi* transition, a higher absorption in the visible spectrum would increase the concentration of reactive triplet state benzophenone and thus the reactivity could be improved.[229]

The UV/Vis spectrum of the new benzophenone derivatives are generally shifted into the visible region compared to the Yang Ketone (*black,* Figure 2.4.9). Benzoyl ferrocene (**97**, red line) has a broad feature at 470 nm. Benzoylpyrene (**98**, *yellow*) does not show much absorption until 420 nm. Benzoylparacyclophane (**99**, *purple*), was red shifted in comparison to the yang ketone, with the absorption beginning at 390 nm and increasing considerably. CsOBP (**100**, *blue*) was a bright yellow powder. However, when solubilised in THF a cloudy white solution is formed, therefore **100** was generated *in situ* by mixing 1 equivalent of CsOH with 4-hydroxybenzophenone in THF to give a bright yellow solution. Dilution of this solution for analysis by UV/Vis spectroscopy produced a gel which solubilised in acetone and gave the recorded spectra which shows absorption at 362 nm.

Enantioselective C-H

2.4.10. Application to the reaction

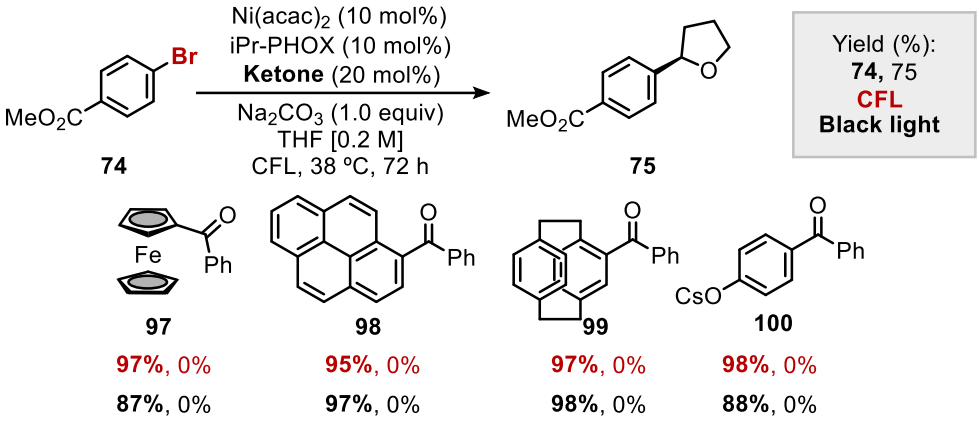

Figure 2.4.10. Reaction conditions: (74) (0.1 mmol), Ni(acac)₂ (0.01 mmol) iPr-Phox (0.01 mmol), Ketone (0.02 mmol), Na_2CO_3 (0.1 mmol), THF (0.5 mL), 38 °C under CFL lights or 15 °C under 390 nm irradiation. GC conversion/yield determined using decane as internal standard, ee% determined by SFC of crude reaction mixture. Cz = Carbazole.

Application of the synthesised ketones to the reaction was conducted under both CFL and black light conditions (Figure 2.4.10), in this regard we can be sure that the reactivity is not limited to the light source employed. The Yang Ketone works under both conditions. Disappointingly, all synthesised ketones failed to produce any **75** upon application to the standard reaction.

This is most likely due to the loss of the ^{T}**BP**[n, π*]. transition which is essential for the reactivity of the benzophenone catalysts. It is known that naphthalene quenches the triplet excited state of molecules.[230] By introducing the π extended systems the excited state likely resides at a π-π* transition which is unproductive. The caesium salt of hydroxy benzophenone did not afford any product either.

The use of a *red-shifted* biarylketones was set aside as a venture that was not worth exploring further. The electronics of the benzophenone catalysts could still be explored but it was decided that a co-photocatalyst could be used, akin to the works of Molander and Liu.[172, 215] This was to be used as a starting point if the reaction could not be optimised further by other means (*vide infra*).

2.4.11. Co-photocatalyst

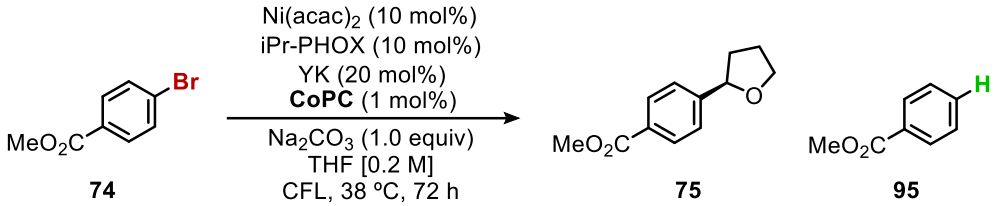

74 **75** **95**

Entry	*Co-PC (1 mol%)*	**74** (%)	**75** (%)	**95** (%)	ee (%)
0	*none*	52	14	0	89
1	$[Ir(ppy)_2(dtbbpy)]PF_6$	46	21	6	- [a]
2	$Ru(bpy)_3Cl_2$	75	16	4	89
3	4CzIPN	89	6	0	-

Figure 2.4.11. Reaction conditions: (74) (0.1 mmol), Ni(acac)₂ (0.01 mmol) iPr-Phox (0.01 mmol), Ketone (0.02 mmol), Co-photocatalyst (0.001 mmol) Na₂CO₃ (0.1 mmol), THF (0.5 mL), 38 °C under CFL lights. [a]An inseperable peak in the SFC meant that it was not possible to record an appropriate enantiodetermination.

To assess this, three photoredox catalysts were added to the reaction to ascertain their impact (Figure 2.4.11). The introduction of $[Ir\text{-}1]PF_6$ increased the reactivity slightly, 21% yield and the enantioselectivity of the reaction was unchanged. The lack of enantioselectivity change may suggest that the phosphine ligand is not oxidised under the reaction conditions. The increase in reactivity could be due to an energy transfer from the iridium photocatalyst to the ketone. Although the triplet energy values are not particularly well matched between $[Ir\text{-}1]PF_6$ (61.5 kcal mol^{-1}) and the yang ketone (67.7 kcal mol^{-1}).[231] It could also be a triplet energy transfer to form the bromide radicals, similar to the work of Molander. The use of $Ru(bpy)_3Cl_2$ (*entry 2*) had negligible impact on the reactivity and 4CzIPN provided **75** in reduced yield.

Whilst the co-photocatalyst screen showed that they are compatible, the use of a secondary photocatalyst would be counterintuitive with such low improvement to the reactivity.

2.5. Light Source

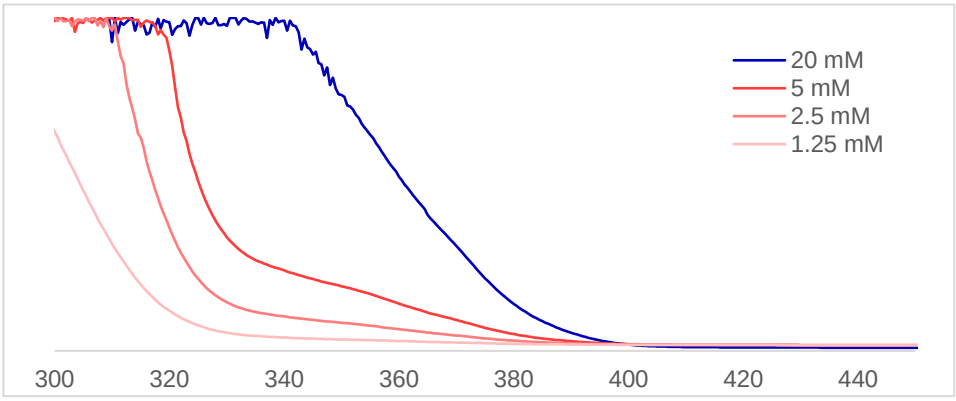

Figure 2.5.1. Blue line is the yang ketone at reaction concentration. Red lines under more dilute conditions.

The yang ketone has a significant dependence on the concentration. At reaction concentrations (blue line, Figure 2.5.1), the absorption tails into the region of 380 nm, under CFL irradiation there is a peak at this wavelength that is likely to give the reactivity that we observe. However, the use of a more suitable light source centred around this wavelength may be highly beneficial to the reaction.

The wavelengths of 390 nm are classed as long wavelength UV (UVA), commonly referred to as black light. However, the use of black light has been avoided in modern photoredox catalysis due to the higher energy and possibility to directly photoexcite the substrates within the reaction, which may lead to problems with side reactions and substrate decomposition. Although the energy difference between high intensity blue (440 nm) or purple (427 nm) LEDs and long wave UVA light irradiation at 390 nm is not likely to cause too many problems with side reactions. The work by Noel and co-workers using high energy 390 nm irradiation in flow is exemplary as the substrate scope of these reactions is not limited.[232]

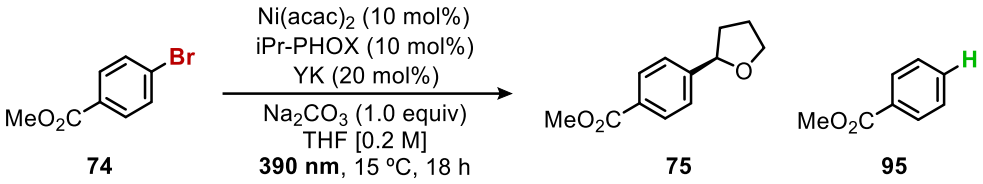

74 **75** **95**

Entry	*General Condition*	**74** (%)	**75** (%)	**95** (%)	ee (%)
0	CFL, 3 days	52	14	0	90
1	Kessil @ ~38 °C	34	30	10	89
2	Reactor @ 15 °C	81	14	0	90

Figure 2.5.2. Reaction conditions: (74) (0.1 mmol), Ni(acac)$_2$ (0.01 mmol) iPr-Phox (0.01 mmol), Yang Ketone (0.02 mmol), Na_2CO_3 (0.1 mmol), THF (0.5 mL). Entry 1 under kessil at ~ 38 °C. Entry 2, 15 °C in temperature controlled reactor.

To this end (Figure 2.5.2), we attempted the reaction under both high (*entry 1,* 35 W) and low power (*entry 2,* 1 W) irradiation for 18 h. *Entry 1* gave significantly better yields but was not a clean reaction with multiple unidentifiable side products. On the other hand, because the low power irradiation could be temperature controlled, the reaction was much cleaner, and all peaks could be accounted for.

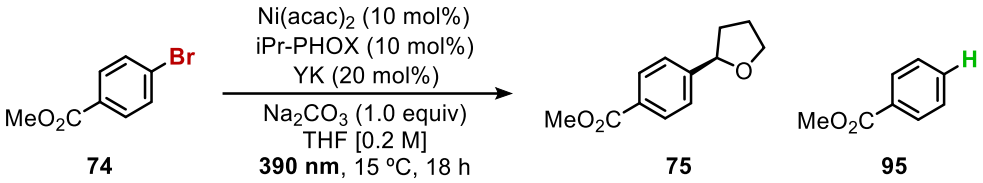

74 **75** **95**

Entry	*General Condition*	**74** (%)	**75** (%)	**96** (%)	ee (%)
0	*none*	81	14	0	89
1	K_2CO_3	62	3	0	-
2	Cs_2CO_3	81	3	0	-
3	Actone (25 ul)	79	15	0	88
4	Acetone (100 ul)	86	16	0	90
5	PhH	79	12	0	89
6	KBr (1 equiv)	87	12	0	90
7	$NiCl_2$	80	18	0	90

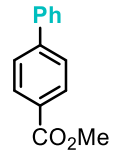

101

Figure 2.5.3. Reaction conditions: (74) (0.1 mmol), Ni(acac)$_2$ (0.01 mmol) iPr-Phox (0.01 mmol), Yang Ketone (0.02 mmol), Na_2CO_3 (0.1 mmol), THF (0.5 mL), 15 °C in temperature controlled reactor 390 nm.

The initial test for black light irradiation using the temperature-controlled reactor was to assess some of the best conditions from the CFL reaction screen (Figure 2.5.3). Gratifyingly the yield for the reaction was reached in just 18 h (CFL 3 days = 15% yield) the enantiomeric ratio had not been affected, a drop of 1% ee is negligible (*entry 0*). The use of potassium and caesium salts that were promising with regards to maintaining mass balance did not yield the desired product in any appreciable yields (*entry 1 + 2*). The use of acetone as cosolvent had a marginal impact on the reactivity. (*entry 3 + 4*).

Enantioselective C-H

Benzene did not affect the bond forming reaction (*entry 5*), although a small quantity of the formal Friedel crafts arylation was observed, **101**. The use of one equivalent of potassium bromide maintained the reactivity (*entry 6*). The use of nickel dichloride as pre-catalyst was slightly beneficial to the reaction (*entry 7*). With these promising results in hand, we decided to switch our efforts to the 390 nm photoreactor.

2.5.1. Ketone

We hypothesised that since the black light emitted at 390nm, well within many of the biarylketones absorption bands, therefore the lifetime or absorbance of the ketone may not have such an impact on the reactivity. By varying the electronic parameters of the ketone, we could also ascertain a rough trend that could aid in ketone design.

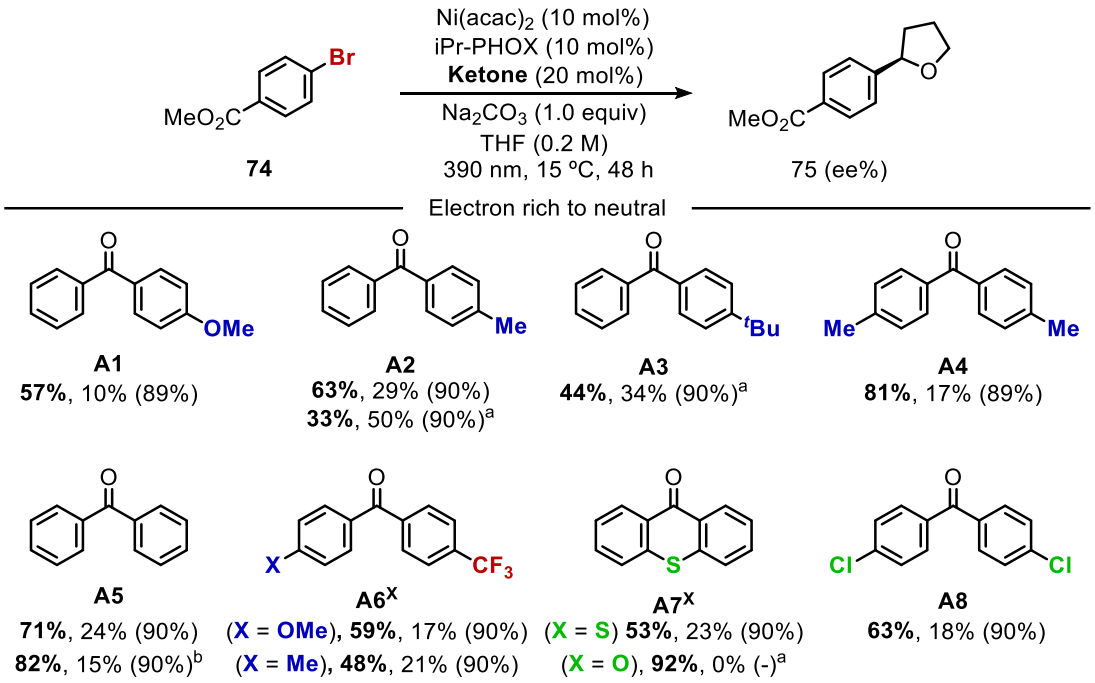

*Figure 2.5.4. [**recovered 74 (%),** Yield of 75 (%), (ee%).] Reaction conditions: (74) (0.1 mmol), Ni(acac)$_2$ (0.01 mmol) iPr-Phox (0.01 mmol), Ketone (0.02 mmol), Na_2CO_3 (0.1 mmol), THF (0.5 mL), 15 °C in temperature controlled reactor 390 nm. a) Run at 20 °C. b) Ketone (0.01 mmol). c) around 50% of the ketone was reduced*

The results of the ketone screen were very promising and have been split into two categories for discussion. The first results were from the more electron rich series (Figure 2.5.4), although the influence on the reactivity is not clearly defined. The formation of **75** in the presence of **A1** gave poorer yields than the original yang ketone (**A6^{OMe}**) 10% *vs* 17% yield. Changing the methoxy unit to the methyl derivative **A2** increased the yield of the desired cross coupling product to 29%, a dramatic increase for what could be considered a minor change to the electronics of the aryl ring.

Ketone **A2** was also run at a higher temperature of 20 °C, which led to an increase in yield to 50% without erosion of the enantiomeric excess. Increasing the electron donation **A3** at 20 °C was detrimental to the reactivity (34% vs 50%). Introducing the symmetrical methyl substituent **A4** reduced the yield at 15 °C (17% vs 29%). **A2** can be viewed as "push-neutral" whereas **A4** is a "push-push" ketone which may have a detrimental effect on the reactivity. Benzophenone **A5** gave reasonable yields of **75** and was used to assess whether a lower loading of photocatalyst could be used under these conditions, at 10 mol% the yield decreased by slightly less than half from 24% to 15%. So, the reaction can still be performed at a lower loading of benzophenone catalyst.

The traditional "push-pull" catalyst **A6^{OMe}** (yang ketone) had consistent yields at 17%. Ketone **A6^{Me}** was designed with the idea that the reactivity of **A2** was considerably better than **A1**, although the reactivity of **A6^{Me}** was only marginally better than that of **A6^{OMe}**. Xanthone type ketones, thioxanthone **A7^{S}** and xanthone **A7^{O}** have been used within the modern photochemical sphere.[233] Although in this reaction **A7^{O}** did not provide any reactivity, whereas **A7^{S}** produced 23% of the desired product, with high conversions. Ketone **A8** has been used by Molander in cross-coupling scenarios.[203] The use within our system provided the desired cross coupling product in 18% yield.

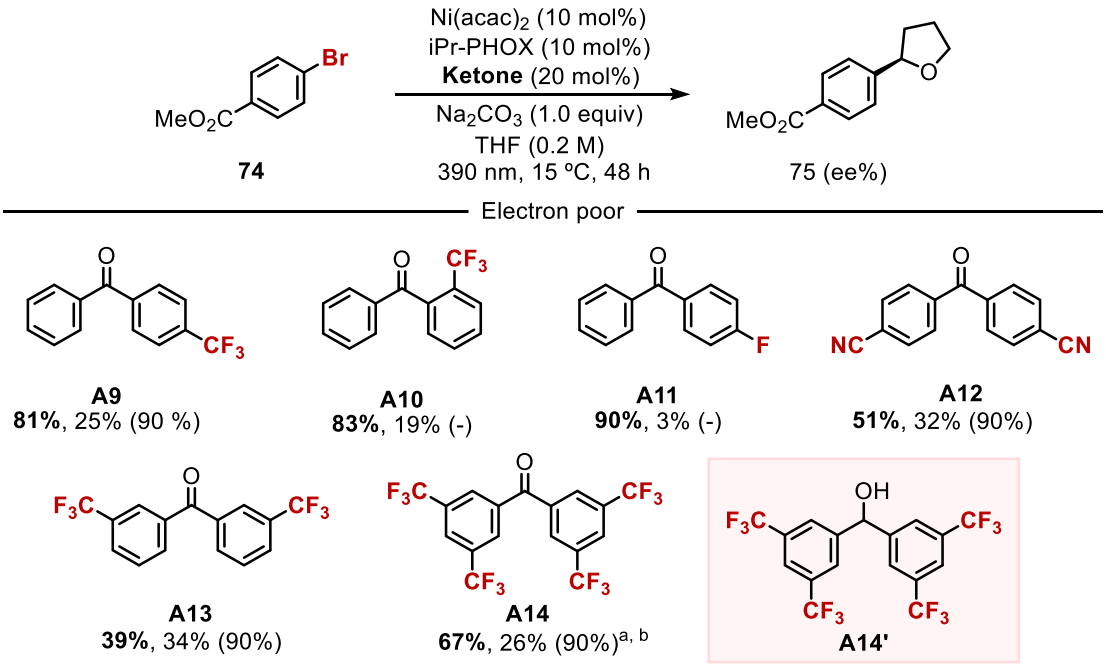

*Figure 2.5.5. [**recovered 74 (%),** Yield of 75 (%), (ee%).] Reaction conditions: (74) (0.1 mmol), Ni(acac)$_2$ (0.01 mmol) iPr-Phox (0.01 mmol), Ketone (0.02 mmol), Na_2CO_3 (0.1 mmol), THF (0.5 mL), 15 °C in temperature controlled reactor 390 nm. a) Run at 20 °C. b) around 50% of the ketone was reduced.*

Enantioselective C-H

The second section is electron poor in nature (Figure 2.5.5). The substitution pattern of the trifluoromethyl site was assessed between **A9** and **A10**. It was hypothesised that the *ortho* substitution of **A10** would be highly detrimental to the reactivity since it would push the aryl rings out of the plane due to steric crowding however this was not the case and reactivity was only slightly worse in comparison. The reactivity of **A11** was unexpected, the presence of the fluorine atom directly attached to the benzophenone seems to have a detrimental impact on reactivity. Both **A12** and **A13** worked very effectively at 15 °C and should be taken forward in the temperature screen. A general trend was observed that increasing the electron withdrawing nature of the substituents generally increased the reactivity, **A13 > A9 > A5 > A1**. The use of *tet*CF_3 **A14** was predicted to have the greatest reactivity from this trend, however over the course of the reaction the ketone was reduced to the biaryl alcohol **A14'**. We believe that the formation of this alcohol was highly detrimental to the reactivity. We propose that the changes in the reactivity are unlikely to be from the inability for the benzophenone catalyst to abstract a hydrogen but are more likely due to triplet state lifetimes or visible light absorption at 390 nm.[234]

2.5.2. Current best conditions

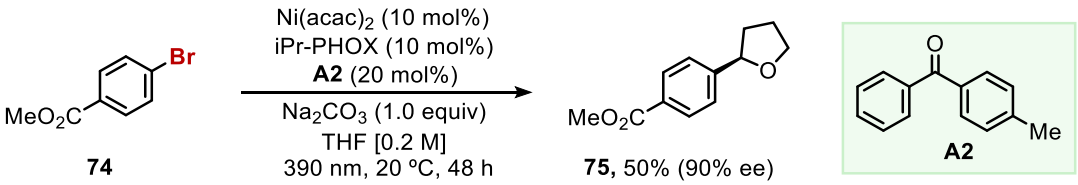

Figure 2.5.6. The current optimised conditions.

The best optimised conditions up to now are the ones shown in Figure 2.5.6, the use of the push-neutral ketone at 20 °C achieved a respectable yield of 50%. Maintaining the enantioinduction at 90% is beneficial. The next steps of the optimisation will be to design and screen more ketones to try to ascertain whether there is any structure-activity relationship. A temperature screen will also assist in the reaction, however as we have seen with the high-power Kessel lamps, it may lead to deleterious side reactions. Finally, the commercially available phox ligand has a number of derivatives that can be readily synthesised from amino acids. To this end ligand development could also be an option. It is likely that the high electron density imbued by the phosphine donor may decrease the electrophilicity of the nickel centre, thus limiting the radical addition and bond forming reaction.

2.6. Summary of Chapter 2

In this chapter we have presented the preliminary optimization of an enantioselective C(sp^3)-H arylation of THF. The work is based on a metallatriplet platform developed within the group. The protocol enables the creation of chiral products from simple starting materials.

Development of the reaction conditions showed that the chiral ^{i}Pr-PHOX ligand achieved the best enantiocontrol over the system although the reactivity was slow under CFL irradiation. Attempts to boost the reactivity by common screening patterns did not improve the overall reactivity but highlighted that acetone and potassium bromide could be potential additives to aid in controlling the side products formed. Switching to a 390 nm wavelength LED boosted the reactivity profile, affording the same conversions and yields within 18 h, when compared to 72 h under CFL irradiation. A small screen of ketones showed that the electron deficient ketone **A2** affords the best yield at 20 °C, 50% of **75**, whilst maintaining enantioinduction at 90% ee.

These results will enable the scope of the reaction after some minor improvements to the reactivity are seen. The information gained through careful screening should allow for any issues arising within the scope to be assessed and overcome. Furthermore, since the reaction is based on the metallatriplet protocol which also afforded the cross-coupling reaction with alkyl bromides, it may be possible to extend this work to encompass an enantioselective C(sp^3)-C(sp^3) bond forming reaction.

2.7. Supporting Information

2.7.1. General considerations

Analytical. 1H NMR and 13C NMR spectra were recorded on a Bruker 400 spectrometer at 20 °C. The chemical shifts are reported in ppm relative to solvent residual peak. All 13C NMR spectra are reported in ppm relative to TMS, were calibrated using the signal of residual CHCl3 (77.16 ppm) and were obtained with 1H decoupling unless otherwise indicated. Coupling constants, J, are reported in Hertz. Mass spectrometry was performed on a Waters LCT Premier spectrometer or on a MicroTOF Focus, Bruker Daltonics spectrometer. Infrared spectra (FT-IR) measurements were carried out on a Bruker Optics FT-IR Alpha spectrometer equipped with a DTGS detector, KBr beamsplitter at 4 cm-1 resolution using a one bounce ATR accessory with diamond windows. Gas chromatographic analyses were performed on Hewlett-Packard 6890 gas chromatography instrument with an FID detector using 25m x 0.20 mm capillary column with cross-linked methyl siloxane as the stationary phase. Column chromatography was performed on silica gel 60 (40-63 μm). Melting points were measured using open glass capillaries in a Büchi B540 apparatus. Enantiodetermination was conducted using an Agilent 1260 Infinity II SFC System

Reagents. Reactions were carried out under argon or nitrogen, unless stated otherwise. Anhydrous solvents were obtained from the solvent purification system Puresolv MD-7 or purchased from Acros Organics. All commercial solvents, reagents, nickel sources, and ligands were used as received without further purification. Na_2CO_3 (anhydrous), Acetone (anhydrous) were purchased from Acros Organics. $Ni(acac)_2$ (anhydrous, 95% purity) was purchased from Strem. iPr-PHOX was purchased from BLDPharm.

(4-methoxy)(4'-trifluoromethyl)benzophenone,[235] benzoylferrocene,[236] benzoylpyrene,[237] benzoylparacyclophane,[238] were prepared according to literature procedures.

2.7.2. Reactor setup

CFL, 2 CFL light bulbs were placed 3 cm from a wire rack which could accomodate 8 round-bottom Schlenk tubes, due to the fluctuation in temperature within the lab, no fan cooling was applied, the reactions were magnetically stirred (~ 500 rpm).

390nm LEDs were installed at the bottom of a custom-made 8 flat-bottom Schlenk tubes holder (the distance between the flat-bottom Schlenk tube and the light source was measured to be ~7 mm), equipped with a water cooling system (the thermostat was set at 15 °C) and magnetically stirred (~ 500 rpm).

2.5.3. Optimisation details

CFL reactor

An oven dried 8 mL Schlenk tube containing a stirrer bar was charged with Na_2CO_3 (0.1 mmol, 10.1 mg, 1.0 equiv), (4-methoxy)(4'-trifluoromethyl)benzophenone (0.02 mmol, 2.8 mg, 20 mol%) and methyl 4-bromobenzoate (0.1 mmol, 21.2 mg, 1 equiv). The Schlenk was transferred to a glovebox where $Ni(acac)_2$ (0.01 mmol, 2.5 mg, 10 mol%), and iPr-PHOX (0.01 mmol, 3.7 mg, 10 mol%) were added. The Schlenk tubes were removed from the glovebox and attached to a Schlenk line, evacuated, and back filled three times with Argon. Under a positive pressure of argon, THF (0.5 mL) was added, the Schlenk sealed and stirred for 15 minutes before being placed under CFL irradiation for 72 h. The mixture was quenched with EtOAc (10 mL). Decane (0.1 mmol, 14.2 mg, 1 equiv) was added as internal standard and filtered through a short plug of silica into a GC vial which was analysed by calibrated GC-FID. The same vial was then evaporated on the rotary evaporator and then diluted with HPLC grade MeCN for SFC analysis. Yields below 10% were not reliably recorded.

390 nm reactor

An oven dried 8 mL Schlenk tube containing a stirrer bar was charged with Na_2CO_3 (0.1 mmol, 10.1 mg, 1.0 equiv), (4-methoxy)(4'-trifluoromethyl)benzophenone (0.02 mmol, 2.8 mg, 20 mol%) and methyl 4-bromobenzoate (0.1 mmol, 21.2 mg, 1 equiv). The Schlenk was transferred to a glovebox where $Ni(acac)_2$ (0.01 mmol, 2.5 mg, 10 mol%), and iPr-PHOX (0.01 mmol, 3.7 mg, 10 mol%) were added. The Schlenk tubes were removed from the glovebox and attached to a Schlenk line, evacuated, and back filled three times with Argon. Under a positive pressure of argon, THF (0.5 mL) was added, the Schlenk sealed and stirred for 15 minutes before being placed under 390 nm irradiation for 48 h. The mixture was quenched with EtOAc (10 mL). Decane (0.1 mmol, 14.2 mg, 1 equiv) was added as internal standard and filtered through a short plug of silica into a GC vial which was analysed by calibrated GC-FID. The same vial was then evaporated on the rotary evaporator and then diluted with HPLC grade MeCN for SFC analysis. Yields below 10% were not reliably recorded.

Enantioselective C-H

2.5.4. Analytical data

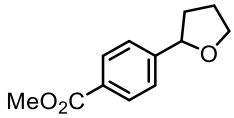

Methyl 4-(tetrahydrofuran-2-yl) benzoate (**75**)

Prepared according to the reported literature procedure:[235] An oven dried 8 mL Schlenk tube containing a stirrer bar was charged with Na_2CO_3 (0.15 mmol, 15.6 mg, 1.0 equiv), 5,5'dimethylbipyridine (0.015 mmol, 2.8 mg, 10 mol%), $Ni(acac)_2$ (0.015 mmol, 3.9 mg, 10 mol%), (4-methoxy)(4'-trifluoromethyl)benzophenone (0.015 mmol, 4.2 mg, 10 mol%) and methyl 4-bromobenzoate (0.15 mmol, 32.2 mg, 1 equiv). The Schlenk was attached to a Schlenk line, evacuated, and back filled three times with Argon. Under a positive pressure of argon, THF (0.75 mL) was added, stirred for 15 minutes, and placed under CFL irradiation for 72 h. The mixture was quenched with 1M HCl (2 mL) and extracted with EtOAc (10 mL). The organic phase was washed with 10 mL brine, dried with $MgSO_4$, evaporated, purification by column chromatography. Affording the title compound as a colourless oil (29.1 mg, 94% yield) using pentane:EtOAc (85:15) as eluent.

^{1}H NMR (300 MHz, $CDCl_3$) δ 7.99 (d, *J* = 8.4 Hz, 2H), 7.38 (d, *J* = 8.4 Hz, 2H), 4.93 (t, *J* = 7.2 Hz, 1H), 4.13-4.06 (m, 1H), 3.98-3.93 (m, 1H), 3.90 (s, 3H), 2.40-2.29 (m, 1H), 2.04-1.94 (m, 2H), 1.81-1.69 (m, 1H) ppm.

^{13}C NMR (75 MHz, $CDCl_3$) δ 167.07, 149.04, 129.74, 129.00, 125.51, 80.26, 68.93, 52.10, 34.79, 26.05 ppm. The enantiomeric ratio was determined by SFC analysis

SFC: CHIRALPAK IA-3 (3mm x 100 mmL, particle size 3 µm), 1.2 mL/min, CO_2/MeCN Gradient 5-40%. λ =230 nm; tR (enantiomer A) = 2.360 min, tR (enantiomer B) = 2.470 min.

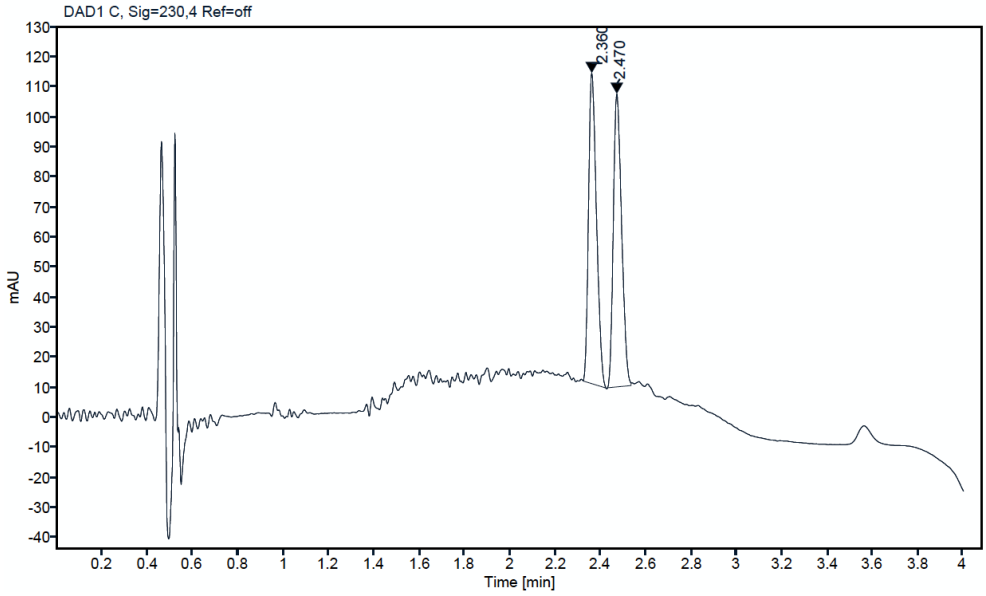

Signal: DAD1 C, Sig=230,4 Ref=off

RT [min]	Type	Width [min]	Area	Height	Area%	Name
2.360	MM	0.0404	250.4572	103.2105	50.3641	
2.470	MM	0.0422	246.8361	97.3955	49.6359	
		Sum	497.2932			

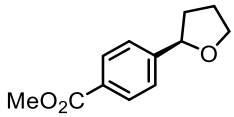

Methyl 4-(tetrahydrofuran-2-yl) benzoate (**75'**)

An oven dried 8 mL Schlenk tube containing a stirrer bar was charged with Na_2CO_3 (0.2 mmol, 20.2 mg, 1.0 equiv), (4-methoxy)(4'-trifluoromethyl)benzophenone (0.04 mmol, 5.6 mg, 20 mol%) and methyl 4-bromobenzoate (0.2 mmol, 43.0 mg, 1 equiv). The Schlenk was transferred to a glovebox where $Ni(acac)_2$ (0.02 mmol, 5.12 mg, 10 mol%), and iPr-PHOX (0.02 mmol, 7.5 mg, 10 mol%) were added. The Schlenk tubes were removed from the glovebox and attached to a Schlenk line, evacuated, and back filled three times with Argon. Under a positive pressure of argon, THF (1.0 mL) was added, stirred for 15 minutes, and placed under CFL irradiation for 72 h. The mixture was quenched with 1M HCl (2 mL) and extracted with EtOAc (10 mL). The organic phase was washed with 10 mL brine, dried with $MgSO_4$, evaporated, purification by column chromatography. Affording the title compound as a colourless oil (5.0 mg, 12% yield) using pentane:EtOAc (85:15) as eluent. Analytical data matched the pure sample above, application to the SFC procedure, showed an enantiomeric ratio of 95:5.

SFC: CHIRALPAK IA-3 (3mm x 100 mmL, particle size 3 µm), 1.2 mL/min, CO_2/MeCN Gradient 5-40%. λ =230 nm;
tR (enantiomer A) = 2.360 min, tR (enantiomer B) = 2.451 min. (the slight change in tR is likely due to small amount of $CDCl_3$)
Spectral data from the SFC confirm the peaks are identical with >99.9% accuracy

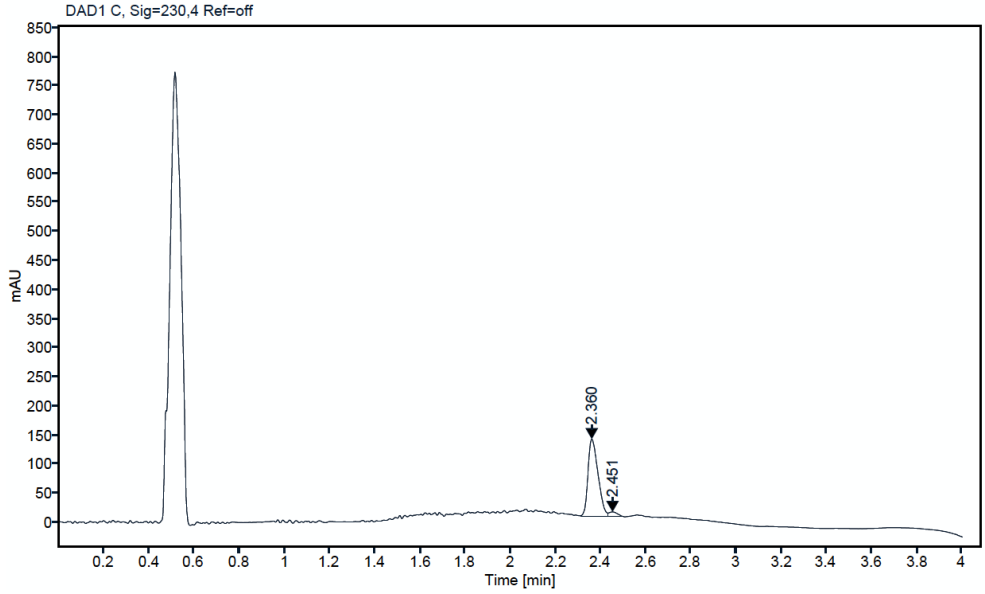

Signal: DAD1 C, Sig=230,4 Ref=off

RT [min]	Type	Width [min]	Area	Height	Area%	Name
2.360	MF	0.0512	407.9903	132.6855	95.6505	
2.451	FM	0.0406	18.5526	7.6232	4.3495	
		Sum	426.5429			

Enantioselective C-H

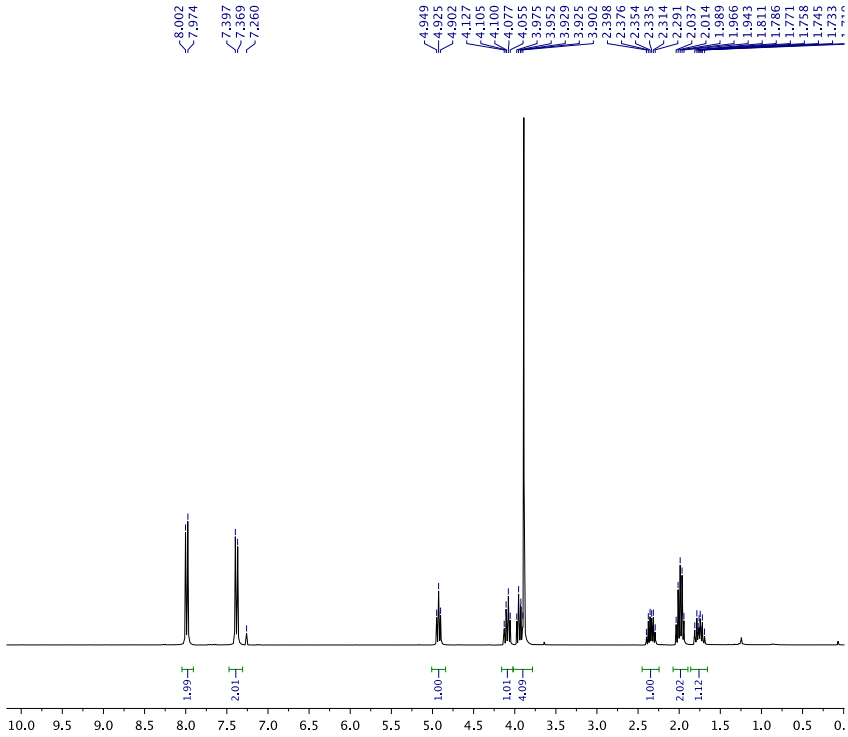

^{1}H NMR spectrum (300 Hz) of **75**

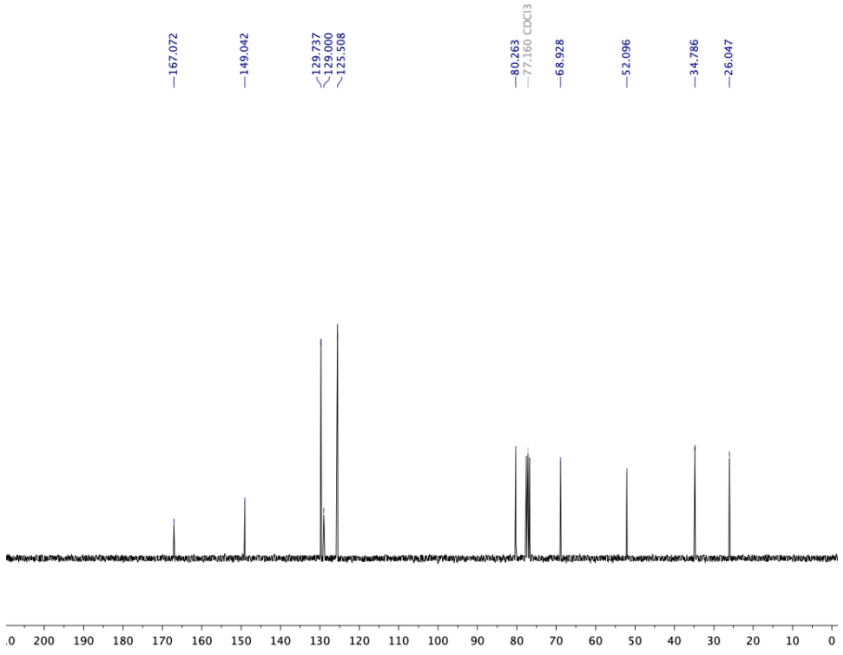

^{13}C NMR spectrum (75 Hz) of **75**

2.8. References

107. Hartwig, J. F. Evolution of C-H Bond Functionalization from Methane to Methodology. *Journal of the American Chemical Society* **2016**, *138* (1), 2–24. https://doi.org/10/f8pcnj.

108. Davies, H. M. L.; Morton, D. Recent Advances in C-H Functionalization. *Journal of Organic Chemistry* **2016**, *81* (2), 343–350. https://doi.org/10.1021/acs.joc.5b02818.

109. a) Chen, K.; Eschenmoser, A.; Baran, P. S. Strain Release in C-H Bond Activation? *Angewandte Chemie International Edition* **2009**, *48* (51), 9705–9708. https://doi.org/10/bck3sk.
b) Huang, X.; Bergsten, T. M.; Groves, J. T. Manganese-Catalyzed Late-Stage Aliphatic C–H Azidation. *J. Am. Chem. Soc.* **2015**, *137* (16), 5300–5303. https://doi.org/10/ggpj2z.
c) Guo, S.; Zhang, X.; Tang, P. Silver-Mediated Oxidative Aliphatic C□H Trifluoromethylthiolation. *Angewandte Chemie International Edition* **2015**, *54* (13), 4065–4069. https://doi.org/10/f258dv.
d) Schmidt, V. A.; Quinn, R. K.; Brusoe, A. T.; Alexanian, E. J. Site-Selective Aliphatic C–H Bromination Using N-Bromoamides and Visible Light. *J. Am. Chem. Soc.* **2014**, *136* (41), 14389–14392. https://doi.org/10/f6mms6.
e) Halperin, S. D.; Fan, H.; Chang, S.; Martin, R. E.; Britton, R. A Convenient Photocatalytic Fluorination of Unactivated C□H Bonds. *Angewandte Chemie International Edition* **2014**, *53* (18), 4690–4693. https://doi.org/10/f2qr3p.
f) Liu, W.; Groves, J. T. Manganese Porphyrins Catalyze Selective C−H Bond Halogenations. *J. Am. Chem. Soc.* **2010**, *132* (37), 12847–12849. https://doi.org/10/bpgx4b.
g) Chen, M. S.; White, M. C. Combined Effects on Selectivity in Fe-Catalyzed Methylene Oxidation. *Science* **2010**, *327* (5965), 566–571. https://doi.org/10/frc83w.

110. a) Lewis, J. C.; Coelho, P. S.; Arnold, F. H. Enzymatic Functionalization of Carbon–Hydrogen Bonds. *Chem. Soc. Rev.* **2011**, *40* (4), 2003–2021. https://doi.org/10/d4gbrp.
b) Li, F.; Zhang, X.; Renata, H. Enzymatic C-H Functionalisations for Natural Product Synthesis. *Current Opinion in Chemical Biology* **2019**, *49*, 25–32. https://doi.org/10/gnjj88.

111. Lang, K.; Torker, S.; Wojtas, L.; Zhang, X. P. Asymmetric Induction and Enantiodivergence in Catalytic Radical C–H Amination via Enantiodifferentiative H-Atom Abstraction and Stereoretentive Radical Substitution. *J. Am. Chem. Soc.* **2019**, *141* (31), 12388–12396. https://doi.org/10/ghj3gw.

112. a) Godula, K.; Sames, D. C-H Bond Functionalization in Complex Organic Synthesis. *Science* **2006**, *312* (5770), 67–72. https://doi.org/10.1126/science.1114731.
b) Yamaguchi, J.; Yamaguchi, A. D.; Itami, K. C-H Bond Functionalization: Emerging Synthetic Tools for Natural Products and Pharmaceuticals. *Angewandte Chemie - International Edition* **2012**, *51* (36), 8960–9009. https://doi.org/10.1002/anie.201201666.
c) Wencel-Delord, J.; Glorius, F. C–H Bond Activation Enables the Rapid Construction and Late-Stage Diversification of Functional Molecules. *Nature Chem* **2013**, *5* (5), 369–375. https://doi.org/10/f4t955.
d) Cannalire, R.; Pelliccia, S.; Sancineto, L.; Novellino, E.; Tron, G. C.; Giustiniano, M. Visible Light Photocatalysis in the Late-Stage Functionalization of Pharmaceutically Relevant Compounds. *Chem. Soc. Rev.* **2021**, *50* (2), 766–897. https://doi.org/10/gkzhzs.

113. Jana, R.; Begam, H. M.; Dinda, E. The Emergence of the C–H Functionalization Strategy in Medicinal Chemistry and Drug Discovery. *Chem. Commun.* **2021**, *57* (83), 10842–10866. https://doi.org/10/gqfdbg.

114. Gaich, T.; Baran, P. S. Aiming for the Ideal Synthesis. *J. Org. Chem.* **2010**, *75* (14), 4657–4673. https://doi.org/10/ch3qpf.
Wender, P. A. Toward the Ideal Synthesis and Transformative Therapies: The Roles of Step Economy and Function Oriented Synthesis. *Tetrahedron* **2013**, *69* (36), 7529–7550. https://doi.org/10/gqfr8t.

115 Jenck, J. F.; Agterberg, F.; Droescher, M. J. Products and Processes for a Sustainable Chemical Industry: A Review of Achievements and Prospects. *Green Chem.* **2004**, *6* (11), 544–556. https://doi.org/10.1039/B406854H.
Dalton, T.; Faber, T.; Glorius, F. C–H Activation: Toward Sustainability and Applications. *ACS Cent. Sci.* **2021**, *7* (2), 245–261. https://doi.org/10/ggh7hn.
Laskar, R.; Pal, T.; Bhattacharya, T.; Maiti, S.; Akita, M.; Maiti, D. Sustainable C–H Functionalization under Ball-Milling, Microwave-Irradiation and Aqueous Media. *Green Chem.* **2022**, *24* (6), 2296–2320. https://doi.org/10/gqh7hm.

116. Newhouse, T.; Baran, P. S. If C-H Bonds Could Talk: Selective C-H Bond Oxidation. *Angewandte Chemie International Edition* **2011**, *50* (15), 3362–3374. https://doi.org/10.1002/anie.201006368.

117. Brückl, T.; Baxter, R. D.; Ishihara, Y.; Baran, P. S. Innate and Guided C-H Functionalization Logic. *Accounts of Chemical Research* **2012**, *45* (6), 826–839. https://doi.org/10.1021/ar200194b.

118. For example, the work of Knochel: Lin, W.; Baron, O.; Knochel, P. Highly Functionalized Benzene Syntheses by Directed Mono or Multiple Magnesiations with TMPMgCl·LiCl. *Org. Lett.* **2006**, *8* (24), 5673–5676. https://doi.org/10/fbtw8z.
b) Bertallo, C. R. d. S.; Arroio, T. R.; Toledo, M. F. Z. J.; Sadler, S. A.; Vessecchi, R.; Steel, P. G.; Clososki, G. C. C-H Activation/Metalation Approaches for the Synthesis of Indolizine Derivatives. *European Journal of Organic Chemistry* **2019**, *2019* (31–32), 5205–5213. https://doi.org/10/ggpj48.

119. Chinchilla, R.; Nájera, C. Recent Advances in Sonogashira Reactions. *Chem. Soc. Rev.* **2011**, *40* (10), 5084–5121. https://doi.org/10/bkd33c.

120. a) Lyons, T. W.; Sanford, M. S. Palladium-Catalyzed Ligand-Directed C−H Functionalization Reactions. *Chem. Rev.* **2010**, *110* (2), 1147–1169. https://doi.org/10/bbr2kt. ~
b) Li, B.; Dixneuf, P. H. Sp2 C–H Bond Activation in Water and Catalytic Cross-Coupling Reactions. *Chem. Soc. Rev.* **2013**, *42* (13), 5744. https://doi.org/10/ggpj6j.

121. pKa of toluene is ~43, whereas of methane it is ~56. a) Bordwell, F. G.; Algrim, D.; Vanier, N. R. Acidities of Anilines and Toluenes. *J. Org. Chem.* **1977**, *42* (10), 1817–1819. https://doi.org/10/bbgj8w.
b) Bordwell, F. G. Equilibrium Acidities in Dimethyl Sulfoxide Solution. *Acc. Chem. Res.* **1988**, *21* (12), 456–463. https://doi.org/10/chmzf6.

122 a) Arndtsen, B. A.; Bergman, R. G.; Mobley, T. A.; Peterson, T. H. Selective Intermolecular Carbon-Hydrogen Bond Activation by Synthetic Metal Complexes in Homogeneous Solution. *Acc. Chem. Res.* **1995**, *28* (3), 154–162. https://doi.org/10/brfk5v.
b) Shilov, A. E.; Shul'pin, G. B. Activation of C-H Bonds by Metal Complexes. *Chemical Reviews* **1997**, *97* (8), 2879–2932. https://doi.org/10/c9rqff.

123. a) Crabtree, R. H.; Lei, A. Introduction: CH Activation. *Chem. Rev.* **2017**, *117* (13), 8481–8482. https://doi.org/10/gdgx62.
b) Rogge, T.; Kaplaneris, N.; Chatani, N.; Kim, J.; Chang, S.; Punji, B.; Schafer, L. L.; Musaev, D. G.; Wencel-Delord, J.; Roberts, C. A.; Sarpong, R.; Wilson, Z. E.; Brimble, M. A.; Johansson, M. J.; Ackermann, L. C–H Activation. *Nat Rev Methods Primers* **2021**, *1* (1), 1–31. https://doi.org/10/gqhbg5.

Rogge, T.; Kaplaneris, N.; Chatani, N.; Kim, J.; Chang, S.; Punji, B.; Schafer, L. L.; Musaev, D. G.; Wencel-Delord, J.; Roberts, C. A.; Sarpong, R.; Wilson, Z. E.; Brimble, M. A.; Johansson, M. J.; Ackermann, L. C–H Activation. *Nature Reviews Methods Primers* **2021**, *1* (1). https://doi.org/10.1038/s43586-021-00041-2.
b) Gensch, T.; Hopkinson, M. N.; Glorius, F.; Wencel-Delord, J. Mild Metal-Catalyzed C–H Activation: Examples and Concepts. *Chem. Soc. Rev.* **2016**, *45* (10), 2900–2936. https://doi.org/10/gqfq54.

124. a) Curto, J. M.; Kozlowski, M. C. Chemoselective Activation of Sp^3 vs Sp^2 C–H Bonds with Pd(II). *J. Am. Chem. Soc.* **2015**, *137* (1), 18–21. https://doi.org/10/gnmn92.
b) Hu, Y.; Zhou, B.; Wang, C. Inert C–H Bond Transformations Enabled by Organometallic Manganese Catalysis. *Acc. Chem. Res.* **2018**, *51* (3), 816–827. https://doi.org/10/gc9csr.

125 For reviews on transition metal catalysed-directed functionalisations: a) Liu, B.; Romine, A. M.; Rubel, C. Z.; Engle, K. M.; Shi, B.-F. Transition-Metal-Catalyzed, Coordination-Assisted Functionalization of Nonactivated C(Sp3)–H Bonds. *Chem. Rev.* **2021**, *121* (24), 14957–15074. https://doi.org/10/gqfhrb.
b) Sambiagio, C.; Schönbauer, D.; Blieck, R.; Dao-Huy, T.; Pototschnig, G.; Schaaf, P.; Wiesinger, T.; Zia, M. F.; Wencel-Delord, J.; Besset, T.; Maes, B. U. W.; Schnürch, M. A Comprehensive Overview of Directing Groups Applied in Metal-Catalysed C–H Functionalisation Chemistry. *Chem. Soc. Rev.* **2018**, *47* (17), 6603–6743. https://doi.org/10/gfqcz9.
Selected examples: Xu, Y.; Yan, G.; Ren, Z.; Dong, G. Diverse Sp3 C-H Functionalization through Alcohol β-Sulfonyloxylation. *Nature Chemistry* **2015**, *7* (10), 829–834. https://doi.org/10.1038/nchem.2326.
Shabashov, D.; Daugulis, O. Auxiliary-Assisted Palladium-Catalyzed Arylation and Alkylation of Sp2 and Sp3 Carbon-Hydrogen Bonds. *Journal of the American Chemical Society* **2010**, *132* (11), 3965–3972. https://doi.org/10.1021/ja910900p.

126. a) Akhtar, M.; Pechet, M. M. The Mechanism of the Barton Reaction. *J. Am. Chem. Soc.* **1964**, *86* (2), 265–268. https://doi.org/10/c7cxrz.
b) Shkunnikova, S.; Zipse, H.; Šakić, D. Role of Substituents in the Hofmann–Löffler–Freytag Reaction. A Quantum-Chemical Case Study on Nicotine Synthesis. *Org. Biomol. Chem.* **2021**, *19* (4), 854–865. https://doi.org/10/gqp2j4.

127. Transient directing group strategies have become a relevant platform, but still require a functional group for interaction.
a) Zhao, Q.; Poisson, T.; Pannecoucke, X.; Besset, T. The Transient Directing Group Strategy: A New Trend in Transition-Metal-Catalyzed C–H Bond Functionalization. *Synthesis* **2017**, *49* (21), 4808–4826. https://doi.org/10/gcg52r.
b) Liao, G.; Zhang, T.; Lin, Z.-K.; Shi, B.-F. Transition Metal-Catalyzed Enantioselective C−H Functionalization via Chiral Transient Directing Group Strategies. *Angewandte Chemie International Edition* **2020**, *59* (45), 19773–19786. https://doi.org/10/gqpj2w.
c) Zu, B.; Guo, Y.; Ke, J.; He, C. Transient- and Native-Directing-Group-Enabled Enantioselective C–H Functionalization. *Synthesis* **2021**, *53* (12), 2029–2042. https://doi.org/10/gqpj2v.

128. Chu, J. C. K.; Rovis, T. Complementary Strategies for Directed C(Sp3)−H Functionalization: A Comparison of Transition-Metal-Catalyzed Activation, Hydrogen Atom Transfer, and Carbene/Nitrene Transfer. *Angewandte Chemie International Edition* **2018**, *57* (1), 62–101. https://doi.org/10/gcnswh.
Davies, H. M. L.; Manning, J. R. Catalytic C-H Functionalization by Metal Carbenoid and Nitrenoid Insertion. *Nature* **2008**, *451* (7177), 417–424. https://doi.org/10.1038/nature06485.

129. Mader, E. A.; Davidson, E. R.; Mayer, J. M. Large Ground-State Entropy Changes for Hydrogen Atom Transfer Reactions of Iron Complexes. *Journal of the American Chemical Society* **2007**, *129* (16), 5153–5166. https://doi.org/10.1021/ja0686918.

130. Fagnoni, M.; Ravelli, D.; Protti, S. *2.6 Generation of Carbon-Centered Radicals by Photochemical Methods*, 1st ed.; Thieme Verlag, 2021. https://doi.org/10.1055/sos-SD-233-00118.

131. Sarkar, S.; Shing Cheung, K. P.; Gevorgyan, V. C–H Functionalization Reactions Enabled by Hydrogen Atom Transfer to Carbon-Centered Radicals. *Chemical Science* **2020**, *11* (48), 12974–12993. https://doi.org/10/gqpj9q.
Capaldo, L.; Ravelli, D. Hydrogen Atom Transfer (HAT): A Versatile Strategy for Substrate Activation in Photocatalyzed Organic Synthesis. *European Journal of Organic Chemistry* **2017**, *2017* (15), 2056–2071. https://doi.org/10/gqfdbq.
Mayer, J. M. Hydrogen Atom Abstraction by Metal−Oxo Complexes: Understanding the Analogy with Organic Radical Reactions. *Acc. Chem. Res.* **1998**, *31* (8), 441–450. https://doi.org/10/fsj8w8.
Salamone, M.; Bietti, M. Tuning Reactivity and Selectivity in Hydrogen Atom Transfer from Aliphatic C–H Bonds to Alkoxyl Radicals: Role of Structural and Medium Effects. *Acc. Chem. Res.* **2015**, *48* (11), 2895–2903. https://doi.org/10/ghgc8k.

132. Evans, M. G.; Polanyi, M. Inertia and Driving Force of Chemical Reactions. *Trans. Faraday Soc.* **1938**, *34* (0), 11–24. https://doi.org/10/djd5kx.
Roberts, B. P. Understanding the Rates of Hydrogen-Atom Abstraction Reactions: Empirical, Semi-Empirical and Ab Initio Approaches. *Journal of the Chemical Society, Perkin Transactions 2* **1996**, No. 12, 2719. https://doi.org/10.1039/p29960002719.

133 (BDE, the enthalpic value that derives from the homolysis of a bond at zero-point energy) Bond dissociation energies are zero-point energy corrected enthalpies, but the terms are often used interchangeably

134. Roberts, B. P.; Steel, A. J. An Extended Form of the Evans–Polanyi Equation: A Simple Empirical Relationship for the Prediction of Activation Energies for Hydrogen-Atom Transfer Reactions. *J. Chem. Soc., Perkin Trans. 2* **1994**, No. 10, 2155–2162. https://doi.org/10.1039/P29940002155.

135. Mayer, J. M. Understanding Hydrogen Atom Transfer: From Bond Strengths to Marcus Theory. *Accounts of Chemical Research* **2011**, *44* (1), 36–46. https://doi.org/10/fgxhpk.

136. a) Blanksby, S. J.; Ellison, G. B. Bond Dissociation Energies of Organic Molecules. *Acc. Chem. Res.* **2003**, *36* (4), 255–263. https://doi.org/10/dzhp7q.
b) Luo, Y.-R. *Comprehensive Handbook of Chemical Bond Energies*, 1st ed.; CRC Press, 2007. https://doi.org/10.1201/9781420007282.

137. Zavitsas, A. A. Activation Energy Requirements in Hydrogen Abstractions. Quantitative Description of the Causes in Terms of Bond Energies and Infrared Frequencies. *J. Am. Chem. Soc.* **1972**, *94* (8), 2779–2789. https://doi.org/10/dn4phq.

138. a) De Vleeschouwer, F.; Van Speybroeck, V.; Waroquier, M.; Geerlings, P.; De Proft, F. Electrophilicity and Nucleophilicity Index for Radicals. *Organic Letters* **2007**, *9* (14), 2720–2724. https://doi.org/10.1021/ol071038k.
b) Parsaee, F.; Senarathna, M. C.; Kannangara, P. B.; Alexander, S. N.; Arche, P. D. E.; Welin, E. R. Radical Philicity and Its Role in Selective Organic Transformations. *Nature Reviews Chemistry* **2021**, *5* (7), 486–499. https://doi.org/10.1038/s41570-021-00284-3.

139. Roberts, B. P. Polarity-Reversal Catalysis of Hydrogen-Atom Abstraction Reactions: Concepts and Applications in Organic Chemistry. *Chemical Society Reviews* **1999**, *28* (1), 25–35. https://doi.org/10.1039/a804291h.

140. Paul, V.; Roberts, B. P.; Willis, C. R. Homolytic Reactions of Ligated Boranes. Part 12. Amine–Alkylboranes as Polarity Reversal Catalysts for Hydrogen-Atom Abstraction by t-Butoxyl Radicals. *J. Chem. Soc., Perkin Trans. 2* **1989**, No. 12, 1953–1961. https://doi.org/10/b37gpz.

141. Tedder, J. M. Which Factors Determine the Reactivity and Regioselectivity of Free Radical Substitution and Addition Reactions? *Angewandte Chemie International Edition in English* **1982**, *21* (6), 401–410. https://doi.org/10/c9qb3g.

142. Paul, V.; Roberts, B. P. Polarity Reversal Catalysis of Hydrogen Atom Abstraction Reactions. *J. Chem. Soc., Chem. Commun.* **1987**, No. 17, 1322. https://doi.org/10/bdnpt6.
Lei, G.; Xu, M.; Chang, R.; Funes-Ardoiz, I.; Ye, J. Hydroalkylation of Unactivated Olefins via Visible-Light-Driven Dual Hydrogen Atom Transfer Catalysis. *J. Am. Chem. Soc.* **2021**, *143* (29), 11251–11261. https://doi.org/10/gk757j.

143. Arndtsen, B. A.; Bergman, R. G.; Mobley, T. A.; Peterson, T. H. Selective Intermolecular Carbon-Hydrogen Bond Activation by Synthetic Metal Complexes in Homogeneous Solution. *Acc. Chem. Res.* **1995**, *28* (3), 154–162. https://doi.org/10/brfk5v.

144. Morris, M.; Chan, B.; Radom, L. Effect of Protonation State and Interposed Connector Groups on Bond Dissociation Enthalpies of Alcohols and Related Systems. *J. Phys. Chem. A* **2014**, *118* (15), 2810–2819. https://doi.org/10/f5zqkk.

145. a) Chu, J. C. K.; Rovis, T. Amide-Directed Photoredox-Catalysed C–C Bond Formation at Unactivated Sp3 C–H Bonds. *Nature* **2016**, *539* (7628), 272–275. https://doi.org/10/f9b2mf.
b) Twilton, J.; Christensen, M.; DiRocco, D. A.; Ruck, R. T.; Davies, I. W.; MacMillan, D. W. C. Selective Hydrogen Atom Abstraction through Induced Bond Polarization: Direct α-Arylation of Alcohols through Photoredox, HAT, and Nickel Catalysis. *Angew. Chem. Int. Ed.* **2018**, *57* (19), 5369–5373. https://doi.org/10/gc95b3.
c) Ye, J.; Kalvet, I.; Schoenebeck, F.; Rovis, T. Direct α-Alkylation of Primary Aliphatic Amines Enabled by CO2 and Electrostatics. *Nature Chem* **2018**, *10* (10), 1037–1041. https://doi.org/10/gfbp4f.

146. Salamone, M.; Bietti, M. Tuning Reactivity and Selectivity in Hydrogen Atom Transfer from Aliphatic C–H Bonds to Alkoxyl Radicals: Role of Structural and Medium Effects. *Acc. Chem. Res.* **2015**, *48* (11), 2895–2903. https://doi.org/10/ghgc8k.

147. Dondi, D.; Ravelli, D.; Fagnoni, M.; Mella, M.; Molinari, A.; Maldotti, A.; Albini, A. Regio- and Stereoselectivity in the Decatungstate Photocatalyzed Alkylation of Alkenes by Alkylcyclohexanes. *Chemistry – A European Journal* **2009**, *15* (32), 7949–7957. https://doi.org/10/c5gjxv.
Oswood, C. J.; MacMillan, D. W. C. Selective Isomerization via Transient Thermodynamic Control: Dynamic Epimerization of *Trans* to *Cis* Diols. *J. Am. Chem. Soc.* **2022**, *144* (1), 93–98. https://doi.org/10/gnvqtt.

148. Ref [3a]

149. Ueda, M.; Kamikawa, K.; Fukuyama, T.; Wang, Y.-T.; Wu, Y.-K.; Ryu, I. Site-Selective Alkenylation of Unactivated C(Sp3)−H Bonds Mediated by Compact Sulfate Radical. *Angewandte Chemie International Edition* **2021**, *60* (7), 3545–3550. https://doi.org/10/gpfsj9.

150. Macmillan?

151. Sarkar, S.; Cheung, K. P. S.; Gevorgyan, V. C–H Functionalization Reactions Enabled by Hydrogen Atom Transfer to Carbon-Centered Radicals. *Chem. Sci.* **2020**, *11* (48), 12974–12993. https://doi.org/10/gqpj9q.

152. a) Duh, Y.-S.; Kao, C.-S.; Lee, W.-L. W. Chemical Kinetics on Thermal Decompositions of Di-Tert-Butyl Peroxide Studied by Calorimetry. *J Therm Anal Calorim* **2017**, *127* (1), 1071–1087. https://doi.org/10/f9ptf9.
b) Ueno, R.; Ikeda, Y.; Shirakawa, E. Tert-Butoxy-Radical-Promoted α-Arylation of Alkylamines with Aryl Halides. *European Journal of Organic Chemistry* **2017**, *2017* (28), 4188–4193. https://doi.org/10/gqpj9r.

153. Scaiano, J. C.; Wubbels, G. G. Photosensitized Dissociation of Di-Tert-Butyl Peroxide. Energy Transfer to a Repulsive Excited State. *J. Am. Chem. Soc.* **1981**, *103* (3), 640–645. https://doi.org/10/dss245.

154. Mayer, Ref 135, states that unpaired spin density is not always an indicator of HAT ability, noting TEMPO as an example as well as several other viable HAT reagents, however in the cases which we will consider, the abstracting agent has an unpaired spin.

155. Xiao, W.; Wang, X.; Liu, R.; Wu, J. Quinuclidine and Its Derivatives as Hydrogen-Atom-Transfer Catalysts in Photoinduced Reactions. *Chinese Chemical Letters* **2021**, *32* (6), 1847–1856. https://doi.org/10/gqpj9v.
Chen, D. F.; Chrisman, C. H.; Miyake, G. M. Bromine Radical Catalysis by Energy Transfer Photosensitization. *ACS Catalysis* **2020**, *10* (4), 2609–2614. https://doi.org/10/gqfdbm.
Wang, B.; Ascenzi Pettenuzzo, C.; Singh, J.; Mccabe, G. E.; Clark, L.; Young, R.; Pu, J.; Deng, Y. Photoinduced Site-Selective Functionalization of Aliphatic C–H Bonds by Pyridine N-Oxide Based HAT Catalysts. *ACS Catal.* **2022**, *12* (16), 10441–10448. https://doi.org/10/gqpj9s.
Schlegel, M.; Qian, S.; Nicewicz, D. A. Aliphatic C–H Functionalization Using Pyridine N-Oxides as H-Atom Abstraction Agents. *ACS Catal.* **2022**, *12* (16), 10499–10505. https://doi.org/10/gqpj9t.
Ciszewski, Ł.; Gryko, D. *Pyridine N-Oxides as HAT Reagents for Photochemical C-H Functionalization of Electron-Deficient Heteroarenes*; preprint; Chemistry, 2022. https://doi.org/10.26434/chemrxiv-2022-j348w.

156. a) Mayer, J. M. Proton-Coupled Electron Transfer: A Reaction Chemist's View. *Annual Review of Physical Chemistry* **2004**, *55*, 363–390. https://doi.org/10.1146/annurev.physchem.55.091602.094446.
b) Choi, G. J.; Zhu, Q.; Miller, D. C.; Gu, C. J.; Knowles, R. R. Catalytic Alkylation of Remote C-H Bonds Enabled by Proton-Coupled Electron Transfer. *Nature* **2016**, *539* (7628), 268–271. https://doi.org/10.1038/nature19811.
c) Chu, J. C. K.; Rovis, T. Amide-Directed Photoredox-Catalysed C-C Bond Formation at Unactivated Sp 3 C-H Bonds. *Nature* **2016**, *539* (7628), 272–275. https://doi.org/10.1038/nature19810.

157. Ma, Z. Y.; Li, M.; Guo, L. N.; Liu, L.; Wang, D.; Duan, X. H. Sulfonamide as Photoinduced Hydrogen-Atom Transfer Catalyst for Regioselective Alkylation of C(Sp3)-H Bonds Adjacent to Heteroatoms. *Organic Letters* **2021**, *23* (2), 474–479. https://doi.org/10/gjmx6h.

158. Mayer, J. M. Hydrogen Atom Abstraction by Metal−Oxo Complexes: Understanding the Analogy with Organic Radical Reactions. *Acc. Chem. Res.* **1998**, *31* (8), 441–450. https://doi.org/10/fsj8w8.

159. a) Mondal, P.; Pirovano, P.; Das, A.; Farquhar, E. R.; McDonald, A. R. Hydrogen Atom Transfer by a High-Valent Nickel-Chloride Complex. *J. Am. Chem. Soc.* **2018**, *140* (5), 1834–1841. https://doi.org/10/gcv58f.
b) An, Q.; Wang, Z.; Chen, Y.; Wang, X.; Zhang, K.; Pan, H.; Liu, W.; Zuo, Z. Cerium-Catalyzed C–H Functionalizations of Alkanes Utilizing Alcohols as Hydrogen Atom Transfer Agents. *J. Am. Chem. Soc.* **2020**, *142* (13), 6216–6226. https://doi.org/10/ggkstk.
c) Dai, Z.-Y.; Zhang, S.-Q.; Hong, X.; Wang, P.-S.; Gong, L.-Z. A Practical FeCl3/HCl Photocatalyst for Versatile Aliphatic C–H Functionalization. *Chem Catalysis* **2022**, *2* (5), 1211–1222. https://doi.org/10/ggkstb.

160. Both *i*-HAT and *d*-HAT were coined by Fagnoni in his review and we will use this notation for the thesis where appropriate:
Capaldo, L.; Ravelli, D.; Fagnoni, M. Direct Photocatalyzed Hydrogen Atom Transfer (HAT) for Aliphatic C-H Bonds Elaboration. *Chemical Reviews* **2021**. https://doi.org/10/gmf5np.

161. a) Jin, J.; MacMillan, D. W. C. Direct α-Arylation of Ethers through the Combination of Photoredox-Mediated C-H Functionalization and the Minisci Reaction. *Angewandte Chemie - International Edition* **2015**, *54* (5), 1565–1569. https://doi.org/10.1002/anie.201410432.
b) Huie, R. E.; Clifton, C. L.; Kafafi, S. A. Rate Constants for Hydrogen Abstraction Reactions of the Sulfate Radical, SO4-: Experimental and Theoretical Results for Cyclic Ethers. *J. Phys. Chem.* **1991**, *95* (23), 9336–9340. https://doi.org/10/bhg3gs.

162. McNally, A.; Prier, C. K.; MacMillan, D. W. C. Discovery of an α-Amino C–H Arylation Reaction Using the Strategy of Accelerated Serendipity. *Science* **2011**, *334* (6059), 1114–1117. https://doi.org/10/cbt4km.

163. Stevenson, B. G.; Spielvogel, E. H.; Loiaconi, E. A.; Wambua, V. M.; Nakhamiyayev, R. V.; Swierk, J. R. Mechanistic Investigations of an α-Aminoarylation Photoredox Reaction. *J. Am. Chem. Soc.* **2021**, *143* (23), 8878–8885. https://doi.org/10/gkcktf.

164. a) Dénès, F.; Pichowicz, M.; Povie, G.; Renaud, P. Thiyl Radicals in Organic Synthesis. *Chem. Rev.* **2014**, *114* (5), 2587–2693. https://doi.org/10/ghcdzj. Breder, A.; Depken, C. Light-Driven Single-Electron Transfer Processes as an Enabling Principle in Sulfur and Selenium Multicatalysis. *Angewandte Chemie International Edition* **2019**, *58* (48), 17130–17147. https://doi.org/10/gftqhq.
b) Pryor, W. A.; Gojon, G.; Church, D. F. Relative Rate Constants for Hydrogen Atom Abstraction by the Cyclohexanethiyl and Benzenethiyl Radicals. *J. Org. Chem.* **1978**, *43* (5), 793–800. https://doi.org/10/dd7xt3.
c) Pryor, W. A.; Gojon, G.; Stanley, J. P. Hydrogen Abstraction by Thiyl Radicals. *J. Am. Chem. Soc.* **1973**, *95* (3), 945–946. https://doi.org/10/czdsp2.
d) Schmidt, U. Free Radicals and Free-Radical Reactions of Monovalent and Divalent Sulfur. *Angew. Chem. Int. Ed. Engl.* **1964**, *3* (9), 602–608. https://doi.org/10/brkrp3.
e) Janssen, M. J. *Organosulfur Chemistry: Reviews of Current Research*; Interscience-Wiley: Chichester, 1967. pp 33.

165. Qvortrup, K.; Rankic, D. A.; MacMillan, D. W. C. A General Strategy for Organocatalytic Activation of C-h Bonds via Photoredox Catalysis: Direct Arylation of Benzylic Ethers. *Journal of the American Chemical Society* **2014**, *136* (2), 626–629. https://doi.org/10.1021/ja411596q.

166. Ochiai, M.; Yamane, S.; Hoque, Md. M.; Saito, M.; Miyamoto, K. Metal-Free α-CH Amination of Ethers with Hypervalent Sulfonylimino-Λ3-Bromane That Acts as an Active Nitrenoid. *Chem. Commun.* **2012**, *48* (43), 5280. https://doi.org/10/gqjp9x.

167. Hager, D.; Macmillan, D. W. C. Activation of C-H Bonds via the Merger of Photoredox and Organocatalysis: A Coupling of Benzylic Ethers with Schiff Bases. *Journal of the American Chemical Society* **2014**, *136* (49), 16986–16989. https://doi.org/10.1021/ja5102695.

168. Jin, J.; MacMillan, D. W. C. Alcohols as Alkylating Agents in Heteroarene C-H Functionalization. *Nature* **2015**, *525* (7567), 87–90. https://doi.org/10.1038/nature14885.

169. Jin, J.; MacMillan, D. W. C. Direct α-Arylation of Ethers through the Combination of Photoredox-Mediated C-H Functionalization and the Minisci Reaction. *Angewandte Chemie – International Edition* **2015**, *54* (5), 1565–1569. https://doi.org/10.1002/anie.201410432.

170. Shaw, M. H.; Shurtleff, V. W.; Terrett, J. A.; Cuthbertson, J. D.; MacMillan, D. W. C. Native Functionality in Triple Catalytic Cross-Coupling: Sp3 C-H Bonds as Latent Nucleophiles. *Science* **2016**, *352* (6291), 1304–1308. https://doi.org/10.1126/science.aaf6635.

171. Maity, B.; Zhu, C.; Yue, H.; Huang, L.; Harb, M.; Minenkov, Y.; Rueping, M.; Cavallo, L. Mechanistic Insight into the Photoredox-Nickel-HAT Triple Catalyzed Arylation and Alkylation of α-Amino Csp3–H Bonds. *J. Am. Chem. Soc.* **2020**, *142* (40), 16942–16952. https://doi.org/10.1021/jacs.0c05010.

172. Heitz, D. R.; Tellis, J. C.; Molander, G. A. Photochemical Nickel-Catalyzed C-H Arylation: Synthetic Scope and Mechanistic Investigations. *Journal of the American Chemical Society* **2016**, *138* (39), 12715–12718. https://doi.org/10/f86xmf.

173. Shields, B. J.; Doyle, A. G. Direct C(Sp3)-H Cross Coupling Enabled by Catalytic Generation of Chlorine Radicals. *Journal of the American Chemical Society* **2016**, *138* (39), 12719–12722. https://doi.org/10.1021/jacs.6b08397.

174. Ishida, N.; Masuda, Y.; Ishikawa, N.; Murakami, M. Cooperation of a Nickel–Bipyridine Complex with Light for Benzylic C−H Arylation of Toluene Derivatives. *Asian Journal of Organic Chemistry* **2017**, *6* (6), 669–672. https://doi.org/10/gqfdbt.

175. Simmons, E. M.; Hartwig, J. F. On the Interpretation of Deuterium Kinetic Isotope Effects in C-H Bond Functionalisations by Transition-Metal Complexes. *Angewandte Chemie International Edition* **2012**, *51* (13), 3066–3072. https://doi.org/10/fz4nqf.

176. a) Hwang, S. J.; Anderson, B. L.; Powers, D. C.; Maher, A. G.; Hadt, R. G.; Nocera, D. G. Halogen Photoelimination from Monomeric Nickel(III) Complexes Enabled by the Secondary Coordination Sphere. *Organometallics* **2015**, *34* (19), 4766–4774. https://doi.org/10/f7vbn6.
b) Hwang, S. J.; Powers, D. C.; Maher, A. G.; Anderson, B. L.; Hadt, R. G.; Zheng, S. L.; Chen, Y. S.; Nocera, D. G. Trap-Free Halogen Photoelimination from Mononuclear Ni(III) Complexes. *Journal of the American Chemical Society* **2015**, *137* (20), 6472–6475. https://doi.org/10.1021/jacs.5b03192.

177. Nielsen, M. K.; Shields, B. J.; Liu, J.; Williams, M. J.; Zacuto, M. J.; Doyle, A. G. Mild, Redox-Neutral Formylation of Aryl Chlorides through the Photocatalytic Generation of Chlorine Radicals. *Angewandte Chemie International Edition* **2017**, *56* (25), 7191–7194. https://doi.org/10/gpnft6.

178. Joe, C. L.; Doyle, A. G. Direct Acylation of C(sp3)−H Bonds Enabled by Nickel and Photoredox Catalysis. *Angewandte Chemie International Edition* **2016**, *55* (12), 4040–4043. https://doi.org/10/f3k339.

179. Griller, D.; Howard, J. A.; Marriott, P. R.; Scaiano, J. C. Absolute Rate Constants for the Reactions of Tert-Butoxyl, Tert-Butylperoxyl, and Benzophenone Triplet with Amines: The Importance of a Stereoelectronic Effect. *J. Am. Chem. Soc.* **1981**, *103* (3), 619–623. https://doi.org/10/dfpf99.

180 Huang, H.; Strater, Z. M.; Lambert, T. H. Electrophotocatalytic C-H Functionalization of Ethers with High Regioselectivity. *Journal of the American Chemical Society* **2020**, *142* (4), 1698–1703. https://doi.org/10.1021/jacs.9b11472.

181. Itoh, A. Quinones. In *Catalytic Science Series*; WORLD SCIENTIFIC (EUROPE), 2019; Vol. 18, pp 39–70. https://doi.org/10.1142/9781786346056_0002.

182. Yan, D.-M.; Chen, J.-R.; Xiao, W.-J. New Roles for Photoexcited Eosin Y in Photochemical Reactions. *Angewandte Chemie International Edition* **2019**, *58* (2), 378–380. https://doi.org/10/gp568h.

183. a) Jaynes, B. S.; Hill, C. L. Selective Ethylation and Vinylation of Alkanes via Polyoxotungstate Photocatalyzed Radical Addition Reactions. *J. Am. Chem. Soc.* **1993**, *115* (25), 12212–12213. https://doi.org/10/b2hnjq.
b) Dondi, D.; Fagnoni, M.; Albini, A. Tetrabutylammonium Decatungstate-Photosensitized Alkylation of Electrophilic Alkenes: Convenient Functionalization of Aliphatic C-H Bonds. *Chemistry - A European Journal* **2006**, *12* (15), 4153–4163. https://doi.org/10.1002/chem.200501216.
c) S.; Fagnoni, M. Decatungstate Anion for Photocatalyzed "Window Ledge" Reactions. *Acc. Chem. Res.* **2016**, *49* (10), 2232–2242. https://doi.org/10.1021/acs.accounts.6b00339.

184. Wagner, P. J. Chemistry of Excited Triplet Organic Carbonyl Compounds. In *Triplet States III*; Topics in Current Chemistry; Springer-Verlag: Berlin/Heidelberg, 1976; Vol. 66, pp 1–52. https://doi.org/10.1007/BFb0047763.

185. a) Bäckström, H. L. J.; Sandros, K.; Lindgren, J.-E.; Varde, E.; Westin, G. Transfer of Triplet State Energy in Fluid Solutions. I. Sensitized Phosphorescence and Its Application to the Determination of Triplet State Lifetimes. *Acta Chem. Scand.* **1960**, *14*, 48–62. https://doi.org/10/fqjk9b.
b) Moore, W. M.; Hammond, G. S.; Foss, R. P. Mechanisms of Photoreactions in Solutions. I. Reduction of Benzophenone by Benzhydrol. *J. Am. Chem. Soc.* **1961**, *83* (13), 2789–2794. https://doi.org/10/dcw3nf.

186. a) Castro, G.; Blanco, S.; Giordano, O. UV Spectral Properties of Benzophenone. Influence of Solvents and Substituents. *Molecules* **2000**, *5* (12), 424–425. https://doi.org/10/d96tgd.
b) Venkatraman, R. K.; Orr-Ewing, A. J. Photochemistry of Benzophenone in Solution: A Tale of Two Different Solvent Environments. *J. Am. Chem. Soc.* **2019**, *141* (38), 15222–15229. https://doi.org/10/gqffj2.

187. The n→pi* transition hypsochromic shift with increasing polarity has been used to identify these transitions for some time. The underlying principle is the increased solvent polarity stabilises the ground state and/or destabilises the "Franck-Condon excited state" which is the excited state upon excitation of the electron, *before* the rearrangement of the solvent cage.

188. Hoffmann, R.; Swenson, J. R. Ground- and Excited-State Geometries of Benzophenone. *J. Phys. Chem.* **1970**, *74* (2), 415–420. https://doi.org/10/b7pntx.

189. Wilkinson, F.; Kelly, G. P.; Ferreira, L. F. V.; Freire, V. M. M. R.; Ferreira, M. I. Benzophenone Sensitization of Triplet Oxazine and of Delayed Fluorescence by Oxazine in Acetonitrile Solution. *Faraday Trans.* **1991**, *87* (4), 547. https://doi.org/10/bktvhr.

190. Gersdorf, J.; Mattay, J.; Goerner, H. Radical Cations. 3. Photoreactions of Biacetyl, Benzophenone, and Benzil with Electron-Rich Alkenes. *J. Am. Chem. Soc.* **1987**, *109* (4), 1203–1209. https://doi.org/10.1021/ja00238a033.
Shoute, L. C. T.; Huie, R. E. Reactions of Triplet Decafluorobenzophenone with Alkenes. A Laser Flash Photolysis Study. *J. Phys. Chem. A* **1997**, *101* (19), 3467–3471. https://doi.org/10/b6rk2h.
Li, H.-F.; Cao, W.; Ma, X.; Xie, X.; Xia, Y.; Ouyang, Z. Visible-Light-Driven [2 + 2] Photocycloadditions between Benzophenone and C═C Bonds in Unsaturated Lipids. *J. Am. Chem. Soc.* **2020**, *142* (7), 3499–3505. https://doi.org/10/gqpkbf.

191. Walling, Cheves.; Gibian, M. J. Hydrogen Abstraction by the Triplet State of Benzophenone. *J. Am. Chem. Soc.* **1964**, *86* (18), 3902–3903. https://doi.org/10/cgqms8.

192. a) Pitts, J. N.; Letsinger, R. L.; Taylor, R. P.; Patterson, J. M.; Recktenwald, G.; Martin, R. B. Photochemical Reactions of Benzophenone in Alcohols. *J. Am. Chem. Soc.* **1959**, *81* (5), 1068–1077. https://doi.org/10/d2bhqn.
b) Hammond, G. S.; Turro, N. J. Organic Photochemistry. *Science* **1963**, *142* (3599), 1541–1553. https://doi.org/10/d4pgc8.

193. Cohen, S. G.; Parola, A.; Parsons, G. H. Photoreduction by Amines. *Chem. Rev.* **1973**, *73* (2), 141–161. https://doi.org/10/fj98hj.

194. The first reported example: Cookson, R. C.; Hudec, J.; Mirza, N. A. Photochemical Addition of Amines to Conjugated Olefins. *Chem. Commun. (London)* **1968**, No. 4, 180a. https://doi.org/10/bjqhf6.

a) Bertrand, S.; Hoffmann, N.; Pete, J.-P. Highly Efficient and Stereoselective Radical Addition of Tertiary Amines to Electron-Deficient Alkenes − Application to the Enantioselective Synthesis of Necine Bases. *European Journal of Organic Chemistry* **2000**, *2000* (12), 2227–2238. https://doi.org/10/dmrxmk.
b) Cossy, J.; Belotti, D. Generation of Ketyl Radical Anions by Photoinduced Electron Transfer (PET) between Ketones and Amines. Synthetic Applications. *Tetrahedron* **2006**, *62* (27), 6459–6470. https://doi.org/10/ddx7ht.
c) Bertrand, S.; Glapski, C.; Hoffmann, N.; Pete, J.-P. Highly Efficient Photochemical Addition of Tertiary Amines to Electron Deficient Alkenes. Diastereoselective Addition to (5R)-5-Menthyloxy-2[5H]-Furanone. *Tetrahedron Letters* **1999**, *40* (16), 3169–3172. https://doi.org/10/dsqfkj.
d) Bertrand, S.; Hoffmann, N.; Humbel, S.; Pete, J. P. Diastereoselective Tandem Addition−Cyclization Reactions of Unsaturated Tertiary Amines Initiated by Photochemical Electron Transfer (PET). *J. Org. Chem.* **2000**, *65* (25), 8690–8703. https://doi.org/10/cs2bnj.
e) Photocatalysed Addition of Pyrrolidines to Butenolides: a Concise Synthesis of…

195. Amaoka, Y.; Nagatomo, M.; Watanabe, M.; Tao, K.; Kamijo, S.; Inoue, M. Photochemically Induced Radical Alkenylation of C(Sp3)–H Bonds. *Chem. Sci.* **2014**, *5* (11), 4339–4345. https://doi.org/10/gqjwf7.

196. Paul, S.; Guin, J. Radical C(Sp3)-H Alkenylation, Alkynylation and Allylation of Ethers and Amides Enabled by Photocatalysis. *Green Chemistry* **2017**, *19* (11), 2530–2534. https://doi.org/10/gfwnh2.

197. Xia, J.; Zhu, C.; Chen, C. Visible Light-Promoted Metal-Free C–H Activation: Diarylketone-Catalyzed Selective Benzylic Mono- and Difluorination. *Journal of the American Chemical Society* **2013**, *135* (46), 17494–17500. https://doi.org/10/f5jpt9.

198. a) Chow, Y. L.; Buono-Core, G. E. Photoreduction of Bis(Acetylacetonato)Nickel(II) Sensitized by Triplet State Ketones. *J. Chem. Soc., Chem. Commun.* **1985**, No. 9, 592–594. https://doi.org/10/fq7xg5.
b) Chow, Y. L.; Buono-Core, G. E.; Lee, C. W. B.; Scaiano, J. C. Sensitized Photoreduction of Bis(Acetylacetonato)Nickel(II) by Triplet-State Aromatic Ketones. *J. Am. Chem. Soc.* **1986**, *108* (24), 7620–7627. https://doi.org/10/djphgf.

199. Masuda, Y.; Ishida, N.; Murakami, M. Aryl Ketones as Single-Electron-Transfer Photoredox Catalysts in the Nickel-Catalyzed Homocoupling of Aryl Halides. *European Journal of Organic Chemistry* **2016**, *2016* (35), 5822–5825. https://doi.org/10/f3shn7.

200. Shen, Y.; Gu, Y.; Martin, R. Sp3 C-H Arylation and Alkylation Enabled by the Synergy of Triplet Excited Ketones and Nickel Catalysts. *Journal of the American Chemical Society* **2018**, *140* (38), 12200–12209. https://doi.org/10.1021/jacs.8b07405.

201 (a) Kalinowski, M. K.; Grabowski, Z. R.; Pakula, B. Reactivity of Ketyl Free Radicals. Part 1.-Acid Dissociation of Aromatic Ketyls and Pinacols. Trans. Faraday. Soc., 1966, 62, 918.
(b) Lund, T.; Wayner, D. D. M. Jonsson, M.; Larsen, A.; Daasbjerg, K. Oxidation Potentials of a-Hydroxyl Radicals in Acetonitrile Obtained by Photomodulated Voltammetry. J. Am. Chem. Soc. 2001, 123, 12590.
(b) Tang, X.; Studer, A. Alkene 1,2-Difuntionalization by Radical Alkenyl Migration. Angew. Chem. Int. Ed. 2018, 57, 814.

202. There is an alternative mechanism which avoids the full reduction to the Ni(0) intermediate. Ni(0) has been proposed to be unfavourable in some scenarios. The alternative mechanistic pathway proceeds via a single electron reduction from nickel (II) to form a nickel (I) intermediate. Oxidative addition to form a Ni(III) species, and reduction to nickel (II) by the ketyl radical, nickel (II) can intercept the THF radical and reductive elimination affords the product and regenerates Ni(I).

203. Dewanji, A.; Krach, P. E.; Rueping, M. The Dual Role of Benzophenone in Visible-Light/Nickel Photoredox-Catalyzed C−H Arylations: Hydrogen-Atom Transfer and Energy Transfer. *Angewandte Chemie International Edition* **2019**, *58* (11), 3566–3570. https://doi.org/10.1002/ANIE.201901327.

204. a) Krach, P. E.; Dewanji, A.; Yuan, T.; Rueping, M. Synthesis of Unsymmetrical Ketones by Applying Visible-Light Benzophenone/Nickel Dual Catalysis for Direct Benzylic Acylation. *Chem. Commun.* **2020**, *56* (45), 6082–6085. https://doi.org/10/ggkt49
b) Ren, C.-C.; Wang, T.-Q.; Zhang, Y.; Peng, D.; Liu, X.-Q.; Wu, Q.-A.; Liu, X.-F.; Luo, S.-P. Photoinduced Activation of Unactivated C(Sp3)-H Bonds and Acylation Reactions. *ChemistrySelect* **2021**, *6* (10), 2523–2528. https://doi.org/10/ggkt46.

205. Campbell, M. W.; Yuan, M.; Polites, V. C.; Gutierrez, O.; Molander, G. A. Photochemical C–H Activation Enables Nickel-Catalyzed Olefin Dicarbofunctionalization. *J. Am. Chem. Soc.* **2021**, *143* (10), 3901–3910. https://doi.org/10.1021/jacs.0c13077.

206. Huo, H.; Shen, X.; Wang, C.; Zhang, L.; Röse, P.; Chen, L. A.; Harms, K.; Marsch, M.; Hilt, G.; Meggers, E. Asymmetric Photoredox Transition-Metal Catalysis Activated by Visible Light. *Nature* **2014**, *515* (7525), 100–103. https://doi.org/10.1038/nature13892.

207. Proctor, R. S. J.; Chuentragool, P.; Colgan, A. C.; Phipps, R. J. Hydrogen Atom Transfer-Driven Enantioselective Minisci Reaction of Amides. *J. Am. Chem. Soc.* **2021**, *143* (13), 4928–4934. https://doi.org/10.1021/jacs.1c01556.

208. Großkopf, J.; Plaza, M.; Seitz, A.; Breitenlechner, S.; Storch, G.; Bach, T. Photochemical Deracemization at Sp3-Hybridized Carbon Centers via a Reversible Hydrogen Atom Transfer. *J. Am. Chem. Soc.* **2021**, *143* (50), 21241–21245. https://doi.org/10/gqpj9p.

209. *Asymmetric Functionalization of C-H Bonds*; You, S.-L., Ed.; RSC catalysis series; Royal Society of Chemistry: Cambridge, UK, 2015.

210. Davies, H. M. L.; Hansen, T.; Churchill, M. R. Catalytic Asymmetric C-H Activation of Alkanes and Tetrahydrofuran. *Journal of the American Chemical Society* **2000**, *122* (13), 3063–3070. https://doi.org/10.1021/ja994136c.

211. Ahneman, D. T.; Doyle, A. G. C-H Functionalization of Amines with Aryl Halides by Nickel-Photoredox Catalysis. *Chemical Science* **2016**, *7* (12), 7002–7006. https://doi.org/10/f9ksnv.

212. Zhang, C.; Li, Z. L.; Gu, Q. S.; Liu, X. Y. Catalytic Enantioselective C(Sp 3)–H Functionalization Involving Radical Intermediates. *Nature Communications* **2021**, *12* (1). https://doi.org/10/gjjh5c.

213. Cheng, X.; Lu, H.; Lu, Z. Enantioselective Benzylic C–H Arylation via Photoredox and Nickel Dual Catalysis. *Nature Communications* **2019**, *10* (1), 1–7. https://doi.org/10/gh53wd.

214. Zhang, W.; Shu, X.; Huan, L.; Cheng, B.; Huo, H. Enantioselective β-C(Sp 3)–H Arylation of Amides *via* Synergistic Nickel and Photoredox Catalysis. *Org. Biomol. Chem.* **2021**, *19* (43), 9407–9409. https://doi.org/10/gnhn2x.

215 Cheng, X.; Li, T.; Liu, Y.; Lu, Z. Stereo- and Enantioselective Benzylic C–H Alkenylation via Photoredox/Nickel Dual Catalysis. *ACS Catal.* **2021**, *11* (17), 11059–11065. https://doi.org/10/gmnmcb.

216. Xu, J.; Li, Z.; Xu, Y.; Shu, X.; Huo, H. Stereodivergent Synthesis of Both *Z* - and *E* -Alkenes by Photoinduced, Ni-Catalyzed Enantioselective C(Sp 3)–H Alkenylation. *ACS Catal.* **2021**, *11* (21), 13567–13574. https://doi.org/10/gnhn2z.

217. The authors highlight the elegant works of Yoon and Meyer:
a) Farney, E. P.; Chapman, S. J.; Swords, W. B.; Torelli, M. D.; Hamers, R. J.; Yoon, T. P. Discovery and Elucidation of Counteranion Dependence in Photoredox Catalysis. *J. Am. Chem. Soc.* **2019**, *141* (15), 6385–6391. https://doi.org/10/gqkvjw.
b) Li, G.; Swords, W. B.; Meyer, G. J. Bromide Photo-Oxidation Sensitized to Visible Light in Consecutive Ion Pairs. *J. Am. Chem. Soc.* **2017**, *139* (42), 14983–14991. https://doi.org/10/gqkvjx.

218. Ananikov, V. P. Nickel: The "Spirited Horse" of Transition Metal Catalysis. *ACS Catal.* **2015**, *5* (3), 1964–1971. https://doi.org/10/gjs84r.

219. Shu, X.; Huan, L.; Huang, Q.; Huo, H. Direct Enantioselective C(Sp3)–H Acylation for the Synthesis of α-Amino Ketones. *J. Am. Chem. Soc.* **2020**, *142* (45), 19058–19064. https://doi.org/10/gj2mtj.

220. Huan, L.; Shu, X.; Zu, W.; Zhong, D.; Huo, H. Asymmetric Benzylic C(Sp3)−H Acylation via Dual Nickel and Photoredox Catalysis. *Nat Commun* **2021**, *12* (1), 3536. https://doi.org/10/gkhvmv.

221. Kawasaki, T.; Yamazaki, K.; Tomono, R.; Ishida, N.; Murakami, M. Photoinduced Carbamoylation of C(Sp3)–H Bonds with Isocyanates. *Chem. Lett.* **2021**, *50* (9), 1684–1687. https://doi.org/10/gqh73m.

222. Shu, X.; Zhong, D.; Lin, Y.; Qin, X.; Huo, H. Modular Access to Chiral α-(Hetero)Aryl Amines via Ni/Photoredox-Catalyzed Enantioselective Cross-Coupling. *J. Am. Chem. Soc.* **2022**, *144* (19), 8797–8806. https://doi.org/10/gqh73n.

223. a) Connon, R.; Roche, B.; Rokade, B. V.; Guiry, P. J. Further Developments and Applications of Oxazoline-Containing Ligands in Asymmetric Catalysis. *Chem. Rev.* **2021**, *121* (11), 6373–6521. https://doi.org/10/gj5kjd.
b) Bausch, C. C.; Pfaltz, A. PHOX Ligands. In *Privileged Chiral Ligands and Catalysts*; John Wiley & Sons, Ltd, 2011; pp 221–256. https://doi.org/10.1002/9783527635207.ch6.

224. Cabré, A.; Riera, A.; Verdaguer, X. P-Stereogenic Amino-Phosphines as Chiral Ligands: From Privileged Intermediates to Asymmetric Catalysis. *Acc. Chem. Res.* **2020**, *53* (3), 676–689. https://doi.org/10/gqkvjr.

225. Synthesised by visiting student Pascal Eisele.

226. Naguib, Y. M. A.; Steel, Colin.; Cohen, S. G.; Young, M. A. Photoreduction of Benzophenone by Acetonitrile: Correlation of Rates of Hydrogen Abstraction from RH with the Ionization Potentials of the Radicals R.Cntdot. *J. Phys. Chem.* **1987**, *91* (11), 3033–3036. https://doi.org/10/cgwxhr.

227. Side reaction of radical addition into acetonitrile and α-arylation of acetone.
a) Engel, P. S.; Lee, W. K.; Marschke, G. E.; Shine, H. J. The Reactions of 1-Adamantyl Radicals with Acetonitrile and Their Bearing on the Oxidative Decomposition of 1,1'-Azoadamantane. *J. Org. Chem.* **1987**, *52* (13), 2813–2817. https://doi.org/10/cz5vhf.
b) Derhamine, S. A.; Krachko, T.; Monteiro, N.; Pilet, G.; Schranck, J.; Tlili, A.; Amgoune, A. Nickel-Catalyzed Mono-Selective α-Arylation of Acetone with Aryl Chlorides and Phenol Derivatives. *Angewandte Chemie International Edition* **2020**, *59* (43), 18948–18953. https://doi.org/10/gqpkbk.

228. Using Chloride and iodide salts have liberated the aryl chloride or iodide from the aryl bromide.

229. a) Ortica, F.; Romani, A.; Favaro, G. Light-Induced Hydrogen Abstraction from Isobutanol by Thienyl Phenyl, Dithienyl, and Thienyl Pyridyl Ketones. *J. Phys. Chem. A* **1999**, *103* (10), 1335–1341. https://doi.org/10/dbkmbc.
b) Wagner, P. J.; Kemppainen, A. E.; Schott, H. N. Effects of Ring Substituents on the Type II Photoreactions of Phenyl Ketones. How Interactions between Nearby Excited Triplets Affect Chemical Reactivity. *J. Am. Chem. Soc.* **1973**, *95* (17), 5604–5614. https://doi.org/10/bc5zb6.
c) Cavaleri, J. J.; Prater, K.; Bowman, R. M. An Investigation of the Solvent Dependence on the Ultrafast Intersystem Crossing Kinetics of

Xanthone. *Chemical Physics Letters* **1996**, *259* (5–6), 495–502. https://doi.org/10/fv5np8.
d) Naguib, Y. M. A.; Steel, Colin.; Cohen, S. G.; Young, M. A. Photoreduction of Benzophenone by Acetonitrile: Correlation of Rates of Hydrogen Abstraction from RH with the Ionization Potentials of the Radicals R.Cntdot. *J. Phys. Chem.* **1987**, *91* (11), 3033–3036. https://doi.org/10/cgwxhr.
e) Bhasikuttan, A. C.; Singh, A. K.; Palit, D. K.; Sapre, A. V.; Mittal, J. P. Laser Flash Photolysis Studies on the Monohydroxy Derivatives of Benzophenone. *J. Phys. Chem. A* **1998**, *102* (20), 3470–3480. https://doi.org/10/b2vswh.
f) Galian, R. E.; Litwinienko, G.; Pérez-Prieto, J.; Ingold, K. U. Kinetic Solvent Effects on the Reaction of an Aromatic Ketone π,Π* Triplet with Phenol. Rate-Retarding and Rate-Accelerating Effects of Hydrogen-Bond Acceptor Solvents. *J. Am. Chem. Soc.* **2007**, *129* (30), 9280–9281. https://doi.org/10/dd7xz7.

230. Natarajan, P. Quenching of Benzophenone Triplets by Naphthalene. A Physical-Organic Chemistry Experiment. *J. Chem. Educ.* **1976**, *53* (3), 200. https://doi.org/10/cn2zwt.

231. a) Schmid, L.; Glaser, F.; Schaer, R.; Wenger, O. S. High Triplet Energy Iridium(III) Isocyanoborato Complex for Photochemical Upconversion, Photoredox and Energy Transfer Catalysis. *J. Am. Chem. Soc.* **2022**, *144* (2), 963–976. https://doi.org/10/gqffmf.
b) Leigh, W. J.; Arnold, D. R.; Humphreys, R. W. R.; Wong, P. C. Merostabilization in Radical Ions, Triplets, and Biradicals. 4. Substituent Effects on the Half-Wave Reduction Potentials and *n* ,π* Triplet Energies of Aromatic Ketones. *Can. J. Chem.* **1980**, *58* (23), 2537–2549. https://doi.org/10/cq2bv6.

232. a) Granados, A.; Cabrera-Afonso, M. J.; Escolano, M.; Badir, S. O.; Molander, G. A. Thianthrenium-Enabled Sulfonylation via Electron Donor-Acceptor Complex Photoactivation. *Chem Catalysis* **2022**, *2* (4), 898–907. https://doi.org/10/gqp2t2.
b) Majhi, J.; Dhungana, R. K.; Rentería-Gómez, Á.; Sharique, M.; Li, L.; Dong, W.; Gutierrez, O.; Molander, G. A. Metal-Free Photochemical Imino-Alkylation of Alkenes with Bifunctional Oxime Esters. *J. Am. Chem. Soc.* **2022**, jacs.2c07170. https://doi.org/10/gqp2tx.
c) Laudadio, G.; Govaerts, S.; Wang, Y.; Ravelli, D.; Koolman, H. F.; Fagnoni, M.; Djuric, S. W.; Noël, T. Selective C(Sp3)−H Aerobic Oxidation Enabled by Decatungstate Photocatalysis in Flow. *Angewandte Chemie International Edition* **2018**, *57* (15), 4078–4082. https://doi.org/10/gc5tjb.
d) Laudadio, G.; Deng, Y.; van der Wal, K.; Ravelli, D.; Nuño, M.; Fagnoni, M.; Guthrie, D.; Sun, Y.; Noël, T. C(Sp3)–H Functionalizations of Light Hydrocarbons Using Decatungstate Photocatalysis in Flow. *Science* **2020**, *369* (6499), 92–96. https://doi.org/10/gpm4sz.

233. a) Ref 92.
b) Ishida, N.; Masuda, Y.; Sun, F.; Kamae, Y.; Murakami, M. A Strained Vicinal Diol as a Reductant for Coupling of Organyl Halides. *Chem. Lett.* **2019**, *48* (9), 1042–1045. https://doi.org/10/gqpkbm.

234. Hoffmann, N.; Görner, H. Photoinduced Electron Transfer from N-Methylpyrrolidine to Ketones and Radical Addition to an Electron-Deficient Alkene. *Chemical Physics Letters* **2004**, *383* (5–6), 451–455. https://doi.org/10/dzf6j4.

235. Shen, Y.; Gu, Y.; Martin, R. Sp3 C-H Arylation and Alkylation Enabled by the Synergy of Triplet Excited Ketones and Nickel Catalysts. *Journal of the American Chemical Society* **2018**, *140* (38), 12200–12209. https://doi.org/10.1021/jacs.8b07405.

236. García-Barrantes, P. M.; Lamoureux, G. V.; Pérez, A. L.; García-Sánchez, R. N.; Martínez, A. R.; San Feliciano, A. Synthesis and Biological Evaluation of Novel Ferrocene–Naphthoquinones as Antiplasmodial Agents. *European Journal of Medicinal Chemistry* **2013**, *70*, 548–557. https://doi.org/10/f5rj3t.

237. Rawe, B. W.; Brown, C. M.; MacKinnon, M. R.; Patrick, B. O.; Bodwell, G. J.; Gates, D. P. A C-Pyrenyl Poly(Methylenephosphine): Oxidation “Turns On” Blue Photoluminescence in Solution and the Solid State. *Organometallics* **2017**, *36* (14), 2520–2526. https://doi.org/10/gbssvp.

238. Zippel, C.; Hassan, Z.; Parsa, A. Q.; Hohmann, J.; Bräse, S. Multigram-Scale Kinetic Resolution of 4-Acetyl[2.2]Paracyclophane *via* Ru-Catalyzed Enantioselective Hydrogenation: Accessing [2.2]Paracyclophanes with Planar and Central Chirality. *Adv. Synth. Catal.* **2021**, *363* (11), 2861–2865. https://doi.org/10/gqpr8r.

UNIVERSITAT ROVIRA I VIRGILI
CATALYTIC TRANSFORMATIONS ENABLED BY DUAL NICKELPHOTOREDOX MANIFOLDS
Bradley Higginson

UNIVERSITAT ROVIRA I VIRGILI
CATALYTIC TRANSFORMATIONS ENABLED BY DUAL NICKELPHOTOREDOX MANIFOLDS
Bradley Higginson

CHAPTER 3.

C(sp3)-H functionalisation of allyic C-H bonds

This work was completed in collaboration with
Dr Mikkel B. Buendia from DTH
Published in: ACS Catal. 2022, 12, 7, 3815–3820

Allylic C-H

3.1. Introduction

3.1.1. General

Accessed on gigaton scales by ethylene oligomerisation, terminal olefins are versatile feedstock chemicals used as precursors to industrially relevant materials.[240] The abundance of terminal olefins means they are commonly used as a platform in academic laboratories to assess new methods to produce value added chemicals.[241] Typical approaches to olefin functionalisation rely on the innate reactivity of the C=C bond present (Figure 3.1.1),[242] with important examples including metathesis (**103**),[243] hydro-functionalisation (**104** or **Y = H**),[244] and di-functionalisation (**104, X** and **Y** ≠ H).[245] Complementary to the aforementioned synthetic techniques is the allylic C(sp^3)-H functionalisation manifold (**105**). Allylic C(sp^3)-H functionalisation can be divided into two classes, carbon-heteroatom bond (C-X) and carbon-carbon bond (C-C) forming reactions. Allylic C-X bond forming reactions have been widely studied,[246] with oxidation of allylic C(sp^3)-H bonds receiving substantial attention.[247] In contrast to C-X construction from allylic C(sp^3)-H bonds, C-C bond formation is somewhat less developed.

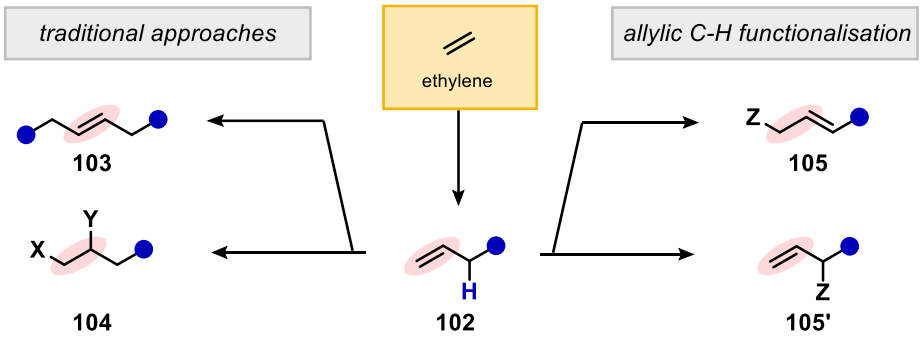

Figure 3.1.1. Formation and chemical manipulation of terminal olefins.

The functionalisation at the allylic position is more facile than simple alkanes because of the presence of the unsaturated system. The π system has a number of effects, the first is the lowered BDE of the C(sp^3)-H bond (83 kcal mol^{-1}) when compared to an unfunctionalized secondary alkyl C(sp^3)-H (97 kcal mol^{-1}), the stabilisation of the radical through the pi system is responsible for this lower BDE.

Secondly, the π system also reduces the pKa value of the allylic C(sp^3)-H (pKa = 44), allowing for strong bases to deprotonate this site, reactivity of both the radical or anion generated can delocalise through the π system to give the terminal **102c** or retained products **102c'**. Finally, the unsaturated system can coordinate to, and facilitate interactions with, transition metal centres. The coordination to a metal centre can further lower the pKa of the C(sp^3)-H bond.

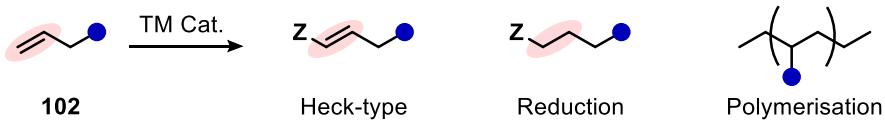

Figure 3.1.2. Chemoselectivity issues associated with the double bond.

Although the presence of the double bond increases the reactivity of the allylic C(sp^3)-H bond, it also introduces a number of problems. A system that is reactive enough to functionalise the C(sp^3)-H bond may also undergo reactivity at the olefin such as the formal C(sp^2)-H functionalisation of the olefin,[248] or hydrofunctionalisation. Additionally, it is well known that transition metals can form polymers from olefins (Figure 3.1.2).[249] These deleterious side reactions can have a significant impact on the overall selectivity of the C(sp^3)-H functionalisation. However, the complementarity of allylic C(sp^3)-H functionalisation cannot be understated, by retaining the versatile olefin functionality, downstream synthetic applications are retained.

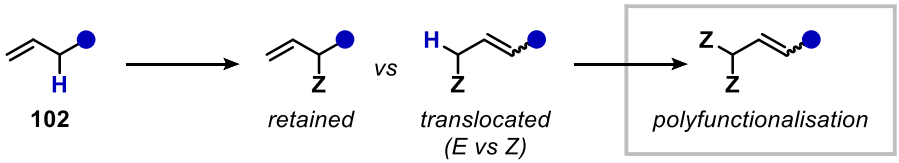

Figure 3.1.3. Regioselectivity issues associated with allylic C(sp^3)-H functionalisation

Outside of biasing chemoselectivity towards C-C bond formation at the allylic C(sp^3)-H position over other reactivity sites, the issue of product isomerization must still be addressed. Reactive intermediates formed at the allylic site can delocalise across the π-system, which may result in possible bond forming reactions at two positions: either the initial C(sp^3)-H site (*retained*) or at the terminal position (*translocated*). Furthermore, in the case of the translocated product geometric isomerization is present between its E and Z forms. Finally, the olefin is also present in the products of the reaction which can lead to overreaction if stoichiometry or reactivity is not controlled effectively (Figure 3.1.3).

Despite these difficulties, the synthetic community has developed some excellent approaches to enable this transformation. We will primarily focus on the formation of C(sp^3)-C(sp^3) bond forming reactions, although where relevant C(sp^3)-C(sp^2) bond forming reaction will also be detailed.

Allylic C-H

3.1.2. Metal-catalysed oxidative coupling

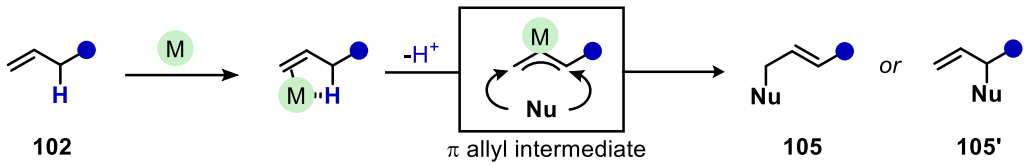

Figure 3.1.4. Seminal work by trost (top), C-C bond formation by π-allyl activation of allylic C(sp³)-H bonds (bottom).

Transition metal catalysed allylic alkylation is a broad field of study, the coordination of a metal to the alkene can greatly acidify the allylic proton allowing for facile deprotonation or activation by a metal centre (Figure 3.1.4).

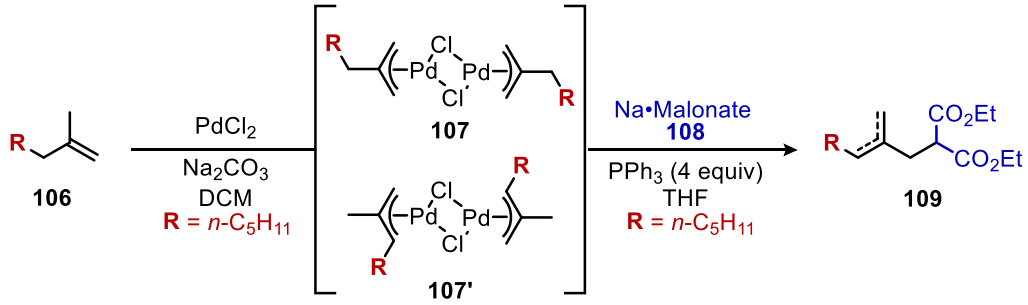

Figure 3.1.5. Stoichiometric studies by Trost are among the first allylic C(sp³)-H functionalisations.

The first example of this was observed by Trost in 1973 (Figure 3.1.5),[250] stoichiometric palladium dichloride reacts with one equivalent of olefin (**106**) in the presence of sodium carbonate to generate a mixture of allylpalladium species (**107:107',** 38:62). Exposing this mixture to sodium malonate (**108**) and four equivalents of PPh_3 yields a mixture of the allylic alkylation products (**109**, 63% yield). This seminal work has led to considerable development by the community, with fundamental works by Bäckvall and Darlington being highly influential.[251] Expanding the scope of nucleophilic partners and developing enantioselective variants.

Historically the reaction required stoichiometric palladium due to difficulties surrounding the reoxidation of the palladium but individual reports by White and Shi in 2008 unlocked a catalytic version by employing a stoichiometric oxidant and sulfoxide-based ligands.[252] Although advances in this technique have been made,[253] there are still some limitations to this approach. For example, only weakly nucleophilic species are employed in this reaction, enolate-type chemistry. This is most likely due to the necessary binding of the olefin to the metal centre which could be displaced by stronger nucleophilic species. Although there are limitations to the pi-allyl approach with palladium, the overarching idea to use the coordination of the olefin to a metal centre has been employed in several scenarios.[254]

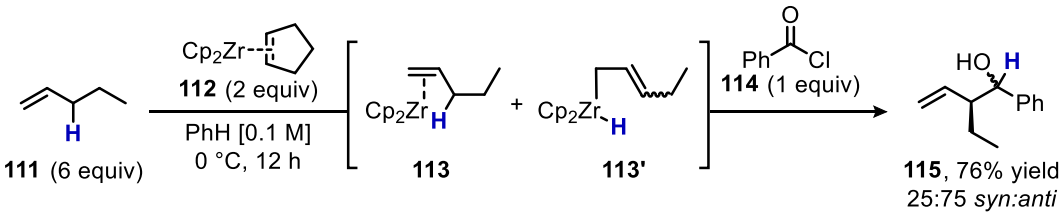

Figure 3.1.6. Nucleophilic allylic C(sp³)-H functionalisation technique with zircocene.

Additionally, whilst many π-allyl species are electrophilic, techniques to enable a nucleophilic π-allyl species have been developed, Oshima and co-workers demonstrated this in 2004 (Figure 3.1.6).[255] Terminal olefin **111** displaces the cyclopentene at zirconocene **112** to form two Zr-olefin species that are in equilibria, **113** and **113'**. Reaction with benzoyl chloride affords the homo-allylic product **115** in high yields and reasonable regioselectivities. Other limited classes of allylic C(sp³)-H alkylation have been developed for example the copper catalysed trifluoromethylation.[256] Additionally, the use of metal carbenes have been used to enable C(sp³)-H functionalisation across a broad range of C(sp³)-H bonds and have also seen extension to the allylic C(sp³)-H bond.[257]

3.1.3. Preoxidation

Although the reactivity of the allylic C(sp³)-H bond is greater than a simple alkyl C(sp³)-H bonds, it is still not too reactive. Preoxidation of terminal olefins using a highly selective oxidant to generate a more reactive intermediate could enable a much broader range of reactions to be accessed. To this end Tambar and co-workers employed a novel sulfinamide oxidant (**117**) in a two-step approach to the functionalisation of allylic C(sp³)-H bonds (Figure 3.1.7).[258]

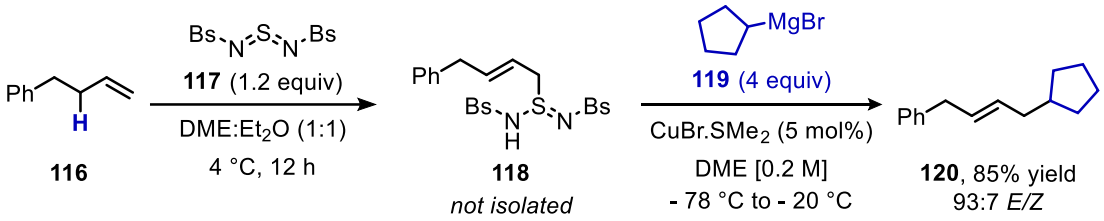

Figure 3.1.7. Tambar and co-workers terminal selective allylic C(sp³)-H functionalisation

The initial oxidation of terminal olefin **116** by sulfinamide forms the activated allylic species (**118**). **118** then undergoes a copper catalysed coupling with Grignard reagents (**119**) to form the alkylated olefin **120** at the *translocated* site with high regioselectivities and E:Z ratios.

Allylic C-H

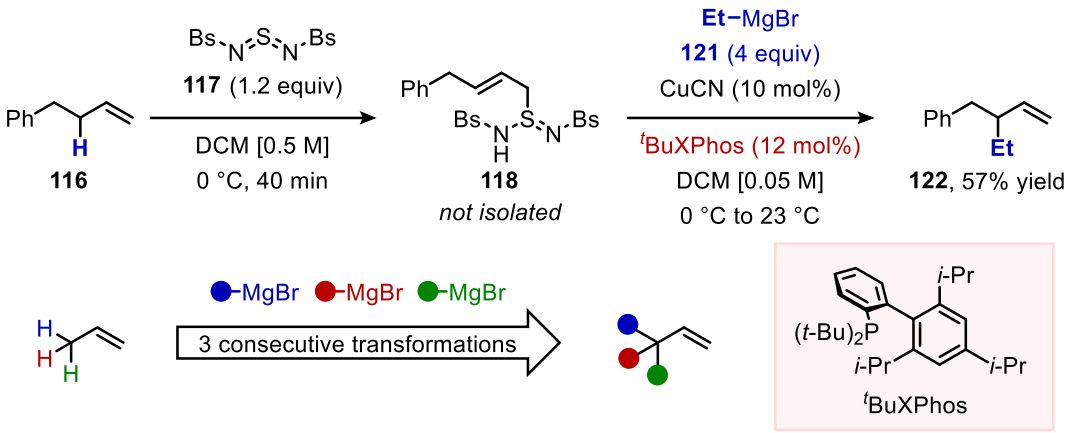

Figure 3.1.8. Retained allylic C(sp^3)-H functionalisation developed by Tambar

In 2019 Tambar and co-workers expanded the *translocated* work to obtain the *retained* isomer by employing a bulky phosphine ligand (Figure 3.1.8).[259] The phosphine ligand is highly influential in delivering the retained isomer **122** in >20:1 ratio. The highly selective nature of this transformation for the *retained* isomer was critical in showing the applicability of this protocol. By regenerating the terminal olefin in the product, the reaction could be conducted iteratively to access quaternary centres, starting from terminal olefins. This was exemplified by the functionalisation of propene to form the allylic quaternary centre after three consecutive C(sp^3)-H functionalisations.

3.1.4. Cross Dehydrogenative Coupling

Cross dehydrogenative coupling (CDC) represents the pinnacle in atom efficiency of C(sp^3)-H functionalisation techniques, with the only by-product formally being molecular hydrogen. Although currently limited to sp^2-sp^3 bond forming reactions, Glorius and co-workers developed an elegant system to achieve a non-directed CDC arylation of allylic bonds with heteroaromatics.[260] Additionally, work by Larossa and co-workers also enabled the cross dehydrogenative coupling of benzylic C(sp^3)-H bonds.[261]

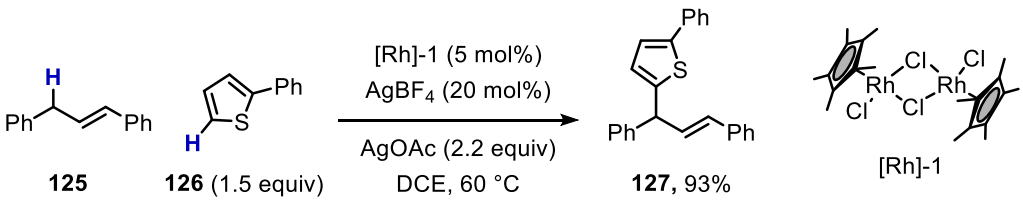

Figure 3.1.9 Glorius and co-workers´ CDC of unactivated olefins and sp^2-centres.

Outside of these seminal techniques there have been several other works on C-C bond functionalization of allylic C(sp^3)-H bonds,[262] but a broadly applicable and selective method to functionalise allylic C(sp^3)-H bonds still remains elusive.

The use of HAT could afford a selective allylic C(sp^3)-H functionalisation because the presence of the olefin dramatically lowers the BDE of the desired C(sp^3)-H bond. Internal olefins have a BDE between 82 and 85 kcal.mol^{-1} this is considerably lower than many of the HAT catalysts which were discussed in Chapter 2. Merging photoredox chemistry and allylic C(sp^3)-H functionalisation would be an ideal opportunity to test this hypothesis because of the readily accessible open shell intermediates in photoredox processes.

3.2. HAT and photochemistry

As we have discussed in Chapter 2, photoredox chemistry has established itself as a versatile C(sp^3)-H functionalisation platform due to the ability to access radical intermediates.[263] Whilst α-heteroatoms like nitrogen and oxygen generate localised and highly nucleophilic radical species through hyperconjugation, the π system stabilises through resonance (Figure 3.2.1).

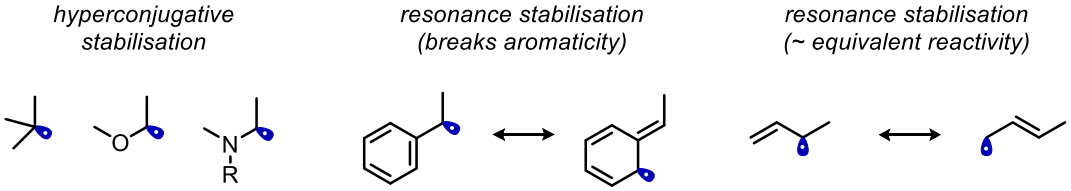

Figure 3.2.1. hyperconjugative stabilisation of radicals versus resonance stabilisation.

Delocalisation to resonance stabilised positions for benzylic sites is of no consequence to the regioselectivity of the reaction because reactivity at the delocalised site breaks aromaticity. However, the corresponding resonance form in an allylic system has a similar reactivity profile as at the initial radical site or is potentially more reactive. If the reactivity is similar, then this can lead to regioselectivity issues.

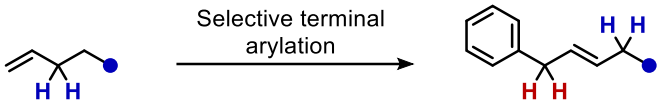

Figure 3.2.2. Potential issues arising from activation of the product C(sp^3)-H bonds

Upon C(sp^3)-H functionalisation of the allylic bond, the olefin remains within the product. Although the steric environment is different, it is possible that the substrate has more activated C(sp^3)-H bonds than the starting material. This could be the case with a selective terminal arylation, where the presence of the aryl ring lowers the BDE of the **red** hydrogens (Figure 3.2.2) leading to overreaction or possibly isomerisation to the conjugated allylarene.

Allylic C-H

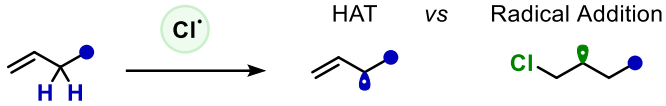

Figure 3.2.3. Possible side reaction includes the addition into an alkene.

Another issue that comes with photoredox mediated HAT is that issues may arise when an electrophilic HAT agent adds into the olefin (Figure 3.2.3). This has been observed where the electrophilic HAT agent is a halide radical.[264] Although there are several issues surrounding the use of photoredox HAT catalysis, the arena has seen development over the past decade.

3.2.1. C(sp³)-C(sp²) bond forming reactions

The seminal work by Macmillan and co-workers in this arena,[265] highlights this regioselectivity issue. The organocatalytic C(sp³)-C(sp²) bond formation between olefins and benzonitrile derivatives (Figure 3.2.4), using thiol HAT catalyst **131**. Here Macmillan and co-workers use an identical system to those seen in chapter 2. As we have discussed the $Ir(ppy)_3$/benzonitrile system is an effective platform for the discovery of oxidative methods to generate radicals.

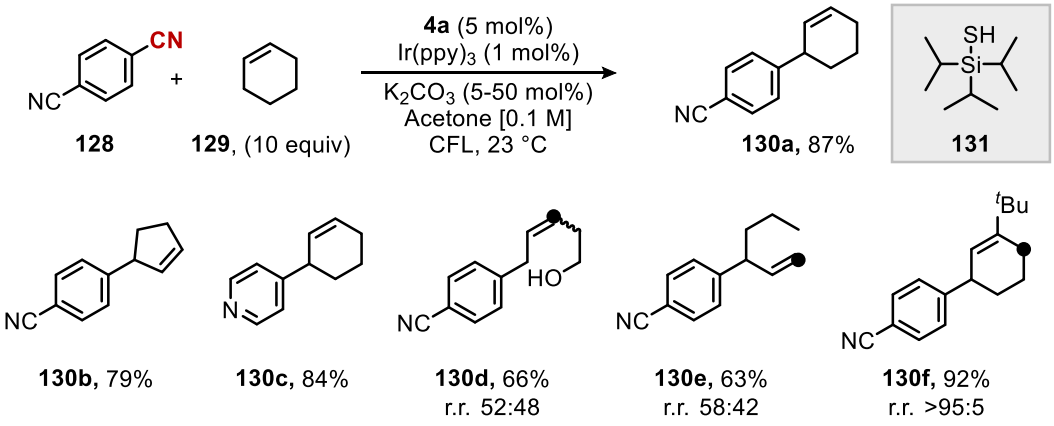

Figure 3.2.4. Thiol mediated allylic C(sp³)-H arylation through radical-radical coupling.

When employing symmetrical substrates, such as cyclohexene (**130a, 130c**) or cyclopentene (**130b**), there are no site selectivity issues. However, moving to unsymmetrical olefins (**130d**, **130e**), the selectivity between the two possible reaction sites is poor with close to statistical amounts of the linear and branched products being produced. The major isomer is shown, and the corresponding isomer is highlighted by the black dot. However, substrates that show considerable steric bias such as **130f** exhibit much greater selectivity to the less hindered site, with regioisomeric ratios being greater than 95:5. However, due to the early transition state of most radical reactions, steric influences are not as strong as their polar counterparts.

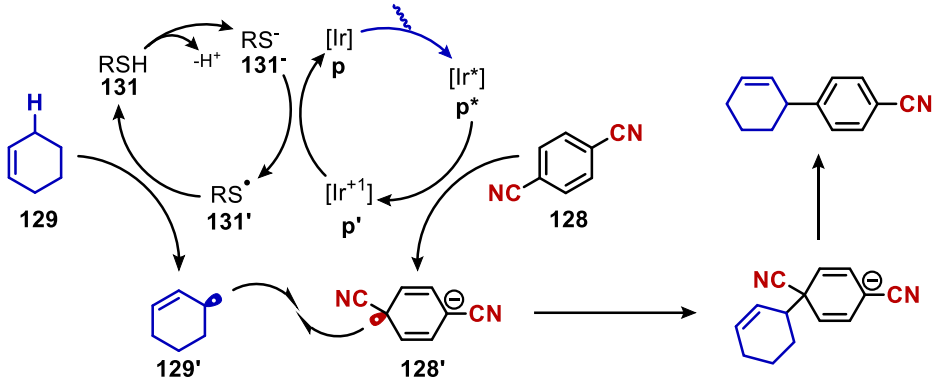

Figure 3.2.5. Mechanistic proposal of the thiol mediated allyic arylation.

The mechanistic proposal (Figure 3.2.5) follows an initial excitation of the iridium photocatalyst to generate a highly reducing excited state ($E[Ir^{IV}/*Ir^{III}]$ = - 1.73 V *vs* SCE). Electron deficient arenes such as 1,4-dicyanobenzenes (**128**, E_{red} = - 1.61 V *vs* SCE) can readily quench the excited state through single electron transfer to produce a persistent radical anion (**128'**) and the oxidised photocatalyst (**p'**). Butane thiol (**131b**) is used as a surrogate to the employed catalyst (**131**) for the mechanistic rationale. The oxidised photocatalyst ($E[Ir^{IV}/Ir^{III}]$ = + 0.77 V *vs* SCE) is unlikely to be able to oxidise the thiol directly, (**131b**, E_{red} = + 1.12 V *vs* SCE), however deprotonation to the thiolate would allow an oxidation event to occur (**131b**$^-$, E_{red} = - 0.85 V *vs* SCE),[266] forming the thiyl radical (**131b'**). The bond dissociation energy of the S-H bond ($BDE_{(SH)}$ = 87 kcal mol^{-1}) is greater than the allylic C(sp^3)-H bond ($BDE_{(CH)}$ = 83.2 kcal mol^{-1}), so the abstraction is thermodynamically favourable. Furthermore, the electrophilic nature of the thiol radical means that abstraction of the electron rich allylic C(sp^3)-H is philicity matched and so kinetically rapid. Coupling of the persistent radical anion (**128'**) and the transient allylic radical (**129'**), followed by rearomatisation by elimination of the cyanide anion to form the allylated (hetero)aromatic product. The elimination of the cyanide anion allows the base to be used in a catalytic fashion because the anion is sufficiently basic to deprotonate the thiol (pKa (thioglycolate) = 7.91).[267]

The (hetero)aromatic coupling partner in this reaction is not widely available and is limited to electron poor aromatic that can be readily reduced. Additionally, the stoichiometric generation of hydrogen cyanide by-product is not attractive for scale-up.

Allylic C-H

3.2.2. Metallaphotoredox C(sp^3)-C(sp^2) bond forming reactions

Merger of transition metal catalysis with photoredox catalysis has been discussed previously and enables the use of widely available aryl halides in place of electrophilic coupling partners like Michael acceptors. The use of aryl halides in an allylic C(sp^3)-H functionalisation technique would avoid the requirement for an arene with low reduction potentials. Using the combination of nickel and photoredox catalysis, Rueping published a C(sp^3)-H arylation of the allylic position of olefins using aryl- and vinyl bromides as coupling partners (Figure 3.2.6).[268]

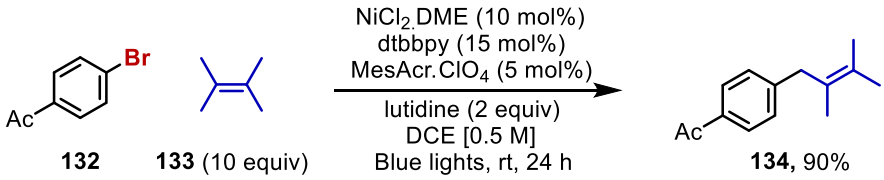

Figure 3.2.6. The conditions developed by Rueping and co-workers.

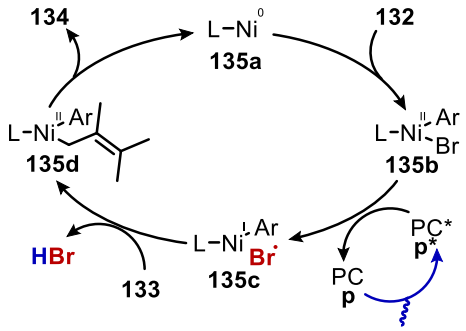

Figure 3.2.7. Reaction mechanism based on EnT.

Oxidative addition of aryl bromide **132** to an *in situ* formed nickel (0) species **135a**, would form a nickel (II) aryl bromide complex **135b** (Figure 3.2.7). The initially proposed mechanism proceeds through an EnT type mechanism from the photoexcited acridinium photocatalyst **p*** to **135b** which in turn generates a bromide radical and a nickel (I) species (**135c**). The bromide radical can abstract the hydrogen from the terminal olefin because it is electronically matched, and the bond dissociation energies of the species render a thermodynamically favourable event ($BDE_{(HBr)}$ = 87 kcal mol^{-1} *vs* $BDE_{(CH)}$ = 85 kcal.mol^{-1}). Addition of the allylic radical to **135c** forms a nickel (II) aryl alkyl species (**135d**) which undergoes reductive elimination to afford the cross-coupling product (**134**) and regenerates nickel (0) species **135a**. However, this scenario does not account for the lack of disubstituted or terminal olefins, bromide radicals should readily undergo a HAT event with both of these species.

The highly oxidising nature of the excited state photocatalyst (E[*$Acr^{+}/Acr^{\cdot+}$] = + 2.06 V *vs* SCE) has been shown to oxidise tri- and tetrasubstituted olefins by SET. Indeed, the oxidation of tetramethylethlyene (E_{ox} = + 1.53 V) is well within the range of this highly oxidising catalyst.

Trisubstituted olefin, 2-methylpent-2-ene has a higher oxidation potential (E_{ox} = + 1.91 V *vs* SCE). Moving to less alkylated olefins, increases the oxidation potential.[269] This pushes the oxidation potential higher than that of the photocatalyst can reach, and is possibly why the scope does not include di-substituted or terminal olefins.

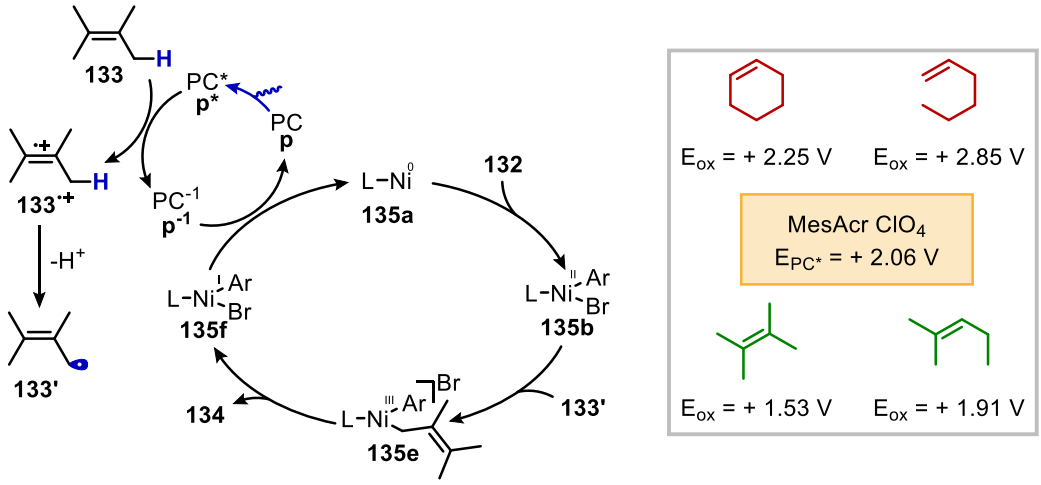

Figure 3.2.8. Oxidation of the olefin by the excited state photocatalyst. Oxidation potentials of four olefins.

This has led to a different mechanism (Figure 3.2.8) to be proposed where **p*** oxidises **133** to form the radical cation (**133**$^{\cdot+}$), deprotonation of this intermediate would generate the allylic radical (**133'**). Radical addition of species **133'** into the nickel aryl complex (**135b**) would form a nickel (III) aryl alkyl intermediate (**135e**) facile reductive elimination to the allylated benzene derivative (**134**) and nickel (I) (**135f**). Reduction of **135f** by **p'** would generate the initial nickel (0) (**135a**) and the ground state photocatalyst to close both catalytic cycles (Figure 3.2.8).

However, this hypothesis is countered by the claims of the authors who state that the use of the photocatalyst [$Ir(dF(CF_3)ppy)_2(bpy)]PF_6$ (E[*Ir^{III}/Ir^{II}] = + 1.21 V) readily furnishes the product. Additionally, the reduced photocatalyst (E[$Acr^{+}/Acr^{\cdot+}$] = - 0.57 V) may not be able to reduce **135f.** The intricacies of the mechanism are subject to debate, but the considerable excess of the olefinic partner and the limitation to electron rich olefins means that the synthetic utility of this protocol is limited on several fronts.

Allylic C-H

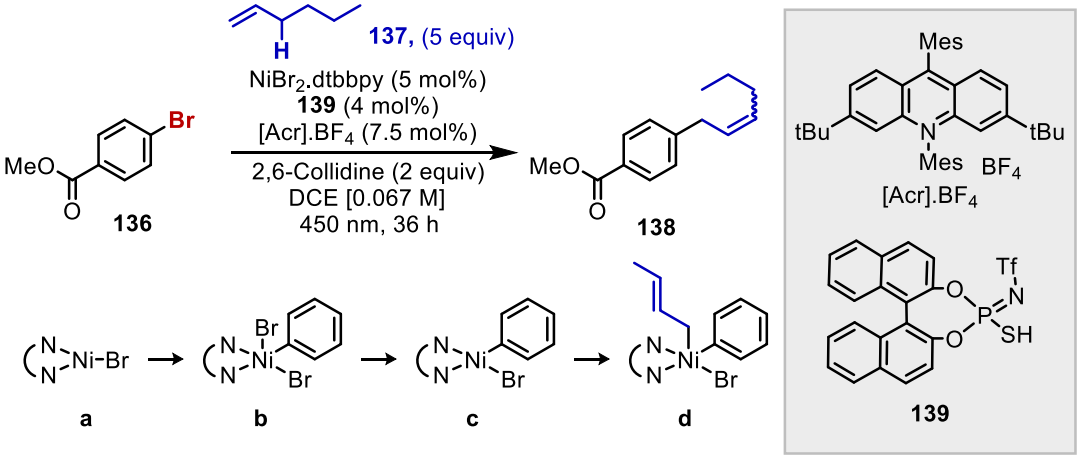

Figure 3.2.9. C(sp³)-H bond arylation of terminal alkenes using ternary catalysis.

In 2022, Glorius and co-workers extended the reactivity of allylic C(sp³)-H arylation using a triple catalytic manifold (Figure 3.2.9).[270] The authors combine a HAT/photoredox system **139/**MesAcrBF$_4$ with nickel catalysis to enable the arylation of terminal olefins at the terminal position (*translocated*). The use of thiophosphoric imide was critical for the reactivity because switching to simple thiol HAT catalysts like Methyl thioglycolate or TIPSSH shut down the reaction. The reaction was supported by detailed DFT studies which revealed that the likely reaction pathway proceeds through an initial Ni (I) species (**a**), oxidative addition of the aryl bromide forms the nickel (III) aryl bromide species **b**. Single electron transfer by the reduced state photocatalyst to generate nickel (II) aryl bromide species **c**. Radical addition of the allylic radical (HAT by the thiophosphoric imide catalyst) at the terminal position would generate nickel (III) **d**, rapid reductive elimination affords the cross coupled product and the nickel (I) species **a**. The selective formation the terminal position or *translocated* was highlighted in the paper. The authors state that "reductive elimination determines the regioselectivity", thus the transition state of this process was analysed and found that the reductive elimination at the *retained* site was 8.2 kcal mol^{-1} higher in energy than at the terminal position.

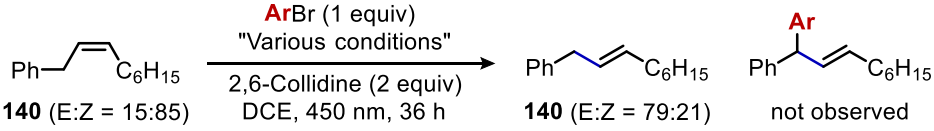

Figure 3.2.10. Submission of Z isomer leads to E isomers

140 was submitted to the reaction conditions and no further arylation could be detected, which suggests that there are no further HAT events on the products of this reaction (Figure 3.2.10). Isomerisation was observed from Z to E, the authors propose this is due to a photocatalytic isomerisation.

3.2.3. C[sp³]-C[sp³] bond forming reactions

The examples presented thus far in a photochemical framework are C(sp²)-C(sp³) bond forming reactions. The ability to generate C(sp³)-C(sp³) bonds would be a beneficial expansion of current technologies because the formation of C(sp³) linkages is a cornerstone of chemistry. Methods to introduce more C(sp³) hybridisation into a molecule whilst maintaining valuable synthetic handles are highly desirable; allylic C(sp³)-H functionalisation with sp³ hybridised entities would enable such a transformation. Although the work surrounding this endeavour from photochemical perspective is quite limited. One of the first sp³-sp³ bond forming reactions was developed by Wu and co-workers, the reaction proceeds through radical conjugate addition of an allylic or benzylic radical into an electron-deficient olefin (Figure 3.2.11).[271]

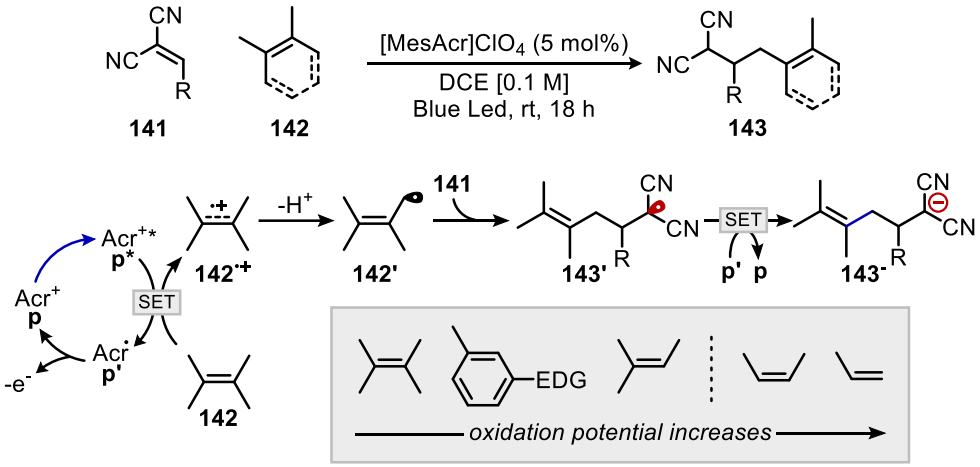

Figure 3.2.11. Radical conjugate addition of α-allyl radical into electron deficient Michael acceptors

Following the proposed mechanism, upon photoexcitation of the $MesAcr^+$ (**p***) a highly oxidising state is accessed (**p***, $E[^*Acr^+/Acr^{\bullet+}]$ = + 2.06 V *vs* SCE) which readily oxidises the tetrasubstituted olefin (**142**, E_{red} ~ + 1.51 V *vs* $Ag/AgNO_3$) to form the olefinic radical cation (**142**$^{\bullet+}$) and reduced state photocatalyst. Deprotonation of the radical cation provides the α-radical which regioselectivity adds into the electron deficient olefin to form radical adduct **c**$^{\bullet}$. Single electron reduction of **143'** to **143**$^-$ by the reduced state photocatalyst (**p'**, $E[Acr^+/Acr^{\bullet}]$ = - 0.57 V *vs* SCE) regenerates the mesityl acridinium and the dimalonate anion. This potential-gated technique is particularly limited because it is limited by both the oxidation potential of the olefin/aromatic, but also by the radical adduct **143'**, because the reduction potential of the acridinium catalyst is low, only activated systems can be used. Having the substrates impose potential gates on a photoredox reaction limits the available bond forming reactions.

Allylic C-H

Chromium catalysed.

The formation of C(sp^3)-C(sp^3) bonds through the allylation of aldehydes has been achieved by employing dual or triple catalytic manifolds with chromium (II) catalysts.[272] The most recent report by Kanai and co-workers uses a triple catalytic system to achieve the diastereoselective allylation of aldehydes to generate the homoallylic alcohols.[273] The technique was also extended to an enantioselective variation by incorporation of a chiral ligand **L33** (Figure 3.2.12).

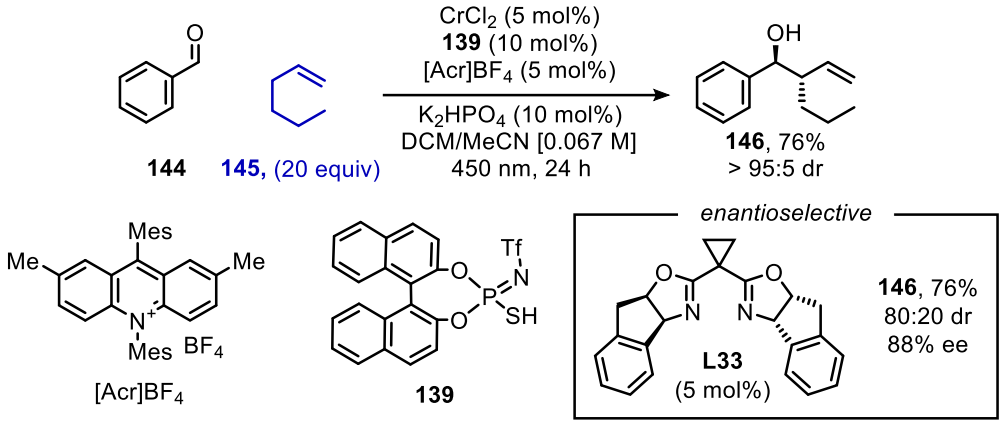

Figure 3.2.12. The diastereoselective allylation of aldehydes using chromium catalysis.

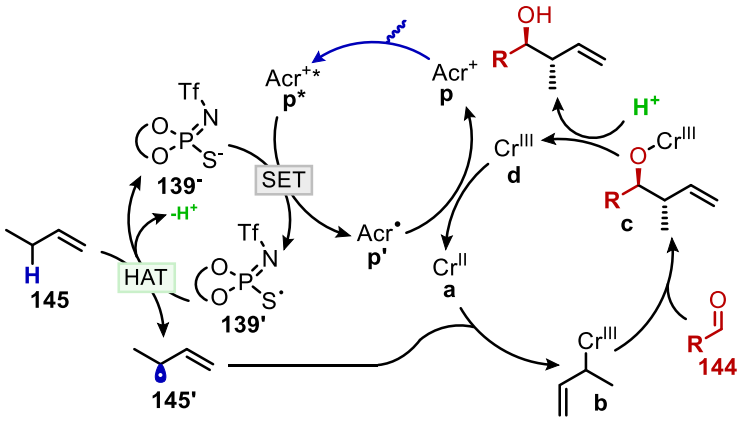

Figure 3.2.13. The proposed mechanistic cycle for ternary chromium catalysis.

Photoexcitation of the $MesAcr^+$ catalyst to the highly oxidising excited state (**p***, E[*$Acr^+/Acr^{\cdot+}$] > + 2 V *vs* SCE) enables the oxidation of deprotonated **139**,[274] to thiyl radical **139'** (Figure 3.2.13). The HAT event is thermodynamically and kinetically favourable due to the bond-dissociation energies and a philicity matched event. Allylic radical **145'** combines with chromium (II) catalyst **a** to form the chromium (III)-allyl complex **b**. Addition into the aldehyde followed by protonation of **c** (by the HAT catalyst) liberates free chromium (III) **d**, reduction by the photocatalyst closes both catalytic cycles (E[Cr^{III}/Cr^{II}] = − 0.41 V *vs* SCE *vs* E[$MesAcr^+/MesAcr^{\cdot+}$] = − 0.46 V *vs* SCE).

Yoon was able to develop a similar protocol that extended the work to activated α-keto esters.[275]

Radical-radical coupling.

A less explored endeavour in the functionalisation of allylic C(sp^3)-H bonds is the use of electron donor-acceptor complexes. Melchiorre and co-workers (Figure 3.2.14) exploited the formation of an EDA complex between dithiophosphoric acid (**149**) and electron deficient radical precursors (**147**) to afford the direct benzylation of allylic C(sp^3)-H bonds.[276]

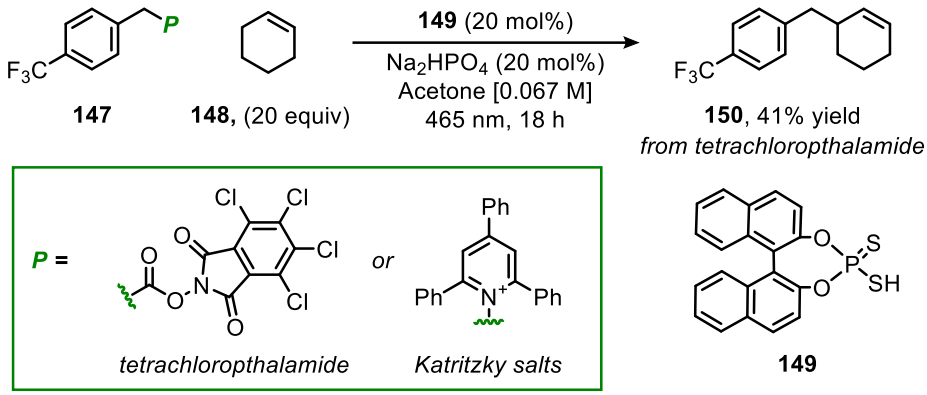

Figure 3.2.14. The radical precursor-thiol EDA complex approach from Melchiorre and co-workers

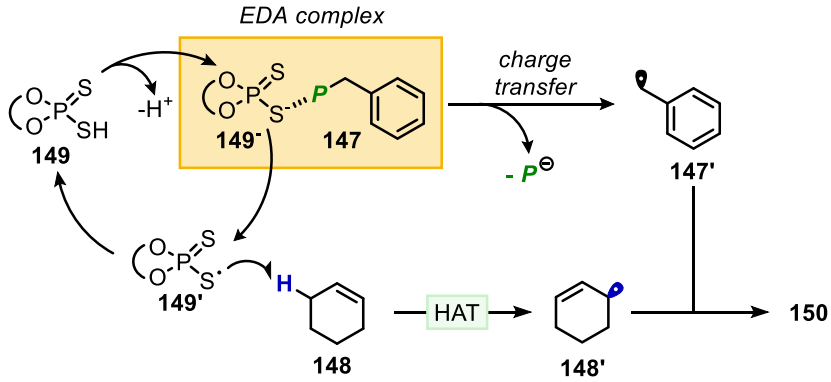

Figure 3.2.15. Proposed mechanistic cycle by Melchiorre and co-workers.

The EDA complexation between the deprotonated catalyst (**149**$^-$) and **tCIP ester** (**147**) was confirmed by UV/Vis spectroscopy. Visible light excitation (435 nm) and charge transfer through a single electron transfer from **149**$^-$ to **147** creates the radical anion of **147**$^{\bullet-}$, and thiyl radical (**1c**$^\bullet$)**.** **147**$^{\bullet-}$ readily fragments into the neutral benzylic radical, either by loss of CO2 and anionic phthalmide (*wrt tCLP esters*), or loss of neutral 2,4,6 triphenyl pyridine (*wrt Katritzky salts*). The thiyl radical generated is polarity matched to abstract the allylic C(sp^3)-H bond of **1b** to form the allylic radical (**1b**$^\bullet$). Radical-radical coupling of **1b**$^\bullet$ with **1c**$^\bullet$ produces the desired homoallyl benzene products.

3.2.4. Accessing a more general electrophile

Although the aforementioned techniques generate a wide range of $C(sp^3)$-$C(sp^3)$ linkages the bond forming reactions are still limited in scope. To this end we envisioned that a transition metal catalysed cross-coupling using a sp^3 electrophile and terminal olefin could enable a more broadly applicable approach to this problem. Prior to our investigation, only the works of Rueping were published on a dual catalytic system but highlighted that the analogous $C(sp^3)$-$C(sp^2)$ cross coupling reaction is viable. By exchanging the aryl bromide electrophile to an alkyl bromide, it could be possible to access the complementary $C(sp^3)$-$C(sp^3)$ cross coupling reaction.

However, the transition from aryl bromide to alkyl bromide is not a trivial task, the development of $C(sp^3)$-$C(sp^3)$ cross-coupling reactions has historically been quite challenging. One of the key issues with this technique is the instability of the alkyl-metal complex. Alkyl-metal complexes can undergo β-hydride elimination pathways, which can lead to undesirable site selectivity issues or problematic alkene formation. The reversible nature of β-hydride can however be used in a positive light to afford chain-walking products.

We decided upon a nickel-photoredox dual catalysis platform because the development of $C(sp^3)$-$C(sp^3)$ bond forming reactions has used nickel effectively.[277] Additionally, the synergy of nickel with photoredox catalysis cannot be understated, it is one of the main metals in this field. Finally, we believed that the photoexcitation of a putative nickel halide species could generate halide radicals which could act as a HAT reagent, removing the need for an additional HAT catalyst, such as thiophosphoric imide or quinuclidine.

3.3. General aim of the project

Prior to our investigations there was a distinct lack of sp^3-sp^3 cross coupling regimes between allylic C(sp^3)-H bonds and a general sp^3 electrophile. Reports by Macmillan and Rueping highlighted that the sp^3-sp^2 coupling was viable, the added complexity of a sp^3 electrophile would be of considerable synthetic value in this scenario. Additionally, we could take advantage of the development of C(sp^3)-C(sp^3) cross coupling reactions to enable a robust transformation.[278]

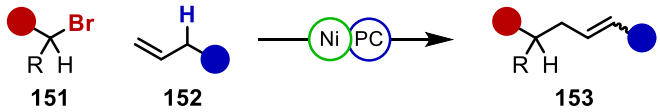

Figure 3.3.1. General scheme of the reaction

The proposed reaction would couple both secondary and primary alkyl bromides with terminal olefins under a dual catalytic system using a ligated nickel catalyst and photocatalyst. The control of the regioselectivity of both site selectivity and E:Z ratio would hopefully be controlled by the ligand employed.

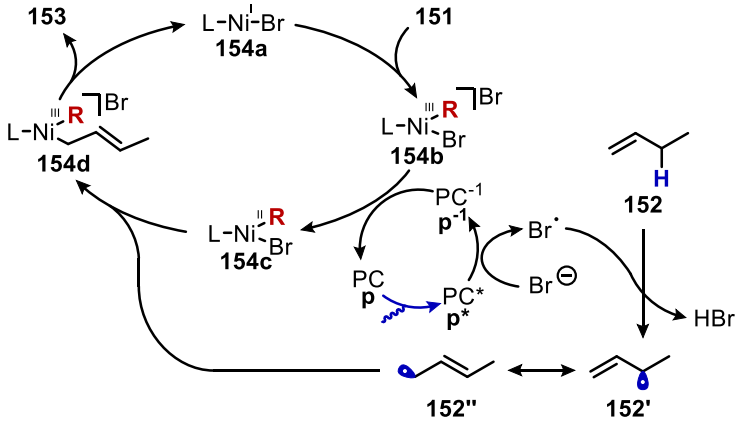

Figure 3.3.2. Mechanistic proposal for alkylation of allylic C(sp^3)-H bonds.

The mechanistic proposal consists of a putative nickel (I) species **154a**, which would undergo oxidative addition with alkyl bromide **151** to form nickel (III) alkyl species **154b**. Oxidation of bromide anion by an excited state photocatalyst **p***, would render the reduced photocatalyst **p^{-1}** and bromide radical. The bromide radical abstracts an allylic proton from the olefin (BDE_{HBr} = 87 kcal mol^{-1} *vs* BDE_{CH} = 83.2 kcal mol^{-1}). Allyl **152'** is resonance stabilised between **152'** and **152''**. **p^{-1}** reduces **154b** to nickel (II) alkyl species **154c**. With judicious choice of ligand, we should be able to control the regioselective addition of **152''** into **154c**, to afford nickel (III) alkyl-alkyl species **154d**. Reductive elimination to the desired cross coupled product and regenerate **154a**.

Allylic C-H

3.4. Optimisation

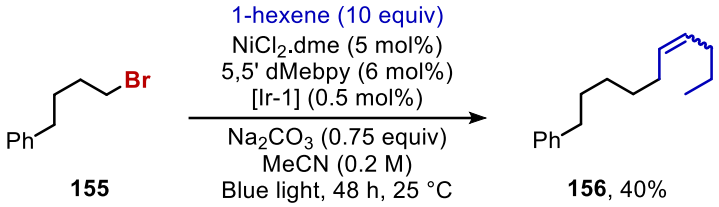

Figure 3.4.1. GC Yield with decane as internal standard.

The initial conditions were discovered with the primary alkyl bromide series,[279] these conditions were used to begin the optimisation of the secondary series using a higher loading of nickel and photocatalyst under blue light (451 nm) irradiation. The alkyl bromide used was cyclohexyl bromide (**157**) with 1-octene (**158**) as the olefin. An initial ligand screen was conducted to assess the influence of sterics on the reaction.

3.4.1. Preliminary ligand Screen

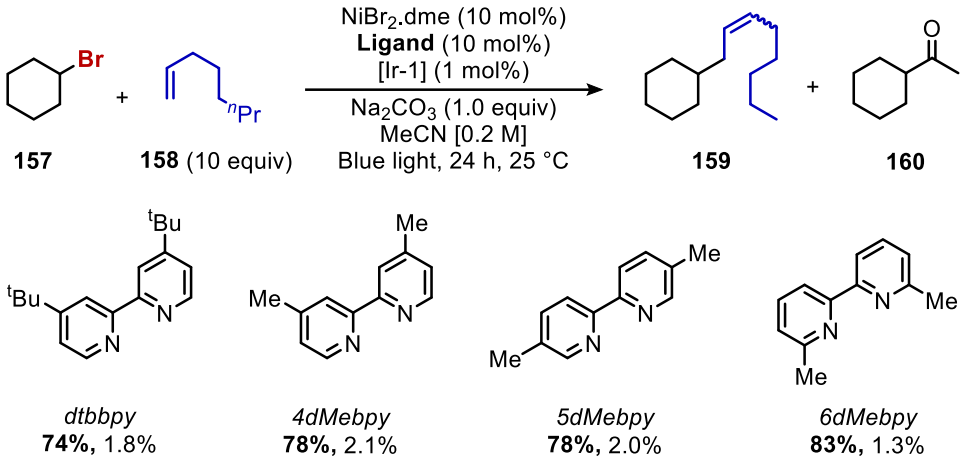

Figure 3.4.2. Ligand screening. Cyclohexyl bromide (0.2 mmol), 1-octene (2.0 mmol), $NiBr_2$ (0.02 mmol), ligand (0.02 mmol), Ir-1 ($[Ir(dFCF_3ppy)_2(dtbbpy)]PF_6$, 2 µmol), Na_2CO_3 (0.2 mmol), MeCN (1 mL), 451 nm reactor at 25 °C for 24 h. recovered xa (%) in bold, xb (%). GC conversion/yield determined using pentamethyl benzene as internal standard.

The initial ligand screen conducted used typical bidentate bipyridines found in many nickel catalysed reactions, additionally the preliminary reaction was obtained with 5dMebpy. The low yielding results of this initial screen was quite unusual due to the success of the primary bromide series (40% yield). The observation of **160** by GC analysis of the crude reaction mixture indicated that a solvent change may be highly beneficial to the reaction conditions. Thus, 4dMebpy would be used to assess the solvent scree before a more rigorous ligand screen could be conducted.

3.4.2. Solvent screen

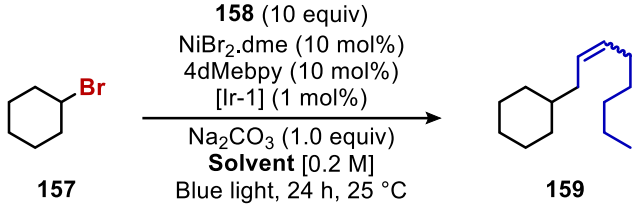

Entry	*Solvent*	**157**	**159**
1	MeCN	76	2
2	Acetone	87	2
3	DMF	79	3
4	DMA	89	5
5	EtOAc	62	1

Figure 3.4.3. Solvent screening. Cyclohexyl bromide (0.2 mmol), 1-octene (2.0 mmol), $NiBr_2$ (0.02 mmol), 4dMebpy (0.02 mmol), Ir-1 ($[Ir(dFCF_3ppy)_2(dtbbpy)]PF_6$, 0.002 mmol), Na_2CO_3 (0.2 mmol), Solvent (1 mL), 451 nm reactor at 25 °C for 24 h. GC conversion/yield determined using pentamethyl benzene as internal standard.

The solvent screen (Figure 3.4.3) was conducted, a repeat of the initial hit (*entry 1*) provided an almost identical reaction profile. Changing the solvent to acetone (*entry 2*) gave lower conversion. Whereas amide solvents like DMF (*entry 3*) and DMA (*entry 4*) gave slightly greater reactivity. With DMA yielding the highest amount of product **159** at 5%. Additionally, DMA also gave a cleaner reaction profile. Ethyl acetate (*entry 5*) provided higher conversions but with no identifiable peaks on GC or by NMR.

3.4.3. Ligand denticity

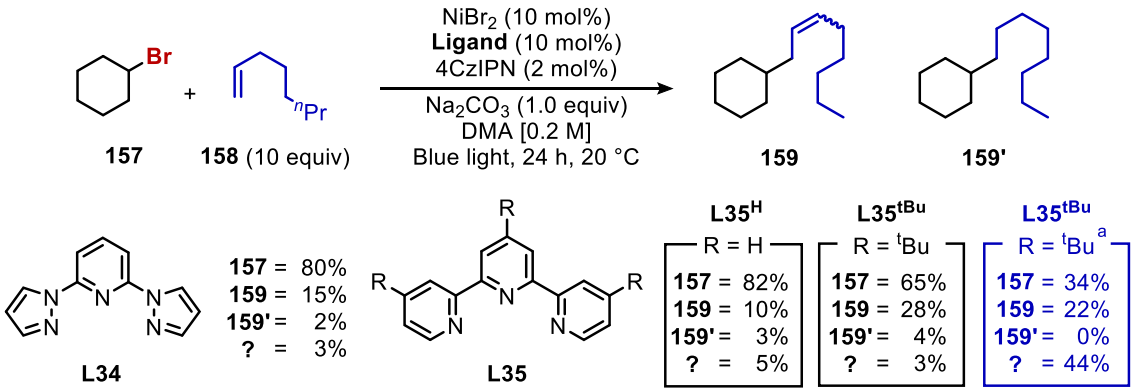

Figure 3.4.4. Denticity. Cyclohexyl bromide (0.2 mmol), 1-octene (2.0 mmol), $NiBr_2$ (0.02 mmol), Ligand (0.02 mmol), 4CzIPN (4 µmol), Na_2CO_3 (0.2 mmol), DMA (1 mL), 451 nm reactor at 20 °C for 24 h. GC conversion/yield determined using pentamethyl benzene as internal standard. a) Ir-1 photocatalyst (1 mol%).

After the solvent screen, we decided to assess the denticity of the ligand (Figure 3.4.4). There is some evidence that tridentate ligands can be very effective for the alkyl series of reactions.[280] We also chose to screen 4CzIPN as a photocatalyst in place of Ir-1. The tridentate ligands (**L1, $L2^H$, $L2^{tBu}$**) were assessed under the conditions given about and gave significantly better yields than the corresponding bidentate system.

Allylic C-H

L1 gave higher yields than the 4dMebpy (15% vs 5%) and the product yield closely matched the conversion. **L2^{H}** however gave lower yield than **L1** and slightly more of the mass balance was unaccounted for. However, increasing the electron density on the ligand **L2^{tBu}** enhanced the product forming reaction significantly, to 28% yield. The control reaction with [Ir-1] was conducted (blue box) and whilst the reaction gave a reasonable yield (22%) there was a considerable discrepancy between recovered **157** and the product **159**. Thus, 4CzIPN and ttbtpy were taken forward.

3.4.4. General parameters

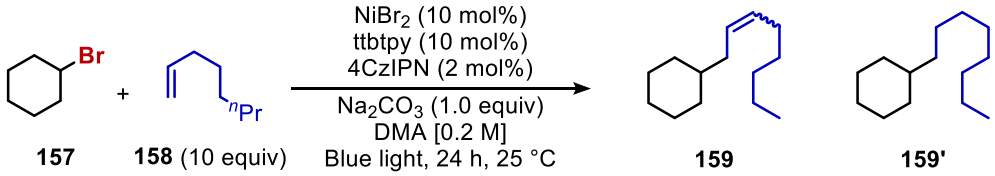

Entry	*General changes*	**157**(%)	**159**(%)	**159'**(%)	**missing**(%)
0	*none*	65	28	4	3
1	PC (1 mol%)	58	15	0	28
2	PC (4 mol%)	50	43	2	5
3	Na_2CO_3 (0.5 equiv)	46	29	0	20
4	Na_2CO_3 (1.5 equiv)	27	42	5	26
5	2 days	28	65	6	0
6	1-octene (2 equiv)	90	7	0	0

Figure 3.4.5. General conditions. Cyclohexyl bromide (0.2 mmol), 1-octene (2.0 mmol), $NiBr_2$ (0.02 mmol), ttbtpy (0.02 mmol), 4CzIPN (4 µmol), Na_2CO_3 (0.2 mmol), DMA (1 mL), 451 nm reactor at 25 °C for 24 h. GC conversion/yield determined using pentamethyl benzene as internal standard.

Some general parameters were then assessed (Figure 3.4.5). Each of the parameters should be compared to *entry 0*. Lowering the photocatalyst loading reduced the mass balance and also the overall yield of **159** (*entry 1*). Conversely increasing the photocatalyst loading increased the formation of **159** (*entry 2*). The equivalents of base had noticeable impact on the reactivity (*entry 3* + *4*), the use of 0.5 equivalents of sodium carbonate only increased the missing material, whereas using 1.5 equivalents improved the yield of **159**, from 28% yield to 42%. An extended reaction time (*entry 5*) also improved the yield of **159**, whilst maintaining the mass balance. Disappointingly, lowering the equivalents of olefin was severely limiting to the reactivity (*Entry 6*).

3.4.5. Base screen

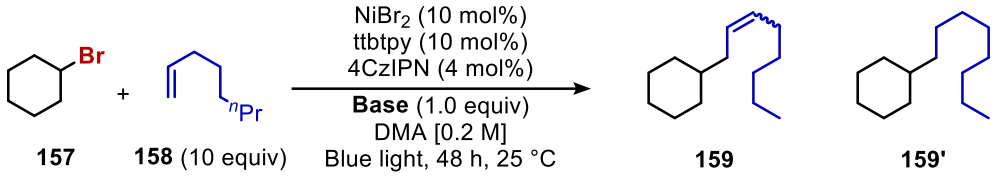

157 **158** (10 equiv) **159** **159'**

Entry	*Base*	**157**(%)	**159**(%)	**159'**(%)	**missing**(%)
1	Na_2CO_3	28	65	6	0
2	K_2CO_3	5	71	5	19
3	Cs_2CO_3	15	59	1	25
4	KOMe	26	0	0	74
5	Na_2HPO_4	33	45	3	19
6	K_3PO_4	43	27	0	30
7	K_2HPO_4	25	45	2	28

Figure 3.4.6. Base screen. Cyclohexyl bromide (0.2 mmol), 1-octene (2.0 mmol), $NiBr_2$ (0.02 mmol), ttbtpy (0.02 mmol), 4CzIPN (4 µmol), Base (0.2 mmol), DMA (1 mL), 451 nm reactor at 25 °C for 48 h. GC conversion/yield determined using pentamethyl benzene as internal standard.

A base screen (Figure 3.4.6) showed that the use of potassium carbonate (*entry 2*) was more reactive than both sodium and caesium carbonate bases (*entry 1 + 3*), with a slightly improved yield of **159** and better ratio of **159: 159'**. Stronger base potassium methoxide (*entry 4*) gave very high conversions but as with most of the reactions we could not identify any new NMR peaks and there were no new GC peaks. We believe that it is likely to be as a result of elimination of the bromide. Phosphate bases (*entry 5-7*) afforded the reaction in reasonable yields but with lower conversions and considerably more missing starting material.

3.4.6. Nickel precatalyst

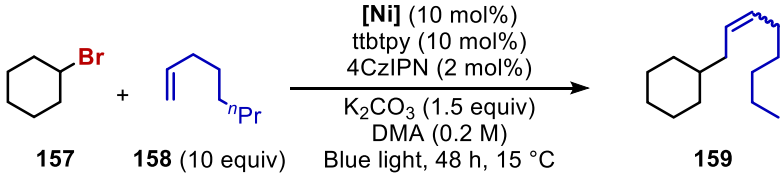

157 **158** (10 equiv) **159**

Entry	*Nickel precat*	**157**(%)	**159**(%)	**missing**(%)
1	$NiBr_2$	5	79	16
2	$NiBr_2$ (5 mol%)	44	41	15
3	$NiBr_2$.DME	29	58	13
4	$NiBr_4$.2TBA	56	23	21
5	$NiCl_2$.DME	4	68	28
6	NiI_2	91	0	8

Figure 3.4.7. Nickel precatalyst screen. Cyclohexyl bromide (0.2 mmol), 1-octene (2.0 mmol), [Ni source] (0.02 mmol), ttbtpy (0.02 mmol), 4CzIPN (4 µmol), K_2CO_3 (0.2 mmol), DMA (1 mL), 451 nm reactor at 15 °C for 48 h. GC conversion/yield determined using pentamethyl benzene as internal standard.

Allylic C-H

We decided to assess a temperature change in conjunction with a nickel precatalyst screen. By lowering the temperature, the hydrofunctionalisation **159'** product was eliminated (*entry 1*). Lowering the nickel loading was detrimental to the reaction (*entry 2*), at 48 h, the reaction mass balance was considerably poorer and extended reaction times would be detrimental to the applicability of the protocol. More soluble precatalysts like glyme coordinated nickel dibromide and the anionic NiTBA complex did not improve the formation of **159** (*entry 3 + 4*). Chloride complex was amenable to the transformation whereas the corresponding iodide did not provide any of the product (*entry 6 vs 7*). Since no better nickel precatalysts were found, $NiBr_2$ was used for a co-solvent screen.

3.4.7. Cosolvent screen

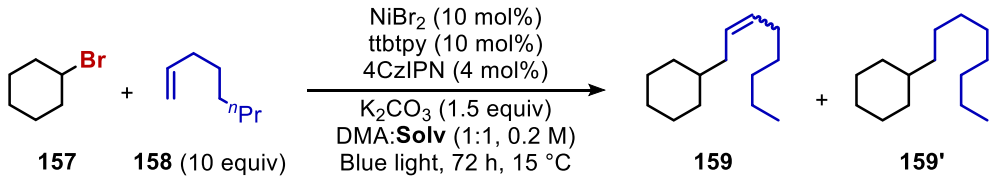

157 **158** (10 equiv) **159** **159'**

Entry	*Change*	**157**(%)	**159**(%)	**159'**(%)	**missing**(%)
0	DMA	5	79	0	16
1	DMA:IPA	22	51	14	13
2	DMA:MeCN	50	39	0	11
3	DMA:EtOAc	64	19	0	17
4	DMA:$PhCF_3$	0	68	0	32
5	DMA:PhH	0	98	0	2

Figure 3.4.8. Co-solvent screen. Cyclohexyl bromide (0.2 mmol), 1-octene (2.0 mmol), $NiBr_2$ (0.02 mmol), ttbtpy (0.02 mmol), 4CzIPN (4 µmol), K_2CO_3 (0.2 mmol), DMA (0.5 mL), solvent (0.5 mL) 451 nm reactor at 15 °C for 72 h. GC conversion/yield determined using pentamethyl benzene as internal standard.

The co-solvent screen provided some interesting results, the use of IPA (entry 1) dramatically increased the formation of the hydrofunctionalisation product **159'**, this could enable the use of olefins as alkylating agents.[281] Both acetonitrile and ethyl acetate were particularly detrimental to the reactivity. Whereas the use of triflurotoluene (*entry 4*) led to an increase in the missing mass balance. However, the use of a cosolvent of benzene increased both selectivity and yield to exclusively form the product.

3.4.8. Optimised reaction conditions.

Secondary bromides

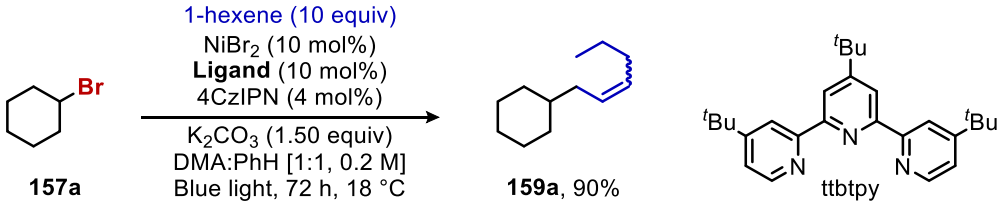

Figure 3.4.9. Cyclohexyl bromide (0.2 mmol), 1-octene (2.0 mmol), $NiBr_2$ (0.02 mmol), ttbtpy (0.02 mmol), 4CzIPN (4 µmol), K_2CO_3 (0.2 mmol), DMA (0.5 mL), PhH (0.5 mL) 451 nm reactor at 15 °C for 72 h.

The secondary series of alkyl bromides uses super stoichiometric amount of terminal olefin (10 equiv) in the presence of $NiBr_2$ and electron rich tridentate terpyridine ligand ttbtpy. The photocatalyst 4CzIPN provided the optimal yields. potassium carbonate base provided the best yields, although other carbonate bases could also afford appreciable amounts of **159**. The cosolvent of DMA and benzene greatly enhanced the reactivity. The temperature was essential for limiting the deleterious hydrofunctionalisation reaction.

Primary bromides

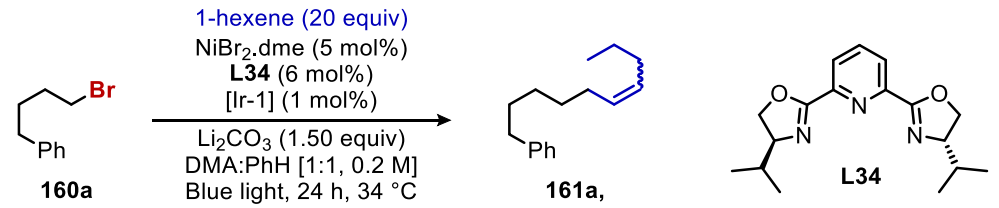

Figure 3.4.10. Alkyl bromide (0.3 mmol), 1-hexene (6.0 mmol), $NiBr_2$.DME (0.015 mmol), L34 (0.018 mmol), $[Ir\text{-}1]PF_6$ (3 µmol), Li_2CO_3 (0.45 mmol), DMA (0.75 mL), PhH (0.75 mL) Hepatochem reactor 34 °C for 24 h. Isolated yields.

The primary series was optimised with some slight changes to the reaction parameters.* The main difference is the ligand employed, the ^{i}Pr-PyBox (**L34**) ligand employed is more sterically demanding than the ttbtpy and is critical in limiting the homocoupling of the alkyl bromide.

The ligand also influences the photocatalyst used, 4CzIPN was not effective in this transformation, so $[Ir\text{-}1]PF_6$ was used. A change in base was also required, lithium carbonate provided the most appropriate yields. Additionally, the alkene is required in greater stoichiometry (20 equiv). The higher temperature and lower reaction times are likely due to a different photoreactor set up.

* These conditions were developed by Mikkel B Buendia @ DTH

Allylic C-H

3.5. Substrate scope

3.5.1. Alkyl bromide scope

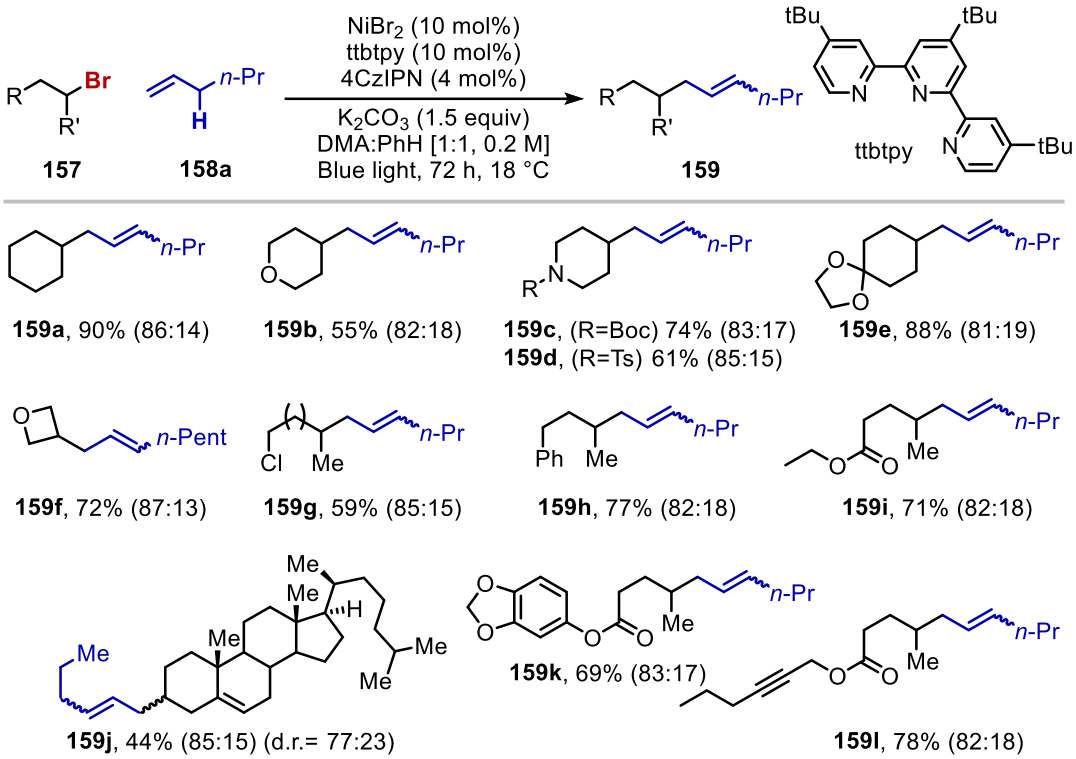

Figure 3.5.1. alkyl bromide (0.2 mmol), 1-hexene (2.0 mmol), $NiBr_2$ (0.02 mmol), ttbtpy (0.02 mmol), 4CzIPN (4 μmol), K_2CO_3 (0.2 mmol), DMA (0.5 mL), PhH (0.5 mL) 451 nm reactor at 15 °C for 72 h. Isolated yields. a) using tBuOH in place if PhH for 86 h. b) starting from single diastereomer.

The scope of the secondary bromides encompasses a good range of functional groups (Figure 3.5.1). The cross coupling of both cyclic and acyclic secondary bromides (**159a**−**159f**), containing carbamates (**159c**), sulfonamides (**159d**), acetals (**159e**), and esters (**159i**, **159k, 159l**) were all well tolerated. Alkynes (**159l**) are well known to bind to nickel centres, additionally the alkynyl C(sp^3)-H bonds have a similar BDE (76 kcal mol^{-1}) to the allylic position but did not affect the reactivity. Additionally, the α-proton of an acetal group (**159e**, **159k**) is known to be abstracted under photocatalytic conditions, but this was not observed under these reaction conditions.[282] Alkyl chloride (**159g**) was also amenable to the reaction conditions and is a valuable synthetic handle for further functionalisations. In addition, cholesterol derivative (**159j**) was easily within reach using tBuOH as solvent under otherwise identical reaction conditions. **159j** is diastereomerically pure, whereas the d.r. of this reaction is reduced to 77:23 which suggests that the oxidative addition may proceed through a radical type of mechanism.

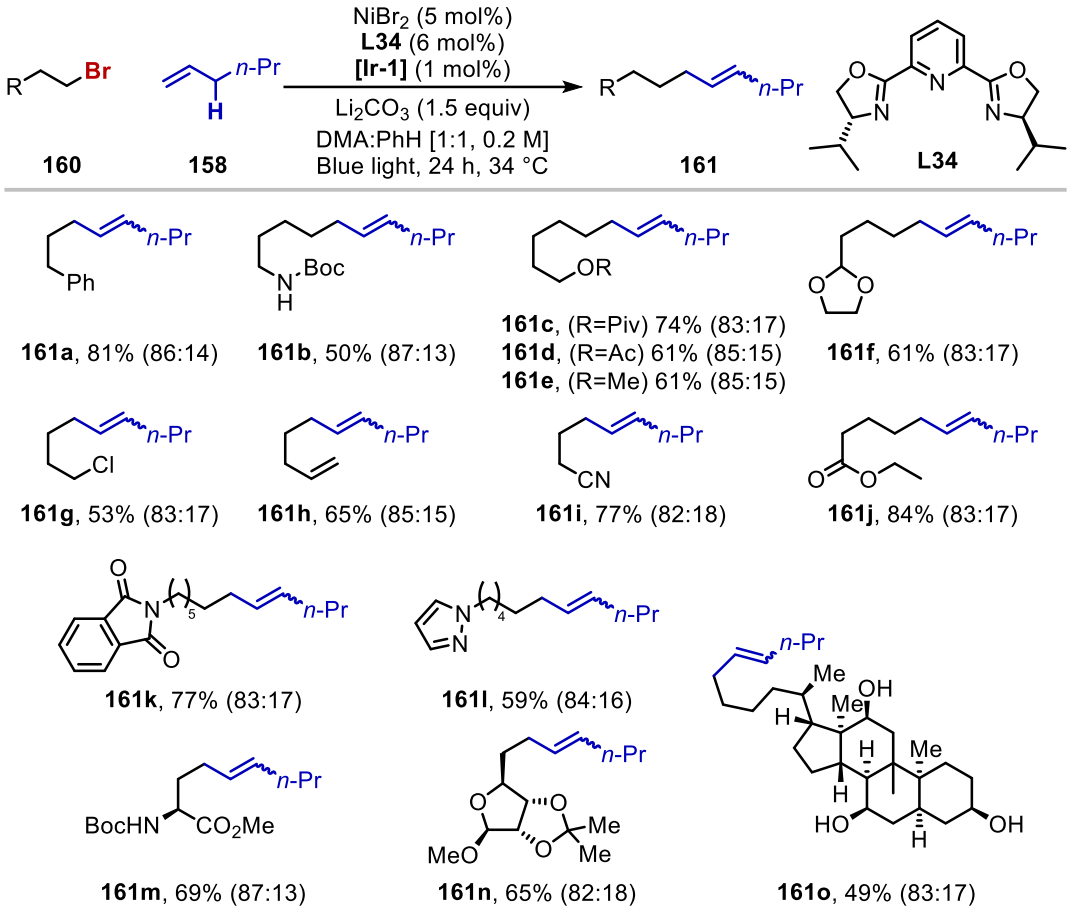

Figure 3.5.2. Performed by Dr Mikkel B. Buendia. Alkyl bromide (0.3 mmol), 1-hexene (6.0 mmol), $NiBr_2$.DME (0.015 mmol), L3434(0.018 mmol), [Ir-1]PF_6 (3 μmol), Li_2CO_3 (0.45 mmol), DMA (0.75 mL), PhH (0.75 mL) Hepatochem reactor 34 °C for 24 h. Isolated yields.

The chemoselectivity profile of the primary series (Figure 3.5.2) encompasses a wide variety of unactivated alkyl halides bearing carbamates (**161b**), esters (**161c**, **161d, 161j**), ethers (**161e**), acetals (**161f**), nitriles (**161i**) and amides (**161k**). Nitrogen containing heterocycles (**161l**) did not cause any issues with the reactivity. Pendant functional groups that are amenable for further functionalisation such as chlorides (**161g**) and olefins (**161h**) posed no issues. Advanced intermediates could be well accommodated, amino acids (**161m**), saccharides (**161n**), and steroid-type fragments containing free aliphatic alcohol motifs (**161o**) gave good yields.

Allylic C-H

3.5.2. Alkene scope

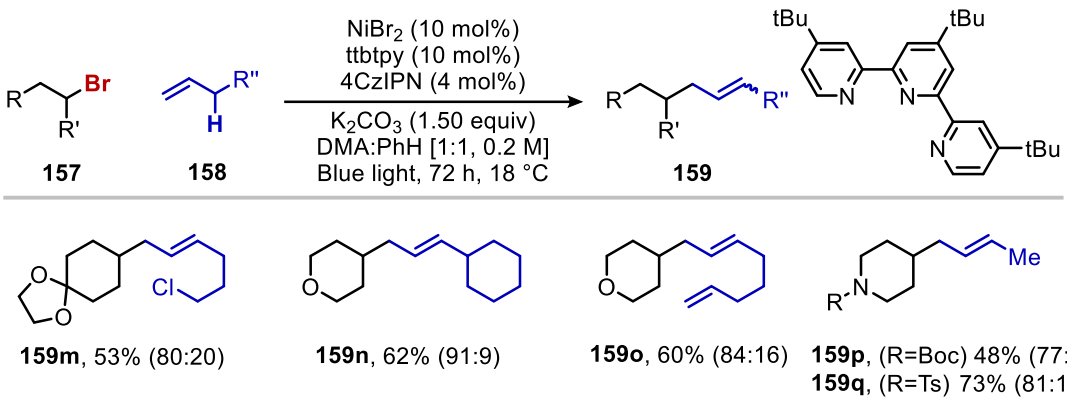

Figure 3.5.3. alkyl bromide (0.2 mmol), olefin (2.0 mmol), $NiBr_2$ (0.02 mmol), ttbtpy (0.02 mmol), 4CzIPN (4 µmol), K_2CO_3 (0.2 mmol), DMA (0.5 mL), PhH (0.5 mL) 451 nm reactor at 15 °C for 72 h. Isolated yields. a) using butene (1 atm).

Cyclic secondary alkyl bromides were chosen to assess some substituted unactivated olefins (Figure 3.5.3). Alkyl chloride **159m** was not detrimental to the reaction even in the presence of ten equivalents of chloride. The secondary position β to the olefin increased the selectivity of the E isomer (**159n**). Butene was amenable to the reaction conditions under ambient pressure to the desired cross coupled product (**159p, 159q**).

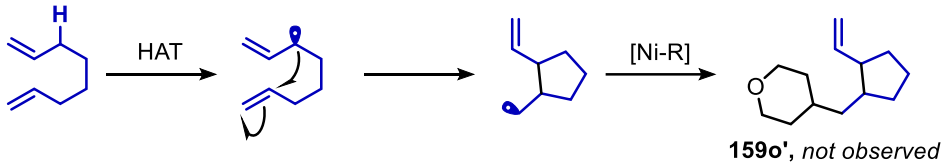

*Figure 3.5.4. The formation of ring closed **159o'** was not observed by GC or NMR.*

1,7-octadiene provided the product cleanly (**159o**), with no overreaction or ring closing to the pendant olefin (**159o'**). The use of allyl-trimethyl silane generated the vinyl silane in excellent regioselectivities (>20:1) and was directly transformed into the corresponding *trans*-vinyl iodide with almost complete retention of configuration using N-iodo succinimide (NIS) in HFIP (**159r**).

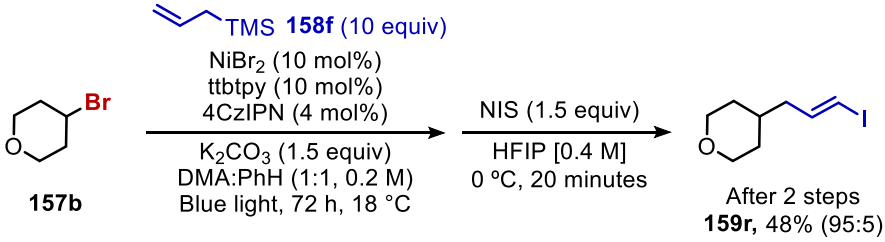

Figure 3.5.5. Telescoped reaction to form vinyliodides.

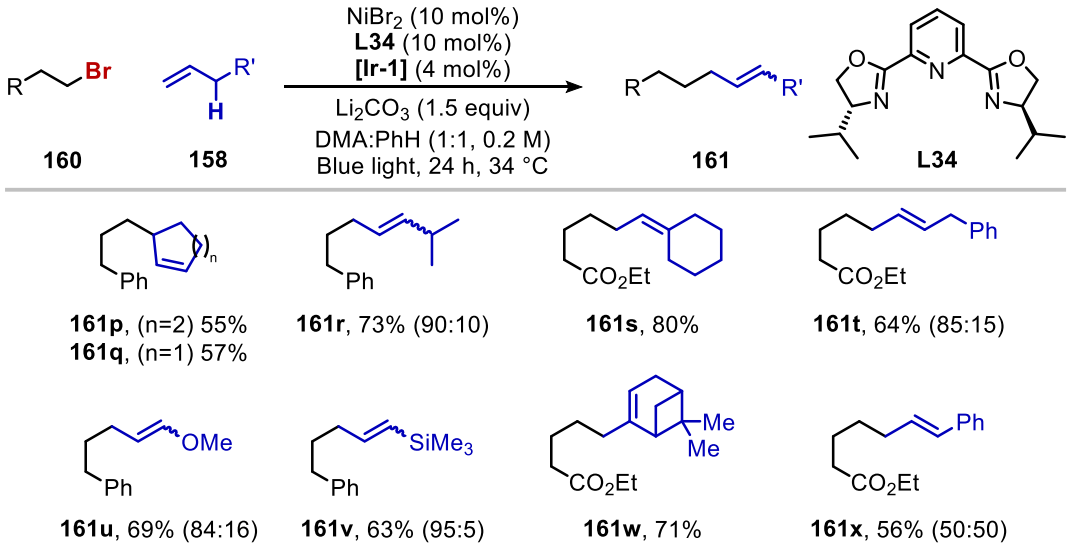

Figure 3.5.6. Performed by Dr Mikkel B. Buendia alkyl bromide (0.3 mmol), olefin (6.0 mmol), $NiBr_2$ (0.015 mmol), L34 (0.018 mmol), $[Ir\text{-}1]PF_6$ (3 µmol), Li_2CO_3 (0.45 mmol), DMA (0.75 mL), PhH (0.75 mL) Hepatochem reactor 34 °C for 24 h. Isolated yields.

The primary bromide series (Figure 3.5.6) enabled the coupling of primary to secondary sp^3 sites is (**161p** and **161q**). The increased size of *iso*-propyl (**161r**) and TMS (**161v**) dramatically increased the selectivity of the reaction to favour the E isomer. Tertiary C(sp^3)-H site could also be abstracted without increasing the number of CH equivalents, yielding 80% (**161s**). Notably, the presence of a more activated C(sp^3)-H group in **161t** was not detrimental to the reaction profile. Additionally, no olefin isomerization of **161t** to the more thermodynamically stable styrene derivative was detected. The formation of vinyl ether (**161u**) worked well. As well as the naturally derived β-pinene (**161w**). Allylbenzenes are amenable for this transformation (**161x**), although the regioselectivity is low when compared to the other examples, the steric bulk of the phenyl ring is unlikely to be the reason. We suspect that the lower ratio is most likely due to a photoisomerization of the styrene.[283]

Allylic C-H

3.5.3. Allylic alcohol

The use of allylic alcohols to access the corresponding aldehyde or ketone would be a good extension of the reactivity profile. Application of allylic alcohol (**162a**) to the reaction resulted in appropriate yields without the need for optimisation. Cholesteryl derivative (**164a**) proceeded cleanly, as did cyclohexyl bromide (**164b**) and straight chain alkyl bromide (**164c**). The propanal derivatives are interesting because Giese addition to acrolein is not possible due to acrolein's poor stability and toxicity.

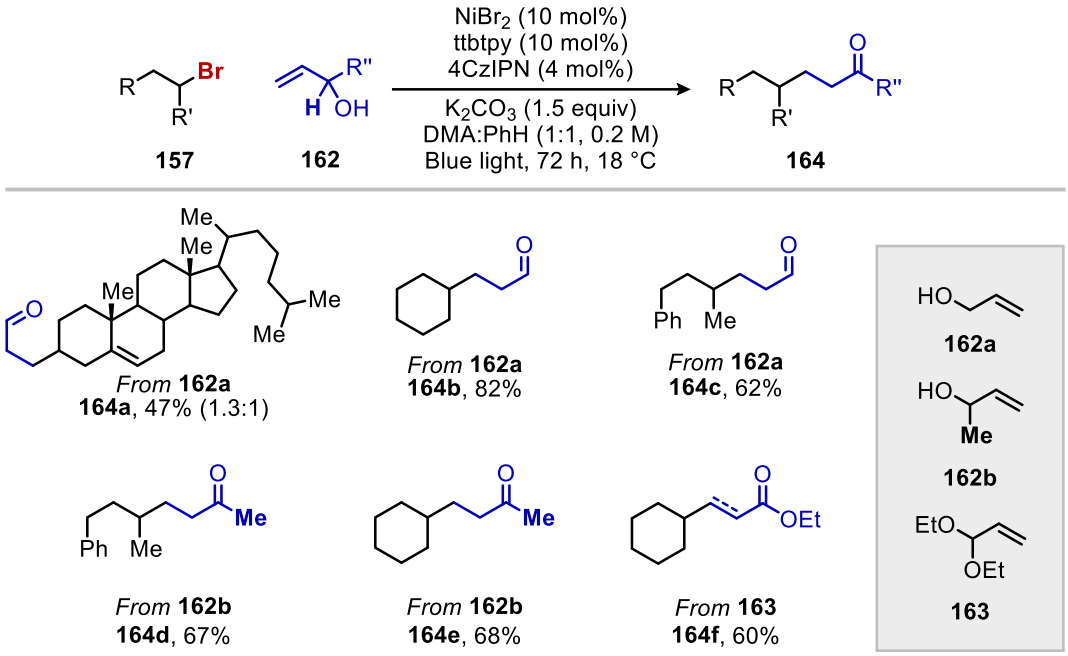

Figure 3.5.7. alkyl bromide (0.2 mmol), allylic alcohol (2.0 mmol), $NiBr_2$ (0.02 mmol), ttbtpy (0.02 mmol), 4CzIPN (4 μmol), K_2CO_3 (0.2 mmol), DMA (0.5 mL), PhH (0.5 mL) 451 nm reactor at 15 °C for 72 h. Isolated yields.

Employing methyl vinyl carbinol (**162b**) gratifyingly provided the methyl ketones in good yields (**164d** and **164e**). The use of acrolein diethyl acetal (**163**) formed the ester (**164f**) upon quenching the reaction with water, however an inseparable mixture of ester and α-β unsaturated ester was obtained. We believe this to have been formed by HAT by the bromide radical from $\mathbf{164f_1}$ which creates the radical $\mathbf{164f_2}$. SET to the cation could form the unsaturated product through elimination of ethyl bromide (Figure 3.5.8).

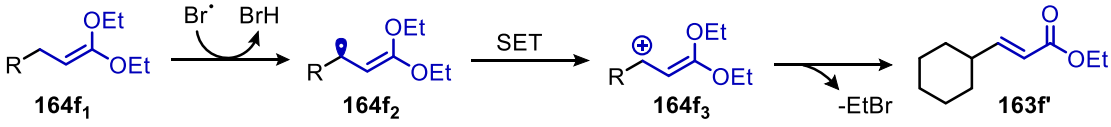

*Figure 3.5.8. possible mechanism for the formation of **164f'***

With a suitable scope in hand with respect to both the alkyl bromide and olefinic coupling partner, it was decided that the aryl bromide series could be used as cross-coupling partners to achieve the sp^2-sp^3 bond forming reaction.

3.5.4. Aryl bromide series

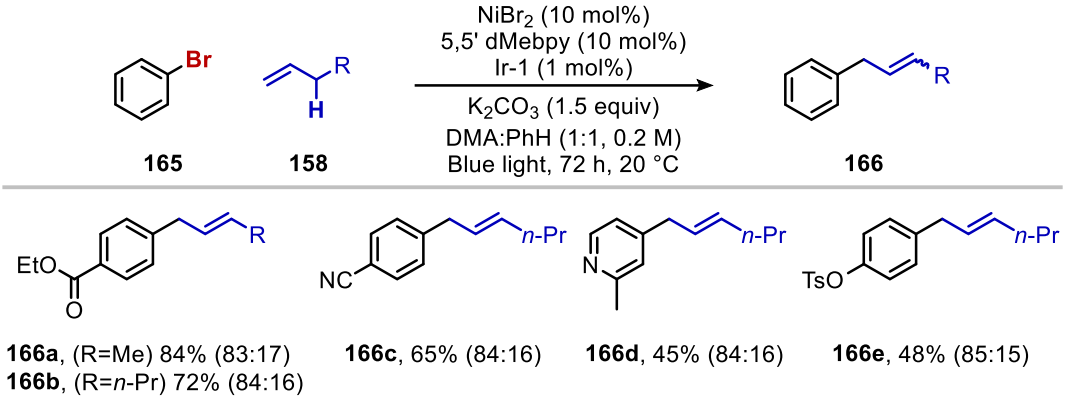

166a, (R=Me) 84% (83:17) **166c**, 65% (84:16) **166d**, 45% (84:16) **166e**, 48% (85:15)
166b, (R=*n*-Pr) 72% (84:16)

Figure 3.5.9. aryl bromide (0.2 mmol), 1-hexene (2.0 mmol), $NiBr_2$ (0.02 mmol), 5,5' dMebpy (0.02 mmol), $[Ir\text{-}1]PF_6$ (4 µmol), K_2CO_3 (0.2 mmol), DMA (0.5 mL), PhH (0.5 mL) 451 nm reactor at 15 °C for 72 h. Isolated yields. a) butene (1 atm) b) 5 days reaction time.

Indeed, the aryl bromide series was compatible with the reaction parameters using a slight adjustment of the reaction conditions (Figure 3.5.9). Bipyridine ligand 5,5'dMebpy was much more effective than the terpyridine series. The use of electron deficient ester worked particularly well with both 1-hexene (**166a**), and 1-butene (**166b**). Electron deficient benzonitrile derivative (**166c**) and heterocyclic systems (**166d**) were tolerated under the reaction conditions. However, tosylate (**166e**) provided 48% yield after an extended reaction period of 5 days. The reaction was monitored at 3 days but there was still considerable amounts of starting aryl bromide remaining.

Allylic C-H

3.5.5. Failed alkyl bromides

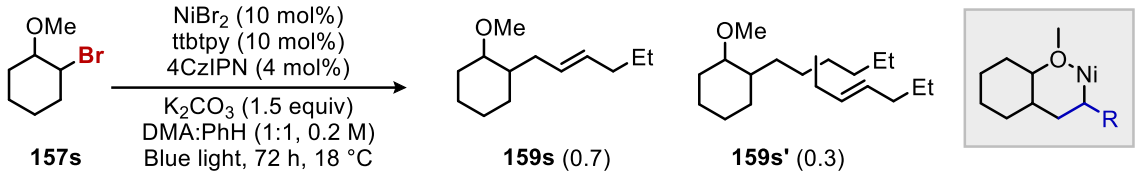

*Figure 3.5.10. Under standard reaction conditions, [Area of **159s** peak / Area of **159s+159s'**]*

Although the substrate scope of the alkyl bromides is broad, there are two failed substrates that warrant discussion (Figure 3.5.10 and Figure 3.5.11). When α-methoxy bromide (**157s**) was exposed to the reaction conditions, two products were observed by GC. The desired product accounted for the majority of the mass balance (~70% of the product mixture). However, a second peak was identified as the "double addition" of 1-hexene by GC-MS analysis (~30% of the product mixture). We hypothesise that the coordinating effect of the methoxy unit may form a six membered nickelacycle that allows a second equivalent of the olefin to react.

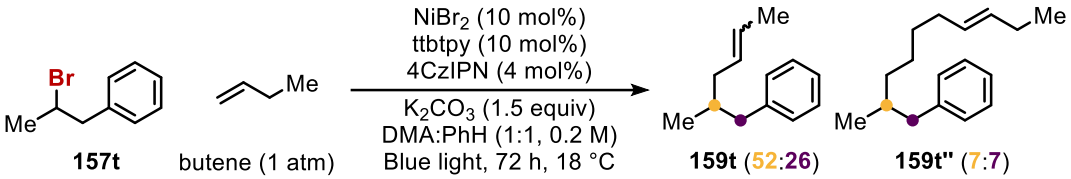

*Figure 3.5.11. The uncalibrated GC product distributions from the alkylation of homobenzylic bromide **xb**. Using decane as internal standard.*

Homobenzylic bromide produced a complex mixture of products when used in conjunction with butene. Analysis of the GC(-MS) and NMR of this reaction showed that alongside the reaction at the initial site, there was a second peak that corresponded to alkylation at the benzylic position as well as multiple additions of the olefin. The benzylic functionalisation is likely due to a facile β-hydride elimination and reinsertion event to afford the nickel at the benzylic site.

The observation of this product in this scenario is likely for two reasons, the first is the use of butene as a gas which slows the kinetics of the reaction, allowing for chain walking event to occur. The second is that the benzylic position is thermodynamically favourable.

However, this result could lead to a chain walking allylation protocol which would be the formal sp^3-sp^3 coupling of two C(sp^3)-H bonds. Controlling the regioselectivity as well as the possible olefin dimers that are also seen could be a challenging but worthwhile endeavour.

3.5.6. Failed alkene substrates using secondary alkyl bromides

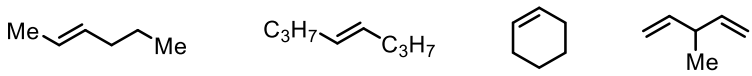

158n **158o** **158p** **158q**

Figure 3.5.12. The failed alkenes with secondary systems. cyclohexyl bromide (0.2 mmol), alkene (2.0 mmol), $NiBr_2$ (0.02 mmol), ttbtpy (0.02 mmol), 4CzIPN (4 µmol), K_2CO_3 (0.2 mmol), DMA (0.5 mL), PhH (0.5 mL) 451 nm reactor at 15 °C for 72 h.

Internal alkenes such as 2-hexene (**158n**) afforded small quantities of the desired cross-coupled product but the majority of the products were from degradation of the starting material, primarily homo-coupling and some dehalogenation of the alkylbromide species. 3-octene (**158o**) on the other hand did not afford even traces of the cross coupled product. Cyclohexene (**158p**) produced only cyclohexene dimers and trimers with no desired cross coupling product observed. This is unusual because the cross coupled product forms with primary bromides (**161p**, 55%). Skipped diene (**158q**) exclusively formed the hydrodehalogenated product.

158r **158s** **158t** **158u**

Figure 3.5.13. The failed gaseous alkenes with secondary systems. cyclohexyl bromide (0.2 mmol), alkene (1 atm), $NiBr_2$ (0.02 mmol), ttbtpy (0.02 mmol), 4CzIPN (4 µmol), K_2CO_3 (0.2 mmol), DMA (0.5 mL), PhH (0.5 mL) 451 nm reactor at 15 °C for 72 h.

Attempts were made to extend the range of gaseous alkene feedstocks, however the reactivity with these species was particularly poor. 3-methyl butene (**158r**) afforded a complex mixture of products. Propene (**158s**) was not amenable to this transformation, recovery of the starting material and some hydrodehalogenated products were obtained. Piperylene (**158t**) gave exclusively the diels-alder products, which likely prevented the productive pathway from occurring. Finally, 1,1-disubstitued olefin (**158u**) was not reactive in the secondary alkyl bromide series.

Allylic C-H

3.5.7. Fragrance molecules

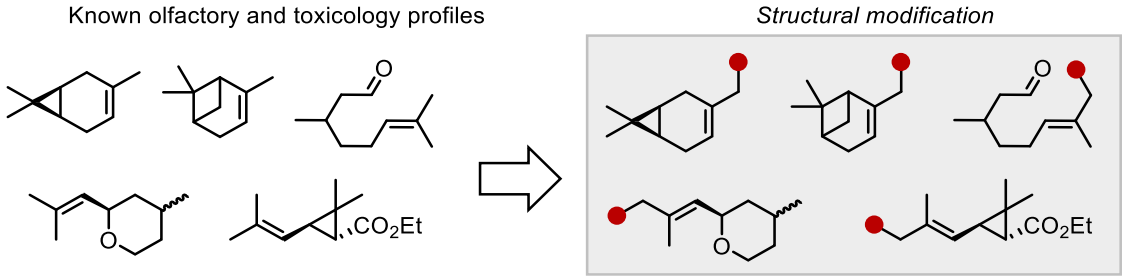

Figure 3.5.14. Relevant fragrance molecules.

The alkenes used so far are petrochemical derivatives. Naturally derived terpenes are an additional bank of feedstock chemicals (Figure 3.5.14), playing a huge part in the fragrance industry. Many actively used or patent protected terpenes could benefit from subtle changes to their organic skeleton, either to improve or change the olfactory properties or overcome patent protection. An example of this smell modification is the well-known chemistry of esters and is taught to many high-school students. Simply changing from methyl propanoate to ethyl propanoate, changes the olfactory properties of the ester from a rum-like odour to that of pineapple. To be able to rapidly access and test alkylated terpenes could enable new perfume leads to be rapidly assessed.

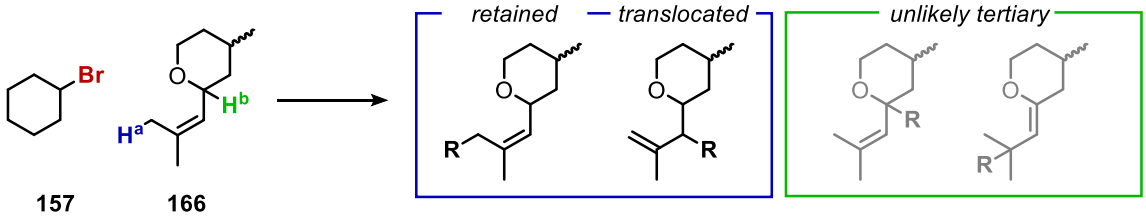

Figure 3.5.15. The issues surrounding using a trisubstituted olefin and secondary bromide.

Rose Oxide, a tri-substituted olefin **166**, was chosen as a starting point, with cyclohexyl bromide. This reaction system upon re-evaluation was not the most appropriate starting point. There are two C(sp^3)-H environments which can be abstracted: the terminal position **H^a**, and the tertiary α-ether position **H^b**. The terminal C(sp^3)-H **H^a** has a slightly higher BDE than the internal allylic C(sp^3)-H. Additionally, we had seen considerably reduced reactivity when using alkenes such as 2-hexene within the secondary alkyl bromide series (**158n**, Figure 3.5.12). In the typical reaction, the *translocated* position is alkylated due to the steric considerations with coupling of the two secondary positions at the *retained* site. Thus, the considerable steric bulk of a trisubstituted olefin may not be an ideal starting point. The outcome of abstraction at the α-ether C(sp^3)-H **H^b** generates either a tertiary or tertiary *O*-stabilized radical.

The abstraction at this site would be unlikely to generate a productive coupling event because we know that that secondary-secondary bonds do not form under the reaction conditions, so a tertiary-secondary bond forming reaction could only occur under a considerably different mechanistic scenario.

Additionally, the use of the 4CzIPN photocatalyst seemed to be specific for the ttbtpy ligand, whereas with other ligands it was considerably less effective. On the other hand, the iridium photocatalyst produced reactivity with several more ligands. Thus, the screen should have been conducted with [Ir-1]PF_6.

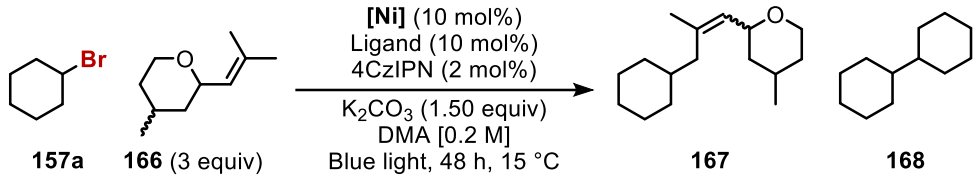

Entry	*Base*	**157a**(%)	**168**(%)	**missing**(%)
1	tpy	50	35	5
2	2,6-diimidazoyl pyridine	32	64	3
3	6Me-tpy	76	23	0
4	bpy	85	15	0
5	dtbbpy	0	60	9
6	55dMe-bpy	100	0	0
7	55dCF_3-bpy	100	0	0
8	2Me-phen	100	0	0
9	2-Picoline	60	0	0
10	DMAP	30	0	5
11	*trans*-Stilbene	100	0	0
12	Methyl Fumerate	90	0	3

Figure 3.5.16. An initial screen of reaction conditions. cyclohexyl bromide (0.2 mmol), rose oxide (0.6 mmol), $NiBr_2$ (0.02 mmol), ttbtpy (0.02 mmol), 4CzIPN (4 µmol), K_2CO_3 (0.2 mmol), DMA (1 mL) 451 nm reactor at 15 °C for 72 h. GC yields using decane as internal standard.

Due to the gem dimethyl group on rose oxide, 6 equivalent C(sp^3)-H environments, we hypothesised that only three equivalents would be required.[284] To our disappointment, none of the desired cross coupled product could be detected under any of the tested experimental conditions. Attempts at reducing the electron density, denticity, or steric demand of the ligands made little difference to the outcome. Incorporating different ligand classes like the stilbene (*entry 11*) and fumarate motif (*entry 12*) were not particularly beneficial.

Allylic C-H

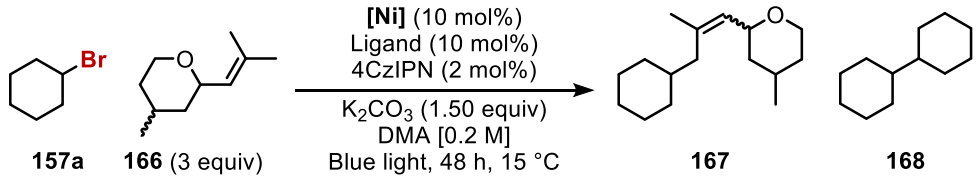

157a **166** (3 equiv) **167** **168**

Entry	*Change*	**157a**(%)	**168**(%)	**missing**(%)
1	No ligand, Air	100	0	0
2	No ligand, Argon	100	0	0
3	Picolinic Acid	90	0	10
4	Veratrole	95	0	5
5	2-methoxybenzoic acid	100	0	0
6	Norbornadiene	100	0	0
7	TMEDA	40	0	20
8	DMAP (1 equiv)	60	0	0
9	DMAP w/ ttbtpy	100	0	0
10	$Ni(acac)_2$	100	0	0
11	$NiBr_2(PMe_3)_2$	100	0	0

Figure 3.5.17. A second screen of reaction conditions. cyclohexyl bromide (0.2 mmol), rose oxide (0.6 mmol), $NiBr_2$ (0.02 mmol), ttbtpy (0.02 mmol), 4CzIPN (4 µmol), K_2CO_3 (0.2 mmol), DMA (1 mL) 451 nm reactor at 15 °C for 72 h. GC yields using decane as internal standard.

In the second round of screening, there was still no observation of even traces of the product. Due to the time constraints, it was decided that the functionalisation of terpenes and terpene like molecules would require considerable development outside of the scope of this thesis. Although the benefits of this work were high, the difficulties in accessing the secondary-secondary coupling or abstracting the terminal C(sp^3)-H bond may require a different approach and screening.

3.6. Mechanistic understandings

Some preliminary mechanistic understanding was gathered to propose a reaction pathway. An initial Stern-Volmer quenching study was conducted by Mikkel. The studies showed that neither alkyl bromide, nor alkene quenched the [Ir-1]PF_6, but a LiBr additive did. The quenching by LiBr could suggest that bromide anions are being oxidised to the radical. Indeed, the reduction potentials of the photocatalyst [Ir-1]PF_6 ($E[*Ir^{III}/Ir^{II}]$ = + 1.21 V *vs* SCE **or** $E[Ir^{IV}/Ir^{III}]$ = + 1.69 V *vs* SCE) and bromide anion ($E[Br^{\bullet}/Br^{-}]$ = + 1.22 V *vs* SCE) match.[285] Additionally, bromide radicals have been hypothesised to behave as HAT agents and could reasonably abstract the internal C(sp^3)-H bond of a terminal olefin. The bond dissociation energies of the internal allylic C(sp^3)-H ($BDE_{(CH)}$ = 82 kcal mol^{-1}) and bromide ($BDE_{(HBr)}$ = 87 kcal mol^{-1}) would render an exergonic HAT. Additionally, bromide radicals are electrophilic and the allylic C(sp^3)-H is nucleophilic so the philicities match.

3.6.1. Proposed Mechanism

We propose a mechanism that involves bromide radicals as the HAT reagent. Although the reaction needs considerably more mechanistic work to fully elucidate the mechanism. We will take the primary bromide series as the representative reaction. Photoexcitation of the iridium photocatalyst generates an excited state ($E[*Ir^{III}/Ir^{II}]$ = + 1.21 V *vs* SCE) which oxidises a bromide anion to the bromide radical ($E[Br^{\bullet}/Br^{-}]$ = + 1.22 V *vs* SCE) and reduced state photocatalyst.

We propose that the nickel (II) complex **a** ($E[Ni^{II}/Ni^{I}]$ = − 1.37 V *vs* $Ag/AgNO_3$)[286] can be reduced by the **p'** ($E[Ir^{III}/Ir^{II}]$ = − 1.37 V *vs* SCE) to generate a ligated nickel (I) bromide species **b**. Oxidative addition of the alkyl bromide would form a nickel (III) intermediate **c** that could feasibly undergo an SET event with the reduced state photocatalyst **p'** ($E[Ni^{III}/Ni^{II}]$ = + 1.11 V *vs* SCE).[287] An electrophilic nickel (II) alkyl complex **d** is thus formed. Concomitant abstraction of the allylic C(sp^3)-H bond by the bromide radical would form an allylic radical that is delocalised across the π-system. Allyl radical addition to **d** at the *terminal* position due to steric considerations forms an nickel (III) alkyl alkyl species **e**. Rapid reductive elimination of **e** would liberate the product and regenerate the initial nickel (I) bromide.

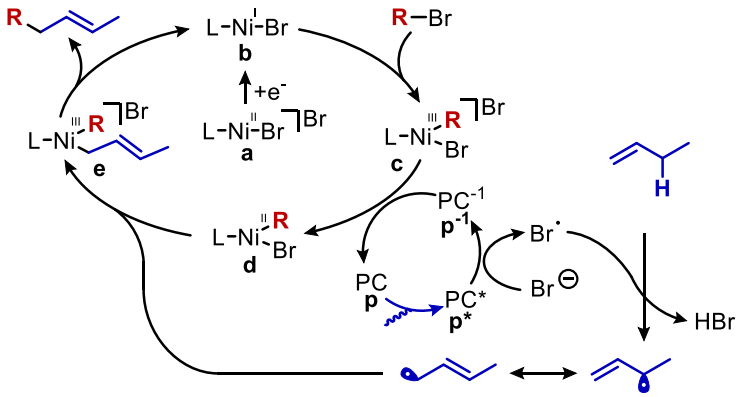

Figure 3.6.1. The proposed mechanism.

3.7. Summary of Chapter 3.

In summary, we have developed a redox-neutral allylic C-H alkylation enabled by photocatalysis. The protocol is mild, robust, and tolerant of a broad range of functionalities. Optimization highlighted the divergency between primary and secondary alkyl bromides. The primary series required a more sterically demanding ligand which in turn necessitated the use of a different photocatalyst and base. The secondary series was slower in reaction time but did not require as high a loading of C-H precursor.

Exquisite site selectivity for the translocated C-C bond forming reaction is a highlight of this work. Although the E:Z selectivities were not readily controlled, this may be inherently due to the photoredox platform employed. The extension of this work to use allylic alcohols expands the synthetic applicability of the protocol. Furthermore, butene could be applied effectively within the protocol. Extension of this work to aryl bromide series was also conducted, although this work was curtailed due to the publication of a paper by Glorius during the finalization of the manuscript. Some preliminary mechanistic understandings were conducted, and it is proposed that bromide radicals are responsible for the HAT event. For further works on this topic, the alkylation of more sterically demanding tri-substituted olefins, such as terpenes, would be highly beneficial.

3.8. Supporting Information

3.8.1. General considerations

The primary series was produced by Mikkel Buendia and spectral data can be viewed online at https://pubs.acs.org/doi/10.1021/acscatal.2c01057.

Analytical. ^{1}H NMR and ^{13}C NMR spectra were recorded on a Bruker 400 spectrometer at 20 °C. The chemical shifts are reported in ppm relative to solvent residual peak. All ^{13}C NMR spectra are reported in ppm relative to TMS, were calibrated using the signal of residual $CHCl_3$ (77.16 ppm), and were obtained with ^{1}H decoupling unless otherwise indicated. Coupling constants, J, are reported in Hertz. Mass spectrometry was performed on a Waters LCT Premier spectrometer or on a MicroTOF Focus, Bruker Daltonics spectrometer. Infrared spectra (FT-IR) measurements were carried out on a Bruker Optics FT-IR Alpha spectrometer equipped with a DTGS detector, KBr beamsplitter at 4 cm^{-1} resolution using a one bounce ATR accessory with diamond windows. Gas chromatographic analyses were performed on Hewlett-Packard 6890 gas chromatography instrument with a FID detector using 25m x 0.20 mm capillary column with cross-linked methyl siloxane as the stationary phase.Column chromatography was performed on silica gel 60 (40-63 μm). Melting points were measured using open glass capillaries in a Büchi B540 apparatus.

Reagents. Reactions were carried out under argon or nitrogen, unless stated otherwise. Anhydrous solvents were obtained from the solvent purification system Puresolv MD-7 or purchased from Acros Organics. All commercial solvents, reagents, nickel sources, and ligands were used as received without further purification. HBr in AcOH and K_2CO_3 (anhydrous) were purchased from Acros Organics. Benzene (sequencing solvent) was purchased from TCI chemicals. $NiBr_2$, $NiBr_2$·glyme, [Ir-1]PF_6, ttbtpy, and **L34** were purchased from Sigma Aldrich. All substrates were either obtained commercially or prepared according to literature procedures.

3.8.2. Reactor setup

OSRAM Oslon® SSL 80 royal- blue LEDs installed at the bottom of a custom-made 8 flat-bottom Schlenk tubes holder (the distance between the flat-bottom Schlenk tube and the light source was measured to be ~7 mm), equipped with a water-cooling system (the thermostat was set at 20 °C) and magnetically stirred (~ 500 rpm).

3.8.3. Optimisation details

An oven dried 8 mL Schlenk tube containing a stirrer bar was charged with K_2CO_3 (0.3 mmol, 41.4 mg, 1.5 equiv), **ttbtpy** (0.02 mmol, 8.02 mg, 10 mol%), $NiBr_2$ (0.02 mmol, 4.4 mg, 10 mol%), and 4CzIPN (0.008 mmol, 6.3 mg, 4 mol%). The Schlenk was attached to a Schlenk line, evacuated, and back filled three times with Argon. Under a positive pressure of argon, **157** (0.2 mmol, 1 equiv) and **158b** (2 mmol, 10 equiv) were added followed by DMA (0.5 mL, anhydrous) and PhH (0.5 mL), stirred for 15 minutes and placed in a preheated reaction vessel at 20 ºC (see picture below) allowed to stir for 48 hours under blue light irradiation. The mixture was quenched with 1M HCl (2 mL) and extracted with EtOAc (10 mL). Decane was added as an internal standard and quantified by calibrated GC-FID analysis.

Allylic C-H

3.8.4. General procedures for allylic alkylation:

Procedure A (2° alkyl bromides): An oven dried 8 mL Schlenk tube containing a stirrer bar was charged with K_2CO_3 (0.3 mmol, 41.4 mg, 1.5 equiv), ttbtpy (0.02 mmol, 8.02 mg, 10 mol%), $NiBr_2$ (0.02 mmol, 4.4 mg, 10 mol%), and 4CzIPN (0.008 mmol, 6.3 mg, 4 mol%) and **157** *if solid* (0.2 mmol, 1 equiv). The Schlenk was attached to a Schlenk line, evacuated, and back filled three times with Argon. Under a positive pressure of argon, **157** i*f liquid* (0.2 mmol, 1 equiv) and **158** (2 mmol, 10 equiv) were added followed by DMA (0.5 mL, anhydrous) and PhH (0.5 mL), stirred for 15 minutes and placed in a preheated reaction vessel at 20 ºC (see picture below) allowed to stir for 48 hours under blue light irradiation. The mixture was quenched with 1M HCl (2 mL) and extracted with EtOAc (10 mL). The organic phase was washed with 10 mL brine, dried with $MgSO_4$ and evaporated, purification by column chromatography. E/Z ratio determined by ^{13}C NMR or by GC-FID analysis.

Procedure B (light alkenes): An oven dried 8 mL Schlenk tube containing a stirrer bar was charged with K_2CO_3 (0.3 mmol, 41.4 mg, 1.5 equiv), ttbtpy (0.02 mmol, 8.02 mg, 10 mol%), $NiBr_2$ (0.02 mmol, 4.4 mg, 10 mol%), and 4CzIPN (0.008 mmol, 6.3 mg, 4 mol%) and **157** *if solid* (0.2 mmol, 1 equiv). The Schlenk was attached to a Schlenk line, evacuated, and back filled three times with Argon. Under a positive pressure of argon, **157** *if liquid* (0.2 mmol, 1 equiv) was added followed by DMA (0.5 mL, anhydrous) and PhH (0.5 mL) and stirred for 5 minutes. The Schlenk was then placed in liquid nitrogen to freeze the solvent, evacuated, and backfilled with an atmosphere of the corresponding gaseous alkene (**158**). The Schlenk was then sealed, warmed to room temperature stirred for 15 minutes, placed in a preheated reaction vessel at 20 ºC (see picture below) and allowed to stir for 48 hours under blue light irradiation. The mixture was opened, hissing can be heard as the reaction is under pressure. Quenched with water and extracted with EtOAc (15 mL). The organic phase was washed with 10 mL brine, dried with $MgSO_4$ and evaporated, purification by column chromatography. *To avoid over pressure of gaseous alkene. The Schlenk* ***must*** *be taken out of the liquid nitrogen bath before opening the valve to the alkene, this prevents too much condensation. It is recommended that as soon as the Schlenk has been filled, the valve to the bottle of alkene is closed and the Schlenk is sealed quickly, the positive pressure from the evaporating alkene should be sufficient to prevent air from entering the vessel.*

Procedure C (Aryl bromides): Inside An oven dried 8 mL Schlenk tube containing a stirrer bar was charged with K_2CO_3 (0.3 mmol, 41.4 mg, 1.5 equiv), ttbtpy (0.02 mmol, 3.7 mg, 10 mol%), $NiBr_2$ (0.02 mmol, 4.4 mg, 10 mol%), and [**Ir-1**]PF_6 (0.002 mmol, 2.3 mg, 1 mol%) and **165** *if solid* (0.2 mmol, 1 equiv). The Schlenk was attached to a Schlenk line, evacuated, and back filled three times with Argon. Under a positive pressure of argon, **165** i*f liquid* (0.2 mmol, 1 equiv) and **158** (2 mmol, 10 equiv) were added followed by DMA (0.5 mL, anhydrous) and PhH (0.5 mL), stirred for 15 minutes and placed in a preheated reaction vessel at 20 ºC (see pictures) allowed to stir for 48 hours under blue light irradiation. The mixture was quenched with 1M HCl (2 mL) and extracted with EtOAc (10 mL). The organic phase was washed with 10 mL brine, dried with $MgSO_4$ and evaporated, purification by column chromatography. E/Z ratio determined by ^1H NMR.

3.8.5. Product data

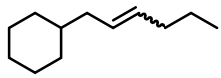

(E)-Hex-2-en-1-ylcyclohexane (159a). The title compound was prepared according to General Procedure A from Cyclohexyl bromide (157a) (32.8 mg, 0.2 mmol, 1 equiv) and 1-hexene (158a) (168 mg, 2 mmol, 10 equiv.), affording the title compound as a colorless oil (30.0 mg, 90% yield) using pentane as eluent. **^{1}H NMR** (400 MHz, $CDCl_3$) δ = 5.37 (m, 2H), 2.05 – 1.92 (m, 2H), 1.92 – 1.84 (m, 2H), 1.73 – 1.60 (m, 5H), 1.38 (m, 2H), 1.28 – 1.09 (m, 5H), 0.88 (4H).**^{13}C NMR** (101 MHz, $CDCl_3$) δ = 131.2, 129.0, 40.7, 38.1, 34.7, 33.1, 26.7, 26.4, 22.8, 13.7. **HRMS** m/z (APCI+) calculated for $C_{12}H_{23}$ [M+H$^+$]: 167.1794, found: 167.1771. **IR (neat):** 2938, 2918, 2849, 1447, 966. **E/Z** ratio determined by ^{13}C NMR to 86:14

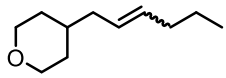

4-((*E*)-Hex-2-en-1-yl)tetrahydro-2*H*-pyran (159b). The title compound was prepared according to General Brocedure B from 4-bromotetrahydro-*2H*-pyran (157b) (32.7 mg, 0.2 mmol, 1 equiv) and 1-hexene (158a) (168 mg, 2 mmol, 10 equiv.), affording the title compound as a colorless oil (18.4 mg, 55% yield) using pentane:EtOAc (98:2) as eluent. **^{1}H NMR** (400 MHz, $CDCl_3$) δ 5.50 – 5.27 (m, 2H), 3.94 (dt, *J* = 11.5, 1.1 Hz, 2H), 3.35 (td, *J* = 11.8, 2.1 Hz, 2H), 2.05 – 1.88 (m, 4H), 1.61 – 1.59 (m, 2H), 1.58 – 1.55 (m, 1H), 1.49 (m, 2H), 1.41 – 1.32 (m, 2H), 1.30 – 1.19 (m, 3H), 0.88 (t, 3H). **^{13}C NMR** (101 MHz, $CDCl_3$) δ = 132.1, 127.7, 68.1, 40.1, 35.4, 34.7, 32.9, 22.7, 13.7. **HRMS** m/z (APCI$^+$) calculated for $C_{12}H_{21}O$ [M+H$^+$]: 169.1587, found: 169.1582. **IR (neat):** 2924, 2922, 2836, 1441, 1230, 1093, 1132, 1011, 966, 849. **E/Z** ratio determined by ^{13}C NMR to 82:18

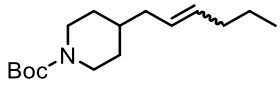

***tert*-Butyl 4-((*E*)-hex-2-en-1-yl)piperidine-1-carboxylate (159c)**. The title compound was prepared according to General Procedure A from *tert*-butyl 4-bromopiperidine-1-carboxylate (157c) (52.6 mg, 0.2 mmol) and 1-hexene (158a) (168 mg, 2 mmol, 10 equiv.), affording the title compound as a colorless oil (39.4 mg, 74% yield) using pentane:EtOAc (9:1) as eluent. **^{1}H NMR** (400 MHz, $CDCl_3$) δ 5.46 – 5.30 (m, 2H), 4.06 (b, 2H), 2.66 (t, *J* = 12.7 Hz, 2H), 1.95 (m, 3H), 1.64 (m, 2H), 1.45 (s, 9H), 1.36 (q, *J* = 7.3 Hz, 2H), 1.26 (s, 2H), 1.08 (m, 2H), 0.88 (t, *J* = 7.3 Hz, 3H). **^{13}C NMR** (101 MHz, $CDCl_3$) δ = 154.9, 132.2, 127.8, 79.1, 39.7, 36.4, 34.7, 31.9, 28.5, 22.7, 13.7. **HRMS** m/z (ESI$^+$) calculated for $C_{16}H_{29}NO_2Na$ [M+Na]: 290.2091, found: 290.2090 **IR (neat):** 2955, 2923, 2854,1691, 1418, 1363, 1163, 1159, 965. **E/Z** ratio determined by ^{13}C NMR to 83:17

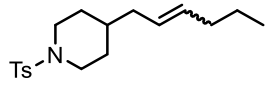

4-((*E*)-Hex-2-en-1-yl)-1-tosylpiperidine (159d). The title compound was prepared according to General Procedure A from 4-bromo-1-tosylpiperidine (4f) (63.4 mg, 0.2 mmol, 1 equiv) and 1-hexene (158a) (168 mg, 2 mmol, 10 equiv), affording the title compound as a colorless oil (39.2 mg, 61% yield) using gradient of pentane:EtOAc (9:1 to 5:1) as eluent. **^{1}H NMR** (300 MHz, $CDCl_3$) δ 7.63 (d, *J* = 8.3 Hz, 2H), 7.30 (d, *J* = 8.0 Hz, 2H), 5.46 – 5.17 (m, 2H), 3.84 – 3.63 (m, 2H), 2.42 (s, 3H), 2.19 (t, *J* = 11.7 Hz, 2H), 1.91 (m, 3H), 1.68 (m, 2H), 1.32 (m, 3H) 1.20 (m, 3H), 0.85 (m, 4H). **^{13}C NMR** (75 MHz, $CDCl_3$) δ = 143.3, 133.2, 132.5, 127.7, 127.4, 46.5, 39.1, 35.6, 34.7, 31.2, 22.6, 21.5, 13.7. **HRMS** m/z (ESI$^+$) calculated for $C_{18}H_{28}NO_2S$ [M+H$^+$]: 322.1835, found: 322.1833. **IR (neat):** 2949, 2921, 2845, 1338, 1162, 1092, 929, 814, 722. **E/Z** ratio determined by ^{13}C NMR to 85:15

Allylic C-H

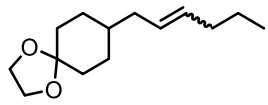

8-((E)-Hex-2-en-1-yl)-1,4-dioxaspiro[4.5]decane (159e). The title compound was prepared according to General Procedure A from 8-bromo-1,4-dioxaspiro[4.5]decane (4d) (44 mg, 0.2 mmol, 1 equiv.) and 1-hexene (158a) (168 mg, 2 mmol, 10 equiv.), affording the title compound as a colorless oil (39.3 mg, 88% yield) using pentane as eluent. **^{1}H NMR** (400 MHz, $CDCl_3$) δ 5.37 (m, 2H), 3.93 (s, 4H), 2.00 – 1.88 (m, 4H), 1.76 – 1.68 (m, 4H), 1.51 (td, *J* = 13.0, 4.4 Hz, 2H), 1.36 (q, *J* = 7.3 Hz, 2H), 1.33 – 1.17 (m, 4H), 0.88 (t, *J* = 7.4 Hz, 3H). **^{13}C NMR** (101 MHz, $CDCl_3$) δ = 131.6, 128.7, 109.2, 64.2, 64.2, 39.4, 36.7, 34.7, 34.5, 29.9, 22.7, 13.7. **HRMS** m/z (APCI$^+$) calculated for $C_{14}H_{25}O_2$ [M+H$^+$]: 225.1849, found: 225.1848. **IR (neat):** 2923, 2857, 1444, 1103, 1033, 965, 922. **E/Z** ratio determined by ^{13}C NMR to 81:19

3-((*E*)-Oct-2-en-1-yl)oxetane (159f). The title compound was prepared according to General Procedure A from 3-bromooxetane (4f) (27.2 mg, 0.2 mmol, 1 equiv) and 1-octene (158b) (224 mg, 2 mmol, 10 equiv), affording the title compound as a colorless oil (24.1 mg, 71% yield) using pentane:EtOAc (97:3) as eluent. **^{1}H NMR** (400 MHz, $CDCl_3$) δ 5.43 (m, 1H), 5.33 (m, 1H), 4.76 (dd, *J* = 7.7, 5.9 Hz, 2H), 4.36 (t, *J* = 6.0 Hz, 2H), 3.01 (m, 1H), 2.35 (m, 2H), 2.00 – 1.91 (m, 2H), 1.37 – 1.20 (m, 7H), 0.93 – 0.82 (m, 3H). **^{13}C NMR** (101 MHz, $CDCl_3$) δ = 132.4, 126.2, 77.1, 36.5, 34.6, 32.5, 31.3, 29.1, 22.5, 14.0. **HRMS** m/z (APCI$^+$) calculated for $C_{12}H_{21}O$ [M+H$^+$]: 169.1587, found: 169.1593. **IR (neat):** 2952, 2922, 2857, 978, 849. **E/Z** ratio determined by ^{13}C NMR to 87:13

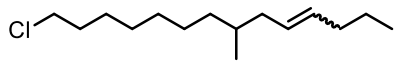

(*E*)-14-Chloro-7-methyltetradec-4-ene (159g). The title compound was prepared according to general Procedure A from 8-bromo-1-chlorononane (4h) (48.0 mg, 0.2 mmol, 1 equiv) and 1-hexene (158a) (168 mg, 2 mmol, 10 equiv), affording the title compound as a colorless oil (28.7 mg, 59% yield) using pentane as eluent. **^{1}H NMR** (400 MHz, $CDCl_3$) δ 5.51 – 5.26 (m, 2H), 3.55 (t, *J* = 6.8 Hz, 2H), 2.08 – 1.93 (m, 3H), 1.87 – 1.74 (m, 3H), 1.50 – 1.17 (m, 14H), 1.13 – 0.94 (m, 2H), 0.94 – 0.77 (m, 6H). **^{13}C NMR** (101 MHz, $CDCl_3$) δ = 131.4, 129.0, 45.2, 40.1, 36.5, 34.8, 33.2, 32.7, 29.7, 28.9, 27.0, 26.9, 22.8, 19.5, 13.6. **HRMS** m/z (EI) calculated for $C_{15}H_{29}Cl$ [M]: 244.1948, NOMINAL MASS found: 244.2. **IR (neat):** 2952, 2923, 2853, 1457, 966, 724. **E/Z** ratio determined by ^{13}C NMR to 85:15

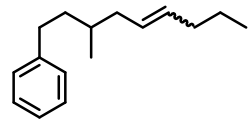

(*E*)-(3-Methylnon-5-en-1-yl)benzene (159h). The title compound was prepared according to General Procedure A from 2-bromo-4-phenyl butane (157g) (42.3 mg, 0.2 mmol, 1 equiv) and 1-hexene (158a) (168 mg, 2 mmol, 10 equiv), affording the title compound as a colourless oil (33.1 mg, 78% yield) using pentane:EtOAc (99:1) as eluent. **^{1}H NMR** (400 MHz, $CDCl_3$) δ = 7.33 – 7.26 (m, 2H), 7.23 – 7.14 (m, 3H), 5.56 – 5.27 (m, 2H), 2.76 – 2.52 (m, 2H), 2.13 – 1.86 (m, 4H), 1.70 – 1.62 (m, 1H), 1.56 – 1.50 (m, 1H), 1.50 – 1.34 (m, 3H), 0.97 – 0.87 (m, 6H). **^{13}C NMR** (101 MHz, $CDCl_3$) δ = ^{13}C NMR (101 MHz, $CDCl_3$) δ 143.1, 131.7, 128.6, 128.4, 128.3, 125.5, 40.0, 38.4, 34.8, 33.5, 32.9, 22.8, 19.4, 13.7. **HRMS** m/z calculated for ($C_{16}H_{25}$) [M+H$^+$]: 217.1961, found: 217.1944. **IR (neat):** 3024, 2954, 2921, 2868, 1494, 1453, 1375, 966, 742, 696. **E/Z** ratio determined by ^{13}C NMR to 82:18

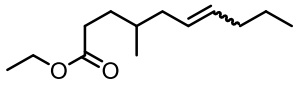

(*E*)-Ethyl 4-methyldec-6-enoate (159i). The title compound was prepared according to general Procedure A from Ethyl 4-bromo-valerate (157i) (41.5 mg, 0.2 mmol, 1 equiv) and 1-hexene (158a) (168 mg, 2 mmol, 10 equiv), affording the title compound as a colorless oil (29.9 mg, 71% yield) using pentane:EtOAc (95:5) as eluent. **^{1}H NMR** (400 MHz, $CDCl_3$) δ 5.46 – 5.29 (m, 2H), 4.12 (q, *J* = 7.2 Hz, 2H), 2.39 – 2.20 (m, 2H), 2.07 – 1.90 (m, 3H), 1.90 – 1.80 (m, 1H), 1.53 – 1.31 (m, 4H), 1.25 (t, *J* = 7.1 Hz, 4H), 0.93 – 0.81 (m, 6H). **^{13}C NMR** (101 MHz, $CDCl_3$) δ = 174.1, 132.0, 128.3, 60.2, 39.7, 34.7, 32.8, 32.2, 31.4, 22.7, 19.1, 14.2, 13.6. **HRMS** *m/z* [APCI$^+$] calculated for $C_{13}H_{25}O_2$ [M+H$^+$]: 213.1849, found 213.1843. **IR (neat):** 2955, 2923, 2856, 2854, 1735, 1171, 967. **E/Z** ratio determined by GC-FID to 82:18

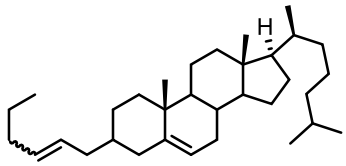

(10*R*,13*R*,17*R*)-3-((*E*)-Hex-2-en-1-yl)-10,13-dimethyl-17-((*R*)-6-methylheptan-2-yl)-2,3,4,7,8,9,10,11,12,13,14,15,16,17-tetradecahydro-1*H*-cyclopenta[*a*]phenanthrene (**159j**). The title compound was prepared according to General Procedure A, with a slight modification, 0.5 mL of *tert*-Butyl alcohol were used in place of 0.5 mL of benzene, from cholesteryl Bromide (157j) (90.0 mg, 0.2 mmol, 1 equiv) and 1-hexene (158a) (168 mg, 2 mmol, 10 equiv), affording the title compound as a mixture of diastereoisomers (38.6 mg, 43% yield) using pentane as eluent. **^{1}H NMR** (400 MHz, $CDCl_3$) δ 5.49 – 5.33 (m, 2H), 5.33 – 5.23 (m, 1H), 2.06 – 1.91 (m, 7H), 1.90 – 1.81 (m, 3H), 1.60 (m, 2H), 1.53 (m, 3H), 1.45 – 1.35 (m, 7H), 1.32 – 1.23 (m, 6H), 1.21 – 1.08 (m, 10H), 1.03 (m, 2H), 1.00 (m, 4H), 0.96 – 0.92 (m, 6H), 0.91 (s, 2H), 0.90 (m, 5H), 0.88 (m, 4H), 0.70 (s, 4H). **^{13}C NMR** (101 MHz, $CDCl_3$) δ = 143.5, 131.5, 128.6, 119.2, 56.9, 56.9, 56.2, 50.6, 50.5, 42.3, 40.4, 39.9, 39.8, 39.6, 39.5, 39.4, 37.4, 37.2, 36.2, 35.8, 34.8, 34.7, 32.9, 31.9, 28.9, 28.3, 28.0, 24.3, 23.8, 22.8, 22.8, 22.6, 21.0, 20.8, 19.5, 19.5, 18.7, 14.1, 13.7, 11.9. **HRMS** calculated for ($C_{33}H_{57}$)[M+H$^+$]: 453.4455, found: 453.4454**IR (neat):** 2924, 2866, 1457, 1376, 964, 734 **E/Z** ratio determined by ^{13}C NMR to 85:15. **dr** ratio determined by ^{1}H NMR to 77:23

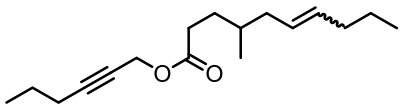

(*E*)-Hex-2-yn-1-yl 4-methyldec-6-enoate (159k). The title compound was prepared according to General Procedure A from hex-2-yn-1-yl 4-bromopentanoate (157k) (52 mg, 0.2 mmol, 1 equiv) and 1-hexene (158a) (168 mg, 2 mmol, 10 equiv.), affording the title compound as a colorless oil (39.6 mg, 78% yield) using pentane:EtOAc (9:1) as eluent. **^{1}H NMR** 400 MHz, $CDCl_3$) δ 5.37 (m, 2H), 4.66 (t, *J* = 2.2 Hz, 2H), 2.45 – 2.25 (m, 2H), 2.20 (tt, *J* = 7.1, 2.2 Hz, 2H), 2.05 – 1.92 (m, 2H), 2.04 – 1.81 (m, 3H), 1.69 (m, 1H), 1.57 – 1.43 (m, 3H), 1.42 – 1.32 (m, 2H), 1.27 (bs, 2H), 0.97 (t, *J* = 7.4 Hz, 3H), 0.91 – 0.83 (m, 6H). **^{13}C NMR** (101 MHz, $CDCl_3$) δ = 173.37, 132.05, 128.20, 87.41, 74.18, 52.69, 39.71, 34.72, 32.76, 31.95, 31.29, 22.70, 21.87, 20.74, 19.06, 13.65, 13.44. **HRMS** m/z (APCI$^+$) calculated for $C_{17}H_{28}O_2Na$ [M+Na$^+$]: 287.1982, found: 287.1979 **IR (neat):** 2957, 2928, 2871, 1739, 1456, 1155, 966, 763. **E/Z** ratio determined by GC-FID to 82:18

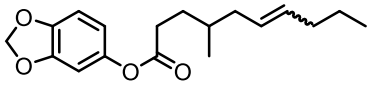

(*E*)-Benzo[*d*][1,3]dioxol-5-yl (*E*)-4-methyldec-6-enoate (159l). The title compound was prepared according to General Procedure A from benzo[*d*][1,3]dioxol-5-yl 4-bromopentanoate (157l) (60.0 mg, 0.2 mmol, 1 equiv) and 1-hexene (158a) (168 mg, 2 mmol, 10 equiv), affording the title compound as a colorless oil (42.0 mg, 69% yield) using pentane as eluent. **^{1}H NMR** (400 MHz, $CDCl_3$) δ 6.79 (d, *J* = 8.4 Hz, 1H), 6.61 (d, *J* = 2.3 Hz, 1H), 6.53 (dd, *J* = 8.3, 2.4 Hz, 1H), 6.00 (s, 2H), 5.54 – 5.32 (m, 2H), 2.64 – 2.46 (m, 2H), 2.08 – 1.99 (m, 2H), 1.94 (m, 1H), 1.86 – 1.76 (m, 1H), 1.60 – 1.51 (m, 2H), 1.40 (m, 2H), 1.34 – 1.27 (m, 1H), 0.98 – 0.88 (m, 6H). **^{13}C NMR** (101 MHz, $CDCl_3$) δ = 172.8, 148.0, 145.3, 145.1, 132.2, 128.1, 113.9, 107.9, 103.8, 101.7, 39.7, 34.7, 32.8, 32.2, 31.3, 22.7, 19.1, 13.7. **HRMS** m/z (ESI$^+$) calculated for $C_{18}H_{24}O_4Na$ [M+Na$^+$]: 327.1568, found: 327.1560. **IR (neat):** 2954, 2923, 2869, 1756, 1481, 1168, 1120, 1035, 933. **E/Z** ratio determined by ^{13}C NMR to 83:17

Allylic C-H

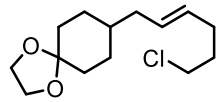

8-((*E*)-6-Chlorohex-2-en-1-yl)-1,4-dioxaspiro[4.5]decane (159m). The title compound was prepared according to general Procedure A from 8-bromo-1,4-dioxaspiro[4.5]decane (157e) (44 mg, 0.2 mmol, 1 equiv.) and 6-chlorohex-1-ene (158c)(240 mg, 2 mmol 10 equiv), affording the title compound as a colorless oil (27.3 mg, 53% yield) using pentane:EtOAc (95:5) as eluent. **^{1}H NMR** (400 MHz, $CDCl_3$) δ 5.54 – 5.30 (m, 2H), 3.95 (s, 4H), 3.54 (t, *J* = 6.7 Hz, 2H), 2.24 – 2.12 (m, 2H), 2.04 – 1.92 (m, 2H), 1.84 (tt, *J* = 6.8, 4.8 Hz, 2H), 1.74 (m, 4H), 1.53 (m, 2H), 1.40 – 1.18 (m, 4H). **^{13}C NMR** (101 MHz, $CDCl_3$) δ = 130.3, 129.5, 109.1, 64.2, 64.2, 44.4, 39.4, 36.6, 34.5, 34.5, 32.3, 29.9, 29.7. **HRMS** m/z (APCI$^+$) calculated for ($C_{14}H_{24}ClO_2$+H$^+$): 259.1459, found: 259.1459. **IR (neat):** 2925, 2858, 1444, 1102, 1033, 967, 921, 755, 730. **E/Z** ratio determined by GC-FID to 80:20

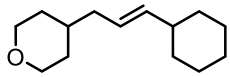

(*E*)-4-(3-Cyclohexylallyl)tetrahydro-2*H*-pyran (159n). The title compound was prepared according to General Procedure A from 4-bromotetrahydro-*2H*-pyran (157b) (32.7 mg, 0.2 mmol, 1 equiv) and allylcyclohexane (158d) (240 mg, 2 mmol, 10 equiv), affording the title compound as a colorless oil (25.7 mg, 62% yield) using pentane:EtOAc (95:5) as eluent. **^{1}H NMR** (400 MHz, $CDCl_3$) δ 5.45 – 5.20 (m, 2H), 3.96 (ddd, *J* = 11.4, 3.9, 1.2 Hz, 2H), 3.37 (td, *J* = 11.8, 2.2 Hz, 2H), 1.94 (t, *J* = 6.4 Hz, 2H), 1.75 – 1.67 (m, 5H), 1.60 (m, 3H), 1.50 (m, 2H), 1.34 – 1.01 (m, 9H). **^{13}C NMR** (101 MHz, $CDCl_3$) δ = 138.4, 124.8, 68.1, 40.7, 40.1, 35.4, 33.3, 33.0, 32.9, 26.2, 26.1. **HRMS** m/z (APCI$^+$) calculated for ($C_{14}H_{24}O$+H$^+$): 209.1900, found: 209.1895. **IR (neat):** 2918, 2845, 1444, 1132, 1091, 966, 851, 754. **E/Z** ratio determined by ^{13}C NMR to 91:9

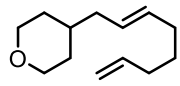

(*E*)-4-(Octa-2,7-dien-1-yl)tetrahydro-*2H*-pyran (5o). The title compound was prepared according to General Procedure A from 4-bromotetrahydro-*2H*-pyran (157b) (32.7 mg, 0.2 mmol, 1 equiv) and 1,7-octadiene (158e)(220 mg, 2 mmol 10 equiv), affording the title compound as a colorless oil (25.0 mg, 65% yield) using pentane:EtOAc (94:6) as eluent. **^{1}H NMR** (400 MHz, $CDCl_3$) δ 5.80 (ddt, *J* = 16.9, 10.2, 6.7 Hz, 1H), 5.39 (m, 2H), 5.07 – 4.93 (m, 2H), 3.94 (m, 2H), 3.35 (td, *J* = 11.8, 2.1 Hz, 2H), 2.11 – 1.93 (m, 6H), 1.70 – 1.54 (m, 3H), 1.54 – 1.43 (m, 3H), 1.38 – 1.17 (m, 4H), 0.88 (m, 1H). **^{13}C NMR** (101 MHz, $CDCl_3$) δ 138.8, 131.9, 127.9, 114.4, 68.1, 40.0, 35.4, 33.2, 33.0, 32.9, 32.0, 28.8. **HRMS** m/z () calculated for $C_{13}H_{23}O$ [M+H$^+$]: 195.1743, found: 195.1742 **IR (neat)**: 2950, 2921, 2836, 1639, 1440, 1230, 1092, 1011, 972, 966, 907, 849. **E/Z** ratio determined by ^{13}C NMR to 5.3:1

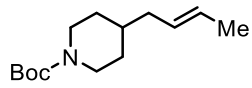

***tert*-Butyl 4-((*E*)-but-2-en-1-yl)piperidine-1-carboxylate (5p).** The title compound was prepared according to General Procedure B from *tert*-butyl 4-bromopiperidine-1-carboxylate (157c) (52.6 mg, 0.2 mmol, 1 equiv) and 1-butene (158f, 1 atmosphere), affording the title compound as a colorless oil (24.8 mg, 50% yield) using pentane:EtOAc (6:1) as eluent. **^{1}H NMR** (400 MHz, $CDCl_3$) δ 5.63 – 5.26 (m, 2H), 4.09 (s, 2H), 2.68 (t, *J* = 12.7 Hz, 2H), 1.94 (m, 2H), 1.70 – 1.63 (m, 4H), 1.47 (s, 9H), 1.33 – 1.25 (m, 2H), 1.09 (m, 2H), 0.86 (m, 1H). **^{13}C NMR** (101 MHz, $CDCl_3$) δ 128.9, 126.6, 79.1, 39.6, 36.4, 31.9, 28.5, 17.9. **HRMS** m/z (APCI$^+$) calculated for $C_{14}H_{25}NO_2Na$ [M+Na$^+$]: 262.1777, found: 262.1773. **IR (neat)**: 2967, 2920, 2851, 1691, 1419, 1363, 1240, 1167, 964. **E/Z** ratio determined by ^{1}H NMR to 77:23

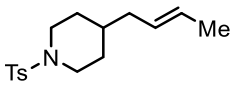

4-((*E*)-But-2-en-1-yl)-1-tosylpiperidine (5q). The title compound was prepared according to General Procedure B from 4-bromo-1-tosylpiperidine (157d) (63.4 mg, 0.2 mmol, 1 equiv) and 1-butene (158f, 1 atmosphere) affording the title compound as a pale yellow oil which solidified to an off-white wax (44.5 mg, 73% yield) using pentane:EtOAc (5:1) as eluent. **^{1}H NMR** (400 MHz, $CDCl_3$) δ 7.65 (d, *J* = 8.4 Hz, 2H), 7.37 – 7.30 (d, *J* = 8.3 Hz, 2H), 5.65 – 5.15 (m, 2H), 3.76 (d, *J* = 11.7 Hz, 2H), 2.44 (s, 3H), 2.22 (m, 2H), 2.02 – 1.85 (m, 2H), 1.76 – 1.68 (m, 2H), 1.63 (dd, *J* = 6.1, 1.3 Hz, 3H), 1.39 – 1.04 (m, 4H). **^{13}C NMR** (101 MHz, $CDCl_3$) δ = 143.3, 133.3, 129.5, 128.4, 127.7, 126.9, 125.5, 46.5, 39.1, 35.5, 31.2, 21.5, 17.9. **HRMS** m/z (ESI^+) calculated for $C_{14}H_{24}NO_2S$ $[M+H^+]$: 294.1522, found: 294.1519. **IR (neat)**: 2918, 2840, 1445, 1335, 1160, 1094, 813, 725. **Melting point:** 52-54 ºC. **E/Z** ratio determined by ^{1}H NMR to 81:19

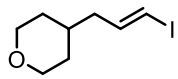

(*E*)-4-(3-Iodoallyl)tetrahydro-2H-pyran (5r). The title compound was prepared according to General Procedure A from 4-bromotetrahydro-*2H*-pyran (157b) (32.7 mg, 0.2 mmol, 1 equiv) and allyl-trimethylsilane (158g) (229 mg, 2 mmol, 10 equiv), affording the vinyl-silane intermediate using pentane:EtOAc (97:3) as eluent, 5 mg was taken to asses purity and the rest was taken on to the next step. To the remaining reactant was added 0.8 mL of dry HFIP under nitrogen, cooled to 0 ºC and NIS (1.5 equiv) was added in one portion, the reaction was allowed to stir at 0 ºC for 20 minutes and then quenched with aqueous sodium sulfite, extracted with EtOAc (3 x 5 mL), the combined extracts were washed once with $NaHCO_3$ and brine. The organic layer was dried with magnesium sulfate and evaporated. Column chromatography afforded the title compound as a colorless oil (23.5 mg, 48% yield over 2 steps) using pentane:EtOAc (96:4) as eluent. **^{1}H NMR (400 MHz, $CDCl_3$)** δ 6.51 (dt, *J* = 14.3, 7.6 Hz, 1H), 6.04 (dt, *J* = 14.3, 1.3 Hz, 1H), 3.97 (ddt, *J* = 11.7, 4.7, 1.2 Hz, 2H), 3.38 (td, *J* = 11.8, 1.9 Hz, 2H), 2.03 (ddd, *J* = 7.6, 6.2, 1.4 Hz, 2H), 1.64 – 1.58 (m, 3H), 1.33 – 1.23 (m, 2H). **^{13}C NMR (101 MHz, $CDCl_3$)** δ 144.2, 77.3, 77.0, 76.7, 75.7, 67.9, 43.3, 34.5, 32.6. **HRMS** m/z ($APCI^+$) calculated for $C_8H_{14}IO$ $[M+H^+]$, 243.0084 found: 253.0083. **IR (neat)**: 2911, 2835, 1440, 1233, 1131, 1090, 1010, 981, 950, 849, 666. **E/Z** ratio determined by ^{1}H NMR to 95:5

Intermediate (trimethyl(3-(tetrahydro-2H-pyran-4-yl)prop-1-en-1-yl)silane) **^{1}H NMR (300 MHz, $CDCl_3$)** δ 5.99 (dt, *J* = 18.4, 6.6 Hz, 1H), 5.66 (dt, *J* = 18.5, 1.3 Hz, 1H), 4.03 – 3.90 (m, 2H), 3.39 (td, *J* = 11.8, 1.9 Hz, 2H), 2.08 (td, *J* = 6.5, 1.3 Hz, 2H), 1.65 – 1.58 (m, 2H), 1.36 – 1.17 (m, 2H), 0.06 (d, *J* = 0.9 Hz, 9H). **^{13}C NMR (101 MHz, $CDCl_3$)** δ 144.4, 132.1, 77.3, 77.0, 76.7, 68.1, 44.3, 34.8, 32.9, -1.2. **E/Z** ratio determined by ^{1}H NMR to >95:5

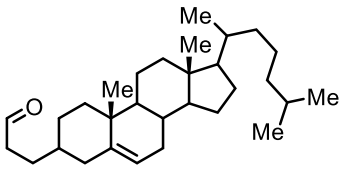

3-((10R,13R,17R)-10,13-Dimethyl-17-((R)-6-methylheptan-2-yl)-2,3,4,7,8,9,10,11,12,13,14,15,16,17-tetradecahydro-1H-cyclopenta[a]phenanthren-3-yl)propanal (164a). The title compound was prepared according to General Procedure A from cholesteryl Bromide (157j) and and allylalcohol (162a) (116 mg, 2 mmol, 10 equiv) were used, affording the title compound as a mixture of diastereoisomers (1.3:1) colourless oil (40.0 mg, 47%) using pentane:EtOAc (95:5) as eluent.**^{1}H NMR** (400 MHz, $CDCl_3$) δ 9.79 (t, 1.9 Hz, 1H), 5.37 – 5.20 (m, 1H), 2.49 – 2.45 (m, 1H), 2.44 – 2.31 (m, 1H), 2.03 (m, 2H), 1.95 (m, 1H), 1.90 – 1.74 (m, 3H), 1.64 – 1.54 (m, 6H), 1.54 – 1.46 (m, 3H), 1.45 – 1.30 (m, 5H), 1.30 – 1.21 (m, 3H), 1.19 – 1.08 (m, 6H), 1.07 (q, *J* = 3.0 Hz, 1H), 1.03 (s, 2H), 0.99 (s, 2H), 0.94 (d, *J* = 6.5 Hz, 3H), 0.89 (dd, *J* = 6.6, 1.8 Hz, 6H), 0.69 (d, *J* = 1.6 Hz, 3H). **^{13}C NMR** (101 MHz, $CDCl_3$) δ 203.1, 202.8, 142.7, 140.0, 121.6, 119.8, 77.3, 77.2, 77.0, 76.7, 56.8, 56.2, 50.5, 42.3, 42.2, 41.5, 39.8, 39.5, 39.4, 39.4, 38.9, 37.4, 37.2, 36.6, 36.2, 35.8, 35.8, 33.9, 33.9, 31.9, 29.1, 28.9, 28.3, 28.0, 26.0, 24.3, 23.9, 23.8, 23.1, 22.8, 22.6, 20.9, 20.8, 19.5, 19.4, 18.7, 11.9, 11.9. **HRMS** m/z ($APCI^+$) calculated for ($C_{30}H_{50}O$) $[M+H^+]$: 427.3934, found: 427.3939 **IR(neat):** 2917, 2864, 1716, 1464, 1436, 1330, 1382. **Melting point:** 84-88 ºC.

Allylic C-H

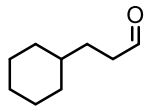

3-Cyclohexylpropanal (164b). The title compound was prepared according to General Procedure A from cyclohexylbromide (157a) (32.8 mg, 0.2 mmol, 1 equiv) and allylalcohol (162a)(116 mg, 2 mmol, 10 equiv), affording the title compound as a colorless oil (22.6 mg 82% yield) using pentane:EtOAc (9:1) as eluent. **^{1}H NMR** (400 MHz, $CDCl_3$) δ 9.76 (m, 1H), 2.42 (td, *J* = 7.7, 1.9 Hz, 2H), 1.69 (m, 4H), 1.63 (m, 1H), 1.52 (q, *J* = 7.2 Hz, 2H), 1.31 – 1.12 (m, 6H), 0.99 – 0.83 (m, 2H). **^{13}C NMR** (101 MHz, $CDCl_3$) δ 203.1, 41.5, 37.2, 33.1, 29.4, 26.5, 26.2. **IR (neat)**: 2919, 2849, 1702, 1447, 1411, 1280. Analytical data is consistent with literature values.[288]

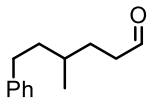

4-Methyl-6-phenylhexanal (164c). The title compound was prepared according to General Procedure A from 2-bromo-4-phenyl butane (157h) (42.3 mg, 0.2 mmol) and allylalcohol (7a)(116 mg, 2 mmol, 10 equiv), affording the title compound as a colorless oil (23.5 mg, 62% yield) using pentane:EtOAc (9:1) as eluent. **^{1}H NMR** (400 MHz, $CDCl_3$) δ 9.77 (t, *J* = 1.8 Hz, 1H), 7.28 (m, 2H), 7.22 – 7.13 (m, 3H), 2.62 (m, 2H), 2.49 – 2.32 (m, 2H), 1.86 – 1.58 (m, 2H), 1.54 – 1.34 (m, 3H), 0.95 (d, *J* = 6.0 Hz, 3H). **^{13}C NMR** (101 MHz, $CDCl_3$) δ 202.8, 142.6, 128.3, 128.3, 125.7, 41.6, 38.6, 33.3, 32.1, 28.8, 19.3. **HRMS** calculated for $C_{13}H_{18}O$ [M]: 190.1358, found: 190.1304. **IR (neat)**: 3024, 2953, 2922, 2857, 1701, 743, 696.

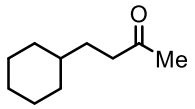

4-Cyclohexylbutan-2-one (164d). The title compound was prepared according to General Procedure A from cyclohexylbromide () (32.8 mg, 0.2 mmol, 1 equiv) and but-3-en-2-ol (162b)(144 mg, 2 mmol, 10 equiv), affording the title compound as a colorless oil (20.9 mg, 68%) using pentane:EtOAc (9:1) as eluent. **^{1}H NMR** (400 MHz, $CDCl_3$) 2.42 (m, 2H), 2.13 (s, 3H), 1.69 (m 4H), 1.62 (m, 1H), 1.46 (m, 2H), 1.19 (m, 6H), 0.88 (m, 2H). **^{13}C NMR** (101 MHz, $CDCl_3$) δ 209.6, 41.4, 37.2, 33.1, 31.2, 29.8, 26.5, 26.2. **IR(neat):** 2918, 2848, 1714, 1447, 1354, 1160. Analytical data is consistent with literature values.[289]

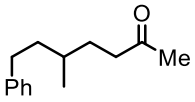

5-Methyl-7-phenylheptan-2-one (164e). The title compound was prepared according to General Procedure A from 2-bromo-4-phenyl butane (157h) (42.3 mg, 0.2 mmol) and but-3-en-2-ol (162b) (144 mg, 2 mmol, 10 equiv), affording the title compound as a colourless oil (27.4 mg, 67% yield) using pentane:EtOAc (9:1) as eluent. **^{1}H NMR** (400 MHz, $CDCl_3$) δ 7.42 – 7.25 (m, 2H), 7.24 – 7.15 (m, 3H), 2.75 – 2.54 (m, 2H), 2.45 (m, 2H), 2.16 (s, 3H), 1.77 – 1.60 (m, 3H), 1.56 – 1.39 (m, 2H), 0.97 (d, *J* = 6.0 Hz, 2H). **^{13}C NMR** (101 MHz, $CDCl_3$) δ = 209.3, 142.8, 128.3, 128.3, 125.7, 41.4, 38.6, 33.3, 32.1, 30.6, 29.9, 19.3. **HRMS** m/z (APCI$^+$) calculated for ($C_{14}H_{21}O$ [M+H$^+$]: 205.1587, found: 205.1587. **IR(neat):** 3024, 2952, 2923, 2856, 1713, 1354, 745, 697.

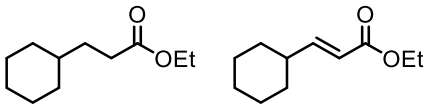

Ethyl 3-cyclohexylpropanoate (164f). The title compound was prepared according to General Procedure A from cyclohexylbromide (4a) (32.8 mg, 0.2 mmol, 1 equiv) and 3,3-diethoxyprop-1-ene (6) (260 mg, 2 mmol, 10 equiv), affording an inseparable mixture of the title compound and 3-cyclohexylacrylate (**5s'**) (21.9 mg) in a 5 to 1 ratio as a colorless oil (21.9 mg, 60% yield) using pentane:EtOAc (9:1) as eluent. **^{1}H NMR** (400 MHz, $CDCl_3$) δ 4.12 (q, *J* = 7.1 Hz, 2H), 2.33 – 2.25 (m, 2H), 1.79 – 1.60 (m, 6H), 1.52 (m, 2H), 1.25 (t, *J* = 7.1 Hz, 10H), 0.90 (m, 3H). **^{13}C NMR** (101 MHz, $CDCl_3$) δ = 174.2, 60.2, 37.3, 33.0, 32.4, 32.0, 31.7, 26.5, 26.2, 14.2. Analytical data of 5s is consistent with literature values.[290]

164f' ^{1}H NMR (400 MHz, $CDCl_3$) δ 6.91 (dd, *J* = 15.8, 6.8 Hz, 1H), 5.76 (dd, *J* = 15.8, 1.5 Hz, 1H) 4.13 (q, J = 7.1 Hz, 2H). Analytical data of 5s' is consistent with literature values.

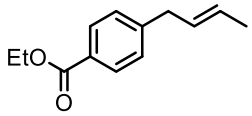

Methyl 4-((*E*)-hex-2-en-1-yl) benzoate (166a). The title compound was prepared according to General Procedure C from Methyl 4-bromobenzoate (8a) (42.8 mg, 0.2 mmol, 1 equiv) and 1-hexene (165a) (168 mg, 2 mmol, 10 equiv), affording the title compound as a colorless oil (36.9 mg, 84%) using pentane:EtOAc (9:1) as eluent. **Note: these aryl-allyl compounds decompose with storage under air, the more electron deficient the aryl ring, the quicker the decomposition, it is advised to store in the freezer under argon**.* **^{1}H NMR** (^{1}H NMR (400 MHz, $CDCl_3$) δ 8.02 – 7.95 (d, *J* = 8.3 Hz, 2H), 7.30 – 7.22 (d, *J* = 8.1 Hz, 2H), 5.65 – 5.47 (m, 2H), 3.92 (s, 3H), 3.40 (d, *J* = 4.9 Hz, 2H), 2.06 – 1.98 (m, 2H), 1.42 (h, *J* = 7.4 Hz, 2H), 0.92 (t, *J* = 7.4 Hz, 3H).**^{13}C NMR** (101 MHz, $CDCl_3$) δ = 167.2, 146.7, 132.8, 129.7, 128.5, 127.9, 52.0, 39.0, 34.6, 22.5, 13.7. **E/Z** ratio determined by ^{1}H NMR to 83:17. Analytical data is consistent with literature values.[291]

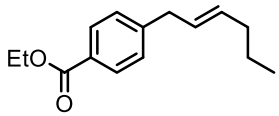

Methyl 4-((*E*)-but-2-en-1-yl) benzoate (166b). The title compound was prepared according to general procedure C, however, 1-butene was added according to general procedure B, from methyl 4-bromobenzoate (165a)(42.8 mg, 0.2 mmol, 1 equiv) and 1-butene (1m, atmosphere), affording the title compound as a colorless oil (36.9 mg, 84%) using pentane:EtOAc (9:1) as eluent. **^{1}H NMR** (^{1}H NMR (400 MHz, $CDCl_3$) δ 7.98 (d, *J* = 8.2 Hz, 2H), 7.26 (d, *J* = 8.3 Hz, 2H), 5.58, (m, 2H), 3.92 (s, 3H), 3.39 (d, *J* = x Hz, 2H), 1.72 (m, 3H). **^{13}C NMR** (101 MHz, $CDCl_3$) δ = 167.1, 146.5, 129.7, 129.0, 128.5, 128.4, 127.2, 52.0, 39.0, 17.9. **E/Z** ratio determined by ^{1}H NMR to 84:16. Analytical data is consistent with literature values.[292]

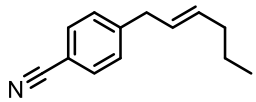

4-((*E*)-Hex-2-en-1-yl)benzonitrile (166c). The title compound was prepared according to general procedure C from 4-bromobenzonitrile (165b) (36.2 mg, 0.2 mmol, 1 equiv) and 1-hexene (158a) (168 mg, 2 mmol, 10 equiv, affording the title compound as an oil (24.0 mg, 65%) using pentane:EtOAc (9:1) as eluent.**^{1}H NMR** (400 MHz, $CDCl_3$) δ 7.57 (d, *J* = 8.5 Hz, 2H), 7.28 (d, *J* = 8.6 Hz, 2H), 5.65 – 5.43 (m, 2H), 3.45 (d, *J* = 7.1 Hz, 2H), 2.11 (dq, *J* = 1.3, 7.3 Hz, 2H), 1.47 – 1.33 (m, 2H), 0.90 (t, *J* = 7.3 Hz, 3H). **^{13}C NMR** (101 MHz, $CDCl_3$) δ = 146.8, 133.5, 132.2, 129.3, 127.1, 119.1, 109.8, 39.1, 34.6, 22.5, 13.7. **E/Z** ratio determined by ^{1}H NMR to 84:16. Analytical data is consistent with literature values.[293]

Allylic C-H

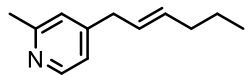

4-((*E*)-Hex-2-en-1-yl)-2-methylpyridine (166d). The title compound was prepared according to general procedure C from 4-bromo-2-methylpyridine (165c) (34.2 mg, 0.2 mmol, 1 equiv) and 1-hexene (158a) (168 mg, 2 mmol, 10 equiv) were used, affording the title compound as a pale yellow oil (16.0 mg, 45%) using pentane:EtOAc (4:1) as eluent. **^{1}H NMR** (400 MHz, $CDCl_3$) δ 8.36 (d, *J* = 5.1 Hz, 1H), 6.97 (s, 1H), 6.91 (d, *J* = 5.1 Hz, 1H), 5.52 (m, 2H), 3.38 – 3.22 (m, 2H), 2.52 (s, 3H), 2.13 – 1.98 (m, 2H), 1.46 – 1.34 (m, 2H), 0.90 (t, *J* = 7.4 Hz, 3H). **^{13}C NMR** (101 MHz, $CDCl_3$) δ = 158.3, 150.4, 149.0, 133.4, 126.9, 123.4, 121.0, 38.3, 34.6, 24.3, 22.5, 13.7. **HRMS** *m/z* (ESI^+) calculated for $C_{12}H_{18}N$ [$M+H^+$] 176.1434, found: 176.1434. **E/Z** ratio determined by ^{1}H NMR to 84:16.

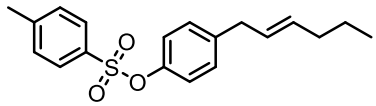

4-((*E*)-Hex-2-en-1-yl) phenyl 4-methylbenzenesulfonate (166e). The title compound was prepared according to general procedure C from 4-bromophenyl 4-methylbenzenesulfonate (165d) (65.2 mg, 0.2 mmol, 1 equiv) and 1-hexene (158a) (168 mg, 2 mmol, 10 equiv) were used, affording the title compound as an oil (31.7 mg, 48%) using pentane:EtOAc (9:1) as eluent. **^{1}H NMR** (400 MHz, $CDCl_3$) δ 7.73 (d, *J* = 8.3 Hz, 2H), 7.36 – 7.30 (d, J = 8.3 Hz, 2H), 7.10 (d, *J* = 8.5 Hz, 2H), 6.90 (d, *J* = 8.6 Hz, 2H), 5.61 – 5.43 (m, 2H), 3.30 (d, *J* = 4.8 Hz, 2H), 2.47 (s, 3H), 2.01 (dtd, *J* = 6.5, 5.4, 2.5 Hz, 2H), 1.41 (m, 2H), 0.91 (t, *J* = 7.4 Hz, 3H). **^{13}C NMR** (101 MHz, $CDCl_3$) δ = 147.8, 145.2, 140.2, 132.5, 129.7, 129.5, 128.5, 128.2, 122.1, 38.3, 34.6, 22.5, 21.7, 13.7. **HRMS** *m/z* (ESI^+) calculated for $C_{19}H_{22}NaO_3S$ [$M+Na^+$]**:** 353.1182, found: 353.1180. **E/Z** ratio determined by ^{1}H NMR to 85:15.

3.8.6. NMR Data

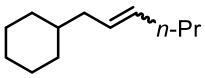

159a

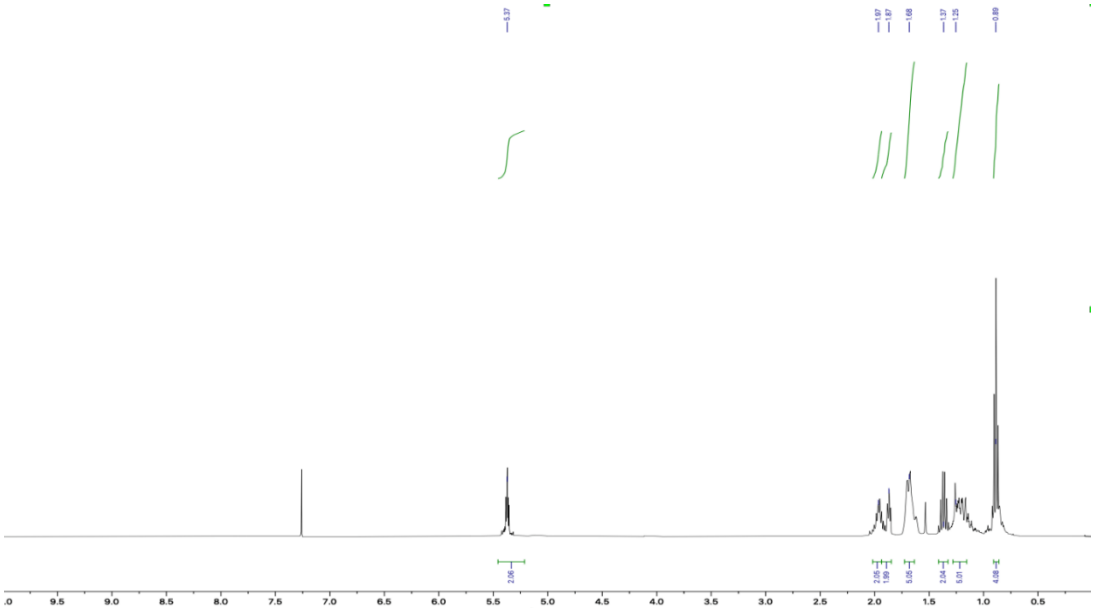

^{1}H NMR spectrum (400 Hz) of **159a**

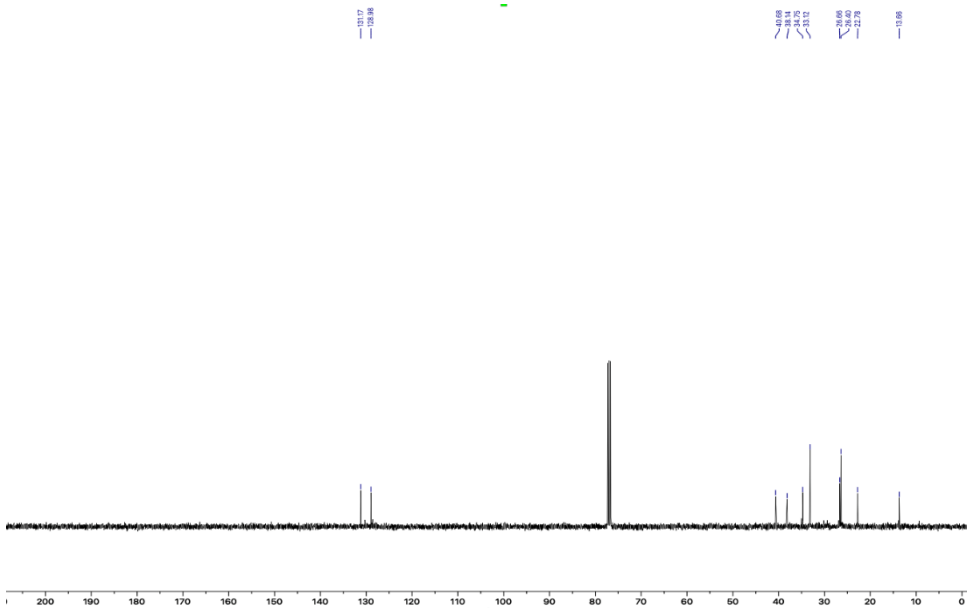

^{13}C NMR spectrum (101 Hz) of **159a**

Allylic C-H

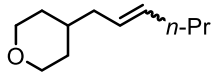

159b

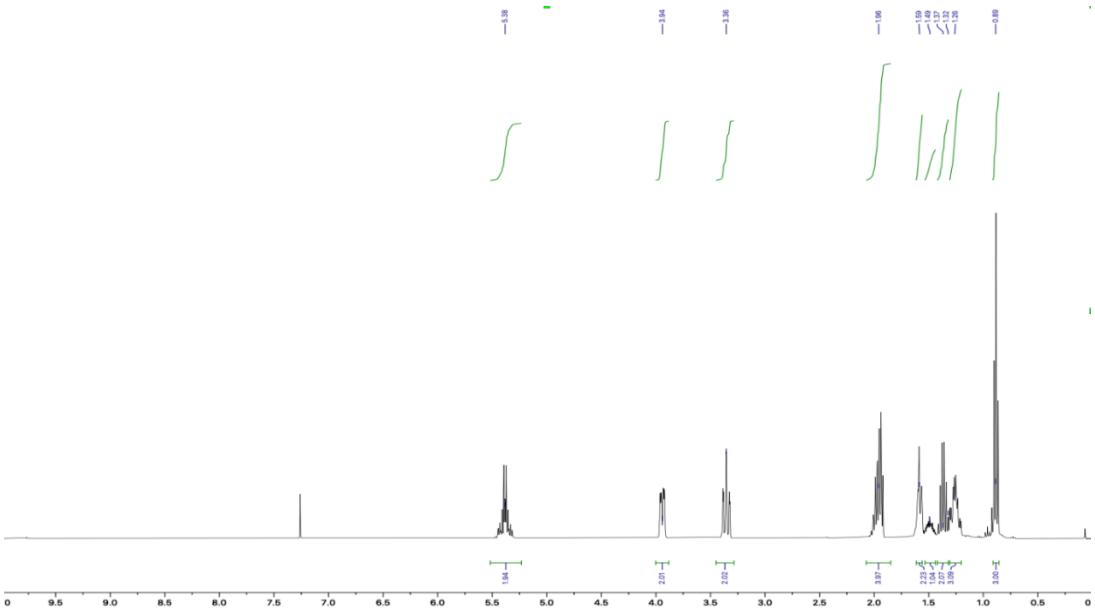

^{1}H NMR spectrum (400 Hz) of **159b**

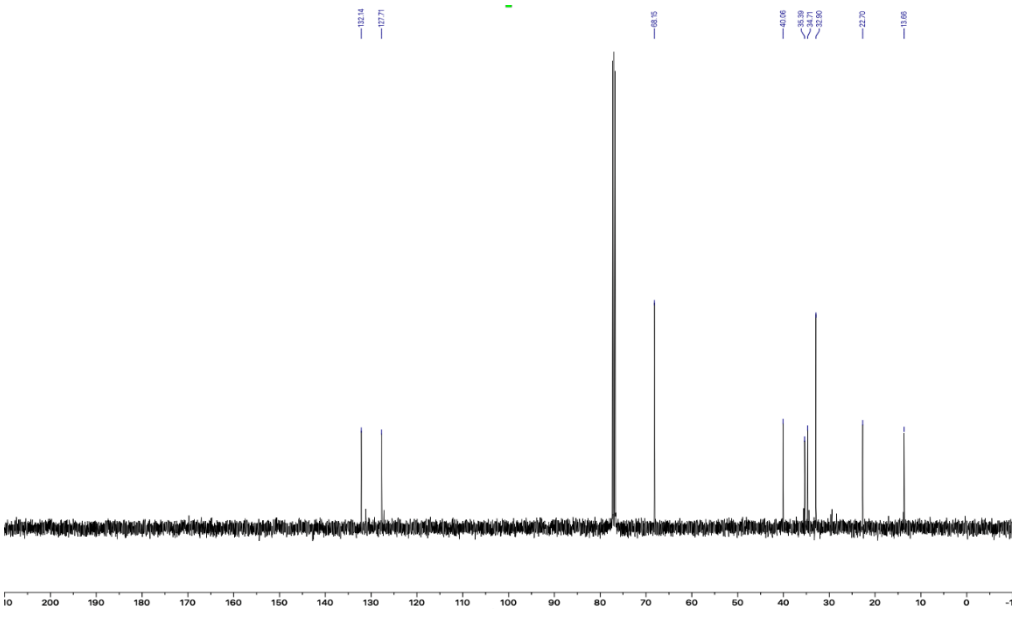

^{13}C NMR spectrum (101 Hz) of **159b**

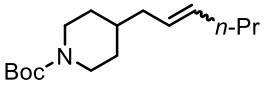

159c

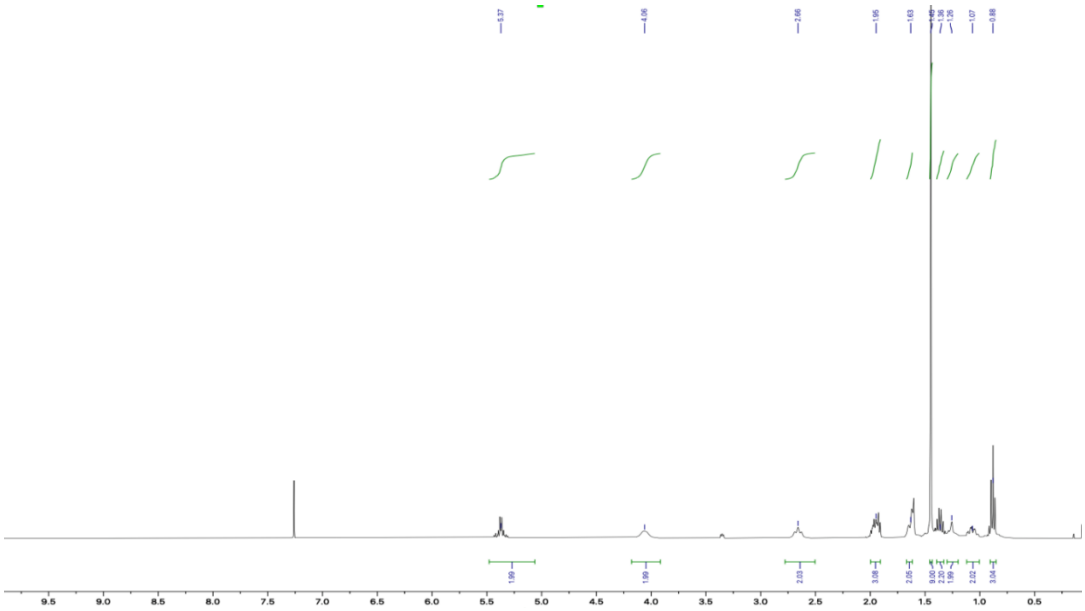

^{1}H NMR spectrum (400 Hz) of **159c**

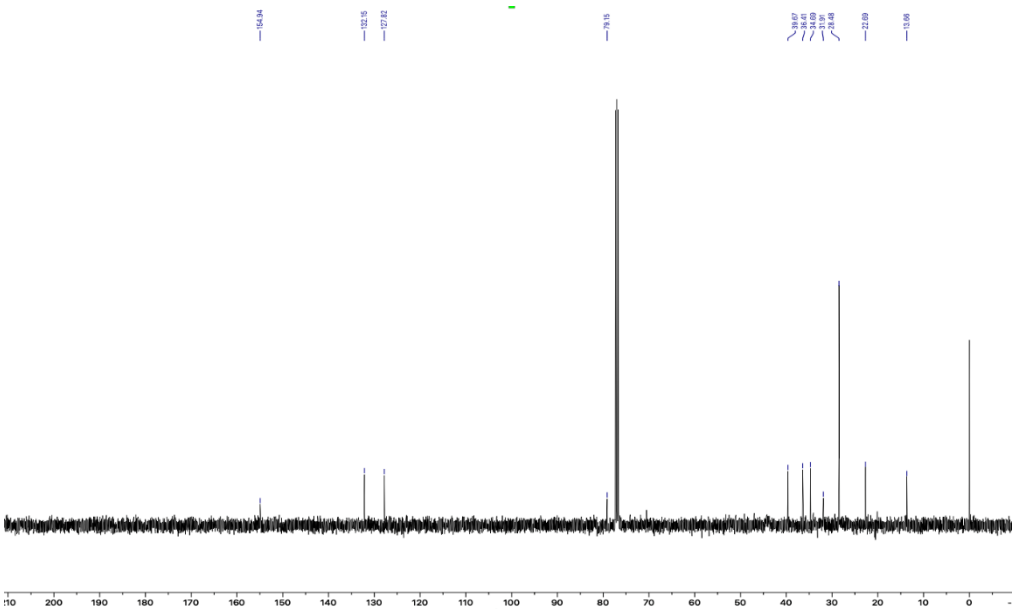

^{13}C NMR spectrum (101 Hz) of **159c**

Allylic C-H

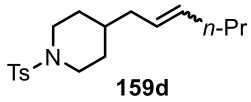

159d

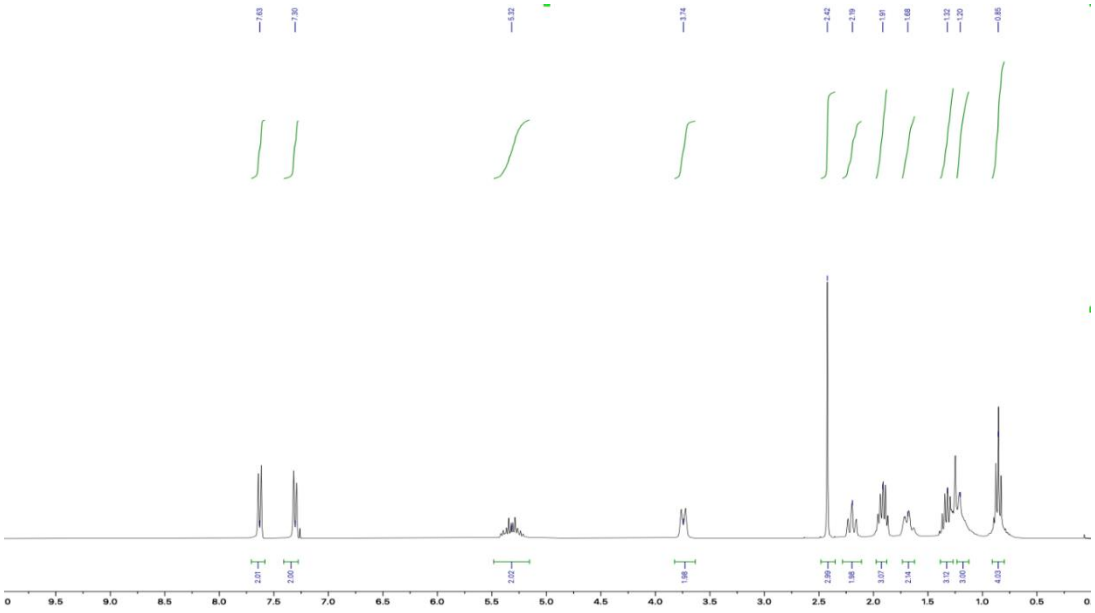

^{1}H NMR spectrum (400 Hz) of **159d**

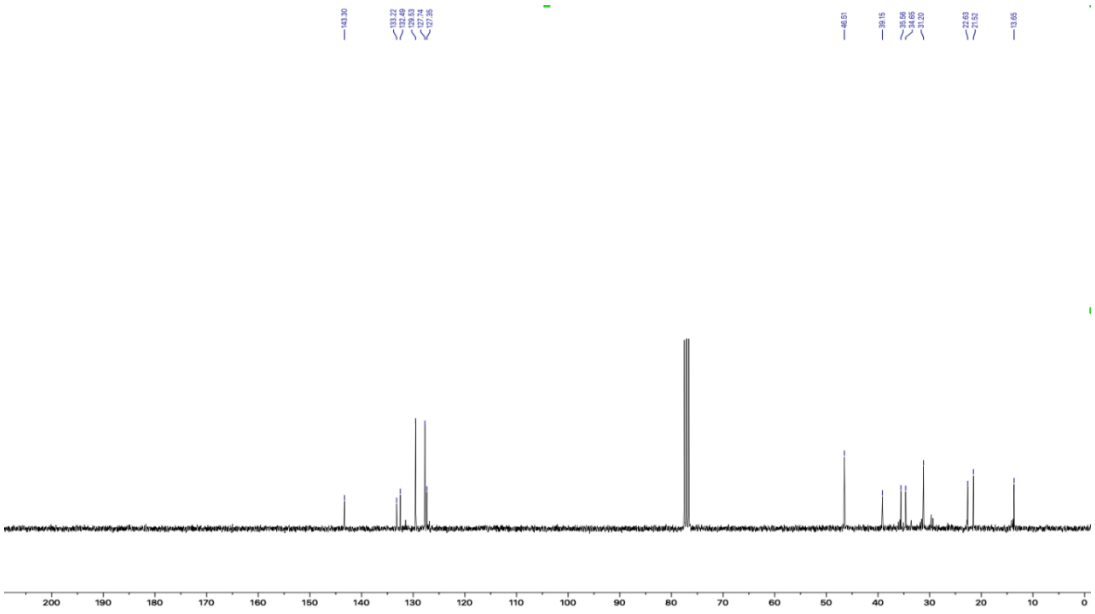

^{13}C NMR spectrum (101 Hz) of **159d**

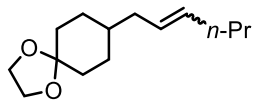

159e

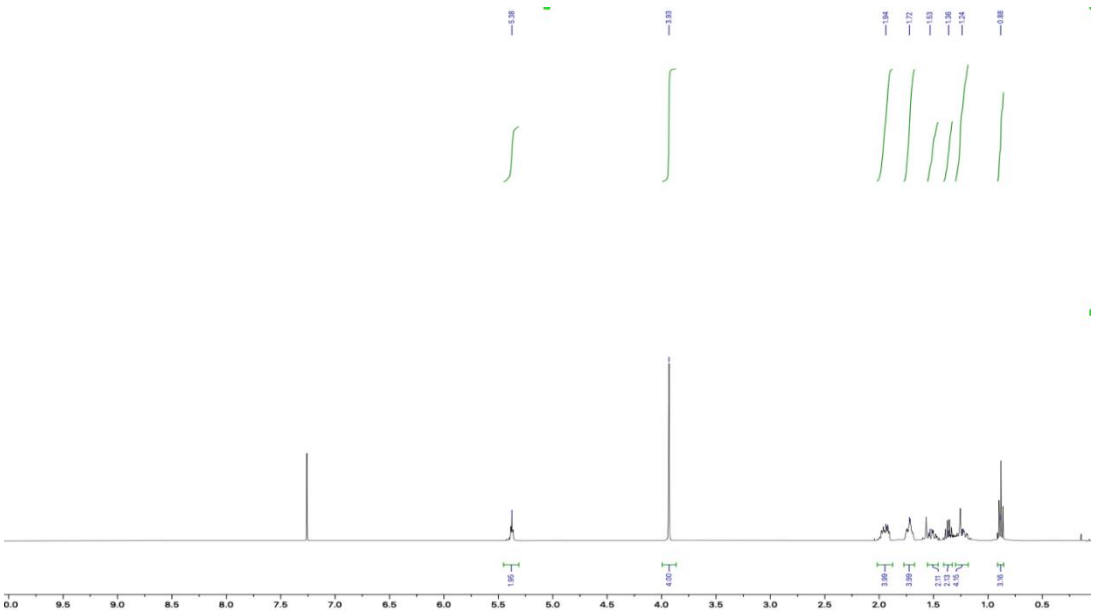

^{1}H NMR spectrum (400 Hz) of **159e**

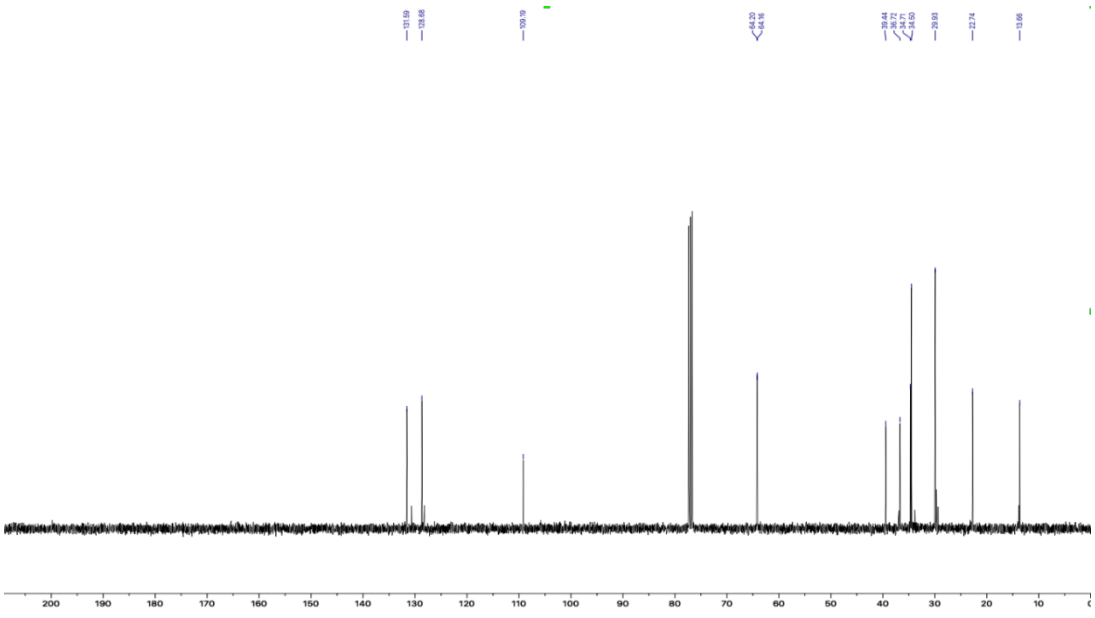

^{13}C NMR spectrum (101 Hz) of **159e**

Allylic C-H

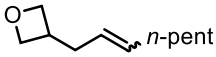

159f

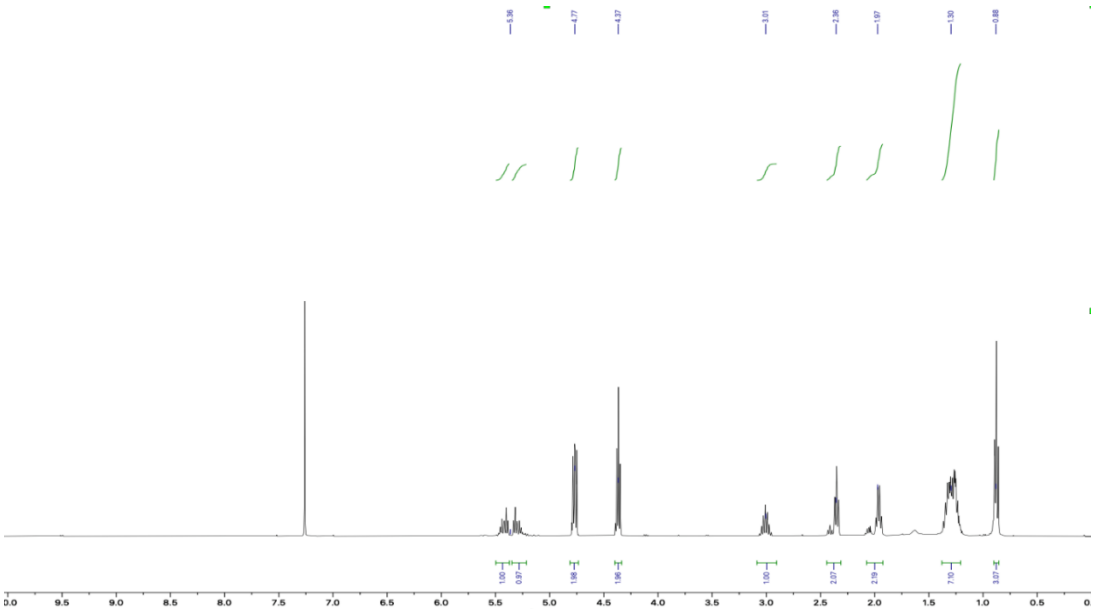

^{1}H NMR spectrum (400 Hz) of **159f**

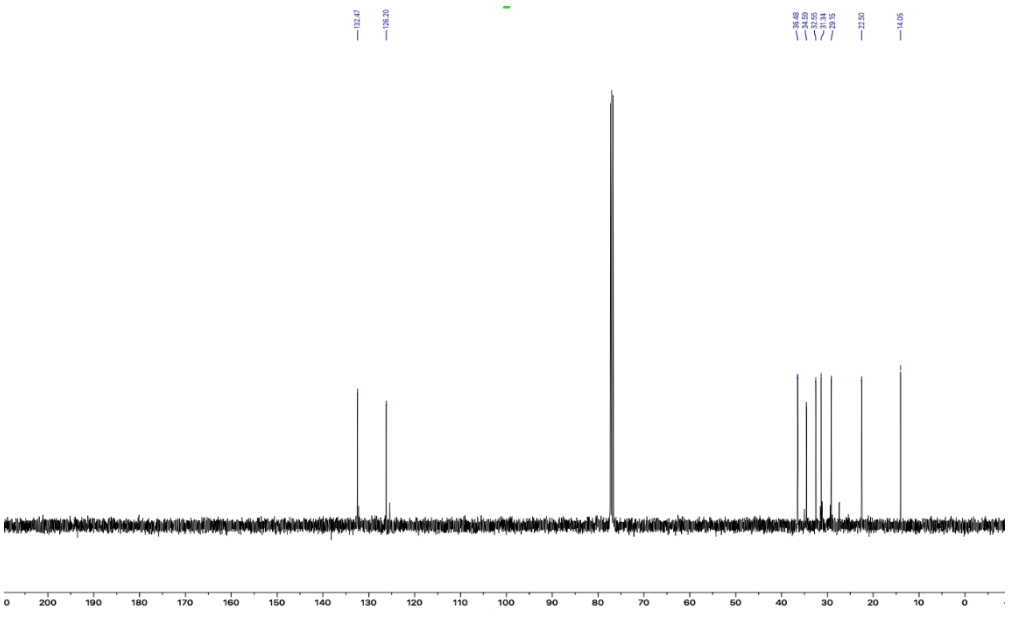

^{13}C NMR spectrum (101 Hz) of **159f**

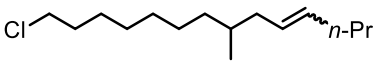

159g

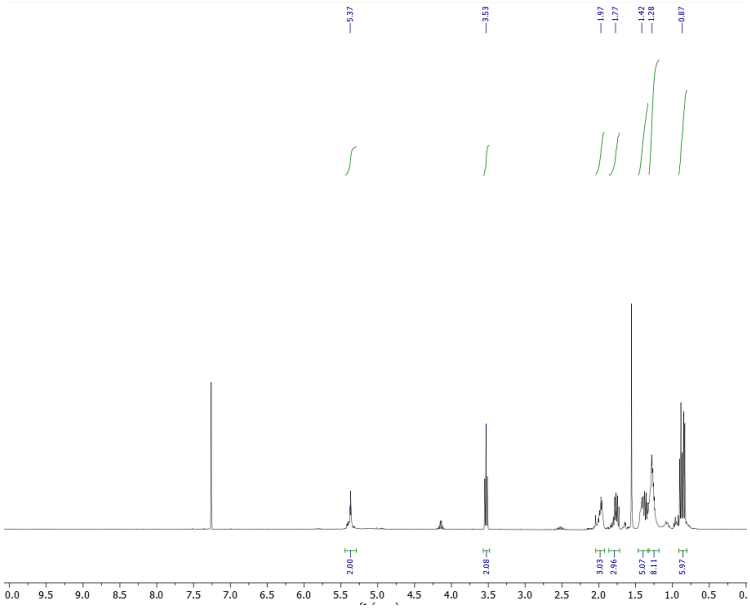

^{1}H NMR spectrum (400 Hz) of **159g**

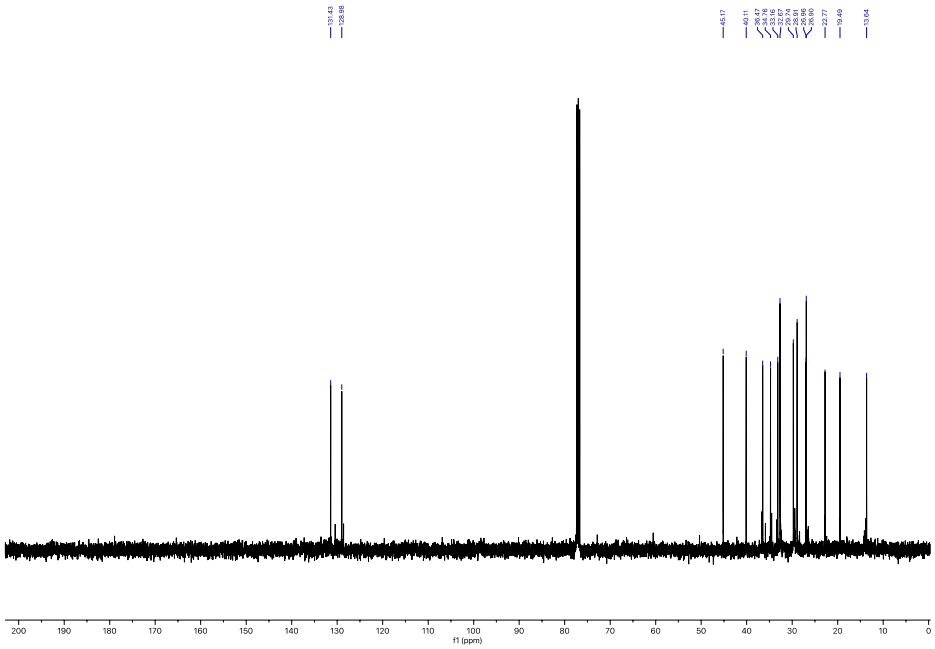

^{13}C NMR spectrum (101 Hz) of **159g**

Allylic C-H

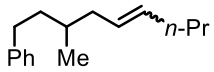

159h

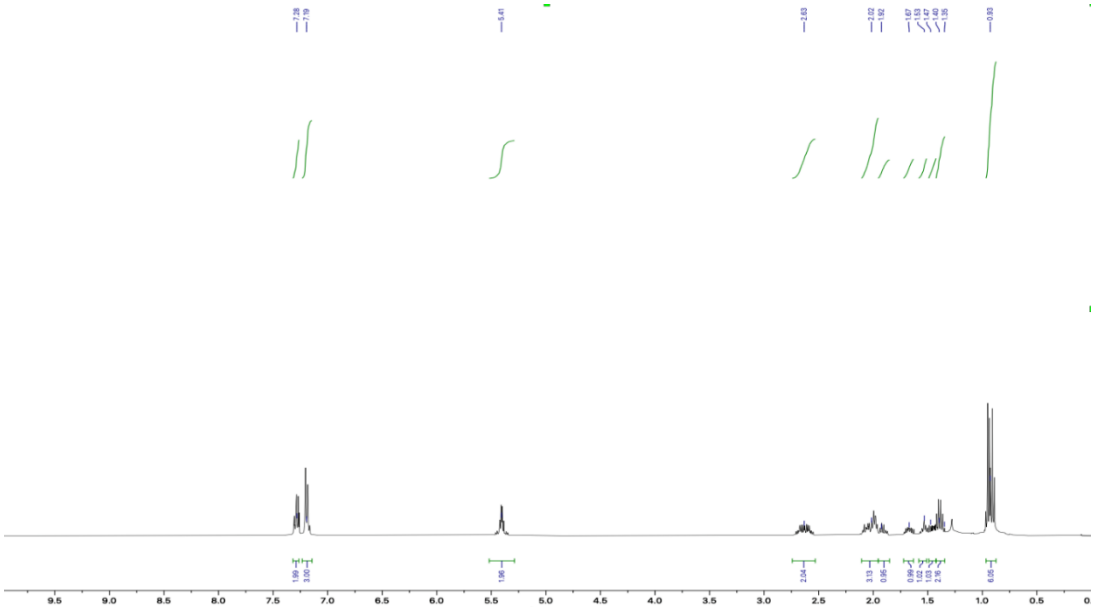

^{1}H NMR spectrum (400 Hz) of **159h**

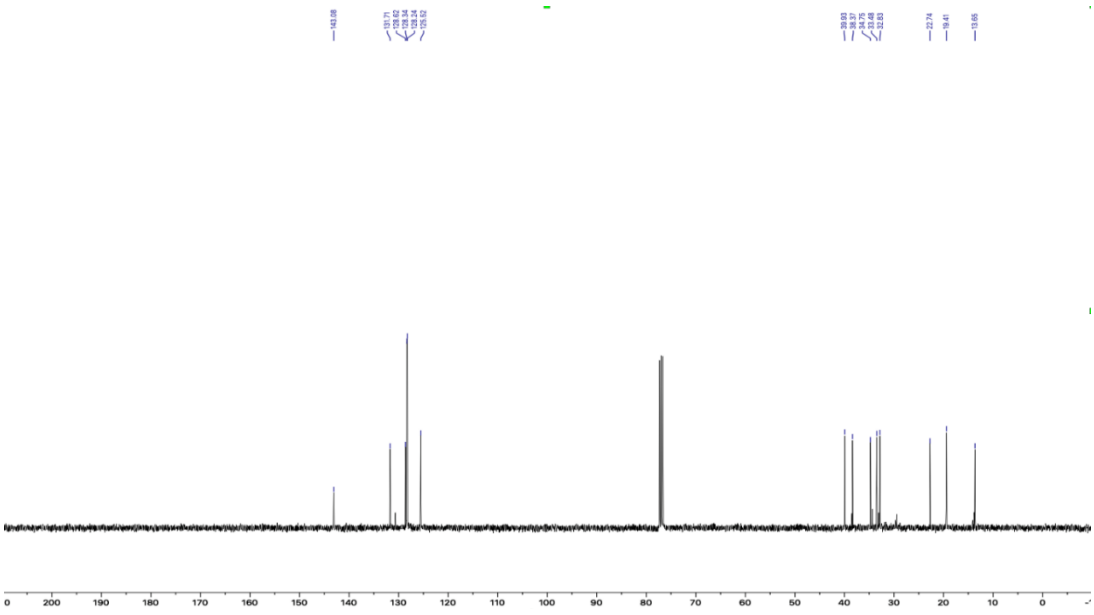

^{13}C NMR spectrum (101 Hz) of **159h**

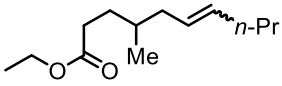

159i

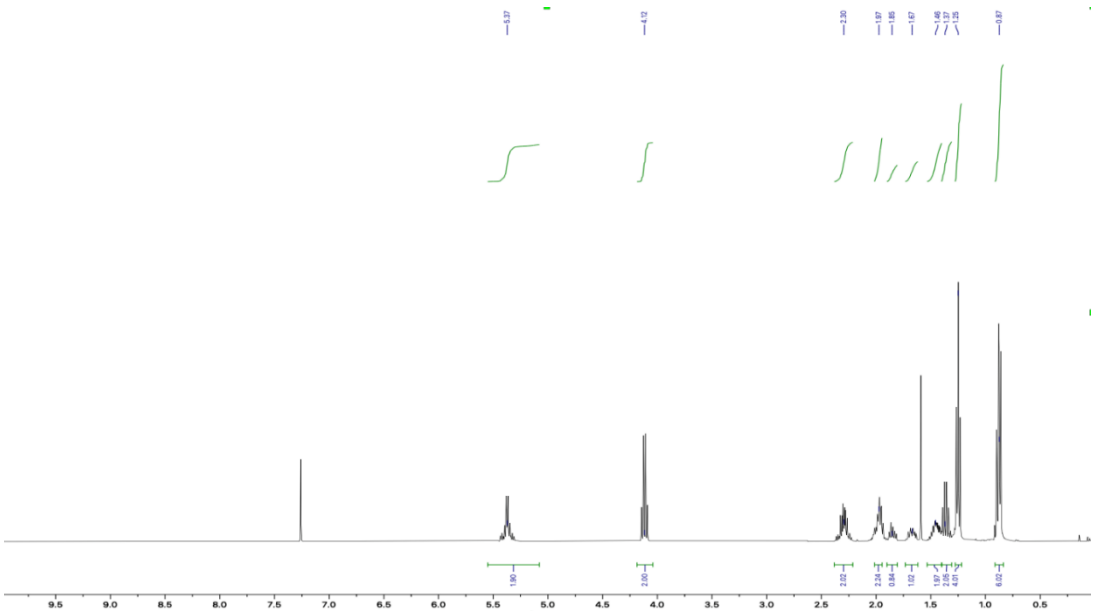

^{1}H NMR spectrum (400 Hz) of **159i**

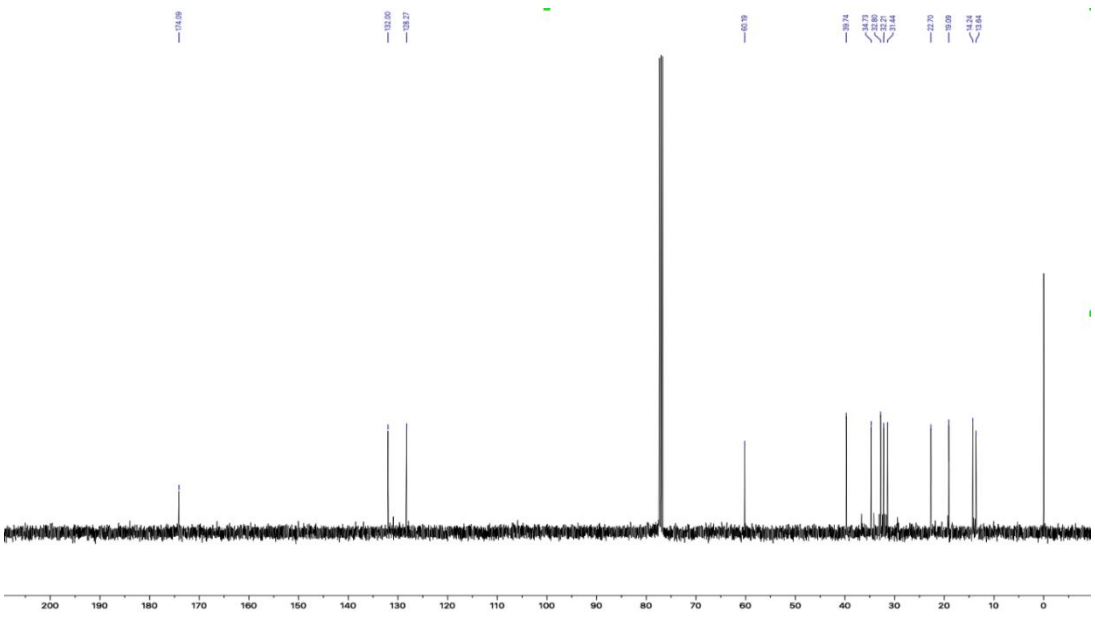

^{13}C NMR spectrum (101 Hz) of **159i**

Allylic C-H

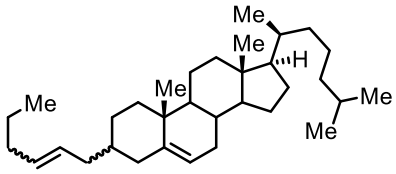

159j

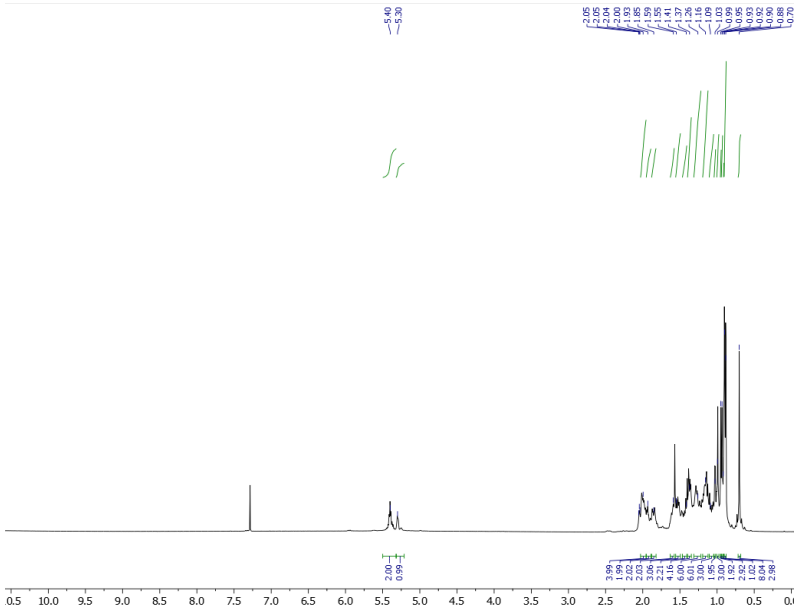

^{1}H NMR spectrum (400 Hz) of **159j**

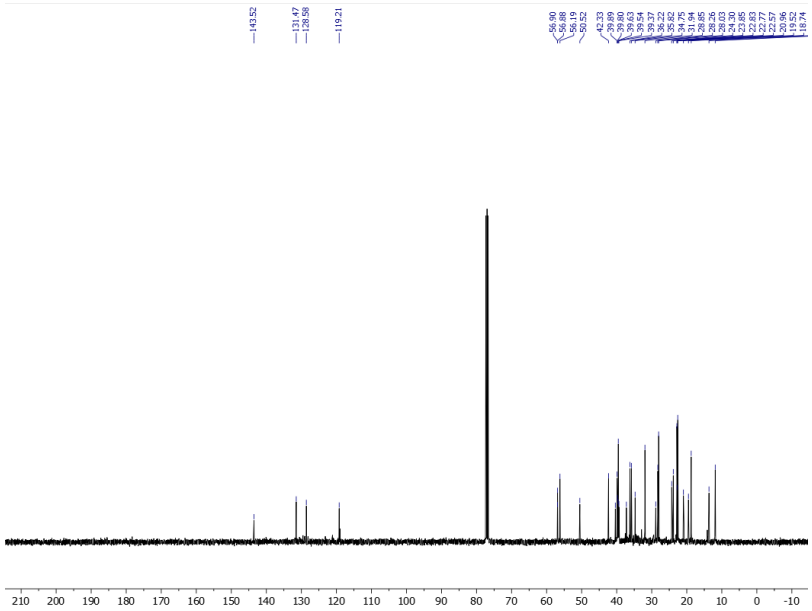

^{13}C NMR spectrum (101 Hz) of **159l**

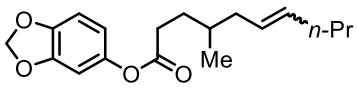

159k

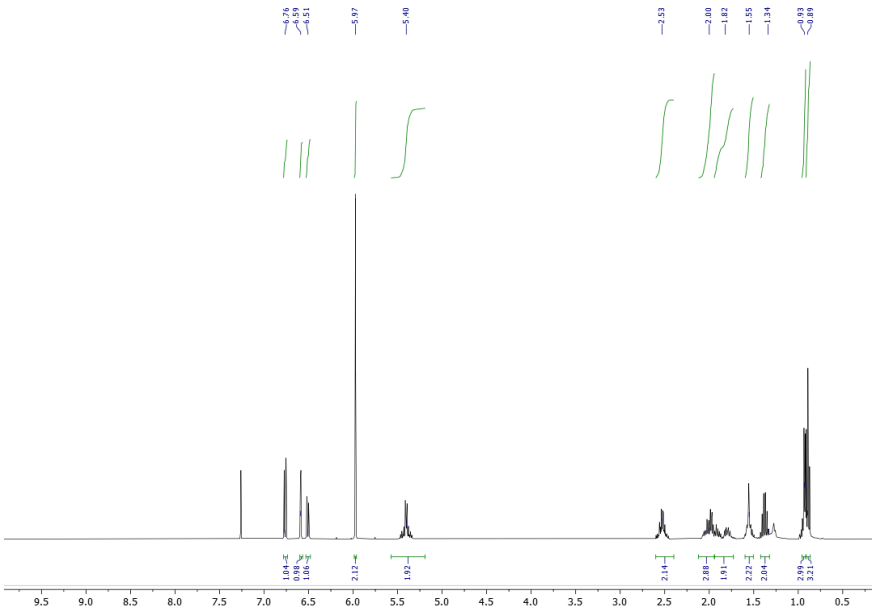

^{1}H NMR spectrum (400 Hz) of **159k**

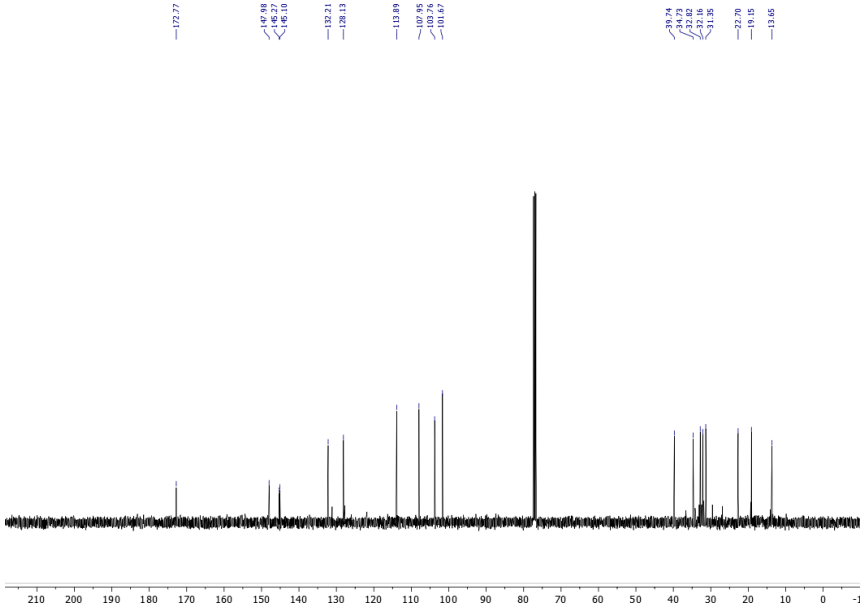

^{13}C NMR spectrum (101 Hz) of **159k**

Allylic C-H

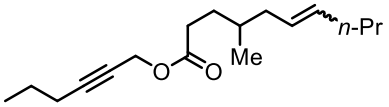

159l

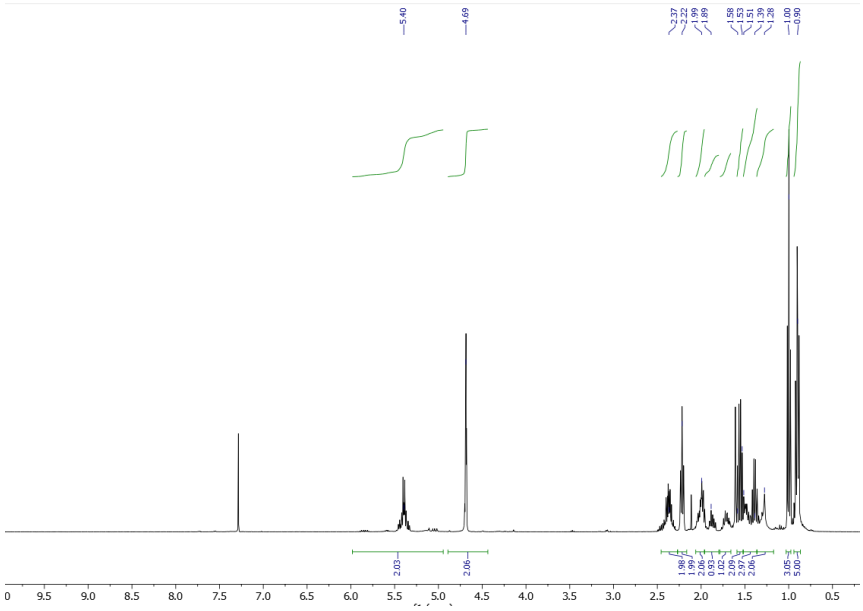

^{1}H NMR spectrum (400 Hz) of **159l**

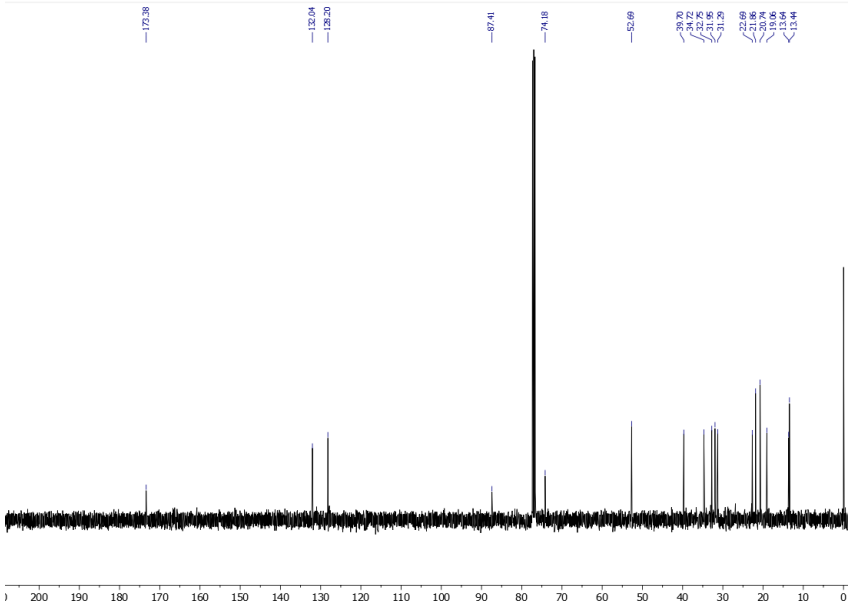

^{13}C NMR spectrum (101 Hz) of **159l**

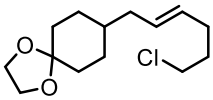

159m

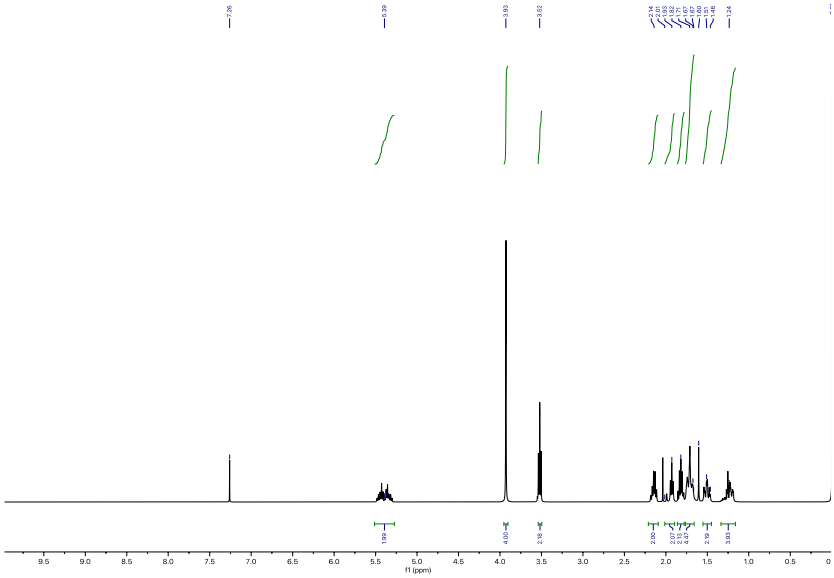

^{1}H NMR spectrum (400 Hz) of **159m**

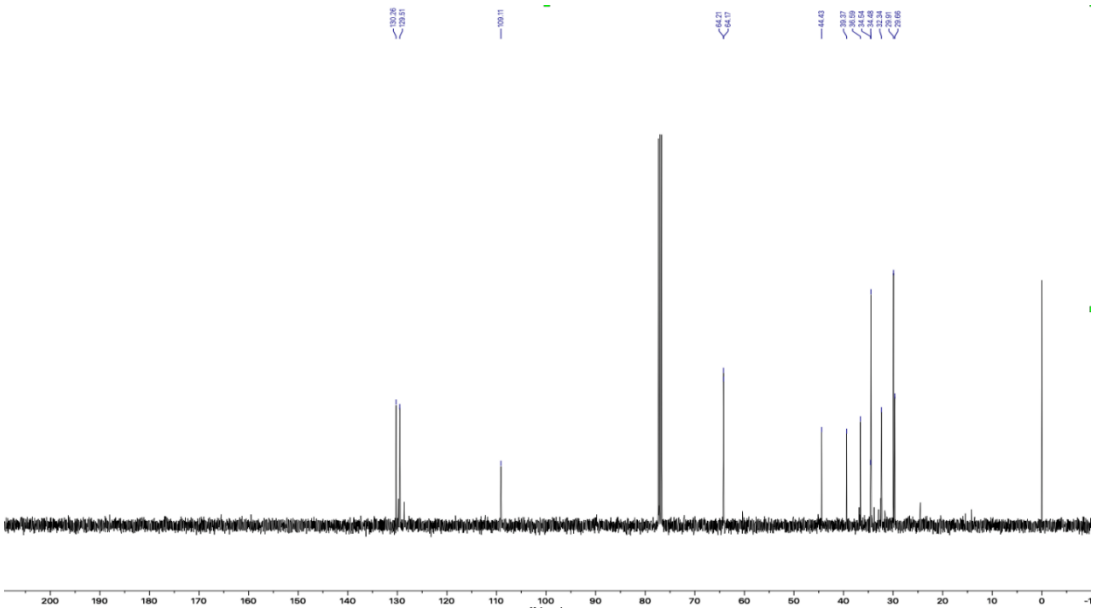

^{13}C NMR spectrum (101 Hz) of **159m**

Allylic C-H

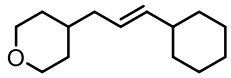

159n

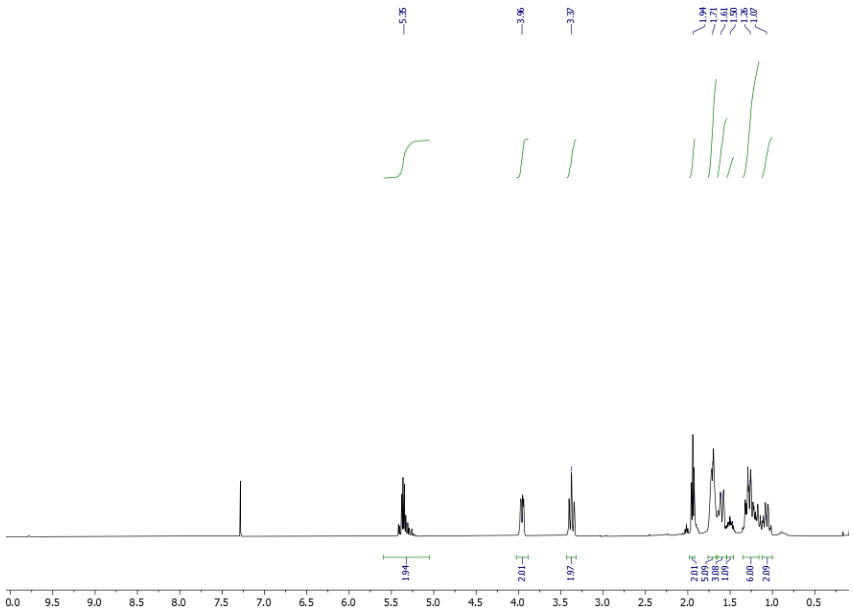

^{1}H NMR spectrum (400 Hz) of **159n**

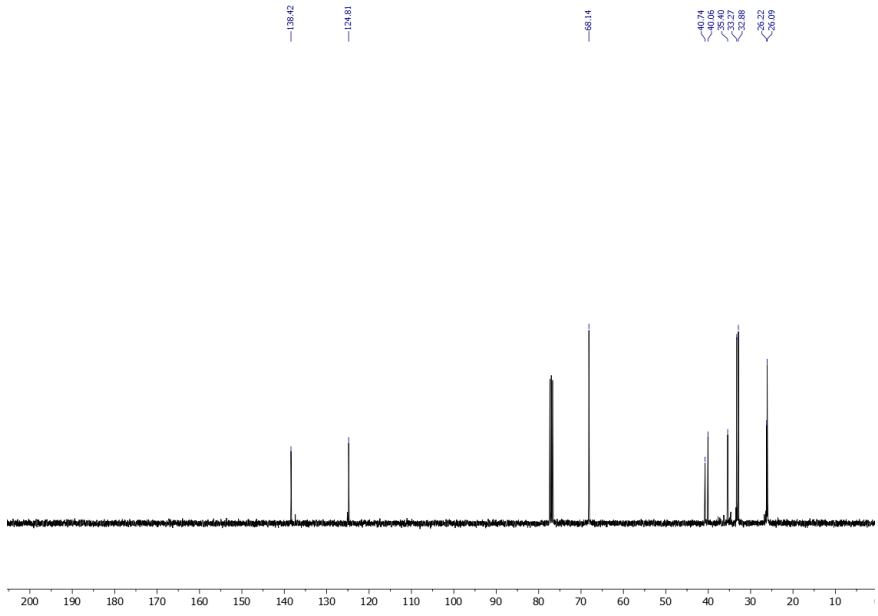

^{13}C NMR spectrum (101 Hz) of **159n**

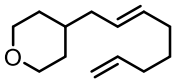

159o

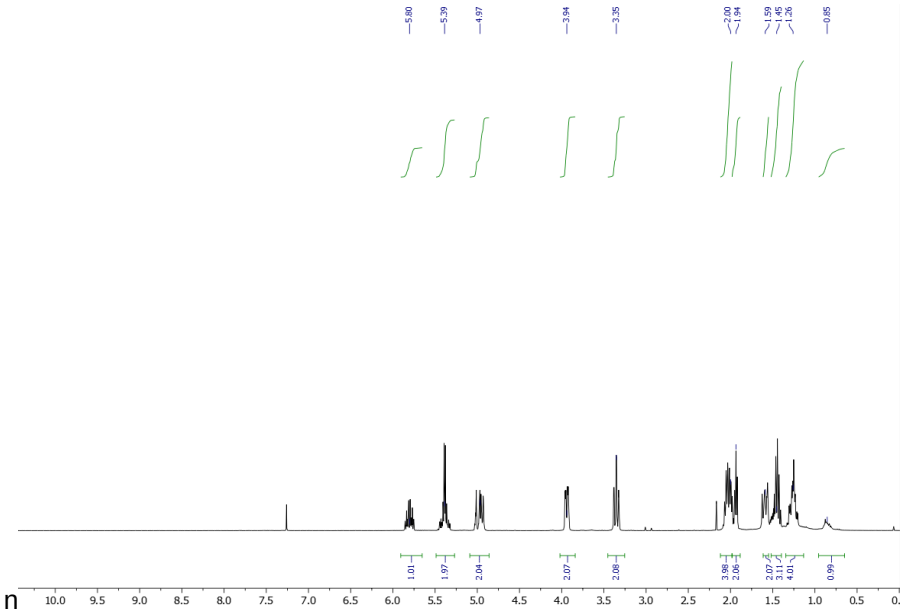

^{1}H NMR spectrum (400 Hz) of **159o**

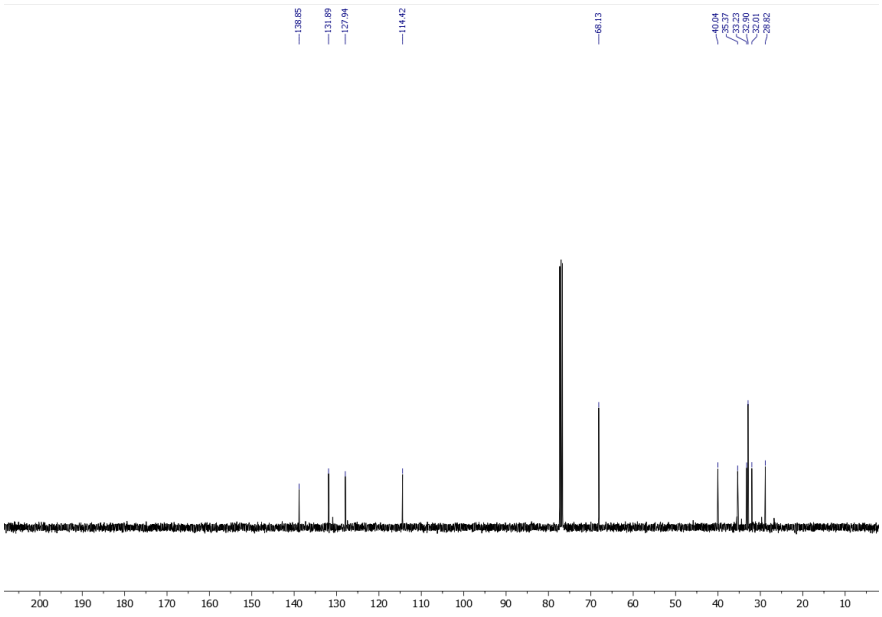

^{13}C NMR spectrum (101 Hz) of **159o**

Allylic C-H

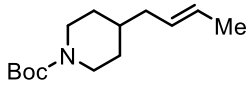

159p

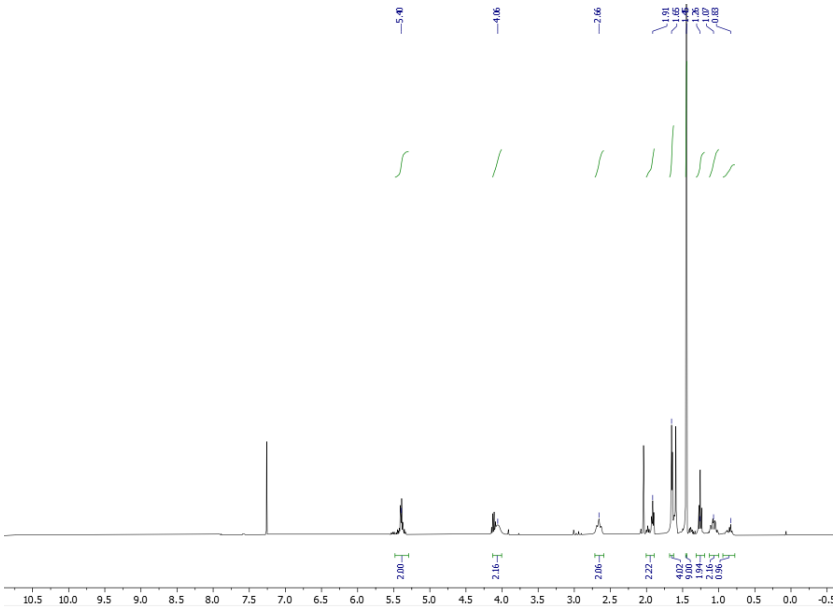

^{1}H NMR spectrum (400 Hz) of **159p**

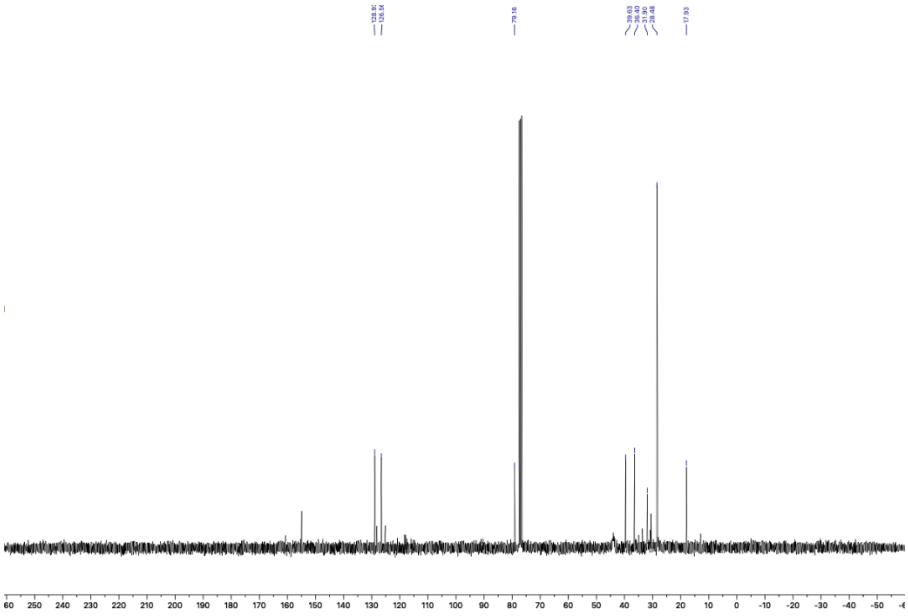

^{13}C NMR spectrum (101 Hz) of **159p**

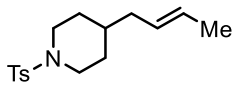

159q

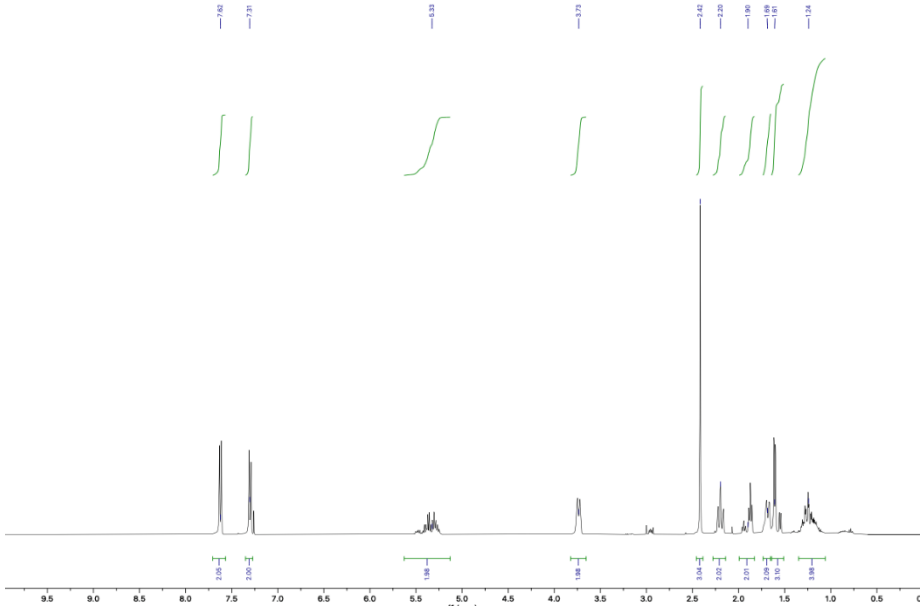

^{1}H NMR spectrum (400 Hz) of **159q**

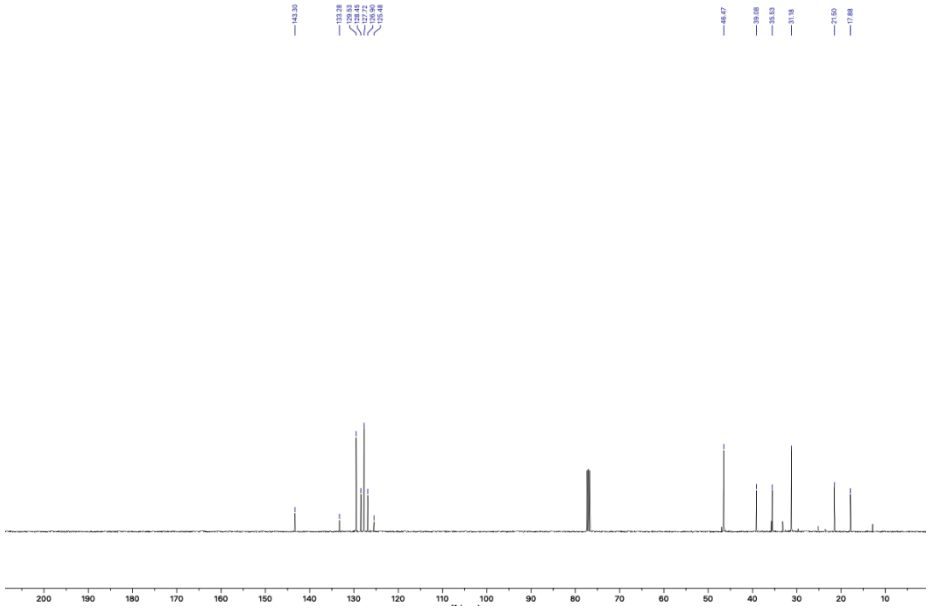

^{13}C NMR spectrum (101 Hz) of **159q**

Allylic C-H

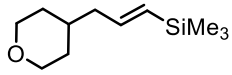

159r(a)

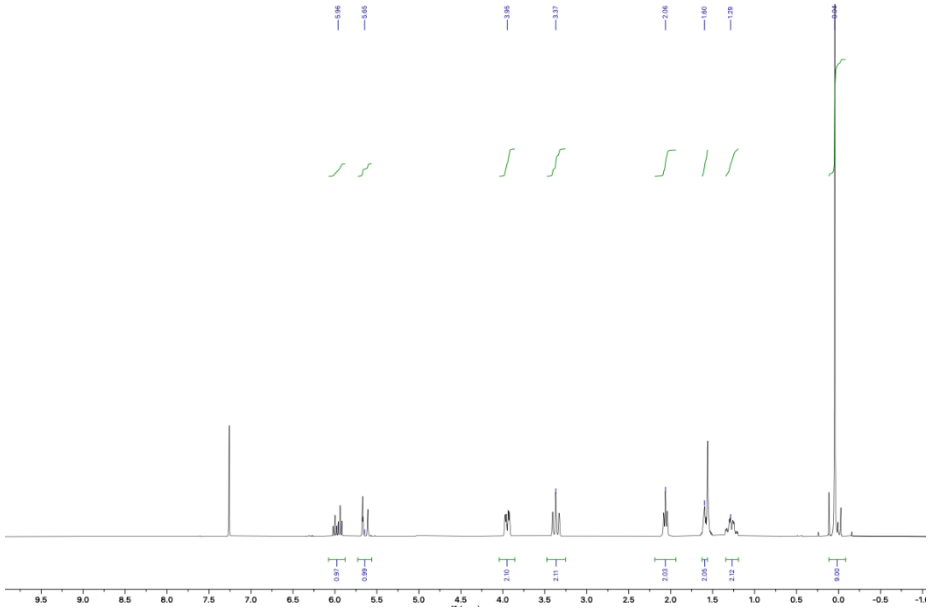

^{1}H NMR spectrum (400 Hz) of **159r(a)**

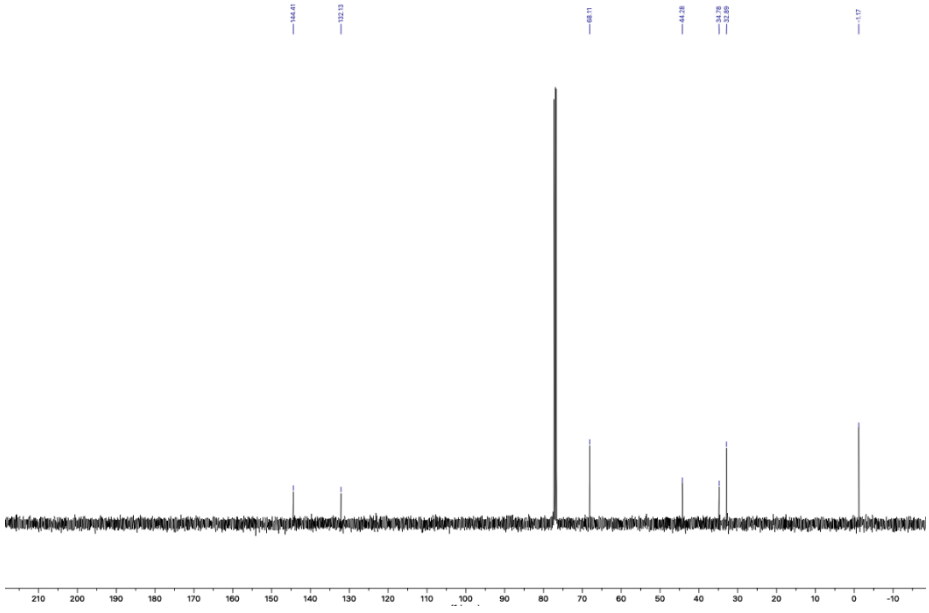

^{13}C NMR spectrum (101 Hz) of **159r(a)**

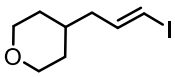

159r

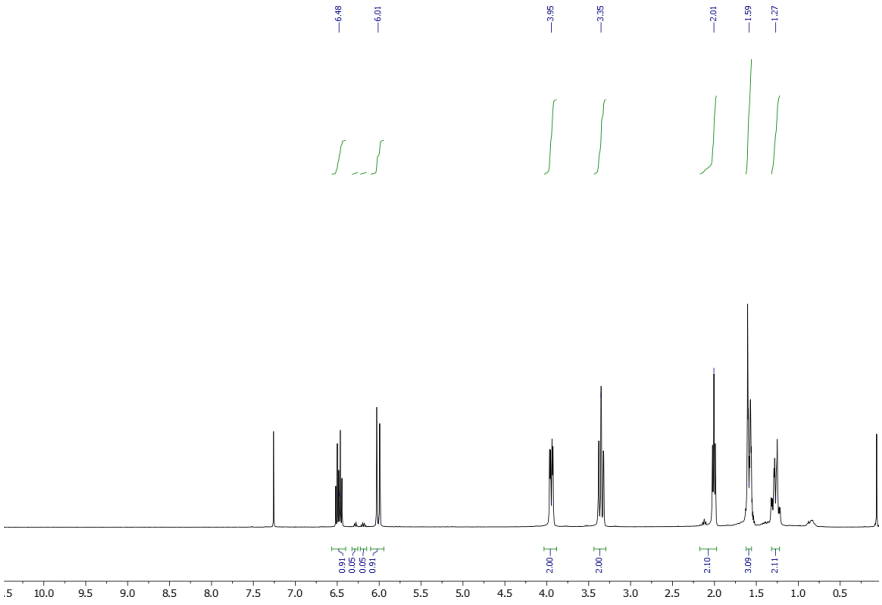

^{1}H NMR spectrum (400 Hz) of **159r**

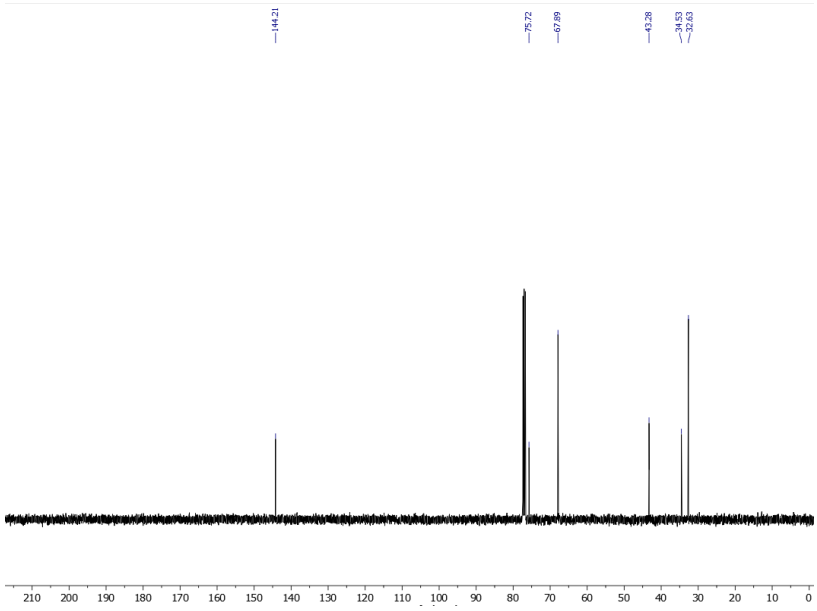

^{13}C NMR spectrum (101 Hz) of **159r**

Allylic C-H

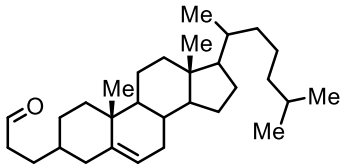

164a

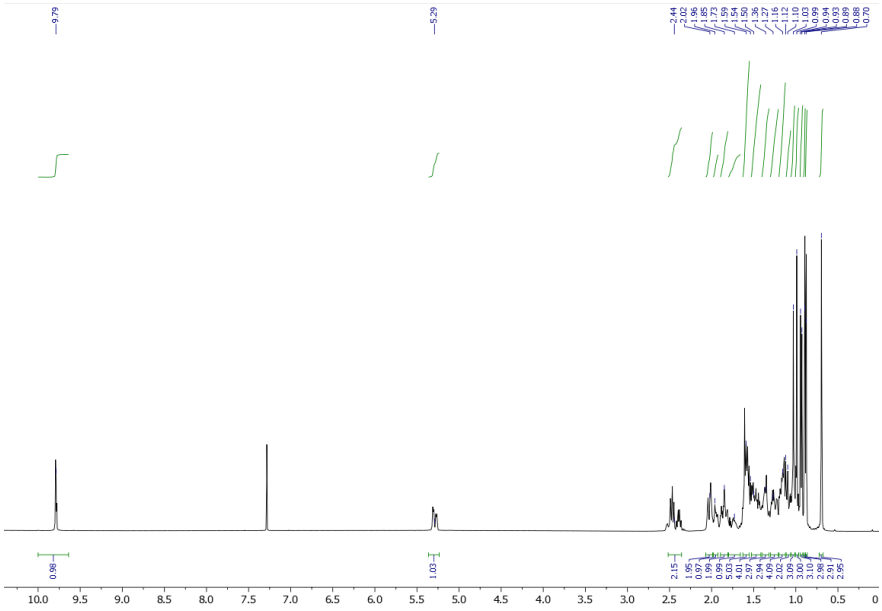

^{1}H NMR spectrum (400 Hz) of **164a**

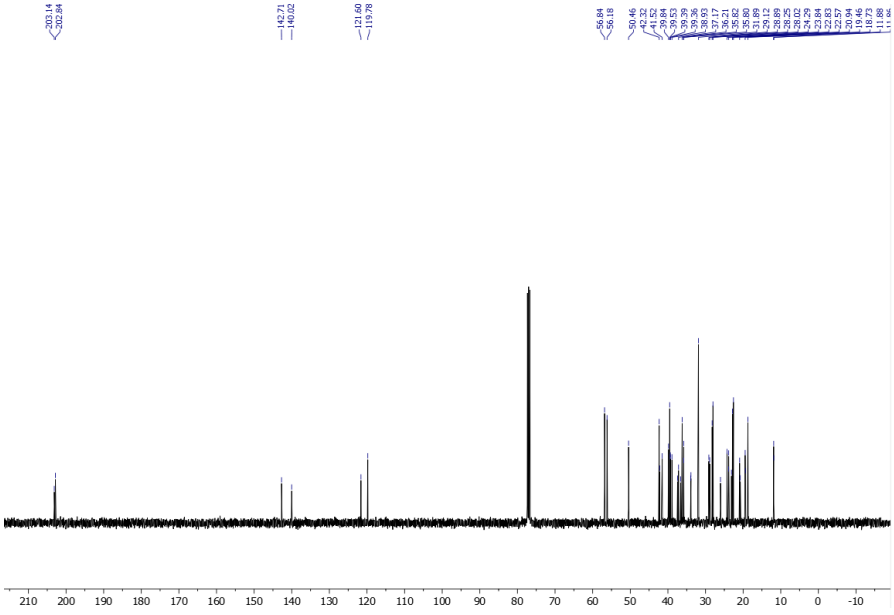

^{13}C NMR spectrum (101 Hz) of **164a**

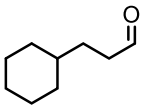

164b

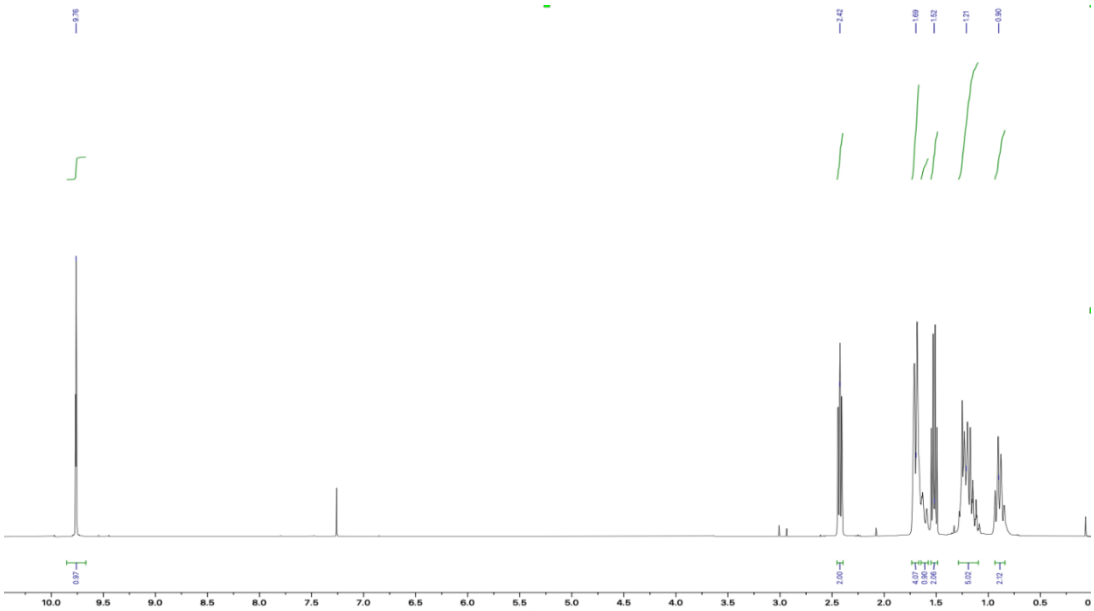

^{1}H NMR spectrum (400 Hz) of **164b**

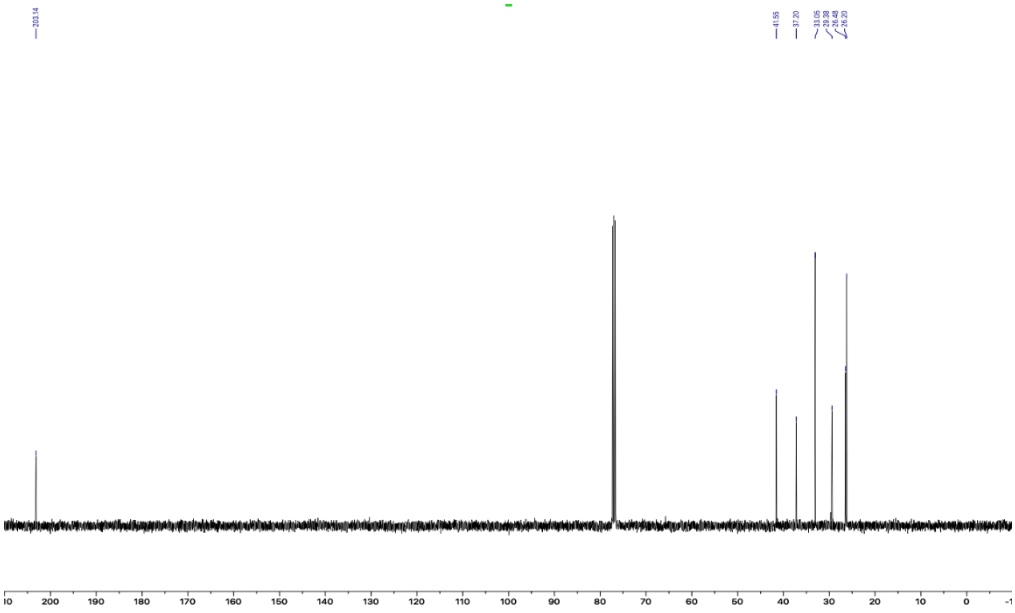

^{13}C NMR spectrum (101 Hz) of **164b**

Allylic C-H

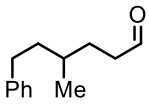

164c

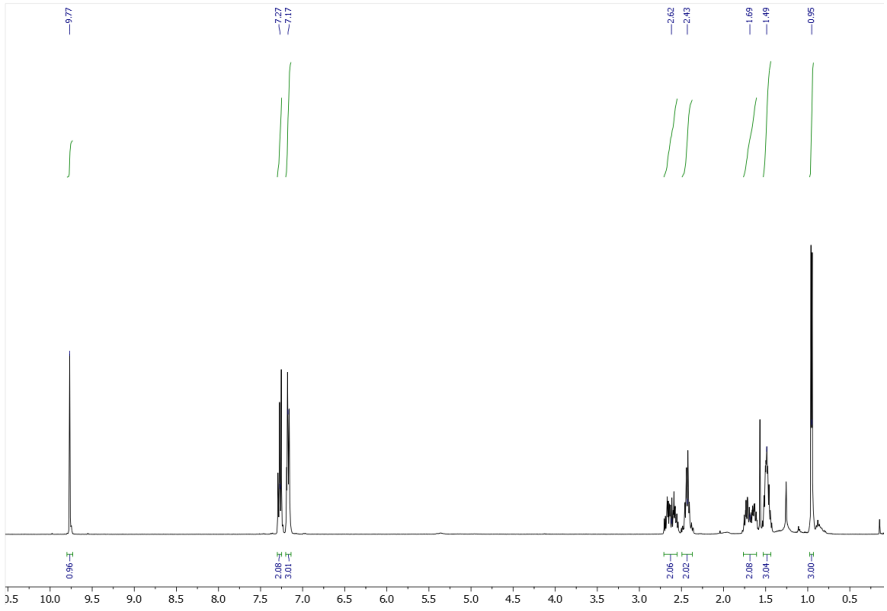

^{1}H NMR spectrum (400 Hz) of **164c**

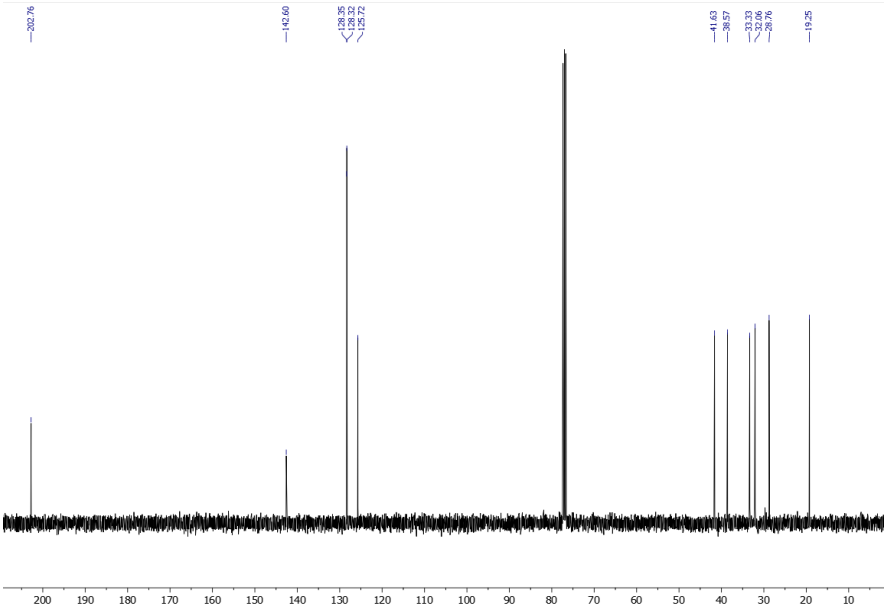

^{13}C NMR spectrum (101 Hz) of **164c**

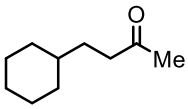

164d

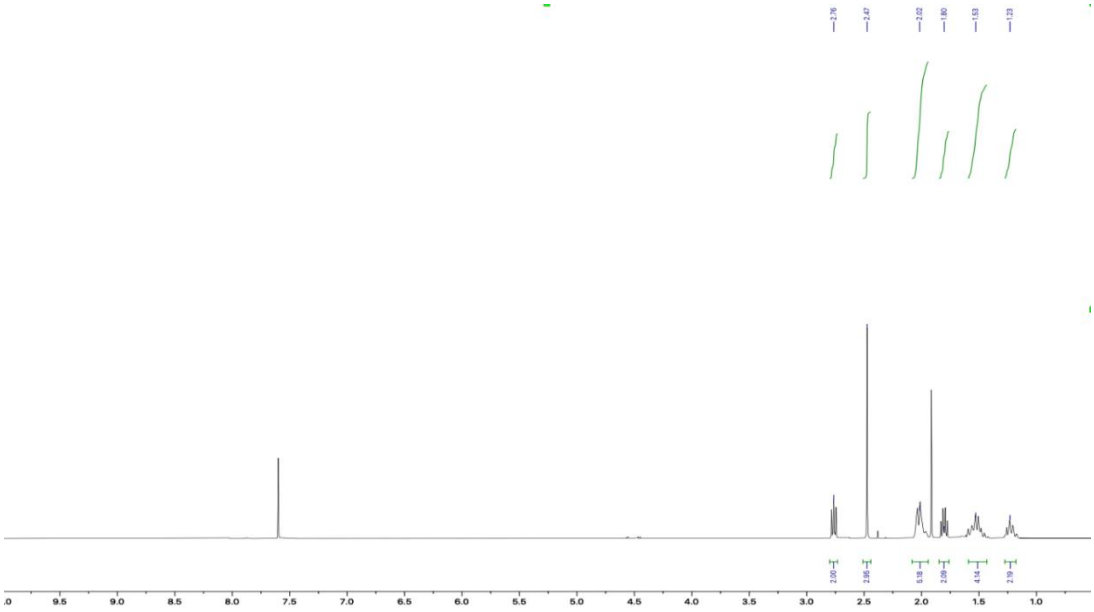

^{1}H NMR spectrum (400 Hz) of **164d**

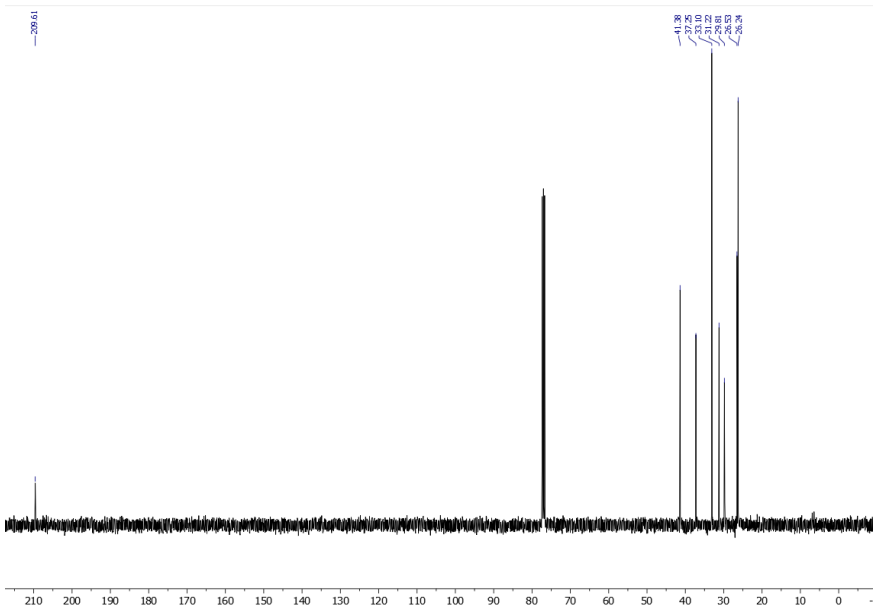

^{13}C NMR spectrum (101 Hz) of **164d**

Allylic C-H

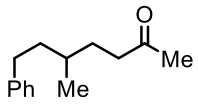

164e

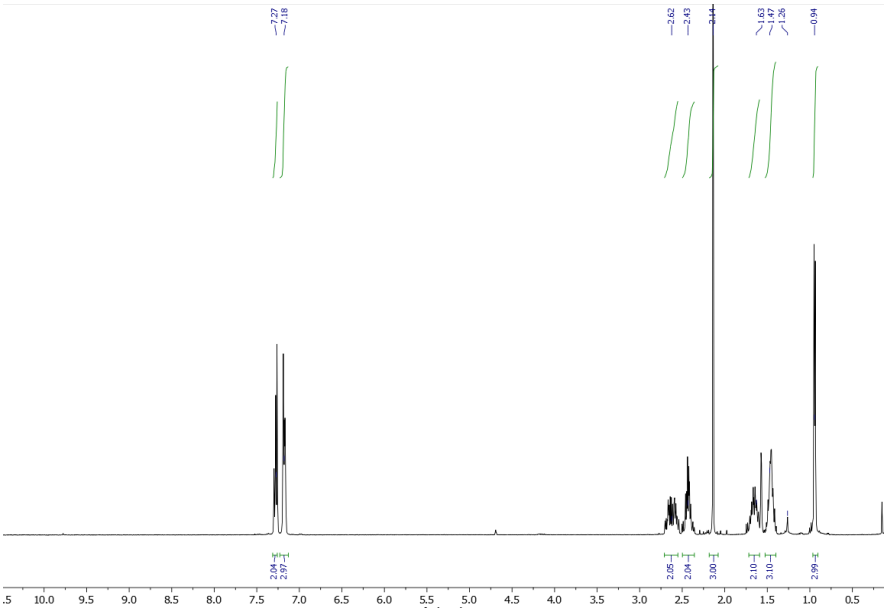

^{1}H NMR spectrum (400 Hz) of **164e**

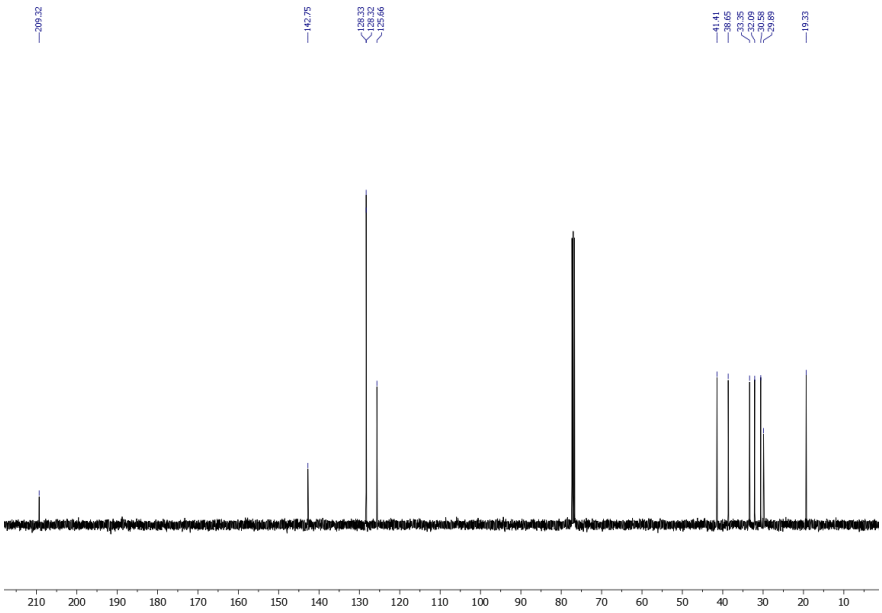

^{13}C NMR spectrum (101 Hz) of **164e**

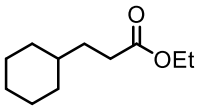

164f

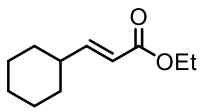

164f'

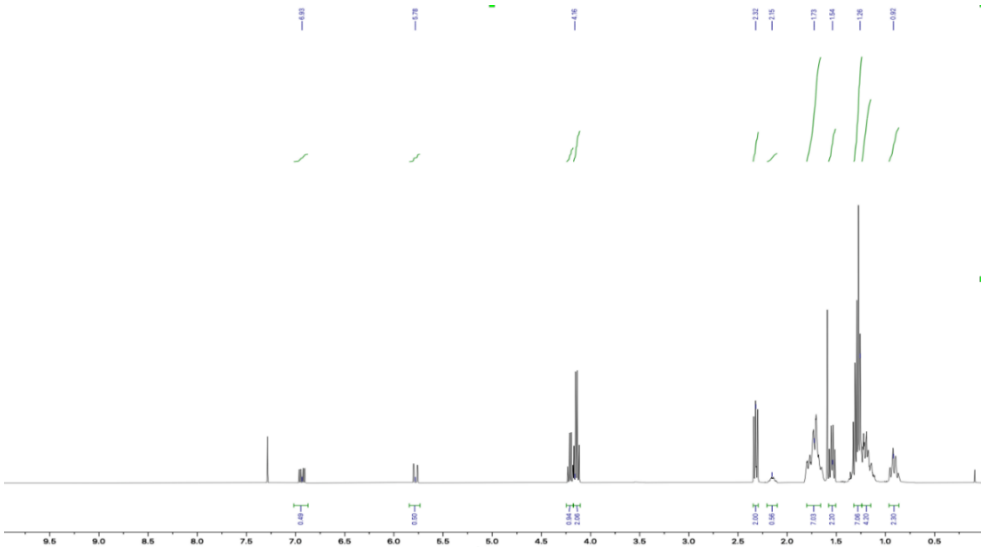

^{1}H NMR spectrum (400 Hz) of **164f**

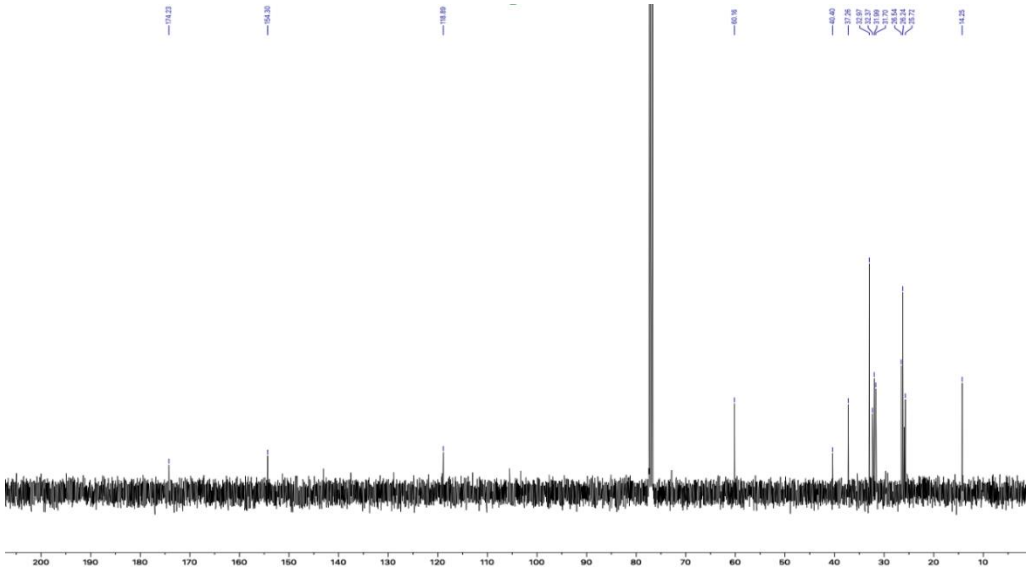

^{13}C NMR spectrum (101 Hz) of **164f**

Allylic C-H

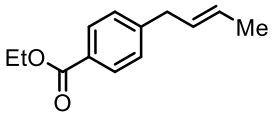

166a

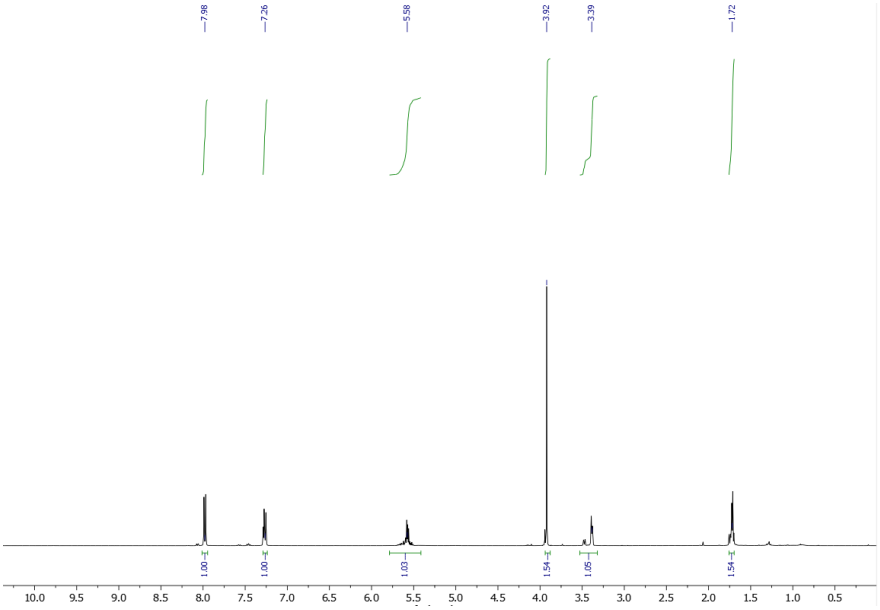

^{1}H NMR spectrum (400 Hz) of **166a**

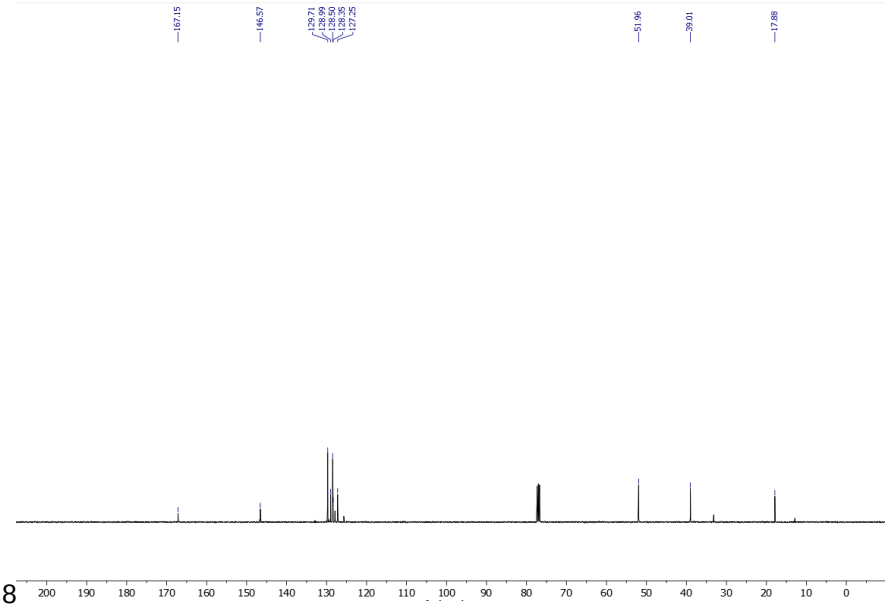

^{13}C NMR spectrum (101 Hz) of **166a**

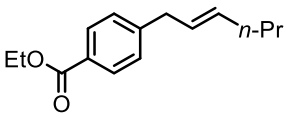

166b

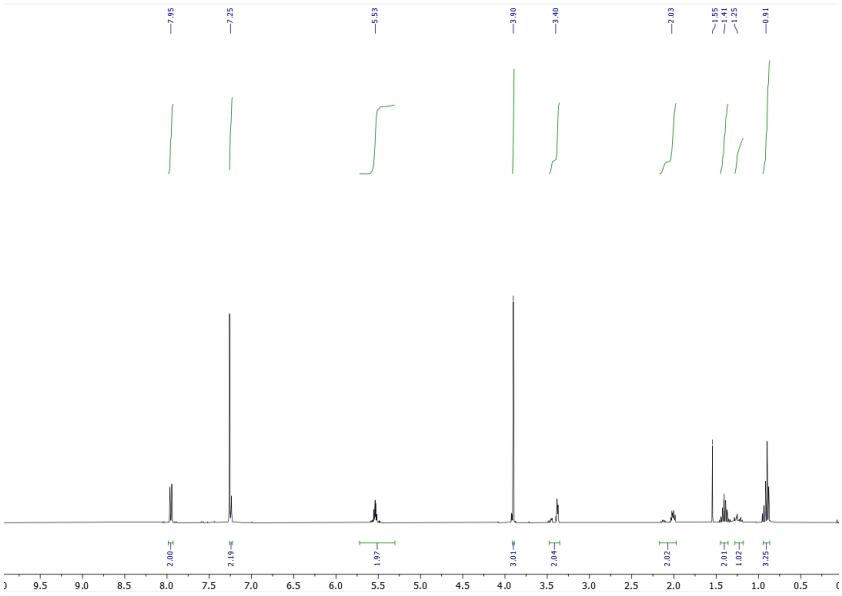

^{1}H NMR spectrum (400 Hz) of **166b**

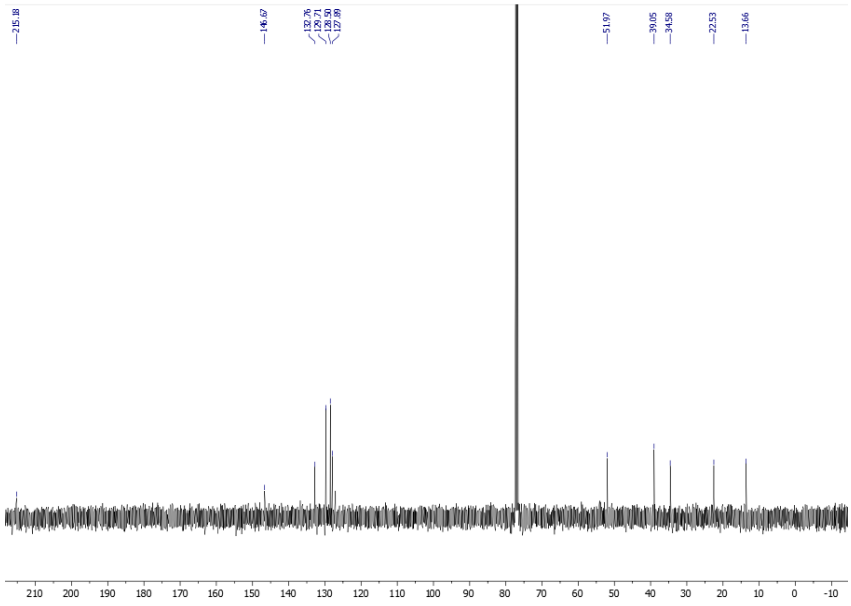

^{13}C NMR spectrum (101 Hz) of **166b**

Allylic C-H

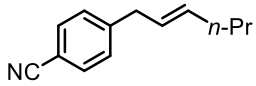

166c

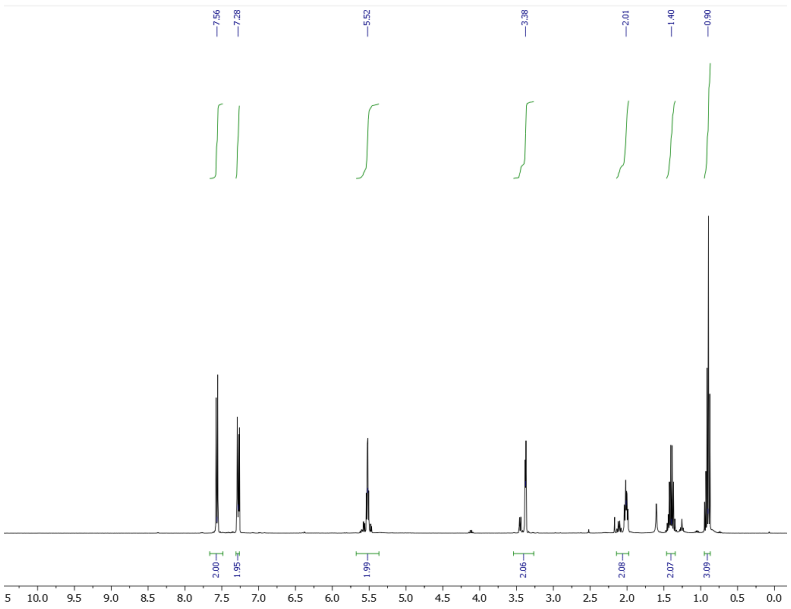

^{1}H NMR spectrum (400 Hz) of **166c**

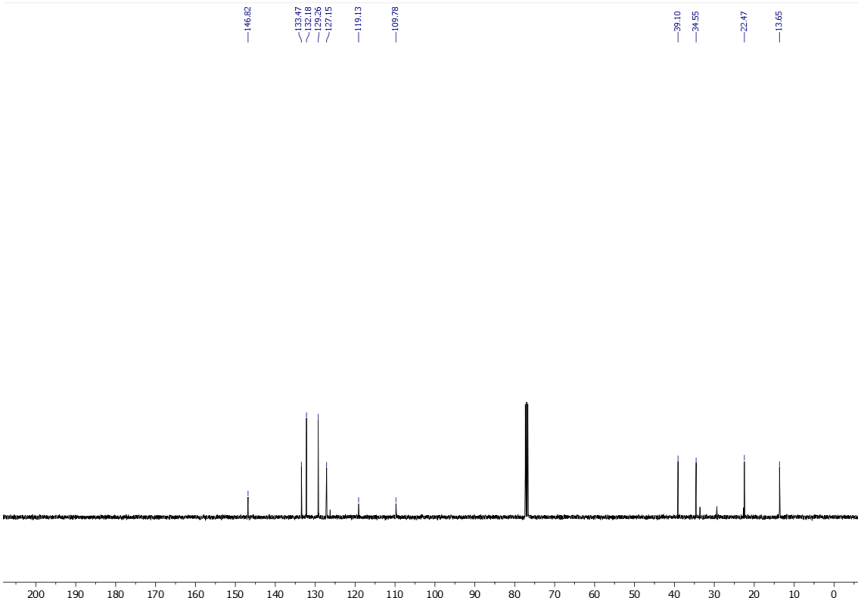

^{13}C NMR spectrum (101 Hz) of **166c**

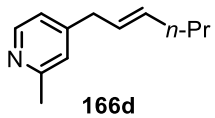

166d

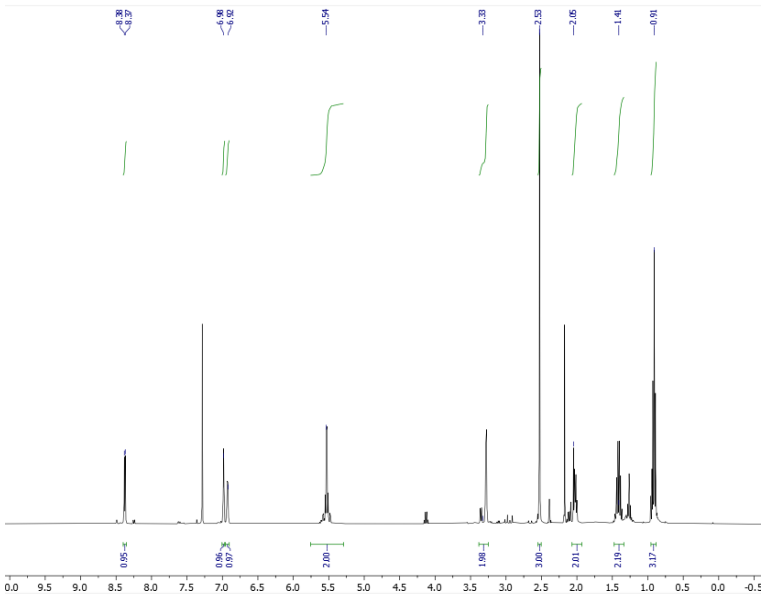

^{1}H NMR spectrum (400 Hz) of **166d**

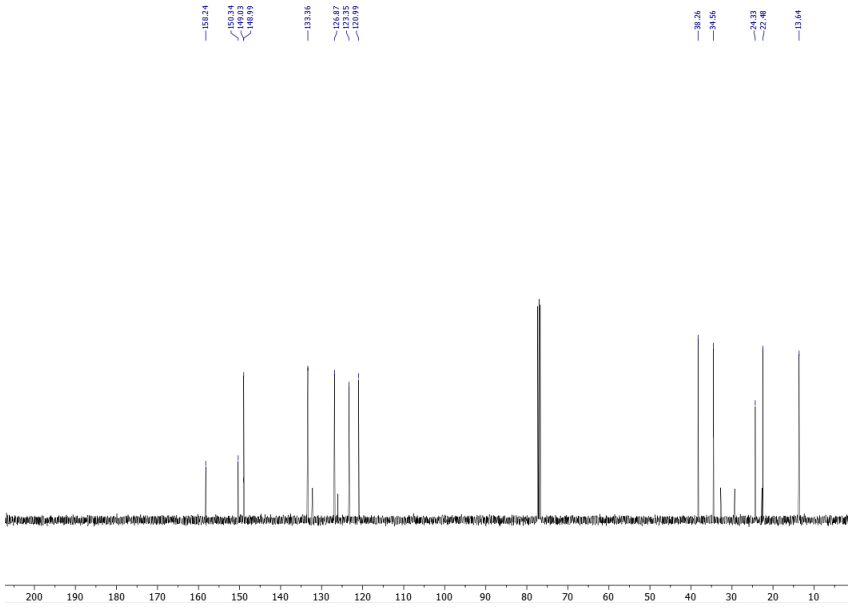

^{13}C NMR spectrum (101 Hz) of **166d**

Allylic C-H

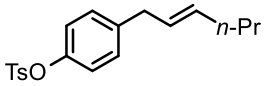

166e

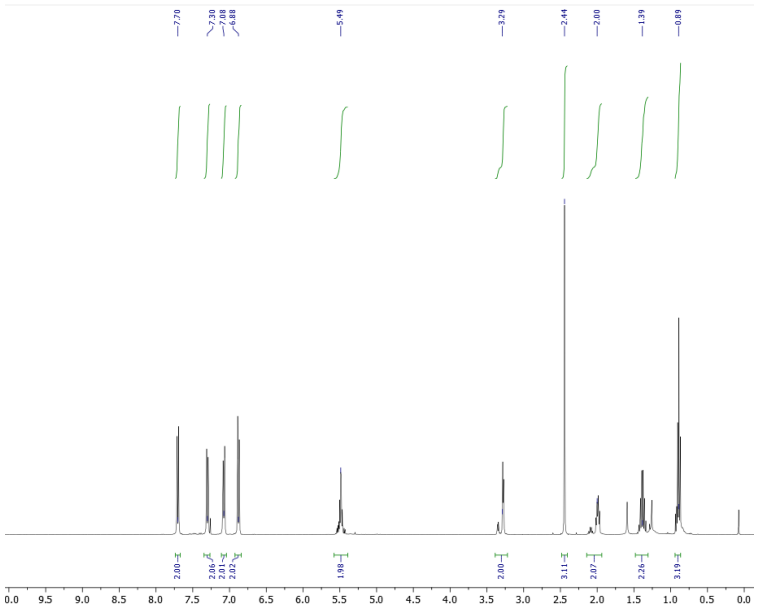

^{1}H NMR spectrum (400 Hz) of **166e**

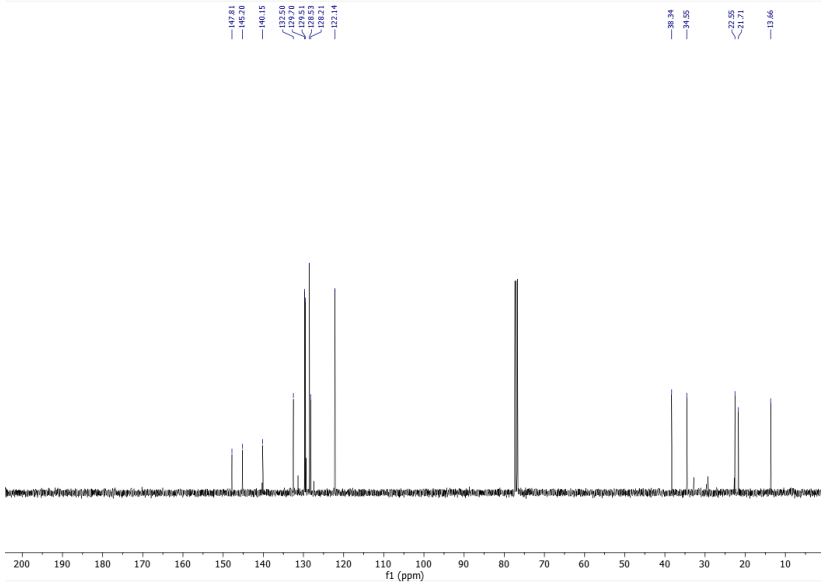

^{13}C NMR spectrum (101 Hz) of **166e**

3.9. References

240. a) Sydora, O. L. Selective Ethylene Oligomerization. *Organometallics* **2019**, *38* (5), 997–1010. https://doi.org/10/gm9cbd.
b) Britovsek, G. J. P.; Malinowski, R.; McGuinness, D. S.; Nobbs, J. D.; Tomov, A. K.; Wadsley, A. W.; Young, C. T. Ethylene Oligomerization beyond Schulz–Flory Distributions. *ACS Catal.* **2015**, *5* (11), 6922–6925. https://doi.org/10/gqfs54.

241. Keim, W. Oligomerization of Ethylene to α-Olefins: Discovery and Development of the Shell Higher Olefin Process (SHOP). *Angew. Chem. Int. Ed.* **2013**, *52* (48), 12492–12496. https://doi.org/10/f2fcqq.

242. Carruthers, W.; Coldham, I. MODERN METHODS OF ORGANIC SYNTHESIS. pp 315 -367. https://doi.org/10/gfvbzj.

243. *Handbook of Metathesis: Grubbs/Handbook of Metathesis, Set*; Grubbs, R. H., Wenzel, A. G., O'Leary, D. J., Khosravi, E., Eds.; Wiley-VCH Verlag GmbH & Co. KGaA: Weinheim, Germany, 2015. https://doi.org/10.1002/9783527674107.

244. Dong, Z.; Ren, Z.; Thompson, S. J.; Xu, Y.; Dong, G. Transition-Metal-Catalysed C-H Alkylation Using Alkenes. *Chemical Reviews* **2017**, *117* (13), 9333–9403. https://doi.org/10/gmw2q8.
Chen, J.; Lu, Z. Asymmetric Hydrofunctionalization of Minimally Functionalized Alkenes *via* Earth Abundant Transition Metal Catalysis. *Org. Chem. Front.* **2018**, *5* (2), 260–272.
https://doi.org/10/gqfs6h. Green, S. A.; Crossley, S. W. M.; Matos, J. L. M.; Vásquez-Céspedes, S.; Shevick, S. L.; Shenvi, R. A. The High Chemofidelity of Metal-Catalyzed Hydrogen Atom Transfer. *Acc. Chem. Res.* **2018**, *51* (11), 2628–2640. https://doi.org/10/gfq6jd.

245. a) Dhungana, R. K.; Kc, S.; Basnet, P.; Giri, R. Transition Metal-Catalyzed Dicarbofunctionalization of Unactivated Olefins. *The Chemical Record* **2018**, *18* (9), 1314–1340. https://doi.org/10/gqpnm9.
b) Li, J.; Luo, Y.; Cheo, H. W.; Lan, Y.; Wu, J. Photoredox-Catalysis-Modulated, Nickel-Catalyzed Divergent Difunctionalization of Ethylene. *Chem* **2019**, *5* (1), 192–203. https://doi.org/10/gqpnnc.
c) Patel, M.; Desai, B.; Sheth, A.; Dholakiya, B. Z.; Naveen, T. Recent Advances in Mono- and Difunctionalization of Unactivated Olefins. *Asian Journal of Organic Chemistry* **2021**, *10* (12), 3201–3232. https://doi.org/10/gqpng8.

246. a) Kazerouni, A. M.; McKoy, Q. A.; Blakey, S. B. Recent Advances in Oxidative Allylic C–H Functionalization *via* Group IX-Metal Catalysis. *Chem. Commun.* **2020**, *56* (87), 13287–13300. https://doi.org/10/gqpm7k.
b) Strambeanu, I. I.; White, M. C. Catalyst-Controlled C–O versus C–N Allylic Functionalization of Terminal Olefins. *J. Am. Chem. Soc.* **2013**, *135* (32), 12032–12037. https://doi.org/10/f472pj.
c) Åkermark, B.; Åkermark, G.; Hegedus, L. S.; Zetterberg, K. Amination of π-allylpalladium Chloride Complexes. A Mechanistic Study. *J. Am. Chem. Soc.* **1981**, *103* (11), 3037–3040. https://doi.org/10/drr5qf.
d) Ali, S. Z.; Budaitis, B. G.; Fontaine, D. F. A.; Pace, A. L.; Garwin, J. A.; White, M. C. Allylic C–H Amination Cross-Coupling Furnishes Tertiary Amines by Electrophilic Metal Catalysis. *Science* **2022**, *376* (6590), 276–283. https://doi.org/10/gqpm8t.

247. Grennberg, H.; Backvall, J.-E., Allylic Oxidations. In¨Transition Metals for Organic Synthesis; Wiley-VCH Verlag GmbH, **2008**; pp 243−265.
b) McMurry, J. E.; Kočotovský, P. A Method for the Palladium-Catalyzed Allylic Oxidation of Olefins. *Tetrahedron Letters* **1984**, *25* (38), 4187–4190. https://doi.org/10/ddjw4b.
c) Heumann, A.; Åkermark, B. Oxidation with Palladium Salts: Catalytic Preparation of Allyl Acetates from Monoolefins Using a Three-Component Oxidation System. *Angewandte Chemie International Edition in English* **1984**, *23* (6), 453–454. https://doi.org/10/ckvwcs.
d) Chen, M. S.; White, M. C. A Sulfoxide-Promoted, Catalytic Method for the Regioselective Synthesis of Allylic Acetates from Monosubstituted Olefins via C−H Oxidation. *J. Am. Chem. Soc.* **2004**, *126* (5), 1346–1347. https://doi.org/10/dv9h3d.

248. a) Gøgsig, T. M.; Kleimark, J.; Nilsson Lill, S. O.; Korsager, S.; Lindhardt, A. T.; Norrby, P.-O.; Skrydstrup, T. Mild and Efficient Nickel-Catalyzed Heck Reactions with Electron-Rich Olefins. *J. Am. Chem. Soc.* **2012**, *134* (1), 443–452. https://doi.org/10.1021/ja2084509.
b) Bhakta, S.; Ghosh, T. Emerging Nickel Catalysis in Heck Reactions: Recent Developments. *Advanced Synthesis & Catalysis* **2020**, *362* (23), 5257–5274. https://doi.org/10/gqpncj.

249. a) Cai, Z.; Xiao, D.; Do, L. H. Fine-Tuning Nickel Phenoxyimine Olefin Polymerization Catalysts: Performance Boosting by Alkali Cations. *J. Am. Chem. Soc.* **2015**, *137* (49), 15501–15510. https://doi.org/10/f8h4m5.
b) Mu, H.; Pan, L.; Song, D.; Li, Y. Neutral Nickel Catalysts for Olefin Homo- and Copolymerization: Relationships between Catalyst Structures and Catalytic Properties. *Chem. Rev.* **2015**, *115* (22), 12091–12137. https://doi.org/10/gqpnb8.

250. Trost, B. M.; Fullerton, T. J. New Synthetic Reactions. Allylic Alkylation. *J. Am. Chem. Soc.* **1973**, *95* (1), 292–294. https://doi.org/10/c8d8gc.
For a comprehensive review of Trost's work in this field: Trost, B. M. Metal Catalyzed Allylic Alkylation: Its Development in the Trost Laboratories. *Tetrahedron* **2015**, *71* (35), 5708–5733. https://doi.org/10/gqhbhz.

251 a) Solladié-Cavallo, A.; Haesslein, J. L.; Bäckvall, J.-E. Asymmetric Palladium-Assisted Alkylation of Olefins. *Tetrahedron Letters* **1982**, *23* (9), 939–942. https://doi.org/10/dsc6vp.
b) Bäckvalĺ, J.-E.; Zetterberg, K.; Åkermark, B. π-Allyl Complexes from Allylic C—H Bond Cleavage in Olefins by Metal Complexes. *Inorganic Reactions and Methods* **1991**, 123–132. https://doi.org/10.1002/9780470145272.ch14.
c) Hegedus, L. S.; Hayashi, T.; Darlington, W. H. Palladium Catalyzed Allylic Alkylation of Olefins. *J. Am. Chem. Soc.* **1978**, *100* (24), 7747–7748. https://doi.org/10/dmwfrk.

252. a) Young, A. J.; White, M. C. Catalytic Intermolecular Allylic C-H Alkylation. *Journal of the American Chemical Society* **2008**, *130* (43), 14090–14091. https://doi.org/10.1021/ja806867p.
b) Lin, S.; Song, C.-X.; Cai, G.-X.; Wang, W.-H.; Shi, Z.-J. Intra/Intermolecular Direct Allylic Alkylation via Pd(II)-Catalyzed Allylic C−H Activation. *J. Am. Chem. Soc.* **2008**, *130* (39), 12901–12903. https://doi.org/10/dq2s4q.

253. a) Trost, B. M.; Donckele, E. J.; Thaisrivongs, D. A.; Osipov, M.; Masters, J. T. A New Class of Non-C2-Symmetric Ligands for Oxidative and Redox-Neutral Palladium-Catalyzed Asymmetric Allylic Alkylations of 1,3-Diketones. *J. Am. Chem. Soc.* **2015**, *137* (7), 2776–2784.

https://doi.org/10/gn7s63.
b) Chen, Y. W.; Liu, Y.; Lu, H. Y.; Lin, G. Q.; He, Z. T. Palladium-Catalyzed Regio- and Enantioselective Migratory Allylic C(Sp3)-H Functionalization. *Nature Communications* **2021**, *12* (1). https://doi.org/10.1038/s41467-021-25978-6.
c) Lin, H. C.; Wang, P. S.; Tao, Z. L.; Chen, Y. G.; Han, Z. Y.; Gong, L. Z. Highly Enantioselective Allylic C-H Alkylation of Terminal Olefins with Pyrazol-5-Ones Enabled by Cooperative Catalysis of Palladium Complex and Brønsted Acid. *Journal of the American Chemical Society* **2016**, *138* (43), 14354–14361. https://doi.org/10.1021/jacs.6b08236.
d) Fan, L. F.; Wang, P. S.; Gong, L. Z. Monodentate Phosphorus Ligand-Enabled General Palladium-Catalyzed Allylic C-H Alkylation of Terminal Alkenes. *Organic Letters* **2019**, *21* (17), 6720–6725. https://doi.org/10/gqfc9w.
e) Wang, K.; Lin, X.; Liu, Y.; Li, C. Palladium-Catalyzed Asymmetric Allylic C–H Functionalization for the Synthesis of Hydroquinolines through Intermolecular [4+2] Cycloadditions. *ACS Catal.* **2021**, *11* (17), 10913–10922. https://doi.org/10/gqdmrh.

254. Wang, R.; Luan, Y.; Ye, M. Transition Metal–Catalyzed Allylic C(Sp3)–H Functionalization via H3-Allylmetal Intermediate. *Chinese Journal of Chemistry* **2019**, *37* (7), 720–743. https://doi.org/10.1002/cjoc.201900140.

255. Fujita, K.; Yorimitsu, H.; Shinokubo, H.; Oshima, K. Transformation of Zirconocene−Olefin Complexes into Zirconocene Allyl Hydride and Their Use as Dual Nucleophilic Reagents: Reactions with Acid Chloride and 1,4-Diketone. *J. Am. Chem. Soc.* **2004**, *126* (21), 6776–6783. https://doi.org/10/db6fds.

256. a) Parsons, A. T.; Buchwald, S. L. Copper-Catalyzed Trifluoromethylation of Unactivated Olefins. *Angewandte Chemie International Edition* **2011**, *50* (39), 9120–9123. https://doi.org/10/c5frzp.
b) Xu, J.; Fu, Y.; Luo, D.-F.; Jiang, Y.-Y.; Xiao, B.; Liu, Z.-J.; Gong, T.-J.; Liu, L. Copper-Catalyzed Trifluoromethylation of Terminal Alkenes through Allylic C–H Bond Activation. *J. Am. Chem. Soc.* **2011**, *133* (39), 15300–15303. https://doi.org/10/fsx5nw.
c) Chu, L.; Qing, F.-L. Copper-Catalyzed Oxidative Trifluoromethylation of Terminal Alkenes Using Nucleophilic CF3SiMe3: Efficient C(Sp3)–CF3 Bond Formation. *Org. Lett.* **2012**, *14* (8), 2106–2109. https://doi.org/10/qhw8gs.
d) Wang, X.; Ye, Y.; Zhang, S.; Feng, J.; Xu, Y.; Zhang, Y.; Wang, J. Copper-Catalyzed C(Sp3)–C(Sp3) Bond Formation Using a Hypervalent Iodine Reagent: An Efficient Allylic Trifluoromethylation. *J. Am. Chem. Soc.* **2011**, *133* (41), 16410–16413. https://doi.org/10/cjx66q.

257. a) Davies, H. M. L.; Morton, D. Guiding Principles for Site Selective and Stereoselective Intermolecular C–H Functionalization by Donor/Acceptor Rhodium Carbenes. *Chem. Soc. Rev.* **2011**, *40* (4), 1857–1869. https://doi.org/10/b2wcx6.
b) Davies, H. M. L.; Ren, P.; Jin, Q. Catalytic Asymmetric Allylic C−H Activation as a Surrogate of the Asymmetric Claisen Rearrangement. *Org. Lett.* **2001**, *3* (22), 3587–3590. https://doi.org/10/cnrgkt.
c) Davies, H. M. L.; Walji, A. M. Direct Synthesis of (+)-Erogorgiaene through a Kinetic Enantiodifferentiating Step. *Angewandte Chemie International Edition* **2005**, *44* (11), 1733–1735. https://doi.org/10/cjt2md.
d) Davies, H. M. L.; Coleman, M. G.; Ventura, D. L. Balance between Allylic C−H Activation and Cyclopropanation in the Reactions of Donor/Acceptor-Substituted Rhodium Carbenoids with Trans-Alkenes. *Org. Lett.* **2007**, *9* (24), 4971–4974. https://doi.org/10/cxv3fh.

258 Bao, H.; Bayeh, L.; Tambar, U. K. Allylic Functionalization of Unactivated Olefins with Grignard Reagents. *Angewandte Chemie - International Edition* **2014**, *53* (6), 1664–1668. https://doi.org/10.1002/anie.201309134.

259. Qin, L.; Sharique, M.; Tambar, U. K. Controllable, Sequential, and Stereoselective C-H Allylic Alkylation of Alkenes. *Journal of the American Chemical Society* **2019**, *141* (43), 17305–17313. https://doi.org/10.1021/jacs.9b08801.

260. a) Jia, C., Wu, N., Li, G., & Cui, X. (2022). Allylation of Arenes via Ruthenium-Catalyzed Cross-Dehydrogenative Coupling. The Journal of Organic Chemistry. https://doi.org/10.1021/acs.joc.2c00332
b) Lerchen, A., Knecht, T., Koy, M., Ernst, J. B., Bergander, K., Daniliuc, C. G., & Glorius, F. (2018). Non-Directed Cross-Dehydrogenative (Hetero)arylation of Allylic C(sp 3)−H bonds enabled by C−H Activation. Angewandte Chemie International Edition, 57(46), 15248–15252. https://doi.org/10.1002/anie.201807047

261. Spencer, A. R. A.; Grainger, R.; Panigrahi, A.; Lepper, T. J.; Bentkowska, K.; Larrosa, I. Transition Metal-Free Cross-Dehydrogenative Arylation of Unactivated Benzylic C–H Bonds. *Chem. Commun.* **2020**, *56* (92), 14479–14482. https://doi.org/10/gqpm6z.

262. a) Jia, C., Wu, N., Li, G., & Cui, X. (2022). Allylation of Arenes via Ruthenium-Catalyzed Cross-Dehydrogenative Coupling. The Journal of Organic Chemistry. https://doi.org/10.1021/acs.joc.2c00332
b) Lerchen, A., Knecht, T., Koy, M., Ernst, J. B., Bergander, K., Daniliuc, C. G., & Glorius, F.; Non-Directed Cross-Dehydrogenative (Hetero)arylation of Allylic C(sp3)-H bonds enabled by C−H Activation. *Angewandte Chemie International Edition,* **2018** *57(46)*, 15248–15252. https://doi.org/10.1002/anie.201807047

263. a) Yue, H.; Zhu, C.; Huang, L.; Dewanji, A.; Rueping, M. Advances in Allylic and Benzylic C–H Bond Functionalization Enabled by Metallaphotoredox Catalysis. *Chem. Commun.* **2022**, *58* (2), 171–184. https://doi.org/10/gnrtqz

264. Zhang, X.; Zeng, R. Neutrally Photoinduced MgCl2-Catalyzed Alkenylation and Imidoylation of Alkanes. *Org. Chem. Front.* **2022**, 10.1039.D2QO01003H. https://doi.org/10/ggkvkz.

265. Cuthbertson, J. D.; MacMillan, D. W. C. The Direct Arylation of Allylic Sp3 C-H Bonds via Organic and Photoredox Catalysis. *Nature* **2015**, *519* (7541), 74–77. https://doi.org/10.1038/nature14255.

266. Ogawa, K. A.; Boydston, A. J. Organocatalyzed Anodic Oxidation of Aldehydes to Thioesters. *Org. Lett.* **2014**, *16* (7), 1928–1931. https://doi.org/10/f5w4tb.

267. Jencks, W. P.; Salvesen, K. Equilibrium Deuterium Isotope Effects on the Ionization of Thiol Acids. *J. Am. Chem. Soc.* **1971**, *93* (18), 4433–4436. https://doi.org/10/d45ss2.

268. Huang, L.; Rueping, M. Direct Cross-Coupling of Allylic C(Sp3)−H Bonds with Aryl- and Vinylbromides by Combined Nickel and Visible-Light Catalysis. *Angewandte Chemie* **2018**, *130* (32), 10490–10494. https://doi.org/10/gqfs6f.

269. Schepp, N. P.; Johnston, L. J. Reactivity of Radical Cations. Effect of Radical Cation and Alkene Structure on the Absolute Rate Constants of Radical Cation Mediated Cycloaddition Reactions 1. *J. Am. Chem. Soc.* **1996**, *118* (12), 2872–2881. https://doi.org/10/chb5rs.

270. Huang, H.-M.; Bellotti, P.; Chen, P.-P.; Houk, K. N.; Glorius, F. Allylic C(Sp3)–H Arylation of Olefins via Ternary Catalysis. *Nat Synth* **2022**, *1* (1), 59–68. https://doi.org/10.1038/s44160-021-00006-z.

271. Zhou, R.; Liu, H.; Tao, H.; Yu, X.; Wu, J. Metal-Free Direct Alkylation of Unfunctionalized Allylic/Benzylic Sp3 C–H Bonds via Photoredox Induced Radical Cation Deprotonation. *Chem. Sci.* **2017**, *8* (6), 4654–4659. https://doi.org/10/gpnf2r.

272. a) Schwarz, J. L.; Schäfers, F.; Tlahuext-Aca, A.; Lückemeier, L.; Glorius, F. Diastereoselective Allylation of Aldehydes by Dual Photoredox and Chromium Catalysis. *J. Am. Chem. Soc.* **2018**, *140* (40), 12705–12709. https://doi.org/10/gqfhtk.
b) Mitsunuma, H.; Tanabe, S.; Fuse, H.; Ohkubo, K.; Kanai, M. Catalytic Asymmetric Allylation of Aldehydes with Alkenes through Allylic C(Sp3)–H Functionalization Mediated by Organophotoredox and Chiral Chromium Hybrid Catalysis. *Chem. Sci.* **2019**, *10* (12), 3459–3465. https://doi.org/10/gpnfs5.

273 Tanabe, S.; Mitsunuma, H.; Kanai, M. Catalytic Allylation of Aldehydes Using Unactivated Alkenes. *J. Am. Chem. Soc.* **2020**, *142* (28), 12374–12381. https://doi.org/10/gqfhtm.

274. Kato, S.; Saga, Y.; Kojima, M.; Fuse, H.; Matsunaga, S.; Fukatsu, A.; Kondo, M.; Masaoka, S.; Kanai, M. Hybrid Catalysis Enabling Room-Temperature Hydrogen Gas Release from N-Heterocycles and Tetrahydronaphthalenes. *J. Am. Chem. Soc.* **2017**, *139* (6), 2204–2207. https://doi.org/10/gqfs6b.

275. Zheng, J.; Dong, X.; Yoon, T. P. Divergent Photocatalytic Reactions of α-Ketoesters under Triplet Sensitization and Photoredox Conditions. *Org. Lett.* **2020**, *22* (16), 6520–6525. https://doi.org/10/gqfht3.

276. Le Saux, E.; Zanini, M.; Melchiorre, P. Photochemical Organocatalytic Benzylation of Allylic C–H Bonds. *J. Am. Chem. Soc.* **2022**, *144* (3), 1113–1118. https://doi.org/10/gn682s.

277. a) Choi, J.; Fu, G. C. Transition Metal-Catalyzed Alkyl-Alkyl Bond Formation: Another Dimension in Cross-Coupling Chemistry. *Science* **2017**, *356* (6334). https://doi.org/10/f9445g.
b) Kim, S.; Goldfogel, M. J.; Gilbert, M. M.; Weix, D. J. Nickel-Catalyzed Cross-Electrophile Coupling of Aryl Chlorides with Primary Alkyl Chlorides. *J. Am. Chem. Soc.* **2020**, *142* (22), 9902–9907. https://doi.org/10/ghjv3c.
c) Johnston, C. P.; Smith, R. T.; Allmendinger, S.; MacMillan, D. W. C. Metallaphotoredox-Catalysed Sp3–Sp3 Cross-Coupling of Carboxylic Acids with Alkyl Halides. *Nature* **2016**, *536* (7616), 322–325. https://doi.org/10/f82jmr.

278. a) Johnston, C. P.; Smith, R. T.; Allmendinger, S.; MacMillan, D. W. C. Metallaphotoredox-Catalysed Sp3–Sp3 Cross-Coupling of Carboxylic Acids with Alkyl Halides. *Nature* **2016**, *536* (7616), 322–325. https://doi.org/10/f82jmr.
b) Dauncey, E. M.; Dighe, S. U.; Douglas, J. J.; Leonori, D. A Dual Photoredox-Nickel Strategy for Remote Functionalization *via* Iminyl Radicals: Radical Ring-Opening-Arylation, -Vinylation and -Alkylation Cascades. *Chem. Sci.* **2019**, *10* (33), 7728–7733. https://doi.org/10/gqjq89.
c) Thullen, S. M.; Treacy, S. M.; Rovis, T. Regioselective Alkylative Cross-Coupling of Remote Unactivated C(*Sp*3)–H Bonds. *J. Am. Chem. Soc.* **2019**, *141* (36), 14062–14067. https://doi.org/10/gqhzhj.

279. Initial discovery made by Dr Mikkel B Buendia.

280. Cong, F.; Lv, X.-Y.; Day, C. S.; Martin, R. Dual Catalytic Strategy for Forging Sp2 – Sp3 and Sp3 – Sp3 Architectures via β - Scission of Aliphatic Alcohol Derivatives. *J. Am. Chem. Soc.* **2020**, *142* (49), 20594–20599. https://doi.org/10/gh53zf.

281. Dong, Z.; Ren, Z.; Thompson, S. J.; Xu, Y.; Dong, G. Transition-Metal-Catalyzed C-H Alkylation Using Alkenes. *Chemical Reviews* **2017**, *117* (13), 9333–9403. https://doi.org/10/gmw2q8.

282. Nielsen, M. K.; Shields, B. J.; Liu, J.; Williams, M. J.; Zacuto, M. J.; Doyle, A. G. Mild, Redox-Neutral Formylation of Aryl Chlorides through the Photocatalytic Generation of Chlorine Radicals. *Angewandte Chemie International Edition* **2017**, *56* (25), 7191–7194. https://doi.org/10/gpnft6.

283. Neveselý, T.; Wienhold, M.; Molloy, J. J.; Gilmour, R. Advances in the E → Z Isomerization of Alkenes Using Small Molecule Photocatalysts. *Chem. Rev.* **2022**, *122* (2), 2650–2694. https://doi.org/10/gqpngv.

284. 3 equivalents correspond to 18 C(sp3)-H equivalents. The protocol requires 20 CH equivalents for secondary bromdies or 40 CH equivalents for primary bromides.

285. Tsai, K. Y.-D.; Chang, I.-J. Oxidation of Bromide to Bromine by Ruthenium(II) Bipyridine-Type Complexes Using the Flash-Quench Technique. *Inorg. Chem.* **2017**, *56* (14), 8497–8503. https://doi.org/10/gqk3pw.

286. Mikhaylov, D.; Gryaznova, T.; Dudkina, Y.; Khrizanphorov, M.; Latypov, S.; Kataeva, O.; Vicic, D. A.; Sinyashin, O. G.; Budnikova, Y. Electrochemical Nickel-Induced Fluoroalkylation: Synthetic, Structural and Mechanistic Study. *Dalton Trans.* **2012**, *41* (1), 165–172. https://doi.org/10/b93n5w.

287. Half-cell potential of NiIII/NiII in acetonitrile *vs* Ag/AgNO3 corrected to the SCE by -0.26 V: Prasad, R.; Scaife, D. B. Electro-Oxidation and Electro-Reduction of Some Iron (II), Cobalt(II) and Nickel(II) Polypyridyl Complexes in Acetonitrile. *Journal of Electroanalytical Chemistry and Interfacial Electrochemistry* **1977**, *84* (2), 373–386. https://doi.org/10/btkkgb.

288 Grünenfelder, C. E.; Kisunzu, J. K.; Wennemers, H. Peptide-Catalyzed Stereoselective Conjugate Addition Reactions of Aldehydes to Maleimide. *Angewandte Chemie International Edition* **2016**, *55* (30), 8571–8574. https://doi.org/10/f3qcwv.

289 Zhang, D.; Iwai, T.; Sawamura, M. Iridium-Catalyzed Alkene-Selective Transfer Hydrogenation with 1,4-Dioxane as Hydrogen Donor. *Org. Lett.* **2019**, *21* (15), 5867–5872. https://doi.org/10/gqp3bb.

290 Aggarwal, V. K.; Fulton, J. R.; Sheldon, C. G.; de Vicente, J. Generation of Phosphoranes Derived from Phosphites. A New Class of Phosphorus Ylides Leading to High E Selectivity with Semi-Stabilizing Groups in Wittig Olefinations. *J. Am. Chem. Soc.* **2003**, *125* (20), 6034–6035. https://doi.org/10/d4c4q9.

291 Meng, Q.-Y.; Schirmer, T. E.; Katou, K.; König, B. Controllable Isomerization of Alkenes by Dual Visible-Light-Cobalt Catalysis. *Angewandte Chemie International Edition* **2019**, *58* (17), 5723–5728. https://doi.org/10/gfwqdt.

292 Wang, S.; Qian, Q.; Gong, H. Nickel-Catalyzed Reductive Coupling of Aryl Halides with Secondary Alkyl Bromides and Allylic Acetate. *Org. Lett.* **2012**, *14* (13), 3352–3355. https://doi.org/10/gjf2jp.

293 Cuthbertson, J. D.; MacMillan, D. W. C. The Direct Arylation of Allylic Sp3 C–H Bonds via Organic and Photoredox Catalysis. *Nature* **2015**, *519* (7541), 74–77. https://doi.org/10/f63bhz.

UNIVERSITAT ROVIRA I VIRGILI
CATALYTIC TRANSFORMATIONS ENABLED BY DUAL NICKELPHOTOREDOX MANIFOLDS
Bradley Higginson

UNIVERSITAT ROVIRA I VIRGILI
CATALYTIC TRANSFORMATIONS ENABLED BY DUAL NICKELPHOTOREDOX MANIFOLDS
Bradley Higginson

CHAPTER 4.

Nickel Mediated Proto- and Deuterodehalogenation of Aryl Bromides Using Visible Light

Published in: Synlett, 2021, 1633-1636

Photodebromination

4.1. Introduction

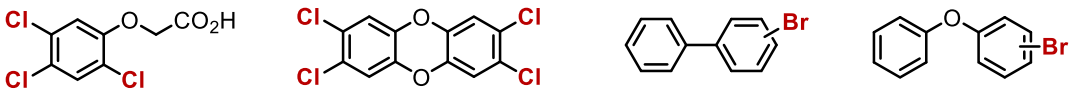

2,4,5-trichloro phenoxyacetic acid
Used as a defoliant in the Vietnam war by the US

TCDD
Acknowledged as the most potent toxin man has ever created.

PBBs
Flame retaradants with cyto- and genotoxicity

PBDEs
Flame retardants that are damaging to fertility

Figure 4.1.1. Some halogenated arenes. Oxidation as a degradation method leads to toxic compounds.

Aryl halides are an invaluable class of organic compounds; the number of transformations possible from these synthetic handles is overwhelming.[294] Their application is not only limited to the synthetic laboratory with widespread use of halogenated compounds in both agrochemical and industrial settings also.[295] The industrial use of halogenated arenes is often because of the general resistance exhibited towards degradation. As such, aryl halides have found application in flame retardants, coatings, and defoliants (Figure 4.1.1).

Figure 4.1.2. Oxidation leads to highly toxic compounds, whereas reduction can allow for incineration

Although the resistance to degradation is what makes these compounds useful, it considerably hinders their disposal. Chemically oxidising methods are not widely developed or applied because of the associated generation of harmful chemicals (Figure 4.1.2). On the other hand, significant attention has been invested into the reduction of these halogenated materials prior to incineration.[296] Chemical reduction methods have been the most widely studied and a review by Yus *et. al.* should be read by those interested in this field.[297]

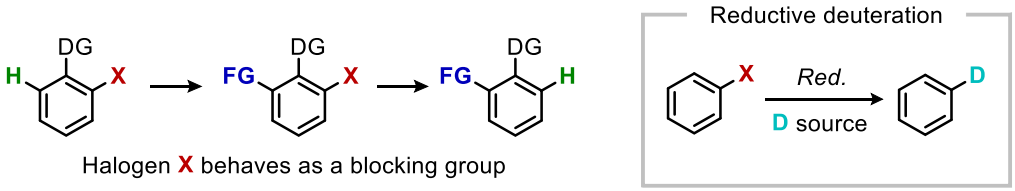

Figure 4.1.3. Blocking groups and reductive deuteration are possible applications for aryl halide reduction.

Furthermore, academia has invested time and resources into developing these reductive transformations because halogens can serve as blocking groups in C(sp^2)-H functionalisation reactions.[298] Finally, the techniques can provide a convenient route to access deuterated compounds by replacing the H-source with the corresponding D-source (Figure 4.1.3).[299]

4.1.1. The nature of the C-X bond

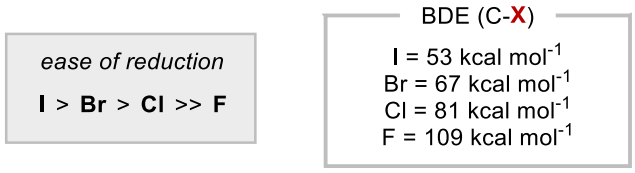

Figure 4.1.4. Bond dissociation energy is a factor that can predict ease of reduction.

The nature of the sp^2 C-X bond plays a key role in the factors governing such a transformation and deserves some consideration (Figure 4.1.4) The ease of reduction closely follows the Bond Dissociation Energy (BDE), is in the order I > Br > Cl >> F, this can enable selective reduction of polyhalogenated compounds.

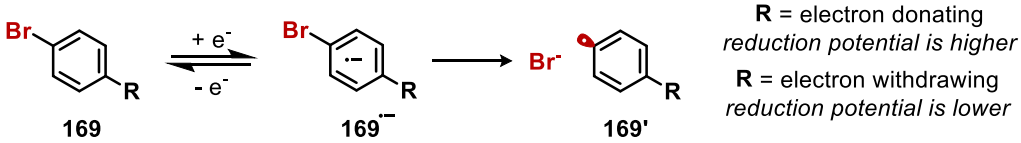

Figure 4.1.5. The reduction potentials of aryl halides are important for understanding trends.

The reduction potentials of ArX are also an indication of the ease of reduction. This potential corresponds to the injection of one electron into the arene to form the radical anion. Generally, rapid fragmentation of the radical anion occurs to generate the phenyl radical and X^-.[300] A high reduction potential means that more strongly reducing conditions are required. Furthermore, the reduction potential is related to the substituents of the aryl ring, more electron donating substituents increase the reduction potential and *vice versa (*Figure 4.1.5*)*.[301] The rapid fragmentation upon electron injection generates an electrophilic aryl radical which can be trapped by an appropriate radical trap. The methods for aryl halide reduction have expanded over the course of chemical history. We will briefly discuss the history of aryl halide reduction.

4.1.2. Historical Methods

Metal-Halogen exchange

Highly reactive alkali metals have previously been used to afford dehalogenated arenes by metal/halogen exchange followed by quenching of the resultant organometallic intermediate with a suitable proton source (Figure 4.1.6).[302] The reaction can either use zero-valent metals (e.g. Li/Li^+ = - 3.04 V *vs* SCE) or preformed organometallic species such as alkyl lithium. Alkyl lithium species such as the isomers of *butyl*-lithium are used due to their relative ease of handling in comparison to lithium metal and ability to readily reduce aryl bromides. Aryl chloride reduction on the other hand is more challenging and requires reactive species such as Li•Napthalinide.[303]

Photodebromination

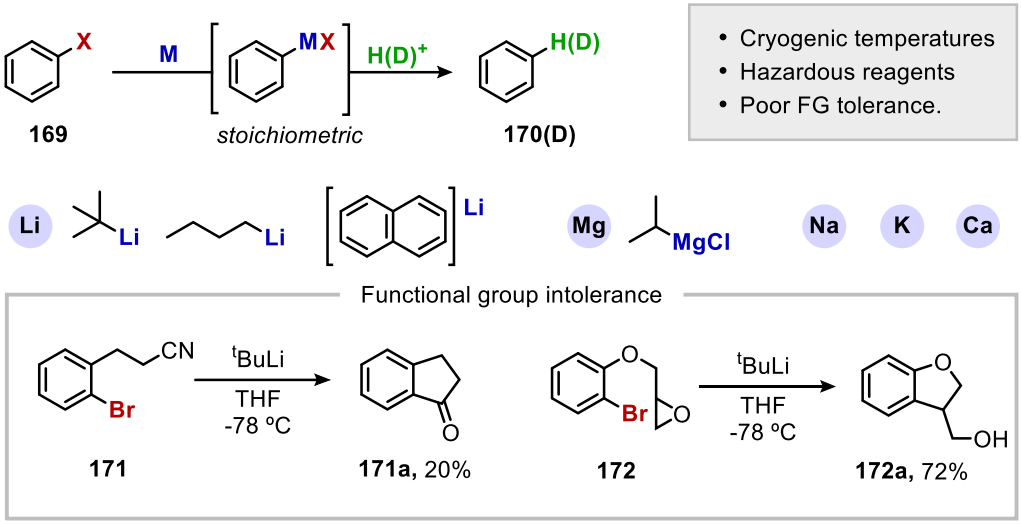

Figure 4.1.6. Representation of metal-halogen exchange mediated dehalogenation. Functionali group incompatibilities demonstrated by Li.

Descending the periodic table to sodium and potassium is accompanied by a decrease in reported methods.[304] The use of these alkali metals has not been as widespread as the use of lithium because of difficulties associated with handling of sodium and potassium, the techniques are generally used in an industrial setting.[305] On the other hand, alkali earth metal magnesium has seen considerable use due to its high reduction potential (- 2.38 V *vs* SCE). As with lithium, techniques have been developed using the zerovalent metal;[306] but preformed alkyl Grignard reagents are preferred due to the kinetics of exchange.[307] Nevertheless, the use of highly reactive species in stoichiometric quantities diminishes the applicability and functional group tolerance of these protocols.

The general intolerance is widely recognised, and Liu highlighted this in 2018 (Figure 4.1.6),[308] the pendant nitrile and epoxide groups both undergo intermolecular cyclisation with the resultant Ar-Li after lithium/halogen exchange with *tert*-butyllithium. Although there are disadvantages to these techniques, for simple molecules on lab scale the reactions are straightforward to perform and should not be overlooked. Particularly because the proton source is often water, enabling deuterated compounds to be accessed from D_2O which is one of the cheapest sources of deuterium.[309]

Group IV hydrides

An alternative to alkali-metal mediated reductions is the use of Group IV hydrides,[310] (silicon, tin, and germanium hydrides). These reducing agents operate by a different mechanism exploiting a radical chain pathway. As a result of the radical nature of this pathway (Figure 4.1.7), the thermodynamic considerations are dramatically altered. In this regard, emphasis should be placed on C-X BDEs rather than the reduction potentials. The trend for Gp^{IV}-H based reductions follows the trend seen in the previous chapters for radical stabilised reactivity:

Benzylic > *tert*-alkyl > *sec*-alkyl > primary-alkyl >> aryl.

Thus, alkyl halides are considerably more amenable to reduction over aryl halides because the corresponding carbon centre radical is much more stable than the aryl. As such, there has been comparatively limited exploration of Gp(IV) hydride mediated dehalogenation of aryl halides.

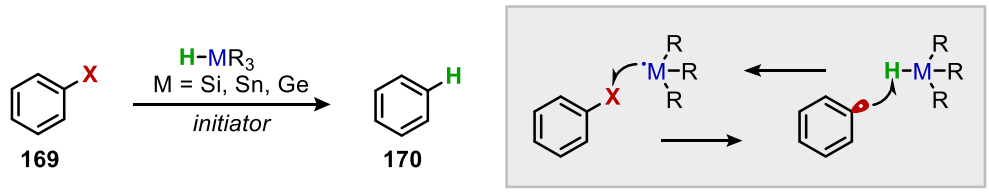

Figure 4.1.7. A general scheme for Gp IV hydride mediated dehalogenation and it's radical chain nature.

Although generally regarded as milder and more tolerant of functionalities, there are several problems associated with these methods. The most prominent is the toxicity and persistence of the by-products, particularly those employing tin hydrides. Additionally, radical initiators are employed and the radical nature of this pathway disfavours aryl halide reduction. The group IV hydrides can however be used in conjunction with transition metals to afford the dehalogenation of several aryl bromides.[311]

4.1.3. Transition metal mediated

Due to the widespread application of transition metal catalysts in chemical society, their extension towards hydrodehalogenation reactions was inevitable. Transition metal chemistry offers an array of variables which can be exploited to control reactivity. Furthermore, the presence of the metal catalyst allows for alternative mechanistic scenarios, such as oxidative addition, which alters the factors dictating reduction. The formation of Metal-Carbon (M-C) bonds alters the properties to the C-X bond. The area has largely been dominated by palladium, although the use of earth abundant metals such as nickel,[312] and iron,[313] are becoming more relevant (Figure 4.1.8).

Photodebromination

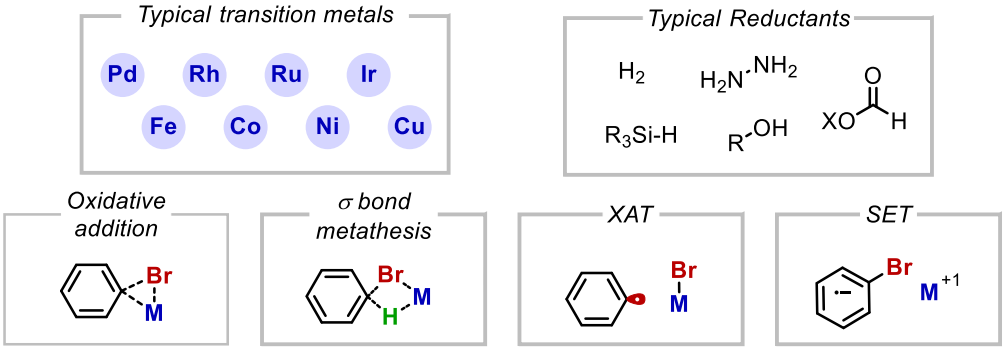

Figure 4.1.8. Typical metals and reductants used in dehalogenation. Four plausible mechanistic scenarios.

As mentioned, palladium's use in this field is broad,[314] with both homogeneous and heterogeneous catalysis playing significant roles. The hydrogen source in these reactions is commonly hydridic in nature such as formate or hydrazine. For homogeneous palladium catalysts, bulky, expensive ligands are often required which dramatically reduces the desirability of these transformations.[315] Many transition metal reactions proceed through the formation of M-Ar bonds which dramatically alters the chemical considerations for reduction due to the changes in BDE and the ability to reductively eliminate with a hydride species.

However, oxidative addition to an aryl halide is not the only way in which transition metal catalysts can react with the Ar-X bond. There are several other activation modes including sigma bond metathesis, halogen atom transfer (XAT), or single electron transfer (SET) (Figure 4.1.8, bottom).

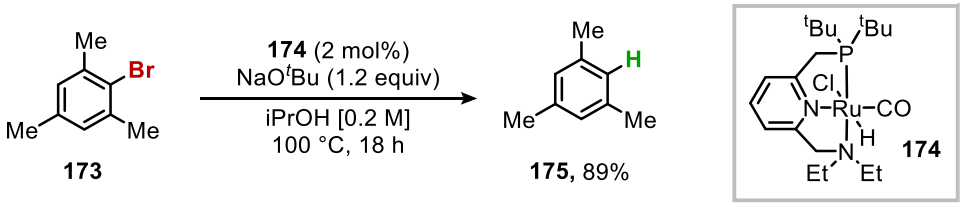

Figure 4.1.9. Dehalogenation using a hydrogen transfer type catalyst.

The use of noble metals in the arena of hydrodehalogenation has not seen widespread application due to the cost of the noble metal and the generally harsher reaction conditions required.[316] However it does enable the unique opportunity to use solvents as the source of hydrogen. Much like transfer hydrogenation by Noyori unlocked the ability to use IPA as a hydrogen surrogate for the reduction of alkenes;[317] Grubbs developed a ruthenium catalyst which uses butanol for the reduction of halogenated arenes (Figure 4.1.9). The ruthenium catalyst developed requires elevated temperatures and stoichiometric amounts of strong base but the reaction tolerates sterically challenging substrates such as **173**.

4.1.4. Miscellaneous

Disilane mediated dehalogenation

Aside from the classical techniques, there have been several approaches which are not strictly part of the previous categories. For example, the potassium methoxide/ disilane mediated deuterodehalogenation of (hetero)aryl bromides developed by Liu (Figure 4.1.10.).[318]

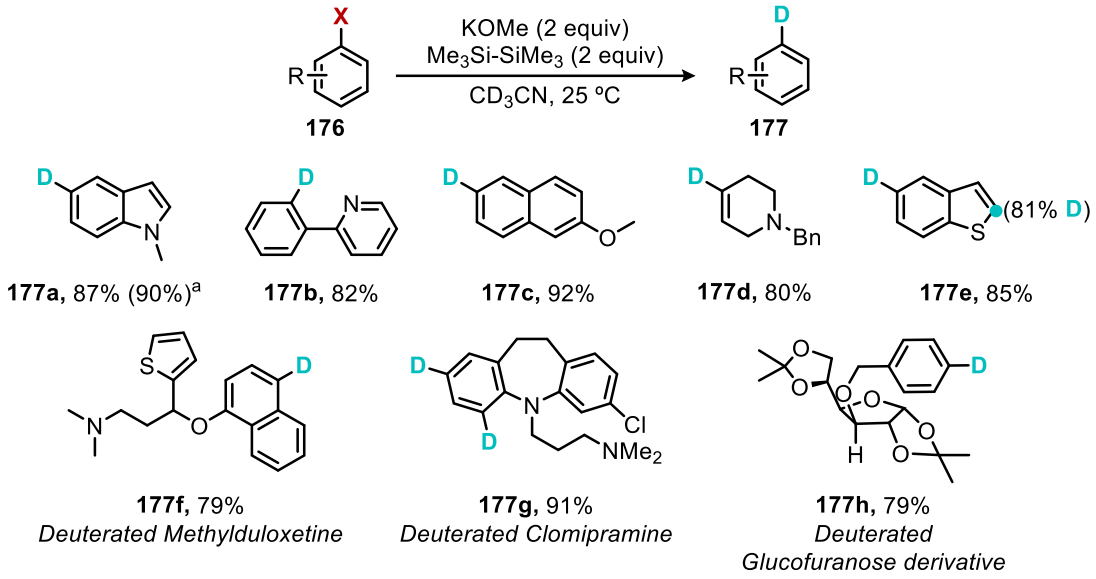

Figure 4.1.10. Deuterodehalogenation of aryl bromides using a potassium methoxide disilane.

Although the technique was principally applied to deuterodehalogenation, the use of non-deuterated solvent also works effectively (*supporting information of the paper*) and is thus representative to the analogous hydrodehalogenation reactions described above. The simple, and mild reaction conditions of this work are exceptional and permit broad functional group compatibility.

Specific deuteration is becoming a valuable technique, particularly to the pharmaceutical industry. Deuterated compounds are being used to combat oxidative degradation, improve pharmacokinetics, lipophilicity, and maintain essential hydrogen bonding.[319] The specific incorporation of deuterium at the *ipso* site of aryl halides provides facile access to mono- or bis-deuterated compounds.

Photodebromination

"Electron" chemistry

The recently coined "electron chemistry" developed by Studer and co-workers uses a strong base in conjunction with elevated temperature to achieve the hydrodehalogenation of a range of aryl halides, including arylfluorides.[320] Although use of NaH is not uncommon in this field, it is the modality of which the reduction is invoked in this reaction which is surprising.[321] The authors propose the formation of a highly reducing dioxane radical anion which transfers the electron to the aryl ring. Fragmentation of the aryl radical anion **178**, creates the aryl radical **178'** which can abstract a hydrogen from the solvent 1,4-dioxane (**180**). As we have discussed in the previous chapters, HAT from the solvent proceeds due to a high thermodynamic driving for (BDE of Ar-H = 112.7 kcal mol^{-1}),[322] additionally the philicities of the radicals are matched, aryl radicals are electrophilic and the dioxane hydrogen is hydridic. The dioxane radical (**180'**), which after deprotonation by NaH, regenerates the radical anion. It is mentioned that the formation of a radical can greatly increase the acidity of the α-protons

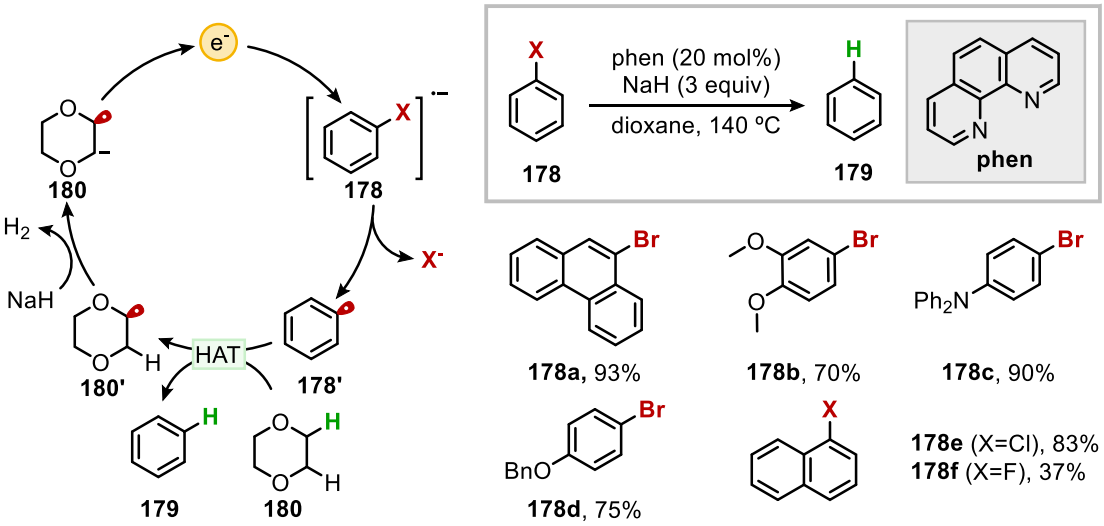

Figure 4.1.11. Dehalogenation afforded by sodium hydride at elevated temperatures.

It should be noted, however, that the use of phenanthroline is essential for the reactivity but it is not included in the proposed electron cycle. Additionally, the reaction is run at elevated temperature (140 °C), well above the boiling point of dioxane, which is not particularly safe or environmentally benign. Despite the mechanistic intricacies, a SET scenario could be a viable opportunity to access a general reductive technique. A milder technique to generate these types of SET processes would be ideal.

4.2. A Photochemical Renaissance

Modern photoredox chemical techniques can readily access open shell intermediates through single electron transfer (SET) events. Therefore, the blending of photochemistry with hydrodehalogenation reactions has the potential to establish novel and mild conditions for the effective dehalogenation of aryl halides. The use of high energy UV has been used on several occasions,[323] but this can lead to deleterious side reactions. With regards to visible light mediated transformations, significant progress into this field has already been made. However, due to the disparity between commonly employed photoredox catalysts and the high reduction potentials typical of aryl halides, the merger of these two fields has not been as trivial as initially anticipated.

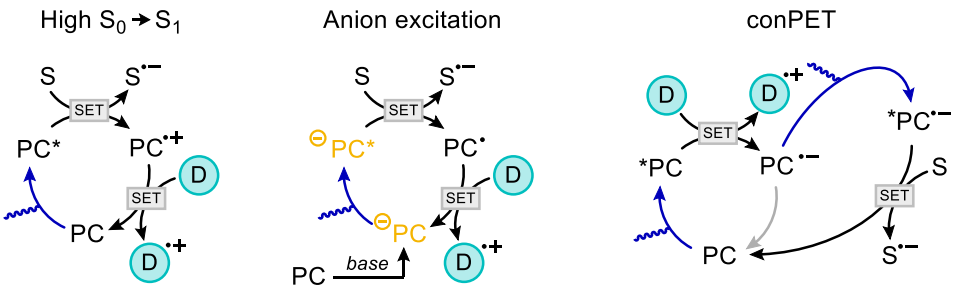

Figure 4.2.1. Some historically highly reducing photocatalysts. Three methods for highly reducing systems all requiring a sacrificial electron donor. The typical method to reduce aryl halides is to generate the radical anion.

The gap between reduction potentials has in part been addressed by significant photocatalyst development. New photocatalysts boasting higher reduction potentials, or larger $S_0 \rightarrow S_1$ transitions has enabled for many reductions to be accessed.[324] Furthermore, unique methods to achieve highly reducing species have been developed such as anion excitation;[325] consecutive photoinduced electron transfer (conPET)[326] or excitation of electrochemically generated radical anions (Figure 4.2.1).[327] More recently there has been an imitation of the Z-scheme employed by nature, using two photocatalysts to enable the reduction of aryl chlorides with low energy red light.[328]

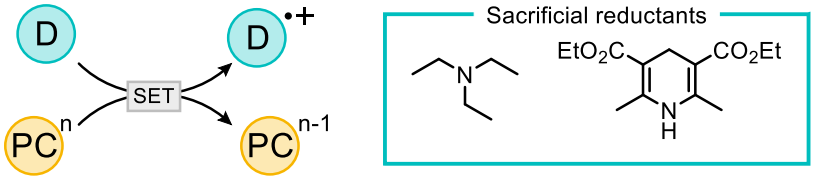

Figure 4.2.2. Sacrificial reductants are necessary

Due to the fundamental nature of photoredox chemistry, requires the use of sacrificial reductants to turn over the photocatalyst (Figure 4.2.2). Typical sacrificial reductants are trialkyl amines and Hanztch esters.

Photodebromination

4.2.1. Highly reducing photocatalysts

The accessible reducing power of a photocatalyst is limited to the energy of the incident light. For blue light (centred at 440 nm) the maximum energy threshold between donor and acceptor is 270 kJ mol^{-1}. Additionally, there are non-negligible energy losses from intersystem crossing and reorganisation energies, so the available energy for transfer is restricted by fundamental photophysical principals. This constraint means that the reductive potential that photocatalysts can reach is also limited.

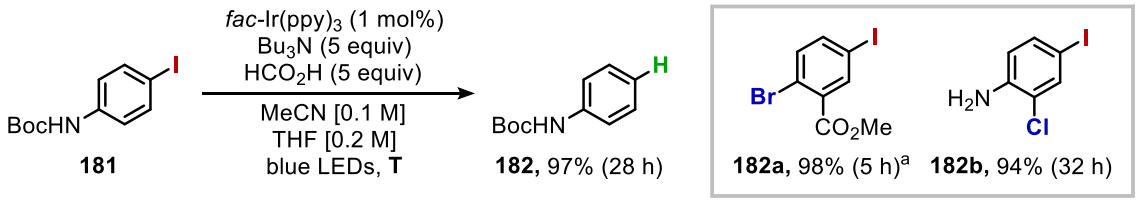

Figure 4.2.3. The halogens in blue do not undergo reduction a) prolonged reaction time leads to some debromination.

The first example of aryl halide reduction by Stephenson and co-workers (Figure 4.2.3),[329] the applied photocatalyst, *fac*-Ir(ppy)$_3$ has one of the highest reduction potentials of the iridium polypyridyl series. (E[Ir^{IV}/*Ir^{III}] = - 1.73 V *vs* SCE). The high reduction potential means that it is able to reduce unactivated alkyl, alkenyl, and aryl iodides selectively in the presence of other halogens such as bromide **182a** and chlorides **182b**. Although extended reaction times do see partial reductions of the bromide from **182a**. The photocatalyst must be regenerated using a sacrificial reductant, in this case the use of tributylamine and formic acid.

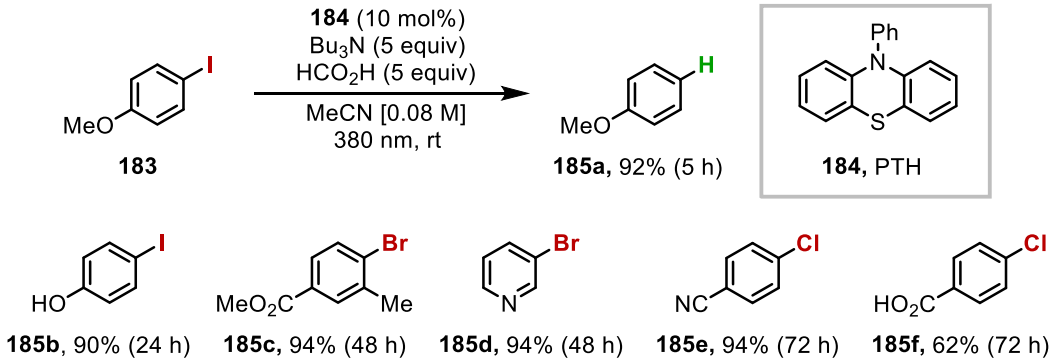

Figure 4.2.4. Reduction of aryl bromides and chlorides afforded by organic photocatalyst PTH.

The *fac*-Ir(ppy)$_3$ catalysts also have a limitation in the sense that they are expensive. An organic molecule that could play a similar role would be highly beneficial. Alaniz and co-workers developed a thiazine catalyst **184** for the application in ATRP (Figure 4.2.4),[330] but found that the reduction potential was high, (E[PTH$^{\bullet+}$/*PTH] = -2.03 V *vs* SCE) application of this photocatalyst in a reductive scenario leads to a promising array of aryl halide reductions.

Electron rich aryl iodides **185a** and **185b** can be readily reduced using PTH in the presence of higher energy UV light (380 nm light), the scope was extended to incorporate, aryl and heteroaryl bromides **185c** and **185d** as well as electron deficient aryl chlorides such as **185e** and **185f**. The scope of the reaction is broader than the initial report by Stephenson because of the higher wavelength of light used. The use of UV also leads us to one of the photophysical concepts as to why the excited state PTH* is a stronger reductant than *fac*-Ir(ppy)$_3$*. The excited state reduction potential can be related to the ground state oxidation potential and the photoluminescence maximum by the equation:

$$E_{red^*} = E_{ox} - \frac{hc}{\lambda_{max}}$$

E_{red*} is the excited state reduction potential, E_{ox} is the ground state oxidation potential, h is Planck's constant, c is the speed of light and λ_{max} is the photoluminescence maximum. Whilst the ground state oxidation potential of PTH ($E[PTH^{\bullet+}/PTH]$ = + 0.68 *vs* SCE) and *fac*-Ir(ppy)$_3$ are quite similar ($E[Ir^{IV}/Ir^{III}]$ = + 0.77 V *vs*. SCE). The significant difference is the photoluminescence maximum of PTH (445 nm) which is considerably lower than *fac*-Ir(ppy)$_3$ (500 nm). This means the reduction potential is higher.

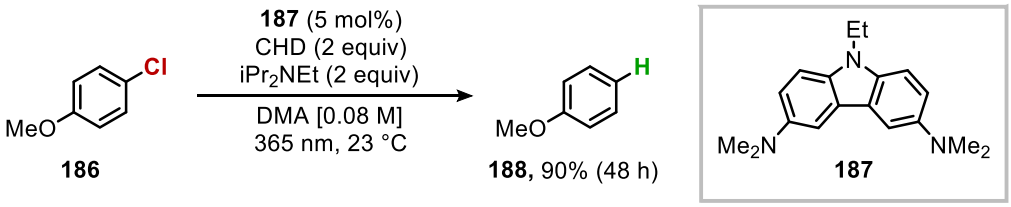

Figure 4.2.5. The use of 365 nm UV light affords the dechlorination of electron rich substrate 186.

Although electron deficient aryl chlorides could be reduced by Alaniz, electron rich aryl chlorides were outside of the reduction potential. However, the concept of using an organic photocatalyst and higher energy UV was extended by Sakata and co-workers (Figure 4.2.5).[331] Using the carbazole derivative **187** in the presence of UVA light (365 nm) afforded the reduction of electron rich aryl chlorides and one example of an aryl fluoride (1-fluoro-4-octylbenzene, 62% yield, 48 h). The transition towards higher energy UV is not particularly desirable because this wavelength can start to directly excite the substrates which may lead to problematic side reactions.

The advantage of photoredox catalysts is the ability to selectively irradiate the photocatalyst. Thus, techniques that exploit other photophysical ideas rather than increasing the $S_0 \rightarrow S_1$ band gap would be appropriate.

Photodebromination

4.2.2.Anionic photocatalysts

The use of ionic photocatalysts has played an important role in the history of photocatalysis. Cationic catalysts like the Fukuzumi catalyst have played a historical role, particularly in oxidative chemistry.[332] König and co-workers believed that, by extension, anionic photocatalysts could play a key role in reductive chemistry. The use of ionic catalysts has significant advantages because upon SET the photocatalyst and substrate are not electrostatically attracted, which is the case for neutral PCs, so back electron transfer (BET) is less of a problem. Anionic photocatalysis is not as widely applied in comparison to the cationic variant but it is a growing field.[333]

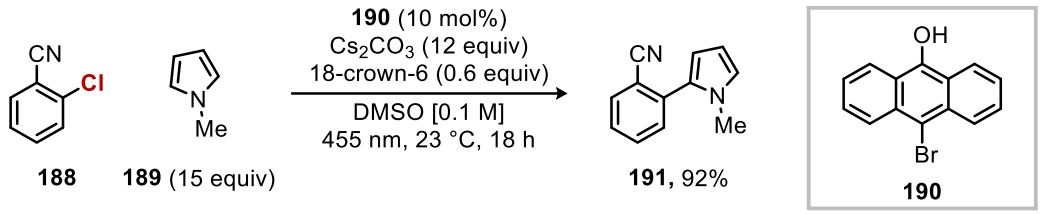

Figure 4.2.6. The conditions developed by Konig for a highly reducing anionic photocatalyst

The anthraquinone photocatalyst **190** was not used to reduce the aryl chloride to the arene, but to form a C-C bond through radical addition to pyrrole **189** to form the coupled product **191** (Figure 4.2.6). Whilst not strictly a reduction the mechanistic scenario is identical to the aforementioned techniques, forming the aryl radical anion which fragments to form the aryl radical. The scenario could be reasonably extended to a reduction by changing the pyrrole trap (**T**) to a source of hydrogen.

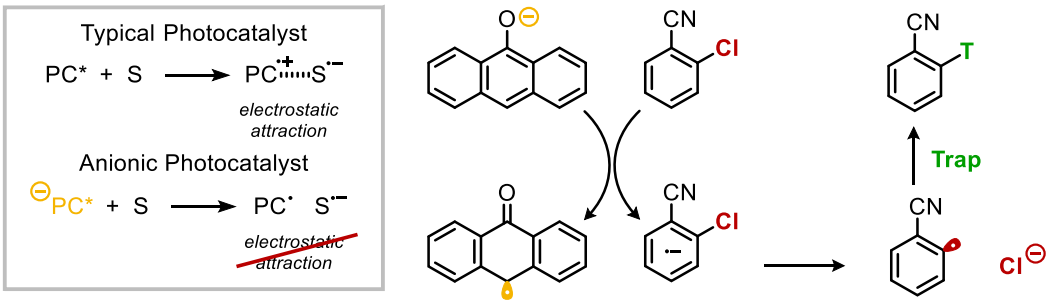

Figure 4.2.7. The mechanism of radical formation through oxidative quenching of the photocatalyst.

4.2.3. Consecutive photoinduced electron transfer

In both simple photocatalytic reductions and the anionic variant, the energy available to the system is constrained to the energy from a single photon. The use of two photons would inevitably increase the energy available. König and co-workers took inspiration from the Z-Scheme of nature (*vide infra*) to develop a dual photon absorption technique.[326] The authors call this consecutive photoinduced electron transfer (conPET)

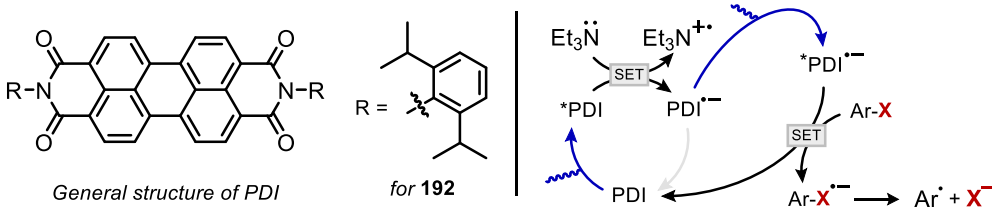

Figure 4.2.8. Structure of PDI and the variation used | Mechanism of conPET.

The photocatalyst used in this work is **PDI**, a well-studied fluorescent dye (Figure 4.2.8). The photoexcitation of PDI by 455 nm light to ***PDI** creates an oxidising state which can be quenched by triethylamine to form the radical anion **PDI$^{\bullet-}$**. A second photoexcitation event of the radical anion to form ***PDI$^{\bullet-}$** creates a highly reducing state that can access reduction potentials greater than those of aryl chlorides.

Single electron transfer to the arene to form the ground state **PDI** and arene radical anion is followed by rapid fragmentation to the aryl radical and halide anion. The arene radical participates in a hydrogen atom abstraction from the solvent or oxidised amine to liberate the reduced aryl halide product. The direct transfer of the electron from ***PDI$^{\bullet-}$** has been observed by transient absorption spectroscopy.[334]

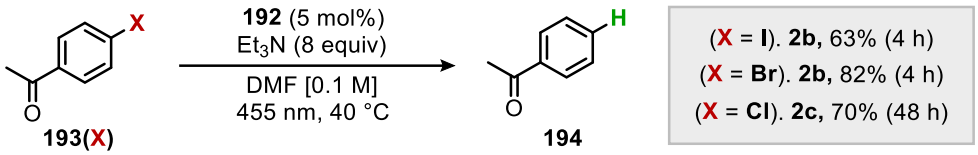

Figure 4.2.9. PDI used in a conPET scenario affords the dehalogenation of iodide, bromide and chloride

This technique requires an initial reduction of the PDI to generate the radical anion, trialkylamines are used in this instance in an oxidative quenching cycle (Figure 4.2.9); but it is possible to inject this electron by electrochemical means.[335] In this manor a dual photo-electrochemical technique to access highly energetic states has been developed and applied in an analogous scenarios.

Photodebromination

4.2.4. Z-Scheme

The Z-Scheme describes the redox events that occur during photosynthesis,[336] it enables highly reducing conditions to be accessed using low energy light. A simplified version of the Z-Scheme is seen in Figure 4.2.10 (left). the absorption of a photon ($h\nu_1$) promotes the enzyme P_{680} to an excited state, a series of electron transfer (ET) events to P_{700}, and a second photon absorption by P700 creates a highly reducing state of $*P_{700}$ which is ultimately responsible for the reduction of $NADP^+$ to NADPH and overall photosynthesis.[337]

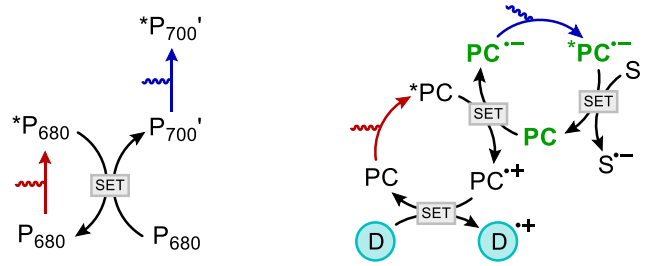

Figure 4.2.10. Schematic of the Z-Scheme and it's man-made analogue

The Z-Scheme has inspired chemists to create an analogous scheme, with applications in man-made problems such as the photo-oxidation of water.[338] SET between photocatalysts followed by photoexcitation forms highly reducing ***PC**•−** (Figure 4.2.10., right).

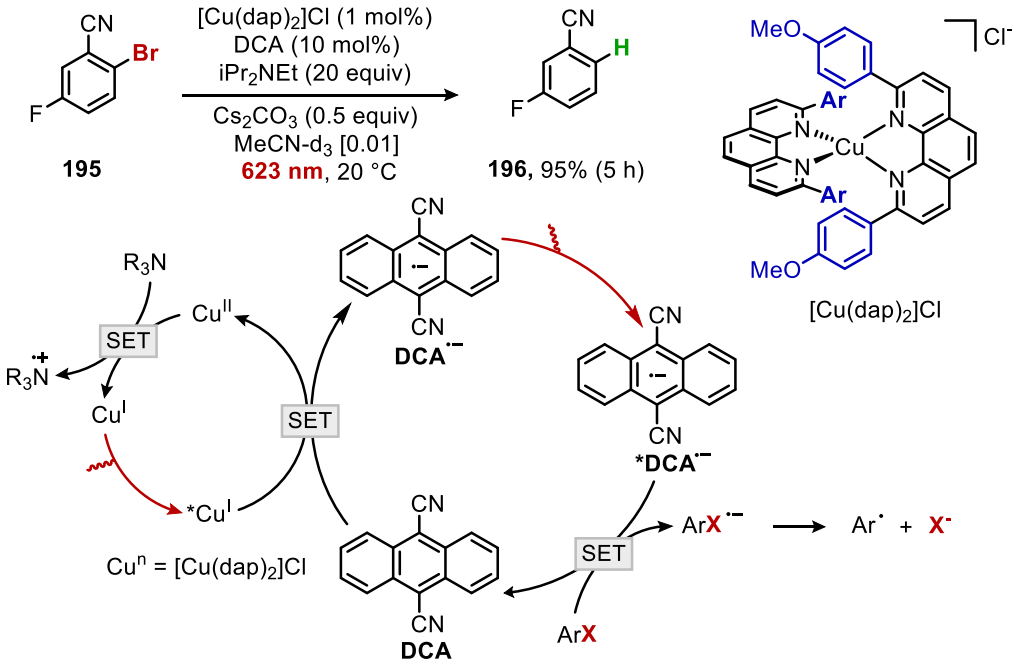

Figure 4.2.11. Two photocatalysts allow for the photodehalogenations of aryl halides with red light.

The highly reducing nature of these excited states could in theory be applied to the photoreduction of aryl halides. Indeed, Wenger and co-workers have exploited this photochemical principal to access the reduction of arylhalides using low energy red light (Figure 4.2.11).[329] The advantage of red light (620 nm = 2.0 eV) is that it is considerably lower in energy when compare to blue light (410 nm = 3.0 eV), this lower energy means that undesirable side reactions through direct photoexcitation of a substrate will not occur. Selective photoexcitation of photocatalysts is essential for controlled reaction systems. The reaction proceeds through photoexcitation of Cu^{I} species to an excited state, electron transfer to the ground state of **DCA**, generates a Cu^{II} intermediate and **DCA**$^{\bullet-}$. The Cu^{II} species oxidises triethylamine to return to its ground state. Whereas DCA absorbs another photon of light to become promoted to ***DCA**$^{\bullet-}$. This is a highly reducing form which can inject an electron into the aryl ring which rapidly fragments and can abstract a hydrogen from the solvent or oxidised triethylamine. The authors also propose a second mechanistic scenario whereby there is a triplet-triplet energy transfer (TTET) between Cu^{I} and DCA. Depending upon the reaction conditions, the contribution from both pathways varies.

A similar idea using CdS quantum dots as highly reducing species has been exploited by Weix and co-workers.[339] Additionally, there has been some interesting work through photon up conversion by triplet-triplet annihilation,[340] however both of these exemplary works are beyond the scope of this thesis.

Each of the aforementioned techniques are able to access highly energetic states one of the key issues is they require they have to generate the aryl radical anion, which often requires very high reduction potentials. Additionally, there is a common issue, the redox nature of the photocatalysts provides simultaneously both an oxidising and reducing environment. For a net reductive environment, an exogenous sacrificial reductant must be employed which perturbs the green metrics of these photodehalogenation techniques. Lastly, because the photocatalyst excited state potentials are correlated to the ground state potentials, if a species has a highly reducing ground state, such as *fac*-$Ir(ppy)_3$ ($E[*Ir^{III}/Ir^{II}]$ = - 2.19 V) the corresponding excited state oxidation potential is low ($E[Ir^{III}/Ir^{II}]$ = + 0.31 V). This is an issue as it limits the applicability of these catalysts as the reaction is now oxidation-potential gated from the sacrificial reductant.

Photodebromination

4.2.5.HAT from Solvent

A reaction that could harness the power of light without the requirement for exogenous reductant would be particularly beneficial. For example, a hydrogen atom transfer (HAT) event from an appropriate solvent, akin to that of the work by Studer and Grubbs could be very useful (Figure 4.1.9 and Figure 4.1.11). The advantages of obtaining the H-atom from the solvent are multifold, not least is that there is an abundance of readily available deuterated solvents that can be employed. But the removal of unnecessary waste material is also highly beneficial. This approach was envisioned and utilised by Chen *et al*.,[341] a photochemical hydro- and deuterodehalogenation using a simple Pd(0) pre catalyst and isopropanol as solvent was developed under visible light irradiation (Figure 4.2.12).

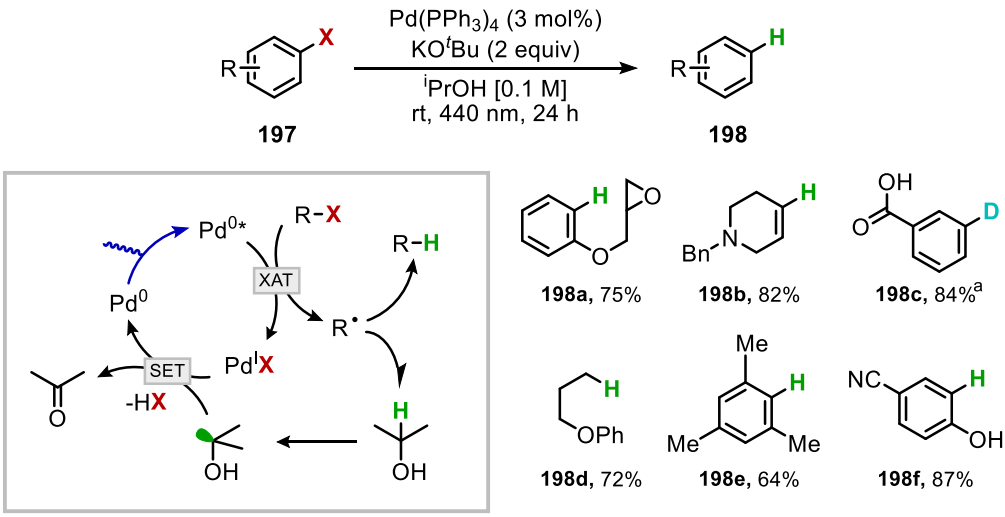

Figure 4.2.12. Dehalogenation using iso-propanol as solvent and hydrogen source. a) using IPA-d_8

The authors propose that the an excited Pd^0 species abstracts the halogen from the aryl or alkyl bromide to form the corresponding radical, radical abstraction from IPA liberates the reduced aryl halide (**198**). The a-oxy radical undergoes a SET event with the PdX species formed. Base deprotonation liberates acetone and regenerates the Pd^0 catalyst.

This work highlights the utility of developing hydrodehalogenation techniques in conjunction with transition metal catalysis. However, the drawbacks of palladium are quite significant, this expensive and rare earth metal is economically unviable for such a reaction. Furthermore, the use of palladium has downstream consequences for both synthetic application and deuteration techniques.

4.2.6. Nickel as an alternative to Palladium

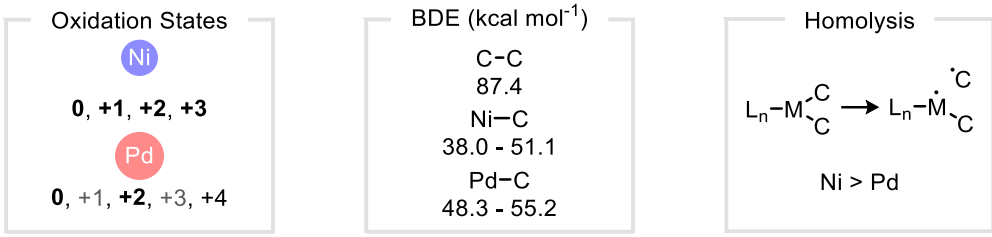

Figure 4.2.13. A comparison of the key differences between nickel and palladium.

Nickel is a relatively cheap and earth abundant metal in comparison to noble metals such as palladium. The chemical properties of nickel also make for a versatile stage to develop reactions. As a first-row transition metal, the energy difference between the d-orbitals is small, allowing for facile absorption of visible light and the ability to access high-spin and odd electronic configurations. Another important factor is the strength of the nickel-carbon (Ni-C) bond, it is generally weaker than the analogous palladium-carbon (Pd-C) bond which can improve the reactivity of nickel-mediated catalysis, although this property can also make reactivity difficult to control. Finally, M-C bond homolysis to form radicals is much more common in nickel catalysis. In this regard, the generation of either halide or aryl radicals could have considerable value in a reduction protocol.

With these factors in mind, we believed that the dehalogenation of aryl bromides could be afforded by a nickel-catalysed process. This was also supported by the observation of dehalogenated arylbromides as a side product in many related photochemical reactions. For example, in the enantioselective C(sp^3)-H functionalisation work (chapter 2), hydrodehalogenation was especially prominent when employing bidentate phosphine ligands.

4.3 General aim of the project

The dehalogenation of aryl bromides is an interesting avenue for exploration due to the prolific use of these compounds in industry and academia. Furthermore, as hydrodehalogenation is a common side-reaction in many visible light mediated transformations, unravelling the origins of this side product could be very beneficial to the community. However, current methods to afford the dehalogenation under visible light use stoichiometric reductants, high energy UV light, or more recently, palladium which is ecologically and economically undesirable.

Early transition metals offer several advantages over rare earth metals, not least is the cost. We envisioned that a nickel-based protocol could afford a broadly applicable dehalogenation of aryl bromides using THF as the hydrogen source under visible light irradiation.

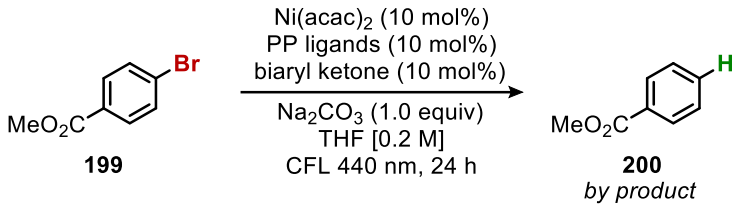

199 **200**
by product

Figure 4.3.1. The observed side products from chapter two.

The platform for this reactivity was discovered in Chapter 2 with diphosphine ligands providing significant amounts of dehalogenated arene (Figure 4.3.1) and was seen as an opportunity to develop a new methodology including a deuterodehalogenation protocol with THF-d_8 . Finally, extension of this work to understand mechanistic underpinnings could lead to enhanced ligand design to avoid the dehalogenation side products in cross-coupling reactions.

4.4 Optimisation.

4.4.1. Reproducing results

This project was initiated by a previous member of the group, Dr Yiting Gu, who provided the optimised reaction conditions. The use of $Ni(acac)_2$ and an inexpensive diphosphine ligand (dppe) in combination with a biaryl ketone as co-catalyst under compact fluorescent light (CFL) bulb irradiation gave **200** in 84% yield.[342]

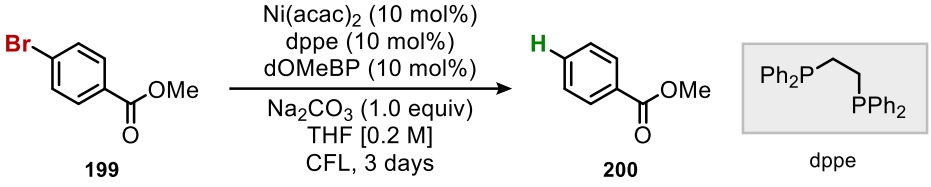

Entry	*Ketone*	**199**	**200**
1	✓	0	84%
2	X	0	80%

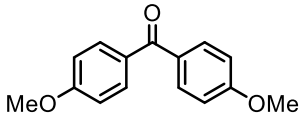

dOMeBP

Figure 4.4.1 Aryl bromide (0.2 mmol), $Ni(acac)_2$ (0.02 mmol), dppe (0.02 mmol), Na_2CO_3 (0.3 mmol), THF (1 mL), CFL light irradiation at 38 °C for 72 h.

The co-catalyst was originally employed because this project was initiated during the C(sp^3)-H functionalisation of ethers using aryl bromides, but it was questioned whether it was necessary for this hydrodebromination reaction. Indeed, removing dimethoxybenzopheone (dOMeBP) had only limited impact on the reactivity of the system (Figure 4.4.1) with electron poor aryl bromide **199**.

4.4.2. Small scope with Conditions A

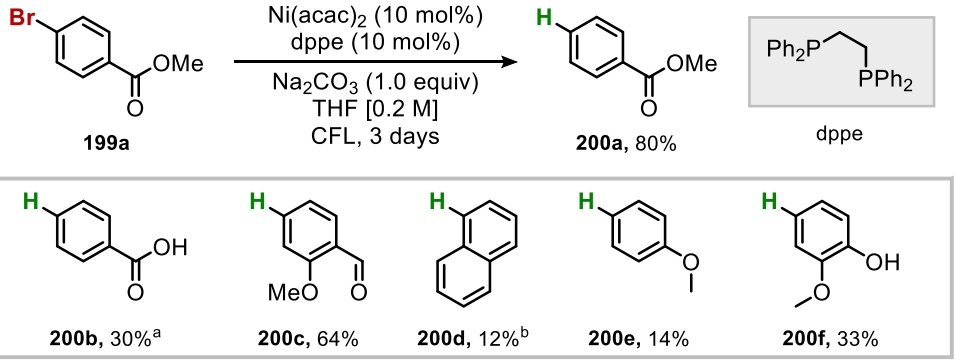

Figure 4.4.2 Small substrate scope using optimised conditions A. Aryl bromide (0.2 mmol), $Ni(acac)_2$ (0.02 mmol), dppe (0.02 mmol), Na_2CO_3 (0.3 mmol), THF (1 mL), CFL light irradiation at 38 °C for 72 h. NMR yields using 1,3,5 trimethoxy benzene as internal standard. a) an additional equivalent of KOtBu (0.2 mmol) b) corrected GC yield using 1,3,5-trimethoxy benzene as internal standard.

Photodebromination

After repeating the initial results, a small assessment of the scope was conducted to see if the results were broadly applicable. Disappointingly, when moving away from the optimised substrate **200a**, the yield dropped significantly. The use of carboxylic acid **200b**, was achieved in 30%, which is significantly lower than the optimised substrate. Methoxy-aldehyde **200c** was the only successful substrate that was employed in this scenario with 64% NMR yield, although the halogenated material was still present. Moving to assess more rich substrates such as **200d** and **200e**, led to poor performance, with less than 20% NMR yield in both cases. Guaiacol derivative **200f** was tolerated to a certain extent. With this in mind, we decided to take a step back and find a set of conditions that could afford a general protocol for the reduction of aryl halides.

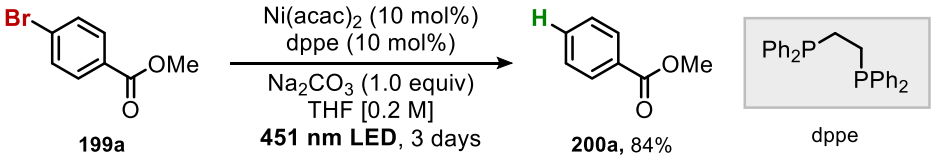

Figure 4.4.3. Reaction conducted under blue light without dOMeBP

Additionally, almost identical yields could be obtained using blue LEDs (Figure 4.4.3, emission centred at 451 nm) which would allow us to use a more controllable system in the form of the custom-made reactors. Electron poor aryl bromide (**199a**) is commonly used to enable the discovery of nickel-mediated photoredox reactions due to its ease of handling - a stable crystalline solid - and propensity to undergo oxidative addition with nickel. Yet to find a general protocol, more challenging electron rich substrates such as 4-bromoanisole **201** should be tolerated so was used as model substrate in the continued optimisation.

4.4.3. Ligand Screen

The electron density of the phosphine ligand plays an important role in the oxidative addition step of a typical nickel cross coupling reaction (which we hypothesise is the mechanistic scenario). We believed that the initial oxidative addition of the aryl bromide was the reason for the poor results of the initial scope. Thus, we decided to explore a range of more electron rich diphosphine ligands.

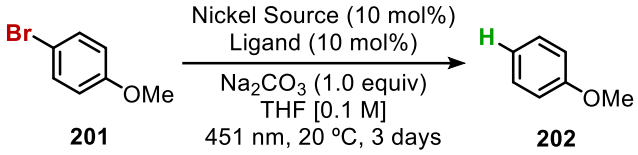

Entry	*Change*	**201**	**202**
1	**L35** with $Ni(acac)_2$	100	0
2	**L36** with $Ni(acac)_2$	53	44
3	**L37** with $Ni(acac)_2$	48	52
4	**L38** with $Ni(acac)_2$	80	5
5	**L39** with $Ni(acac)_2$	98	0
6	**L40** with $Ni(acac)_2$	63	25
7	**L36** with $NiCl_2$	27	63
8	**L36** with $NiBr_2$	0	70
9	**L36** with NiI_2	23	74

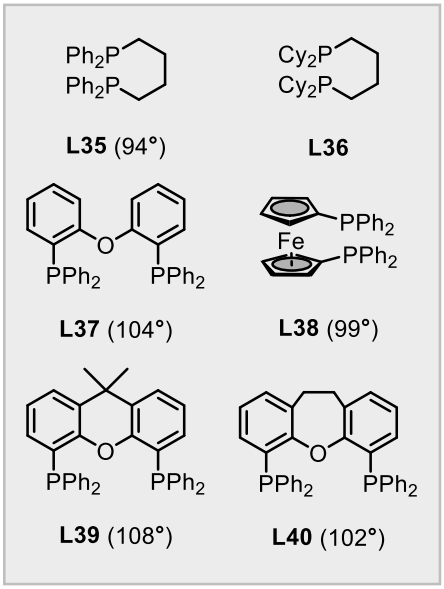

Figure 4.4.4 Ligand screen. Aryl bromide (0.2 mmol), NiI_2 (0.02 mmol), ligand (0.02 mmol), Na_2CO_3 (0.2 mmol), THF (1 mL), 451 nm reactor at 20 °C for 72 h. Corrected GC yields using decane as internal standard.

An initial ligand screen (e*ntry 1 - 6*) was conducted and the bite angles of the ligands are shown (Figure 4.4.4).[343] The more electron rich dicyclohexylphosphine **L36** ligand outperformed the analogous diphosphine **L35** (*entry 2 vs 1*).[344] The bite angle of the ligand dcyb are not so easy to confirm, solid state structures of Rh, Cu, and Co gave bite angles of 98, 101, and 109 respectively.[345]

The use of DPEphos **L37** (*entry 3*) was also shown to be a competent ligand to afford the arene reduction product **202** in slightly higher yield of 52% compared to **L36**. Dppf **L38** and xantphos **L39** (*entry 4 + 5*) provided minimal or no desired hydrodehalogenated product. HOMO-xantphos also afforded the dehalogenated arene in 25% yield (*entry 6*).The nickel (II) source played a nonnegligible role in the outcome of the reaction. With the use of $Ni(acac)_2$, $NiCl_2$ or NiI_2, all mass balance could be accounted for (Entry 2, 7-9) and the highest yield was obtained with NiI_2. When $NiBr_2$ was employed, however, there was a drop in the mass-balance, which could not be observed accounted for by GC, ^1H NMR, or HPLC.

Photodebromination

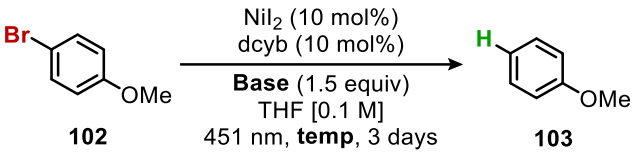

temp	base	**102** (%)	**103** (%)
@ 20 °C	Na_2CO_3	23	74
	K_3PO_4	18	79
@ 30 °C	Na_2CO_3	24	71
	K_3PO_4	10	87

Figure 4.4.5. Aryl bromide (0.2 mmol), NiI_2 (0.02 mmol), dcyb (0.02 mmol), Na_2CO_3 (0.2 mmol), THF (1 mL), 451 nm reactor at 20 °C or 30 °C for 72 h. Corrected GC yields using decane as internal standard.

The reaction could also be afforded using the base K_3PO_4 and increasing the reaction temperature was critical in improving these conditions to afford anisole (**103**) in 87% GC yield.

4.4.4. Small Scope with Conditions B

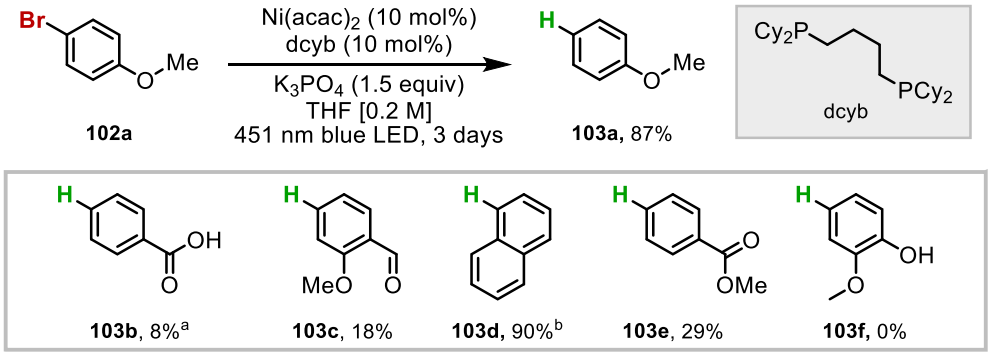

Figure 4.4.6. Small substrate scope using optimised conditions B. Aryl bromide (0.2 mmol), NiI_2 (0.02 mmol), dcyb (0.02 mmol), K_3PO_4 (0.3 mmol), THF (1 mL), 451 nm reactor at 30 C for 72 h. NMR yields using 1,3,5 trimethoxy benzene as internal standard.

However, as with the previous reaction conditions, when we moved to evaluate the scope of the reaction, the conditions were incompatible with certain substrates (Figure 4.4.6). Both carboxylic acid **103b** and aldehyde **103c** were dehalogenated in less than 20% yield. The dehalogenation of napthyl bromide on the other hand proceeded well to produce **103d** in 90% GC yield. Attempts to dehalogenate the previously optimised aryl bromide was met with a disappointing 29% yield.

Since the functional group tolerance was not sufficiently broad for an appropriate substrate scope to be generated. Since it would not be suitable to go through each substrate and optimise the reaction conditions on a case-by-case basis, we instead decided to approach the problem from a different angle. We speculated whether it would be possible to assess the compatibility of the reaction parameters against two electronic environments in one system.

4.4.5. Assessing a system using two bromide environments.

To this end, we designed a simple substrate (**104**) that would allow us to analyse two electronically differentiated environments in the same molecule. By using the predicted ^{13}C environments on chemdraw as a rough indicator of the electron density found at the C-Br position (Figure 4.4.7), we chose two fragments that were reasonably spaced. When combining the two fragments into one molecule, the ^{13}C shift values remained distinct.

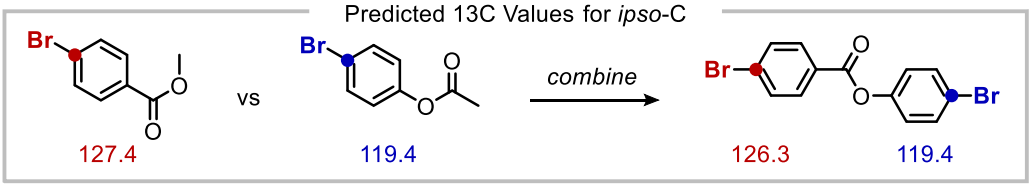

Figure 4.4.7. Predicted ^{13}C environments using the Chemdraw ^{13}C NMR prediction tool.

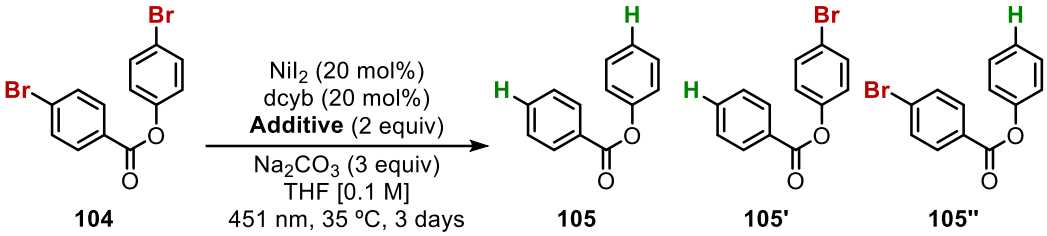

Entry	*Additive*	**104**	**105**	**105'**	**105''**
1	*none*	30	67	0	0
2	NaCl	46	3	13	35
3	NaBr	59	38	0	0
4	NaI	73	2	10	25
5	LiCl	58	0	18	30
6	LiBr	100	0	0	0
7	LiI	0	88	0	0
8	CsI (0.4 equiv)	0	98	0	0
9	TBAI	100	0	0	0
10	Cs_2CO_3	20	24	22	40

Figure 4.4.8 Aryl bromide (0.1 mmol), NiI_2 (0.02 mmol), ligand (0.02 mmol), Na_2CO_3 (0.3 mmol), THF (1 mL), additive (0.2 mmol) 451 nm reactor at 35 °C for 72 h. Corrected GC yields using decane as internal standard.

The dibromo compound (**104**) could therefore be an ideal candidate to test for a broadly reducing system, although partial reduction of the substrate could complicate analysis. The initial reaction system (NiI_2, dcyb) worked reasonably within this system *entry 1*, however there was still room for improvement, so a range of halide additives were assessed (Figure 4.4.8). The addition of chloride and iodide salts generally suppressed the reduction (*Entry 2-6*). On the other hand, lithium iodide (*entry 7*) greatly improved the reaction, affording the fully reduced product (**105**) in high yield.

Photodebromination

However, a small amount of the Finkelstein product from bromide-iodide exchange was observed.[346] Gratifyingly, addition of a sub-stoichiometric amount of cesium iodide liberated 98% GC yield of **105** (*entry 8*). However, yield dropped upon isolation to 78%. The use of TBAI gave very inconsistent results, resulting in high reactivity in some cases and poor reactivity in others. To probe the influence of caesium on the reaction Cs_2CO_3 (*entry 10*) was used in place of Na_2CO_3 but surprisingly poor reduction was observed.

4.4.6. Application of Conditions C to a failed substrate.

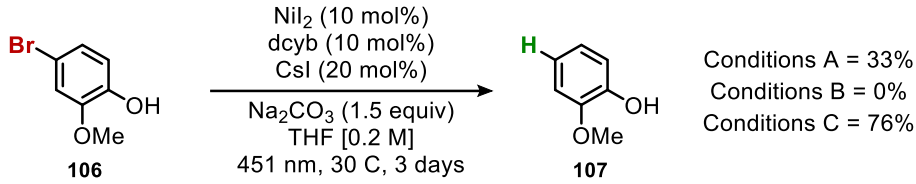

*Figure 4.4.9. Comparison of the yields for **106.***

The application of these conditions to a substrate that worked inadequately in both previous conditions (Figure 4.4.9), yielded **107** in an appropriate 76% isolated yield. Therefore, we believed these to be the most suitable conditions to proceed with the assessment of the scope.

4.5. Scope

4.5.1. Aryl bromide scope

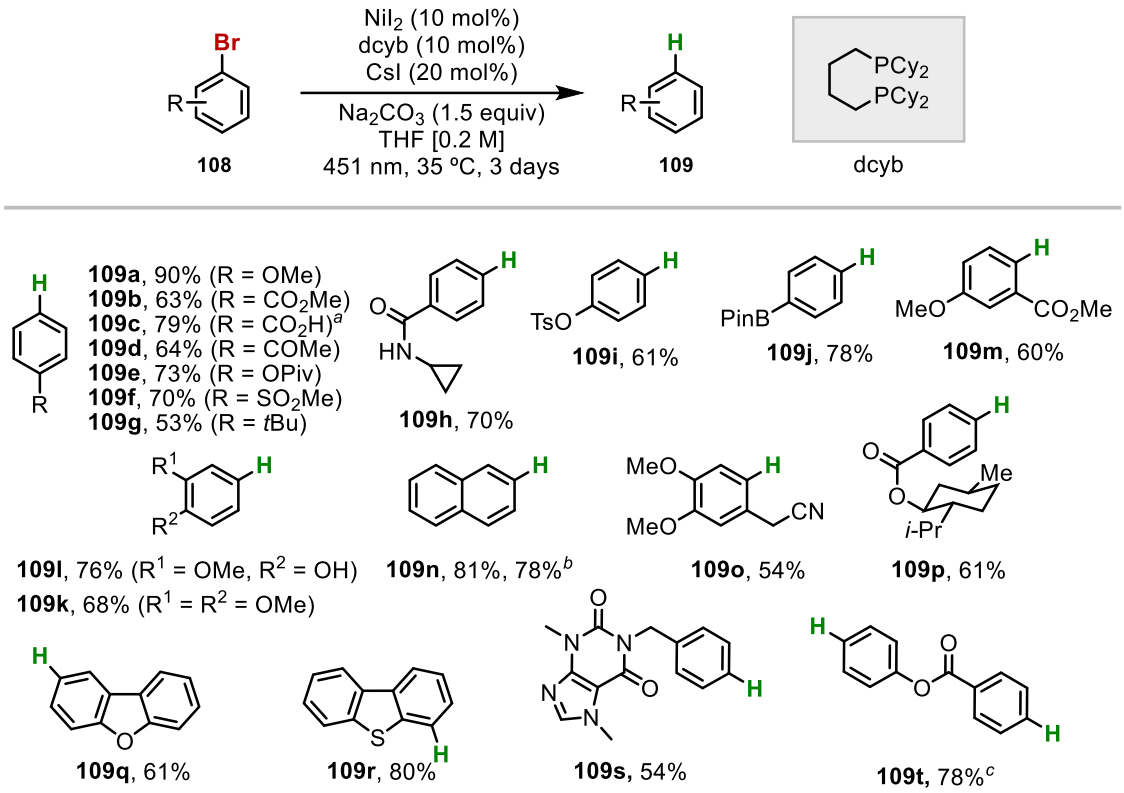

Figure 4.5.1. Aryl bromide (0.2 mmol), NiI_2 (0.02 mmol), dcyb (0.02 mmol), Na_2CO_3 (0.3 mmol), THF (1 mL), CsI (0.04 mmol) 451 nm reactor at 35 °C for 72 h. Isolated yields. a) +1 equivalent of LiOtBu b) 5 mmol scale using 5 mol% NiI_2, 6 mol% dcyb, 30 mol% CsI, Blue light irradiation, 5 days. c) using 20 mol% NiI_2, 20 mol% dcyb, 40 mol% CsI, 3 equiv Na_2CO_3

Firstly, the influence of electronic factors on the reaction outcome was explored (Figure 4.5.1). Both electron rich, (**109a, 109g**) and electron poor (**109b-f**) aryl rings are tolerated. Functional handles like carboxylic acid (**109c**), tosylates (**109i**), and boronic esters (**109j**) are accommodated with commendable yields. Substrates with mildly acidic protons like ketones (**109d**) and amide (**109h**) are also accepted. Noteably, oxidative addition into pivalic esters can occur with electron rich phosphine ligands,[347] but this was not observed (**109e**) under these conditions. *Ortho*-substitution in the form of ester (**109m**) and benzylic nitrile (**109o**), could enable the use of bromine as a blocking group in ortho-directed aryl C-H functionalisation reactions. Guaiacol (**109l**) and veratrole (**109k**) were cleanly obtained with good yield. Furthermore, π-extended systems could be tolerated (**109n**) even on 5 mmol scale as well as heterocyclic compounds, such as benzofuran (**109q**) and its thio- analogue (**109r**). The use of the Menthol-ester (**109p**) showed no change in diastereoselective, and so it is unlikely that any ablation of the chiral units occurred.

Photodebromination

Additionally, theobromine derivative (**109s**) was debrominated in 54% yield. Finally, dibromo compound (**109t**) could be isolated in good yields as the fully dehalogenated product, the conditions employed were used on a *per bromide basis,* although some of the product was lost upon isolation. The next step was to apply this work to more industrially relevant compounds.

4.5.2. Polybrominated diphenyl ethers (PBDEs)

PBDEs are a class of flame retardants that were produced on a relatively large industrial scale.[348] They have since been shown to cause fertility issues, which has led them to be classed as persistent organic pollutants and the Stockholm convention has banned their production.[349]

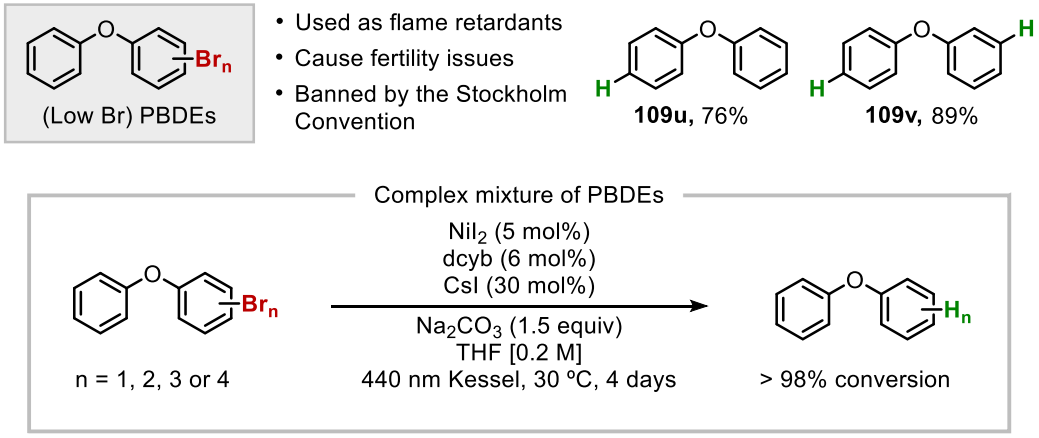

Figure 4.5.2 a) isolated yield, 108u (0.2 mmol), NiI_2 (0.02 mmol), dcyb (0.02 mmol), Na_2CO_3 (0.3 mmol), THF (1 mL), CsI (0.04 mmol) 451 nm reactor at 35 °C for 72 h. b) isolated yield, 108v (0.1 mmol), NiI_2 (0.02 mmol), dcyb (0.02 mmol), Na_2CO_3 (0.3 mmol), THF (1 mL), CsI (0.04 mmol) 451 nm reactor at 35 °C for 72 h. c) Aryl bromide (1 mmol), NiI_2 (0.05 mmol), dcyb (0.06 mmol), Na_2CO_3 (3 mmol), THF (20 mL), CsI (0.3 mmol) Kessel light at 38 °C for 86 h.

The class of compounds is split into two distinct halves, low bromine count PBDEs (n<5) and high bromine count PBDEs (n>5). We decided to assess whether low bromine count PBDEs could be dehalogenated in our protocol. Gratifyingly, using the standard conditions for simple mono- (**109u**) and di-brominated (**109v**) compounds could achieve full dehalogenation in good yields. We then moved to assess whether it would be possible to dehalogenate a complex mixture of low Br PBDEs to obtain a single isolatable product. Diphenyl ether (1 mmol) was brominated in the presence of NBS (2 mmol) to generate a complex mixture which was then submitted to our protocol with minor modifications. After 4 days under Kessil lamp irradiation (centred at 440 nm, 40 W), work up and filtration through a plug of silica yielded 0.51 mmol of diphenyl ether, GC analysis showed no remaining PBDE. Although the substrate scope proved broad, there were some unsuccessful substrates that warrant discussion.

4.5.3. Failed substrates

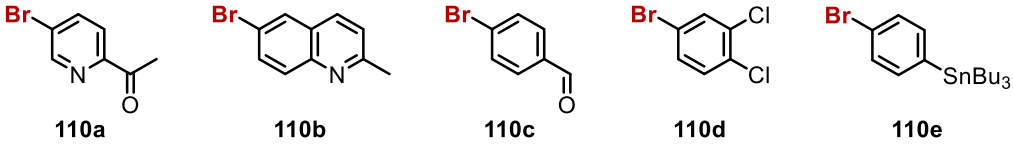

Figure 4.5.3. failed (hetero)aryl bromides.

The most prominent failures were the heteroaryl bromides (**110a, 110b**) we hypothesised that the coordinating nature of pyridine like heterocycles were detrimental to the reactivity. Benzaldehyde derivates (**110c**) underwent hydrodebromination but the reactions were generally unclean, leading to several unidentifiable products and often only generated less than 50% of the desired dehalogenation product. It is likely due to the presence of the aldehyde C-H bonds which can be readily abstracted by radical intermediates. Aryl chlorides (**110d**) could be tolerated to an extent, GC analysis showed 34% yield of the desired bromo-dehalogenation, but there was also PhCl (14%), and PhH (30%) as well as several other unassignable products. Interestingly, tin containing compounds such as **110e** were not tolerated, with Bu_3SnBr isolated in 45% yield. This could be indicative of the formation of bromide radicals within the reaction medium, or more likely as the by-product derived from the cross-coupling reaction.

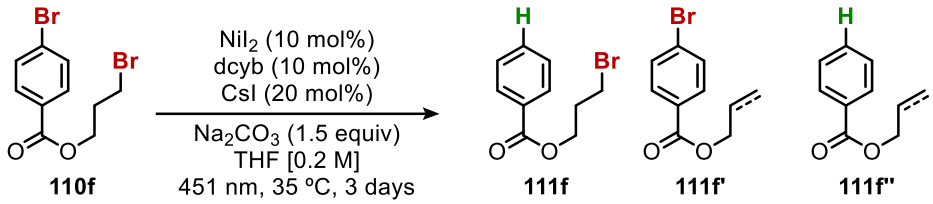

Figure 4.5.4. alkyl bromides were not tolerated.

Mixed, aryl and alkyl bromides (**110f**) underwent the reaction to give a complex mixture of products including the desired aryl debromination **111f**. Additionally, the alkyl bromide was also reduced to the alkene or alkane (**111f'**). Or full reduction of both alkyl and aryl bromide to **111f''**. This complex mixture was not desirable , however, a selective protocol could have been very well received.

With a reasonable number of examples in hand, the next step was to assess the viability of deuterodehalogenation of aryl bromides with the corresponding deuterated solvent.

Photodebromination

4.5.4. Deuterium incorporation

Deuterium incorporation has the potential to be the next step in drug design;[350] incorporating deuterium can dramatically improve the pharmacokinetic profile. By exchanging hydrogen for deuterium, the kinetics of metabolism can be altered significantly due to the kinetic isotope effect. This change allows for essential hydrogen bonding to be maintained whilst preventing negative metabolism. Furthermore, as sp^2 C-D bonds are often used to study the mechanism of arene C-H activation methods, the ability to easily access monodeuterated compounds could be beneficial to this community.

Conceptually, we could modify our reaction to access monodeuterated aryl rings, which would allow for the creation of specifically deuterated building blocks for drug synthesis. We began optimisation using the conditions found in the hydrodehalogenation protocol but employed deuterate solvents. It is worth noting that deuterated solvents are not dried and should be dried before use, for example Karl Fisher analysis of THF-d_8 had a water content of 252 ppm. An initial screen of deuterated solvents, due to the expense of THF-d_8 (Figure 4.5.5),[309] did not provide any more appropriate results. The mass balance was accounted for by the Finkelstein product **112**, as well as homocoupling **113**.

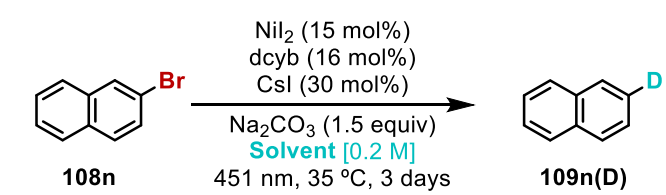

Entry	*Solvent*	**Conv.**	**Yield**
1	THF-d_8	90	60
2	Acetone-d_6	70	5
3	MeOH-d_4	2	0
4	$CDCl_3$	3	0
5	MeCN-d_3	70	3

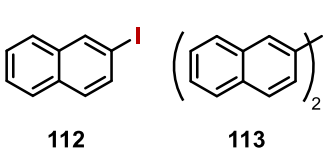

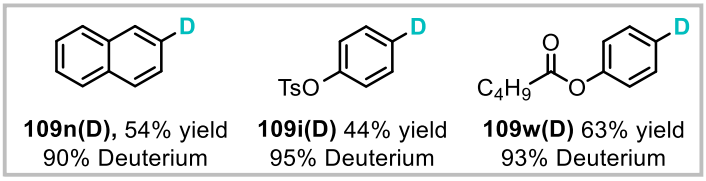

Figure 4.5.5. Aryl bromide (0.2 mmol), NiI_2 (0.02 mmol), dcyb (0.02 mmol), Na_2CO_3 (0.3 mmol), THF (1 mL), CsI (0.04 mmol) THF-d8 (1 mL), 2 x 440 nm kessel at 35 °C for 72 h. Isolated yields.

The use of more intense Kessil light irradiation (440 nm, 40 W) along with dried THF-d_8 with a higher loading of nickel was essential in producing reliable results. The deuterodehalogenation technique was thus extended to encompass two other substrates containing tosylate (**109i(D)**) and ester (**109x(D)**) functionalities. With both a general reaction and the ability to deuterodehalogenate arylbromides demonstrated we decided to evaluate the mechanistic understanding through a comparison with the known literature.

4.5.5. Mechanistic understandings

The mechanistic rationale behind the hydrodehalogenation is important because the product is often an undesired side-reaction of transition metal catalysed cross-coupling reactions. Understanding the mechanism of reduction could aid in both ligand and reaction design to suppress the pathway. There are several mechanistic scenarios that are mechanistically reasonable.

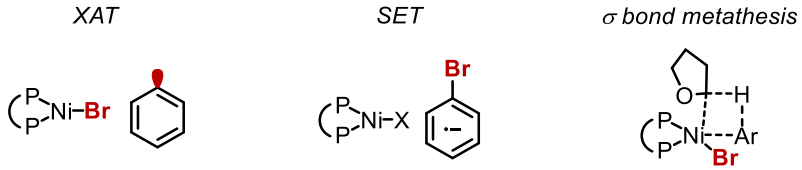

Figure 4.5.6. Possible mechanistic scenarios.

The mechanistic scenarios that we have envisioned are summarised in Figure 4.5.6. A halogen atom abstraction by a nickel species is often proposed in the oxidative addition with electron rich phosphine ligands.[351] The XAT is then quickly followed by radical recombination to form the nickel (II) aryl bromide complex. However, it would be plausible suggest that with the steric bulk of the phosphines and potential coordination of an iodide ligand, that instead of radical recombination of the aryl radical with nickel (II), the aryl ring escapes the encounter complex to abstract a hydrogen from the solvent. Another potential mechanism, although we believe to be unlikely, is the single electron transfer between a nickel species and the aryl halide, however this would require CT from the electron deficient nickel (II) to the aryl bromide to generate the aryl radical anion.

σ-bond metathesis has been suggested in C(sp^3)-H bond functionalisation strategies. The collected works of C(sp^3)-H functionalisation by Doyle, Molander, and Martin all propose that σ-bond metathesis is an unlikely scenario. This clearly does not rule out this pathway because the conditions are considerably different but there is more literature precedence for the final mechanistic scenario, the photo-assisted cleavage of a nickel-X bond.

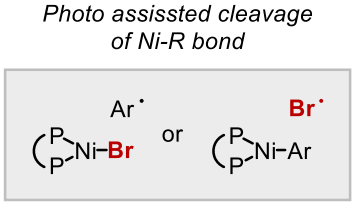

Figure 4.5.7. The most likely scenario is a Ni-R bond homolysis

Of the conceivable scenarios, the photo assisted bond-homolysis has the most literature precedent. There have been several mechanistic investigations that suggest the homolysis of

Photodebromination

nickel bonds under visible light irradiation. The work by Nocera to eject chlorine radicals from nickel (III) species, [352] photoelimination of halide radicals from Molander and co-workers by photosensitisation or through UV irradiation.[353] Additionally, Doyle and co-workers have shown that elimination of aryl radicals is also plausible under visible light irradiation.[354] Thus, the elimination of a radical from a putative nickel intermediate is the most plausible scenario.

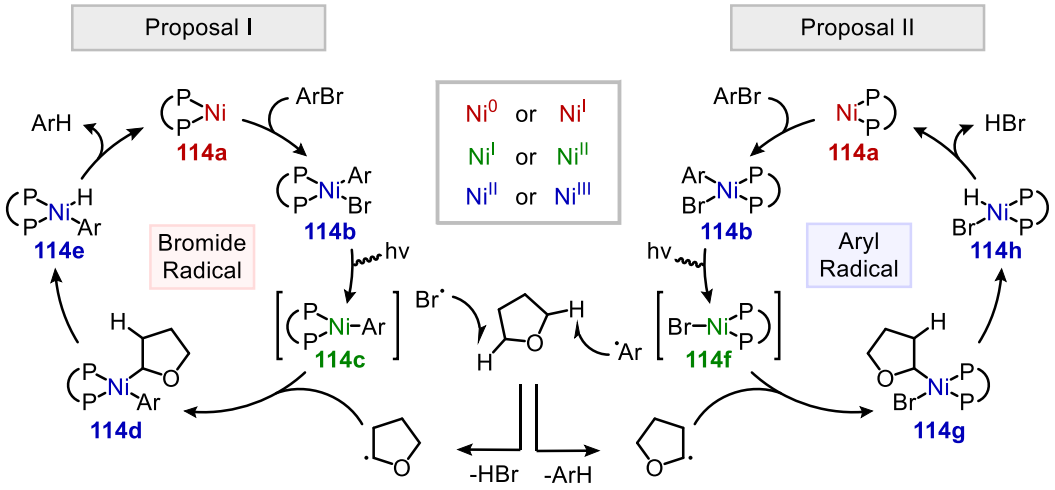

Figure 4.5.8. The two proposals that proceed via photoelimination of one of the ligands.

The two mechanistic scenarios we have envisioned begin with the oxidative addition of the aryl bromide to form a nickel aryl bromide complex (**114b**). The oxidation state of the nickel is unknown at this point, starting from the initial complex **114a**, we propose either a nickel (0) or a nickel (I) species. The generation of these intermediates has not been rationalised. However, from either oxidation state the oxidative addition of arylbromide can occur to give **114b**. from this state we propose that there is an excitation event to generate intermediate **114c** or **114f**, the two species are where the proposals diverge. In the bromide radical cycle, the homolysis of the bromide occurs which can abstract the hydrogen from THF in a “thermoneutral” event, due to the disparity of the bond dissociation energies. From this the THF radical generated can add into **114c** to generate **114d,** this species would then β-hydride eliminate to the nickel aryl hydride (**114e**). Reductive elimination from this species liberates the starting complex **114a** and the reduced aryl halide.

In the alternate, aryl radical cycle, the aryl radical is ejected from the nickel centre and directly abstracts a hydrogen from the THF to liberate the reduced product. steps **114f – 114h** are to generate a species which can undergo a base elimination to regenerate the initial nickel complex **114a**. The role of the iodide salt must also plat a non-neglible part in the reaction as it’s absence dramatically reduces the reactivity.[355]

4.6. Concluding remarks

In summary, we have developed a nickel mediated dehalogenation of aryl bromides under visible light irradiation without the need for external photocatalyst or exogeneous reductant. The broad electronic scope of this visible light mediated technique is complemented by the ability to readily reduce industrially relevant brominated diphenyl ethers as well as access the corresponding monodeuterated aryl rings. Of the possible mechanisms proposed, the most supported by literature is the homolysis of a nickel σ bound ligand to generate an appropriate radical. However, the mechanistic understandings of this reaction await further investigation, the exploration of which could aid in reaction design to prevent deleterious dehalogenation and provide new avenues for method development due to the unusual nature of this reaction.

4.7. Supporting Information

4.7.1. Photoreactor Setup

CFL reactor set up was shown below, two CFL bulbs are placed approximately 3 cm away from a wire rack that can contain up to 8 reactions.

Standard dehalogenation reactions were performed at 0.2 mmol under blue light irradiation using 451 nm LEDs (OSRAM Oslon® SSL 80 royal- blue LEDs), which were installed at the bottom of a custom-made 8 flat-bottom Schlenk tubes holder (the distance between the flat-bottom Schlenk tube and the light source was measured to be ~7 mm), equipped with a water cooling system (the thermostat was set at the appropriate temperature) and magnetically stirred (~ 500 rpm).

For large scale reactions and deuterations, the appropriate vessel was placed 5 cm away from 2 x 440 nm kessel lights, the reaction vessel and cooled with a strong fan and adequate ventilation. The measured temperature under these conditions was 38 ºC on average.

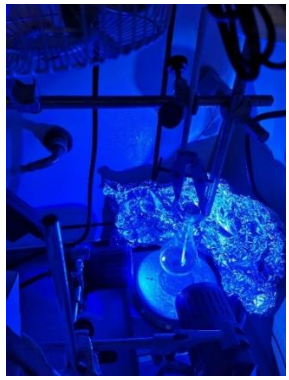

4.7.2. Optimisation Details

Optimisation on Anisole (102)

An oven dried Schlenk tube containing a stir bar was charged with Base (0.3 mmol, 31.8 mg, 1.5 equiv), and nickel salt (0.02 mmol, 6.1 mg, 10 mol%). The Schlenk was transferred to a nitrogen filled glovebox where ligand (0.022 mmol, 11 mol%), additive (0.2 mmol, 1 equiv) and 4-bromoanisole (0.2 mmol, 37.4 mg, 1 equiv) were added followed by anhydrous THF (0.2 M, 1 mL). Once added, the Schlenks were sealed, and the mixture was stirred for 15 minutes. They were then taken out of the glovebox and placed in a preheated reaction vessel at 35 ºC (**PR2**) and stirred for 72 hours under blue light irradiation. The mixture was quenched with 1M HCl (2 mL) and diluted with EtOAc, Decane (0.2 mmol, 28.4 mg, 39 ul) was added as an internal standard and shaken vigorously. An aliquot was taken and filtered through silica, washed with EtOAc, analysed by GC-FID.

Optimisation on dibromocompound (104)

An oven dried Schlenk tube containing a stir bar was charged with and 4-bromophenyl 4-bromobenzoate (0.1 mmol, 35.6 mg, 0.5 equiv), base (0.3 mmol, 1.5 equiv), and nickel salt (0.02 mmol, 10 mol%). The Schlenk was transferred to a nitrogen filled glovebox where ligand (0.022 mmol, 11 mol%), additive (0.2 mmol, 1 equiv) were added followed by anhydrous THF (0.2 M, 1 mL). Once added, the Schlenks were sealed, and the mixture stirred for 15 minutes. They were then taken out of the glovebox and placed in a preheated reaction vessel at 35 ºC (**PR2**) and stirred for 72 hours under blue light irradiation. The mixture was quenched with 1M HCl (2 mL) and diluted with EtOAc, Decane (0.1 mmol, 14.2 mg, 18 ul) was added as an internal standard and shaken vigorously. An aliquot was taken and filtered through silica, washed with EtOAc, analysed by GC-FID.

Photodebromination

4.7.3. Small Scope Assessment

Dr Yiting Gu's Conditions

An oven dried Schlenk tube containing a stir bar was charged with aryl bromide *if solid* (0.2 mmol, 1.0 equiv), Na_2CO_3 (0.2 mmol, 20 mg, 1.0 equiv), $Ni(acac)_2$ (0.02 mmol, 5.4 mg, 10 mol%), dppe (0.02 mmol, 8 mg, 10 mol%). The Schlenk was attached to a Schlenk line, evacuated, and backfilled 3 times with Argon. Then aryl bromide *if liquid* (0.2 mmol, 1 equiv) was added followed by, anhydrous THF (0.2 M, 1 mL). The Schlenks were sealed, placed under CFL irradiation (**PR1**) and stirred for 72 hours. The mixture was quenched with 1M HCl (2 mL) and diluted with EtOAc, trimethoxy benzene (0.066 mmol, 11.2 mg) was added as an internal standard, the water was separated, and the organic fraction was collected in a round bottom flask. 1 cm^3 of Silica was added to the RBF and the solvent removed by rotary evaporation (40 C, 140 mbar). The silica was then placed on a glass frit, washed with EtOAc and the organic layer collected and evaporated. Analysis of by ^1H NMR. *If the silica step is skipped, broad peaks are often observed due to nickel.*

First Optimisation Results

An oven dried Schlenk tube containing a stir bar was charged with aryl bromide *if solid* (0.2 mmol, 1 equiv.) NiI_2 (0.02 mmol, 6.1 mg, 10 mol%). The Schlenk was transferred to a nitrogen filled glovebox where dcyb (0.022 mmol, 11 mol%), K3PO4 (0.3 equiv, 64 mg, 1.5 equiv) and aryl bromide *if liquid* (0.2 mmol, 1 equiv) were added followed by anhydrous THF (0.2 M, 1 mL). Once added, the Schlenks were sealed, and the mixture was stirred for 15 minutes. They were then taken out of the glovebox and placed in a preheated reaction vessel at 30 ºC (**PR2**) and stirred for 72 hours under blue light irradiation. The mixture was quenched with 1M HCl (2 mL) and diluted with EtOAc, trimethoxy benzene (0.066 mmol, 11.2 mg) was added as an internal standard, the water was separated, and the organic fraction was collected in a round bottom flask. 1 cm^3 of Silica was added to the RBF and the solvent removed by rotary evaporation (40 C, 140 mbar). The silica was then placed on a glass frit, washed with EtOAc and the organic layer collected and evaporated. Analysis of by ^1H NMR. *Again, if the silica step is skipped, broad peaks are often observed due to nickel impurities.*

4.4.4. Starting Material Synthesis

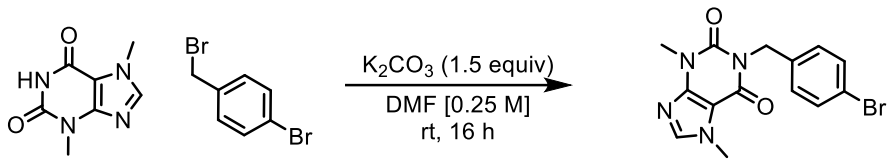

115 **116**, 2 equiv **108s**

Theobromine derivative was synthesised in an analogous procedure.[356] Theobromine (2 mmol, 1 equiv), and K_2CO_3 (3 mmol, 1.5 equiv) was suspended in DMF (5 mL, 0.25 M), to this suspension was added two equivalents of 4-bromo benzyl bromide (4 mmol, 2 equiv) and allowed to stir overnight. The solution was poured into water and the product filtered off to give a white solid (78% yield). **^1H NMR** (400 MHz, DMSO-d_6) δ 8.04 (s, 1H) 7.51 – 7.48 (m, 2H), 7.30 – 7.24 (m, 2H), 5.01 (s, 2H), 3.88 (s, 3H), 3.41 (s, 3H). **^{13}C NMR** (101 MHz, DMSO-d_6) δ 154.8, 151.4, 149.0, 143.7, 137.5, 131.6, 130.3, 120.6, 107.1, 43.4, 33.7, 30.0

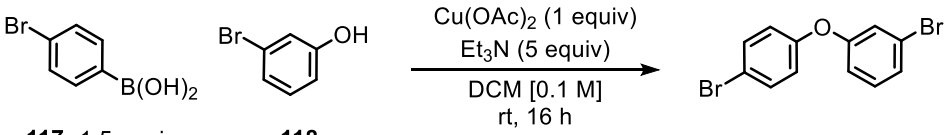

117, 1.5 equiv **118** **108v**

To a round bottom flask was added, copper (II) acetate (1 equiv, 1 mmol), phenol (1 equiv, 1 mmol), and aryl boronic acid (1.5 equiv, 1.5 mmol), to this was added powdered 4 A molecular sieves, and DCM (10 mL), the reaction was stirred, and triethylamine was added. Left to stir at room temperature overnight. Filtration and column chromatography yielded the title compound as a viscous oil. **^1H NMR** (400 MHz, $CDCl_3$) δ 7.46 (d, 2H) 7.22 (m, 2H), 7.13 (m, 1H), 6.94 (m, 1H), 6.91 (d, 2H). **^{13}C NMR** (101 MHz, CDCl3) δ 157.8, 155.6, 132.8, 130.9, 126.62, 123.0, 121.85, 120.9, 117.3, 116.5

4.4.5. General Procedure

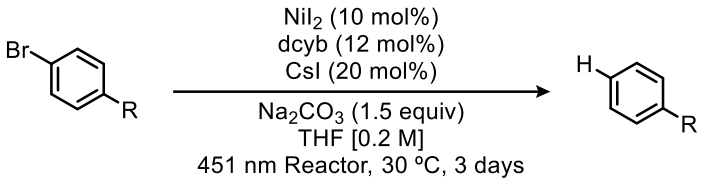

An oven dried Schlenk tube containing a stir bar was charged with aryl bromide *if solid* (0.2 mmol, 1 equiv.) Na_2CO_3 (0.3 mmol, 31.8 mg, 1.5 equiv), NiI_2 (0.02 mmol, 6.1 mg, 0.1 equiv). The Schlenk was transferred to a nitrogen filled glovebox where dcyb (0.022 mmol, 0.1 equiv), CsI (0.04 mmol, 10.4 mg, 0.2 equiv) and aryl bromide *if liquid* (0.2 mmol, 1 equiv) were added followed by anhydrous THF (0.2 M, 1 mL). Once added, the Schlenks were sealed, and the mixture was stirred for 15 minutes. They were then taken out of the glovebox and placed in a preheated reaction vessel at 35 ºC (**Photo2**) and stirred for 72 hours under blue light irradiation. The mixture was quenched with 1M HCl (2 mL) and diluted with EtOAc, aqueous layer extracted, dried and evaporated. Subject to column chromatography.

4.4.6. Product Data

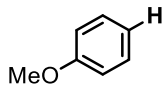

Anisole (109a). Following General Procedure B, 4-bromo anisole **(108a)** (37.4 mg, 0.2 mmol) was used, affording the title compound as a colourless liquid (19.4 mg, 90% yield) using hexane as eluent. **^{1}H NMR (400 MHz, $CDCl_3$)** δ: 7.36 – 7.24 (m, 2H), 7.01 – 6.88 (m, 3H), 3.82 (s, 3H **^{13}C NMR (101 MHz, $CDCl_3$)** δ: 159.5, 129.4, 120.6, 113.9, 55.1. Spectroscopic data in agreement with literature.[357]

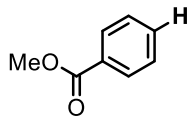

Methyl benzoate (109b). Following General Procedure A, methyl 4-bromobenzoate **(108b)** (43 mg, 0.2 mmol) was used, affording the title compound as a colourless liquid (17.1 mg, 63% yield) by using hexanes:EtOAc (98:2) as eluent. **^{1}H NMR (400 MHz, $CDCl_3$)** δ: 8.11 – 8.03 (m, 2H), 7.58 (m, 1H), 7.47 (m, 2H), 3.95 (s, 3H) **^{13}C NMR (101 MHz, $CDCl_3$)** δ: 167.1, 132.9, 130.2, 129.6, 128.4, 52.1. Spectroscopic data was in agreement with literature.[341]

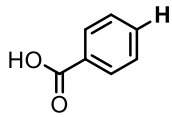

Benzoic acid (109c) Following General Procedure A, 4-bromobenzoic acid **(108c)** (40.2 mg, 0.2 mmol) and lithium *tert*-butoxide (0.2 mmol) was used affording the title compound as a white solid (19.3 mg, 79% yield) by using hexanes:EtOAc (4:1) as eluent **^{1}H NMR (400 MHz, DMSO-d_6)** δ: 7.99 – 7.92 (m, 2H), 7.66 – 7.58 (m, 1H), 7.54 – 7.46 (m, 2H). **^{13}C NMR (101 MHz, DMSO)** δ: 167.8, 133.3, 131.2, 129.7, 129.0. **Melting Point:** 122-124 ºC Spectroscopic data was in agreement with literature.[341]

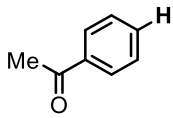

Acetophenone (109d). Following General Procedure A, 4-bromoacetophenone **(108d)** (40.1 mg, 0.2 mmol) was used affording the title compound as a colourless liquid (15.3 mg, 64% yield) by using hexanes:EtOAc (8:1) as eluent. **^{1}H NMR (400 MHz, $CDCl_3$)** δ: 8.00 – 7.93 (m, 2H), 7.61 – 7.53 (m, 1H), 7.47 (m, 2H), 2.61 (s, 3H) **^{13}C NMR (101 MHz, $CDCl_3$)** δ: 137.1, 133.1, 128.6, 128.3, 26.6. Spectroscopic data was in agreement with literature.[343]

Photodebromination

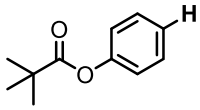

Phenylpivalate (109e). Following General Procedure B, 4-bromophenyl pivalate **(108e)** (48.2 mg, 0.2 mmol) was used affording the title compound as a colourless liquid (23.6 mg, 73% yield) by using hexanes:EtOAc (8:1) as eluent. **^{1}H NMR (400 MHz, $CDCl_3$)** δ: 7.41-7.34 (m, 2H), 7.25-7.18 (m, 1H), 7.08-7.03 (m, 2H), 1.37 (s, 9H) **^{13}C NMR (101 MHz, $CDCl_3$)** δ 177.1, 151.1, 129.3, 125.6, 121.5, 39.1, 27.1. Spectroscopic data was in agreement with literature.[358]

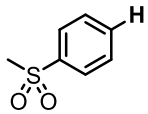

(methylsulfonyl)benzene (109f). Following General Procedure A, 4-bromophenyl methyl sulfone **(108f)** (47.0 mg, 0.2 mmol) was used affording the title compound as white solid (21.9 mg, 70% yield) by using EtOAc as eluent. **^{1}H NMR (400 MHz, $CDCl_3$)** δ: 8.00 – 7.92 (m, 2H), 7.71 – 7.54 (m, 3H), 3.06 (s, 3H). **^{13}C NMR (101 MHz, $CDCl_3$)** δ 140.6, 133.7, 129.4, 127.4, 44.5. **Melting point:** 88-91 ºC Spectroscopic data was in agreement with literature.[359]

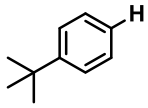

***tert*-butyl benzene (109g).** Following General Procedure A, 1-bromo-4-(*tert*-butyl) benzene **(108g)** (42.6 mg, 0.2 mmol) was used affording the title compound as a colourless liquid (14.2 mg, 53% yield) by using hexanes as eluent. **^{1}H NMR (400 MHz, $CDCl_3$)** δ: 7.43-7.38 (m, 2H), 7.34 – 7.28 (m, 2H), 7.18 (m 1H), 1.34 (s, 9H) **^{13}C NMR: (101 MHz, $CDCl_3$)** δ 129.7, 128.0, 125.4, 125.2, 34.7, 31.3. Spectroscopic data was in agreement with literature.[357]

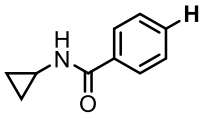

N-cyclopropylbenzamide (109h). Following General Procedure, 4-bromo-N=cyclopropylbenzamide **(108h)** (48.0 mg, 0.2 mmol) was used affording the title compound as a white solid (22.5 mg, 70% yield) by using Hexanes:EtOAc (1:1) as eluent. **^{1}H NMR (300 MHz, CDCl3)** δ: 7.79 – 7.68 (m, 2H), 7.54 – 7.33 (m, 3H), 6.35 (s, 1H), 2.90 (m, 1H), 0.96 – 0.78 (m, 2H), 0.67 – 0.56 (m, 2H**). ^{13}C NMR (101 MHz, $CDCl_3$)** δ 168.9, 134.4, 131.5, 128.5, 126.9, 23.1, 6.8. **Melting Point:** 54-56 ºC Spectroscopic data was in agreement with literature.[360]

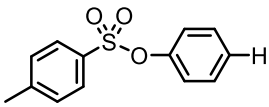

Phenyl 4-methylbenzenesulfonate (109i). Following General Procedure A, 4-bromophenyl tosylate **(108i)** (65.4 mg, 0.2 mmol) was used affording the title compound as an off-white solid (30.3 mg, 61% yield) by using hexanes:EtOAc (7:1) as eluent. **^{1}H NMR (400 MHz, $CDCl_3$)** δ: 7.81 - 7-65 (m, 2H), 7.35 - 7.23 (m 5H), 7.10 - 6.93 (m, 2H), 2.47 (s, 3H) **^{13}C NMR: (101 MHz, $CDCl_3$)** δ: 149.7, 145.3, 132.4, 129.7, 129.6, 128.5, 127.0, 122.4, 21.7. **Melting Point:** 94-96 ºC Spectroscopic data was in agreement with literature.[361]

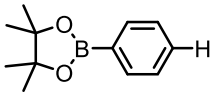

4,4,5,5-tetramethyl-2-phenyl-1,3,2-dioxaborolane (109j). Following General Procedure A, 2-(4-bromophenyl)-4,4,5,5-tetramethyl-1,3,2-dioxaborolane **(108j)** (56.4 mg, 0.2 mmol) was used affording the title compound as a viscous oil (31.8 mg, 78% yield) by using Hexanes:EtOAc (1:1) **^{1}H NMR (400 MHz, CDCl$_3$)** δ 7.86 – 7.79 (m, 2H), 7.55 – 7.42 (m, 1H), 7.42 – 7.33 (m, 2H), 1.36 (s, 12H), **^{13}C NMR (101 MHz, CDCl3)** δ 136.3, 134.7, 131.2, 127.7, 83.7, 24.9. Spectroscopic data was in agreement with literature.[343]

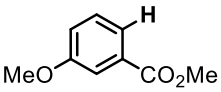

methyl 3-methoxybenzoate (109k). Following General Procedure A, methyl 2-bromo-5-methoxybenzoate **(108k)** (49.0 mg, 0.2 mmol) was used, affording the title compound as a colourless liquid (19.9 mg, 60% yield) by using Hexanes:EtOAc (9:1) as eluent. **^{1}H NMR (400 MHz, CDCl$_3$)** δ: 7.63 (m, 1H), 7.55 (s, 1H), 7.28 (m, 1H), 7.05 (m, 1H), 3.90 (s, 1H) 3.60 (s, 3H), **^{13}C NMR (101 MHz, CDCl$_3$)** δ 167.0, 159.6, 131.4, 129.4, 122.0, 119.5, 113.9, 55.4, 52.1. Spectroscopic data was in agreement with literature.[362]

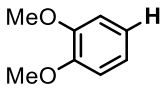

1,2-dimethoxybenzene (109l). Following General Procedure A, 1-bromo-3,4-dimethoxy benzene **(108l)** (43.4 mg, 0.2 mmol) was used affording the title compound as a colourless liquid (28.1 mg, 68% yield) by using Hexanes:EtOAc (9:1 **^{1}H NMR (400 MHz, CDCl$_3$)** δ 6.95 – 6.86 (m, 4H), 3.88 (s, 6H) **^{13}C NMR (101 MHz, CDCl$_3$)** δ 149.0, 120.8, 111.4, 55.8. Spectroscopic data was in agreement with literature.[363]

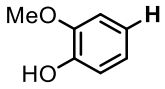

Guaiacol (109mO). Following General Procedure A, 4-bromo-2-methoxyphenol **(108m)** (40. mg, 0.2 mmol) was used, affording the title compound as a colourless oil (18.8 mg, 76% yield) by using Hexanes:EtOAc (4:1) as eluent **^{1}H NMR (400 MHz, CDCl$_3$)** δ 7.02 – 6.47 (m, 4H), 5.61 (s, 1H), 3.89 (s, 3H). **^{13}C NMR (101 MHz, CDCl$_3$)** δ 146.6, 145.7, 121.5, 120.1, 114.5, 110.7, 55.9. Spectroscopic data was in agreement with literature.[364]

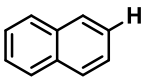

naphthalene (109n). Following General Procedure A, 2-bromonaphthalene **(108n)** (41.4 mg, 0.2 mmol) was used, affording the title compound as a white solid (20.7 mg, 81% yield) by using Hexanes:EtOAc (96:4) as eluent. **^{1}H NMR (400 MHz, CDCl$_3$)** δ 7.86 (dd, *J* = 6.2, 3.3 Hz, 4H), 7.49 (dd, *J* = 6.3, 3.2 Hz, 4H). **^{13}C NMR (101 MHz, CDCl$_3$)** δ 133.4, 127.9, 25.8. **Melting point:** 79-80 ºC. In agreement with literature data.[343]

***Large-scale synthesis of 2n*:** 2-bromonapthalene (1035 mg, 5 mmol, 1 equiv), NiI_2 (0.25 mmol, 0.05 equiv), and Na_2CO_3 (7.5 mmol, 1.5 equiv) were weighed out into a 100 mL round bottomed flask equipped with large stir bar. The RBF was transferred into the glovebox where CsI (1.5 mmol. 0.3 equiv) and dcyb (0.3 mmol, 0.06 equiv) was added. The rbf was secured with a septum and wrapped with blue electrical tape. Anhydrous THF (25 mL) taken from an SPS was added to the reaction mixture and allowed to stir under visible light irradiation. Reaction progress was monitored by GC. After 5 days under visible light irradiation, THF was removed under rotary evaporation, 1 M HCl was added to the crude reaction mixture and extracted with DCM. Column chromatography afforded the title compound as a white solid (499 mg, 78% yield).

Photodebromination

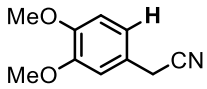

2-(3,4-dimethoxyphenyl)acetonitrile (109o). Following General Procedure A, 2-(2-bromo-4,5-dimethoxyphenyl)acetonitrile **(108o)** (51.2 mg, 0.2 mmol) was used, affording the title compound as a white solid (19.1 mg, 54% yield) by using Hexanes:EtOAc (6:1) as eluent **^{1}H NMR (400 MHz, $CDCl_3$)** δ 6.92 – 6.79 (m, 3H), 3.90 (s, 3H), 3.88 (s, 3H), 3.70 (s, 2H**). ^{13}C NMR (101 MHz, $CDCl_3$)** δ 149.5, 122.2, 120.2, 111.5, 111.0, 77.3, 77.0, 76.7, 56.0, 23.2. **Melting point:** 64-67 ºC Spectroscopic data was in agreement with literature.[365]

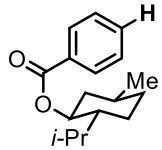

Menthol benzoate (109p). Following General Procedure A, Menthol 4-bromobenzoate **(108p)** (67.8 mg, 0.2 mmol) was used, affording the title compound as a colourless oil (32.2 mg, 61% yield) by using Hexanes:EtOAc (9:1) as eluent. **1H NMR (400 MHz, $CDCl_3$)** δ 8.09 – 8.01 (m, 2H), 7.59 – 7.50 (m, 1H), 7.48 – 7.39 (m, 2H), 4.94 (td, *J* = 10.9, 4.4 Hz, 1H), 2.18 – 2.08 (m, 1H), 2.07 – 1.91 (m, 1H), 1.79 – 1.68 (m, 2H), 1.64 – 1.48 (m, 2H), 1.12 (dtd, *J* = 14.7, 12.4, 9.8 Hz, 2H), 1.02 – 0.86 (m, 7H), 0.80 (d, *J* = 6.9 Hz, 3H). **^{13}C NMR (101 MHz, $CDCl_3$)** δ 166.1, 132.7, 130.9, 129.5, 128.3, 74.8, 47.3, 41.0, 34.3, 31.4, 26.5, 23.6, 22.0, 20.8, 16.5. Spectroscopic data was in agreement with literature.[366]

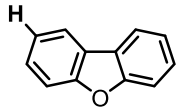

Dibenzofuran (109q). Following General Procedure A, 2-bromodibenzo[b,d]furan **(108q)** (49.4 mg, 0.2 mmol) was used, affording the title compound as a white solid (30.2 mg, 90% yield) by using Hexanes:EtOAc (9:1) as eluent. **^{1}H NMR (400 MHz, $CDCl_3$)** δ 7.97 (dd, J = 7.7, 1.3 Hz, 2H), 7.62 – 7.57 (m, 2H), 7.47 (td, J = 8.3, 7.9, 1.5 Hz, 2H), 7.36 (t, J = 7.5 Hz, 2H). **^{13}C NMR (101 MHz, $CDCl_3$)** δ 156.2, 127.1, 124.2, 122.7, 120.6, 111.6. **Melting Point:** 83-85 ºC Spectroscopic data was in agreement with literature.[363]

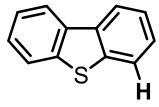

dibenzo[b,d]thiophene (109r). Following General Procedure A, 4-bromodibenzo[b,d]thiophene **(108r)** (52.6 mg, 0.2 mmol) was used, affording the title compound as a yellowish white solid (29.4 mg, 80% yield) by using Hexanes:EtOAc (4:1) as eluent. **^{1}H NMR** (400 MHz, CDCl3) δ 8.21 – 8.13 (m, 2H), 7.91 – 7.82 (m, 2H), 7.51 – 7.42 (m, 4H). **^{13}C NMR** (101 MHz, CDCl3) δ 139.4, 135.6, 126.7, 124.4, 122.8, 121.6. **Melting Point:** 97-99 ºC. Spectroscopic data was in agreement with literature.[367]

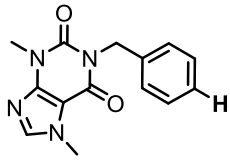

1-benzyl-3,7-dimethyl-3,7-dihydro-1H-purine-2,6-dione (109s) Following General Procedure A, 1-(4-bromobenzyl)-3,7-dimethyl-3,4,5,7-tetrahydro-1H-purine-2,6-dione **(108s)** (70.2 mg, 0.2 mmol) was used, affording the title compound as a white solid (29.9 mg, 54% yield) by using Hexanes:EtOAc (2:1) as eluent. **^{1}H NMR (400 MHz, $CDCl_3$)** δ 7.54 – 7.43 (m, 3H), 7.33 – 7.26 (m, 2H), 7.26 – 7.20 (m, 1H), 5.18 (s, 2H), 3.97 (s, 3H), 3.56 (s, 3H). **^{13}C NMR** (101 MHz, CDCl3) δ 155.2, 151.0, 148.9, 141.5, 137.3, 128.8, 128.4, 127.52, 44.5, 33.6, 29.8 **Melting Point:** 140-142 ºC Spectroscopic data was in agreement with literature.[356]

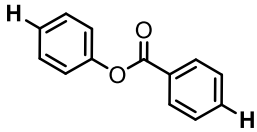

Phenyl benzoate (109t). Following General Procedure A, 4-bromophenyl 4-bromobenzoate **(109t)** (35.6 mg, 0.1 mmol) was used with Na_2CO_3 (0.3 mmol, 31.8 mg, 3.0 equiv), NiI_2 (0.02 mmol, 6.1 mg, 0.2 equiv). The Schlenk was transferred to a nitrogen filled glovebox where dcyb (0.022 mmol, 0.2 equiv), CsI (0.04 mmol, 10.4 mg, 0.4 equiv) in THF (1 mL, 0.1 M) affording the title compound as a white solid (15.6 mg, 78% yield) by using Hexanes:EtOAc (2:1) as eluent. **^{1}H NMR (400 MHz, $CDCl_3$)** δ 8.28 – 8.21 (m, 2H), 7.71 – 7.63 (m, 1H), 7.59 – 7.50 (m, 2H), 7.55 – 7.42 (m, 2H), 7.37 – 7.22 (m, 3H). **^{13}C NMR (101 MHz, $CDCl_3$)** δ 165.2, 151.0, 133.6, 130.2, 129.6, 129.5, 128.6, 125.9, 121.7. **Melting Point:** 70-73 ºC Spectroscopic data was in agreement with literature.[368]

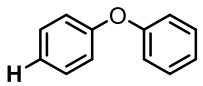

diphenyl ether (109u). Following General Procedure A, **(108u)** (49.4 mg, 0.2 mmol) was used, affording the title compound as a white solid (25.8 mg, 76% yield) by using Hexanes:EtOAc (2:1) as eluent. **^{1}H NMR δ (400 MHz, $CDCl_3$)** δ: 7.39-7.29 (m, 4H), 7.10 (m, 2H). 7.02 (m, 4H). **^{13}C NMR (101 MHz, $CDCl_3$)** δ: 157.2, 129.7, 123.2, 118.9 Spectroscopic data was in agreement literature.[369]

From **(108v)** dibromide (32.8 mg, 0.1 mmol) was used with Na_2CO_3 (0.3 mmol, 31.8 mg, 3.0 equiv), NiI_2 (0.02 mmol, 6.1 mg, 0.2 equiv). The Schlenk was transferred to a nitrogen filled glovebox where dcyb (0.022 mmol, 0.2 equiv), CsI (0.04 mmol, 10.4 mg, 0.4 equiv) in THF (1 mL, 0.1 M) affording the title compound as a white solid (15.1 mg, 88% yield) by using Hexanes:EtOAc (2:1) as eluent. **^{1}H NMR δ (400 MHz, $CDCl_3$)** δ: 7.39-7.29 (m, 4H), 7.10 (m, 2H). 7.02 (m, 4H). **^{13}C NMR (101 MHz, $CDCl_3$)** δ: 157.2, 129.7, 123.2, 118.9

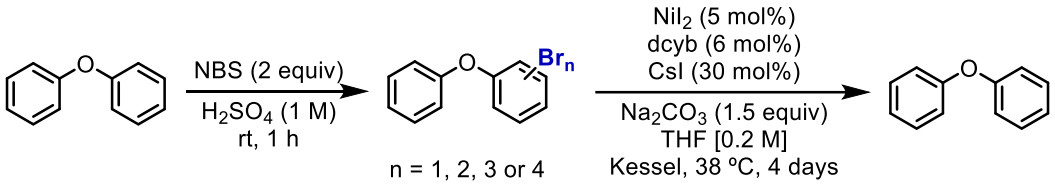

Complex mixture of low bromine count PBDEs. A round bottomed flask was charged with diphenyl ether (170 mg, 1 mmol), and H2SO4 (1 mL), to this was added NBS (2 mmol) and stirred for 30 minutes. Diluted with water and extracted with DCM, washed with sodium sulfite and brine. Evaporation and filtration through a silica plug, used in the next step without further purification. NiI_2 (0.1 mmol, 0.05 equiv), and Na_2CO_3 (3 mmol, 1.5 equiv) were weighed out into a 100 mL round bottomed flask equipped with large stir bar. The RBF was transferred into the glovebox where CsI (0.6 mmol. 0.3 equiv) and dcyb (0.12 mmol, 0.06 equiv) was added. The RBF was secured with a septum and wrapped with blue electrical tape. The complex mixture of polybrominated diphenyl ethers, was solubilised in Anhydrous THF (25 mL) and added to the reaction mixture. This was stirred under visible light irradiation. Reaction progress was monitored by GC. After 5 days under visible light irradiation, THF was removed under rotary evaporation, 1 M HCl was added to the crude reaction mixture and extracted with DCM and dried over anhydrous $MgSO_4$. GC-MS showed complete consumption of bromine containing diphenyl ethers, column chromatography afforded the title compound as a colourless oil (88 mg, 51% yield).

Photodebromination

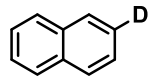

109n(D)

2-d naphthalene (2f-D). An oven dried Schlenk tube containing a stir bar was charged with 2-bromonapthalene (0.2 mmol), Na_2CO_3 (0.3 mmol, 31.8 mg, 1.5 equiv), and NiI_2 (0.03 mmol, 9 mg, 15 mol%). The Schlenk was transferred to a nitrogen filled glovebox where dcyb (0.032 mmol, 13 mg, 11 mol%), CsI (0.06 mmol, 15.4 mg, 30 mol%), and THF d8 (0.2 M, 1 mL) was added. The Schlenk was sealed and the mixture was stirred for 15 minutes. They were then taken out of the glovebox and placed under 2 x 440 nm kessels (**Photo3**) and stirred for 4 days. The mixture was quenched with 1M HCl (2 mL) and extracted with EtOAc, 0.5 cm^3 of silica gel was added to the round bottom flask and evaporated on a rotary evaporator set at 40 ºC and 100 mbar. The crude was then subjected to column chromatography, hexanes:EtOAc (95:5) affording the title compound as a white solid (22.1 mg, 56% yield). Unreacted bromide was also recovered (16.4 mg, 15%) Deuterium incorporation: 90% (^{1}H-NMR) **^{1}H NMR (400 MHz, Chloroform-*d*)** δ 7.86 (m, 4H), 7.49 (m, 3.09 H). **^{13}C NMR (101 MHz, $CDCl_3$)** δ 133.5, 128.0, 127.8, 125.9, 125.8. **^{2}H NMR (500 MHz, Chloroform)** δ 7.56

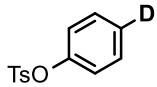

109i(D)

Phenyl-4-d 4-methylbenzenesulfonate (2f-D). An oven dried Schlenk tube containing a stir bar was charged with 4-bromophenyl 4-methylbenzenesulfonate (0.2 mmol), Na_2CO_3 (0.3 mmol, 31.8 mg, 1.5 equiv), and NiI_2 (0.03 mmol, 9 mg, 15 mol%). The Schlenk was transferred to a nitrogen filled glovebox where dcyb (0.032 mmol, 13 mg, 11 mol%), CsI (0.06 mmol, 15.4 mg, 30 mol%), and THF d8 (0.2 M, 1 mL) was added. The Schlenk was sealed and the mixture was stirred for 15 minutes. They were then taken out of the glovebox and placed under 2 x 440 nm kessels (**Photo3**) and stirred for 4 days. The mixture was quenched with 1M HCl (2 mL) and extracted with EtOAc, 0.5 cm^3 of silica gel was added to the round bottom flask and evaporated on a rotary evaporator set at 40 ºC and 100 mbar. The crude was then subjected to column chromatography, hexanes:EtOAc (5:1) affording the title compound as a white solid (22.1 mg, 44% yield). Unreacted bromide was also recovered (16.4 mg, 15%) Deuterium incorporation: 90% (^{1}H-NMR) **^{1}H NMR (400 MHz, Chloroform-*d*)** δ 7.70 (d, J = 8.4 Hz, 2H), 7.29 (t, J = 8.5 Hz, 4.05H), 6.98 (d, J = 8.7 Hz, 2H), 2.45 (s, 3H). **^{13}C NMR (101 MHz, $CDCl_3$)** δ = 149.7, 145.3, 129.7, 129.5, 128.5, 122.4, 21.7. **^{2}H NMR (500 MHz, Chloroform):** δ 7.56

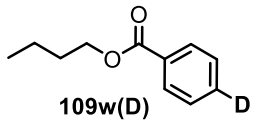

109w(D)

Phenyl-4-d pentanoate (2v-D). An oven dried Schlenk tube containing a stir bar was charged with 4-bromophenyl pentanoate (0.2 mmol), Na_2CO_3 (0.3 mmol, 31.8 mg, 1.5 equiv), and NiI_2 (0.03 mmol, 9 mg, 15 mol%). The Schlenk was transferred to a nitrogen filled glovebox where dcyb (0.032 mmol, 13 mg, 16 mol%), CsI (0.06 mmol, 15.4 mg, 30 mol%), and THF d8 (0.2 M, 1 mL) was added. The Schlenk was sealed, and the mixture was stirred for 15 minutes. They were then taken out of the glovebox and placed in a custom made pre heated reaction vessel at 35 ºC for 4 days. The mixture was quenched with 1M HCl (2 mL) and extracted with EtOAc, 0.5 cm^3 of silica gel was added to the round bottom flask and evaporated on a rotary evaporator set at 40 ºC and 100 mbar. The crude was then subjected to column chromatography, hexanes:EtOAc (96:4) affording the title compound as a clear liquid (22.6 mg, 63% yield). Deuterium incorporation: 93% (^{1}H-NMR) **^{1}H NMR (400 MHz, Chloroform-*d*)** δ 7.39-7.36 (d, J = 8.2 Hz, 2H), 7.22 (t, 0.07H), 7.09-7.07 (d, J = 8.6 Hz, 2H), 2.56 (t, J = 7.5 Hz, 2H), 1.75 (p, J = 7.6 Hz, 2H), 1.52 – 1.40 (m, 2H), 0.98 (t, J = 7.4 Hz, 3H). **^{13}C NMR (101 MHz, $CDCl_3$)** δ 13C NMR (101 MHz, CDCl3) δ = 172.3, 150.8, 129.3, 121.6, 34.1, 27.0, 22.3, 13.7. **^{2}H NMR (400 MHz, Chloroform)** δ 7.58

4.4.7. NMR Data

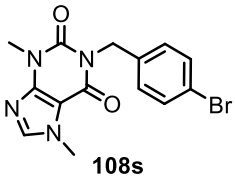

108s

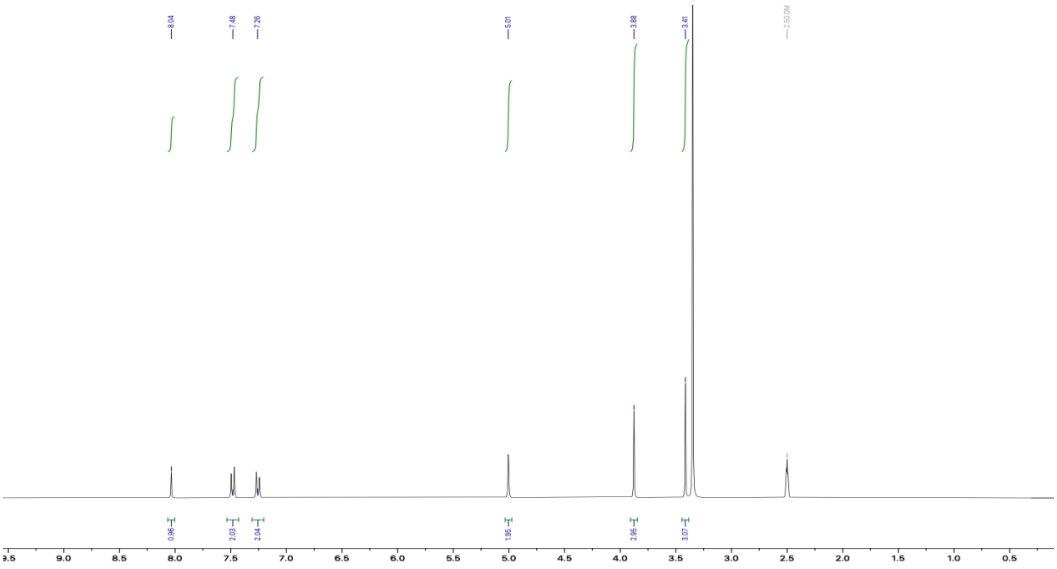

^{1}H NMR spectrum (400 Hz) of **108s**

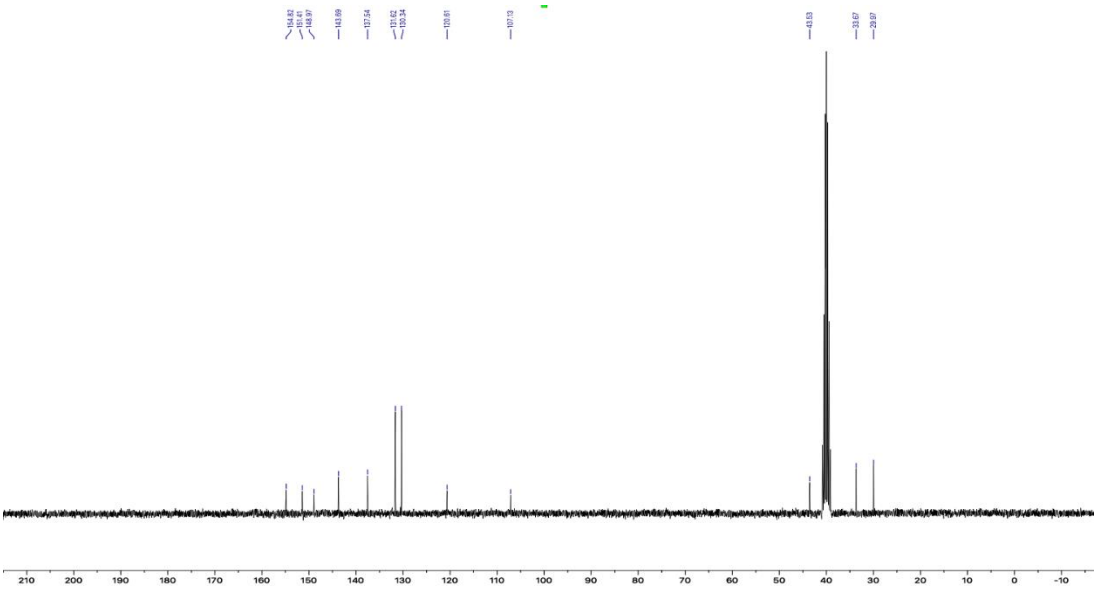

^{13}C NMR spectrum (101 Hz) of **108s**

Photodebromination

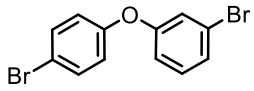

108v

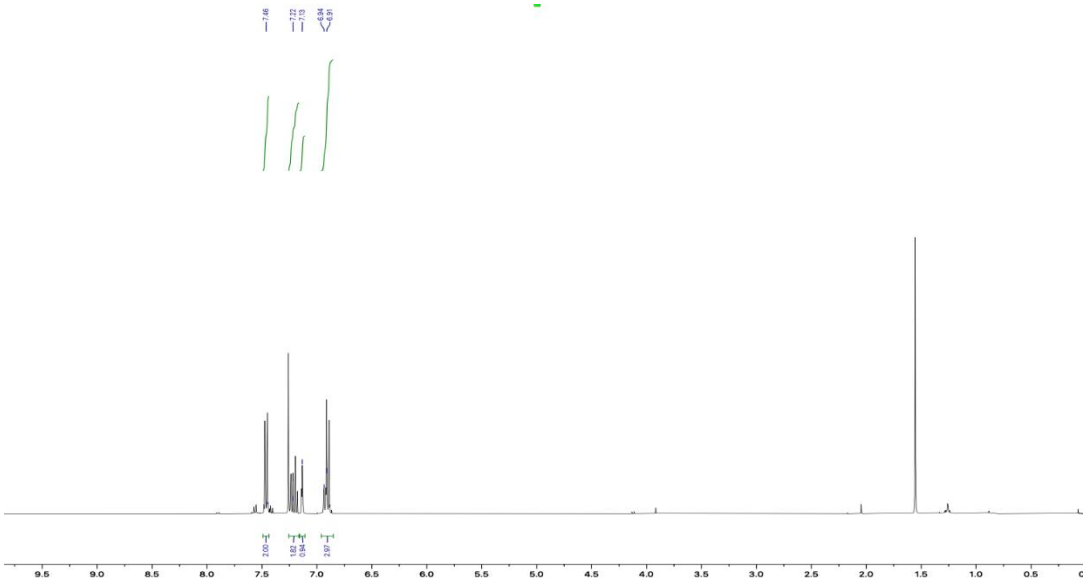

^{1}H NMR spectrum (400 Hz) of **108v**

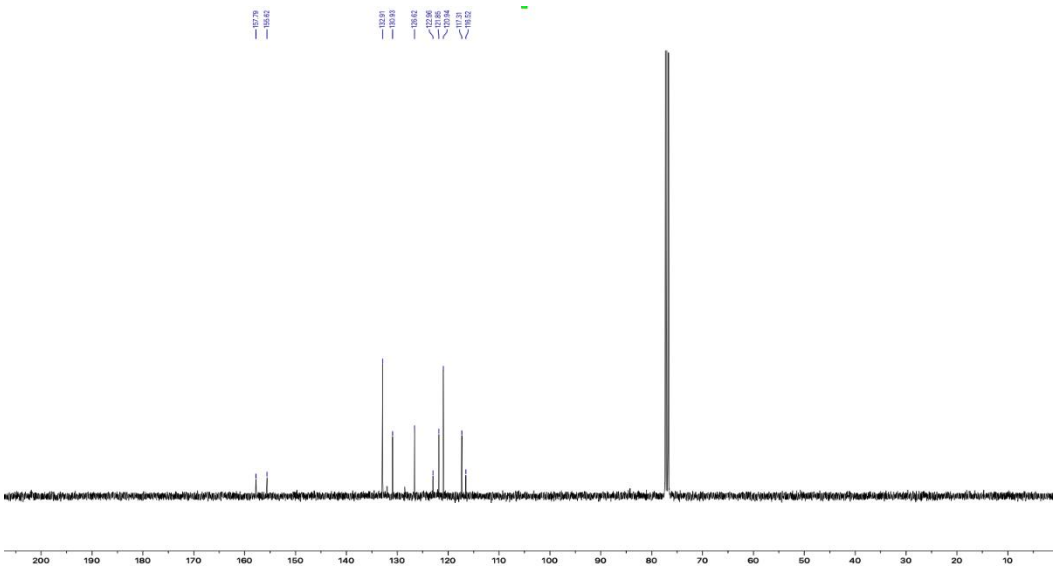

^{13}C NMR spectrum (101 Hz) of **108v**

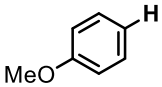

109a

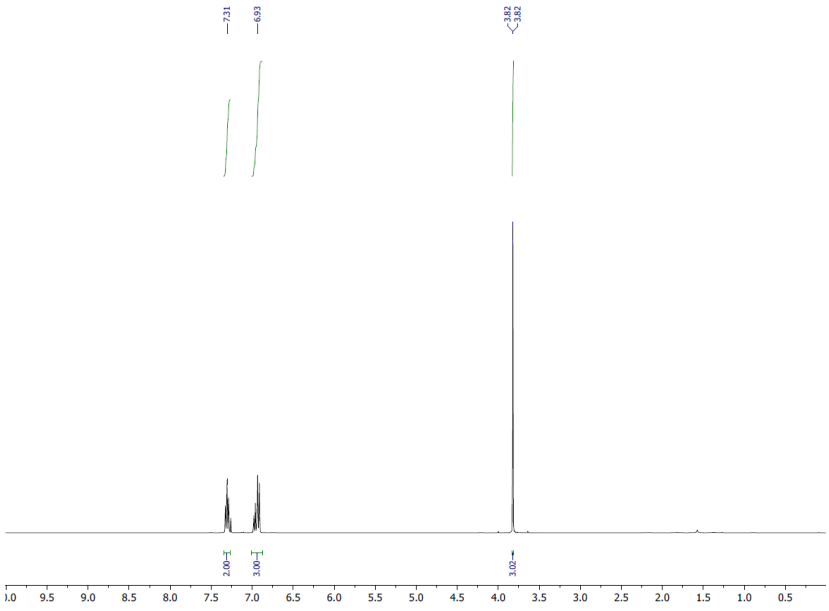

^{1}H NMR spectrum (400 Hz) of **109a**

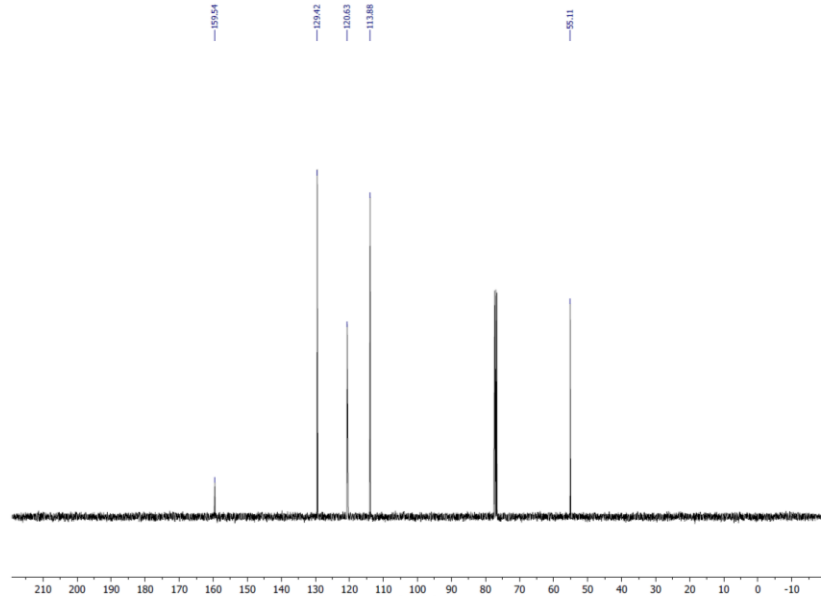

^{13}C NMR spectrum (101 Hz) of **109a**

Photodebromination

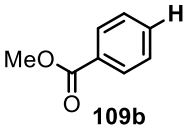

109b

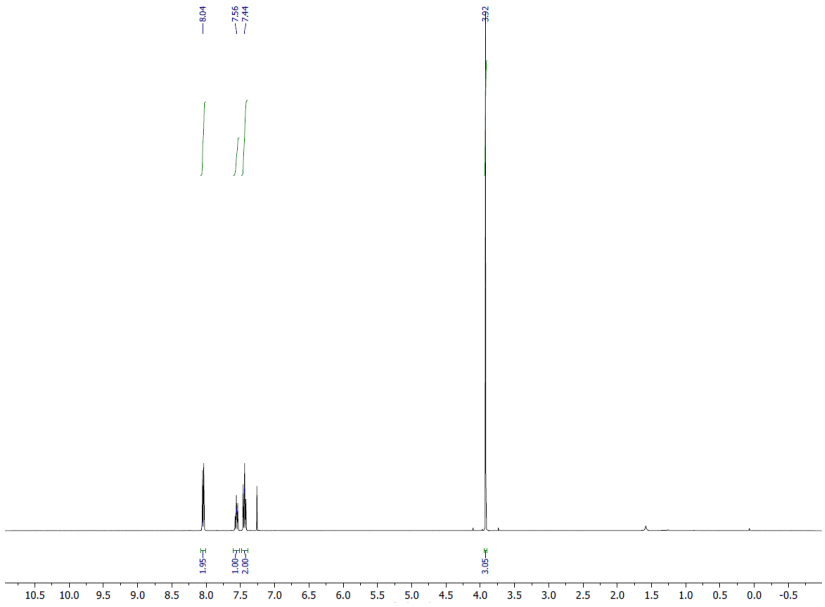

^{1}H NMR spectrum (400 Hz) of **109b**

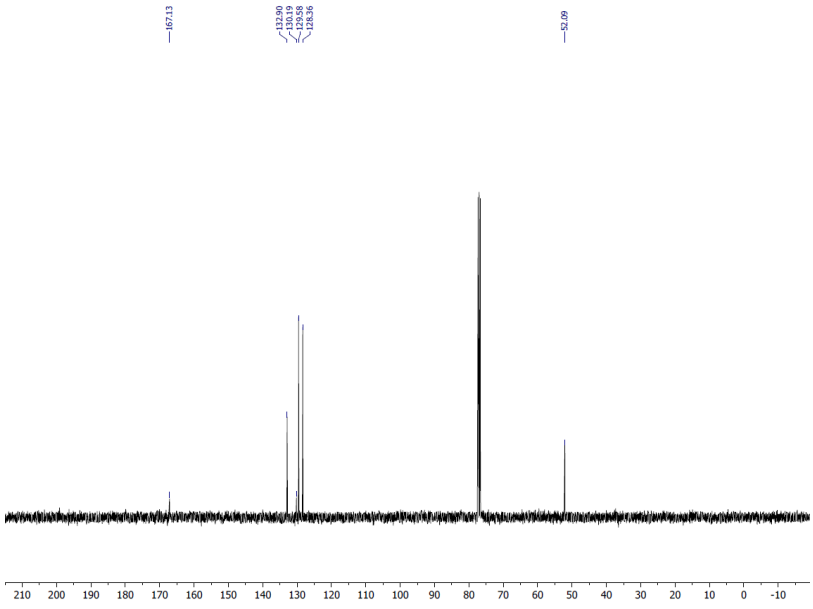

^{13}C NMR spectrum (101 Hz) of **109b**

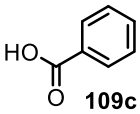

109c

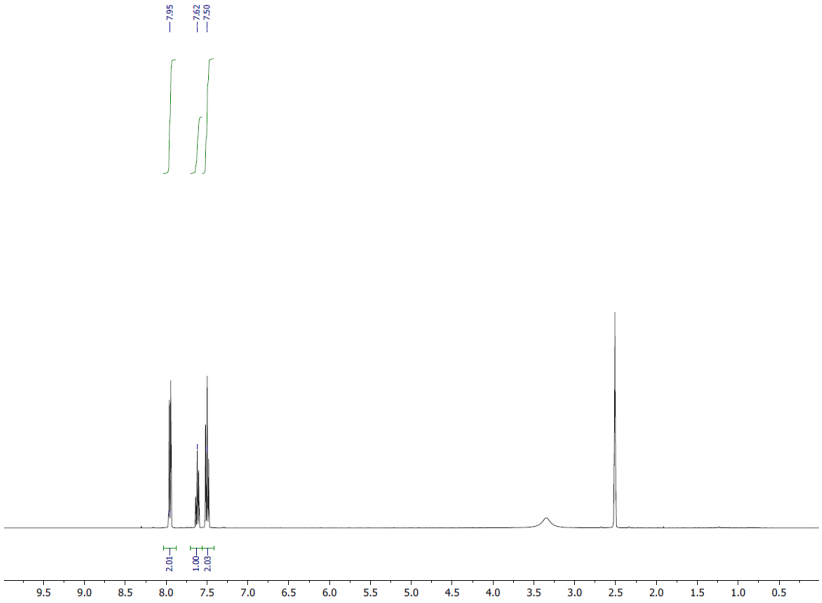

^{1}H NMR spectrum (400 Hz) of **109c**

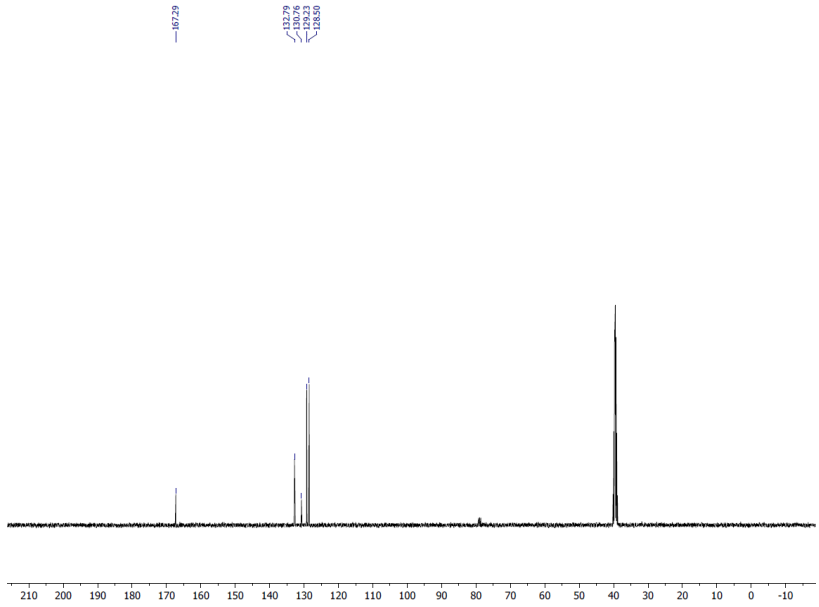

^{13}C NMR spectrum (101 Hz) of **109c**

Photodebromination

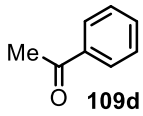

109d

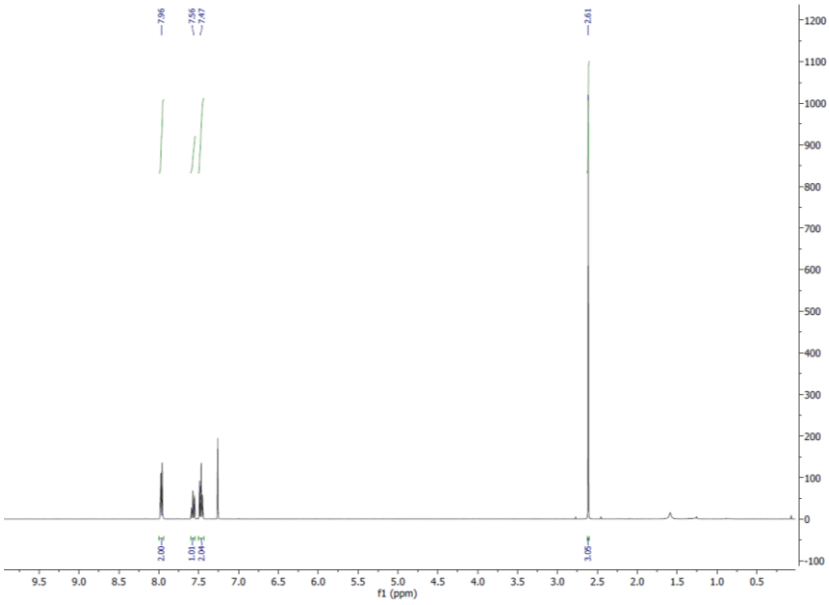

^{1}H NMR spectrum (400 Hz) of **109d**

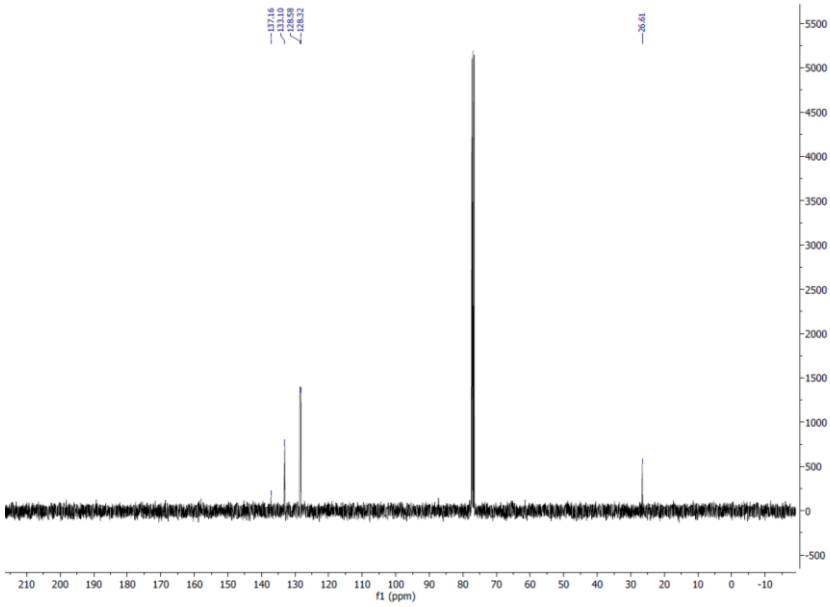

^{13}C NMR spectrum (101 Hz) of **109d**

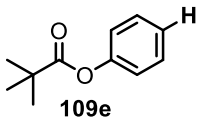

109e

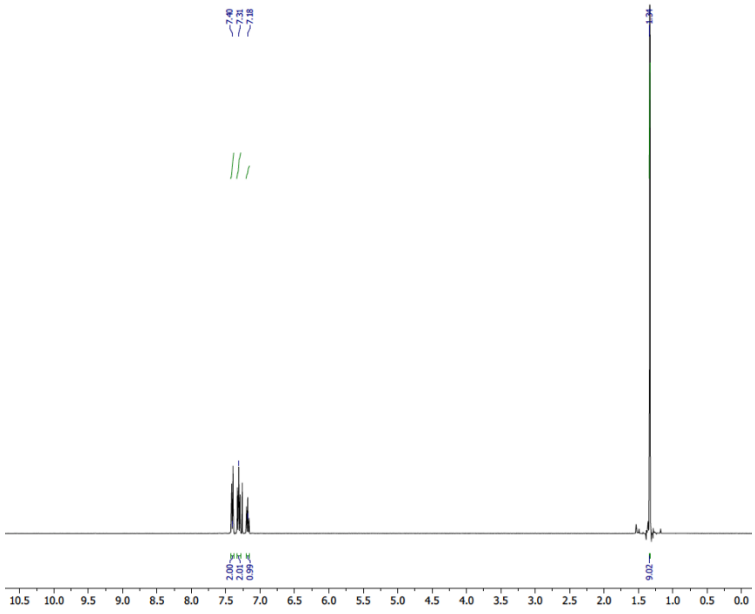

^{1}H NMR spectrum (400 Hz) of **109e**

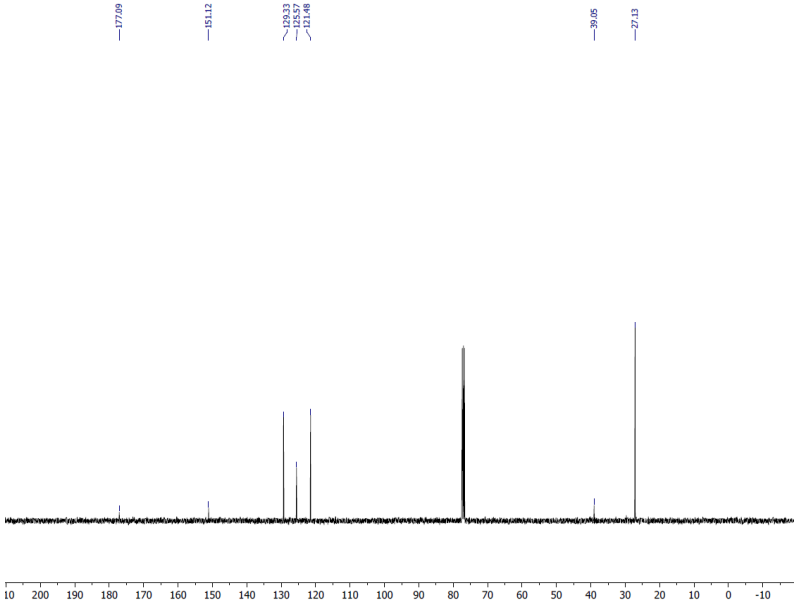

^{13}C NMR spectrum (101 Hz) of **109e**

Photodebromination

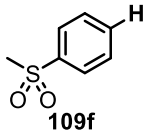

109f

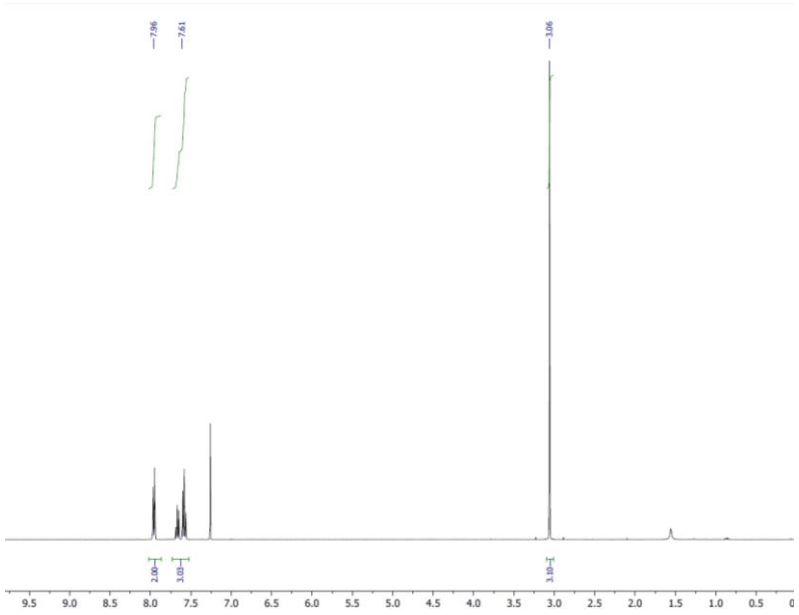

^{1}H NMR spectrum (400 Hz) of **109f**

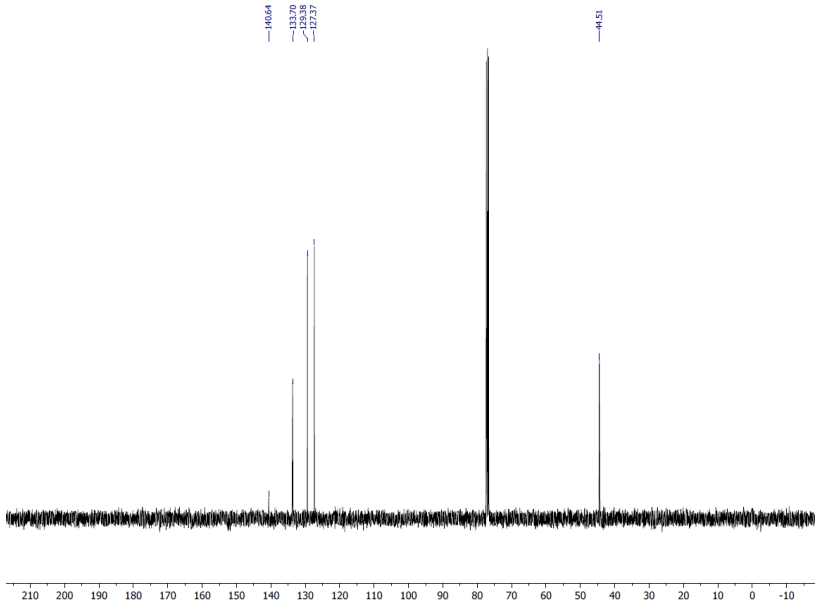

^{13}C NMR spectrum (101 Hz) of **109f**

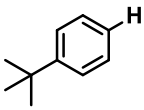

109g

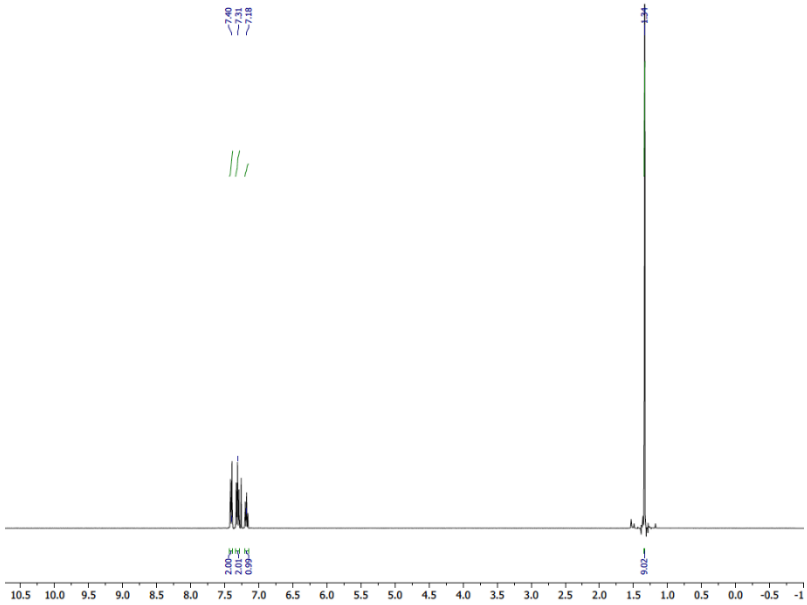

^{1}H NMR spectrum (400 Hz) of **109g**

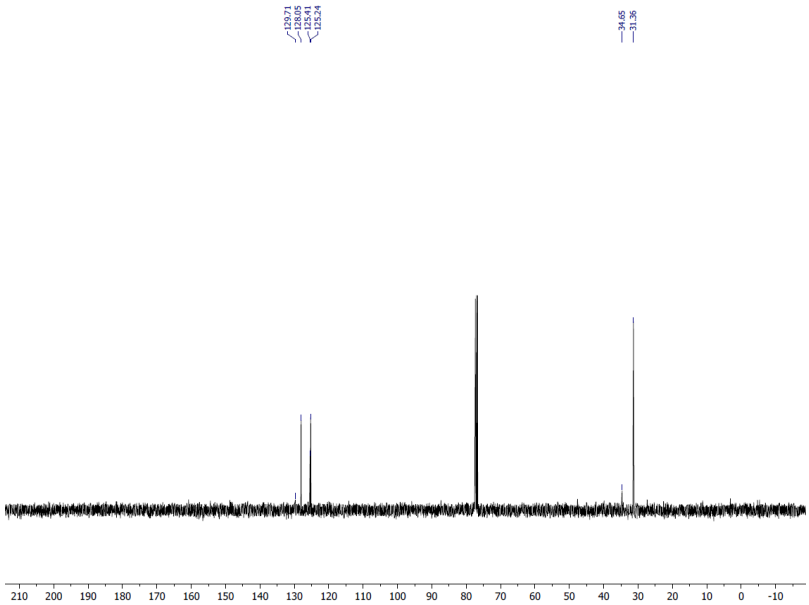

^{13}C NMR spectrum (101 Hz) of **109g**

Photodebromination

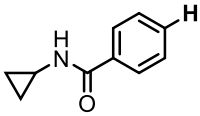

109h

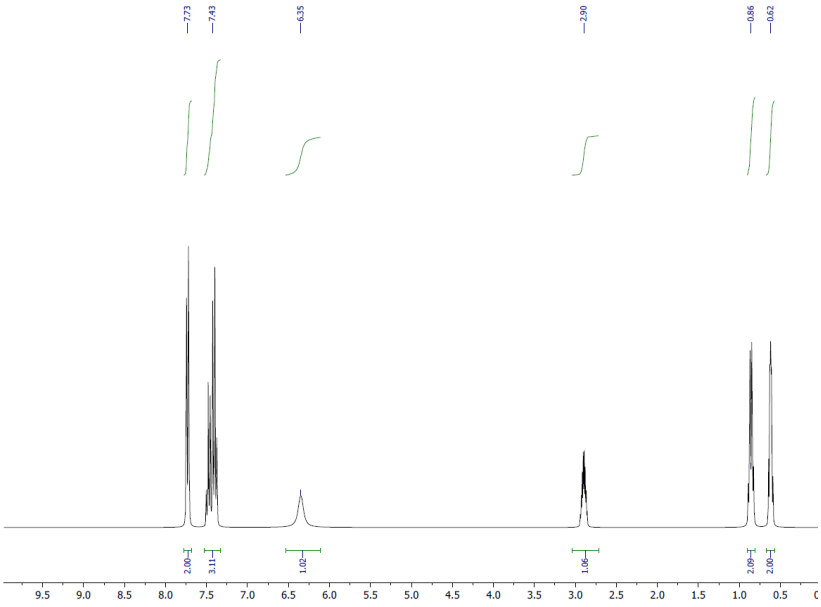

^{1}H NMR spectrum (400 Hz) of **109h**

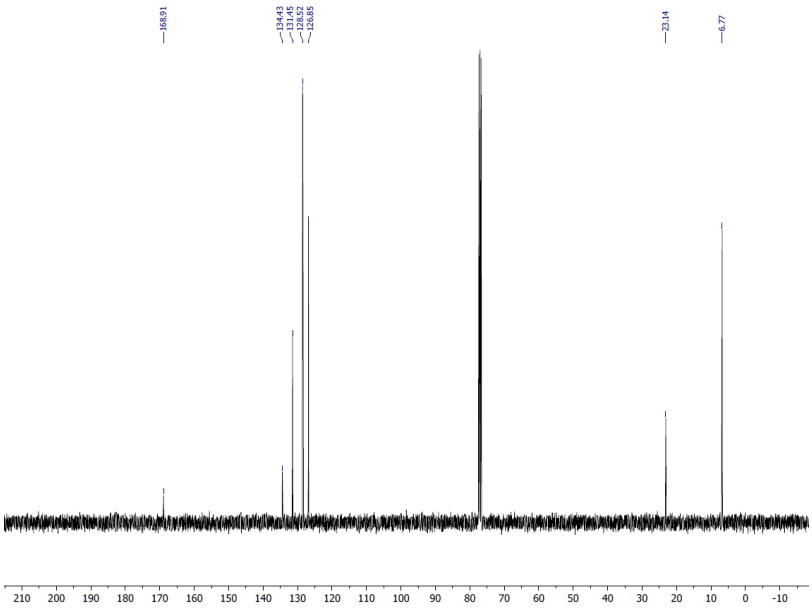

^{13}C NMR spectrum (101 Hz) of **109h**

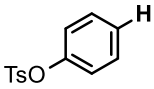

109i

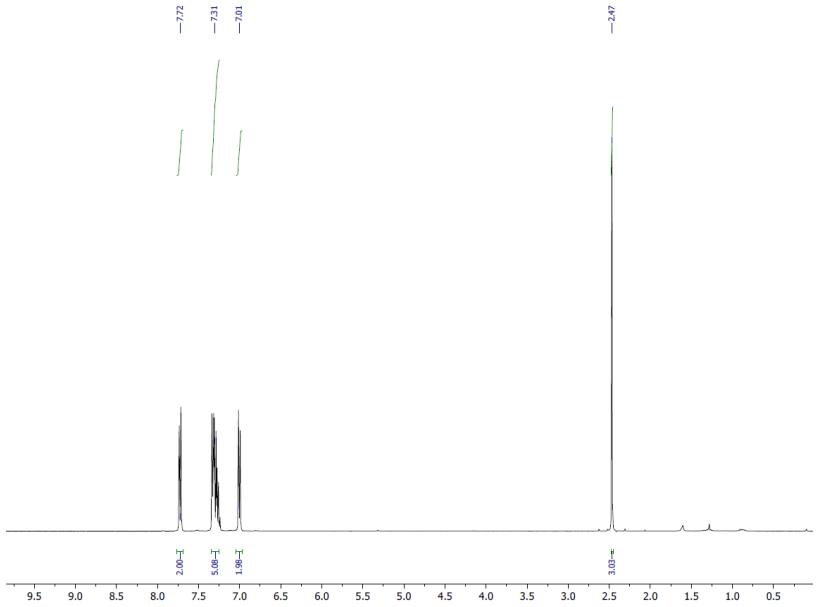

^{1}H NMR spectrum (400 Hz) of **109i**

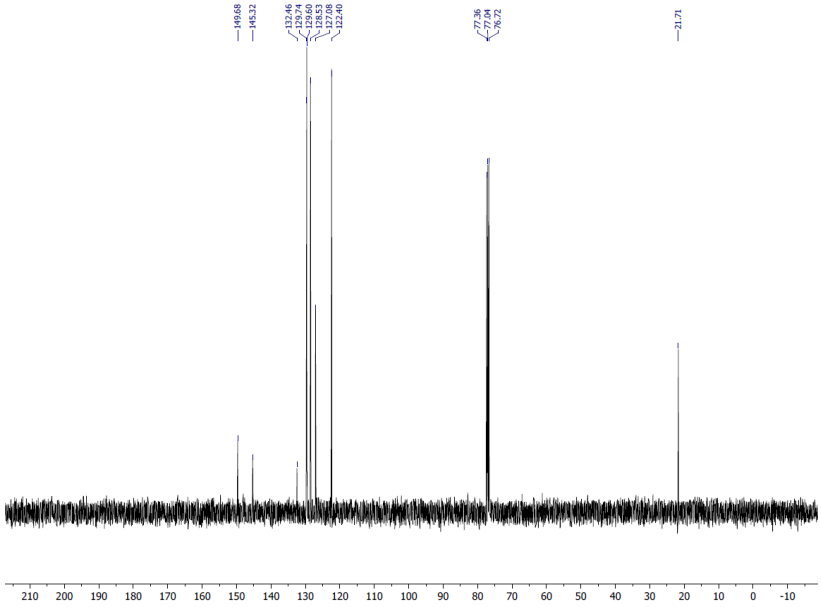

^{13}C NMR spectrum (101 Hz) of **109i**

Photodebromination

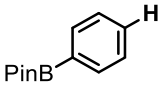

109j

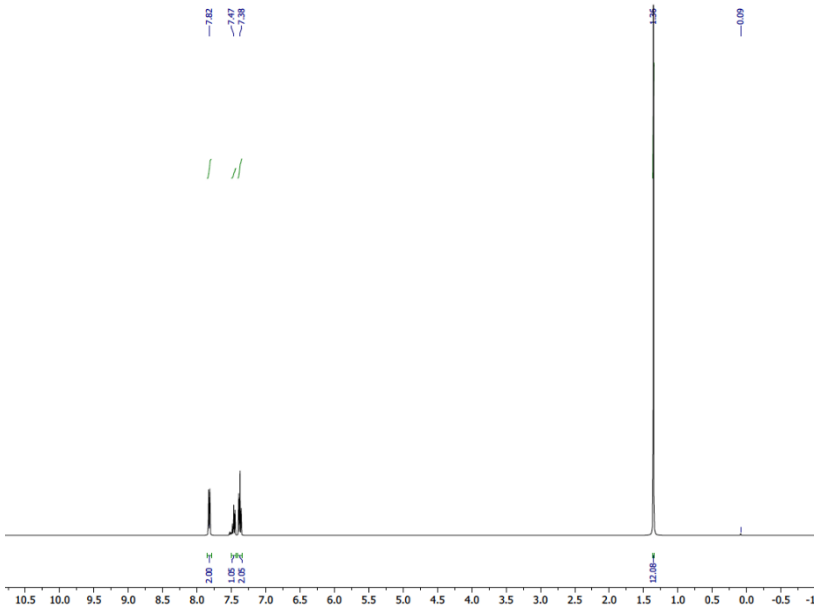

^{1}H NMR spectrum (400 Hz) of **109j**

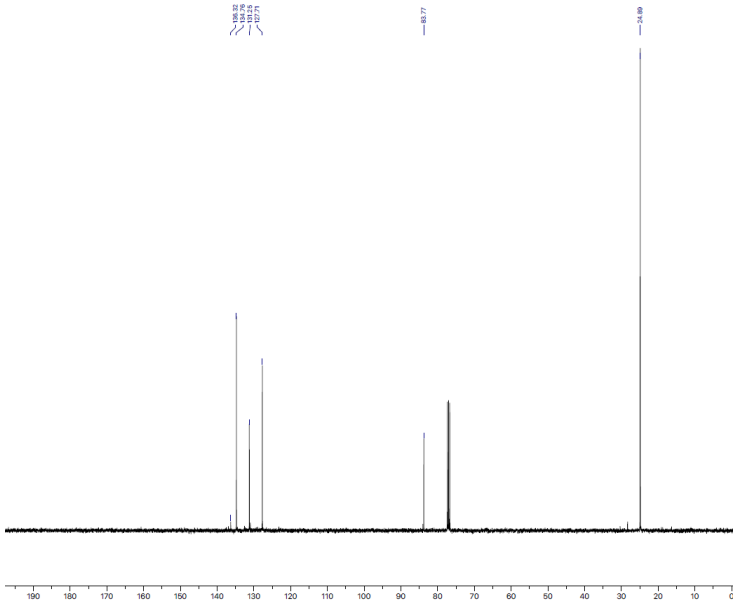

^{13}C NMR spectrum (101 Hz) of **109j**

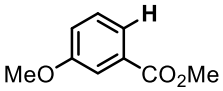

109k

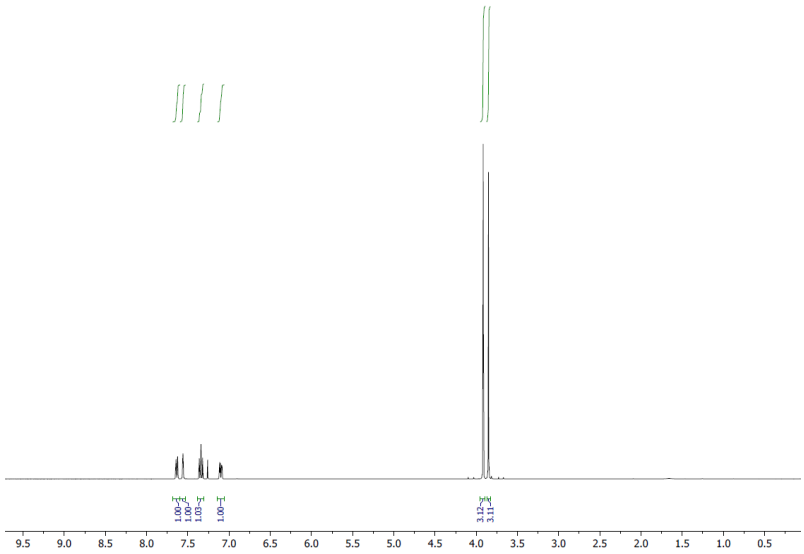

^{1}H NMR spectrum (400 Hz) of **109k**

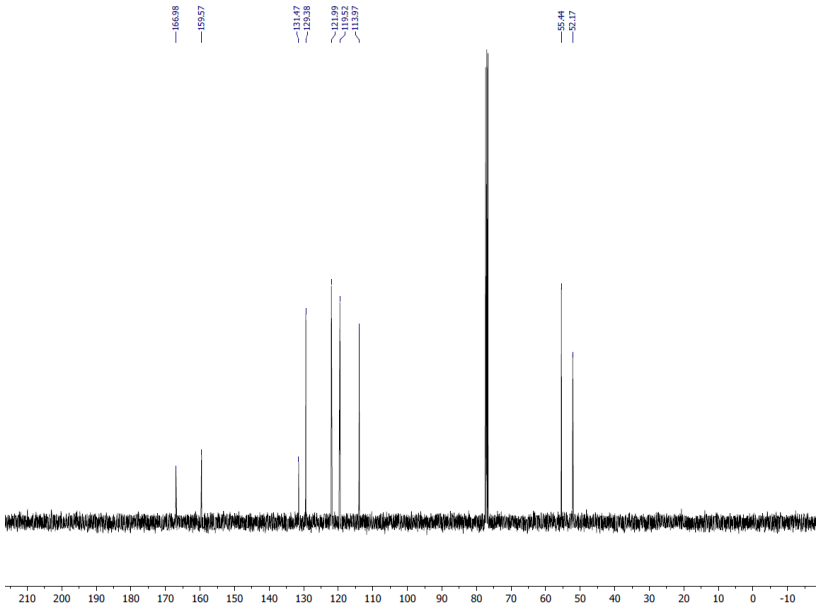

^{13}C NMR spectrum (101 Hz) of **109k**

Photodebromination

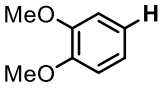

109l

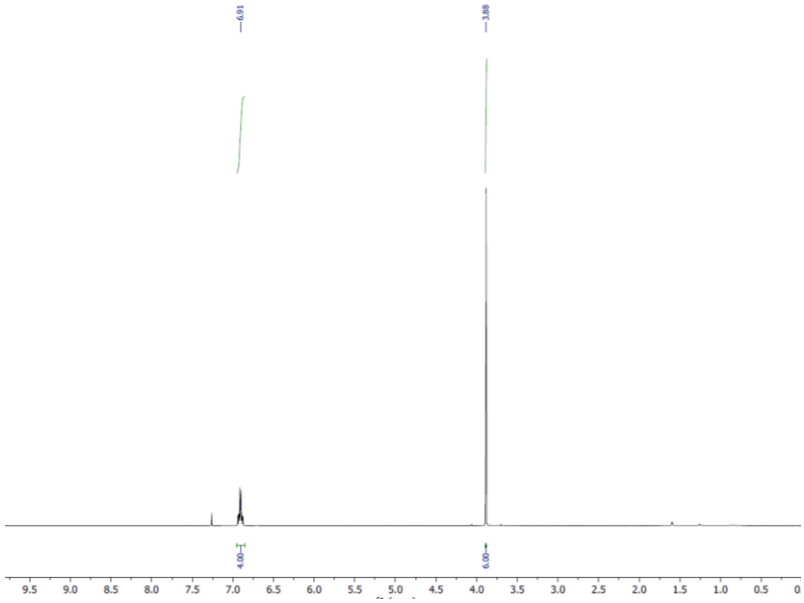

^{1}H NMR spectrum (400 Hz) of **109l**

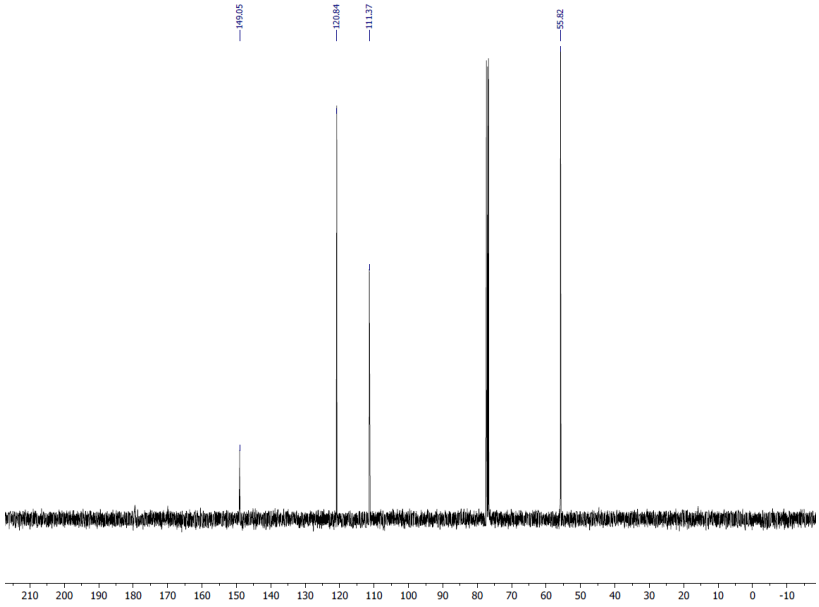

^{13}C NMR spectrum (101 Hz) of **109l**

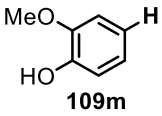

109m

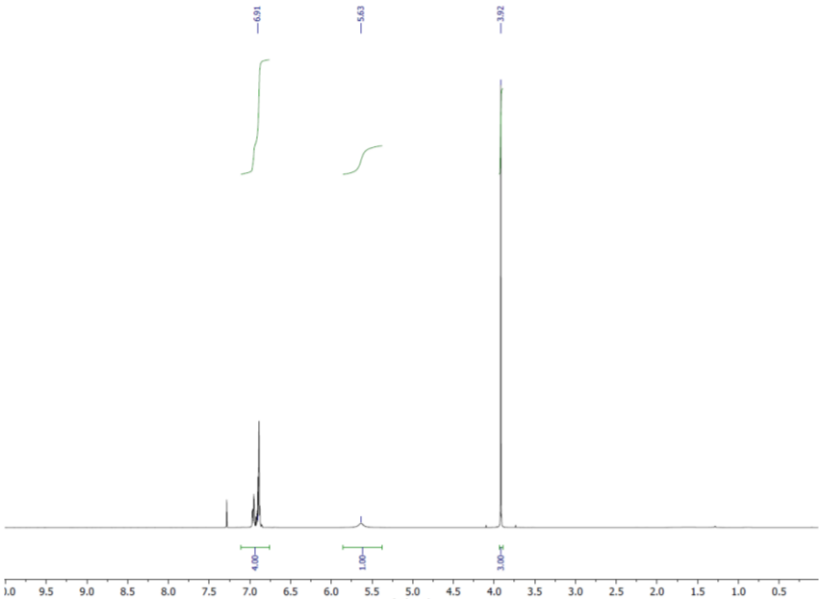

^{1}H NMR spectrum (400 Hz) of **109m**

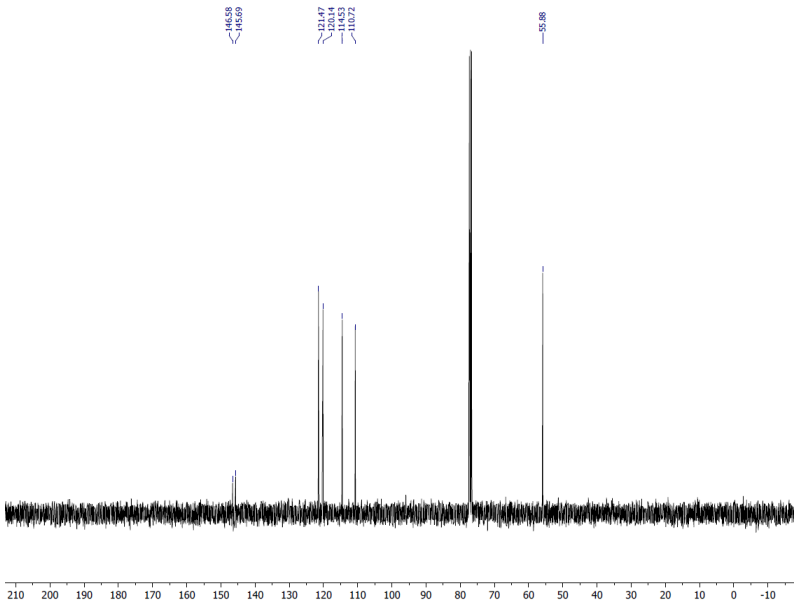

^{13}C NMR spectrum (101 Hz) of **109m**

Photodebromination

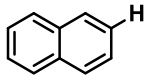

109n

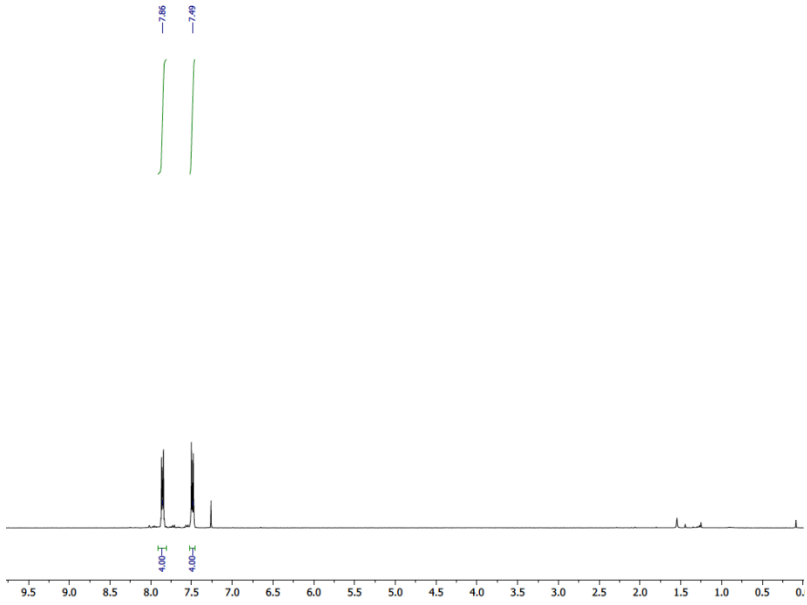

^{1}H NMR spectrum (400 Hz) of **109n**

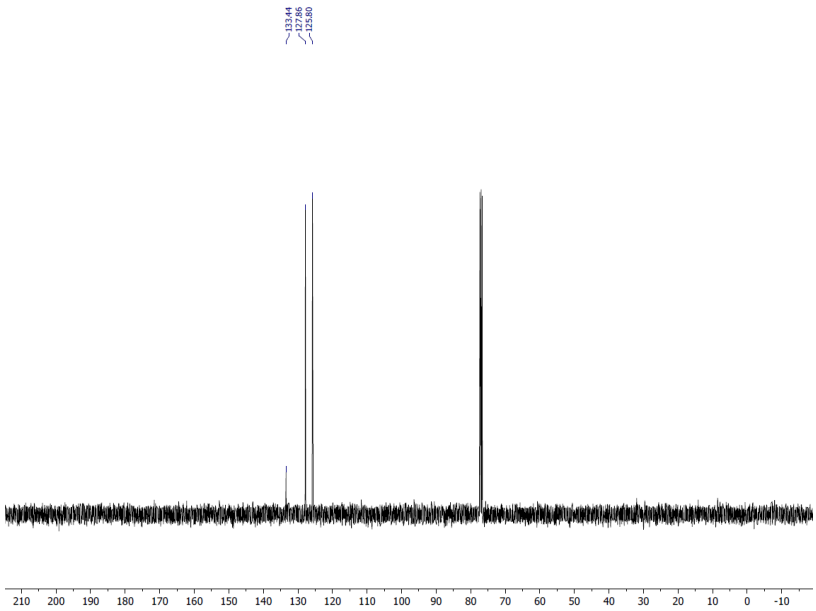

^{13}C NMR spectrum (101 Hz) of **109n**

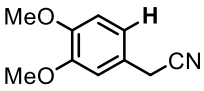

109o

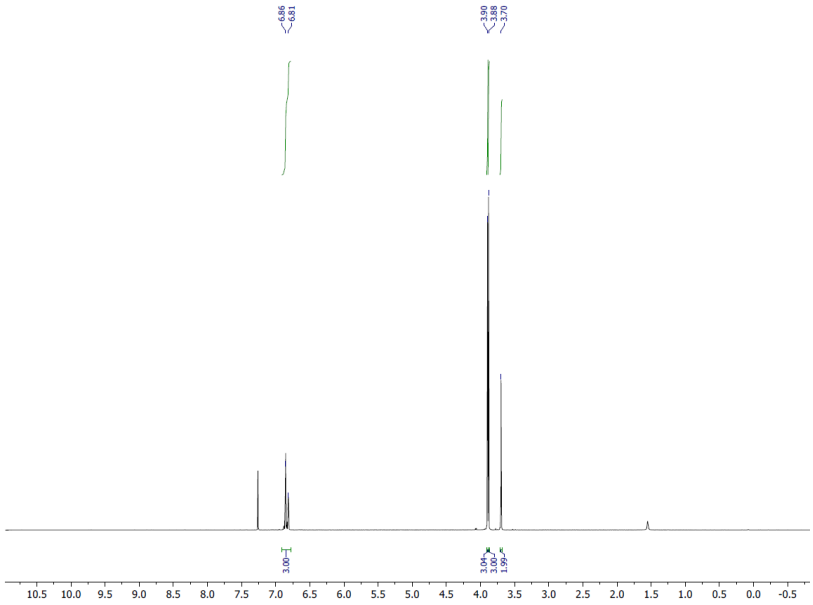

^{1}H NMR spectrum (400 Hz) of **109o**

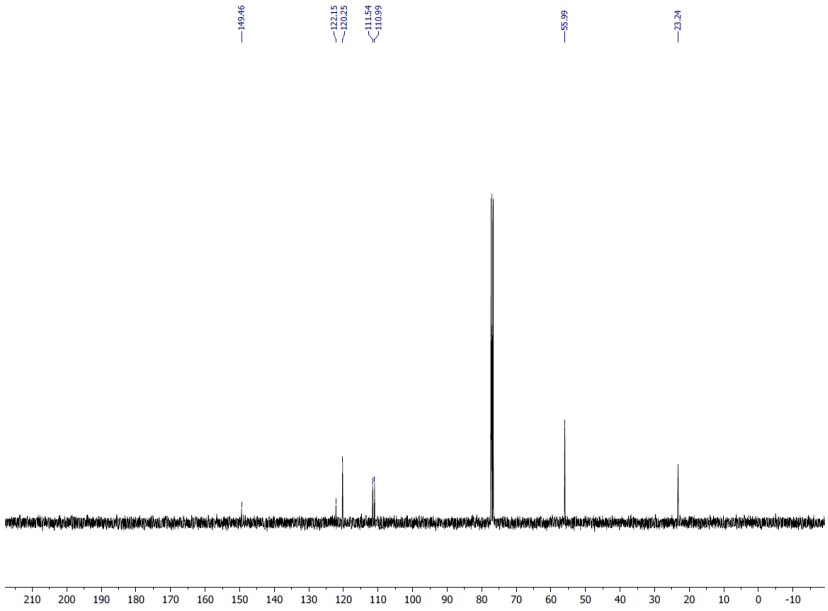

^{13}C NMR spectrum (101 Hz) of **109o**

Photodebromination

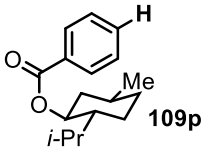

109p

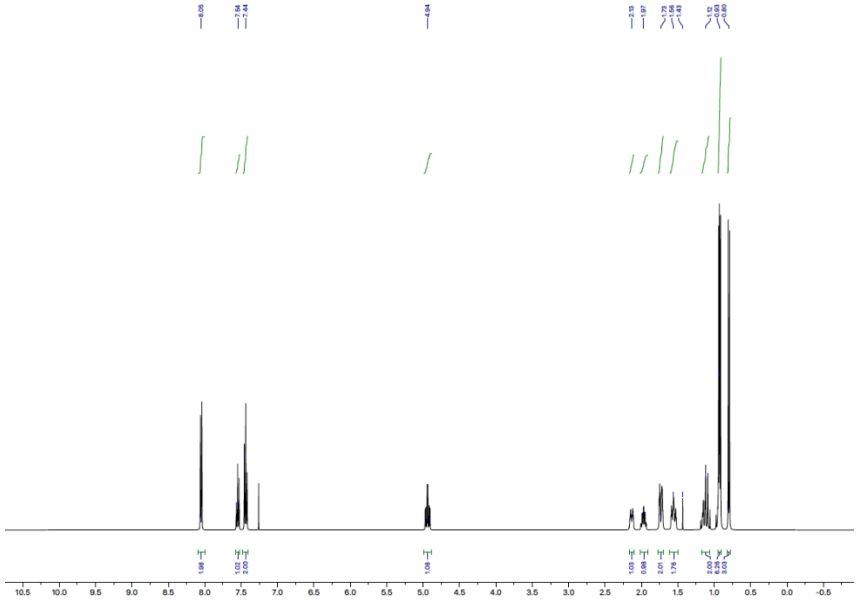

^{1}H NMR spectrum (400 Hz) of **109p**

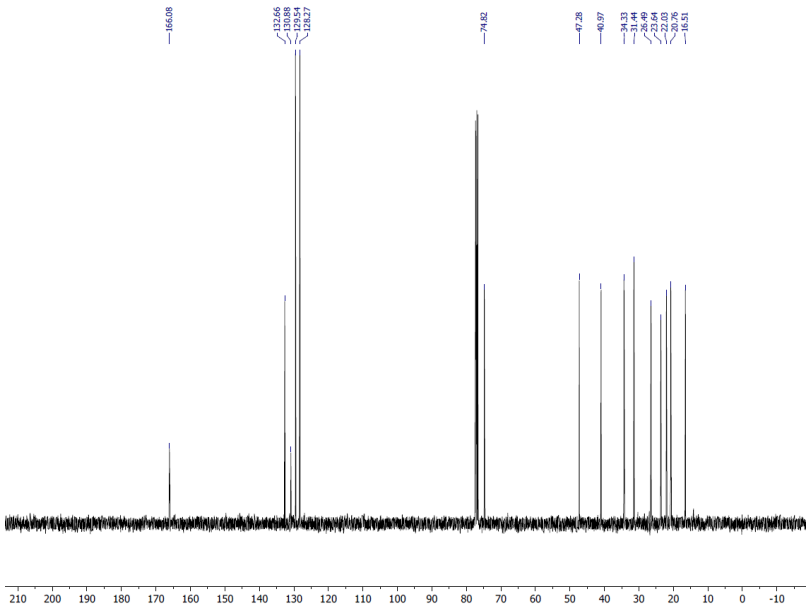

^{13}C NMR spectrum (101 Hz) of **109p**

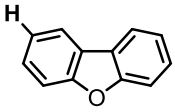

109q

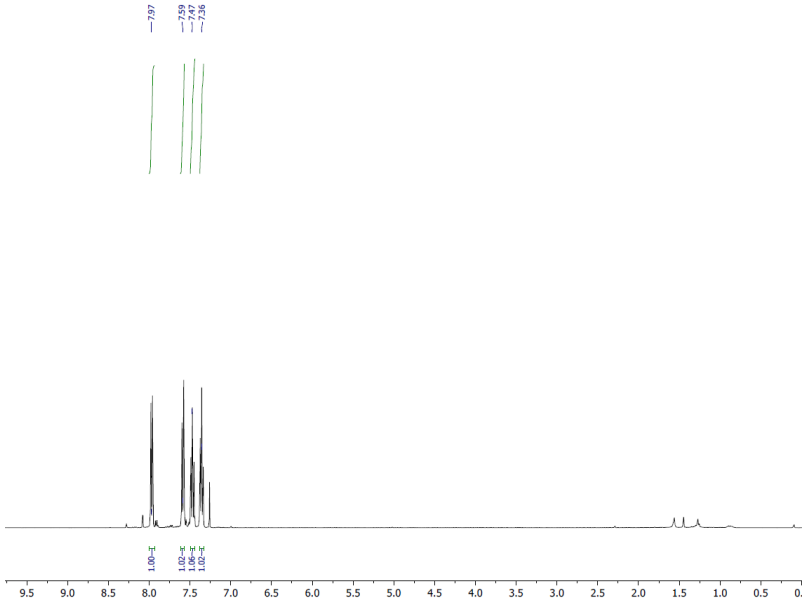

^{1}H NMR spectrum (400 Hz) of **109q**

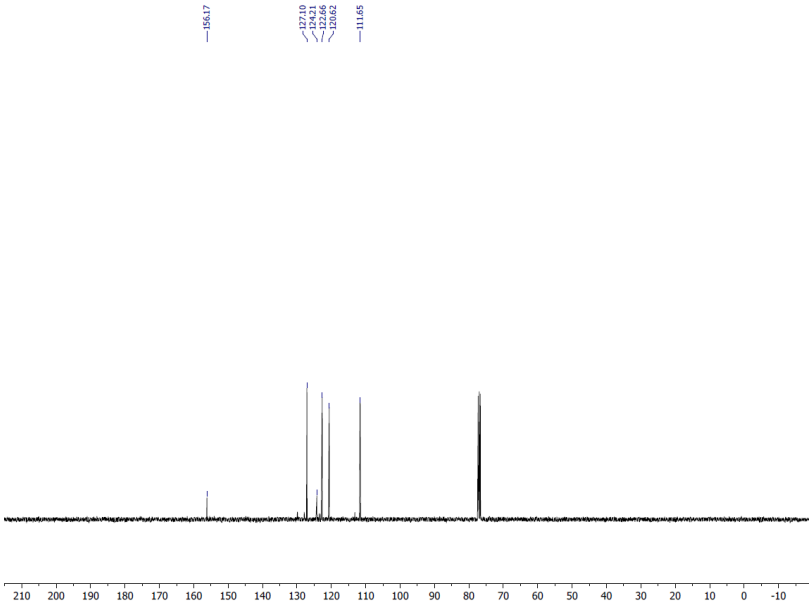

^{13}C NMR spectrum (101 Hz) of **109q**

Photodebromination

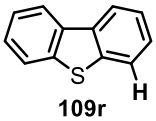

109r

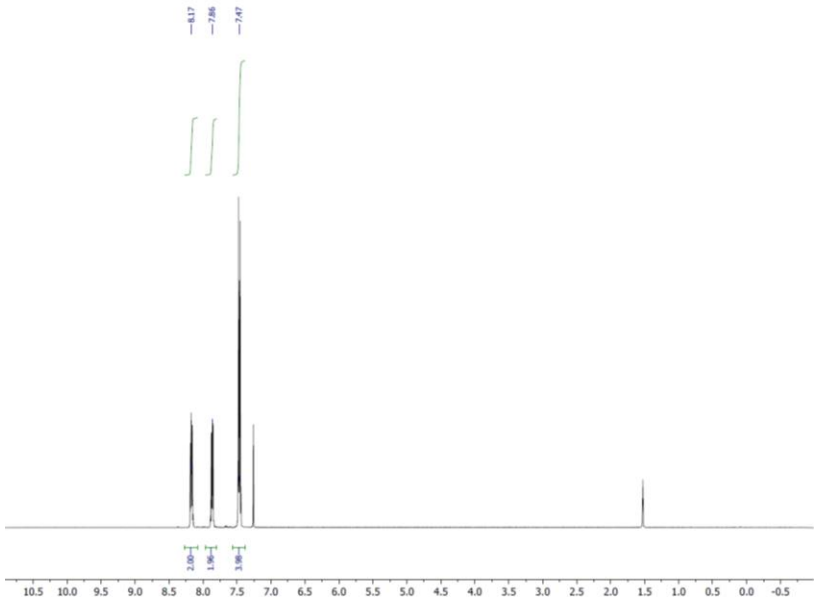

^{1}H NMR spectrum (400 Hz) of **109q**

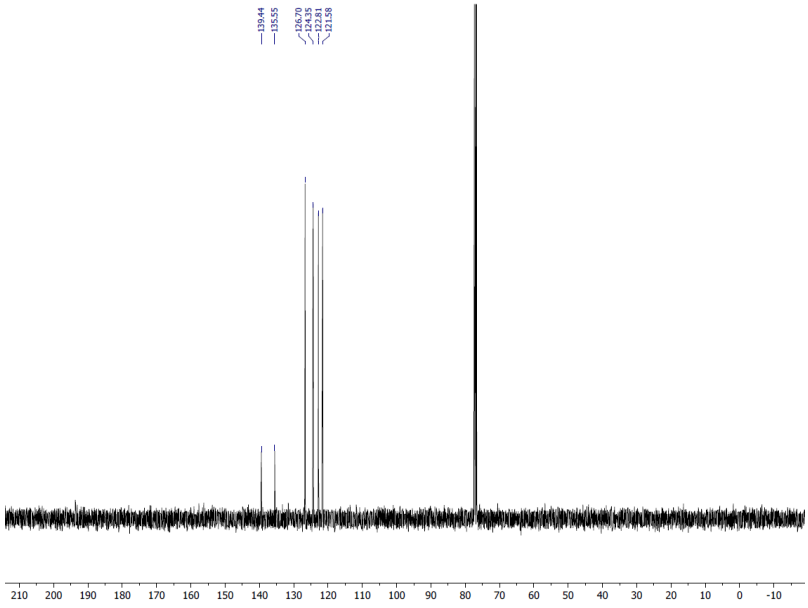

^{13}C NMR spectrum (101 Hz) of **109q**

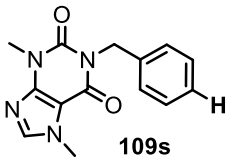

109s

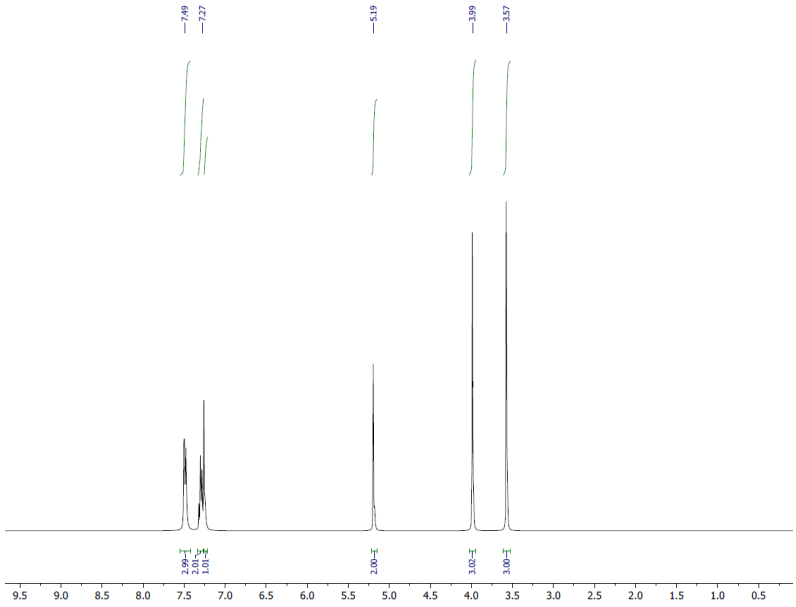

^{1}H NMR spectrum (400 Hz) of **109r**

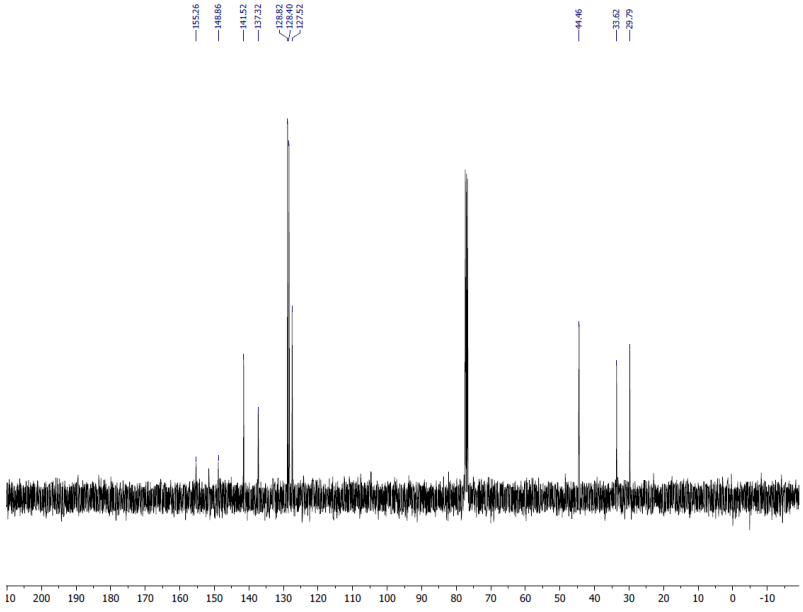

^{13}C NMR spectrum (101 Hz) of **109s**

Photodebromination

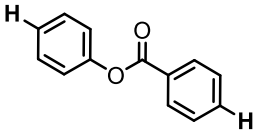

109t

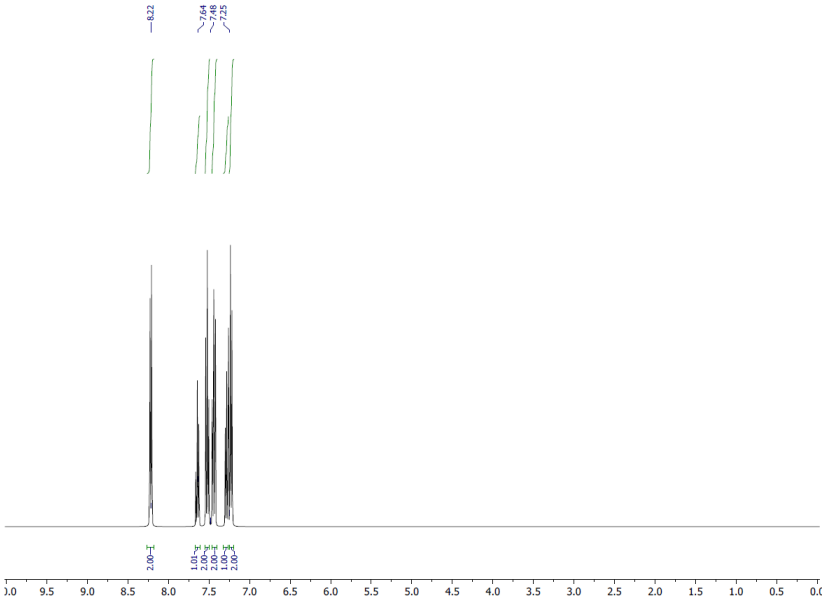

^{1}H NMR spectrum (400 Hz) of **109t**

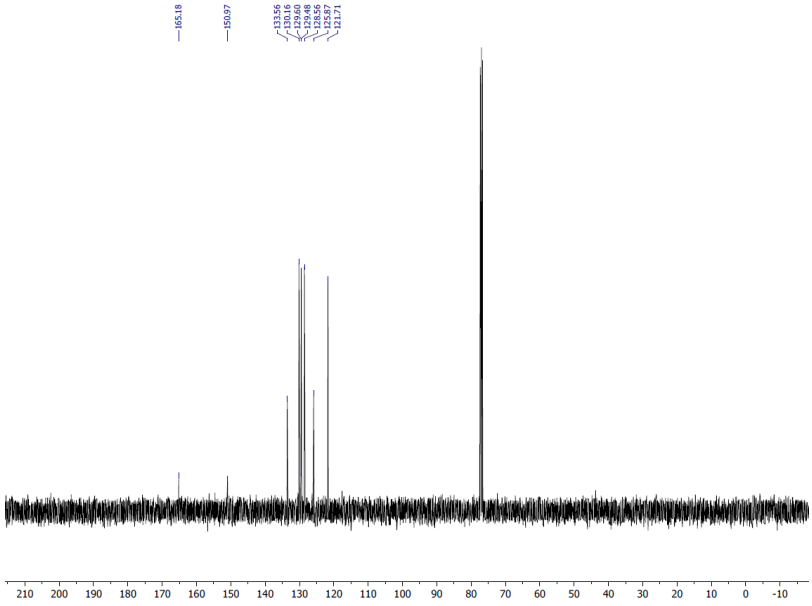

^{13}C NMR spectrum (101 Hz) of **109t**

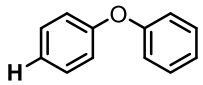

109u

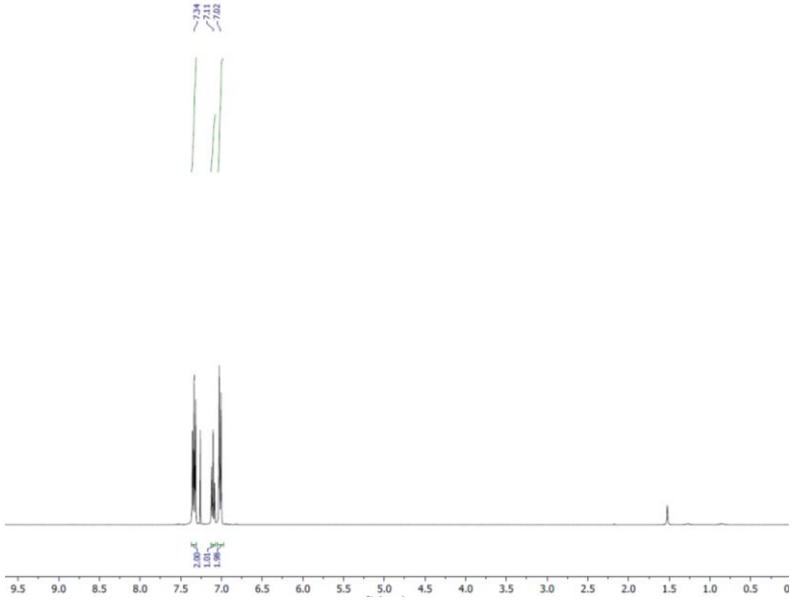

^{1}H NMR spectrum (400 Hz) of **109u**

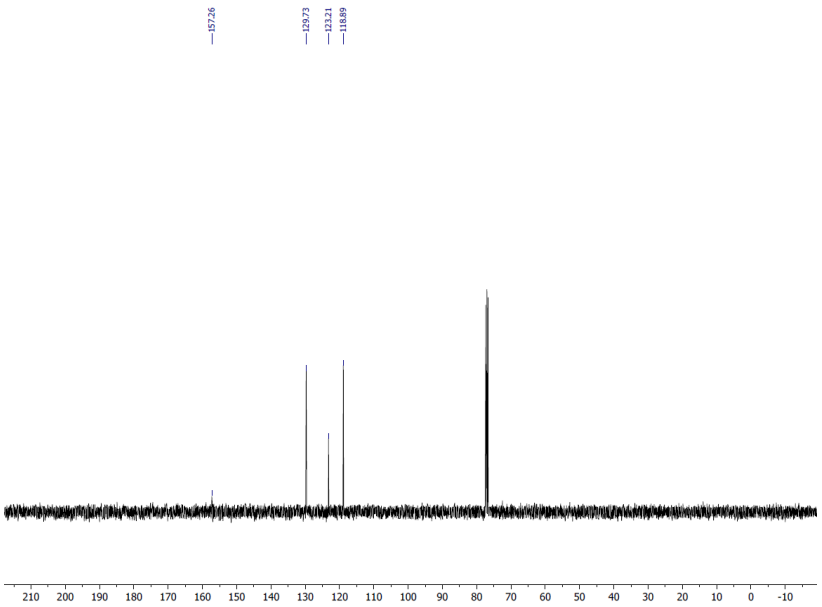

^{13}C NMR spectrum (101 Hz) of **109u**

Photodebromination

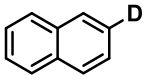

109n(D)

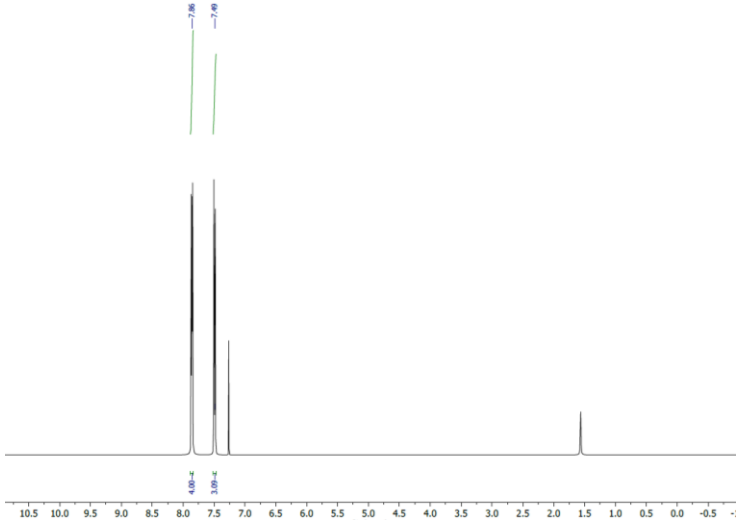

^{1}H NMR spectrum (400 Hz) of **109n(D)**

^{2}H NMR spectrum (400 Hz) of **109n(D)**

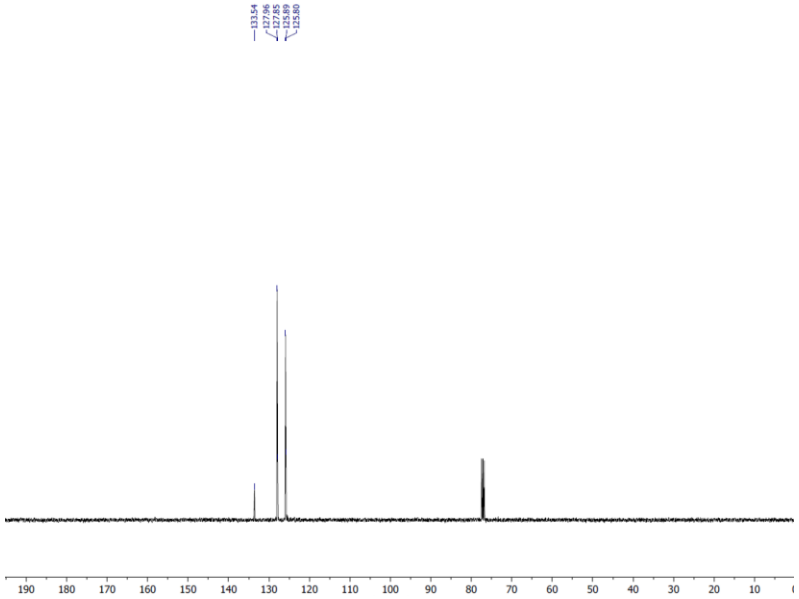

^{13}C NMR spectrum (101 Hz) of **109n(D)**

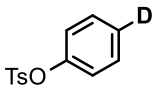

109i(D)

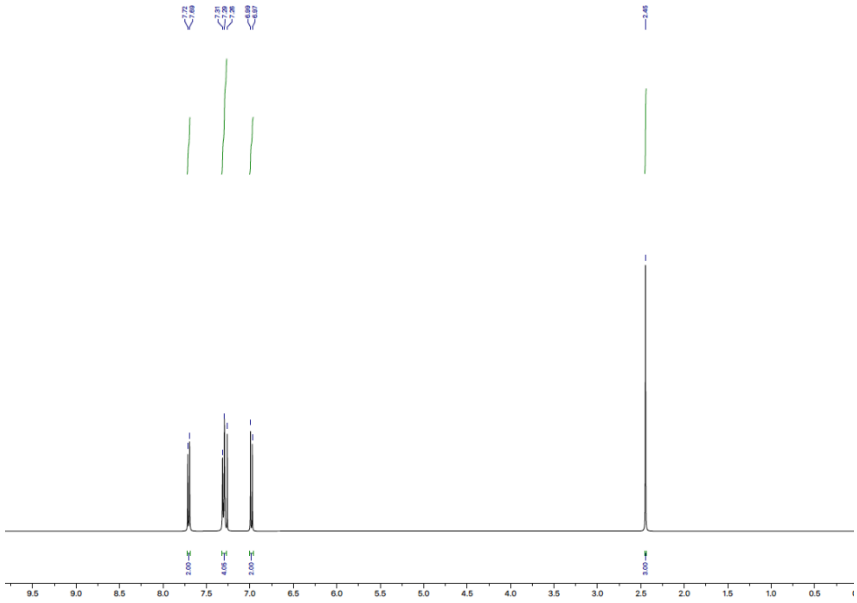

^{1}H NMR spectrum (400 Hz) of **109i(D)**

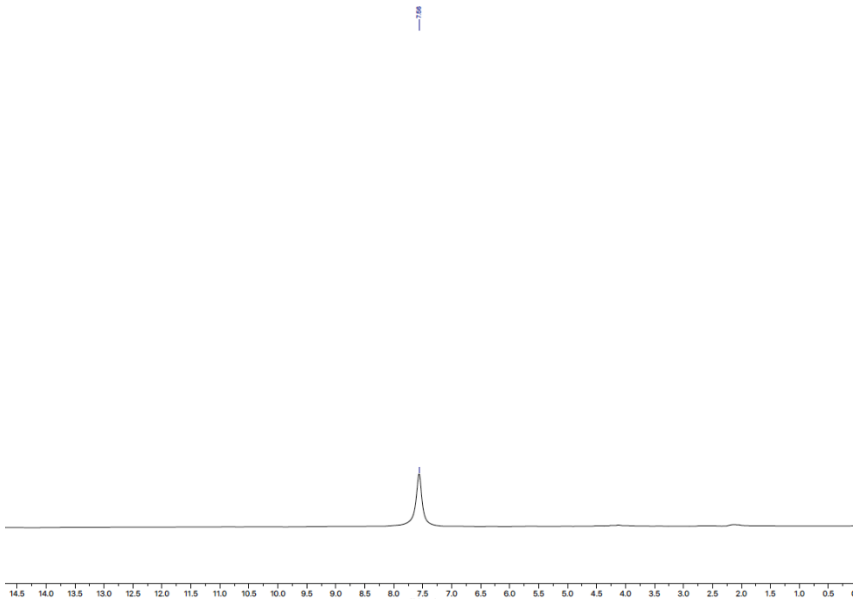

^{1}H NMR spectrum (400 Hz) of **109i(D)**

Photodebromination

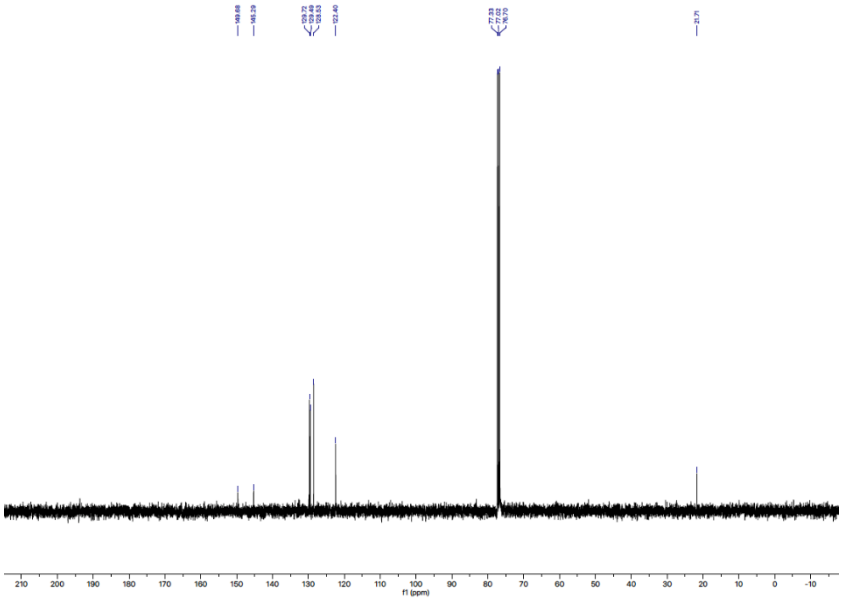

^{13}C NMR spectrum (101 Hz) of **109i(D)**

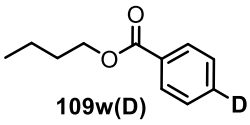

109w(D)

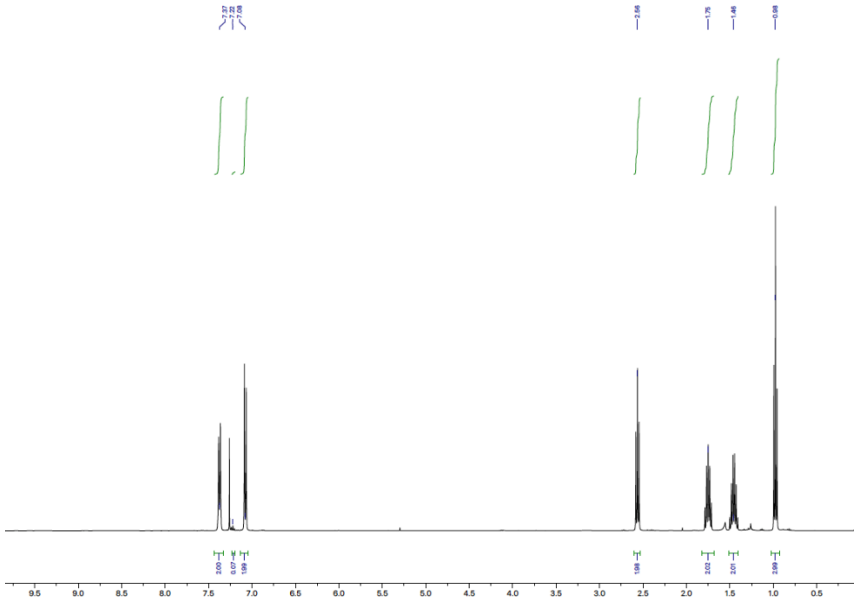

^{1}H NMR spectrum (400 Hz) of **109w(D)**

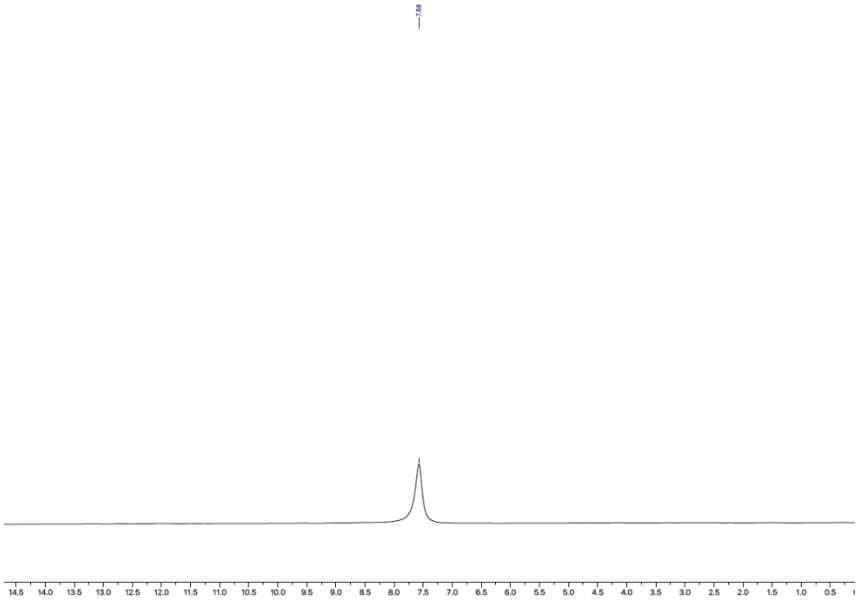

^{2}H NMR spectrum (400 Hz) of **109w(D)**

Photodebromination

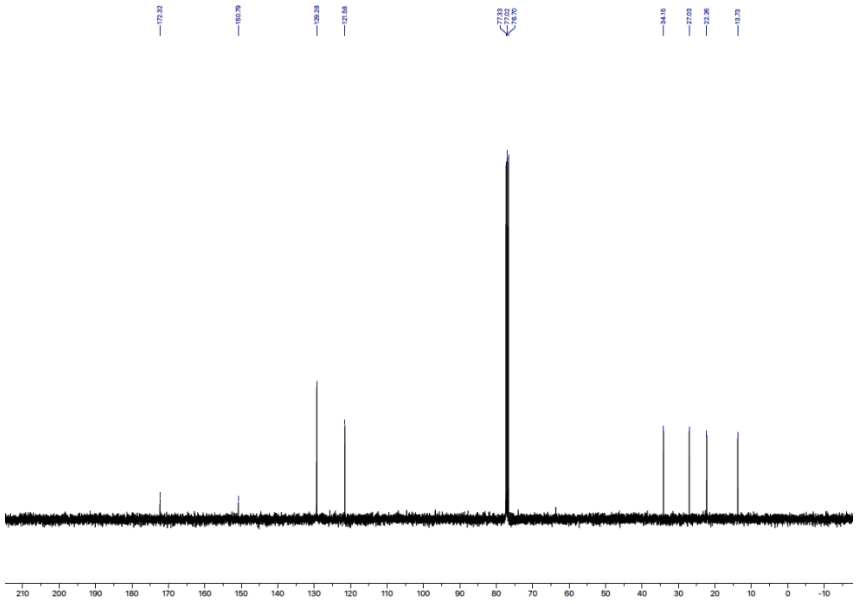

^{13}C NMR spectrum (101 Hz) of **109w(D)**

4.3. References

294. a) *Copper-Mediated Cross-Coupling Reactions*; Evano, G., Blanchard, N., Eds.; Wiley: Hoboken, New Jersey, 2014.
b) Mikami, K.; Hatano, M.; Akiyama, K. Active Pd(II) Complexes as Either Lewis Acid Catalysts or Transition Metal Catalysts. In *Palladium in Organic Synthesis : -/-*; 2005; Vol. 14, p 279.

295. a) Jeschke, P. Manufacturing Approaches of New Halogenated Agrochemicals. *European Journal of Organic Chemistry* **2022**, *2022* (12), e202101513. https://doi.org/10/gqp3jj.
b) Chapter 17 Non-Petroleum Liquids as Lubricants. In *Tribology Series*; Elsevier, 1985; Vol. 9, pp 501–520. https://doi.org/10.1016/S0167-8922(08)70856-3.
c) Torborg, C.; Beller, M. Recent Applications of Palladium-Catalyzed Coupling Reactions in the Pharmaceutical, Agrochemical, and Fine Chemical Industries. *Adv. Synth. Catal.* **2009**, *351* (18), 3027–3043. https://doi.org/10/cj3jnd.

296. Cagnetta, G.; Robertson, J.; Huang, J.; Zhang, K.; Yu, G. Mechanochemical Destruction of Halogenated Organic Pollutants: A Critical Review. *Journal of hazardous materials* **2016**, *313*, 85–102. https://doi.org/10/gpg28b.

297. Alonso, F.; Beletskaya, I. P.; Yus, M. Metal-Mediated Reductive Hydrodehalogenation of Organic Halides. *Chemical Reviews* **2002**, *102* (11), 4009–4092. https://doi.org/10/ft5wxh.

298. Ramanathan, A.; Jimenez, L. S. Reductive Dehalogenation of Aryl Bromides and Chlorides and Their Use as Aryl Blocking Groups. *Synthesis* **2010**, No. 2, 217–220. https://doi.org/10/cqwd2s.

299. Li, W.; Rabeah, J.; Bourriquen, F.; Yang, D.; Kreyenschulte, C.; Rockstroh, N.; Lund, H.; Bartling, S.; Surkus, A.-E.; Junge, K.; Brückner, A.; Lei, A.; Beller, M. Scalable and Selective Deuteration of (Hetero)Arenes. *Nat. Chem.* **2022**, *14* (3), 334–341. https://doi.org/10/gqp3jk.

300 Cole, S. J.; Nicholas Kirwan, J.; Roberts, B. P.; Willis, C. R. Radical Chain Reduction of Alkyl Halides, Dialkyl Sulphides and O-Alkyl S-Methyl Dithiocarbonates to Alkanes by Trialkylsilanes. *Journal of the Chemical Society, Perkin Transactions 1* **1991**, No. 1, 103–112. https://doi.org/10.1039/p19910000103.

301 Isse, A. A.; Lin, C. Y.; Coote, M. L.; Gennaro, A. Estimation of Standard Reduction Potentials of Halogen Atoms and Alkyl Halides. *Journal of Physical Chemistry B* **2011**, *115* (4), 678–684. https://doi.org/10/fmwvc3.

302. Bailey, W. F.; Patricia, J. J. The Mechanism of the Lithium - Halogen Interchange Reaction : A Review of the Literature. *Journal of Organometallic Chemistry* **1988**, *352* (1), 1–46. https://doi.org/10.1016/0022-328x(88)83017-1.

303. Guijarro, A.; Ramón, D. J.; Yus, M. Naphthalene-Catalysed Lithiation of Functionalized Chloroarenes: Regioselective Preparation and Reactivity of Functionalized Lithioarenes. *Tetrahedron* **1993**, *49* (2), 469–482. https://doi.org/10/bvn6dw.

304. Sodium – Miura, Y.; Oka, H.; Yamano, E.; Morita, M. Convenient Deuteration of Bromo Aromatic Compounds by Reductive Debromination with Sodium Amalgam in CH3OD. *The Journal of Organic Chemistry* **1997**, *62* (4), 1188–1190. https://doi.org/10.1021/jo9619037.

305. a) Mackenzie, K.; Kopinke, F.-D. Debromination of Duroplastic Flame-Retarded Polymers. *Chemosphere* **1996**, *33* (12), 2423–2430. https://doi.org/10/cc85gh.
b) Miyoshi, K.; Nishio, T.; Yasuhara, A.; Morita, M. Dechlorination of Hexachlorobiphenyl by Using Potassium–Sodium Alloy. *Chemosphere* **2000**, *41* (6), 819–824. https://doi.org/10/fgb2hq.
c) Boyarskii, V. P.; Sangaranarayanan, M. V.; Khaibulova, T. Sh.; Boyarskaya, I. A. Reduction of Mono- and Dichlorobiphenyls with Sodium-Naphthalene Complex. *Russ J Gen Chem* **2010**, *80* (4), 800–808. https://doi.org/10/fk4jc3.

306. Jouha, J.; Khouili, M.; Hiebel, M. A.; Guillaumet, G.; Suzenet, F. Room Temperature Dehalogenation of (Hetero)Aryl Halides with Magnesium/Methanol. *Tetrahedron Letters* **2018**, *59* (32), 3108–3111. https://doi.org/10/gqfc98.

307. a) Knochel, P.; Dohle, W.; Gommermann, N.; Kneisel, F. F.; Kopp, F.; Korn, T.; Sapountzis, I.; Vu, V. A. Highly Functionalized Organomagnesium Reagents Prepared through Halogen–Metal Exchange. *Angewandte Chemie International Edition* **2003**, *42* (36), 4302–4320. https://doi.org/10.1002/anie.200300579.
b) Nishiyama, H.; Isaka, K.; Itoh, K.; Ohno, K.; Nagase, H.; Matsumoto, K.; Yoshiwara, H. Metal-Halogen Exchange between Polybromoanisoles and Aliphatic Grignard Reagents: A Synthesis of Cyclopenta[b]Benzofurans. *The Journal of Organic Chemistry* **1992**, *57* (1), 407–410. https://doi.org/10.1021/jo00027a078.

(308) Wang, X.; Zhu, M.-H.; Schuman, D. P.; Zhong, D.; Wang, W.-Y.; Wu, L.-Y.; Liu, W.; Stoltz, B. M.; Liu, W.-B. General and Practical Potassium Methoxide/Disilane-Mediated Dehalogenative Deuteration of (Hetero)Arylhalides. *Journal of the American Chemical Society* **2018**, *140* (35), 10970–10974. https://doi.org/10.1021/jacs.8b07597.

309. $CDCl_3$ (0.75 \$ g^{-1}), D_2O (2.39 \$ g^{-1}), DMSO-d_6 (3.50 \$ g^{-1}), MeOD (3.77 \$ g^{-1}), Acetone-d_6 (4.28 \$ g^{-1}), THF-d_8 (43.70 \$ g^{-1})
NMR Solvents - Alfa Aesar. https://www.alfa.com/en/nmr-solvents/ (accessed 2022-08-25).
Tetrahydrofuran-d8 D = 99.5atom 1693-74-9. http://www.sigmaaldrich.com/ (accessed 2022-08-26).

310. Selected silicon hydride mediated techniques:
Cole, S. J.; Nicholas Kirwan, J.; Roberts, B. P.; Willis, C. R. Radical Chain Reduction of Alkyl Halides, Dialkyl Sulphides and O-Alkyl S-Methyl Dithiocarbonates to Alkanes by Trialkylsilanes. *Journal of the Chemical Society, Perkin Transactions 1* **1991**, No. 1, 103–112. https://doi.org/10.1039/p19910000103.
Selected tin hydride mediated techniques:

Maitra, U.; Das Sarma, K. Tri-n-Butylin Hydride Mediated Dehalogenation in Water. *Tetrahedron Letters* **1994**, *35* (42), 7861–7862. https://doi.org/10.1016/0040-4039(94)80137-1.
Selected germanium hydride mediated techniques:
Sakurai, H.; Mochida, K.; Hosomi, A.; Mita, F. Organogermanium Compounds: II. Reduction of Organic Halides with Hydrogermanes. *Journal of Organometallic Chemistry* **1972**, *38* (2), 275–280. https://doi.org/10.1016/s0022-328x(00)83329-x.

311 Donald, C. S.; Moss, T. A.; Noonan, G. M.; Roberts, B.; Durham, E. C. Deuterodehalogenation - A Mild Method for Synthesising Deuterated Heterocycles. *Tetrahedron Letters* **2014**, *55* (22), 3305–3307. https://doi.org/10.1016/j.tetlet.2014.04.025.
Yang, J.; Brookhart, M. Iridium-Catalyzed Reduction of Alkyl Halides by Triethylsilane. *Journal of the American Chemical Society* **2007**, *129* (42), 12656–12657. https://doi.org/10.1021/ja075725i.
Pilli, R.; Balakrishnan, V.; Chandrasekaran, R.; Rasappan, R. Iron-Catalyzed Hydrodehalogenation of Alkyl and Aryl Halides Using Hydrosilanes. *Organic and Biomolecular Chemistry* **2019**, *17* (7), 1749–1753. https://doi.org/10.1039/c8ob02365d.

312. Weidauer, M.; Irran, E.; Someya, C. I.; Haberberger, M.; Enthaler, S. Nickel-Catalyzed Hydrodehalogenation of Aryl Halides. *Journal of Organometallic Chemistry* **2013**, *729*, 53–59. https://doi.org/10.1016/j.jorganchem.2013.01.014.
Ganem, B.; Osby, J. O.; Truce, W. E.; Roberts, F. E.; Perry, F. M.; Strohmeier, W.; Steigerwald, . Z; Naturforschungb ; Karn, J. L.; Busch, D. H.; Curry, J. D. Nickel Complexes as Soluble Catalysts for Reductive Dehalogenation of Aromatic Halides. *J. Am. Chem. Soc* **1994**, *59* (2), 5381–5385.
Lipshutz, B. H.; Tomioka, T.; Sato, K. Nickel-on-Charcoal-Catalyzed Reductions of Aryl Chlorides. *Synlett* **2001**, *2001* (Special Issue), 970–973. https://doi.org/10.1055/s-2001-14636.
Desmarets, C.; Kuhl, S.; Schneider, R.; Fort, Y. Nickel(0)/Imidazolium Chloride Catalyzed Reduction of Aryl Halides. **2002**. https://doi.org/10.1021/om010949.
Colon, I. Reduction of Organic Halides by Water and Zinc Effected by Nickel. *The Journal of Organic Chemistry* **1982**, *47* (13), 2622–2625. https://doi.org/10.1021/jo00134a021.

313. Guo, H.; Kanno, K. I.; Takahashi, T. Iron-Catalyzed Dechlorination of Aryl Chlorides. *Chemistry Letters* **2004**, *33* (10), 1356–1357. https://doi.org/10/bnxrg6.
Czaplik, W. M.; Grupe, S.; Mayer, M.; Wangelin, A. J. V. Practical Iron-Catalyzed Dehalogenation of Aryl Halides. *Chemical Communications* **2010**, *46* (34), 6350–6352. https://doi.org/10.1039/c0cc01980a.
Zhuang, Y.; Ahn, S.; Seyfferth, A. L.; Masue-Slowey, Y.; Fendorf, S.; Luthy, R. G. Dehalogenation of Polybrominated Diphenyl Ethers and Polychlorinated Biphenyl by Bimetallic, Impregnated, and Nanoscale Zerovalent Iron. *Environmental Science & Technology* **2011**, *45* (11), 4896–4903. https://doi.org/10.1021/es104312h.

314 *Heterogeneous Palladium:*
Sajiki, H.; Kume, A.; Hattori, K.; Hirota, K. Mild and General Procedure for Pd/C-Catalyzed Hydrodechlorination of Aromatic Chlorides. *Tetrahedron Letters* **2002**, *43* (40), 7247–7250. https://doi.org/10.1016/s0040-4039(02)01622-2.
Homogeneous:
a) Logan, M. E.; Oinen, M. E. Dechlorination of Aryl Chlorides with Sodium Formate Using a Homogeneous Palladium Catalyst. *Organometallics* **2006**, *25* (4), 1052–1054. https://doi.org/10/d253mn.
b) Hadnagy, E.; Gardner, K. H.; Rauch, L. M. Dechlorination of Polychlorinated Biphenyls, Naphthalenes and Dibenzo-p-Dioxins by Magnesium/Palladium Bimetallic Particles. *Journal of Environmental Science and Health, Part A* **2007**, *42* (6), 685–695. https://doi.org/10.1080/10934520701326222.
c) Moon, J.; Lee, S. Palladium Catalyzed-Dehalogenation of Aryl Chlorides and Bromides Using Phosphite Ligands. *Journal of Organometallic Chemistry* **2009**, *694* (3), 473–477. https://doi.org/10/dzfx8r

315 Janni, M.; Peruncheralathan, S. Catalytic Selective Deuteration of Halo(Hetero)Arenes. *Org. Biomol. Chem.* **2016**, *14* (11), 3091–3097. https://doi.org/10.1039/C6OB00193A.

316 a) Fujita, K. I.; Owaki, M.; Yamaguchi, R. Chemoselective Transfer Hydrodechlorination of Aryl Chlorides Catalyzed by Cp*Rh Complexes. *Chemical Communications* **2002**, No. 24, 2964–2965. https://doi.org/10.1039/b209855e.
b) You, T.; Wang, Z.; Chen, J.; Xia, Y. Transfer Hydro-Dehalogenation of Organic Halides Catalyzed by Ruthenium(II) Complex. *The Journal of Organic Chemistry* **2017**, *82* (3), 1340–1346. https://doi.org/10.1021/acs.joc.6b02222.

317. Wang, D.; Astruc, D. The Golden Age of Transfer Hydrogenation. *Chem. Rev.* **2015**, *115* (13), 6621–6686. https://doi.org/10/gg45w7.

318. Wang, X.; Zhu, M.-H.; Schuman, D. P.; Zhong, D.; Wang, W.-Y.; Wu, L.-Y.; Liu, W.; Stoltz, B. M.; Liu, W.-B. General and Practical Potassium Methoxide/Disilane-Mediated Dehalogenative Deuteration of (Hetero)Arylhalides. *J. Am. Chem. Soc.* **2018**, *140* (35), 10970–10974. https://doi.org/10/gqp3j3.

319. Cargnin, S.; Serafini, M.; Pirali, T. A Primer of Deuterium in Drug Design. *Future Medicinal Chemistry* **2019**, *11* (16), 2039–2042. https://doi.org/10.4155/fmc-2019-0183.
Kopf, S.; Bourriquen, F.; Li, W.; Neumann, H.; Junge, K.; Beller, M. Recent Developments for the Deuterium and Tritium Labeling of Organic Molecules. *Chem. Rev.* **2022**, *122* (6), 6634–6718. https://doi.org/10/gqp3dd.

320. Hokamp, T.; Dewanji, A.; Lübbesmeyer, M.; Mück-Lichtenfeld, C.; Würthwein, E.-U.; Studer, A. Radical Hydrodehalogenation of Aryl Bromides and Chlorides with Sodium Hydride and 1,4-Dioxane. *Angewandte Chemie International Edition* **2017**, *56* (43), 13275–13278. https://doi.org/10.1002/anie.201706534.

321. a) Nelson, R. B.; Gribble, G. W. Reduction of Aryl Iodides with Sodium Hydride. *J. Org. Chem.* **1974**, *39* (10), 1425–1426. https://doi.org/10/cfnt2c.
b) Ong, D. Y.; Tejo, C.; Xu, K.; Hirao, H.; Chiba, S. Hydrodehalogenation of Haloarenes by a Sodium Hydride-Iodide Composite. *Angew. Chem.* **2017**, *129* (7), 1866–1870. https://doi.org/10/f3twcr.

322. Luo, Y.-R. *Comprehensive Handbook of Chemical Bond Energies*, 1st ed.; CRC Press, 2007. https://doi.org/10.1201/9781420007282.

323. a) Fukuyama, T.; Fujita, Y.; Miyoshi, H.; Ryu, I.; Kao, S.-C.; Wu, Y.-K. Electron Transfer-Induced Reduction of Organic Halides with Amines. *Chem. Commun.* **2018**, *54* (44), 5582–5585. https://doi.org/10/gqfdbd.
b) Yoshimi, Y.; Ishise, A.; Oda, H.; Moriguchi, Y.; Kanezaki, H.; Nakaya, Y.; Katsuno, K.; Itou, T.; Inagaki, S.; Morita, T.; Hatanaka, M.

Hydroxide Ion as Electron Source for Photochemical Birch-Type Reduction and Photodehalogenation. *Tetrahedron Letters* **2008**, *49* (21), 3400–3404. https://doi.org/10/d625cd.

324. Speckmeier, E.; Fischer, T. G.; Zeitler, K. A Toolbox Approach to Construct Broadly Applicable Metal-Free Catalysts for Photoredox Chemistry: Deliberate Tuning of Redox Potentials and Importance of Halogens in Donor-Acceptor Cyanoarenes. *Journal of the American Chemical Society* **2018**, *140* (45), 15353–15365. https://doi.org/10.1021/jacs.8b08933.

325. a) Schmalzbauer, M.; Ghosh, I.; König, B. Utilising Excited State Organic Anions for Photoredox Catalysis: Activation of (Hetero)Aryl Chlorides by Visible Light-Absorbing 9-Anthrolate Anions. *Faraday Discuss.* **2019**, *215*, 364–378. https://doi.org/10/ggp3j5.
b) Schmalzbauer, M.; Marcon, M.; König, B. Excited State Anions in Organic Transformations. *Angew. Chem. Int. Ed.* **2021**, *60* (12), 6270–6292. https://doi.org/10/ggfc9s.

326. Ghosh, I.; Ghosh, T.; Bardagi, J. I.; König, B. Reduction of Aryl Halides by Consecutive Visible Light-Induced Electron Transfer Processes. *Science* **2014**, *346* (6210), 725–728. https://doi.org/10.1126/science.1258232.

327 Kim, H.; Kim, H.; Lambert, T. H.; Lin, S. Reductive Electrophotocatalysis: Merging Electricity and Light to Achieve Extreme Reduction Potentials. *Journal of the American Chemical Society* **2020**, *142* (5), 2087–2092. https://doi.org/10.1021/jacs.9b10678.

328. Glaser, F.; Wenger, O. S. Red Light-Based Dual Photoredox Strategy Resembling the Z-Scheme of Natural Photosynthesis. *JACS Au* **2022**, *2* (6), 1488–1503. https://doi.org/10/gqfs7q.

329. Nguyen, J. D.; D'Amato, E. M.; Narayanam, J. M. R.; Stephenson, C. R. J. Engaging Unactivated Alkyl, Alkenyl and Aryl Iodides in Visible-Light-Mediated Free Radical Reactions. *Nature Chem* **2012**, *4* (10), 854–859. https://doi.org/10/f392v5.

330. Treat, N. J.; Sprafke, H.; Kramer, J. W.; Clark, P. G.; Barton, B. E.; Read de Alaniz, J.; Fors, B. P.; Hawker, C. J. Metal-Free Atom Transfer Radical Polymerization. *J. Am. Chem. Soc.* **2014**, *136* (45), 16096–16101. https://doi.org/10/gg2t8b.

331. Matsubara, R.; Yabuta, T.; Md Idros, U.; Hayashi, M.; Ema, F.; Kobori, Y.; Sakata, K. UVA- and Visible-Light-Mediated Generation of Carbon Radicals from Organochlorides Using Nonmetal Photocatalyst. *J. Org. Chem.* **2018**, *83* (16), 9381–9390. https://doi.org/10/gdw7mq.

332. Joshi-Pangu, A.; Lévesque, F.; Roth, H. G.; Oliver, S. F.; Campeau, L.-C.; Nicewicz, D.; DiRocco, D. A. Acridinium-Based Photocatalysts: A Sustainable Option in Photoredox Catalysis. *J. Org. Chem.* **2016**, *81* (16), 7244–7249. https://doi.org/10/f8zfxn.

333. Schmalzbauer, M.; Marcon, M.; König, B. Excited State Anions in Organic Transformations. *Angewandte Chemie - International Edition* **2021**, *60* (12), 6270–6292. https://doi.org/10/ggfc9s.

334. Zeman, C. J.; Kim, S.; Zhang, F.; Schanze, K. S. Direct Observation of the Reduction of Aryl Halides by a Photoexcited Perylene Diimide Radical Anion. *Journal of the American Chemical Society* **2020**, *142* (5), 2204–2207. https://doi.org/10.1021/jacs.9b13027.

335. Kim, H.; Kim, H.; Lambert, T. H.; Lin, S. Reductive Electrophotocatalysis: Merging Electricity and Light to Achieve Extreme Reduction Potentials. *Journal of the American Chemical Society* **2020**, *142* (5), 2087–2092. https://doi.org/10.1021/jacs.9b10678.

336. Photosynthesis. *Wikipedia*; 2022.

337. *The paper*. https://www.life.illinois.edu/govindjee/paper/gov.html (accessed 2022-08-26).
Thursday, November 9, 2000. https://www.life.illinois.edu/govindjee/textzsch.htm (accessed 2022-08-26).

338. a) Sasaki, Y.; Kato, H.; Kudo, A. [Co(Bpy)3]3+/2+ and [Co(Phen)3]3+/2+ Electron Mediators for Overall Water Splitting under Sunlight Irradiation Using Z-Scheme Photocatalyst System. *J. Am. Chem. Soc.* **2013**, *135* (14), 5441–5449. https://doi.org/10/f4smpq.
b) Maeda, K. Z-Scheme Water Splitting Using Two Different Semiconductor Photocatalysts. *ACS Catal.* **2013**, *3* (7), 1486–1503. https://doi.org/10/f45x3j.

339. Widness, J. K.; Enny, D. G.; McFarlane-Connelly, K. S.; Miedenbauer, M. T.; Krauss, T. D.; Weix, D. J. CdS Quantum Dots as Potent Photoreductants for Organic Chemistry Enabled by Auger Processes. *J. Am. Chem. Soc.* **2022**. https://doi.org/10/gqfn3b.

340. Häring, M.; Pérez-Ruiz, R.; von Wangelin, A.; Díaz, D. D. Intragel Photoreduction of Aryl Halides by Green-to-Blue Upconversion under Aerobic Conditions. *Chem. Commun.* **2015**, *51* (94), 16848–16851. https://doi.org/10.1039/C5CC06917C.

341. Zhou, Z.-Z.; Zhao, J.-H.; Gou, X.-Y.; Chen, X.-M.; Liang, Y.-M. Visible-Light-Mediated Hydrodehalogenation and Br/D Exchange of Inactivated Aryl and Alkyl Halides with a Palladium Complex. *Org. Chem. Front.* **2019**, *6* (10), 1649–1654. https://doi.org/10.1039/C9QO00240E.

342. The numbering for the aryl bromides and their reduction will change over the course of the chapter, as we believed it was the clearest way to show the works.

343. van Leeuwen, P. W. N. M.; Kamer, P. C. J.; Reek, J. N. H.; Dierkes, P. Ligand Bite Angle Effects in Metal-Catalyzed C−C Bond Formation. *Chem. Rev.* **2000**, *100* (8), 2741–2770. https://doi.org/10/btpxs3.

344. Liu, K.; Xin, H.; Han, M. Elucidation of Key Factors in Nickel-Diphosphines CatalyzedIsomerization of 2-Methyl-3-Butenenitrile. *Journal of Catalysis* **2019**, *377*, 13–19. https://doi.org/10/gqkjfr.
Birkholz (née Gensow), M.-N.; Freixa, Z.; van Leeuwen, P. W. N. M. Bite Angle Effects of Diphosphines in C–C and C–X Bond Forming Cross Coupling Reactions. *Chem. Soc. Rev.* **2009**, *38* (4), 1099. https://doi.org/10/bqzjv4.

345. Boyd, T. M.; Tegner, B. E.; Tizzard, G. J.; Martínez-Martínez, A. J.; Neale, S. E.; Hayward, M. A.; Coles, S. J.; Macgregor, S. A.; Weller, A. S. A Structurally Characterized Cobalt(I) σ-Alkane Complex. *Angewandte Chemie International Edition* **2020**, *59* (15), 6177–6181. https://doi.org/10/gqkjgk.
Sitte, N. A.; Ghiringhelli, F.; Shevchenko, G. A.; Rominger, F.; Hashmi, A. S. K.; Schaub, T. Copper-Catalysed Synthesis of Propargyl Alcohol and Derivatives from Acetylene and Other Terminal Alkynes. *Advanced Synthesis & Catalysis* **2022**, *364* (13), 2227–2234. https://doi.org/10/gqkjqj.

Photodebromination

346. Evano, G.; Nitelet, A.; Thilmany, P.; Dewez, D. F. Metal-Mediated Halogen Exchange in Aryl and Vinyl Halides: A Review. *Frontiers in Chemistry* **2018**, *6*. https://doi.org/10/gnrphf.

347. a) Muto, K., Yamaguchi, J., Lei, A., & Itami, K. (2013). Isolation, structure, and reactivity of an arylnickel(II) pivalate complex in catalytic C-H/C-O biaryl coupling. *Journal of the American Chemical Society*, *135*(44), 16384–16387. https://doi.org/10.1021/ja409803x
b) Somerville, R. J., Hale, L. V. A., Gómez-Bengoa, E., Burés, J., & Martin, R. (2018). Intermediacy of Ni-Ni Species in sp2 C-O Bond Cleavage of Aryl Esters: Relevance in Catalytic C-Si Bond Formation. *Journal of the American Chemical Society*, *140*(28), 8771–8780. https://doi.org/10.1021/jacs.8b04479

348 Zhuang, Y., Ahn, S., Seyfferth, A. L., Masue-Slowey, Y., Fendorf, S., & Luthy, R. G. (2011). Dehalogenation of polybrominated diphenyl ethers and polychlorinated biphenyl by bimetallic, impregnated, and nanoscale zerovalent iron. Environmental Science and Technology, 45(11), 4896–4903. https://doi.org/10.1021/es104312h

349. a) Siddiqi, M. A.; Laessig, R. H.; Reed, K. D. Polybrominated Diphenyl Ethers (PBDEs): New Pollutants-Old Diseases. *Clinical Medicine & Research* **2003**, *1* (4), 281–290. https://doi.org/10/dzh6bt.
b) Polybrominated Diphenyl Ethers. *Wikipedia*; 2022. https://en.wikipedia.org/wiki/Polybrominated_diphenyl_ethers
c) Scientific Opinion on Polybrominated Diphenyl Ethers (PBDEs) in Food | EFSA. https://www.efsa.europa.eu/es/efsajournal/pub/2156 (accessed 2022-08-26).

350. Harbeson, S. L., & Tung, R. D. (2011). Deuterium in Drug Discovery and Development. In Annual Reports in Medicinal Chemistry (Vol. 46, pp. 403–417). Academic Press Inc. https://doi.org/10.1016/B978-0-12-386009-5.00003-5

Cargnin, S., Serafini, M., & Pirali, T. (2019). A primer of deuterium in drug design. Future Medicinal Chemistry, 11(16), 2039–2042. https://doi.org/10.4155/fmc-2019-0183

351. a) Tsou, T. T.; Kochi, J. K. Mechanism of Oxidative Addition. Reaction of Nickel(0) Complexes with Aromatic Halides. *J. Am. Chem. Soc.* **1979**, *101* (21), 6319–6332. https://doi.org/10/fsgmg4.
b) Nelson, D. J.; Maseras, F. Steric Effects Determine the Mechanisms of Reactions between Bis(N-Heterocyclic Carbene)-Nickel(0) Complexes and Aryl Halides. *Chem. Commun.* **2018**, *54* (75), 10646–10649. https://doi.org/10/gqk57d.

352. a) Hwang, S. J.; Anderson, B. L.; Powers, D. C.; Maher, A. G.; Hadt, R. G.; Nocera, D. G. Halogen Photoelimination from Monomeric Nickel(III) Complexes Enabled by the Secondary Coordination Sphere. *Organometallics* **2015**, *34* (19), 4766–4774. https://doi.org/10/f7vbn6.
b) Hwang, S. J.; Powers, D. C.; Maher, A. G.; Anderson, B. L.; Hadt, R. G.; Zheng, S. L.; Chen, Y. S.; Nocera, D. G. Trap-Free Halogen Photoelimination from Mononuclear Ni(III) Complexes. *Journal of the American Chemical Society* **2015**, *137* (20), 6472–6475. https://doi.org/10.1021/jacs.5b03192.

353. Heitz, D. R.; Tellis, J. C.; Molander, G. A. Photochemical Nickel-Catalyzed C-H Arylation: Synthetic Scope and Mechanistic Investigations. *Journal of the American Chemical Society* **2016**, *138* (39), 12715–12718. https://doi.org/10/f86xmf.

354. Shields, B. J.; Kudisch, B.; Scholes, G. D.; Doyle, A. G. Long-Lived Charge-Transfer States of Nickel(II) Aryl Halide Complexes Facilitate Bimolecular Photoinduced Electron Transfer. *J. Am. Chem. Soc.* **2018**, *140* (8), 3035–3039. https://doi.org/10/gqm2sr

Ting, S. I.; Garakyaraghi, S.; Taliaferro, C. M.; Shields, B. J.; Scholes, G. D.; Castellano, F. N.; Doyle, A. G. 3d-d Excited States of Ni(II) Complexes Relevant to Photoredox Catalysis: Spectroscopic Identification and Mechanistic Implications. *ACS Applied Materials and Interfaces* **2020**, No. Ii. https://doi.org/10.1021/jacs.0c00781.

355 a) One suggestion could be the generation of the aryliodide in situ which may get more easily reduced: Klapars, A.; Buchwald, S. L. Copper-Catalyzed Halogen Exchange in Aryl Halides: An Aromatic Finkelstein Reaction. *J. Am. Chem. Soc.* **2002**, *124* (50), 14844–14845. https://doi.org/10/dj3dkv.
b) Cant, A. A.; Bhalla, R.; Pimlott, S. L.; Sutherland, A. Nickel-Catalysed Aromatic Finkelstein Reaction of Aryl and Heteroaryl Bromides. *Chem. Commun.* **2012**, *48* (33), 3993–3995. https://doi.org/10/gqp3mb.
c) Li, L.; Liu, W.; Mu, X.; Mi, Z.; Li, C.-J. Photo-Induced Iodination of Aryl Halides under Very Mild Conditions. *Nat Protoc* **2016**, *11* (10), 1948–1954. https://doi.org/10/gpfsfq.

356. Scattolin, T.; Caligiuri, I.; Canovese, L.; Demitri, N.; Gambari, R.; Lampronti, I.; Rizzolio, F.; Santo, C.; Visentin, F. Synthesis of New Allyl Palladium Complexes Bearing Purine-Based NHC Ligands with Antiproliferative and Proapoptotic Activities on Human Ovarian Cancer Cell Lines. *Dalton Trans.* **2018**, *47* (38), 13616–13630. https://doi.org/10/gqp3kn.

357. MacKenzie, I. A.; Wang, L.; Onuska, N. P. R.; Williams, O. F.; Begam, K.; Moran, A. M.; Dunietz, B. D.; Nicewicz, D. A. Discovery and Characterization of an Acridine Radical Photoreductant. *Nature* **2020**, *580* (7801), 76–80. https://doi.org/10/ggr9vr.

358. Aukland, M. H.; Šiaučiulis, M.; West, A.; Perry, G. J. P.; Procter, D. J. Metal-Free Photoredox-Catalysed Formal C–H/C–H Coupling of Arenes Enabled by Interrupted Pummerer Activation. *Nat Catal* **2020**, *3* (2), 163–169. https://doi.org/10/gqp3kt.

359. Mangiavacchi, F.; Crociani, L.; Sancineto, L.; Marini, F.; Santi, C. Continuous Bioinspired Oxidation of Sulfides. *Molecules* **2020**, *25* (11), 2711. https://doi.org/10/gqp3kv.

360. Wang, M.-M.; Jeon, S.; Waser, J. Synthesis of Thiochromans via [3+3] Annulation of Aminocyclopropanes with Thiophenols. *Org. Lett.* **2020**, *22* (22), 9123–9127. https://doi.org/10/gqp3kw.

361. Perez, K. A.; Rogers, C. R.; Weiss, E. A. Quantum Dot-Catalyzed Photoreductive Removal of Sulfonyl-Based Protecting Groups. *Angewandte Chemie International Edition* **2020**, *59* (33), 14091–14095. https://doi.org/10.1002/anie.202005074.

362. Tobisu, M.; Yamakawa, K.; Shimasaki, T.; Chatani, N. Nickel-Catalyzed Reductive Cleavage of Aryl–Oxygen Bonds in Alkoxy- and Pivaloxyarenes Using Hydrosilanes as a Mild Reducing Agent. *Chem. Commun.* **2011**, *47* (10), 2946–2948. https://doi.org/10/cbhfwr.

363. Hokamp, T.; Dewanji, A.; Lübbesmeyer, M.; Mück-Lichtenfeld, C.; Würthwein, E.-U.; Studer, A. Radical Hydrodehalogenation of Aryl Bromides and Chlorides with Sodium Hydride and 1,4-Dioxane. *Angewandte Chemie International Edition* **2017**, *56* (43), 13275–13278. https://doi.org/10/gb44r9.

364. Hokamp, T.; Dewanji, A.; Lübbesmeyer, M.; Mück-Lichtenfeld, C.; Würthwein, E.-U.; Studer, A. Radical Hydrodehalogenation of Aryl Bromides and Chlorides with Sodium Hydride and 1,4-Dioxane. *Angewandte Chemie International Edition* **2017**, *56* (43), 13275–13278. https://doi.org/10/gb44r9.

365. Velcicky, J.; Soicke, A.; Steiner, R.; Schmalz, H.-G. Palladium-Catalyzed Cyanomethylation of Aryl Halides through Domino Suzuki Coupling–Isoxazole Fragmentation. *J. Am. Chem. Soc.* **2011**, *133* (18), 6948–6951. https://doi.org/10/fwvcsq.

366. Lyons, D. J. M.; Empel, C.; Pace, D. P.; Dinh, A. H.; Mai, B. K.; Koenigs, R. M.; Nguyen, T. V. Tropolonate Salts as Acyl-Transfer Catalysts under Thermal and Photochemical Conditions: Reaction Scope and Mechanistic Insights. *ACS Catal.* **2020**, *10* (21), 12596–12606. https://doi.org/10/gqp3kz.

367. Samanta, R.; Antonchick, A. P. Palladium-Catalyzed Double C-H Activation Directed by Sulfoxides in the Synthesis of Dibenzothiophenes. *Angewandte Chemie International Edition* **2011**, *50* (22), 5217–5220. https://doi.org/10/c5frdk.

368. Jakob, U.; Mundinger, S.; Bannwarth, W. Efficient Transfer of Chelating Amides into Different Types of Esters and Lactones. *European Journal of Organic Chemistry* **2014**, *2014* (31), 6963–6974. https://doi.org/10/f2t7zh.

369. Tobisu, M.; Nakamura, R.; Kita, Y.; Chatani, N. Rhodium-Catalyzed Reductive Cleavage of Carbon−Cyano Bonds with Hydrosilane: A Catalytic Protocol for Removal of Cyano Groups. *J. Am. Chem. Soc.* **2009**, *131* (9), 3174–3175. https://doi.org/10/b4xtgk.

UNIVERSITAT ROVIRA I VIRGILI
CATALYTIC TRANSFORMATIONS ENABLED BY DUAL NICKELPHOTOREDOX MANIFOLDS
Bradley Higginson

CHAPTER 5.

General Conclusions

5.1. Conclusions

To conclude this thesis, the main points from each of the experimental chapters will be highlighted. The methods disclosed in this thesis are all established within a metallaphotoredox framework which has enabled for mild and selective protocols to be developed.

5.1.1. Chapter 2

- The enantioselective C(sp^3)-H functionalisation has been developed and shows promising reactivity to access synthetically relevant yields.
- The method makes use of a commercially available ^{i}Pr-PHOX ligand which demonstrates excellent control over the enantioninduction on tetrahydrofuran.
- 390 nm wavelength light and the biarylketone photocatalyst were essential in discovering an appropriate platform for further development.

5.1.2. Chapter 3

- A mild, redox neutral platform for the allylic C-H alkylation is developed using alkyl bromides and terminal olefins.
- This platform uses widely accessible alkyl bromides to alkylate at the terminal position in excellent site selectivities and a redox neutral manner.
- The reaction scope could also be extended to a C(sp^3)-C(sp^2) bond forming reaction using aryl bromides.

5.1.3. Chapter 4

- A hydrodehalogenation reaction using the direct photoexcitation of a phosphine ligated nickel is presented.
- The mild access to hydrodehalogenated arenes using THF as the hydrogen donor is broad in scope and can be applied to a range of motifs.
- The applicability of this technique is demonstrated by the dehalogenation of PBDEs and also the deuterodehalogenation of three aryl bromides.
- Mechanistic understandings of this transformation could aid in the development of more robust cross-coupling reactions by eliminating the parasitic hydrodehalogenation reaction. Furthermore, it serves to highlight that direct nickel excitation can be an appropriate platform for bond forming reactions.

Conclusions

UNIVERSITAT
ROVIRA i VIRGILI